STAROST, K.J. 2020. Assessment of nanoparticle emission of polypropylene, polyester and epoxy nanocomposites during automated drilling process. Robert Gordon University [online], PhD thesis. Available from: https://openair.rgu.ac.uk

Assessment of nanoparticle emission of polypropylene, polyester and epoxy nanocomposites during automated drilling process.

STAROST, K.J.

2020

The author of this thesis retains the right to be identified as such on any occasion in which content from this thesis is referenced or re-used. The licence under which this thesis is distributed applies to the text and any original images only – re-use of any third-party content must still be cleared with the original copyright holder.

OpenAIR @RGU

This document was downloaded from https://openair.rgu.ac.uk

CC BY NC

ROBERT GORDON UNIVERSITY ABERDEEN

Assessment of Nanoparticle Emission of Polypropylene, Polyester and Epoxy Nanocomposites during Automated Drilling Process

Kristof Johan Starost

A thesis submitted in partial fulfilment of the
requirements of the
Robert Gordon University
for the degree of Doctor of Philosophy.

Supervisor: Professor James Njuguna

Co-Supervisor: Dr Nadimul Faisal

June 2020

Abstract

Polymer nanocomposites are widely being established within industry due to, among others, their lightweight performance advantages and ability to meticulously target material properties with great control and precision. Despite the beneficial properties introduced, certain nanofillers have shown conceivable health risks and toxicity to humans and the environment. The use and introduction of these materials into the workplace can be hazardous when human exposure is concerned. The risk, exposure and understanding of the influence of embedded nanoparticles within commercial composites have on release during machining processes is yet to be evaluated and quantified.

Four groups of nanocomposites incorporating seven relevant different nanoparticles at different weight concentrations are identified to be utilised within industry and contain potentially harmful nanoparticles if released and exposed. The materials are manufactured and the effect on mechanical properties are investigated through tensile tests, 3-point bend flexural tests, SEM, EDX and FT-IR. An automated drilling methodology in which the background noise is eliminated in the measurements is used for a process approach on the assessment of nanoparticle emissions. The investigation uses real-time measurements using a combination of a Condensation Particle Counter (CPC), Scanning Mobility Particle Sizer Spectrometer (SMPS), a real-time fast mobility particle spectrometer (DMS50) and post-test analytical methods. In this research work, the influence of a variety of nanofillers on nanoparticle release during drilling from three different polymers; polyester (PE), polypropylene (PP) and epoxy (EP) is investigated. For each polymer, respective suitable fillers for the commercial polymer application are chosen and researched with demonstrated modified material properties. The four sets of nanocomposites include PP-based, PE-based, EP-based and a hybrid EP/carbon fibre-based (EP/CF). PP-based samples were reinforced with talcum (Talc), montmorillonite (MMT) and wollastonite (WO). PE-based samples were reinforced with two weight concentrations of nano-silica (SiO_2) and nano-alumina (Al_2O_3). EP-based samples were reinforced with carbon nanotubes (CNT) and carbon nanofibres (CNF). EP/CF-based samples were reinforced with three weight concentrations of graphene oxide (GO).

The fillers utilised within the PP-based samples were ascertained to decrease the material density without significantly affecting the tensile and/or flexural properties. The fillers in the PE-based samples observed minimal effect on the tensile properties; however, all of the reinforcing fillers improved both the flexural modulus and flexural strength. The incorporation of CNFs and CNTs in EP displayed both positive and negative effects on the tensile and flexural properties in comparison to the EP sample. The use of GO within EP/CF demonstrated minimal effect on both the tensile and flexural properties in comparison to the sample without nanoparticle reinforcement.

The study on the PP-based nanocomposites is the first to explore and demonstrate the nanoparticle release from WO and Talc reinforced composites. The nano-filled samples exhibited a 33 % decrease (PP/MMT) or a 30 % increase (PP/WO) on average particle number concentration released in comparison to the virgin PP sample. The size distribution displayed a substantial percentage of the particles released from the PP, PP/WO and PP/MMT samples between 5 nm to 20 nm, whereas the PP/Talc sample emitted larger particle diameters. The results from the PE-based nanocomposites show that the nano-reinforced samples displayed an increase in nanoparticle number concentration by up to 228% compared to virgin PE. The study suggests that the nanofillers adhered to the PE matrix showing a higher concentration of larger particles released (20 nm to 100 nm). The correlation between nanoparticle weight concentration and nanoparticle release can be seen to vary considerably between the SiO_2 and Al_2O_3 samples.

In comparison to the virgin EP, the results revealed that the EP/CNF and EP/CNT samples returned statistically significant differences for all samples and produced an increase of 93% and 211% respectively in average particle number concentration. The particle mass concentration indicated that the release from EP/CNT and EP/CNF samples underlines a vital new perspective needed on CNTs and CNFs embedded within nanocomposite materials to be considered and evaluated for occupational exposure assessment. The incorporation of GO within the EP/CF-based samples displayed a statistically significant increase in nanoparticle release at the three different weight concentrations. However, no relationship between filler weight concentration and nanoparticle release was distinguished. Also, although a statistically significant increase was observed, there was no evidence of the independent fillers in the characterisation and particle size distribution.

Overall, 83 % of the samples investigated exhibited a statistically significant influence on the average particle number concentration with the introduction of nanoparticles within the material. 67 % of the nanocomposites displayed a statistically significant increase, and 17% displayed a statistically significant decrease in the particle number concentration. No clear correlation between mechanical properties and particle number concentration was evident, however revealed to be highly dependent on polymer brittleness and ductility. The results demonstrated that the incorporation of most nanofillers can produce a consequential influence on particle number concentration and therefore may have a detrimental effect on nanoparticle release. It was observed that some samples emitted significant concentrations that surpassed the limits of the CPC instrument on several occasions during the drilling. The significant amount of evidence presented contributes a substantial amount of data on the assessment of nanoparticle release from polymer nanocomposites during drilling.

Keywords: Nanoparticle, emissions, release, drilling, nanocomposite, polymer, nanofiller, mechanical properties

Acknowledgements

Firstly, I would like to express my sincere appreciation to my principal supervisor, Professor James Njuguna, for his extraordinary supervision, support and opportunities provided for me to carry out my research and achievements during my PhD. I am extremely grateful to my second supervisor, Dr Nadimul Faisal, for his supervision, input and approachability at any stage during my research.

My appreciation and acknowledgment goes to the funding bodies of this research. The work was principally funded by part of the European Commission Life project named Simulation of the release of nanomaterials from consumer products for environmental exposure assessment (SIRENA, Pr. No. LIFE 11 ENV/ES/596). I am therefore also grateful to the collaborators on this project especially Maria Blazquez (Inkoa), Ainhoa Egizabal (Tecnalia), Cristina Elizextea (Tecnalia) and Dr Veronica Marchante (Cranfield University). Additionally, I am thankful to the funding from the QualityNano project through Transnational Access (TA Application VITO-TAF-382 and VITO-TAF-500) under the European Commission, Grant Agreement No: INFRA-2010-262163 for the access and use of the facilities at the Flemish Institute for Technological Research (VITO). From this I would like to acknowledge Evelien Frijns, Jo Van Laer and Dr Inge Nelissen. I am also thankful for partial funding by the School of Engineering at Robert Gordon University for my studentship.

Additionally, I would to thank my friends and the entire research community at RGU for their support and entertainment away from academia, especially Dorothy McDonald, Dr Ahmed Salaheldin, Amir Hamedanian, Shohel Siddique, Dr Anil Prathuru and Dr Akshay Nagaraghatta. Furthermore, I would like to thank the assistance of the staff in the School of Engineering at RGU including Allan MacPherson, David Smith, Alan Mclean, Kirsty Stevenson, Catherine Reid, Petrena Morrison and Dr Rosslyn Shanks. A more recent and special thank you goes to Claire Brazier for her belief, unconditional support and merriment away from my studies.

Finally, I would like to extend my most meaningful thank you to my parents, Angela and Graham and two brothers, Stephen and Harry, for their unconditional support and encouragement.

Table of Contents

List of Figures

List of Tables

Nomenclature and Notations

Å	Symbol to represent unit Ångström, equal to 0.1 nm
Al_2O_3	Aluminium oxide, also known as alumina
APS	Aerodynamic particle sizer
ANOVA	Analysis of variance
ASTM	American Society for Testing and Materials
ATO	Antimony-tin oxide
CB	Carbon black
CF	Carbon-fibres
cm	Centimetre
CNF	Carbon nanofibers
CNT	Carbon nanotubes
CPC	Condensation particle counter
CuO	Copper oxide
CV	Coefficient of variation
DMA	Differential mobility analyser
DMS50	Fast mobility particle spectrometer
EDX	Energy-dispersive X-ray spectroscopy
ENM	Engineered nano materials
EP	Epoxy
ESP	Electrostatic precipitator
F	Load
F value	F-statistic used in F-tests and One-Way ANOVA
FMPS	Fast mobility particle sizer
FT-IR	Fourier-transform infrared spectroscopy
ISO	The International Organization for Standardization
kx	Prefix for multiple of magnification i.e. 10^3
L/min	Litres per minute
MMT	Montmorillonite
MWCNTs	Multiwalled carbon nanotubes

NEAT	Nanoparticle Emission Assessment Technique
nm	Nanometres
NIOSH	National Institute for Occupational Safety and Health
OMMT	Organically modified montmorillonite
OPS	Optical particle sizer
PE	Polyester
PP	Polypropylene
SEM	Scanning electron microscope
sp^2	Hybridized atomic orbital binding of one s-orbital and two p- orbitals aligning themselves to a structure with strong binding.
SiO_2	Silica dioxide, also known as silica
SIRENA	European Commission funded project titled: Simulation of the Release of Nanomaterials from Consumer Products for Environmental Exposure Assessment (SIRENA, Pr. No. LIFE 11 ENV/ES/596)SMPS - Scanning Mobility Particle Sizer.
SMPS	Scanning mobility particle sizer
SWCNTs	Single walled carbon nanotubes
TEM	Transmission electron microscope
TiO_2	Titanium dioxide, also known as titania
TSI	TSI Incorporated company headquartered in USA
WO	Wollastonite
wt. %	Weight percentage
XRF	X-ray fluorescence
#/cm^3	Particle number concentration (number of particles/cm^3)

Chapter One

General Introduction

1.1. Introduction

Composite materials are characterized as multi-phase materials comprised of two or more components (*Plueddemann, 2016*). The combination of material constituents in composites come in several forms such as: metallic, ceramic, polymer and bio-based composites (*Vasiliev and Morozov, 2013*). Polymer-based composites are beneficial for lightweight applications due to their strength-to-weight ratio and/or stiffness-to-weight ratio (*Hull and Clyne, 1996*). Polymer composites can be categorised in several comparative ways such as synthetic vs natural or oil resistant vs non-oil-resistant. However, polymers are most regularly characterised as either a thermoset or thermoplastic polymer depending on the behaviour when heated and chemical bonds formed during polymerisation and curing process of the matrix (*Landel and Nielsen, 1993; Pielichowski and Njuguna, 2005*).

Conventional polymer composites are fabricated using a selection of material fillers to modify the properties of the constituent polymer matrix. The size and amount of filler used to transform the characteristics traditionally varies with different composites depending on the resin matrix and the intended application. Due to the combination of ease of manufacture, cost, processing properties and resulting material characteristics, polypropylene (PP), polyester (PE) and epoxy (EP) are three widely used polymer matrices for composite materials. The persistent development, commercial competition and continued pressure to progress within industry has seen a recent influx of composite materials within lightweight applications, such as aerospace as shown in Figure 1 (*Aerospace Technology Institute, 2018*). The transition away from metals is evident within the aeronautical industry with the Airbus A350 jet airliner composed of more than 50% composite materials and the Airbus H160 helicopter third prototype was the first fully composite fuselage in civil rotorcraft demonstrated in 2018 (*Gay, 2014; Breuer, 2016*).

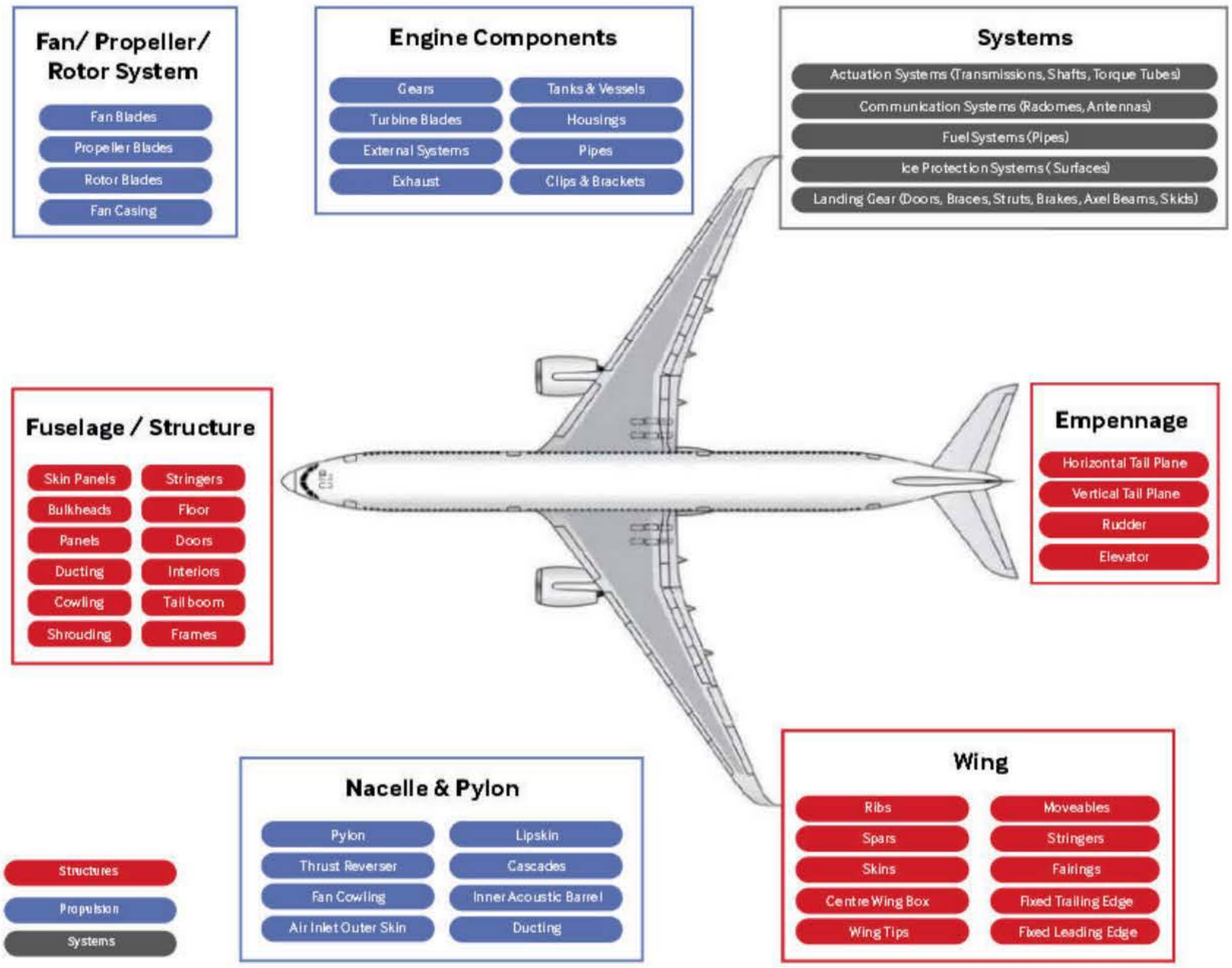

Figure 1: Current aerospace composite products used within industry (*Aerospace Technology Institute, 2018*).

Research into nanotechnology and refining composite materials has led to the introduction of nanocomposites within industry. A nanocomposite is distinct, in that at least one dimension of a filler material is in the nano range: i.e. less than 100 nanometres (*Njuguna et al., 2014; Njuguna and Pielichowski, 2003; Mai and Yu, 2006*). With the development and control of the atomic and molecular structure within nanoparticle synthesis and coating processes, such as surface functionalisation, increasingly more nanocomposite applications are being identified, for example the use of nanoparticles as self-healing polymer nanocomposites (*Urdl et al., 2017*).

The polymers used within the products shown in Figure 2, are all specified as using multiple additives to tailor the material properties to the particular application (*BASF, 2019*). An example is the described *Ultramid Advanced N* material used within gear wheels and structural parts within an automotive application contains a variation of fillers to offer strong and stable mechanical properties at elevated temperatures, dimensional stability, chemical resistance and better processing (*BASF, 2019*). The example demonstrates the vast variation and opportunity for nanocomposites to be used within the

automotive industry (*Mathew et al., 2018*). Figure 2 demonstrates an example of polymer composite use within the automotive industry by BASF.

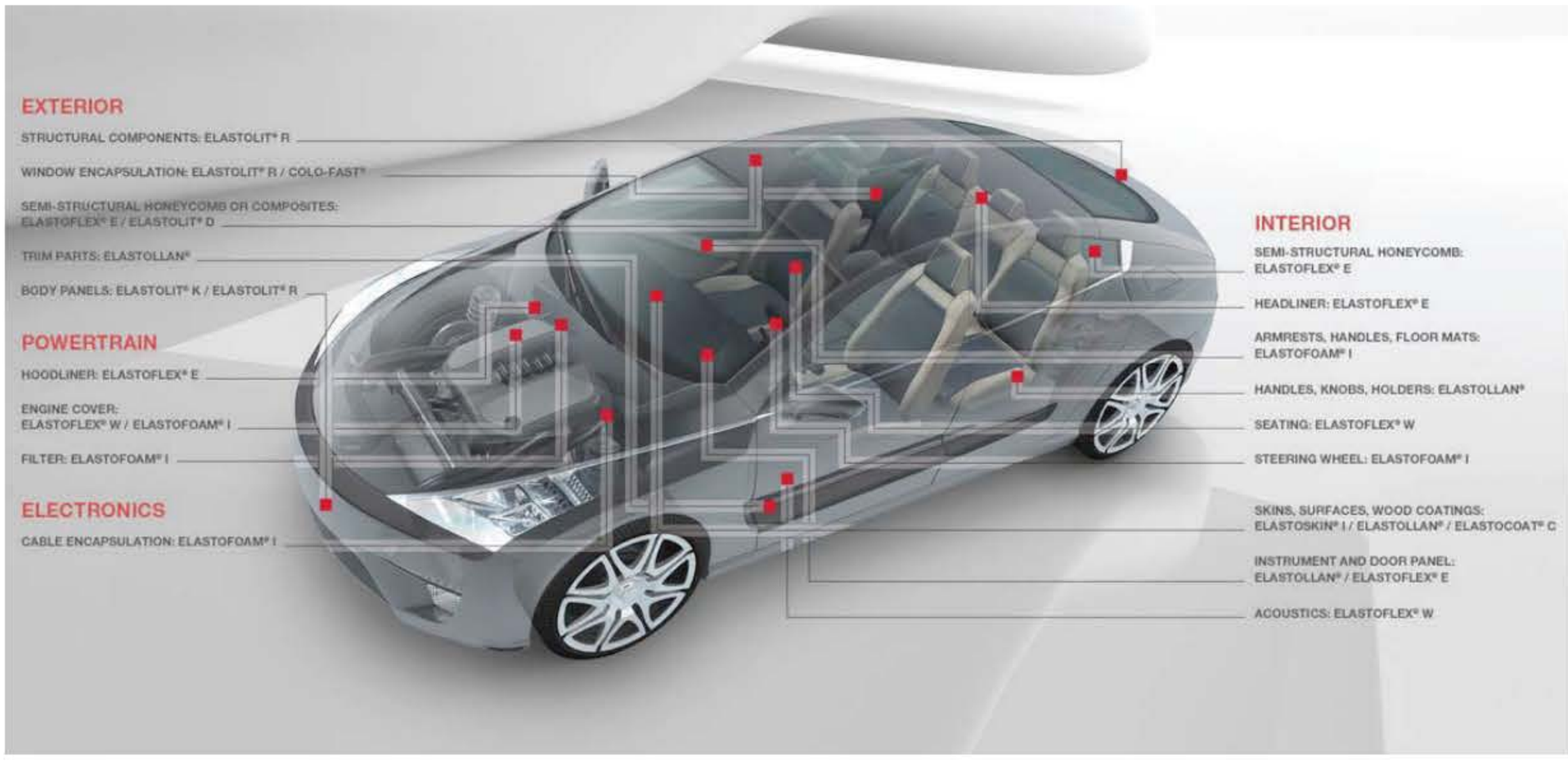

Figure 2: Examples of interior, exterior, electronic or powertrain polymer parts manufactured by BASF within the automotive industry *(BASF, 2019).*

Considered as 21st century advanced materials, nanocomposites are still relatively new materials within industry. Research and development of polymer nanocomposites has recently increased due to three main reasons (*Schadler et al., 2003*). Firstly, recent advances and studies on the resin-filler structure-property effect has provided an extraordinary level of flexibility and control over the material properties. This provides the ability to tailor material properties, through the use of multiple fillers, bespoke to the application (*Paul and Robeson, 2008; Njuguna et al., 2008*). Further to this, another reason for the increase in research is due to the discoveries of more nano-sized fillers, such as carbon nanotubes in the early 1990s, and graphene in 2006 (*Rafiee, 2011*). The individual responsible for the initial discovery of carbon nanotubes is disputed (*Arash et al., 2014*), however only from the 1990s were they synthesised for nanocomposite use (*Ajayan et al., 1994*). A review carried out by *Mittal et al., (2015*) highlights the functional properties and importance of continued research on carbon nanotubes and graphene as nanocomposite fillers for future industrial applications. The more recent discovery of graphene has released a new field of nanoparticle research.

A third reason for the increase in research and use within industry is due to the developments in chemical processing of nanoparticles and synthesis to control the morphology of particles within composites (*Azeez et al., 2013*). Although the notion of improving materials through the addition of other materials is not new, the recent developments in nanotechnology and ease of manufacture have provided a new dimension of material tailoring.

Various industries, such as the automotive and aerospace industry, have already established the use of nanocomposites within their structures (*Njuguna et al., 2012*). An example of this is with a leading automotive manufacturer using 300,000 kg of nanoclay nanocomposites annually for exterior automotive parts, and according to a report in 2015, the global nanoclay market is expected to be worth $ 3.4 billion by 2023 in comparison to $ 1.3 billion in 2014, growing at a compound annual growth rate of 12 % for the period 2015-2023 (*Transparency Market Research, 2015*). A separate report on nanocomposites found the total global market to be valued at $2 billion in 2017, and estimated an increase to reach $7.3 billion by 2022, growing at a compound annual growth rate of 29.5% for the period 2017-2022 (*BCC Research, 2018*).

The use of nanoparticles to reinforce polymer-based materials has shown drastic improvement, control and potential in material performance tailoring, predominantly due to the high aspect ratio, strength and modulus of the nanoparticles (*Koo, 2016; Paul and Robeson, 2008; Azeez et al., 2013; Mittal et al., 2015*). However, along with the many advantages interpolated, the nanoparticles used to enhance the material properties have also shown to be hazardous and toxic to humans and the environment when exposed at a certain dosage (*Love et al., 2012; Yang et al., 2010; Bergin and Witzmann, 2013; Kobayashi et al., 2017*). One potential route for exposure is during composites and components manufacturing stages involving processes such as drilling for joining, integration and assembly of parts. For example, approximately 180,000 holes are drilled to produce a single Airbus A380 wing, and around 60 % of rejected parts are due to defects introduced in holes (*Zitoune et al., 2010*). Composites drilling is therefore an important operation at manufacturing stage that is also prone to causing damage on components as well as lead to generation of dust and potential nanoparticles release, the concern of this thesis.

1.2. Aim and Objectives

The overarching aim of this thesis is to investigate the influence of various nanoparticles utilized within industrial polymer nanocomposites has on nanoparticle emissions during drilling. In order to achieve this principal aim, the thesis objectives are:

a. Literature review on the use of nanoparticles within polymer composite materials and the release of nanoparticles from embedded nanocomposites during drilling.
b. Investigate the influence of the talcum (talc), montmorillonite (MMT), wollastonite (WO), silicon dioxide (SiO_2), aluminium oxide (Al_2O_3), carbon nanotubes (CNT), carbon nanofibers

(CNF) and graphene oxide (GO) nanoparticles have on the corresponding polymer composite mechanical properties (tensile, flexural and morphology).

c. Investigate the influence of selected MMT, WO and talc on nanoparticle emissions from PP-based nanocomposites during automated drilling.

d. Investigate the influence of SiO_2 and Al_2O_3 on nanoparticle emissions from PE-based nanocomposites during automated drilling.

e. Investigate the influence of CNTs and CNFs on EP-based nanocomposites and GO on EP/CF hybrid composites on nanoparticle release during automated drilling.

The objectives given above will evaluate the influence of the nanoparticles inclusion within nanocomposites on the nanoparticle release during drilling as well as the correlation to the tensile and flexural properties of the materials. Focusing on this relationship, the research project will explore the performance of the nanocomposites and the influence of the reinforcing nano-filler and matrix combination have on nanoparticle during an automated drilling scenario.

This project is part of the European collaboration project, SIRENA Life, which is part of the European Commission 7th Framework Programme SIRENA, Pr. No. LIFE 11 ENV/ES/596. SIRENA life project aims to increase the existing knowledge in relation to risk associated to nanocomposites by investigating the simulation of the release of nano-materials from consumer products for environmental exposure assessment. The project has identified the need to develop standardized methods for the assessment of risk of nanocomposites throughout their lifecycle. The work carried out within this thesis is completed by the author unless otherwise stated.

1.3. Methodology Overview

The initial steps are to review the use of nanoparticles use within nanocomposite materials to identify particles that have proven both material benefits and shown to be potentially toxic. Simultaneously a setup for the assessment of nanoparticle release during drilling is chosen along with the setup of an environmentally controlled test chamber. As drilling is the scenario in which nanoparticle release will be assessed, the drilling tool is selected and setup. An outline of the approach demonstrated in Figure 3 highlights this by separating the release test procedure from the nanocomposite selection and manufacture.

The nanoparticle release methodology consists of the background interference control, nanoparticle release instrumentation, and the drill tool selection. The aim of the chamber is to remove any influencing parameters, and only evaluate the influence of the nanoparticles used within the materials

on nanoparticle release during drilling. Without the interference of background particles and noise, the right instrumentation and control over the mechanical process, only the one parameter, varying material, is changed and evaluated. The air within the chamber is cleared to have no particle influencing prior to testing and therefore provide an environmentally controlled test chamber. The drilling procedure is setup so that the drill tool and drill bit does not introduce any particles. With a constant set of drilling parameters, and an environmentally controlled test chamber, the focus of the study is to evaluate the influence the nanoparticle fillers have on the release from the materials.

Figure 3: Workflow diagram demonstrating the approach towards the thesis.

Once the nanofillers and polymer combinations are identified, these are manufactured (at Tecnalia) and then can be evaluated for material mechanical properties and nanoparticle release. The influence of the fillers on tensile properties and flexural properties will be correlated to the data from the nanoparticle release. The influence of the fillers on nanoparticle release during drilling will be

quantified in terms of particle number concentration, particle size distribution, particle mass distribution and an assessment on the deposited particles. The analysis thereafter will evaluate and correlate the data to investigate the influence of the nanoparticle fillers on the nanoparticle emissions.

1.4. Motivation

Despite the many advantages introduced, nanofillers have shown conceivable health risks and toxicity to humans and the environment. Due to the use of nano-sized particles, nanocomposites can introduce a potential toxicological and/or eco-toxicological hazard. With the need to assess each particle for nano-related toxicity, literature has seen a huge increase in publications over the past decade. In a review carried out by *Krug, 2014*, the author found that up until 2011, around 5000 papers had been published on nano-toxicology, whereas, the total number had more than doubled by 2014. Although the substantial number of publications has provided significant enhancement in nanotoxicity knowledge, literature still lacks an all-inclusive comprehension with various conflicting results due to many difficulties in determination of the mechanism of nanotoxicity in cells and in vivo (*Fu et al., 2014*). The nanoparticles identified to have demonstrated potential toxicity effects is included here to substantiate the selection and the necessity to investigate the release of the nanoparticles from nanocomposite materials.

Carbon-based nanofillers have been a key interest within toxicity studies. Many carbon-based nanofillers such as, CNTs and CNFs, have already been established within industry. Despite the beneficial material properties of CNTs and CNFs, the nanofillers have shown conceivable health risks and toxicity to humans and the environment. Studies have validated that certain concentrations of CNT exposure has shown to induce cytotoxicity and apoptosis (*Wang et al., 2011; Bottini et al., 2006*), genotoxicity (*Patlolla et al., 2010; Guo et al., 2011*), systemic immune function alterations (*Mitchell et al., 2007*) and pulmonary damage, inflammation and granuloma lesions (*Chou et al., 2008; Porter et al., 2010; Poland et al., 2008*). Review papers have been released in an attempt to quantify various CNT attributes to the level of toxicity. The many studies, varied types of CNTs, different evaluation methods and different exposure conditions have shown conflicting results as presented by *Liu et al., 2012*. Consequently, we are still, at present, unable to classify and gauge exact level of toxicity factors such as size, shape, purity and functionalisation to CNT toxicity (*Madani et al., 2013*). However, in the findings from *Aschberger et al. (2010)* studies suggest that chronic occupational inhalation; especially during activities involving high CNT release and uncontrolled exposure are the main risks for humans.

Equally, CNFs are increasingly being investigated for toxicity. Studies have shown inhalation or exposure to a varied concentration of CNFs to cause respiratory tract and pulmonary inflammation

(*Delorme et al., 2012; Castranova et al., 2012; Warheit et al., 2011*), DNA damage (*Lindberg et al., 2009*) cell proliferation inhibition and cell death (*Magrez et al., 2006*). Despite the evidence of toxicity and widespread use of CNFs, most studies have investigated CNTs. However, additional to offering economic benefits over CNTs with a better cost to strength ratio, some studies have suggested that CNFs show less toxicity than CNT's (*Delorme et al., 2012; Kisin et al., 2011; Murrary et al., 2012*). Carbon-nanofillers are of big interest within the nanotoxicity literature available due to the beneficial material properties. GO is another carbon-based filler that has demonstrated potential cytotoxicity affects (Akhavan et al., 2012; Matesanz et al., 2013; Seabra et al., 2014; Lalwani et al., 2016; Kang et al., 2017).

Although carbon-based nanofillers have demonstrated to be particularly hazardous materials, other nanofillers such as nano-alumina and nano-silica have shown conceivable health risks and toxicity to humans and the environment. Considered the foremost toxicity mechanism relating to nanoparticle exposure, nano-silica has reported to increase oxidative stress (*Lin et al., 2006; Eom & Choi, 2009*) and pro-inflammatory responses (*Park & Park, 2009; Kaewamatawong et al., 2006*). *Soutar et al. (2000)* summarized a significant number of epidemiological studies linking exposure to silica and carcinogenicity. And an extensive review focused on inhalation exposure to nano-sized silica by *Rabolli et al. (2010)* encapsulates the hazard and physico-chemical properties of nano-silica that can affect cytotoxicity with studies linking nano-silica to causing silicosis, chronic obstructive pulmonary disease (COPD) and pulmonary tuberculosis (*Calvert et al., 2003*).

Similarly, nano-sized aluminium oxide nanoparticles (alumina) are increasingly being investigated for toxicity. Studies have shown nano-alumina to cause cellular toxicity and increase in oxidative stress (*Alshatwi et al., 2013*), and a study in mice has shown nano-alumina to increase the lactate dehydrogenase level in the blood and induced the development of a pathological lesion in the liver and kidneys (*Park et al., 2015*). Studies by *Zhang et al. (2013)* and *Zhang et al. (2011)* have shown nano-alumina to have neurotoxicity effects inducing cell necrosis and apoptosis, including indications of higher cellular toxicity than nano-carbon particles. Hence, it is generally agreed upon throughout literature that nano-silica and nano-alumina have shown toxic effects to humans and the environment.

Likewise, nanoclay fillers such as wollastonite (WO) and montmorillonite (MMT) have also demonstrated toxicity effects. In a study by *Lordan et al. (2011*) two variations of organically modified MMT demonstrated cytotoxicity by inducing intracellular reactive oxygen species (ROS) and increased cell membrane damage to human hepatoma HepG2 cells. In a review article by *Maxim and McConnell, (2005)* a conclusion at that point on WO found it to increase bronchitis and reduced lung function in

morbidity studies. However the limited epidemiological studies demonstrated no significant risk of increased incidence of pulmonary fibrosis, lung cancer or mesothelioma. An updated health surveillance study on workers by the same authors in 2014, found a decrease in toxicity effects which failed to reveal any elevated standardized mortality ratio (SMR) for malignant neoplasms or cancer of the lung and bronchus, which is expected to directly reflect progress in reducing workplace fibre concentrations and exposure (*Maxim et al., 2014*).

As these fillers are mostly already established within industry, it is important to fully understand the potential toxicity associated, and acknowledge that throughout their lifecycle, may undergo mechanical processes that unintentionally release the particles. Therefore, the use and introduction of these materials into the workplace can be hazardous when human exposure is concerned. Throughout its use, a nanocomposite structure will undergo industrial machining where drilling can lead to exposure to the potentially toxic nanoparticles. A full understanding of the inadvertent release of nanoparticles within the workplace poses unknown risks which are yet to be quantified. The current state and gap of knowledge is demonstrated in Figure 4.

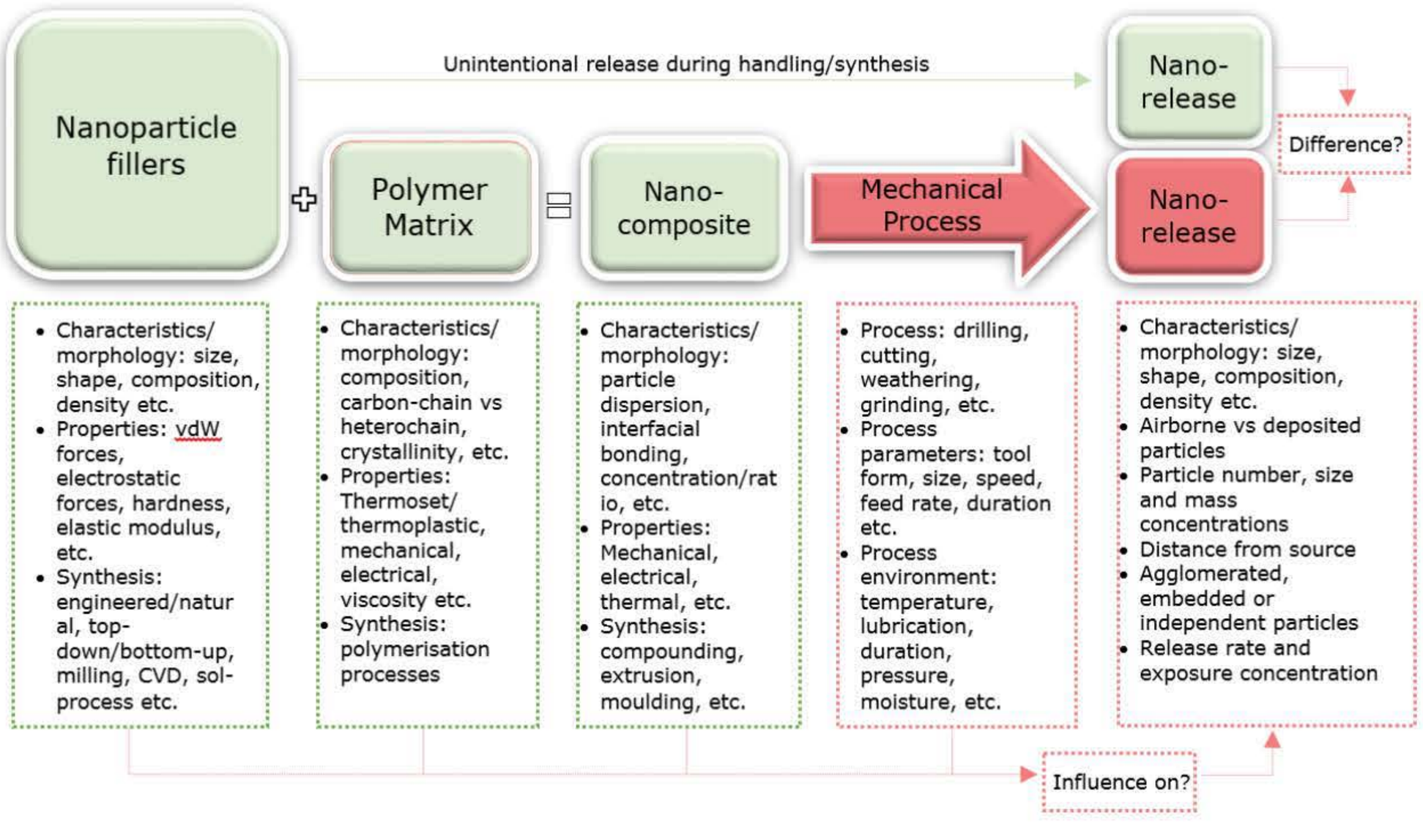

Figure 4*:* Outline demonstrating the current state of the art (featured in green) and gap in knowledge (featured in red) on the nanoparticle release due to mechanical processes from nanocomposites.

Numerous studies have identified and are in unison to control and limit the exposure of unintended nanoparticles released during synthesis and handling. However, the release of nanoparticles from

nanocomposites is less understood or regulated. Research is now comprehensively investigating the potential nanoparticle release and exposure to humans and the environment from nanocomposites. Several studies have investigated the release of nano-sized particles from nanocomposites due to a variety of processes. So far however there is no harmonized conclusion on the particles released and no standardized method established to simulate the release scenarios. From the literature available, including the studies performed on nanocomposite drilling, it can be said that most studies illustrated that nano-sized particles are released during some of the scenarios, but to a certain extent. There is therefore currently a lack of knowledge on release and the influence the filler-matrix combination has on the release due to a mechanical processing on nanocomposites. This study investigates the effect the nanofillers have on nanoparticle release due to mechanical drilling.

Since nanocomposites are manufactured to embed nanoparticles within the material, less literature has been reported on the release of the nanoparticles during machine relative to number of studies on handling independent nanoparticles. It is crucial that any potential health or environmental risks associated with the materials are known and avoided where possible. As described, there is currently conflicting conclusions on the effect nanoparticles have on the particles released and the exposure levels to humans.

1.5. Thesis Structure

Chapter1 is presented as an introduction to the thesis which states the aim, objectives and motivation which leads into an overview of the methodology and structure of the thesis. This introduction allows the reader to have a general scope and the motivation behind the nanoparticle release study carried out as a whole.

Chapter 2 provides an overview of existing relevant research in nanocomposite drilling, presenting the gap in knowledge and the originality of the research project. The latest state of the art knowledge available on nanocomposites are first presented leading into the toxicity and safety concern of the materials. With the hazards identified, the current knowledge on release scenarios and exposure measurements reveal conclusive but incomparable data, accentuating the need for a standardised methodology and more data to understand the nanoparticle release during machining.

Chapter 3 presents the materials chosen, fabrication and mechanical testing of the materials for this thesis. Since the justification and characterisation methods of the materials chosen are related, this chapter goes through the selection and synthesis, followed by the mechanical properties. The

characterisation of the materials is included in this chapter to demonstrate the differences between the materials.

Within *Chapter 4*, the influence of the selected nanoparticles on nanoparticle release from the PP-based nanocomposite samples is presented. The results go through the particle number concentration, particle size distribution, particle mass distribution and deposited particles.

Chapter 5 presents the nanoparticle release experimental investigation of the PE reinforced nanocomposites with nano-sized alumina and silica. The chapter demonstrates the differences and effect of filler on nanoparticles release during drilling. It includes two weight concentrations of similar mechanical performance but varying nanoparticle release data of the two nanofillers.

Chapter 6 presents the nanoparticle release study on the EP reinforced with CNTs and CNF nanocomposites. The investigation is a comparison and effect of CNFs and CNTs to neat EP matrix.

Chapter 7 presents the influence of GO on EP/CF based nanocomposites on nanoparticle released during drilling. Three concentrations of GO are investigated to see the consequential effect on nanoparticle release.

Within Chapter 8, a discussion on the results and an analysis on the correlation of all previous results is presented. This chapter combines the data of all previous chapters to identify the correlation between mechanical properties and nanoparticle release during drilling.

The conclusion of the findings of this thesis and detail of the future work that has been identified from the discussion within each chapter is presented in *Chapter 9*. This is followed by the references and Appendices.

Chapter Two

Literature Review

2.1. Introduction

Over the past decade, polymer nanocomposites have undergone intensive research and development ensued by its increasing implementation within commercial applications (Mittal et al., 2015). The benefits and unique advantages and effect nanoparticles have on the material properties, accompany potential exposure to unique toxic effects within biological systems. Throughout its use, a nanocomposite will undergo industrial machining where drilling, along with other machining scenarios, can lead to material damage and/or release of potentially toxic nanoparticles (Basinas et al., 2018). Within this chapter, a critical literature review on the current knowledge on the release of nanoparticles from nanocomposite drilling is discussed. An overview of the relevant present knowledge and current state of the art is presented, leading into the gap in the knowledge and the contribution of this research project to the field. The use of polymer nanocomposites will first be reviewed providing the developments and significance in a variety of material applications. This will provide an understanding into the influence nanoparticles have on nanocomposite mechanical properties. Although the influence of some nanoparticle fillers is recognised, the effect on mechanical properties of some nanoparticles are still to be evaluated (Kumar et al., 2017; Kotal and Bhowmick, 2015). The assessment of the literature available on nanoparticles released from polymer nanocomposites and release scenarios will then be evaluated. A comparison of the studies will provide the advantages and limitations of methods used to measure, quantify and characterise the nanoparticle release from an assortment of release scenarios. Currently, although considerable amount of studies have investigated machining on conventional composite materials (Liu et al., 2012; Xu et al., 2016; Feito et al., 2018), there is a lack of knowledge on the influence nanoparticle fillers have on release due to drilling (Çelik et al., 2019; Panchagnula and Palanivandi, 2018; Kulkarni et al., 2019). Importantly, previous studies have identified the possibility of potentially toxic nanoparticles to be released from nanocomposites during mechanical processes (Basinas et al., 2018; Harper et al.,

2015; Froggett et al., 2014). It is therefore crucial to develop an understanding on the influence nanoparticles have on material mechanical properties and how these effect the nanoparticle release during drilling.

2.2. Polymer Nanocomposites

As multi-phase materials comprised of two or more constituents, conventional polymer composites are fabricated using a selection of material fillers to improve the properties of the polymer matrix (*Plueddemann, 2016; Vasiliev & Morozov, 2013*). The size and amount of filler used to modify the characteristics traditionally varies with different composites depending on the resin matrix and the intended application. Although the combination of two materials to form a composite has been known for centuries, modern advances over the past several decades have transformed engineered composites (*Hull and Clyne, 1996)*.

The use of conventional polymer composite materials has seen an increase mainly due to the advances in filler materials and improved manufacturing abilities (*Ajayan et al., 2006*). Composite materials offer distinct properties with advantages in strength-to-weight ratio, stiffness-weight, improved fatigue life and corrosion resistance properties compared to other materials (*Campbell, 2010; Njuguna & Pielichowski, 2003*). But the composite material structure of combining performance of individual constituents, allow the material to be flexible in design and tailoring towards the application needs. In theory, this therefore allows for materials to be designed for each application instead of a structural design based on material properties (*Barbero, 2010*).

Fibre reinforced composites have been the prominent combination over other composites due to the increased specific strength, modulus and stiffness in fibrous form (*Reddy and Miravete, 2018*). However, this also results in anisotropic behaviour in the fibre direction. Alternative reinforcement constituents can come in various forms including: particles, flakes, short fibres, continuous fibres, sheets or whiskers (*Chawla, 2013*). The extensive research on fibre-reinforced composites has developed several models in predicting material mechanical properties; however, the models are still limited with no universally accepted failure criterion and employ a probabilistic method to predict the behaviour or the basis of assumptions due to the random nature of fibre strengths (*Tsai, 2018; Hyer and White, 2009*).

Whilst the selection in filler is vital in the influence on material properties, the polymer matrix resin can dictate a major fraction of some material properties (*Barbero, 2010*). Each polymer has its benefits and limitations, which are selected based on the desired application as with normal material selection

criteria (*Plueddemann, 2016*). However, the fillers used to reinforce the polymer are chosen based on compatibility with the polymer as the nature of the interface between the fillers and the matrix has a bearing on the extent of influence on the material properties (Kim and Mai, 1998). The cohesion at the interface between the filler and polymer is achieved through mechanical bonding, physical bonding, chemical bonding or multiple bonds formed through solid solution effects (*Tsai, 2018*).

2.2.1 Nanofillers

Research in development of engineered polymers and fillers to optimise material properties has led to the discovery of nanocomposites (*Koo, 2016*). A nanocomposite is distinct from conventional composites, in that at least one dimension of the reinforcing filler material is in the nano range. (*Njuguna et al., 2014; Njuguna & Pielichowski, 2003; Chapman & Mulvaney, 2001*). Many studies have established that the introduction of nano-sized fillers can significantly further improve multiple properties of traditional polymer composite materials. As an example, carbon nanotubes (CNTs) use within polymer nanocomposites have demonstrated enhanced mechanical (*Ashrafi et al., 2011*), electrical (*Ayatollahi et al., 2011*), thermal (*Guadagno et al., 2011*) and fire-retardant properties (*Wu et al., 2010*) from just a selected number of researches. As a result, worldwide CNT production capacity has increased at least 10-fold since 2006 (*De Volder et al., 2013*), and the CNT market size has more recently been forecast to be worth over $ 8 billion by 2024, growing from over $2 billion in 2017 at a compound annual growth rate of 22% for the period 2018-2024 (Global Market Insights, 2018).

A benefit of a nano-sized filler over a micron-sized filler is attributed to the higher ratio of surface area to volume, aspect ratio and shape of the particles (*Mago et al., 2010*). The higher surface area to volume increases the molecular interface between the filler and the polymer, which in turn controls the material properties. The interfacial region is the defining region at which the properties differ from those of an independent filler and matrix to a combined altered chemistry and structure (*Ajayan et al., 2006; Vaia & Wagner, 2004*). The overall properties of the material are defined by the number of interfacial regions and the interparticle spacing. If the interfacial region is reduced or widened, a different interaction behaviour of the polymer composite will occur. Therefore, when the interfacial region is controlled and manipulated, the material properties can also be controlled.

The developments over the past decades have improved the processing methods to control the particle size and dispersion which will affect the interfacial interactions (*Ajayan et al., 2006*). Many technologies available are attempting new methods to identify and maximising these parameters for material improvement and control (*Zhou et al., 2015; Yoonessi et al., 2014; Alian et al., 2015*). The

advancements in ability to incorporate the nanoscale fillers within polymers has permitted extensive research and progress in targeting specific material properties with great control and precision.

As defined by ISO, nanomaterials involve materials at the nanoscale. The ISO defines the "nanoscale" to mean size range from approximately 1 nm to 100 nm (*ISO/TS 80004-2, 2015*). The shape and size of the nanofillers are critical in the structure and bonding with the polymer matrix. Nanofillers are classified into three categories based on the geometry: nanoparticles, nanofibre or nanoplates (*ISO/TS 80004-2, 2015*). The three categories are defined by the varied shapes and dimensions. A nanoplate is a one-dimension nanofiller, in that the thickness of the plate is less than 100 nm. Nanofibres or nanotubes are classified as having a diameter in the nano range. And a nanoparticle has all dimensions less than 100 nm and is therefore three-dimensional nano (*Koo, 2016*). Due to the high surface to volume ration of the nanoparticles, the nanofillers are commonly dispersed within the polymer at a mass concentration typically between 0.1 - 10 wt. % (*Gupta et al., 2009*).

The nanofiller is one of three said main contributing factors of the composite material. The other two influences are the polymer matrix and the interfacial region. The ascribed properties, different from the individual constituents, are attributed to the interface of the filler to the matrix, and the impact on the matrix radius of gyration, R_g. R_g is understood to be a significant spatial parameter to which the majority of polymer's static and dynamic properties are related (*Sen et al., 2007*). The smaller the particles and increased density of particles causes the distance between particles to become comparable to the interfacial region and thus increasing the volume fraction of interfacial material to the bulk. The low filler aspect ratio is therefore, understood to influence the volume fraction and consequently the interfacial region (*Vaia & Wagner, 2004*). Figure 5 illustrates a log-log plot of the surface area per volume with respect to the aspect ratio (α) and largest dimension of various fillers.

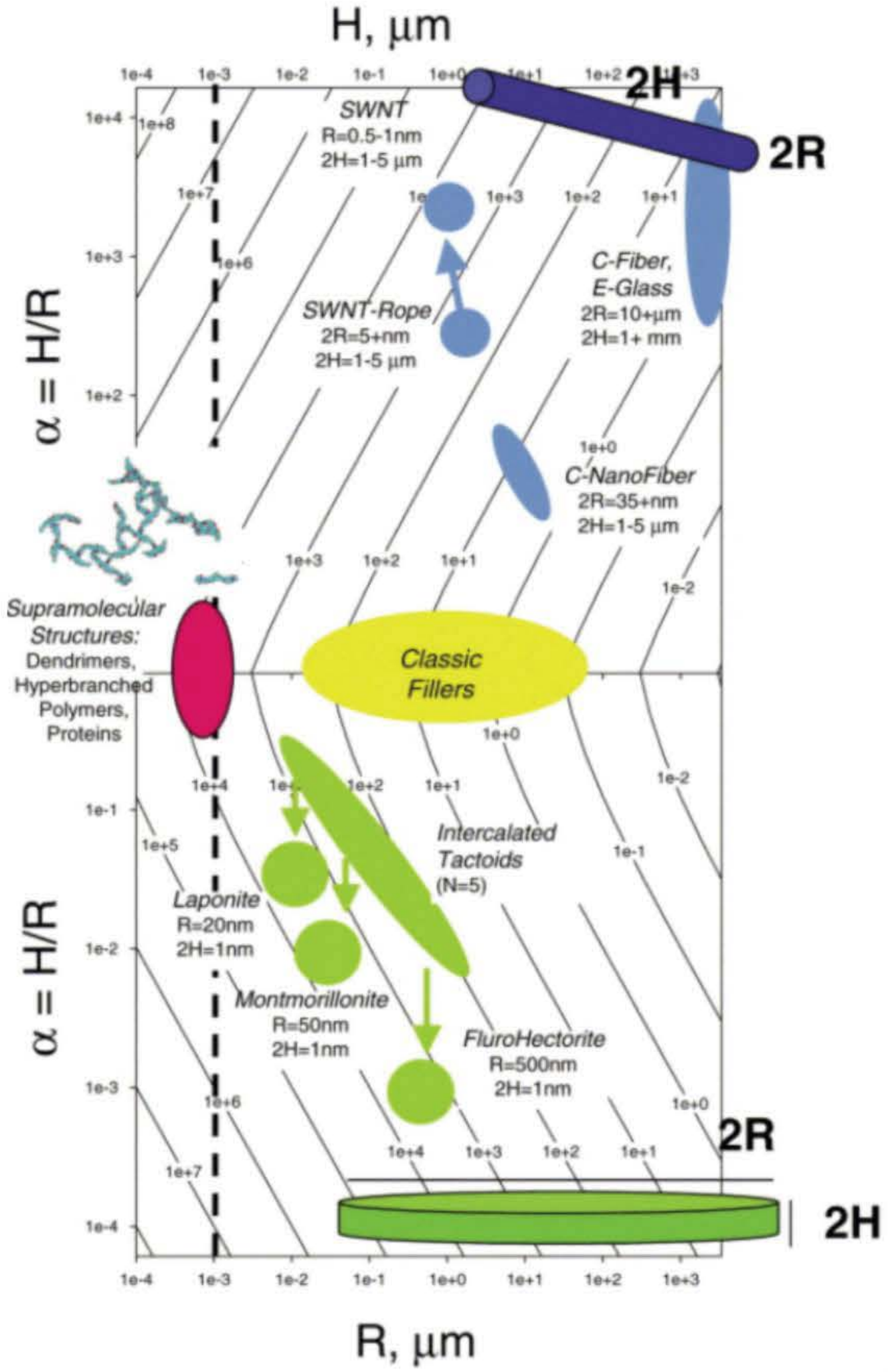

Figure 5*:* Logarithmic map of interfacial (surface) area / volume of particles ($\mu m^{-1} = m^2/ml$) with respect to the aspect ratio, α = H/R, and largest dimension of particle (R = radius, H = height, length) based on approximating particles as cylinders (area/volume =1/H+1/R) (Vaia & Wagner, 2004).

The first real understanding of nanofillers explored polyamide-6 filled with nanoclays (*Okada et al., 1988*) from Toyota, and is now considered a milestone and initiation of the modern nanocomposite era. Nowadays, nanoclays are common nanoparticle fillers in the automotive industry, including car manufacturers General Motors and Maserati (Proveda and Gupta, 2016). A nanoclay is a layered mineral silicate, of which MMT has the broad acceptance within polymer nanocomposite use (*Njuguna et al., 2014*). Other clays researched include WO (*Luyt et al., 2009*), hectorite (*Awad et al., 2009*), and others, but MMT is most readily used due to its natural abundance, high surface area and its well-

known intercalation and exfoliation chemistry (*Pielichowski et al., 2014*). The benefits have lead nanoclays to become a common nano-sized constituent used within automotive components since the early 2000s (*Liu et al., 2005*). The clays can be natural or synthetic, as well as phosphates of transition metals. The most common improvement seen with the introduction of clays are mechanical properties. The clays are a shell-shaped nanoplates with a thickness or one-dimension in the nano range. The crystalline structures and the quantity and position of the ions within the elementary mesh are what classify the clays (*Njuguna et al., 2012*).

Another massive influence in the development in nanocomposites has emerged from carbon-based nanofillers since the discovery of the CNT in 1991 and buckyball, C_{60}, in 1996 providing insight into new carbon nanostructures (*Girifalco et al., 2000*). Stemming from the sp^2 carbon units based on simple geometrical principles, the carbon filler developments have resulted in new symmetries and structures that have intriguing and practical properties. CNFs and CNTs have been of great attraction within research over the past couple of decades and are now widely used within industry. This is due to their exceptional mechanical, electrical and optical characteristics. A CNT is unique in the helicity in the arrangement of the carbon atoms in hexagonal arrays on their surface honeycomb lattices (*Ajayan et al., 2001*). Research has been able to develop a CNT down to a diameter thickness of 3 Å, or 0.3 nm (*Zhao et al., 2004*). The combination of size, structure and topology provides CNTs with important mechanical properties. Furthermore, a one atom thick allotrope of carbon, known as graphene, has been a new focus point within research due to its superior electrical and thermal efficiency characteristics (*Mittal et al., 2015*). CNTs differ from graphene as it consists of layers of graphene wrapped into tubular shapes which can be multiwall (MWCNTs) or single wall (SWCNTs), whereas CNFs are identified as layers of truncated conic sections of graphene (*Gupta et al., 2009*).

The development in carbon based fillers since the discovery of graphene has demonstrated significant improvement over the past decade. However, graphene is highly unstable due to delocalised π electrons, costly synthesis and is challenging to bond with polymers. Graphene is a two-dimensional carbon allotrope with a honeycomb structure of C_6 molecules. The sp_2 hybridised carbon atoms are bonded to neighbouring atoms by three covalent σ-bonds which leaves the π-electrons delocalized and thus causing the instability (Mohan et al., 2018). Research has therefore attempted to overcome these limitations with a derivative of graphene, called GO, a relatively more stable form and less costly to synthesise from graphite. The widely accepted Lerf-Klinowski model of GO proposes a sp_2 and sp_3 C_6 skeleton with epoxide and hydroxyl functionalities on the basal plane and carboxylic acid groups on the edges (He et al., 1998). This has triggered interest and increasing implementation within commercial applications for both textile and engineering hybrid composites (*Nikfar et al., 2014; Njuguna et al., 2008; Njuguna et al., 2009; Khobragade et al., 2016*). The mechanical properties

provided by the carbon fibre to the polymer are currently limited due to the chemical inertness and poor wettability affecting the bonding at the interphase (Hung et al., 2018). Chemical treatment or the use of nanofillers is therefore necessary to reduce de-bonding and improve the interphase. Use of reduced graphene oxide (RGO) and graphene oxide (GO) in EP-carbon fibre reinforced composites is still at the infancy stages and has been limited due to the challenges in processing and dispersion of the fillers along with the high price associated therewith (Mohan et al., 2018). As with other nanofillers, homogeneous dispersion of the filler within the polymer and the strong interfacial interactions required between the filler and the matrix are the two biggest concerns when fabricating polymer nanocomposites (McAllister et al., 2007). The oxygen groups within GO offer and allow for a versatile, less fastidious and enhanced chemical cross-interlocking with the polymer chains. The oxygen functional groups that GO possesses on its basal planes and edges permit it to be manipulated, exfoliated and functionalised to yield well-dispersed solutions of graphene oxide sheets (Dreyer et al., 2010; Park et al., 2008; He et al., 1998; Desai et al., 2013). Researchers have therefore identified the combination of GO nanofillers with the micro-sized carbon fibre fillers to create hybrid composites as a novelty and a future in composite development (Hadden et al., 2015; Jiang et al., 2016; Qin et al., 2016).

Further examples of beneficial nanofillers include ceramic and metallic nanomaterials. Various nanoparticles, such as titanium dioxide (TiO_2), alumina (Al_2O_3), antimony-tin oxide (ATO) and silica (SiO_2) have all shown to improve material properties when integrated at the nanoscale (Ribeiro et al., 2015; Gaminian & Majid, 2015; ; Rusmirović et al., 2016; Georgopanos et al., 2017). Many of these fillers are customarily micron-sized but can be reduced to the nano scale, such as alumina which ranges spherical crystal particles from 20 nm to micrometric sizes. Whereas synthetic nano silica forms particles from 5 nm to 100 nm (*Marquis et al., 2011*). The nanoparticles offer a variety of improved properties depending on the structure and characteristics and are increasingly being researched as a relative cost-effect material to target material properties (*Ajayan et al., 2006*). Two separate reports estimated the global market size of nano silica to be 3348 kilo tonnes in 2015 (Market Research Report, 2017) and the global high purity alumina market size to be over 20 kilo tonnes in 2015 (Market Research Report, 2016).

2.2.2 Nano-reinforced Polymer Nanocomposite Property Behaviour

The sole aim of integrating nano-sized fillers is to develop the characteristics of the primary polymer matrix which therefore, are typically classified as reinforcement agents. Nanocomposites have the

advantage over conventional composite materials in that only small weight concentrations are required to improve the properties and consequently minimising the material weight increase. Composites within industries are predominantly used in lightweight applications and are continuously trying to improve material properties without increasing, and if possible decreasing, material weight (*Njuguna et al., 2008*). The nature and extent of reinforcement is dependent on numerous factors, such as the properties of the matrix, properties and distribution of the filler, and the material preparation method. The introduction of the nanofiller can improve properties such as: mechanical properties (e.g. tensile, flexural, stiffness, toughness), gas barrier, flame retardant properties, dimensional stability, thermal conductivity, electrical, and optical properties. However, the improvement of one property has also shown to have a subsequent negative effect on another. An example of this is common in nanoclays with the improvement of tensile strength and stiffness can decrease the elongation and impact resistance (Svab et al., 2005, Selvakumar et al., 2010).

A governing factor for polymer nanocomposite properties is attributed to the compatibility between the nanofiller and polymer matrix. Principal features such as homogeneous dispersion of the filler within the polymer and the strong interfacial interactions required between the filler and the matrix are the two biggest concerns when fabricating polymer nanocomposites which is directly influenced by the compatibility (*McAllister et al., 2007*). Research has consequently studied chemical modification to manipulate the physical and chemical properties of nano-fillers, as to improve the compatibility, dispersion and interfacial interaction of nanofillers in polymer matrix to influence the properties (*Bao et al., 2011*).

Nanoclays are some of the most extensively investigated nanofillers to be used within composite materials due to their low cost, high aspect ratio, high surface area > 750 m^2/g and high modulus up to 176 GPa (*Baniassadi et al., 2011*). Research has continuously attempted to maximise the properties through preparation and processing techniques to control intercalation and exfoliation (*Ray & Okamoto, 2003*). The clay dispersion within the polymer matrix has been of significant interest within literature, and can be divided into four different describable states: conventional miscible, partially intercalated and exfoliated, fully intercalated and dispersed and finally, fully exfoliated and dispersed (Luo & Daniel, 2003). In a review by *Baniassadi et al., 2011*, fully exfoliated structures, in relation to intercalated ones, were found to give the best performance due to the higher homogeneity of the phase. Clays have therefore since been modified with organic surfactants to increase the exfoliation (also known as d-spacing), such as organic modified montmorillonite (OMMT) giving enhanced properties such as increasing tensile strength from 69 MPa to 107 MPa with 4.2 % modified nanoclay (*Chen et al., 2008*) or increased modulus by approximately 500 % with the addition of 10 wt. %

organoclay (*Becker et al., 2002*). However, where exfoliation has shown to increase stiffness of the nanocomposite with increasing clay content, the impact strength and tensile ductility have shown a decrease (*Tjong, 2006, Park & Jana, 2003*). Therefore, consideration in concentrations volumes are required to balance the material properties. Different nanoclay fillers have observed improved mechanical properties at different weight concentrations, e.g. talc at 20 wt. % (Lapcik et al., 2009), in comparison to studies on WO (*Wetzel et al., 2003*) and MMT (Selvakumar et al., 2010; Kampeerapappun et al., 2005) at 5 wt. %. More research that is recent has progressed with nanoclays utilised to improve fire retardant properties. Although there are currently no commercialized individual fire-resistant materials containing nano-sized materials, there is considerable amount of research being carried out to develop one (*Visakh and Yoshihiko, 2015; Bourbigot et al., 2007*). Heat properties such as thermal conductivity, oxidation resistance, flammability, heat deflection or related properties such as reducing the fraction of radiation absorbed from a fire through reflectivity, are all properties that are being investigated in relation to flame retardant properties (*Cinausero et al., 2008*).

PE-based nanocomposites are tailored with a variety of nanofillers including metallic, ceramic or polymer particles having shown improved material properties such as alumina (*Baskaran et al., 2011;* Ribeiro et al., 2015; Rajesh et al., 2014), silica (*Chen et al., 2003;* Changizi & Haddad, 2015; Rusmirović et al., 2016), zinc oxide (*Liufu et al., 2005*), polyetheretherketone (*Wang et al., 2010*), polytetrafluoroethylene (*McElwain et al., 2008*), halloysite (Saharudin et al., 2016; Lin et al., 2017) and titanium dioxide (Gaminian & Majid, 2015; Patel & Dhanola, 2016). Similar to other polymer nanocomposites, PE-based materials are established in lightweight applications with reinforcement fillers such as ceramic based nano Al_2O_3 or nano SiO_2 used to improve mechanical (*Baskaran et al., 2011; Trinath et al., 2016*), thermal (*Chen et al., 2003; Leszczyńska et al., 2007*), electrical (*Paszkiewicz et al., 2012*) and optical (*Zhao et al., 2007; Zhou et al., 2003*) properties. A study by Rusmirović et al. (2016), observed a 156 % increase in flexural strength with 1 wt. % nano SiO_2 added to a PE-based composite. The same study reported 2 wt. % nano SiO_2 to show similar increase in flexural strength, followed by either a constant or slight decrease with further increase in weight concentrations. In contrast, a study by Baskaran et al. (2011) evaluated the influence of nano Al_2O_3 weight concentrations on PE nanocomposites and concluded a maximum tensile strength at 5 wt. % and any further additions resulted in a tensile strength decrease. The decrease in strength at higher weight concentrations were attributed to a limitation in adhesion between the nano alumina and resin and therefore leading to the formation of agglomerations creating defects and stress concentrations (Chen et al., 2004; Baskaran et al., 2004). A study by Ribeiro et al. (2015) that evaluated both Al_2O_3 and SiO_2, reported an average increase of 19 % in flexural elasticity modulus for different variations in weight concentrations. Although optimum weight concentrations have varied between 1 wt. % to 5 wt. %,

and as with other filler/polymer combinations, the manufacturing process is influential, as the dispersion of both Al_2O_3 and SiO_2 will have a significant effect on the properties (Zou et al., 2008).

Carbon-based fillers within the nanoscale have shown some of the greatest potential mechanical and electrical strengths. CNTs have shown to be the stiffest and strongest fibres known. Literature has presented CNTs to have a Young's modulus of over 1TPa (*Arash et al., 2014*) and with an elongation to failure of 20 % to 30% combined with the stiffness projects a tensile strength well above 100 GPa (possibly higher). In comparison, the Young's modulus of high strength steel is around 200 GPa and tensile strength is 1 GPa to 2 GPa (*Khare & Bose, 2005*). However, the challenge is transferring this into a macroscopic scale in a polymer composite. The individual CNTs have high van der Waal forces making it difficult to avoid agglomeration. However, when dispersed properly, CNTs have shown significant strength and stiffness properties with weight concentration levels of 1 wt. % to 5 wt. % (*Prashantha et al., 2009*). *Spitalsky et al., 2010*, carried out a review on the mechanical strength exhibited from incorporation of CNTs and found that matrices with CNTs bearing covalently attached polymer chains show enhanced mechanical properties. Furthermore, the review identifies the electrical improvements to exceed the mechanical. However, numerous studies found CNTs to increase the maximum tensile strength by over 100 % with small weight concentrations of less than 5 wt. % (*Bhattacharyya et al., 2006; Blake et al., 2004; Liu et al., 2007*). A more recent review study by Liu et al. (2018) highlights similar material property increase, but also concludes there is still a lack in knowledge on how to optimise the interaction between both CNTs and CNFs with the epoxy matrix. CNTs differ from CNFs as they are hollow and better covalent bonds between hexagonal shaped structure (*Ajayan et al., 2001*). The property improvement is therefore seen to be less effective than the use of CNTs with studies such as by Zhu et al. (2010) having demonstrated a 12.6 % improvement in flexural properties with 0.1 wt. % CNFs, 10 % increase in flexural strength with 0.25 wt. % CNFs (Shokrieh et al., 2014), or a 49 % increase in flexural modulus with 1 wt. % CNFs (Bal, 2010) in comparison to neat EP samples. As concluded within the review by Liu et al. (2018), factors seen to affect the varied properties observed within literature include the intrinsic properties of the CNFs or CNTs, dispersion of the fillers, and the interaction between the fillers and epoxy.

CF-based composites have become well-established materials within various lightweight applications, most prominently, aeronautical and automotive. CFs alone typically have an ultimate tensile strength of around 3.5 GPa, compared to an upper limit of around 1 to 1.5 GPa for an EP/CF composite. Various studies have already presented GO to improve the CF/polymer matrix material mechanical properties as summarised in a thorough review study on the modification of CFs using graphene-related materials (Hung et al., 2017). The study highlights that weight concentrations between 0.1 wt. % and 0.5 wt.%

GO have the improved tensile and flexural properties. An underlined study, included in the review, by Ashori et al. (2015) demonstrated an increase in 22.4 % in tensile strength and 76 % in flexural strength with a 0.3 wt. % GO functionalised in CF reinforced EP. Lower improvements were also observed, as shown in He et al. (2016), which revealed a 14 % increase in flexural strength by densely covering the CFs and established insufficient bonding between the polymer and fillers. Studies since the review have shown a similar increasing trend in material properties, as demonstrated by a study by Hung et al. (2019), establishing a flexural property improvement with the deposition of GO onto the surface of CFs. The study found optimum weight concentrations of GO between 0.25 wt. % and 0.5 wt. % demonstrated enhanced flexural strength of up to 29 % and flexural modulus by 55 %. The study also concluded concentrations higher than 0.5 wt. % observed a redundancy in nanoparticles with agglomerations evident. GO is non-stoichiometric and therefore properties can be variable depending on degree of oxidation; as shown by Feicht et al (2017) in a report on how the in-plane modulus of GO produced by Hummers or Brodie methods varied from around 300 GPa to around 500 GPa respectively. However, although GO has shown to improve a conventionally used CF reinforced EP, the particles also pose a potential hazard if unintendedly released into the environment and/or exposed.

2.3 Composite Drilling Operation

Drilling is a common process utilised within the manufacturing industry and cannot be avoided in many structures, such as drilling for rivet and bolt joining, integration and assembly of parts (Hufenbach et al., 2007). The process is classified as a conventional machining process within industry and is required as a material removal process through a combination of rotational and translational movement between the workpiece material and the drilling tool. The increased use of composites within industry, has led to a significant amount of research into the fracture mechanics, stresses and failure analysis behind drilling on composites (Karatas and Hasan, 2018). For most composite applications, such as aerospace, damage-free and precise holes must be drilled to ensure high joint strength and precision (Liu et al., 2012).

Composite materials differ from conventional single-phase materials due to having anisotropic and inhomogeneity material properties that, generally, do not exhibit plastic deformation (Karatas and Hasan, 2018). Furthermore, composites can be composed of highly abrasive and hard reinforcement fillers, which result in difficulty in machining (Abrao et al., 2007; Liu et al., 2012). The interaction between the fillers and cutting tools is therefore distinguishably different from the interfaces during the drilling of metallic materials. The separation of phases within the composite material are therefore

of particular interest. This leads to damage distinctively associated to drilling on composites, such as delamination. Most literature available investigates delamination mechanisms, as this is the leading and major cause of material failure (Liu et al., 2012; Geng et al., 2019). Other damage modes induced by drilling include interlaminar cracking, fibre pull-out and fuzzing, matrix catering and thermal alterations (Tagliaferri et al., 1990). Figure 6 demonstrates various failures due to delamination on fibre-reinforced composite materials.

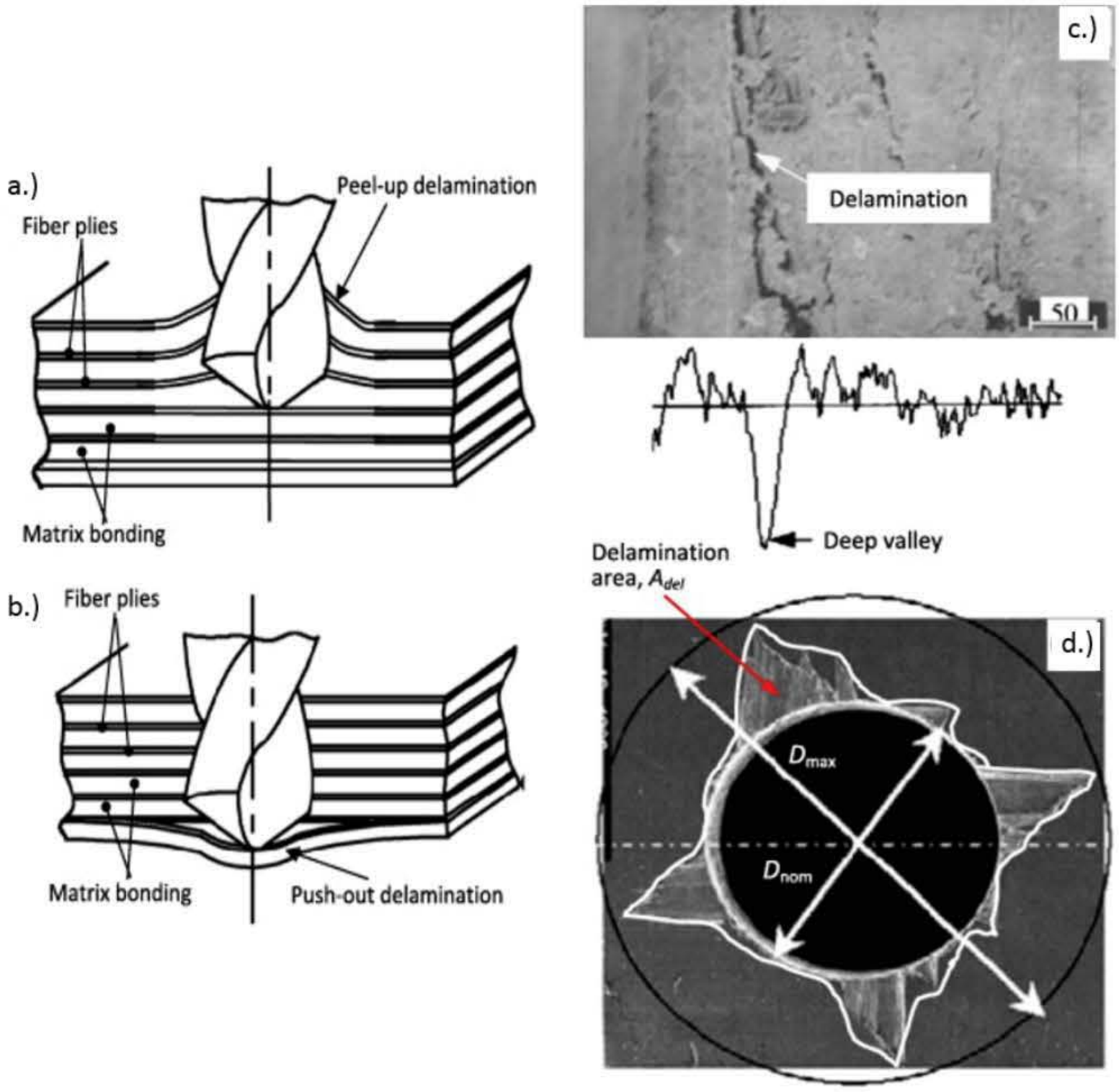

Figure 6: Mechanisms of drilling-induced delamination in fibre-reinforced composite materials shown through a.) peel-up delamination, b.) push-out delamination, c.) an SEM image of delamination intersection of a glass-fibre reinforced composite, and d.) a surface image of carbon-fibre reinforced composite used to measure delamination factor (Liu et al., 2012).

One of the main assumptions in classical lamination theory, is a state of plane stress across all of the layers in the laminate, i.e. all out-of-plane stress components are equal to zero (Isaac and Ori, 1994). However, within composite materials interlaminar stresses or peel stresses incline to separate the laminate layers from each other. The interlaminar stresses can cause interlaminar separation, which is known as delamination (Isaac and Ori, 1994; Jones, 2014; Christensen, 2012). The strength of the composite material to withstand the interlaminar stresses, is known as the interlaminar strength. It is

a well-known assessment that the failure of a composite laminate due to interlaminar stresses is challenging to analyse and model (Jones, 2014). The failure criteria and prediction is a combination of basic lamina strengths, interlaminar shear, interlaminar tensile strengths and fibre orientation (Isaac and Ori, 1994). Furthermore, due to the anisotropic and inhomogeneity material properties, the interlaminar strengths are not constant, and are only known through parametric investigations or qualitative evaluations of performance. The delamination within composites can also lead to interlaminar cracking. The delamination can occur due to the established three modes of failure: opening mode (Mode I), sliding shear mode (Mode II), or tearing mode (Mode III) (Isaac and Ori, 1994). The ability of a material to withstand the delamination growth is expressed as the interlaminar fracture toughness (Christensen, 2012). This is measured by the strain energy release rate dissipated per unit area of delamination growth (Jones, 2014). Despite the definitions of delamination, there is still a challenge in measuring and quantifying it. A study by Abrao et al. (2007) found techniques used within literature vary considerably: some have a tendency to measure damage directly (by means of parameters such as damage width, delaminated area or delamination factor), whilst others measure the damage indirectly through thrust force, torque or power. One of the most common measures of delamination within materials is through the measure of the delamination factor (F_d) which is determined using the equation (Liu et al., 2012):

$$F_d = \frac{D_{max}}{D_0} \qquad \textbf{Equation 2.1}$$

Where:
D_{max} = maximum diameter of the hole,

D_0 = actual diameter of hole.

Several reviews on drilling on composite materials do exist, however, are predominantly on the drilling on fibre-reinforced composite materials (Abrao et al., 2007; Liu et al., 2012; Teti, 2002; Hocheng and Tsao, 2006; Geng et al., 2019). Liu et al. (2012) and Abrao et al. (2007) provide two similar reviews on mechanical drilling on fibre-reinforced composites. The two reviews conclude similar findings stating that although significant improvements have been made in identifying some empirical models on delamination, there is still insufficient knowledge to be able to emphasise the physical meaning of drilling of composite laminates. A study by Teti (2002) provides a comprehensive review of drilling on both fibre-reinforced composite laminates as well as metal matrix composites up until 2001. And a study by Hocheng and Tsao summarises the critical force models of various drill bits for delamination of fibre-reinforced composites. A more recent review study by Geng et al. (2019) reviews the delamination formation, evaluation and suppression during drilling of composites. With a focus purely on delamination, the review article concludes that although present factors (such as tool speed,

thrust, feed rate) affecting delamination are widely used to direct drilling-induced delamination control within industry, a comprehensive understanding of the contributions of damaged area and cracks on delamination is still missing and difficult to evaluate.

As the review studies highlight, there is still a lack in understanding of the behaviour of composites under drilling. Nonetheless, the uniqueness of composite material properties and use within industry has led to numerous studies throughout the past couple decades attempting to model the machinability and behaviour of the more common, fibre-reinforced composite materials (e.g. Kopleve et al., 1983; Lachaud et al., 2001; Che et al., 2014; by Hocheng and Tsao, 2001; 2003a; 2003b).

The first experimental investigation by Kopleve et al., (1983) on chip formation from a carbon-fibre reinforced composite, indicate that fracture and chip formation is a process of serial material fractures. The fracture was suggested to be at the interface between the composite and drilling tool and is related to the tool tip pressure. The work is considered to be one of the first to reveal a different cutting mechanism to that of common metals (Hocheng and Puw, 1993).

The initial penetration of the drill bit on the surface is identified as causing a crack opening mode due to the normal stress perpendicular to the surface (Christensen, 2012). This is the initiation of the hole through the contact of the drill bit tip and workpiece material. The energy from the drill bit exceeds the critical energy required to extend the crack to the work done by the normal force applied and subsequent Mode I crack propagation (Abrate, 1997). The corresponding surface defines the part of the material that is also liable to undergo flexural bending as the drill penetrates the material (Lachaud et al., 2001). Studies have demonstrated how this initial contact and interaction between the drilling tool and material is correlated to the bending stiffness in composite materials (e.g. Zitoune and Collombet, 2007; Lachaud et al., 2001). The thrust force at the tip of the drill bit must exceed the critical force required to cause initial delamination at the surface. The type of drill bit edge has shown to increase the thrust force and consequent normal stresses (Che et al., 2014; Hocheng and Tsao, 2003a). The material is considered to be limited to the performance of the interlaminar strength and bonding between the filler and matrix. The delamination is therefore used as a measure of the performance of the composite under drilling. A model used throughout literature, originating from work by Ho-Cheng and Dharan (1990) provides a critical force F_z at which delamination will occur:

$$F_z = \pi \left[\frac{8 G_{Ic} E}{3(1-v^2)} (h)^3 \right]^{\frac{1}{2}} \qquad \textbf{Equation 2.2}$$

Where:
G_{Ic} = the critical energy release rate in Mode I,
h = workpiece thickness beneath drill,
E = global tensile modulus,

v = homogenised Poisson's ratio.

The expressed model assumes a global tensile modulus, homogenised Poisson's ration, purely elastic and isotropic, and therefore does not take into account the role of anisotropy in inhomogeneity properties (Zitoune and Collombet, 2007). More recent analytical models allow for the initial normal stress and the critical axial force required to exceed the critical energy of propagation of cracks in Mode I crack propagation (tensile stress normal to the plane of crack initiated). Analytical models by Hocheng and Tsao (2003a; 2001; 2003b) are available and correlate the thrust force with the onset delamination. However, the models still employ linear elastic fracture mechanics to solve the critical force for fibre reinforced composites. The models do not account for nonlinear and inelastic material behaviour for other composite materials. Therefore, as concluded within the drilling on composite review studies (Abrao et al., 2007; Liu et al., 2012; Teti, 2002; Hocheng and Tsao, 2006; Geng et al., 2019), empirical models on delamination are based on considerable assumptions but are able to identify present factors (such as tool speed, thrust, feed rate) affecting delamination and are widely used to direct drilling-induced delamination control within industry. There is still insufficient knowledge to be able to reproduce the physical and theoretical prediction of drilling of composite laminates (Abrao et al., 2007; Liu et al., 2012; Geng et al., 2019).

Whilst the current models are still being developed to understand the formation mechanism of drilling-induced delamination (Geng et al., 2019), literature is still unable to model the chip formation from composites during drilling. The creation of chips or material separation from the workpiece, the combination of various forces must exceed the critical delamination force, material strength, including the cutting force, thrust force, shear force, normal force, and frictional force (Abrate, 1997). The only literature available on understanding the formation of nano-sized and micro-sized particles generated from materials during drilling is on metallic materials. The chip formation within metals has been studied within literature mainly due to correlation between chip formation and drill tool wearing (Songmene et al., 2015). Within metals, the variation in chips formed can have a detrimental effect on the drill bit and thus reducing the life and increasing the drilling cost (Niknam et al., 2014). No studies however were found on chip formation due to drilling on nanocomposite materials. Instead, literature available is mainly on the analysis of chip formation to identify the optimal conditions for improving machining and machinability. The knowledge on nano-sized and micro-sized particles generated during drilling on metals could potentially provide a foundation for the necessary research on understanding the mechanism for composite materials.

A study by Xie et al. (1996) was one of the first reports on a coefficient identifying chip segmentation in aluminium drilling, a process that has significant effect on the cutting force fluctuation during

drilling which will affect the tool vibration and tool wear. A more recent study by Songmene et al. (2011) attempted to evaluate the effect on material brittleness on chip formation from aluminium during drilling. The authors observed that both brittle and ductile materials produced continuous and long chips at low cutting speeds. However, the study was able to conclude that the chip length decreases as the cutting speed increases for the aluminium alloys investigated. The authors also concluded a reasonably broad statement that the chip length depends on material properties and cutting conditions. Also, in the study by Songmene et al. (2011), the effect of various parameters and materials on ultrafine particles were evaluated. An isolated system was setup to capture all particles released. The study highlights the particle formation process through two main steps which depend on the material workpiece. The first step occurs during the material separation (i.e. drilling forces exceeding fracture forces), and step two occurs when the chip slides on the tool rake face. The fracture of the material is highly associated to the brittleness of the material. A brittle material will cause chip formation by brittle fracture, with very small chip contact length. The authors also indicate that the contact between the drill bit and irregular chip surface, caused by the brittle fracture, can break up particles from the internal chip surface. In contrast, in more ductile materials, the chip is formed by micro-segments that undergo a local work hardening due to the contact roughness of the drill bit tool. The hardened small part is then separated by a local brittle fracture. The two steps are displayed in Figure 7.

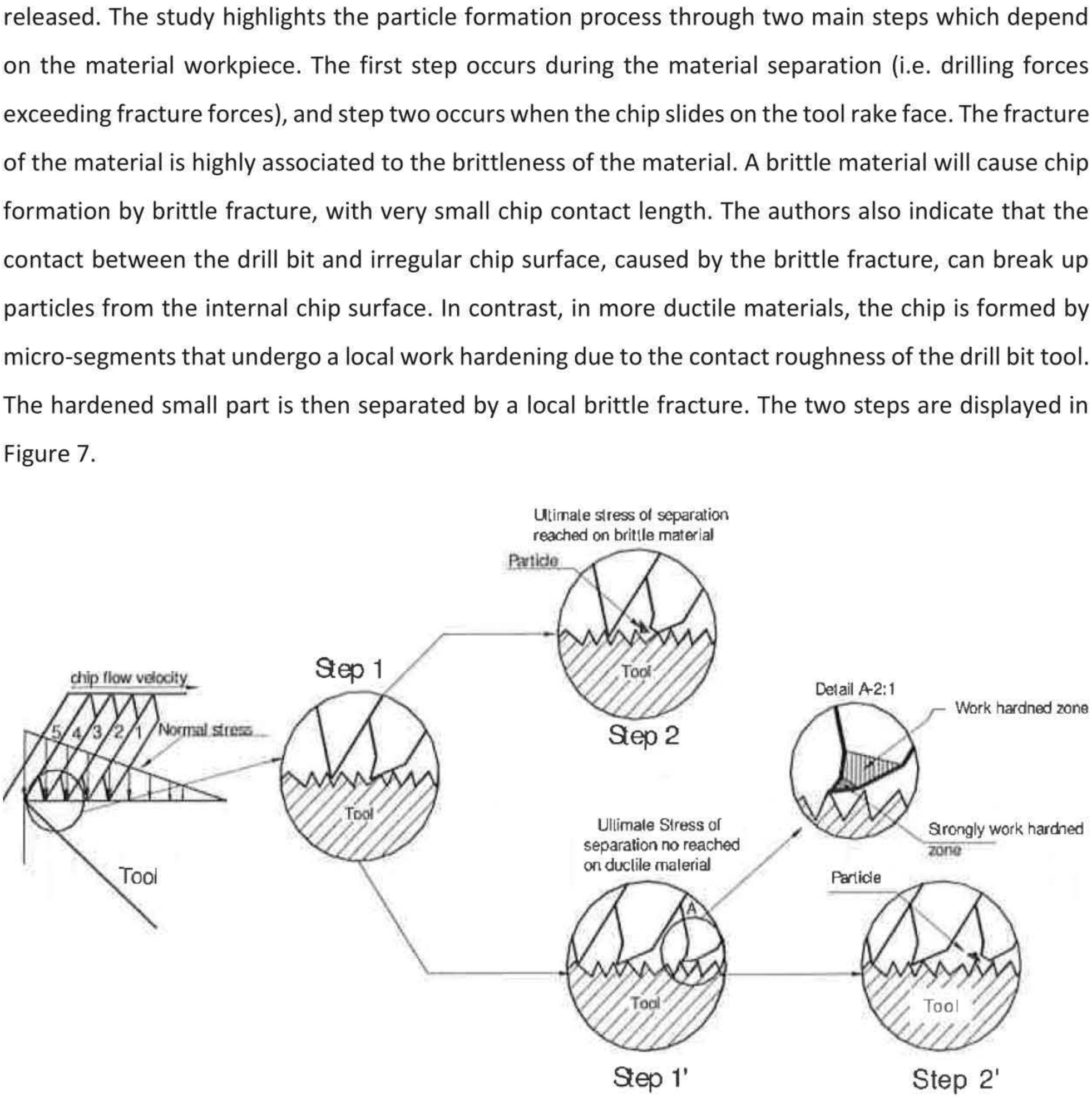

Figure 7: Schematic illustration of chip and dust emissions at drill tool tip-workpiece interface (Songmene et al., 2011).

In contrast however, the influence of nanoparticles within polymer nanocomposites on the material performance during drilling is far less studied. Most frequent reoccurrence of use of nanocomposites and drilling searches returns the use of nanoparticles to alter drilling fluids in oil and gas drilling operations (such as Cheraghian et al., 2018; Sadeghalvaad and Sabbacghi, 2015). Within the separated relevant literature, only one review article was identified to include a review on the influence of nanoparticles within polymer nanocomposites on material performance during drilling (Panchagnul and Palaniyandi, 2018). The article reviews published studies up until 2017 and reported only nine studies to have investigated the influence of nanoparticles within polymer nanocomposites on material performance during drilling. Three of the studies are investigations on the nanoparticle release (Sachse et al., 2012a; Irfan et al., 2013; Bello et al., 2010) and do not relate to the damage or fracture mechanics within the materials. Another article in the review is a paper published from this thesis (see Scientific Contributions section for publications, Starost and Njuguna, 2014). The remaining five articles evaluate the influence of incorporating nanoparticles on either hybrid composites or as coatings on material performance during drilling (Rajakumar et al., 2013; Tan et al., 2015; Li et al., 2015, Gowda et al., 2015; Baker et al., 2002).

The study by Rajakumar et al., (2013) is focused as an investigation on the utilisation of acoustic emissions to monitor the drilling of carbon-fibre reinforced composites. However, the study includes the dispersion of 0.5 - 1.5 wt. % CNFs within the hybrid carbon-fibre/epoxy nanocomposite. The results demonstrated an increase in stiffness with increase in CNF wt. %, and a decrease in delamination factor with an increase in CNFs. The improvement is attributed to the CNFs providing a better interlaminar bond strength. In similar work by Li et al. (2015), a carbon-fibre reinforced epoxy is modified to become a hybrid nanocomposite with the incorporation of 1 wt. % CNTs. The authors demonstrate the nanoparticles are able to decrease the deamination factor by 16 % and the mode I interlaminar fracture toughness increased by more than 66 %. The improved properties are associated to the bonding interface improving with the inclusion of CNTs. Furthermore, the CNTs were attributed to being able to bridge cracks and transfer the load. The remaining studies included within the review article by Panchagnul and Palaniyandi (2018) do not demonstrate the influence of nanoparticles on material performance during drilling, but evaluate hybrid carbon/glass fibres (Tan et al., 2015), optimising drilling parameters for epoxy/silicon nitride (Gowda et al., 2015), and investigate nanocomposite coating on stainless steel (Baker et al., 2002).

Two more studies on evaluating the influence of nanoparticles within polymer nanocomposites on material performance during drilling have since been released (Kumar and Singh, 2019; Buruk Kaybal et al., 2019). The study by Kumar and Singh (2019) investigated drilling on carbon-fibre/epoxy hybrid nanocomposites reinforced with CNTs. Similarly, the study demonstrated a decrease in delamination

factor by up 28.6 % with the inclusion of CNTs. The improvement is attributed to the increase in interlaminar shear strength with the addition of CNTs. In the most recent article, the study by Buruk Kaybal et al. (2019) evaluated drilling on the use of boron nitride nanoparticles within a hybrid carbon-fibre/epoxy nanocomposite. Correspondingly, the study demonstrated how the addition of the nanoparticles were able to reduce the delamination factor. The property improvement was shown to be due to indicated strong interface and interlaminar bonding due to the ceramic structure and hexagonal crystal structure of the nanoparticles.

From the available literature therefore, most studies evaluated the use of nanoparticles to improve the bonding within hybrid nanocomposite materials. The studies thus far, are in agreement, that the nanoparticles used, mostly CNTs or CNFs, are able to improve the interlaminar strength between the micro-sized fibres and the epoxy, as well as providing a potential bridge when cracks form and transfer the stresses. This in subsequence has demonstrated a decrease in delamination factor for the hybrid fibre-reinforced composite materials. The available literature also does not provide sufficient knowledge on the influence of nanoparticles within composite materials on chip formation. Not overlooking the major differences in material characteristics, the literature on drilling on metallic materials might provide a foundation for nanocomposites. As there is still insufficient knowledge to be able to understand the phenomena and reproduce the physical and theoretical prediction of drilling of composite laminates (Liu et al., 2012), the effect on nanocomposites is still required. The literature demonstrates, and as concluded within Panchagnul and Palaniyandi (2018), there is a clear lack of knowledge on the influence of incorporating nanoparticles within polymer nanocomposites on material performance during drilling.

2.4 Nanoparticle Toxicity

Due to the use of the nano-sized particles, nanocomposites introduce a potential toxicological and/or eco-toxicological hazard. Research is comprehensively investigating the potential nanoparticle release and exposure to humans and the environment (Fadeel et al., 2018). In addition to machining the material, mechanical processes such as drilling on nanocomposites has shown to unintentionally release nanoparticles into the environment and/or workplace (Basinas et al., 2018).

Literature recognises that certain nanoparticles at certain dosages have the potential to be hazardous to humans (Fadeel et al., 2018; Brown et al., 2013). The advantages of the nanoparticle physiochemical properties employed for the use within materials also render potential unique toxic effects within biological systems (*Hristozov et al., 2012)*. The use and introduction of these materials into the

workplace can be hazardous when human exposure is concerned (*Njuguna et al., 2009; Njuguna et al., 2014; lee et al., 2019; Froggett et al., 2014; Basinas et al.,* 2018).

It is important to note that not all nanomaterials induce toxic effects. The hypothesis that smaller means more reactive and thus more toxic, cannot be substantiated (*Baalousha & Lead, 2013*). Potential differences in physio-chemical properties compared to the bulk chemical and numerous applications spread over a wide range of fields (Hankin & Reat, 2016), necessitate nano-sized materials to be evaluated on a case-by-case basis (*Aitken et al., 2008; Stone et al., 2010*). However, studies have attempted to classify the key particle characteristics that have exhibited to cause toxicity effects (such as Froehlich, 2012; Gnach et al., 2015; Johnston et al., 2010; Stone et al., 2010). Literature has been able to identify that the physio-chemical properties of the nanoparticles have a strong influence on the adverse health effects (*Vega-Villa et al., 2008*). Figure 8 illustrates some key characteristics identified.

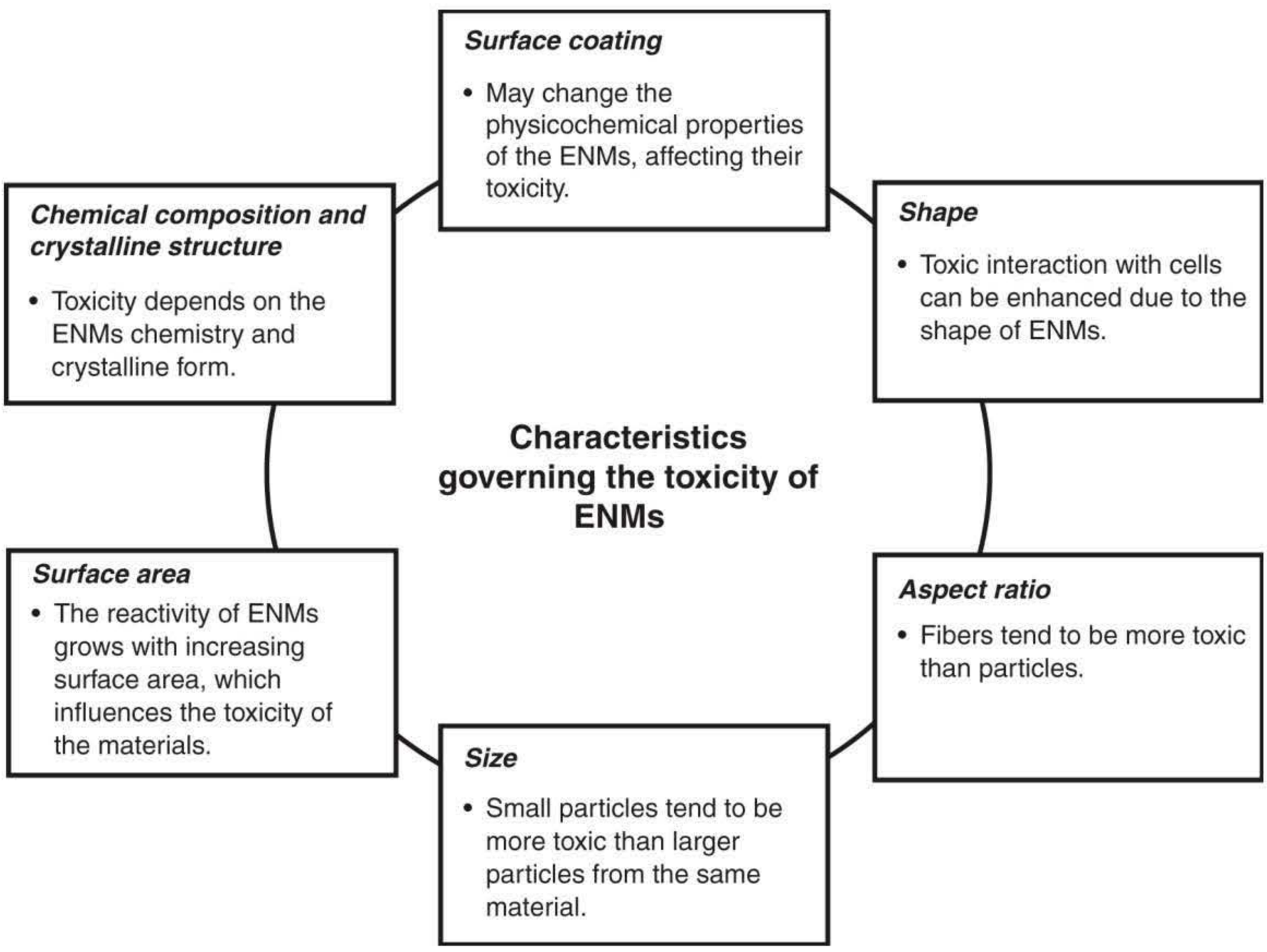

Figure 8*:* A selection of identified nanoparticle characterics that have demonstrated to have an efffect on toxicity (Hristozov et al., 2012).

Particle size has been highlighted to be one of the most influential material properties effecting toxicity. Studies have shown that the size of a particle can be directly linked to toxicity and generate size-dependent genotoxicity (*Jacobsen et al., 2008; Park et al., 2011*). This increased biological

response (whether beneficial or detrimental) to certain nanoparticles compared to that "of the same mass of larger particles of similar chemical composition" is highlighted in the hazard characterization in a recent ISO technical report on "Health and safety practices in occupational settings" (ISO/TR 12885, 2018). However, a study carried out by *Karlsson et al., 2009*, reported an inverse correlation between certain particles on size and toxicity effects. The study found nanoparticles of copper oxide (CuO) to be significantly more toxic when exposed to human cell line A549, compared to CuO micro-sized particles. In contrast, titanium dioxide (TiO_2) micro-sized particles demonstrated more DNA damage compared to the nanoparticles. Separately, two iron oxides (Fe_2O_3 and Fe_3O_4) displayed similar low toxicity and no difference between nano and micro sized particles (*Karlsson et al., 2009*). Therefore, although specific particles have demonstrated to be toxic due to certain characteristics, each particle is different and requires to be individually assessed based on current knowledge. A review on the toxicity of CNTs alone by Aschberger et al., (2010) concluded there is currently inconclusive data to draw definitive conclusions on the genotoxic potential and the dependence on physico-chemical properties, requiring a case-by-case approach for the time being. A more recent study by Obertdoerster et al. (2015) concluded similar findings and the need for more data.

Further to the characteristics mentioned in Figure 8, other factors such as aggregation, agglomeration, solubility, particle uptake and presence of mutagens etc. have been acknowledged to influence toxicity (*Hristozov et al., 2012; Froehlich, 2012; Gnach et al., 2015*). With the dosage established as one of the most crucial characteristics, the particle size, shape, chemical composition and size distribution have shown to be the influential particle characteristics (*Hristozov et al., 2012*). Various studies have attempted to summarise literature findings and narrow down and focus concerns on certain characteristics such as size, composition etc. for example fibres with aspect ratio of more than 3:1 (*NanoPortal, 2017*).

A human can be exposed to nanoparticles into the circulatory system through four main pathways: ingestion, injection, transdermal delivery, and inhalation (*Gnach et al., 2015*). Toxicological studies involve the assessment of the particle effect on the cell type within the pathway of exposure. A challenge therefore is to understand the potential route of nanoparticles once inhaled, with the purpose of subsequently identifying any conclusive assessment on the potential health risks. Figure 9 illustrates a predicted deposition location within the respiratory tract of all nanoparticles that are inhalable based on particle diameter if inhaled through the nose (Oberdoerster *et al., 2005*).

Airborne particles are also classified into separate categories in relation to the probability of the particles penetration: inhalable, thoracic and respirable (Sanchez Jimenez et al., 2012). The inhalable fraction is the mass fraction of total airborne particles that can penetrate the nose and mouth. The

thoracic fraction is the fraction that can penetrate the bronchial region. Whereas, the respirable fraction is the fraction of inhalable particles that reach the alveolar region of the lung (Lidén and Harper, 2007).

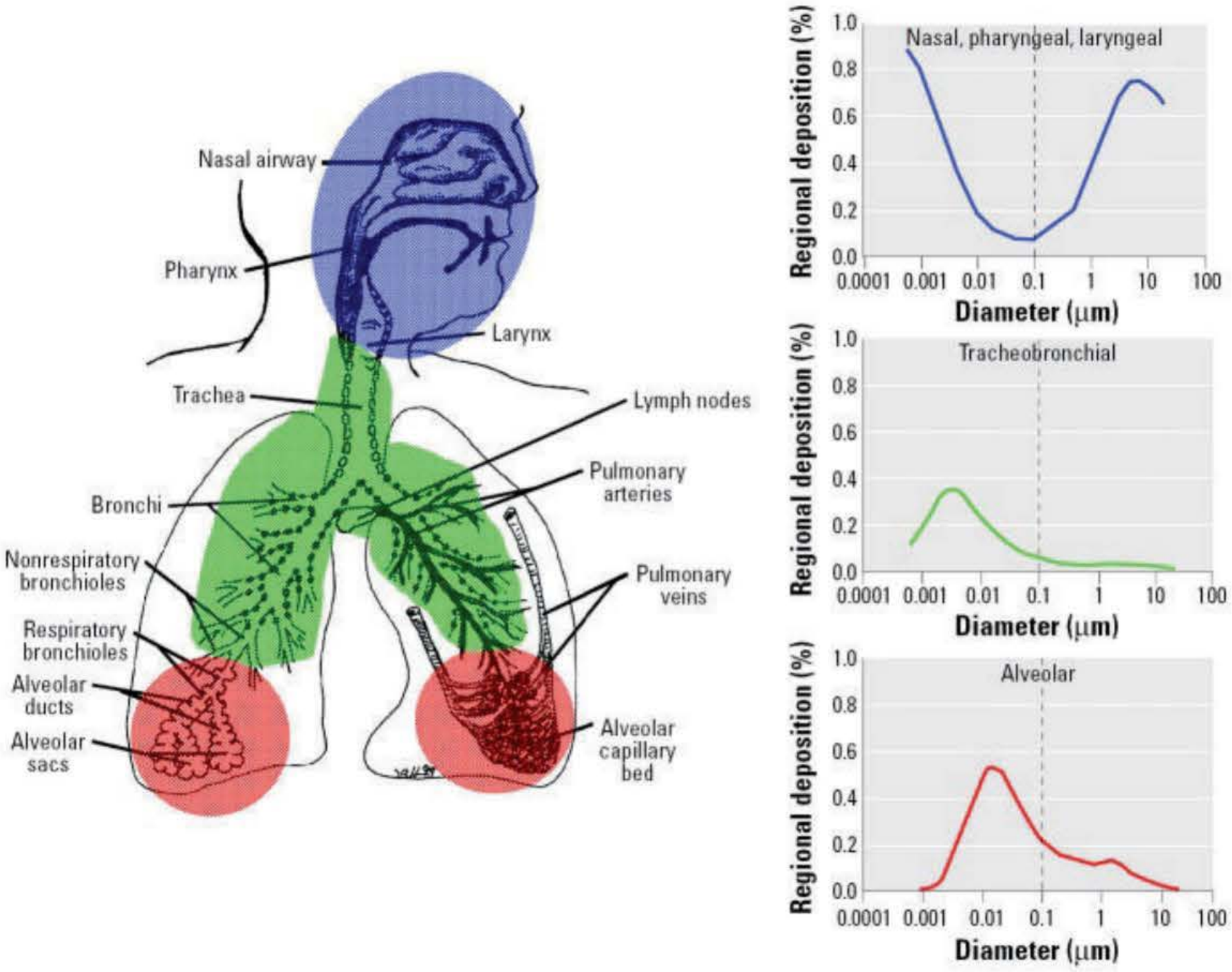

Figure 9*:* Predicted percentile deposition of nanoparticles within respiratory tract if inhaled through the nose in relation to particle diameter *(Oberdoerster et al., 2005).*

The pathway of entry for the particles into the human body has significant effect on the toxicity. Inhalation models of toxicity assessment are the most commonly employed of the four modes of nanoparticle uptake (*Love et al., 2012*) through the use of common lung cell lines. As shown in Figure 9, the particle will deposit at various locations along the respiratory tract depending on the diameter. Significantly, different sizes can target all three regions of the respiratory tract. Once deposited within the pulmonary system, the particles will translocate to reach various organs via different transfer routes and mechanisms such as via the blood circulation or lymphatics (*Oberdorster et al., 2005*). The extent and toxicity effects thereafter are particle-dependent and therefore required to be studied individually.

Healthy skin generally works as a protective barrier, however as summarised in a review article by *Crosera et al. (2009*) numerous studies have shown interaction between human dermal cells and

nano-sized particles. The review nonetheless does call for more studies on nanoparticle skin absorption as the findings thus far have been contradictory. As with particles exposed to human cells through inhalation, and ingestion, it is necessary to study each nanoparticle individually to fully understand the toxicity effects (*Crosera et al., 2009; Hristozov et al., 2012*).

Additionally, projects have developed into databases which provide various toxicity metrics on nanomaterials such as the Hazardous Substances Data Bank assembled by the National Institutes of Health (*NIH, 2017*) or the NanoSafer tool maintained by the Danish National Research Centre for the Working Environment (*NanoSafer., 2017*), both of which are revised after assessment by a scientific review panel.

Due to the significant amount of literature available having established various nanoparticles potentially being toxic, industry and research labs are institutionalising the safe handling, exposure limits and working with nanoparticles. Recommended exposure limits and safe handling handbooks are in place when manufacturing or handling certain nanoparticles (e.g. *NIOSH, 2013; EU-OSHA, 2009; ISO/TS 12901-2, 2014; CEN/TC 352, 2016; OECD, 2017; ASTM E2535, 2018; BSI PD 6699, 2007; WHO, 2017*). An example is by the National Institute for Occupational Safety and Health (NIOSH) in the United States recommending the exposures to CNT and CNF be kept below the recommended exposure limit (REL) of 1 $\mu g/m^3$ of respirable elemental carbon as an 8-hr TWA (*NIOSH No. 2013–145, 2013*). Legislation now instruct the assessment of exposure to certain nanoparticles such as under the European law known as the Regulation on Registration, Evaluation, Authorization and Restriction of Chemical (REACH), requiring manufacturers and chemical importers to carry out a consumer exposure assessment if the chemical is classified as hazardous (*REACH No. 1907/2006, 2017*). However, a systematic review by Mihalache et al. (2017) on occupational exposure limits for manufactured nanomaterials concluded that whilst current OELs can provide a valuable reference point for exposure reduction measures in workplaces, there is a need for more and better supported OELs. The current exposure limits comprise of working solely with the nanoparticles prior to being embedded into materials. The nanoparticles are utilised within polymer nanocomposites and only relatively recently have studies started evaluating the potential release of the nanoparticles from the nanocomposite materials (Basinas et al., 2018).

Literature is also in agreement in that despite studies having demonstrated potential risks to human health and the environment from the manufacture and use of nanoparticles, there is also a lack of knowledge about what the risks might be and how to deal with them (Hankin & Read; 2016). Literature has therefore reported on the challenge in handling the uncertainty and concerns through innovation governance and responsible development (Hankin & Read; 2016; BASF, 2008; EC, 2008). Hankin &

Read (2016) discuss both concepts (among others) in a report along with the challenges and the purpose of governance of nanotechnology in relation to anticipate and realise future developments, ensure safety and sustainability and generate trust and confidence.

2.5 Nanoparticle Release and Exposure Scenarios (Mechanisms)

2.5.1 Routes of Exposure to Engineered Nanoparticles

Although control and regulations on inhalable particles exist, there are currently no exposure limits comprising of nanoparticles released from engineered nanocomposites (Debia et al., 2016; Methner et al., 2007). However, the nanoparticles are also utilised within nanocomposites and only relatively recently have studies started evaluating the potential release of the nanoparticles from the materials (*Basinas et al., 2018; Debia et al., 2016; Froggett et al., 2014)*. Since nanoparticles are manufactured to be embedded within the polymer composite, the nanoparticles cannot be released without an energy input. Throughout its lifecycle, after synthesis and manufacturing, nanocomposites may encounter potentially degrading mechanical, thermal and/ or chemical energy inputs that results in the unintentional release of the nanoparticles (*Froggett et al., 2014*). Although the unintentional release may occur randomly and due to unrepeatable events throughout its life, some of the causes may take place on a more regular basis, such as within the workplace when working with the materials on a daily basis. The toxicity of the nanoparticles thereby becomes critical when considering exposure during the workplace. Figure 10 illustrates the various elements to consider in an occupational exposure scenario (*Ding et al., 2017*).

As can be seen in Figure 10, there are a considerable number of factors and elements to consider when evaluating the release of nanoparticles. When not taking place within a controlled environment, parameters such as the ventilation, room volume, distance from personnel, personal protective equipment (PPE) etc., all need to be included in the assessment of occupational exposure.

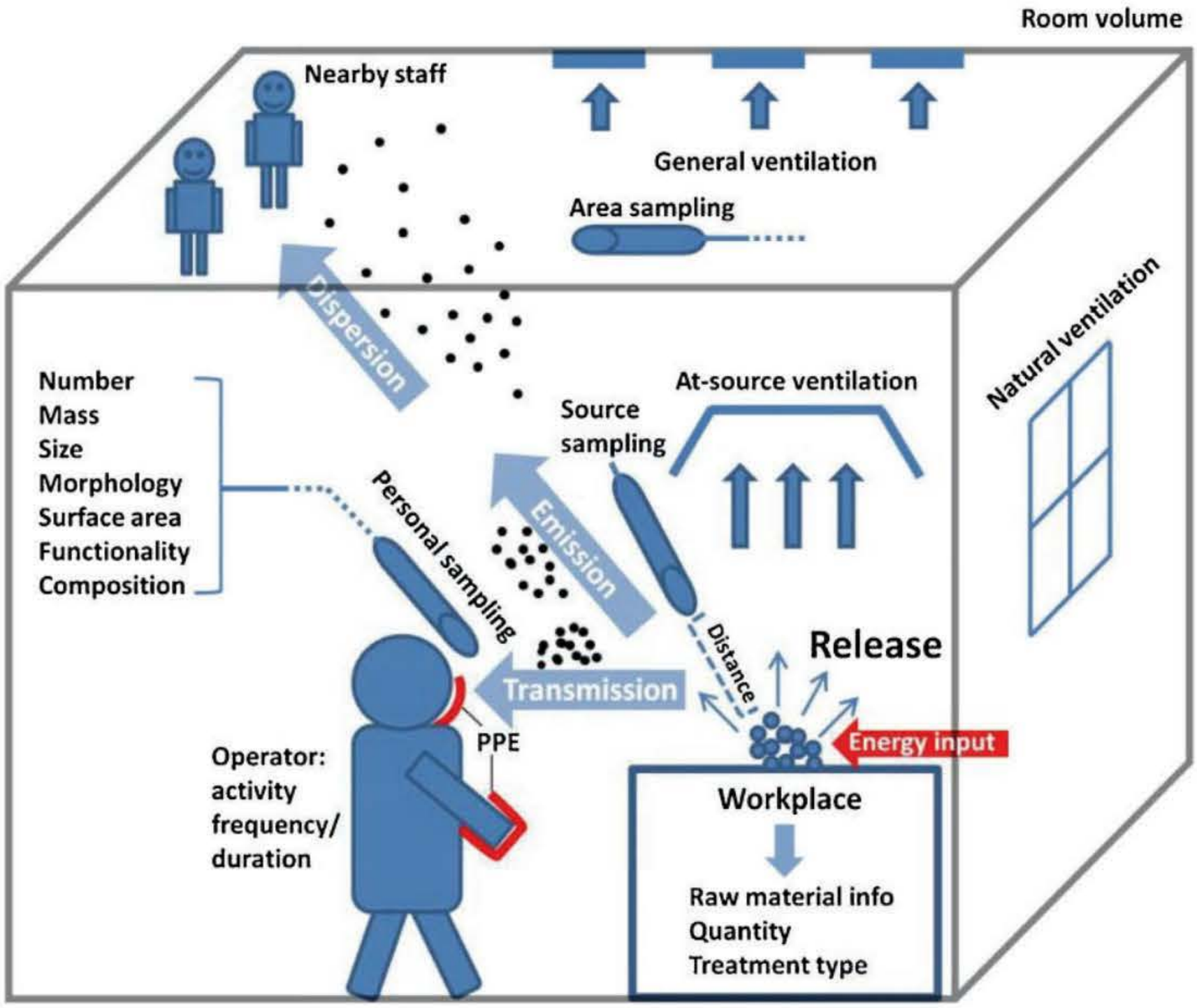

Figure 10: Diagram representing various elements and processes in an occupational exposure scenario *(Ding et al., 2017).*

Various studies have investigated the release of the particles from nanocomposite materials. As the quantification of the release is carried out due to the concerns of release of potentially toxic nanoparticles, studies have attempted to integrate current literature to identify likely scenarios of nanoparticle exposure. Three similar studies have collated the findings of numerous papers on the routes and forms of exposure to ENMs (Froggett et al., 2014; Basinas et al., 2018; Debia et al., 2016).

Another earlier study by Van Duuren-Stuurman et al. (2010) evaluates the assessment of ENM dermal exposures. The study groups the exposure likelihood with the identified activities. The findings however are limited to dermal exposure and provide few details on the scenario conditions in the assessment. The findings from the study conclude that the likelihood of exposure is increased when feeding into a process, packing and extruding. The synthetisation of materials showed little likelihood of exposure, and no information is provided on the assessment from machining on ENMs.

In contrast, a review study by Froggett et al. (2014) summarised the existing nanoparticle release studies up until 2014, highlighting the current gap in knowledge with 54 publications covering the release from solid non-food nanocomposites. From the experimental studies, 96% demonstrated

release of nanomaterial from the nanocomposites. The review divided the type of release scenario into five categories: machining, weathering/UV, washing, contact and incineration. The summary of the investigated studies is demonstrated in Figure 11.

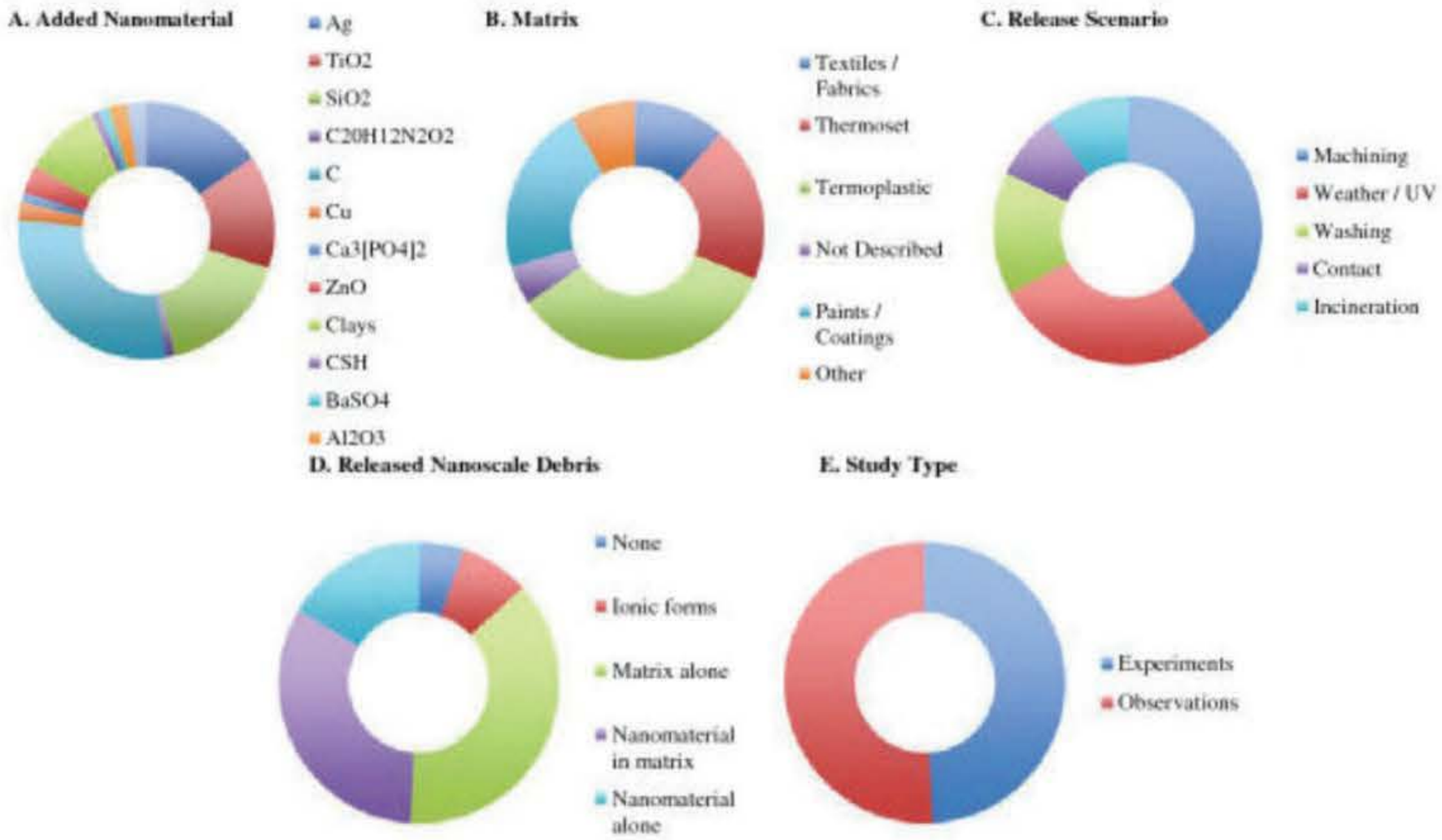

Figure 11: Summary of 54 reviewed articles by Froggett et al., 2014, concerning the release of nanomaterials from solid nanocomposites.

As can be seen in Figure 11, a large variety of nanomaterials, matrixes, release scenarios and exposure study types have been considered. Machining was found to be the most examined scenario with 43% of the studies including machining. This is due to the high energy input required for machining and thus higher expected quantity of particles released. This scenario is therefore covered in the following section.

The second most investigated release scenario, with 32 % of the studies, was due to weathering such as UV exposure (*Nguyen et al., 2012; Gorham et al., 2012*), fluorescent lamps (*Hsu & Chein, 2007*) and saline water contact (*Zann et al., 2010*). The review found and concluded that a broad range of nanocomposites and matrices were tested via different setups and exposures. 94 % of the weathering studies found the release debris to be the nanocomposite alone and 65 % found the nanoparticles embedded within the debris (*Froggett et al., 2014*). The studies show contrasting evidence, with Nguyen et al., 2012, presenting clear evidence of nanosilica released from epoxy/nanosilica nanocomposites exposure to UV light within a controlled environmental chamber, whereas other studies such as *Al-Kattan et al. (2013*) showed low release quantities of nano-TiO_2 close to the background values. A more recent study by *Nguyen et al. (2017*) found MWCNTs to form a dense entanglement layer on the surface of the material due to UV light exposure, but resisted release.

As seen in Figure 11, other studies have investigated the release due to washing (Pasricha et al., 2012; Lorenz et al., 2012), contact (Von Goetz et al., 2013; Moreau et al., 2012) and incineration (Motzkus et al., 2011; Bouillard et al., 2013). Washing studies demonstrated almost no evidence of identifiable separate nanoparticles. Whereas contact scenarios reported some evidence of release dissociated nanomaterials (Von Goetz et al., 2013), whilst others reported none or the matrix alone (Moreau et al., 2012). The incineration studies identified within the available literature mostly focused on the addition of CNTs to thermoplastics, and only one study reported the release of the nanomaterial (Bouillard et al., 2013). However, it was also noted that the incineration process makes it difficult to distinguish the released particles from combustion (Motzkus et al., 2011). The limited literature available highlights the current understanding being in a preliminary stage where, although a slight majority of the studies did not report identified release of separate nanomaterial, the contrasting results raise interesting data of potential release. More data, analysis and correlation between the materials and methodology are required.

A review study by Debia et al., (2016) focused on literature on reported exposure to engineered nanomaterials. The study evaluated literature available between 2000 and 2015 and found 306 exposure situations in the workplace. The paper follows a strict set of criteria in assessing exposure studies, following another study (Brouwer et al., 2009), in meeting the inclusion criteria only selecting studies with high methodological strength. To simplify the presentation and ease of understanding the results in terms of the nanoparticles, the data is grouped into nanoparticle fillers as opposed to exposure scenario. The results from the study found exposure to occur in 83 % (N=107) involving carbonaceous ENMs, in 73 % (N=120) involving metallic ENMs and in 100% (N=6) involving nanoclays. The study concluded therefore that a potential for occupational exposure to nanoparticles, especially during handling tasks, is consistently reported in literature. Furthermore, given the limitations found in studies, e.g. evaluating differences across different seasons or days, the review emphasised the urgent need for more and better exposure data.

In a more recent study by Basinas et al. (2018), a systematic review found 174 articles to meet a rigorous selection criteria on literature published between 2000-2015 on measurements studies on inhalation or dermal exposure from ENMs. Not only does the study report an increase in research on release from ENM materials, but also concludes the lack of high-quality data. The authors found that in certain life-cycle scenarios, there is sufficient evidence to conclude that there is no likelihood of exposure to the nanoparticles. For example, from 27 studies reviewed, CNTs and CNFs were concluded to not show inhalation exposure during synthesis. However, from 37 studies, the data showed there was a sufficient evidence showing a likelihood of exposure during machining and abrasion to CNTs and CNFs. Similarly, from 6 studies found to meet the inclusion criteria, Si-based fillers results were

"unclear", whilst evidence from 17 studies on other nanofillers were also "unclear". Furthermore, results from large and pilot production exposure assessment situations for CNTs and CNFs provided evidence that inhalation exposure occurs when the process is of high-energy input, manual, and dry. Additionally, the study concludes that although there is a lack of measurement data for ENM exposure and with limitations between data, the results of the study suggest that all three routes of exposure (i.e. inhalation, dermal and ingestion) are relevant for workers in the manufacturing of ENMs (Bainas et al., 2018).

2.5.2 Nanoparticles Released due to Machining

Within the life cycle analysis of nanocomposites, studies (e.g. Bainas et al., 2018; Debia et al., 2016; Froggett et al., 2014) have identified that machining is a key relevant scenario where the embedded nanoparticles can potentially be released due to the high energies involved. Throughout its life-cycle, a nanocomposite material will undergo various machining processes during assembly operations to fabricate and regulate to its corresponding application where the nanofillers could unintentionally be released and exposed to workers and/or consumers. Various studies have looked into nanoparticle release due to a variety of mechanical processes nanocomposite materials will go through such as cutting (*Methner et al., 2012*), abrasion (*Schlagenhauf et al., 2012*), sanding (*Saber et al., 2012*), sawing (*Gomez et al., 2014*) and drilling (*Sachse et al., 2012a, b*). *Froggett et al. (2014)* reported twenty-three studies to have investigated the release due to machining methods. Of the studies on machining, 30% of studies reported the identification of dissociated nanomaterial alone among the release debris. However, in contrast, 91% of the studies reported the release measurement of matrix alone and 87% reported identified nanomaterial within the matrix. Drilling, abrasion, sanding, cutting and grinding scenarios all demonstrated release of individual nanoparticles. However, studies carried out using the same scenarios also reported no evidence nanoparticle release (*Froggett et al., 2014*). As with the previous section 2.5, it is difficult to draw comparisons and distinct conclusions due to the varied material and methodologies. A general conclusion that can be drawn from review would be the limited literature highlights a need for a harmonised methodology in order to compare the materials and processes. The review also concludes that whilst the data currently indicates a high portion of the release to be partially or fully embedded nanomaterials, there is a shortage of research into the release of manufactured nanomaterials. From the few studies available, literature has indicated that fragments of polymer matrix with protrusions of ENMs, have shown no more toxicity than fragments of control polymer without the nanofiller (e.g. Wohlleben et al., 2011; Wohlleben et al., 2013, Saber et al., 2012; Saber et al., 2012, Schlagenhauf et al., 2015).

A similar earlier review study by *Kuhlbusch et al. (2011)* reviewed the current studies in nanoparticle exposure in workplaces. The authors found a similar conclusion on the difficulty in comparison of the results. A lack of coherent approach towards exposures assessment, measurement metrics and major drawbacks such as differentiating background particles from nanomaterial related particles, and instrument sensitivity, all made it challenging to compare studies. A key challenge is the ability to relate the simulated and workplace scenarios. The summary of findings observed agglomerations of nanomaterials of < 100 nm to be released in only a few cases, but a regular release of > 300 nm was observed (*Kuhlbusch et al., 2011*).

The review of reported exposure scenarios by Debia et al., (2016) identified several industrial processes in which the exposure to nanoparticles were investigated. The study focuses on the nanoparticles used as opposed to exposures scenario and groups all activities under industrial handling tasks, which include pouring, weighing, drilling, sanding, sawing etc. As a result, the machining processes are not separated and many of the studies crossover with the studies reported in Froggett et al. (2014).

In the review study by Basinas et al. (2018) on routes and forms of exposure to ENMs, the authors put emphasis on a clear lack in data from studies relating to machining and abrasion scenarios. From the studies found on machining (Mazzuckelli et al., 2007; Takaya et al., 2012; Lo et al., 2012; Ono-Ogasawara et al., 2013) on CNTs/CNFs, the authors conclude that the studies "provide a clear evidence that inhalation exposure occurs when the process is of high-energy input, manual, and dry". The process include cutting, abrasion, drilling, sawing and weaving. The authors also found that literature provides high-quality evidence that dermal exposure is likely during machining and abrasion in 15 assessments.

As demonstrated in Figure 11 in the review by Froggett et al. (2014), Debia et al. (2016) and Basinas et al. (2018), a variety of machining processes have been investigated within available literature. From the results, drilling has been identified as a fundamental and significant machining process used during assembly operations which can produce nanoparticles. An Airbus A350 will undergo 16000 holes drilled per composite wing set (Griffiths, 2013). However, only six studies were identified to have investigated the release of nanoparticles from nanocomposite materials during drilling (Bello et al., 2010; Sachse et al., 2012a, b; Irfan et al., 2013; Gendre et al., 2015; Ding et al., 2017). All six studies demonstrated nanoparticles to be released.

In the work carried out by *Sachse et al (2012a*), the release of polyamide 6 reinforced with SiO_2 nanoparticles and micro-sized glass fibres is investigated. The findings displayed that with a 5 wt. % SiO_2 reinforced nanocomposite, fifty-six times more nanoparticles were released in comparison to the

neat polyamide. However, the study also observed the majority of the particles released to be in the same size range 22.6 nm to 42.5 nm. The silica reinforcement therefore was not reported to have introduced particles at a new size range, but instead, increase the concentration at the same size range as the neat polyamide 6. In the similar study carried out by the same authors, but with the use of 5 wt. % MMT as a nanofiller for the polyamide 6 resin, a reverse trend was observed. The reinforced nanocomposite was seen to release twenty times fewer airborne nanoparticles than the neat polyamide, but double the number of deposited nanoparticles (*Sachse et al., 2012b*). The authors associate the reduction in airborne nanoparticle release to the exfoliation of the nanoparticles within the matrix.

In a similar study by *Irfan et al. (2013)* and using the same equipment, polyamide and polypropylene were reinforced with 5 wt. % SiO_2 and MMT. The study found polyamide nanocomposites displayed up to ten times more nanoparticles generated than from polypropylene nanocomposites. The matrix can therefore be seen to have a significant effect. The study also reported silica nanoparticles increased the nanoparticles released, whereas MMT was found to decrease the release of nanoparticles, and therefore demonstrated corresponding findings to both Sachse et al. (2012a and 2012b) studies. The study also evaluated the cytotoxicity of the particles released in human lung epithelial A549 cells. The authors concluded the polyamide-based nanoparticles released were much more toxic than the polypropylene-based nanoparticles and that the toxicity however, was much less than that induced by the individual SiO_2 nanoparticles.

In the drilling study by *Bello et al. (2010)*, hybrid composites incorporating Al_2O_3 fibres and graphite with reinforced CNTs within epoxy were investigated for nanoparticle release during drilling. The study reports the inclusion of CNTs demonstrated an increase in geometric mean particle number concentration when included in both the Al_2O_3 fibres and graphite hybrid composites. Two different drilling speeds were evaluated for the comparison of including CNTs within the Al_2O_3 fibres samples. At 725 rpm, the CNT reinforced sample displayed a 70 % increase in geometric mean particle number concentration in comparison to the Al_2O_3 fibre epoxy sample without CNTs. In contrast, the inclusion of CNTs within the graphite epoxy sample displayed a 35 % reduction in geometric mean particle number concentration in comparison to the graphite fibre epoxy sample. The microscopy analysis revealed aggregates of CNTs in the emissions after drilling on CNT-alumina and CNT-carbon nanocomposites. Furthermore, with a similar study on the same materials using cutting, drilling demonstrated significant differences and an increase in overall nanoparticle release *(Bello et al., 2009; Bello et al. 2010)*. The particle release measurements were taken and compared for both the unmodified and carbon nanotube reinforced samples. The studies observed that nanoparticles were detected regardless of the composite type and presence of the CNT fillers. 1% to 10% of particles

released were shown to be within the nanometre range (<100nm), whilst 71% to 89% were in the 1 µm to 10µm range. When examined using scanning electron microscopy (SEM) and transmission electron microscope (TEM), the released nanoparticles from the cutting experiment exposed no clearly distinguishable CNTs, contrasting the findings from the drilling experiment. The data suggests the nano-fillers continue to be embedded within the polymer resin. The authors therefore reported the need to assess different processes in evaluating the nanoparticle release from CNT reinforced nanocomposite materials and recommended effective exposure controls for both processes.

The study by Gendre et al. (2015) replicates similar nanofillers used by Sachse et al. (2012a and 2012b) and *Irfan et al. (2013).* The paper investigates the nanoparticle release from hybrid micro-sized glass fibre polyamide composites reinforced with nano SiO_2 and MMT at different weight concentrations. The authors found the different weight concentrations of both SiO_2 and MMT to demonstrate different particle number concentrations. However, the author's main findings from the study is the variability of the process. Measurements were taken on different days of the week and found different values for the same sample on different days. This was due to the lab air changing each day, producing a variable background of airborne particles before the drilling experiment is initiated. The study therefore concluded the necessity of a controlled environment. Furthermore, the authors also utilised a handheld drill and demonstrated the variability of results depending on the feed rate of the user. The study therefore also concludes the need for a controlled drilling process in order to evaluate the release of the nanoparticles during drilling.

The final study available within literature, by Ding et al. (2017), investigated the influence of 0.09 wt. % multiwalled CNTs, carbon black (CB) and SiO_2 within polyurethane nanocomposites on nanoparticle release during drilling. The weight concentrations are substantially lower than the other studies, but are correlated to beneficial electrical conductivity properties. The introduction of the SiO_2 and CB demonstrated minor increases in particle number concentration in relation to the neat PU, whilst the PU/CNT sample demonstrated the lowest number of particles released. The authors also observed a difference in particle number concentration due to different drilling speeds and drill tool size. The study concludes, that apart from the PU/CNT sample, the other materials did not have substantial influences on the release results. No free nanoparticle fillers separate from the matrix were observed, apart from protrusions on the surface. The same materials were compared to sawing tests, and concluded the drilling to produce higher particle number concentrations. The study concludes the need to evaluate the influence of different nanofiller weight concentrations within the nanocomposite, due to the low concentration investigated.

The results from the six studies on drilling exhibited agreement with the general findings in the machining review articles (*Froggett et al., 2014; Kuhlbusch et al., 2011, Basinas et al., 2018*). A finding recurrently mentioned within studies is that there is currently a lack of systematic harmonised methods to compare the results and identified the need of a standardised method to test and quantify the release and exposure of nanoparticles from nanocomposites during a machining lifecycle scenario. The differences in study approaches and conditions make it challenging to make conclusions of the effect of various parameters such as matrix or filler due to drilling. However, all studies also emphasised the current lack in data and knowledge on the influence nanoparticles have on nanoparticle release from nanocomposite due to both machining and drilling. From the literature available on nanocomposite drilling however, all studies illustrated that nano-sized particles are released, but differ in the quantity.

A summary and comparison of the materials used and maximum nanoparticle release concentrations observed are displayed in Table 1. As the half of the studies (Sachse et al., 2012a and 2012b; Irfan et al., 2013) were investigated using similar instrumentation and setup, the materials can also be seen to be comparable. The studies conclude unanimously that the introduction of SiO_2 increased the particle number concentration in comparison to the neat polyamide. The study by Ding et al., (2017), also observed a minor increase with the incorporation of SiO_2 nanoparticles. Studies agree that the use of MMT observed to reduce the particle number concentration during drilling (Sachse et al., 2012a and 2012b, Irfan et al., 2013). The maximum quantity of nanoparticle release concentration varies quite significantly. The similar compositions of materials used in Irfan et al., (2013) and Sachse et al. (2012a and 2012b), demonstrated substantial differences in particle number concentration, which is likely to be due to the same conclusion drawn in Gendre et al. (2015): variability due to variation in lab air and manual drilling tool.

Table 1: Overview of materials and maximum nanoparticle release concentrations observed during drilling in current studies on the effect nanofillers have on nanoparticle release during drilling on nanocomposites.

Materials		Nanoparticle Release Concentration [#/cm³]	Release findings in comparison to no nano reinforcement	Reference
Base Polymer Material	Nano filler			
Polyamide	5 wt. % SiO_2	> 1.4 x 10^6	Integration of nano SiO_2 strongly suggest changes in particles emitted during drilling displaying 56 times the neat polyamide.	Sachse et al. (2012a)
Epoxy-alumina & Epoxy-graphite hybrids	Around 2 wt. % CNT (between 1.3 – 2.2 wt. %)	>1.1 x 10^7	Introduction of CNTs demonstrated a 70% increase over neat epoxy-alumina and a 35 % reduction over the epoxy-graphite.	Bello et al. (2010)
Polyamide	5 wt. % MMT	>2 x 10^4	Airborne particles of MMT reinforced sample displayed 20 times lower particle number concentration but doubled the deposited number of particles in comparison to the neat polyamide.	Sachse et al. (2012b)
Polyamide & Polypropylene	5 wt. % MMT 5 wt. % SiO_2	> 1.75 x 10^6	Inclusion of SiO_2 increased the nanoparticles released significantly, whereas MMT was found to decrease the release of nanoparticles.	Irfan et al. (2013)
Polyamide – glass fibre hybrid	5-10 wt. % MMT 0.5 - 3 wt. % SiO_2	> 7 x 10^5	No comparison to neat material without nano reinforcements and concluded variability due to variation in lab air and manual drilling tool.	Gendre et al. (2015)
Polyurethane	0.09 wt.% CNT 0.09 wt.% CB 0.09 wt.% SiO_2	> 2.2 x 10^9	SiO_2 and CB demonstrated minor increases in particle number concentration in relation to the neat PU, whereas the CNT sample demonstrated the lowest number of particles released.	Ding et al. (2017)

The studies demonstrate the incorporation of nanofillers to have either a positive or a negative influence on the nanoparticle release. Within the data that showed the fillers to have a positive increase in particle number concentration (Bello et al., 2010; Sachse et al., 2012a, b; Irfan et al., 2013; Ding et al., 2017), only Bello et al. (2010) reported of evidence found in microscopy analysis of separated nanofillers. Other studies reported of the nanoparticles to be either embedded or extruding

from the matrix. The released nanoparticles identified to be embedded within the matrix are less likely to be harmful (Debia et al., 2016). Although some studies have demonstrated no increased toxicity (e.g. Wohlleben et al., 2011; Wohlleben et al., 2013; Saber et al., 2012; Saber et al., 2012; Schlagenhauf et al., 2015), there is still a lack of understanding whether most embedded nanoparticles within the matrix are toxic as they have not been investigated due to the complexity and variations in material phases (Froggett et al., 2014; Debia et al., 2016). The toxicity studies previously reported within this thesis report the understanding and toxicity of only the individual nanoparticles as opposed to a matrix/filler combination. Additionally, the identification of release of the embedded hazardous nanoparticles must also be linked to the exposure of the released particles for toxicological assessments (*Kuhlbusch et al., 2011*).

Various studies (e.g. *Vorbau et al., 2009; Guiot et al., 2009; Gendre et al., 2015)* have attempted to control the experiments to be able to create a repeatable methodology for other researchers to use. The machining is moderately simple in terms of parameters control and following standardised testing methods for certain types of machining, e.g. taber abrasion. Two studies by *Vorbau et al. (2009)*, and *Guiot et al. (2009)*, adapted the standardised testing method for taber abrasion (ASTM D 4060, 2007) and added a small enclosure around the test sample to measure the particles released. However, due to the different materials, lab environment, measuring equipment and background interference, the studies show varying results. The authors conclude that even with a small enclosure placed around the test sample, particle number concentrations were variable and therefore concluded the need for a modified test rig which can have a controlled environment.

Although some similar conclusions can be drawn up from the studies investigating drilling on nanocomposites, the studies also utilised different drilling parameters and setups. Table 2 demonstrates some of the differences between the collected data. As discussed, a connected group of authors are responsible for three of the studies (*Sachse et al., 2012a, b; Irfan et al., 2013*), and therefore have similar setups. Noticeably, *Irfan et al. (2013)* was the only drilling study to directly investigate the particles collected for a toxicity study. The particles showed indications of toxicity in human lung epithelial A549 cells, however, the results suggest much less toxicity than that induced by the individual SiO_2 nanoparticles. The approach demonstrates the possibility of the assessment of nanoparticle release integrated with a nanoparticle toxicity study (*Irfan et al., 2013*). Other studies have carried out a similar approach in evaluating the release directly for toxicity from machining scenarios (e.g. Wohlleben et al., 2011). Fewer details on the drilling parameters are known for the study by *Bello et al. (2010)* as well as the real-time nanoparticle release equipment being placed at the breathing zone within a lab environment instead of a test chamber in the other studies.

Table 2: Overview of drilling parameters used and measurement techniques in current studies on the effect of drilling on nanocomposites.

Drilling parameters			Nanoparticle Release				Reference
Speed [rpm]	Feed rate	Drill bit Diameter	Nanoparticle Concentration	Nanoparticle Characterization	Toxicity study	Experiment (E) or observation (O)	
1800	Unknown (Manually controlled)	10 mm	x	x		E	Sachse et al. (2012a)
1355	Unknown (Weight controlled)	9.5 mm	x	x		O	Bello et al. (2010)
1800	Unknown (Manually controlled)	10 mm	x	x		E	Sachse et al. (2012b)
1800	Unknown (Manually controlled)	10 mm	x	x	x	E	Irfan et al. (2013)
1800	Unknown (Manually controlled)	5 mm & 8 mm	x	x		E	Gendre et al. (2015)
1200, 1550 & 1880	Unknown (Spring controlled)	4 mm & 8 mm	x	x		E	Ding et al. (2017)

As also highlighted in the review studies on machining (Basinas et al., 2018; Debia et al., 2016; Froggett et al., 2014), studies have approached the nanoparticle release investigation as either an exposure or an experimental release measurement. Table 2 shows that from the studies that investigated the nanoparticle release during drilling, only one study (Bello et al. 2010) used an observation approach. All five other studies created an experimental setup to evaluate a simulation of the release during a drilling scenario. As also shown, a variation in drill bit diameters, speeds and feed rates were used. Two studies (Gendre et al., 2015; Ding et al., 2017) included the comparison of release data using different drill bit diameters. Both studies demonstrated a clear influence in particle number concentration with a different drill bit diameter. Ding et al. (2017) determined the number of particles

to increase with the larger drill bit diameter from 4mm to 8mm. The particles released soared from 4.3 x 10^7 #/cm^3 to 65.2 x 10^7 #/cm^3 (roughly 15.2 times higher) with the increase in drill bit diameter. The authors demonstrated both an increase and decrease with different nanocomposite samples in particle number concentration with an increase in drill bit speeds. The authors therefore concluded the drilling speed to have an effect, but was dependent on the material. The variation in drill bit diameter in the study by Gendre et al. (2015) was unable to draw conclusive evidence on the influence on nanoparticle release due to the variation in data from the differentiating lab air and manual feed control of the drill.

Two of the studies also compared the results from drilling with another machining method. Ding et al. (2017) compared the same materials with sawing. The authors concluded that the process clearly demonstrated an influence in the number and size of particles release and can therefore be classified as process-dependant. Drilling observed an increase in particle number concentration in comparison to sawing. In the study by Bello et al. (2010), the materials were evaluated during drilling and cutting. The authors concluded major differences noted in the size distribution, fibre concentration, particle morphology and observation of CNT aggregates. The only similarities the authors were able to find were the transitional nature of exposures consistent with short task durations, high peak exposure levels and the generation of inhalable fibres and nanofibers. The two studies therefore agree with similar findings to those presumed from the review articles (Basinas et al., 2018; Debia et al., 2016; Froggett et al., 2014), in the release of nanoparticles from nanocomposites to be process-dependent.

As shown, the studies identify the nanoparticle filler, matrix, process, drilling parameters, and environment to all have an effect on the nanoparticle release data. The evidence of nanoparticle release to be process-dependent highlights a need for more data on nanoparticle release from nanocomposites that have not been investigated. Nano SiO_2 has been demonstrated to increase the particle number concentration in comparison to the neat polymer, whereas MMT has be reported twice to reduce the particle number concentration during drilling. There is however, a lack in data on the influence of particle filler concentration on the nanoparticle release during drilling. The study by Ding et al. (2017) utilised a 0.09 wt. % SiO_2 in polyurethane and only observed a minimal increase in particle number concentration, in comparison to a 56 times increase in particle number concentration with 5 wt. % SiO_2 in polyamide (Sachse et al., 2012a). Ding et al., (2017) associates the minimal effect to the low weight concentrations investigated and concludes the need to evaluate the influence of different nanofiller weight concentrations. Studies (Sachse et al., 2012a; Gendre et al., 2015; Bello et al., 2010) also concluded the need for a controlled drilling process and environment in order to evaluate the release of nanoparticles during drilling. The study by Irfan et al. (2013) is the only study

to investigate more than one polymer base material for nanoparticle release during drilling. The study concludes the polymer to have a substantial influence in nanoparticle release as the PP demonstrate substantially less particles released in comparison to the polyamide. The difference in concentration values observed between the six studies and different polymer materials suggests the polymer matrix has a significant effect on the nanoparticle release. However, this could also be associated to the different environment, drilling setup, drilling parameters etc. The influence of the polymer matrix on nanoparticle release during drilling is therefore also needed. The findings from the six studies on influence of nanoparticles on nanoparticle release during drilling are in general agreement with the future work needed that is reported in other machining studies (Basinas et al., 2018; Debia et al., 2016; Froggett et al., 2014).

2.6 Sampling and Measurement of Release Nanoparticles and Debris

Currently within the relevant detailed literature, there is still an insufficient and in depth understanding of the full result of nanoparticle release and exposure (*Clark et al., 2012*). In order to assess the exposure and quantify any risks, studies have investigated several characteristics of the released particles such as the particle concentration, particle size distribution and particle mass distribution. The method and even apparatus used to measure the same release or exposure characteristics can differ quite significantly. Different approaches are used throughout studies depending on the process, equipment, methodology and parameters used. Due to the variation in approaches reported within literature, this study will review the methods and measurements in use.

2.6.1 Instrumentation

The equipment used to assess nanoparticles can commonly be categorized between local, in situ, and external, ex situ, measurement techniques. The full characterization of the released particles cannot be fully achieved in situ from the material, and must therefore also be analysed using ex situ characterisation equipment. In the case of released nanoparticles, several studies categorise the characterisation into the assessment of airborne particles and deposited particles. Due to the considerably small size and densities of particles released, a majority of the released particles will not drop to the surface (*Kuhlbusch et al., 2011*). As will be reviewed, it is comparatively simpler to characterize the released deposited nanoparticles, however, the airborne particles are critical for exposure assessment.

Since there are currently limited established occupational exposure limits or regulations specific to engineered nanomaterials (ENMs) (*Methner et al., 2010a*), it is still unknown which exact particle characteristics to measure in contributing terms of exposure and/or toxicity. Whilst there are numerous factors such as size, shape, morphology, resin matrix, concentration and quantity, all relating to the actual individual particle characteristics, there are also other factors including exposure time, distance and location, PPE equipment etc. (*Hristozov et al., 2012*). As mentioned within the previous section, studies have identified the influential factors contributing to exposure and potential toxicity. These have been chosen as particle concentration, particle size distribution, particle chemistry and particle mass distribution.

Reviews on nanoparticle measurement instrumentation have previously been carried out, such as the review by *Kuhlbusch et al. (2011)*. Table 3 illustrates the particle measuring parameters, size range and functionality of the selected in situ instrumentation for airborne nanoparticles. The information in Table 3 is collected from various sources (*Hornsby & Pryor, 2014; Kulkarni et al., 2011; Methner et al., 2010a; Wiedensohler et al., 2012*).

The principles behind each instrumentation to quantitatively or qualitatively characterise the particles differ, and characterise, depending on the geometric, electrical or mass properties of the particles. As shown in Table 3, the instrumentation offer several measuring parameters, size ranges and principles behind the measurement. The selection of the instrumentation is therefore dependent on the methodology and nature of the nanoparticle assessment. Frequently instrumentation can be combined together to gather more detailed data. The SMPS and CPC are most commonly linked to give the size distribution and number concentration as exemplified in Table 4.

The instrumentation shown in Table 3 collect data in real time. Other devices are then used to characterize nanoparticles for ex-situ assessment. Most studies use electron microscopy to determine the morphology and surface topography of the nanoparticles through either an SEM or TEM. An electrostatic precipitator or thermal precipitator has also been used for chemical analysis and morphology characterization.

Table 3: Principle airborne nanoparticle measuring instrumentation (in situ).

Instrumentation	Measuring Parameters	Size range	Functionality
Condensation Particle Counter (CPC)	Particle number concentration	2 nm to 1 µm	Counts particles after enlarging particle nucleus through vapour condensation (aka Nucleation)
Scanning Mobility Particle Sizer (SMPS)	Particle Size distribution	2.5 nm to 1 µm	Particle electrical mobility diameter is used to measure paticle size. Linked with a CPC, particle concentration at the size can be found. If particle charge and density is known, mass concentration can also be calculated
Fast Mobility Particle Sizer (FMPS)	Particle size Distribution	5.6 nm to 560 nm	Using similar electrical mobility measurement, but linked with electrometers instead of CPC. Time resolution of 1s (SMPS >30s)
Optical Particle Counter (OPC)	Particle Number Concentration	>300 nm	Measures particles through either light scattering or direct imaging. Can be used in combination with CPC for particles <300nm
Aerodynamic Particle Sizer (APS)	Particle Size Distribution	500 nm to 20 µm	Using principles of inertia, particles are accelerated through an airflow to calculate particle sizes
Diffusion Charger (DC)	Particle Surface Area	20 nm to 1µm	Ions are attached to the particle via diffusion which allows for the “Fuchs” surface area to be determined
Electrical Low Pressure Impactor (ELPI)	Particle Size Distribution	7nm to 10 µm	Particles are electrically charged and collected in different low pressured impactor stages according to surface area to give size distribution

In-situ instrumentation can quantify the airborne released nanoparticles in real time, but there is yet to be a method to analyse the chemical composition and morphology of airborne particles in real-time. For nanoparticle assessment, a more qualitative characterisation of the nanoparticles is generally required to back up the findings of the real-time data. The in situ equipment is able to quantify the particles and the size and mass distribution, but ex situ analysis is required to be able to identify the content of the release. This is especially important in the assessment of nanoparticles embedded within a matrix. The in situ instruments are unable to differentiate embedded and independent nano-fillers. Studies have therefore observed the deposited particles through either an SEM or TEM. Since airborne particles are currently not able to be analysed for chemical composition and morphology in real time, deposited particles have to be evaluated. This however, does highlight a limitation in equipment, as deposited particles cannot fully represent the airborne particle characteristics.

A condensation particle counter (CPC) is the most commonly used instrument to measure the particle number concentration (*Hameri et al., 2002*). The CPC works on the principle of enlarging the particles through the process of nucleation via condensation with use of another fluid. Particles are initially continuously drawn into the CPC via an external pump at the specific flow rate. The particles are then grown by creating a vapour from a working fluid (e.g. water) onto the particles to allow them to be optically counted. Conventional optical techniques are currently unable to accurately measure particles down to the 7 nm lower range of the CPC (*Collings et al., 2014*). This is why the particles are required to go through the nucleation via condensation. A common TSI 3783 model uses the water-based condensation growth technique. The particles pass through a growth tube where heated wetted walls produce an elevated pressure resulting in a thermodynamic supersaturation condition. The particles in the flow stream act as nuclei for condensation (nucleation) and grow into micron sized droplets to be optically quantified. The droplets pass through a laser beam and create a large light pulse. Each pulse is detected and counted (*TSI CPC-003-A4, 2014*). Figure 12 below demonstrates a basic flow schematic of the TSI CPC model 3783.

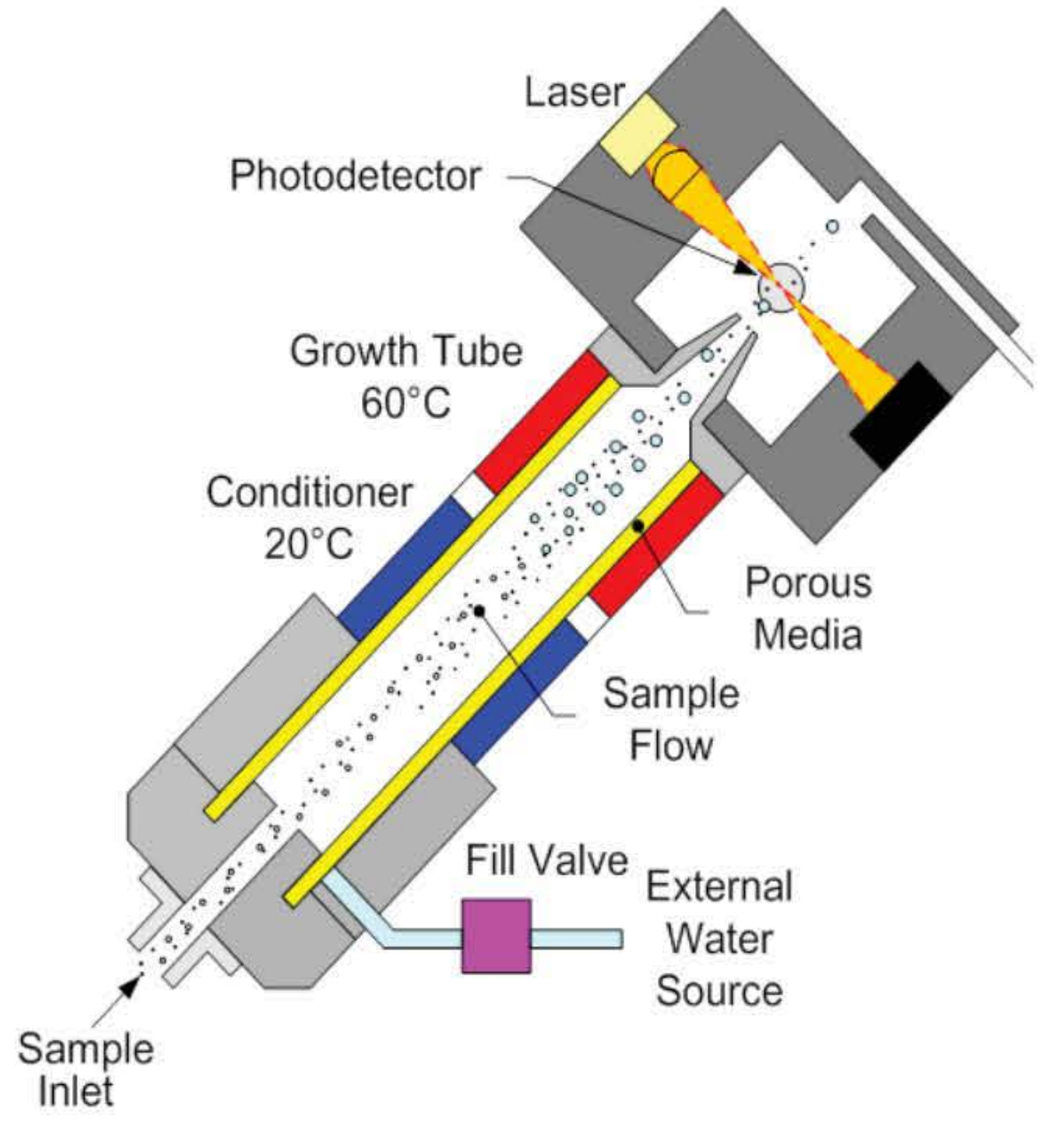

Figure 12*:* Basic flow schematic of TSI Environmental Particle Counter (CPC) model 3783 *(TSI CPC-003-A4, 2014).*

The concentration is a fraction of the total particle count over the sampling time and flow rate as shown in Equation 2.3 (*TSI CPC-003-A4, 2014*).

$$concentration\ \left[\frac{particle}{cm^3}\right] = \frac{CPC\ Counts\ [particles]}{Sample\ Time\ [s] * CPC\ Flow\ rate\ \left[\frac{Liter}{s}\right] * 1000\left[\frac{cm^3}{Liter}\right]}$$

- **Equation 2.3**

The total particle number concentration will be limited to the size range capability of the CPC. Any particles outside of the range will not be included in the concentration. The flow rate and sample time can change between CPCs and as shown above, will have an effect on the particle number concentration. Literature has reported on taking the sample time and flow rate into consideration will allow for comparison between any technical differences of various CPC models (*Hameri et al., 2002*).

The particle size distribution is measured using a scanning mobility particle sizer spectrometer (SMPS), fast mobility particle sizer (FMPS) or an aerodynamic particle sizer (APS). The instruments differ in method of size measurement using electrical mobility or optical sizing. The SMPS is the commonly used aerosol nanoparticle sizer in literature although it has limitations for fast changes in the particle

size distributions due to its time resolution (*Kuhlbusch et al., 2011*). Figure 13 illustrates a schematic of the process for a TSI 3080 Electrostatic Classifier SMPS.

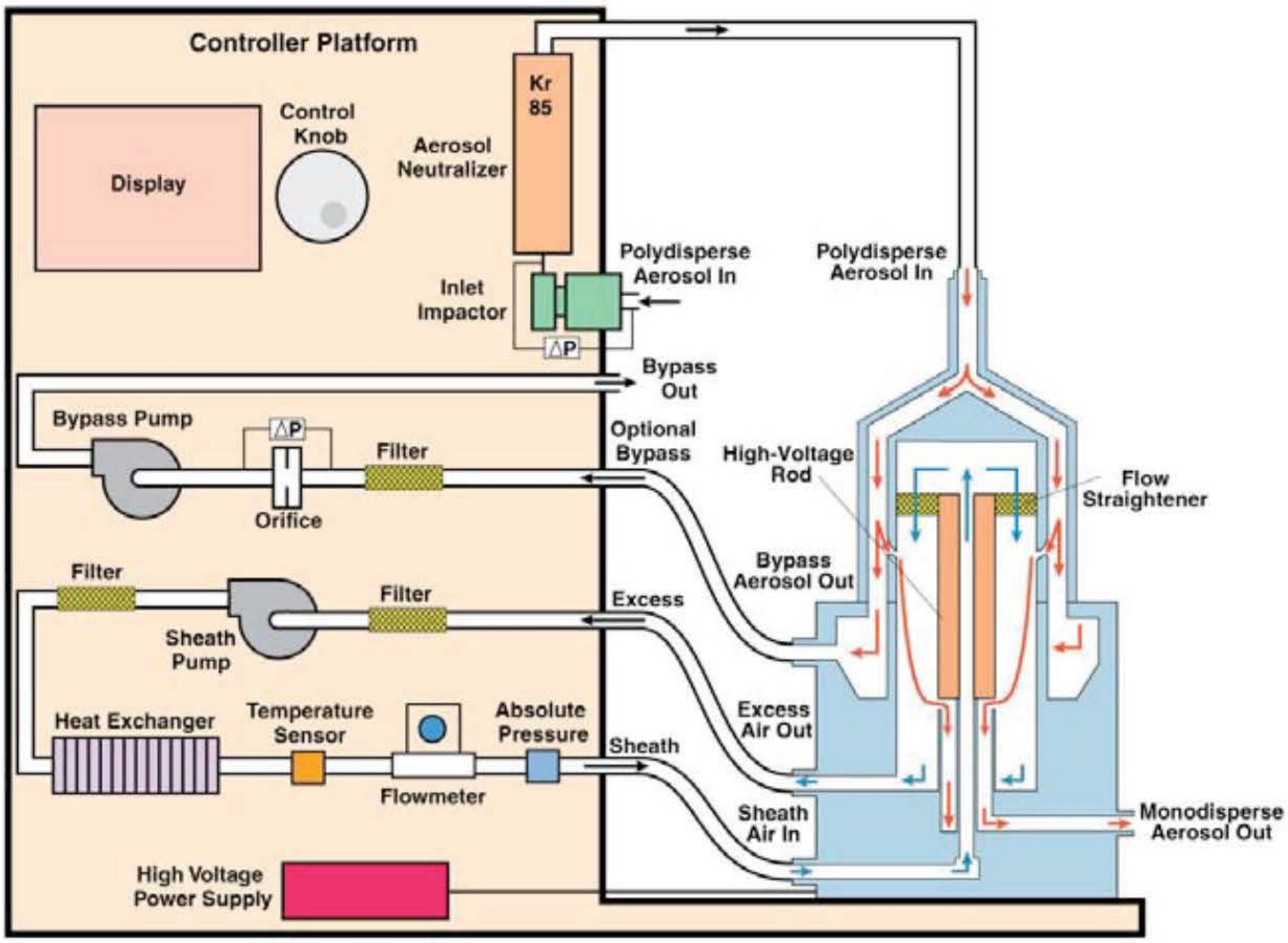

Figure 13*:* Basic schematic of SMPS TSI model 3080 Electrostatic Classifier utilizing a nano DMA *(TSI P/N 1933792, 2009).*

The principle of the TSI CPC Model 3080 Electrostatic Classifier with the differential mobility analyser (DMA) is based on the monotonic relationship between electrical mobility and particle size with singly charged particles. This parameter is inversely related to particle size and proportional to number of charges on the particles.

The polydisperse aerosol particles go through a process of bipolar charging or "neutralization" through a radioactive bipolar charger, creating a bipolar equilibrium charge level on the particles. The particles are then classified with the DMA based on their electrical mobility. Firstly, the polydisperse aerosol and sheath air are introduced into the DMA. Two concentric metal rods within the DMA create an electric field as one is maintained at a negative voltage whilst the other is electrically grounded. This electric field causes the charged particles to be attracted through the sheath air to the negatively charged collector rod. According to their electrical mobility, particles precipitate along the rod, and particles within a narrow range of electrical mobility exit through the small slit at the bottom of the

negatively charged rod as shown in Figure 13. The particles exit with the monodisperse air flow to a condensation counter where the particle concentration at that electrical mobility is determined. The given particle size distribution is therefore corresponding to the electrical mobility of the particles. Other small subsystems are required to control the system as shown (*TSI P/N 1933792, 2009*).

If the particle is carrying electrical charges within an electric field, it experiences an electric force causing it to move through the fluid it is suspended in. The resulting drag force on the particle is given by Stokes law and can be equated to the electrical force to determine the electrical mobility of the particle. The electrical mobility Z_p is defined as shown in Equation 2.3.2 (*TSI P/N 1933792, 2009)*:

$$Z_p = \frac{neC}{3\pi\mu D_p}$$ - **Equation 2.4**

Where:

n = number of elementary charges on the particle
e = elementary charge (1.6×10^{-19} Coulomb)
C = Cunningham slip correction = $1 + Kn[\alpha+\beta \exp(-\gamma/Kn)]$

α= 1.142
β= 0.558
γ= 0.999 (Allen & Raabe, 1985)
kn = Knudsen Number = $2\lambda/Dp$
λ= gas mean free path = $\lambda_r = \left(\frac{P_r}{P}\right)\left(\frac{T}{T_r}\right)\left(\frac{1+{}^{S}/_{T_r}}{1+{}^{S}/_{T}}\right)$

S= Sutherland Constant (K)
T = temperature (K)
T_r = reference temperature (K)

μ = gas viscosity (dyne s/cm^2) poise $= \mu_r \left(\frac{T_r+S}{T+S}\right)\left(\frac{T}{T_r}\right)^{\frac{3}{2}}$
D_P = particle diameter (cm)

The gas mean free path and gas viscosity parameters are based on values for S and T which are consistent values. The values for common gases can be found in Radar (1990) with explanations of the gas equations in Kulkarni et al. (2011). The relationship between the electrical mobility and classifier parameters to give the particle diameter are given in Equation 2.3.3 and Equation 2.3.4 (*TSI P/N 1933792, 2009*):

$$Z_p{}^* = \frac{q_{sh}}{2\pi VL} ln\left(\frac{r_2}{r_1}\right)$$ - ***Equation 2.5***

And mobility bandwidth:

$$\Delta Z_p = \frac{q_a}{q_{sh}} Z_p{}^* \qquad \textbf{- Equation 2.6}$$

Where:

$Z_p{}^*$ = set mobility (if $q_a = q_{sh}$ then $Z_p = Z_p{}^*$)
q_a = aerosol flow rate through the classifier (*qs + qp*, monodisperse flow rate and the polydisperse flow rate)
q_{sh} = sheath air flow rate (equal to excess air flow rate)
r_2 = outer radius of annular space = 1.905 cm (for Nano DMA)
r_1 = inner radius of annular space = 0.937 cm (for Nano DMA)
V = average voltage on the inner collector rod (volts)
L = length between exit slit and polydisperse aerosol inlet = 4.987 cm (for Nano DMA)
b = gap spacing between plates

Combining the two equations gives the direct relation of the particle diameter to negative rod voltage, number of charges on particle, classifier flow rate and geometry for the nano DMA as shown in Equation 2.3.5 (*TSI P/N 1933792, 2009*).

$$\frac{D_p}{C} = \frac{2ne\bar{V}L}{3\mu q_{sh} ln\frac{r_2}{r_1}} \qquad \textbf{- Equation 2.7}$$

Once the particles have gone through the SMPS and are classified according to electrical mobility, the concentration is measured using a CPC. The SMPS uses the assumption of spherical particles which is a limitation when investigating the release of non-spherical nanoparticles such as nanotubes or nanofibers. However, from the diameters of the particle size distribution measured, and the material density of the nanocomposites, the particle mass size distribution can be estimated. The data from the SMPS will therefore be able to provide a particle size and particle mass distribution which are both influencing parameters when investigating nanoparticle exposure (*TSI P/N 1933792, 2009*).

A somewhat different technique in gathering the particle size distribution is using an FMPS. The technique uses similar electrical mobility principles, but with either fewer size ranges or a relatively lower accuracy. However, it is capable of giving a particle size distribution quicker than the slower SMPS, e.g. every second instead of every minute (*Hornsby & Pryor, 2014*). The Cambustion DMS50 fast particle size spectrometer utilizes a unipolar corona charger placing positive charges on each particle which are then classified along electrometer detectors based likewise on mobility and hence particle size. The charge is conducted via an electrometer amplifier whose output indicates the flux of particles giving the particle concentration at that given particle size. The outlet of the DMA is linked

to a CPC to give the particle number concentrations of a given mobility diameter (*Cambustion DMS50 MKII, 2008*). A basic schematic of the theory of operation is displayed in Figure 14.

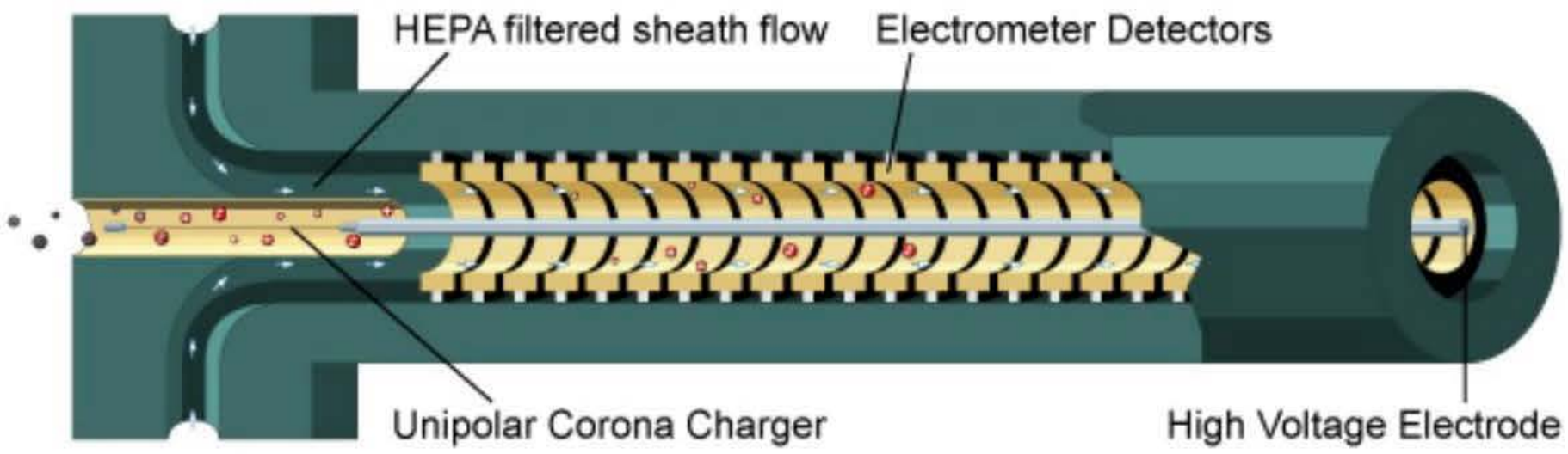

Figure 14: Basic schematic of Cambustion DMS50 fast particle size spectrometer *(Cambustion DMS50 MKII, 2008).*

Since the classification of particles according to their differing electrical mobility takes place in parallel (rather than in series as in the SMPS) the DMS50 is able to offer the faster sampled particle size distribution. This allowed for a size distribution every second compared to the SMPS TSI model 3080 of 1 minute period and therefore an accurate representation of the particles being released from the sample in a given time.

Particle characterisation is carried out ex situ with more conventional instruments such as an SEM, TEM, etc. The method and instrumentation used to measure the released particles varies throughout studies, by reason of the selection of instrumentation having direct influence on the detection of the nanoparticles. Table 4 identifies some of the techniques used to characterize the nanoparticles released in a selected sample of studies.

For the studies carried out by *Sachse et al. (2012a, b)* the airborne particle size distribution was measured using an SMPS+C, comprising of a CPC with classifier Vienna DMA 5.5-U, Grimm, Aerosol Germany. The SMPS+C measured sub micrometer particles generated during the drilling process over a particle size range of 5.6 nm to 1083 nm and a particle size total resolution of 32 channels. An Electrostatic Precipitator was utilized to sample the generated airborne particles. The deposited particles were attracted to a sampling plate to then be studied separately. Dynamic Light Scattering (DLS) was used to measure the deposited particle size distribution, and furthermore, the particle characterization was investigated using a TEM, an SEM, powder X-ray diffraction (XRD), small angle X-ray diffraction (SAXD), and differential scanning calorimetry (DSC). As with most nanoparticle assessment research, an enclosure was used to contain the particles without contamination from the

surroundings. The data acquired and results from the equipment will be discussed in the following sections.

Table 4*:* Instrumentation used in selected mechanical studies to identify and characterise released nanoparticles.

Mechanical Process	Deposited Particles	Airborne Particles	Reference
Dry drilling	SEM, TEM	SMPS, CPC,	*Sachse et al. (2012a,b)*
Wet & dry drilling	SEM, TEM	FMPS, APS, CPC,	*Bello et al. (2010)*
Grinding	SEM	SMPS, CPC, Nuclepore membrane filters	Ogura et al. (2013)
Sanding	TEM	CPC, OPC	Cena & Peters (2011)
Abrasion	SEM, TEM, EDX	FMPS, APS, SMPS, CPC	Schlagenhauf et al. (2012)
Abrasion	SEM, TEM	SMPS, CPC	Vorbau et al. (2009)

In comparison, the similar study assessing the effects of drilling on nanocomposites by *Bello et al. (2010)* used alternative apparatus. The measurement of the airborne particles were attained using an FMPS for particle size distribution in the range of 5.6 nm to 560 nm, an APS with a size range of 0.5 µm to 20 µm, and a CPC for particle number concentration within the range of 10 nm to 1 µm. Similar to the studies by *Sachse et al. (2010a, b),* particles were sampled for electron microscopy characterisation but with a thermophoretic precipitator (TP) and sampling filters. In comparison *Cena & Peters (2011)*, used a CPC with size range of 0.01 µm to 1 µm and an optical particle counter with 15 channels from 0.3 µm to 20 µm. Although a lot of the studies use similar equipment, the size ranges and measurement technique varies.

Additional to characterising the deposited particles on the surface of the chamber, airborne particles were collected within the chamber for characterisation in most studies. *Ogura et al. (2013)* collected aerosol particles on Nuclepore membrane filters to be observed using an SEM. The procedure will not

characterise the particles in real time, but the morphology of the airborne particles can be analysed separately from the particle sizer, particle counter and deposited particles on the surface.

2.6.2 Controlled Environment for Particle Measurement

In order to utilize the instrumentation, the methodology must also be considered when assessing nanoparticle release. Alternative approaches are used depending on the nature of the particle assessment. The strategy on nanoparticle release assessment will determine the selection of instrumentation and its implementation. Parameters, accuracy and relevant metrics are to be identified in order to classify the methodology. In the work carried out by *Kuhlbusch et al. (2011)* several approaches were identified and categorized as: personal exposure approach, process related approach, or toxicological approach. The three approaches are highlighted in Figure 15.

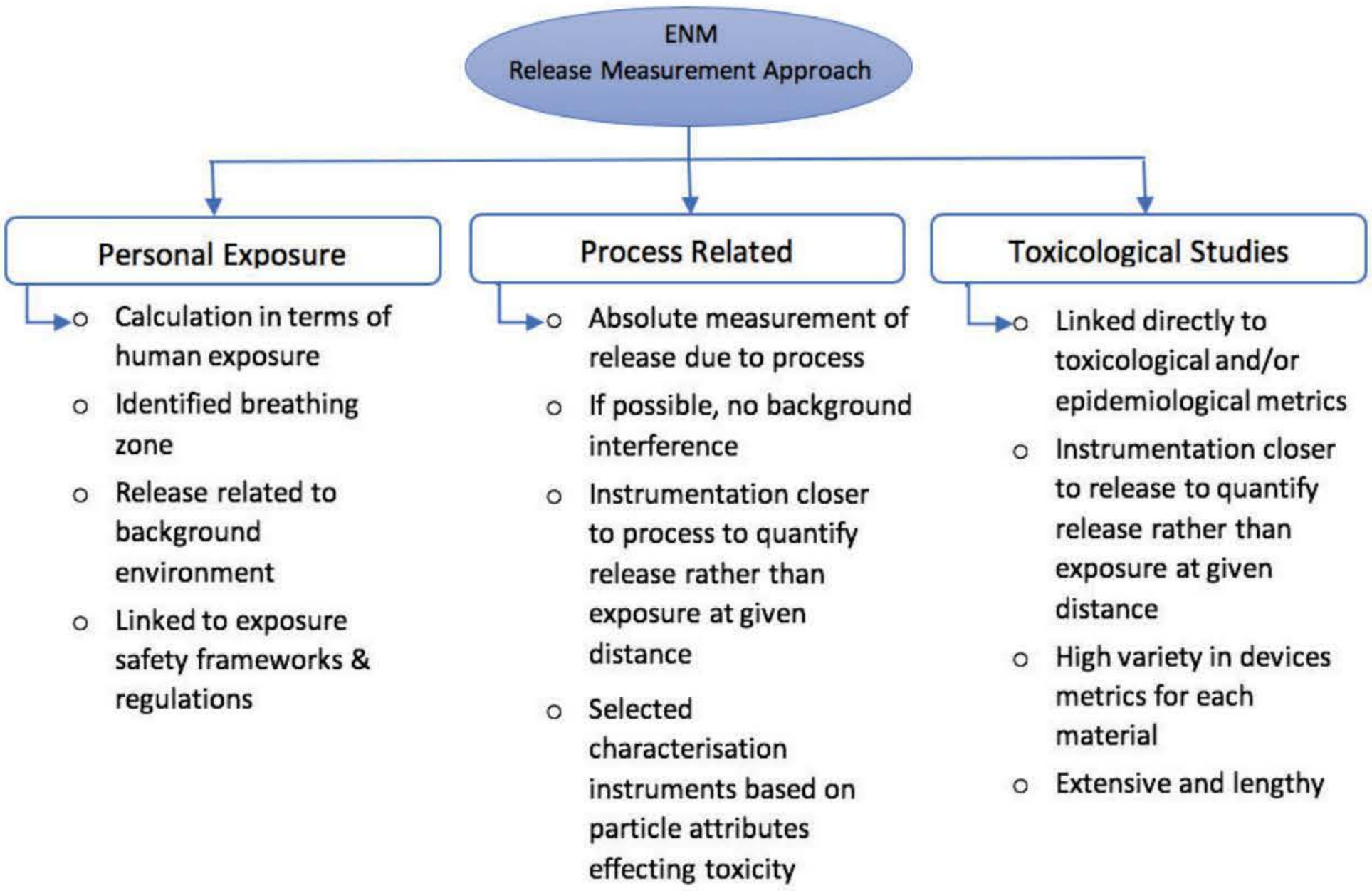

Figure 15*:* Approaches towards measurement of engineered nanomaterial released from a lifecycle scenario (modified from Kuhlbusch et al. 2011).

The breakdown of approach is to maximise efficiency in terms of cost effectiveness for the desired measurements. A full study or investigation into an ENM may be necessary and could take all three approaches into consideration. However, this would come at a substantial financial and time cost. The three tiered hierarchal approaches are developed to increase financial effectiveness.

The personal exposure approaches are methodologies that are targeted towards assessing the airborne nanoparticles that people are exposed to. An ideal design of this approach would involve taking measurements at a workplace to investigate the personal exposure of an industrial scenario. This consists of a combination of selecting the necessary metrics and positioning the sampling within an identified breathing zone (*Maynard & Aitken, 2007*). The end calculation is therefore in terms of personal exposure and could therefore also be defined as an exposure assessment. This can then be directly related to exposure safety frameworks and regulations. Thus far, this approach has been used mostly for occupational exposure scenarios in observational studies instead of experimental. The method provides a good exposure observation for the particular case, however can be limited in use as comparison due each workplace having dissimilar environmental conditions and air quality; hence a different background. The approach requires the distinction of nanomaterial released from the background. Numerous studies (e.g. Brouwer et al., 2011; Ding et al. 2016) have investigated the most suitable mathematical method at tackling the distinction. The approach is most suited when tackling materials with known maximum exposure limits from toxicity studies (although little is known about exposure limits for embedded nanoparticles within matrix resins) and could therefore be identified as an occupational exposure assessment (*Kuhlbusch et al. 2011)*.

The process related approach is designed to give more of an absolute enumerated measurement through the use of several measurements. This may differ from the personal exposure approach by placing the sampling instrumentation closer to the release process to quantify any nanoparticle release rather than the exposure at a given distance (*Kuhlbusch et al., 2011*). Furthermore, since the approach isn't directly related to a worker's exposure, it is possible to exclude the background environment i.e. a controlled environment. Therefore, a full and absolute measurement of the particles released can be assessed. The process approach therefore, provides a worst case scenario of the nanoparticles released, and is task-based scenario instead of an exposure scenario. A toxicological study and personal exposure study could be avoided if an absolute measurement of the material and process would indicate no release of hazardous material. This approach can therefore be taken as an initial measurement to indicate if any further analysis is needed.

Toxicological approaches aim at gathering data which can be linked to toxicological metrics. A full understanding of the toxicological effects of all ENMs is still under debate and therefore difficult to select for each ENM. A considerable amount of research has been directed into identifying the biological and physical attributes of nanoparticles with potential toxicological and eco-toxicological hazards. This approach towards the nanoparticle assessment will include the various attributes to select the measurement device metrics directly relating to the health effects. Additionally, particles could be collected so as to directly use in a toxicological study (*Kuhlbusch et al., 2011)*. This approach

could therefore provide an accurate result of toxicity given the exposed dosage for the particular process.

Alternatively, the National Institute for Occupational Safety and Health developed a more general approach for a standardized assessment of nanoparticle release known as: Nanoparticle Emission Assessment Technique (NEAT) (*Methner et al., 2010a, b*). In the study, a common set of parameters were set out to be then tested across numerous laboratories as validation. The approach consists of using the in situ instrumentation with an SMPS and CPC to give the particle number concentration. If the in situ instrumentation demonstrates a given increase and distinction in nanoparticle release related to regular background data, further comprehensive analysis would take place. The personal exposure, process related or toxicological approaches would then be taken into consideration for the release assessment (*Methner et al., 2010a*, *b*).

The NEAT is an example of a tiered approach involving the three identified approaches in the study by *Kuhlbusch et al. (2011).* An alternative 3 tier approach has been suggested by a collaboration of authors within Europe (*IUTA et al., 2011*). The first step involved evaluating the possibility if nanoscale aerosols would be released through the information on the case. If there is a possibility of release, a basic exposure assessment is carried out e.g. with a CPC. Finally, if there is enough evidence, a more advanced, expert exposure assessment would be performed including an SMPS, CPC, filter etc. (*IUTA et al., 2011*). The concept of using a tiered approach would ideally avoid any unnecessary data collection where the risk of nanoparticle release or exposure is established to be insignificant.

A key influence in the data thus far, also mentioned in the NEAT approach (*Methner et al., 2010a*, *b)*, is the distinction of nanoparticle release and background particles. Within any environment nanoparticles will naturally be airborne and therefore influencing the particles released from any material tested (*Brouwer et al., 2009*). Studies thus far have been unable to eliminate or control the background interference and studies have instead developed background distinction models and approaches. All of the approaches have drawbacks and limitations, and in a study by *Brouwer et al. (2012)*, the authors concluded that none one of the approaches would be suitable for all scenarios and would therefore require the use of different approaches depending on the scenario.

Kuhlbusch et al. (2011) identified four approaches towards background distinction for the measurement strategies:

- time series approach,
- spatial approach,
- approach based on comparative studies with and without nanomaterial
- (size resolved) chemical and/or morphological analysis

The approaches differ and it is still unclear if the background measurements should be subtracted from the data or reported separately (*Brouwer et al. 2012*). However, the strategy and approaches towards measurement and background distinction are directly interconnected. A time series approach would take the background count during no activity and then any increase over time is assumed to be the release from the nanomaterial and process. Conversely, spatial analysis assumes a background measurement location is representative for the background at the workplace of interest. Any difference between the determined background and workplace concentrations is linked to the work activity and the nanomaterial investigated (*Kuhlbusch et al., 2011*). Within the review studies by *Kuhlbusch et al. (2011),* more than 50% of the studies utilised a combined time series and spatial approach. Studies have also compared materials with and without nanomaterial in an attempt to neglect the background (*Bello et al., 2009*). A comparison with morphological analyses are generally included to complement and validate the real time measurements.

With a gaugeable background present, the interaction between the nanoparticles released and the background cannot be represented or fully understood for each environment. Altering the environment can have a different influence on the particles released. The testing of identical processes and materials in different environments could potentially give dissimilar data.

The approach and distinction of the background to the nanoparticles released varies in most studies. The details of approach and background distinction from a selected 10 studies are shown in Table 5.

The studies were selected based on availability of the required details and presenting a variety of mechanical processes. The columns provide the particle number concentrations details as well as the measurement approach and background distinction approach. Quite often some of the samples were backed up with chemical and/or morphological analysis, however this has not been included in Table 5.

Table 5*:* Study measurement strategy and background distinction methods in 10 selected mechanical studies to identify and characterize released nanoparticles from a mechanical process.

Process	PNC (range)	Max PNC [particles/cm^3]	Measurement strategy	Distinction from background	Background control	Process setup	Reference
Dry drilling	5.6 nm to 512 nm	20,000	Time series	1000 particles/cm^3 before drilling	Enclosed within chamber	Process external to chamber	*Sachse et al. (2012a,b)*
Wet & dry drilling	5.6 nm to 1µm	10,000,000	Time series & spatial	Comparison with and without nanomaterial	No enclosure	Influence unknown	*Bello et al. (2010)*
Grinding	10 nm to 1µm	2,500,000	Time series	Comparison with and without nanomaterial	Enclosed within chamber	Process external to chamber	*Ogura et al. (2013)*
Sanding	10 nm to 1µm	3,889 (Geometric mean)	Time series & spatial	Process-to-background ratio	Enclosed within chamber	Process within chamber	*Cena & Peters (2011)*
Abrasion	13nm to 20 µm	20,000	Time series	Subtraction of average background	Enclosed within chamber	Process external to chamber	*Schlagenhauf et al. (2012)*
Abrasion	16 nm to 626 nm	300	Time series	Background below SMPS limit of detection	Enclosed within chamber	Process external to chamber	*Vorbau et al. (2009)*
Sanding & sawing	4.5nm to 3 µm	460,000	Time series & spatial	<3,000 particles/cm^3 before process	Enclosed within chamber	Influence unknown	*Gomez et al. (2014)*
Dry drilling	5.6 nm to 512 nm	1,800,000	Time series	1,000 particles/cm^3 before task	Enclosed within chamber	Process external to chamber	*Irfan et al. (2013)*
Sanding, friction, wind erosion	6 nm to 10 µm	57,000	Time series & spatial	Background elimination < 0.01 particles/cm^3	Enclosed within chamber	Process within chamber	*Göhler et al. (2013)*
Grinding and cutting	20 nm to 300 nm	491,599	Spatial	Subtraction of average background before and after task	No enclosure	Influence unknown	*Methner et al. (2012)*

From the selected studies in Table 5 it can be seen that the variety in data collected clearly differs between all of the studies. Although the particle number concentration is a commonly measured characteristic and usually appears to be one of the only equivalent parameters measured, numerous influences of the characteristic can still be observed in the studies. The particle number concentrations

can be seen to not be entirely comparably due to the contrasting size ranges of the particles measured, measurement strategy and the influencing background measurements.

Almost every study has a different approach towards the background distinction. Few studies were able to reduce the background count to negligible (*Göhler et al., 2013; Vorbau et al., 2009*), whilst other studies subtracted an average background count from the data (*Schlagenhauf et al., 2012; Methner et al., 2012*). Furthermore an enclosure of the nanoparticles released was not always used such as in *Bello et al. (2010)*, as well as the unknown influence of the process mechanism on generating nanoparticles. Previous studies have found nanoparticle readings produced entirely by the mechanical process (*Brouwer et al. 2012)*.

The methodology and background distinction approach selection is directly dependent on the nature of the nanoparticle assessment. Identifying the necessary metrics is vital for the approach towards assessing the nanoparticle release. If a more comprehensive and conclusive approach is required, a combination of the methodologies could be beneficial. Ideally, a methodology that could completely eliminate the background interference would be beneficial. This would be through a controlled environment to measure the nanoparticles released.

As stated, the evidence of nanoparticles potentially being toxic, has led to industry and research labs institutionalising the safe handling, exposure and working with nanoparticles. Recommended exposure limits and safe handling handbooks are in place when manufacturing or handling certain nanoparticles (e.g. *NIOSH, 2013; EU-OSHA, 2009; ISO/TS 12901-2, 2014; CEN/TC 352, 2016; OECD, 2017; ASTM E2535, 2018; BSI PD 6699, 2007; WHO, 2017*). Similarly, various test guidelines on exposure assessments are available to assist in carrying out an adequate approach. The OECD has published numerous reports concerning the physico-chemical properties and characterisation, exposure assessment and control of nanomaterials, including reports titled “Preliminary Analysis of Exposure Measurement and Exposure Mitigation in Occupational Settings: Manufactured Nanomaterials” (OECD ENV/JM/MONO, 2009a), “Consumer And Environmental Exposure To Manufactured Nanomaterials - Information used to characterize exposures: Analysis of a Survey” (OECD ENV/JM/MONO, 2017), “Emission Assessment for Identification of Sources and Release of Airborne Manufactured Nanomaterials in the Workplace: Compilation of Existing Guidance” (OECD ENV/JM/MONO, 2009b), “Harmonized Tiered Approach To Measure And Assess The Potential Exposure To Airborne Emissions Of Engineered Nano-Objects And Their Agglomerates And Aggregates At Workplaces” (OECD ENV/JM/MONO, 2015), and “Physical-Chemical Decision Framework To Inform Decisions For Risk Assessment Of Manufactured Nanomaterials” (OECD ENV/JM/MONO, 2019). The reports provide substantial information on approaches towards the exposure assessment of

nanoparticles from manufactured nanomaterials. A review article by Rasmussen et al., (2016) summarises some main achievements and guidelines of the OECD group. The reports are available to the public to help provide guiding principles in conducting studies, in addition to promoting consistent data reporting. As stated within the report by OECD (2019), which provides a framework for approaches, "the document is not intended for risk assessment" but to be "utilised to guide and prioritise" and "expert judgment is require to determine if the hazard assumptions of each nanomaterials are valid". The guidelines, reports and frameworks have provided a significant set of beneficial principles to follow, but emphasise the current lack in a harmonised approach.

ISO have similarly produced technical reports and guidelines on exposure to nanoparticles. ISO/TR 19601 (2017) provides a complement to the OECD guidelines and relevant documents. The TR provides information on inhalation studies to assist researchers to choose appropriate aerosol generator for their target nano-objects and their aggregates and agglomerates. The TR identifies three aspects to consider when designing and conducting nanomaterial inhalation toxicity studies: 1) uniform and reproducible nano-objects generation that is relevant to realistic exposures; 2) thorough characterization of nanomaterials throughout the duration of testing including starting and generated materials; 3) use of occupational exposure limits (OEL). An article which reviews the TR by Ahn et al., (2017), states that whilst the TR provides aid in selecting appropriate aerosol generators to fulfil a proposed toxicology study design, the TR does not provide guidance for specific aerosol generation and is mainly focused on the synthesis procedures. ISO (ISO/TS 12901-2, 2014) also provides another approach in controlling the workplace exposure to possibly hazardous agents through control banding. The approach is based on grouping controls with the level of risk. The risk management is applied on the concept of the greater the potential for harm, the greater the levels of protection needed for exposure control. The approach is regarded as being useful for the current level of uncertainty in work-related potential health risks to nanoparticles.

Although the various test guidelines and reports on exposure assessments have made remarkable progress and are available to assist in carrying out an adequate approach, there is no available standard or harmonised method in assessment of nanomaterial release during machining (Bainas et al., 2018; Debia et al., 2016; Froggett et al., 2014). The literature available and the incomparability highlight the need for a standardised approach towards measurement and background distinction (*Brouwer et al. 2012)*. The two approaches are directly linked and it is essential for them to be defined if comparisons between studies and assessments are to be carried out. Numerous studies have agreed with this deduction (*Froggett et al., 2014*; *Brouwer et al. 2012; Kuhlbusch et al., 2011; Methner et al., 2010a*, *b;* Bainas et al., 2018; Debia et al., 2016*).*

2.7 Safety by Design of Polymer Nanocomposites

With a better understanding of the emissions and exposure introduced from nanocomposites, materials can be manufactured to be safer by design. The data collected for the nanoparticle release can be used towards developing materials which will avoid or minimise the release the potentially toxic nanoparticles and hence, reduce exposure for workers and consumers. It is now recognised that safety by design concepts allow bridging the gap between the rapid developments in nanotechnology and nanosafety concerns (e.g. Varsou et al., 2019; Lynch et al., 2016; Hjorth et al., 2017; *Njuguna et al. 2014; Falk et al., 2016; Bastus and Puntes, 2018; Lin et al., 2018*). The studies on the implementation of safety by design concepts for nanomaterials highlight however that there is still a lack of knowledge on the release of nanoparticles and its mechanism from nanocomposites undergoing industrial machining such as a mechanical drilling process. Considering nanocomposites are still relatively new to industry, there is still a lack in knowledge on how the material will perform over its entire life cycle. But With the better understanding of the release characteristics, the hazard can be reduced. Figure 16 illustrates a risk mitigation matrix of the concept.

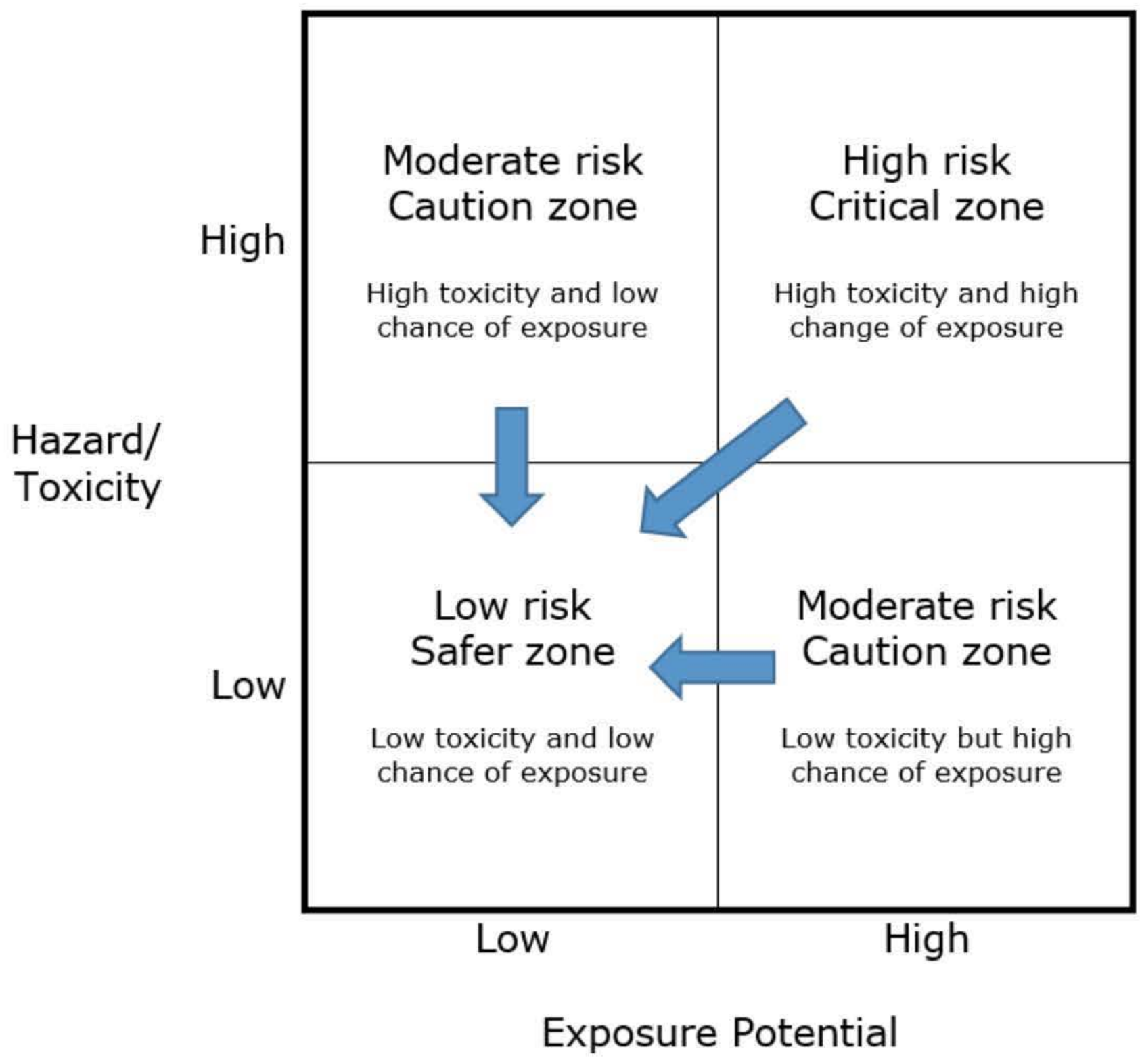

Figure 16*:* Risk mitigation matrix of nanoparticle release adapted from Morose *(2010).*

The process is thought to originate from processes used in drug discovery and development (Damoiseaux et al., 2011; NANoREG; 2015) and has since been a touted aspiration in the field of nanotoxicity and exposure (Hjorth et al., 2016). When there is a higher risk of either exposure and/or hazard, a natural approach is to reduce the relevant risk. *Morose et al., 2010*, developed a strategy composed of five principles towards the design for safer nanotechnology. The aim of the paper is to mitigate the health risk associated to nanoparticles by either reducing the hazard and/or exposure potential. The general principles were structured as: "size, surface and structure", "alternative materials", "functionalisation", "encapsulation" and "reduce the quantity". The size, surface and structure are three major characteristics attributed to the toxicity, and if these could be modified, the toxicity could also be reduced. The second principle involves the approach towards identifying an alternative material to reduce the toxicity. Thirdly, functionalising the material and nanoparticles in different ways might reduce the hazard and/or exposure potential if the release characteristics are affected. The fourth approach involves the enclosure and control over the release of the nanomaterial and therefore reducing the exposure. The final approach involves attempting to use smaller quantities of the hazardous nanoparticles whilst simultaneously maintaining the product functionality (*Morose et al., 2010)*.

The nanoparticle release characteristics play a vital role in all of the principles mentioned by *Morose et al. (2010).* If the release or exposure can be reduced/controlled, the risk can be minimised. Aligning to similar material design processes such as self-principles in design (Xia, 2016), the inputs into the design will determine the output. The knowledge on release can be used towards developing and designing the materials which will reduce the release of the potentially toxic nanoparticles and hence, reduce exposure for workers and consumers. Although there are different ideas towards the concept and approach, the general concept refers to anticipating potential impacts and pre-emptively addressing safety concerns early in the innovation process through altering the product design (Hjorth et al., 2016).

In an article by Lynch et al. (2016), the authors highlight how EU projects are "increasing focus on safety-by-design consideration for nanomaterials". Another article, by NSC et al., (2016) concludes "the focus of investment and research has moved increasingly towards predictive and high throughput approaches to nanosafety, including safety-by-design…". The attention towards the implementation of safety by design concepts is therefore increasing within literature, and evident in existing FP7 projects (Lynch, 2014; 2015; 2016b), as well as an emphasis continuing into the Horizon 2020 projects (Hjorth et al., 2016). An article by Falk et al. (2016) reviewing the roadmap of nano-product and nano-enabled applications, identifies safety by design concepts as an "interesting option" as it enables the number of considered solutions without increasing costs. A review of the concepts and application

within nanosafety by Hjorth et al. (2016), concludes that safety by design concepts provides a good starting point on the road towards developing innovate new products and would best adopt similar approaches (relating to safety by design concepts implemented in drug discovery development). The article does conclude however, that the field should also acknowledge the limitations and challenges in implementing such concepts into practice. As with the implementation within drug discovery development, the article states that despite the best intentions and the best design, no drug is without side effects, and should therefore also be taken into consideration in safety by design for engineered nanomaterials. The concept therefore is widely becoming a recognised strategy towards facilitating design of nanomaterials. The knowledge on release can be used towards developing and designing the materials to minimise the release of the potentially toxic nanoparticles and hence, reduce exposure for workers and consumers. Research on the nanoparticle release from nanocomposite materials during drilling presents an opportunity to provide data that could be implemented within safety by design strategies.

2.8 Conclusion

The benefit of nanoparticle fillers has caused a surge in investment and research across the world. The nanocomposite developments and research are continuously trying to improve the tailoring of material properties, including the mechanical and potentially, the safety of the materials. Industries are increasing looking towards the use of small weight concentrations of nanoparticles to tailor material properties whilst simultaneously reducing the weight.

However, the nanoparticles providing material improvement, have also been established to exhibit potential toxic effects to humans and the environment at certain dosages. The use of these nanoparticles within nanocomposite materials has therefore consequently increased the risk of nanoparticle release and exposure. Regulatory and safety bodies have introduced exposure limits and handling procedures for handling of independent nanoparticles such as CNTs and CNFs. The procedures and handling of the independent nanoparticles prior to embedding within the material can be relatively controlled. However, the unintended release from nanocomposites during a mechanical process is yet to be fully evaluated or understood. It is crucial that more data on nanoparticle release during machining is investigated in order for any potential health or environmental risks associated with the materials to be better understood and characterized.

From the literature, several key findings were found:

- Discoveries and improvements in nanoparticle technology has led to an increase into nanoparticle inclusion within composite materials. Small weight concentrations have demonstrated significant improvement in material properties. Despite the increased use and number of studies, there is no common rule or model to predict the material properties with the addition of nanoparticles within nanocomposite materials. There is therefore a lack in knowledge on the full influence on property behaviour with the addition of nanoparticles, and is unique for each nanocomposite combination. Literature has identified homogeneous dispersion of the filler within the polymer and the strong interfacial interactions required between the filler and the matrix as the two biggest concerns when fabricating polymer nanocomposites which is directly influenced by the compatibility of the filler and matrix.
- The phenomena associated to the drilling mechanism on composite materials has been studied and models developed to predict delamination and critical forces required. However, the models are still limited due to the material assumptions and are restricted to mainly fibre-reinforced composites. The fracture mechanics and mechanism behind nano-sized chip formation to predict the nanoparticle emissions during drilling has only been reported on

metallic materials. The studies highlight the brittleness of metallic materials to be the major factor in particle generation. The literature on drilling on nanocomposite materials demonstrates that there is a clear lack of knowledge on the influence of incorporating nanoparticles within polymer nanocomposites on material performance during drilling.

- Nanotoxicology has demonstrated the potential toxicity of nanoparticles and some exposure limits have been introduced for working with independent nanoparticles. However, no current regulations are available on the exposure limit of nanoparticles that have been embedded within nanocomposites. Literature has therefore reported on the challenge in handling the uncertainty and concerns through innovation governance and responsible development.
- Three review studies (Froggett et al., 2014; Basinas et al., 2018; Debia et al., 2016) on the release of nanoparticles during machining on polymer nanocomposite materials all concluded similar findings that high quality evidence has demonstrated all three routes of exposure are relevant during machining. Whilst in some cases synthesis of nanoparticles has shown to not present evidence of clear nanoparticle exposure, processes of high-energy input have provided evidence that inhalation exposure occurs (Bainas et al., 2018; Debia et al., 2016). From the studies available, there is also a clear lack in data on nanoparticle release during machining.
- Studies have demonstrated that nanoparticles are released from composite materials reinforced with nanoparticles, but there is still a lack in understanding in the release. The unintentional release of nanoparticles has demonstrated conflicting results within studies, with some observing substantial nanoparticle release and identification of independent nanoparticles, whilst others showing minimal release and no free standing nanoparticles. The observed nanoparticle release studies have highlighted the potential hazard and exposure to humans which needs to be understood. From studies that have investigated different machining processes on the same nanocomposites, drilling demonstrated the higher quantity of nanoparticle release. There is a lack in data on the influence of filler/polymer and filler concentration on nanoparticle release during machining and is therefore, yet to be understood.
- The current studies have used multiple methodologies, materials and approaches towards the nanoparticle release control, which present limitations and challenges in the comparison. Although the various test guidelines and reports on exposure assessments have made remarkable progress and are available to assist in carrying out an adequate approach, there is no available standard or harmonised method in assessment of nanomaterial release during machining. A need for a standardised methodology that can easily be repeated and controlled

to give consistent results is necessary. A methodology that can allow for a variety of materials, control over the background environment, repeatable and reliable is critical in the understanding of nanoparticle release and the conceivable health risks and toxicity hazard to humans and the environment.

A key concept which can be found within literature as an alternative approach to handling the data from release of potentially toxic materials, is to adopt safety by design concepts. Understanding the release characteristics of the materials and reducing the hazard is required to improve the safe use of nanocomposites. Further, there is currently conflicting and/or incomparable data from available release studies. Due to different methodologies, materials and environments, the data is challenging to compare and draw confident conclusions. Therefore, accepting the limitations and challenges to implement in practice, knowledge on release has potential to be used towards developing and designing the materials to minimise the release of the potentially toxic nanoparticles and hence, reduce exposure for workers and consumers. The findings from the literature review demonstrate that although remarkable progress has been made in understanding the influence of nanoparticles on nanocomposite properties and release of nanoparticles, the review also highlights the urgent need for continued development and more data.

Chapter Three

Mechanical Properties of EP-based, PE-based and PP-based Nanocomposite Materials

3.1. Introduction

As demonstrated within the literature review, the use of nanoparticles to reinforce polymer materials has demonstrated beneficial material properties. The use of micron-sized fillers is established within industry, with high-end applications, due to the relative significant cost benefit, making use of the advantage of high strength-to weight ratio composite materials offer. More recently, with progress in nanoparticle synthesis and manufacturing, nanoparticles have started to be implemented into composite materials and therefore become nanocomposite materials. Another benefit nanoparticles offer composite materials as particulate fillers is the uniform strength in multiple directions and therefore becoming quasi-isotropic composites (Chawla, 2012). The overall philosophy behind the study of composite materials is to optimise material composition and performance. This chapter will therefore evaluate the influence of selected nano-sized fillers in polymers on mechanical properties.

PP is an extensively established thermoplastic used within various industries, though most significantly within the automotive industry (Cantor et al., 2008). According to a report in 2018, PP is also the most sought-after polymer type, representing 19.3 % of all plastics demand within Europe (PlasticsEurope Market Research Group, 2018). Furthermore, according to a different report published in December 2018, the global PP compound market is expected to reach an estimated $11.7 billion by 2023 with a compound annual growth rate of 3.7 % from 2018 to 2023 (Lucintel, 2018). The high consumer demand for the thermoplastic is mainly due to its simplicity in processing, lightweight, low cost and high recyclability (Liang et al., 2016). To improve the materials properties, PP is usually modified with inorganic fillers, such as talc (Lapcik et al., 2009; Weon and Sue., 2006), MMT (Selvakumar et al., 2010;

Ghasemi et al., 2016), metallic powders (Esthappan et al., 2015; Shimpi et al., 2017), calcium carbonate (Payandehpeyman et al., 2017; Yong et al., 2011), glass fibres (Ashori et al., 2016; Luo et al., 2017), wood powder (AlMaadeed et al., 2012; Haque et al., 2019) and WO (Luyt et al., 2009; Ding et al., 2019). Identified from the review of literature and to follow common uses within the automotive industry, talc, MMT and WO are used as fillers within PP in this study.

PE is a widely used thermoset within polymer engineering and composite materials. A report on the use within industry expects the industry to surpass $14.5 billion by 2024 at a compound annual growth rate of 7.5% (Graphical Research, 2018). PE resin is a comparatively low-cost with strong mechanical properties and high heat-resistance. This has led PE into being widely used within the construction industry and expected to grow at a rate of around 6% over 2018-2024 within the industry alone (Graphical Research, 2018). PE is a commonly used resin within composites and is widely researched within literature (Li et al., 2015). In order to tailor and enhance mechanical properties, PE has been combined with various fillers in composite development, including: Al_2O_3 (Ribeiro et al., 2015; Rajesh et al., 2014), SiO_2 (Changizi & Haddad, 2015; Rusmirović et al., 2016), halloysite (Saharudin et al., 2016; Lin et al., 2017), TiO_2 (Gaminian & Majid, 2015; Patel & Dhanola, 2016), natural fibres (Manalo et al., 2015; Gopinath et al., 2014; Saba et al., 2016) and glass fibres (Luo et al., 2014). As identified from the literature, Al_2O_3 and SiO_2 are used as nanofillers to alter the mechanical properties of PE within this study.

EP resin is one of the most extensively used thermosets within industry, and according to a report, the global EP resin market is forecast to increase to $10.2 billion by 2022 with a compound annual growth rate of 6.2% between 2016-2022 (Sahu, 2016). A similar later report from a different publisher, estimates the global EP resin market to be $10.6 billion by 2023 with a slightly slower compound annual growth rate of 5.24% during 2017-2023 (Cooked Research Reports, 2017). EP is commonly used due to its beneficial mechanical strength, heat resistance, chemical resistance, adhesive properties, and electrical insulating superior properties in relation to other polymers and are often used within the aeronautical and automotive industry (Zheng et al., 2010). Similar to PP and PE, EP is continuously being researched to enhance the mechanical properties with use of various micron-sized and nano-sized fillers, including: CNTs (Yue et al., 2014; Gardea et al., 2014), CNFs (Ahmadi et al., 2015; Shokrieh et al., 2014), graphene (Chandrasekaran et al., 2014; Ahmadi-Moghadam et al., 2015), GO (Wan et al., 2014; Shen et al., 2014), carbon fibre (Kafi et al., 2014; Zhang et al., 2015) and glass fibre (Dong & Davies, 2015; Borrego et al., 2014). As identified within literature, the use of CNTs and CNFs as nanofillers within neat EP and combining a hybrid nanocomposite with conventional carbon fibre reinforced EP with nano-sized GO will be included within this study.

The selection of the materials links directly to the appropriate use within industry and demonstrated potential improvement in material properties. The materials are therefore commercially relevant and representative of a wide range of material characteristics. The chosen nanoparticles have also all demonstrated potential toxicity effects and will therefore be investigated for nanoparticle release in subsequent chapters. The material manufacture, characterisation and material mechanical properties are included within this chapter. An overall discussion and link of the results to other chapters is included in Chapter Eight.

3.2. Experiment

The industry sectors selected as representative of application of the chosen materials are the aeronautical, construction and automotive industries with EP, EP/CF, PE and PP as the polymers. The following sections will detail the material manufacturing, characterisation and testing techniques used for the subsequent results section.

3.2.1. Materials and Manufacture

The review of the literature identified CNTs and CNFs commonly used nanoparticles to reinforce EP. From the available literature, a relatively large variation of weight percentage was reported to improve the mechanical properties (Gantayat et al., 2018). Therefore, as highlighted within several of the studies (Yue et al., 2014; Ahmadi et al., 2015), weight concentrations of 0.5 wt. %, 1 wt. % and 2 wt. % were chosen as the filler concentrations for CNTs and CNFs. Similarly, EP is vastly reported and used within industry to be reinforced with more conventional, micron-sized carbon fibre. Whilst studies have demonstrated the benefit of graphene-based fillers in EP, only recently have some nanoparticles been incorporated into hybrid carbon fibre and epoxy composites (Hadden et al., 2015; Jiang et al., 2016; Qin et al., 2015). For that reason, this study investigates the combination of established carbon fibre reinforcement with nano-sized GO to further enhance the hybrid material mechanical properties. Therefore, based on literature (Shen et al., 2013; Wan et al., 2014; Bortz et al., 2011), GO was chosen as a filler with concentrations of 0.05 wt. %, 0.1 wt. % and 0.5 wt. %.

As previously discussed, Al_2O_3 and SiO_2 are chosen as the reinforcing fillers for the PE-based composites materials due to their demonstrated potential improvement in mechanical properties. Literature has demonstrated that mechanical properties have shown to peak at around 5 wt. % for both nanoparticles for various polymer composite (Kaskaran et al., 2011; Ribeiro et al., 2015; Rusmirović et al., 2016), which has therefore led to two chosen concentrations of 2 wt.% and 5 wt. % nanofillers to compare. Conversely, PP has shown to be used within the automotive industry and established to be reinforced with Talc. The 20 wt. % Talc reinforced PP is therefore used as an

additional reference material representative of the automotive industry, and compared against the use of 5 wt. % nanofillers MMT and WO. However, these fillers are also highlighted as a reinforcing fillers as they will potentially decrease the density of the material without significantly affecting the mechanical properties (Dasari et al., 2004; Hadal et al., 2004). The material manufacturing process for the mechanical testing and nanoparticle release study is included below.

Polypropylene Nanocomposites

The PP-based materials are manufactured at Tecnalia, Donostia (Spain). A commercially available PP homopolymer (Moplen HP648T, Lyondell Basell Industries, Netherlands) was selected to represent the automotive industry. The reinforcements and concentrations chosen were 20 wt. % talc as a common filler within industry and 5 wt. % WO (Harwoll 7ST5, Nordkalk, Finland) and 5 wt. % of MMT (Nanomer I30T, Nanocor Corporation, USA). Neat samples of the PP were chosen to be used as reference materials as a comparison to evaluate the influence of the nanofillers.

The Coperion ZSK 26 MEGA compounder twin-screw extruder was used for homogenization of the nanocomposites. The extruded pellets of the materials were moulded by injection process by means of an Arburg All Rounder 270C-300-100 Injection Machine. Due to the diverse polarity nature of the polypropylene and the MMT and WO, a coupling agent (POLYBOND 3200 from ADDIVANT) was used to ensure adhesion between the nanofillers and the polymer.

Therefore, four sets of samples were fabricated: PP, PP with 20% talc (PP/Talc), PP with 5wt. % MMT and 2 wt. % coupling agent (PP/MMT), and PP with 5 wt. % WO with 2 wt. % coupling agent (PP/WO). A common sample size of 70mm x 45mm x 5mm were prepared for the drilling investigations. The corresponding standard sample was fabricated for the polymer reference standard ASTM D 3039/D tensile test (*ASTM D3039, 2017*) and reference standard ASTM D 7264/M flexural test (ASTM D7264M, 2015).

Polyester Nanocomposites

The materials are manufactured at Tecnalia, Donostia (Spain). A commercially available unsaturated orthophthalic PE (RESICHIM-Resina Poliéster, Gazechim Composites, France) was chosen as the matrix polymer due to its common use within industries such as the energy and construction industry. The polyester was reinforced with unmodified nano-sized SiO_2 (61Va11 Type 1 ,TORRECID S.A., Spain) and nano-sized Al_2O_3 (30VA12 Type 1, TORRECID S.A., Spain). Neat samples of the PE were chosen to be used as reference materials to demonstrate the influence of the nanofillers.

Two weight concentrations of 2 wt. % and 5 wt. % of SiO_2 (PE/SiO_2), and 2 wt.% and 5 wt.% of Al_2O_3 (PE/AL_2O_3) was chosen based on performance (*Liu and Kontopoulou, 2006; Allahverdi et al., 2012*).

The SiO_2 and Al_2O_3 nanofillers were added to the liquid PE resin (Cobalt salt pre-accelerated resin combined with a tyxotropic agent) and the samples were prepared using a dispermat high speed mixer to create a homogeneous concentration within the polyester resin, followed by casting processes. The materials were cured at room temperature in a mould. A common sample size of 70mm x 45mm x 5mm were prepared for the drilling tests. The corresponding standard sample was fabricated for the polymer reference standard ASTM D 3039/D tensile test (*ASTM D3039, 2017*) and reference standard ASTM D 7264/M flexural test (ASTM D7264M, 2015).

Therefore, five sets of samples were fabricated: neat PE (PE), PE with 2 wt. % SiO_2 (PE/SiO_2 2 wt. %), PE with 5 wt. % SiO_2 (PE/SiO_2 5 wt. %), PE 2 wt. % Al_2O_3 (PE/Al_2O_3 2 wt. %) and PE with 5 wt. % of Al_2O_3 (PE/Al_2O_3 5 wt. %).

Epoxy Nanocomposites

The materials are manufactured at Tecnalia, Donostia (Spain). An aeronautical grade and commercially available bi-component EP resin system (MVR444R, CYTEC Solvay Group, UK) was selected as the representative polymer for the aeronautical industry. The EP was reinforced with unmodified multi-walled CNTs with an average diameter of 10 nm to 15 nm (Multi-walled Graphistrength C100, Arkema Inc., USA) and unmodified CNFs with an average fibre diameter of 100 nm (PYROGRAF PR24-XT-LHT, Applied Sciences Inc., USA) due to their electrical properties.

A concentration of 2 wt. % of CNTs (EP/CNT) and 2 wt. % of CNFs (EP/CNF) were dispersed in the epoxy matrix through calendaring using a commercially available laboratory scale three-roll mill (EXAKT 80E, EXAKT Technologies Inc., USA) and cured in an oven process. The process involves employing repeated high shear stresses generated by the gap within the three rollers to disperse the CNTs and CNFs homogeneously in the epoxy. Manufactured sample measuring 70mm x 45mm x 5mm were prepared for the drilling tests. The corresponding standard sample was fabricated for the polymer reference standard ASTM D 3039/D tensile test (*ASTM D3039, 2017*) and reference standard ASTM D 7264/M flexural test (ASTM D7264M, 2015). Neat samples of the Epoxy were chosen to be used as reference materials to demosntrate the influence of the nanofillers. Therefore, three sets of samples were fabricated: neat EP (EP), EP with 2 wt. % CNTs (EP/CNT) and EP with 2 wt. % CNFs (EP/CNF).

Epoxy Carbon Fibre Nanocomposites

The materials are manufactured at RGU. A commercially available high performance bisphenol-A-(epichlorhydrin) based epoxy resin specifically formulated for use in vacuum resin infusion from Easycomposites (IN2 Epoxy Infusion Resin) combined with a polyoxypropylendiamin based hardenerfrom Easycomposites (AT30 Epoxy Hardener –Slow) was chosen for the matrix. Graphene oxide (GO) flakes, 15-20 sheets with 4-10 % edge-oxidized from Sigma-Aldrich (796034 Aldrich) was

employed in this investigation. The 3k 2/2 twill woven carbon fibre was obtained from Easycomposites (Carbon Fibre 2/2 Twill 3k 210g).

The composite samples were manufactured through the vacuum resin infusion method. Concentrations of 0.05 wt. %, 0.1 wt. % and 0.5 wt. % were initially dispersed within methanol with the use of a sonication bath for 1 hour to allow for later dispersion of the GO in the Epoxy. Once fully dispersed, the solution was then homogenously dispersed within the bisphenol-A-(epichlorhydrin) based epoxy and placed in a vacuum oven for 2 hours at 60 ^{O}C to allow for slow solvent evaporation. The solution was then mixed together with the hardener using a magnetic stirrer and manual mixing. This was followed by the vacuum resin infusion process with 6 layers of the carbon fibre textile layered within a mould and left to cure for 7 days at room temperature. The corresponding standard sample was fabricated for the polymer reference standard ASTM D 3039/D tensile test (*ASTM D3039, 2017*) and reference standard ASTM D 7264/M flexural test (ASTM D7264M, 2015). A reference sample without any GO was also manufactured (EP/CF), with 0.05 wt. % GO (EP/CF/GO 0.05 wt. %), with 0.1 wt. % GO (EP/CF/GO 0.1 wt. %) and with 0.5 wt. % GO (EP/CF/GO 0.5 wt. %).

An outline of the chosen material combinations representing the industrial sectors are displayed in Table 6.

Table 6*:* Polymer materials selected and chosen nanofiller and weight concentrations.

Composite Polymer	Properties to be improved	Nanoparticle reinforcements	Reference Material	Nanocomposite formulation
Epoxy (EP)	Mechanical properties (flexural and tensile)	CNTs CNFs	Neat Epoxy	EP + 0.5 wt. % CNTs EP + 1 wt. % CNTs EP + 2 wt. % CNTs EP + 0.5 wt. % CNFs EP + 1 wt. % CNFs EP + 2 wt. % CNFs
Polyester (PE)	Mechanical properties (flexural and tensile)	SiO_2 Al_2O_3	Neat Polyester	P + 2 wt. % SiO_2 P + 5 wt. % SiO_2 P + 2 wt. % Al_2O_3 P + 5 wt. % Al_2O_3
Polypropylene (PP)	Density, mechanical properties (flexural and tensile)	WO MMT	Neat Polypropylene	PP + 20% Talc PP + 5 wt. % WO PP + 5 wt. % MMT
Epoxy reinforced with carbon fibre (EP/CF)	Mechanical properties (flexural and tensile)	GO	Epoxy/carbon fibre	EP/CF + 0.05 wt. % GO EP/CF + 0.1 wt. % GO EP/CF + 0.5 wt. % GO

3.2.2. Characterisation

The materials were characterised to demonstrate the nanofiller and nanocomposite materials structure and morphology. Both a Zeiss EVO LS10 Variable Pressure Scanning Electron Microscope and an SEM/EDX (FEI Quanta 200F) with a beam current of 208 µA and voltage of 10 kV were used in the upcoming study and cross-checked using an electron probe microanalyser (EPMA) JEOL JXA-8621MX, with beam current of 30 nA and voltage of 15 kV. SEM samples of the materials were prepared using sputter coating of an ultra-thin coating of gold to minimize charging. The materials were further investigated using a NICOLET iS10, Thermo Scientific ATR-FT-IR.

The average densities of the materials were also calculated using the mass and volume of the samples. The volume was calculated from measurements using Draper Expert Digital Vernier Callipers with ± 0.1mm and the mass was calculated using a Kern ABT Analytical Balances Model 120-5DM with a resolution of 0.1 mg.

3.2.3. Mechanical Testing

Materials selected were investigated for mechanical properties (tensile and flexural). The influence of the addition of the nanofillers is evaluated and compared. To achieve this, the materials underwent a tensile test in accordance to ASTM D 3039/D tensile test (ASTM D3039, 2017) and 3-point flexural test in accordance with reference standard ASTM D 7264/M flexural test (ASTM D7264M, 2015). The tests were carried out with the use of an Instron 3382 universal testing system with a 100 kN load range. Raw data was collected using the Bluehill 3 software as measured in terms of load and extension. As per the respective standards, a constant head-speed of 2mm/min for the tensile test and 1mm/min for the flexural test was used, and data is collected at 10 Hertz. The equations used to convert the data from the load and extension to stress vs strain and relevant material properties is explained in Appendix E.

The Instron 3382 universal testing system setup for the tensile test in accordance to ASTM D 3039/D tensile test (ASTM D3039, 2017) and 3-point flexural test in accordance with ASTM D 7264/M flexural test (ASTM D7264M, 2015) used is shown in Figure 17.

a.)

b.)

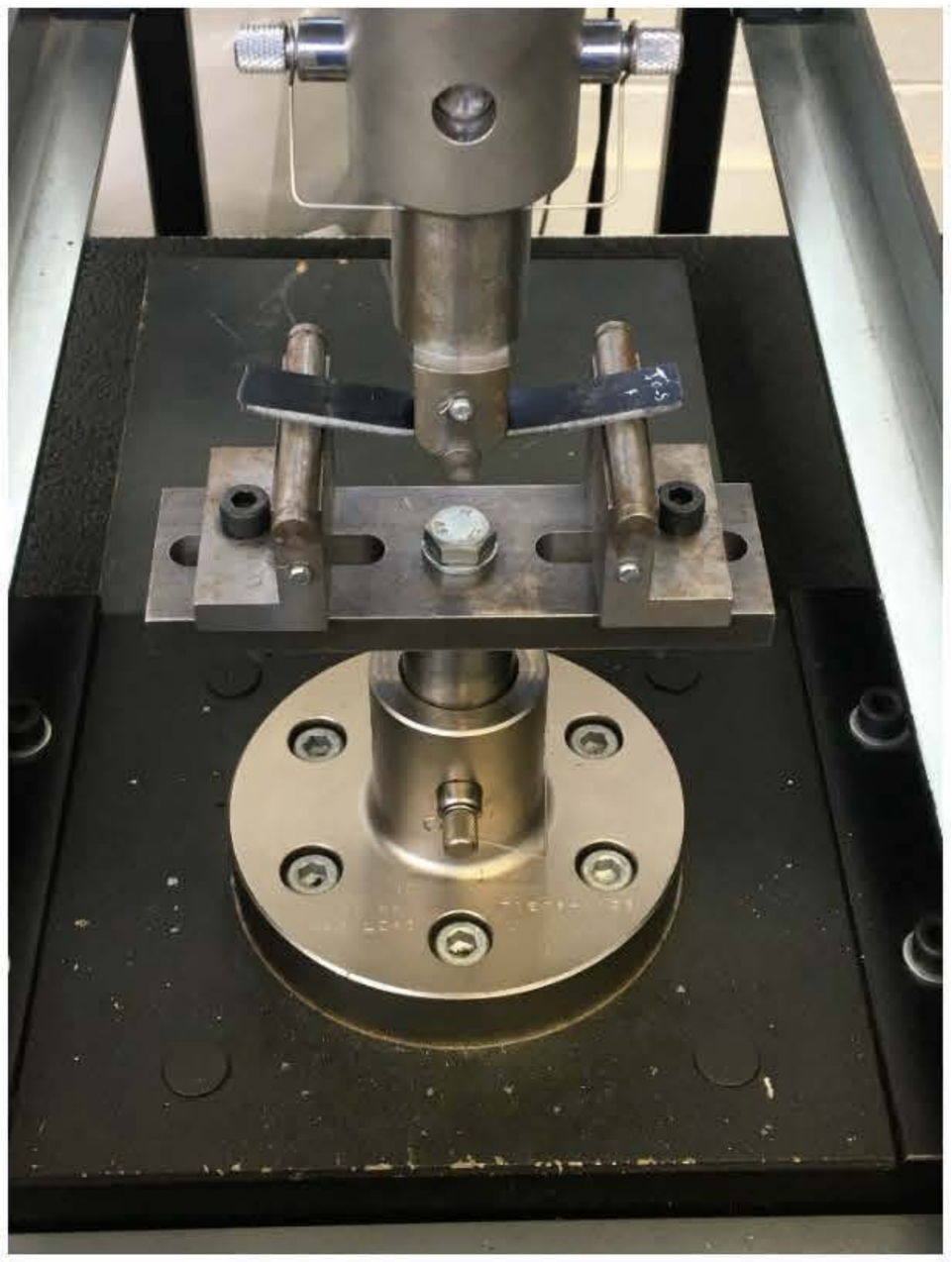

Figure 17: Instron 3382 universal testing system used for a.) tensile test (ASTM D3039, 2017) and b.) 3-point flexural test (ASTM D7264M, 2015).

3.2.4. Statistical Data Analysis

As per the standards (ASTM D3039, 2019; ASTM D7264, 2019), statistical analysis on the number of samples incudes the sample mean, $\bar{x}$, the standard deviation, s_{n-1}, and the coefficient of variation, CV, for each property determined; i.e. Young's Modulus, flexural chord modulus, ultimate tensile strength, ultimate flexural strength, strain at ultimate flexural strength and the strain at ultimate tensile strength using (ASTM D3039, 2019; ASTM D7264, 2019):

$$\bar{x} = \frac{\left(\sum_{i=1}^{n} x_i\right)}{n} \quad \textbf{- Equation 3.1}$$

$$s_{n-1} = \sqrt{\frac{\left(\sum_{i=1}^{n}(x_i^2 - x^2)\right)}{n-1}} \quad \textbf{- Equation 3.2}$$

$$CV = 100 \times \frac{s_{n-1}}{\bar{x}} \quad \textbf{- Equation 3.3}$$

Where:
n = number of specimens
x_i = measured property

The statistical data determined is presented in a table following the presented of the stress vs strain data for each specimen. To compare the reference polymer with the reinforced samples, the percentage change is also determined using (ASTM D3039, 2019; ASTM D7264, 2019):

$$Percentage\ change = \frac{x_{Sample} - x_{reference}}{x_{reference}} \times 100 \qquad \textbf{- Equation 3.4}$$

Where:
$x_{reference}$ = measured property from reference sample
X_{sample} = measured property from comparative sample

Further to the mean, standard deviation, coefficient of variance, a direct comparison between samples can be obtained using inferences on the sample mean. When assessing the data for each material, the variation in property value can be used to provide confidence interval construction and hypothesis testing. These are two fundamental techniques of statistical inference (*Shao, 2008*). A commonly used statistical analysis and given that the data collected is a sample valuation of the data with unknown population variance, the estimated mean, standard deviations and variance can be projected in a t-distribution. From the distribution, a confidence interval can be constructed giving an inference of a chosen confidence interval of the population mean will lie in (from sample collected). The calculation carried out to identify the 90% confidence interval for the measured property is as follows (*DeCoursey, 2003*):

$$\textit{Confidence limits} = \bar{x} \pm t\left(\frac{s}{\sqrt{n}}\right) \qquad \textbf{- Equation 3.5}$$

$\bar{x}$ = mean of measured property: $\bar{x} = \frac{(\sum_{i=1}^{n} x_i)}{n}$
s = standard error (standard deviation) where variance: $s^2 = \frac{1}{n-1}\sum_{i=1}^{n}(x_i - \bar{x})^2$
n = sample size
t = t-score value for 90% confidence interval = 1.645

The calculated confidence intervals will provide the upper and lower limit values of a 90% confidence the mean of peak concentration will sit within. This deduction provides the inference about one sample mean. The t-test can also be used to evaluate the two samples with a two samples t-test. This is also called a two samples test of significance. The samples are assessed by performing a hypothesis test between the two samples to identify if there is a statistically significant difference. The description of the method used for the test is displayed in Equation 3.6 and Equation 3.7.

$$t = \frac{\bar{x}_1 - \bar{x}_2}{\sigma_{\bar{x}-\bar{x}}} \quad \textbf{- Equation 3.6}$$

Where:
$\overline{x}_1$= mean of measured property of first sample
$\overline{x}_2$= mean of measured property of second sample
The mean of the difference between samples means will be zero: $\mu_{\bar{x}-\bar{x}} = 0$
$\sigma_{\bar{x}-\bar{x}}$ = standard error defined by the mean of difference equal to zero

$$\sigma_{\bar{x}-\bar{x}} = \sqrt{\frac{(n_1-1){s_1}^2+(n_2-1){s_2}^2}{n_1+n_2-2}}\sqrt{\frac{n_1+n_2}{n_1 n_2}} \quad \textbf{- Equation 3.7}$$

The t-score is referred with the critical values of a t-distribution to see if it lies within a 90% confidence interval. If the t–score is within the 90% confidence interval critical values, the t-test is classified as statistically insignificant and demonstrated possibility of no change. If the t-score is not inward of the 90% interval, the sample means are not within the confidence interval and are therefore deemed statistically significantly different to one other.

The t-test can be performed to assess the differences between any additional samples. However, when dealing with more than two samples, the equality of means can be tested all at once using analysis of variance F-test. This is a popular approach and is commonly known as the one-way Analysis of Variance (ANOVA). The ANOVA procedure evaluates a null hypothesis that the samples are the same and perform equally (*Montgomery, 2001*).

Principally, one-way ANOVA compares the amount of variation between the samples with the amount of variation within the samples as shown in Equation 3.2.14.

$$F = \frac{variance\ between\ samples}{variance\ within\ samples} \quad \textbf{-Equation 3.8}$$

Where:

Total sum of squares (TSS) = $\sum x_i^2 - n\bar{x}^2$

Variance between samples = $\frac{sum\ of\ squares\ between\ (SSB)}{degrees\ of\ freedom} = \frac{\sum n_s(\overline{x_s}-\bar{x})^2}{k-1}$

Variance within samples = $\frac{sum\ of\ squares\ within\ (SSW)}{degrees\ of\ freedom\ from\ each\ of\ k} = \frac{\mathrm{TSS}-\mathrm{SSB}}{n-k}$

$$= \frac{\sum x_i^2 - n\bar{x}^2 - \sum n_s(\overline{x_s}-\bar{x})^2}{n-k}$$

$\overline{x_s}$= mean for given sample
n_s= number of cases in given sample
k = number of samples

The calculation returns an F-ratio which is compared to the critical values from an F-score table to identify the exact significance level and whether or not to accept the null hypothesis of no difference. If found true, the result indicates that the sample means (accounting standard deviations and errors) have a probability of being equal to each other. If the hypothesis is rejected, the materials can be regarded significantly different. The approach returns the probability that the observation could have been due to random error alone on top of accepting or rejecting the hypothesis that the samples displayed a difference (*Montgomery, 2001*). As a universal method of statistically evaluating the variance between results, several software tools are available such as MS Excel, which is used to execute this analysis.

This data analysis provides a statistical comparison between the materials. The hypothesis testing measures the probability that a relationship between the data is caused by the one variable factor that is being changed (i.e. in this case, the change in material) and not random chance. The confidence intervals inference the range the mean value will be with a confidence interval of 90%. When measuring the effect of a change in parameter, as with material filler, this analysis is essential.

3.3. Results & Discussion

3.3.1. Morphology study

Polypropylene Based Samples and Fillers

MMT and WO are the two representative nanofillers used as reinforcing particles for the PP samples. This section includes the SEM and EDX analysis of the fillers to demonstrate the morphology and chemical composition. Two magnifications of the fillers are illustrated in Figure 18.

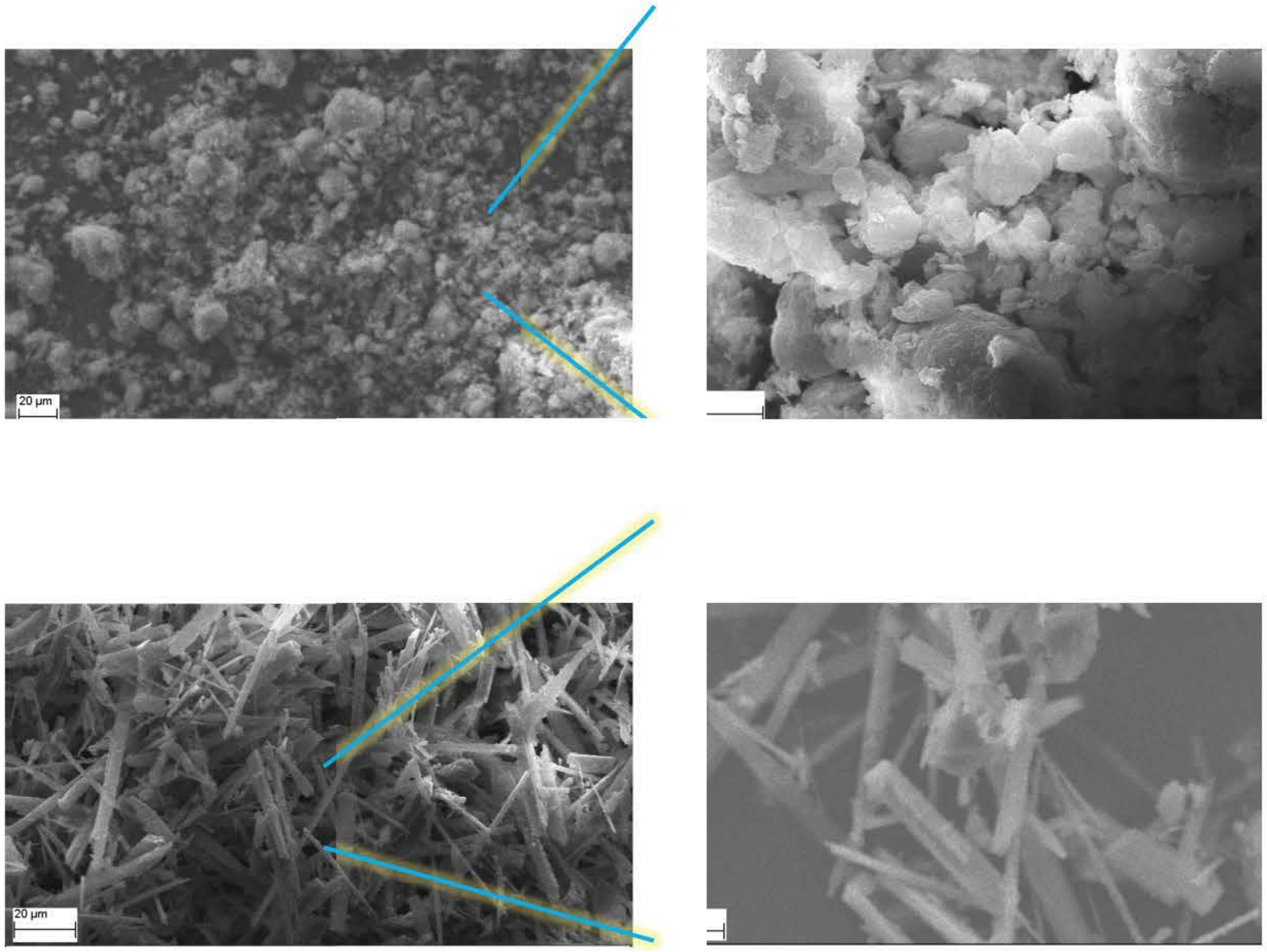

Figure 18: SEM images taken using Zeiss EVO LS10 of nanofillers used within PP-based samples. Images represent two magnifications a.) and b.) of MMT particles and c.) and d.) of WO particles.

WO is a calcium silicate ($CaSiO_3$) and is used as a functional filler in polymer materials. WO is the only naturally occurring white mineral that is wholly acicular (Svab et al., 2005), and can therefore be seen in Figure 18 in fibrous forms. The aspect ratio however will vary and depend on natural conditions and preparation techniques (Ding et al., 2013). In contrast, MMT is composed of silicate layers with nm thicknesses. The structure consists of fused silica tetrahedral sheets with octahedral sheets of Al_2O_3 sandwiched in-between (Kampeerapappun et al., 2007) and therefore be visible as more circular plate-like particulates. As MMT is a clay containing phyllosilicate group of minerals and composed of two tetrahedral sheets of silica sandwiched a central sheet of alumina the material has the formula: $(Na,Ca)_{0.33}(Al,Mg)_2(Si_4,O_{10})$.

The fillers demonstrate two forms of nanoparticles. The MMT can be seen to be composed of crystals with a diameter close to 1 µm and average thickness around 10 nm. The thicknesses and diameters vary significantly as visible in both Figure 18a and 18b. Agglomerations and larger particles of both nanofillers can also be observed in Figure 18. In contrast to the MMT, the WO fillers are in the form

of fibres with a diameter in the nano-range but up to 4.5 µm. The variation in filler shape and composition will therefore offer a different interfacial bonding to the polymer and subsequent material properties (Chen et al., 2003; Svab et al., 2005). Both the MMT and WO SEM images correspond to fillers used in similar studies (Delva et al., 2014; Luyt et al., 2009; Dasari et al., 2004).

Using EDX analysis, the elemental characterisation of the fillers is achieved and shown in Figure 19. A high-energy beam of charged particles was focused over an area shown in Figure 19a to simulate the emission spectrum from the fillers.

a.)

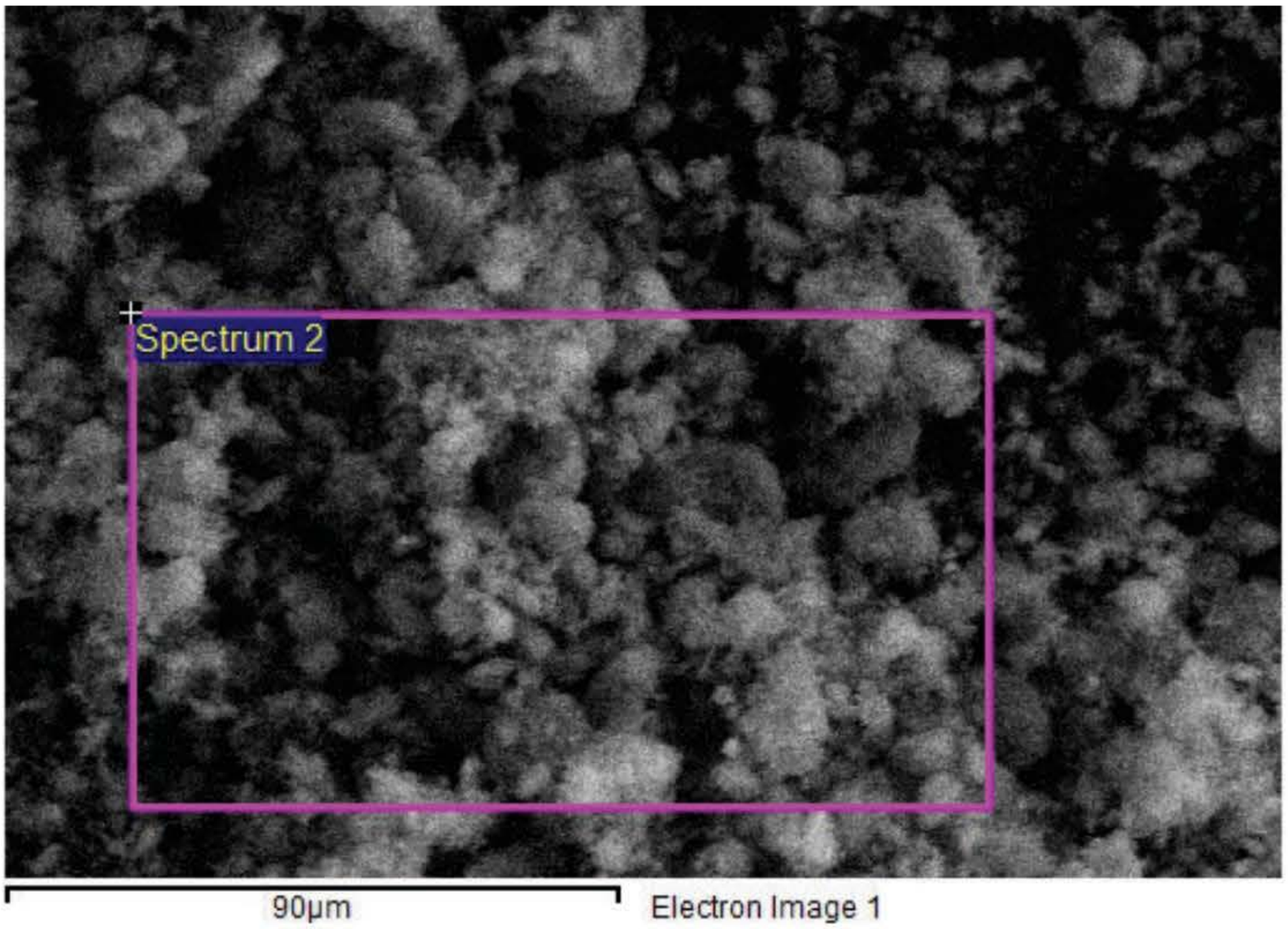

b.)

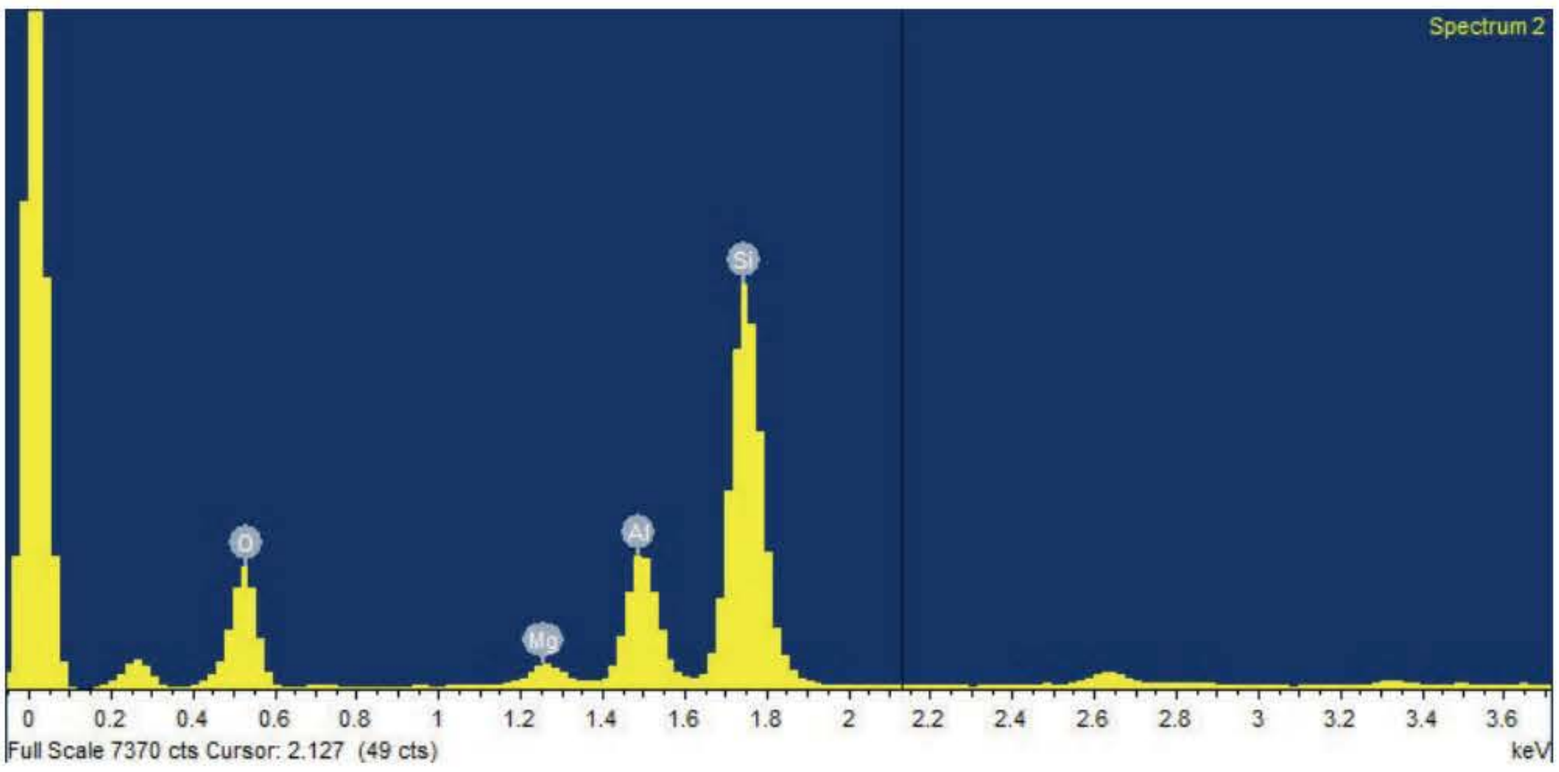

Figure 19: SEM image using Zeiss EVO LS10 of a.) representing the location of b.) EDX spectrum analysis of MMT particles used to reinforce PP samples.

The EDX analysis as presented in Figure 19 detected the four main elements in silicon (Si), aluminium (Al), magnesium (Mg) and oxygen (O). Of the significant elements identified, the values represented in the spectrum in Figure 19 consisted of 60.6 wt. % O, 1.5 wt. % Mg, 8.2 wt. % Al and 29.7 wt. % Si. As expected, the Si and O represented the two highest weight concentrations as they act as the sandwiching sheets of the particles. The peak at 0 energy value in Figure 19 is an electron noise peak. The EDX analysis on WO is illustrated in Figure 20b.

a.)

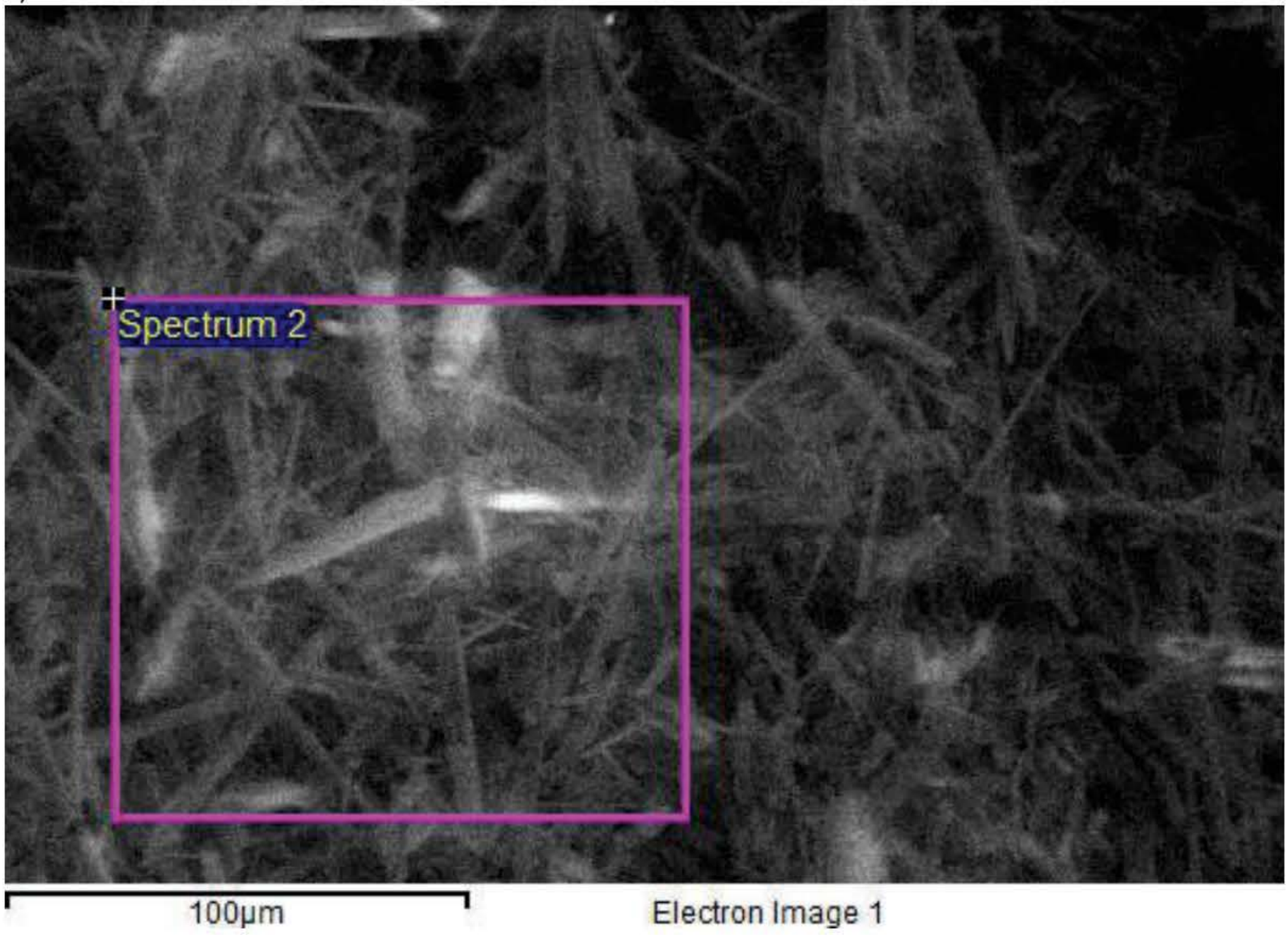

b.)

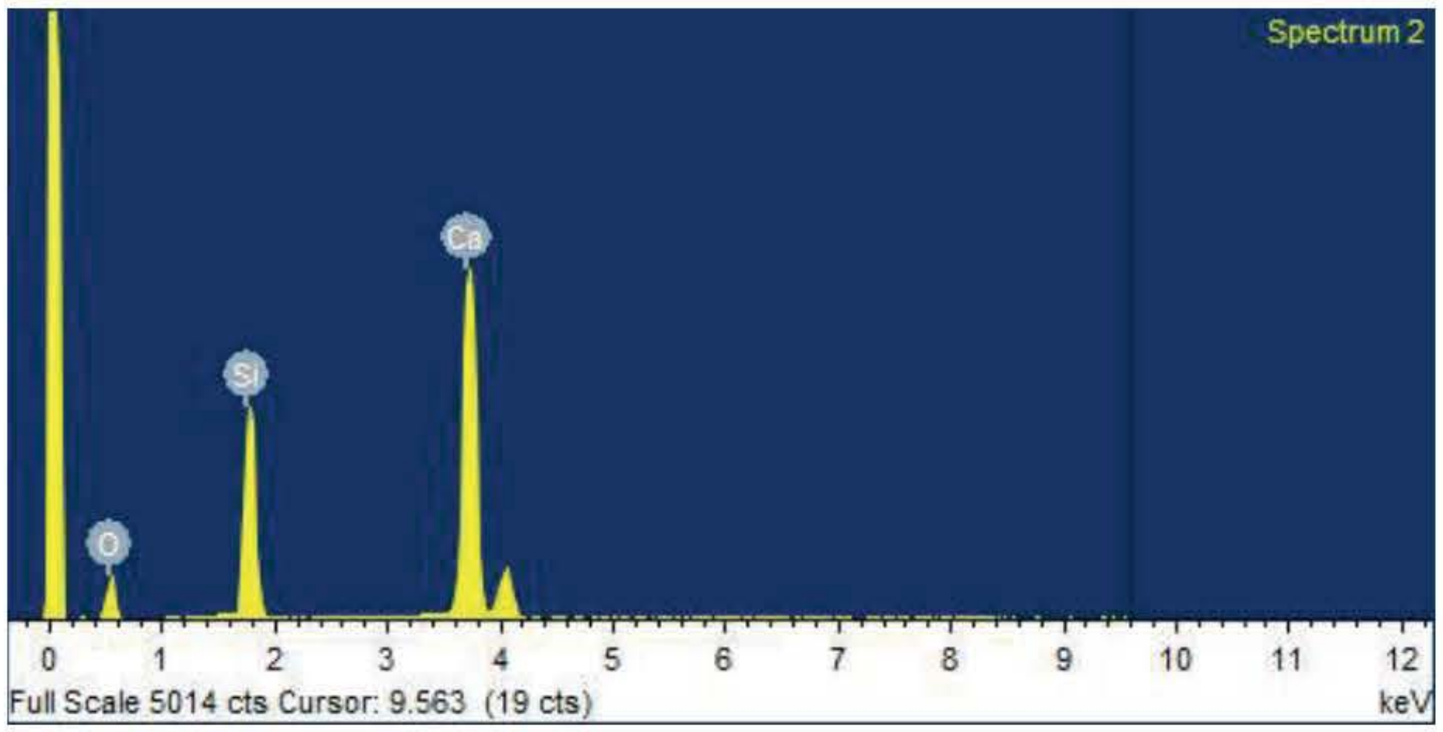

Figure 20 SEM image using Zeiss EVO LS10 of a.) representing the location of b.) EDX analysis of WO filler used to reinforce PP samples.

WO is a calcium silicate mineral with a chemical formula of $CaSiO_3$. The EDX analysis of the fibres illustrated in Figure 20, confirms the three elements in WO: calcium (Ca), silicon (Si) and oxygen (O). The atomic weight concentration of the EDX analysis presented in Figure 20 consists of 53.4 wt. % O, 15.6 wt. % Si and 31 wt. % Ca. A pure $CaSiO_3$ particle can expect to be nearly half CaO and half SiO_2 (Ding et al., 2013). The SEM images of the surface is shown in Figure 21.

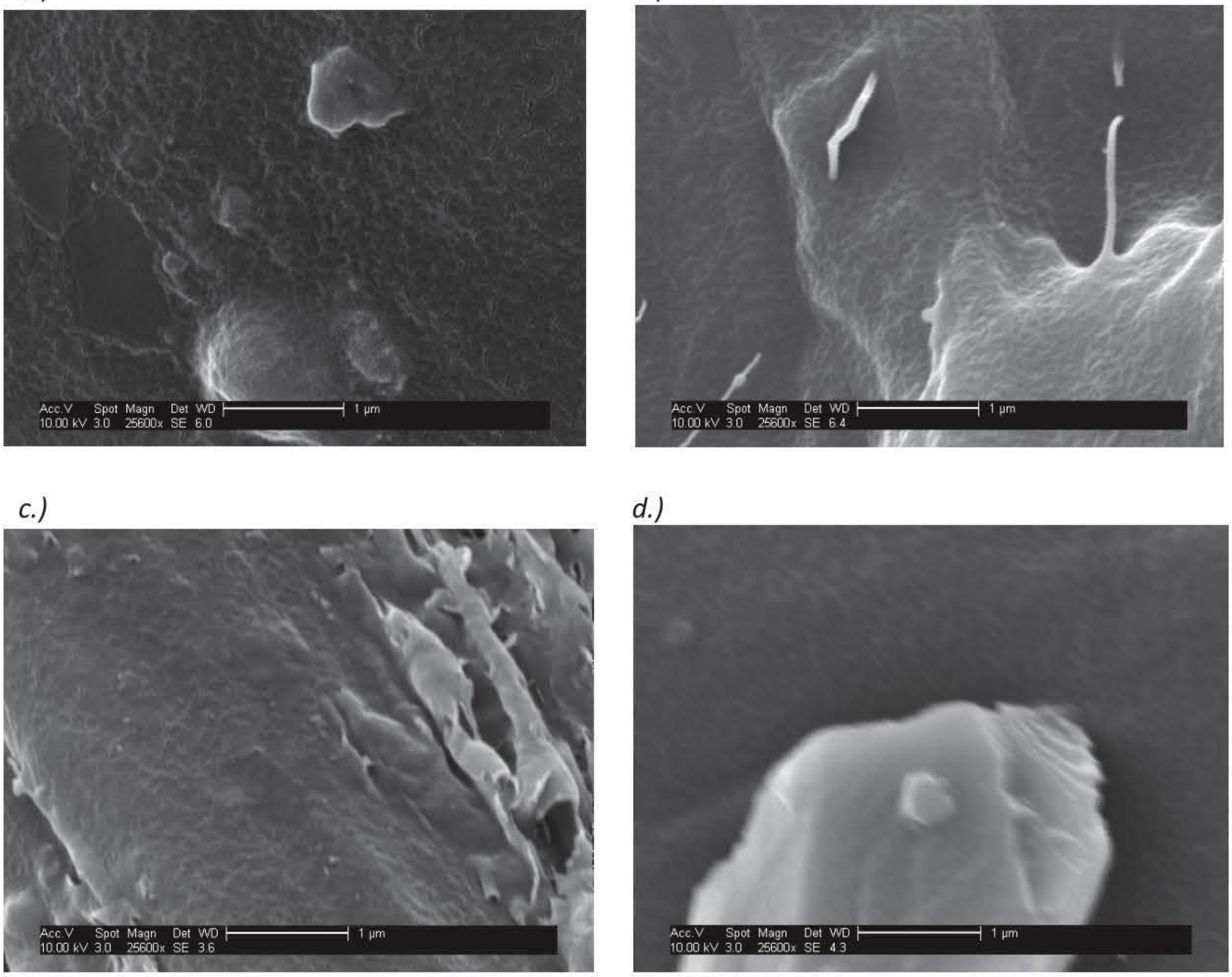

Figure 21*:* SEM images at same magnitude of the surfaces of manufactured samples a.) neat PP, b.) PP/Talc, C.) PP/MMT and d.) PP/WO.

Figure 21 presents the SEM images of the surfaces from the manufactured PP based samples carried out using at SIRENA collaboration partners Cranfield University. Spherical nanoparticles can mainly be seen on the PP/MMT sample and in a smaller proportion on the neat PP sample. In comparison the PP/WO sample illustrates particles with diameter larger than 500 nm. The PP/Talc sample has the largest fillers and displays presence of short filaments of Talc with diameters of around 100 nm. Therefore, the SEM analysis was unable to identify the WO fibres on the surface of the material, most likely due to the low weight concentration. This is a common observation reported within literature (Luyt et al., 2009; Dev et al., 2015; Dasari et al., 2004).

Polyester Based Samples and Fillers

Equally, the nanofillers and surfaces of the PE-based samples were examined using an SEM and EDX. The nano-sized silica and alumina are displayed in Figure 22.

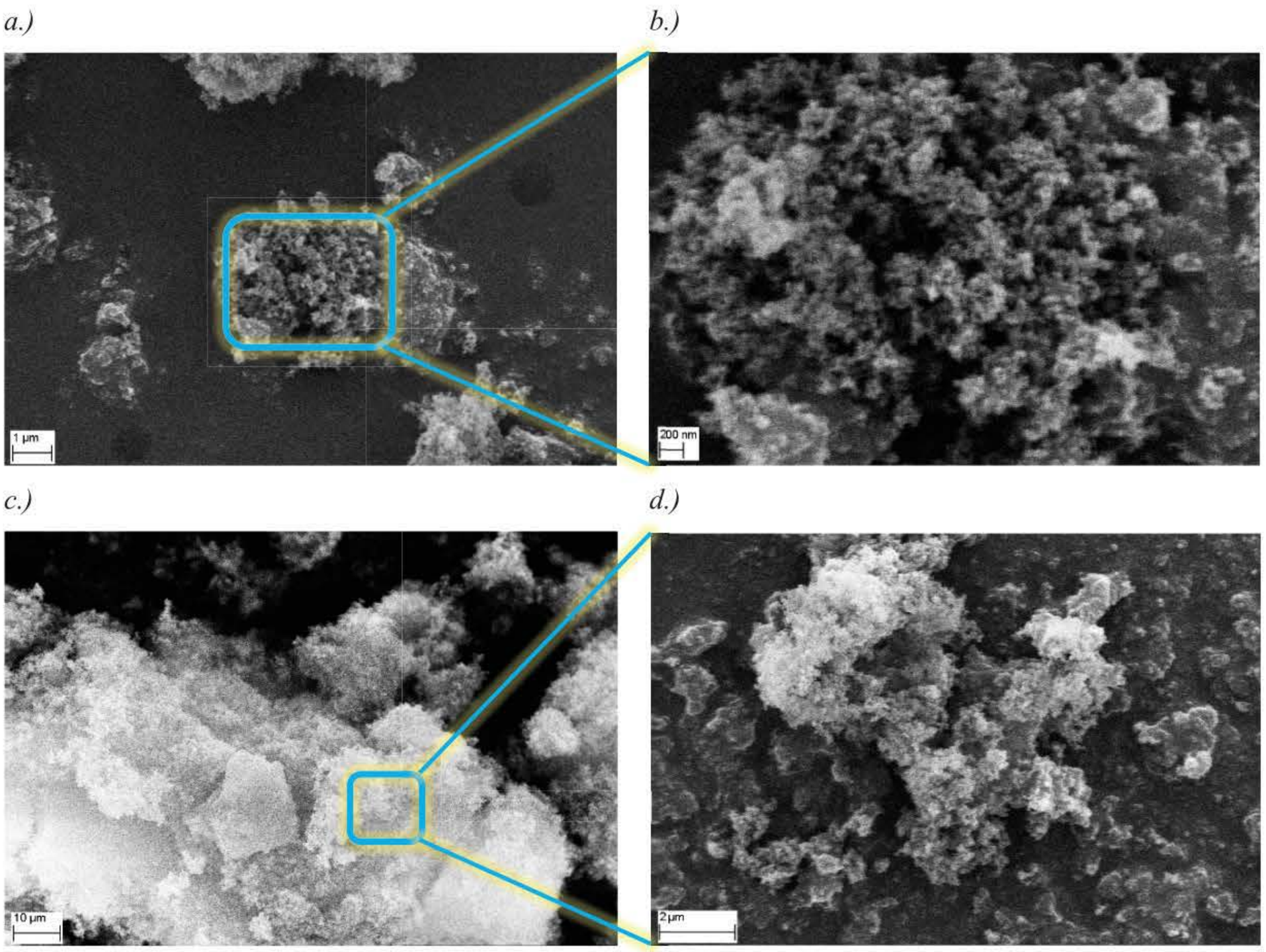

Figure 22: SEM images taken using Zeiss EVO LS10 of nanofillers used within PE-based samples. Images demonstrate two magnifications of the a.) and b.) Al_2O_3 filler and c.) and d.) SiO_2 filler.

Due to the small size and limited resolution of the SEM, individual particles are harder to identify. Both the Al_2O_3 and SiO_2 have particle diameters below 50 nm, which is not entirely observable through the resolution of the images in Figure 22. Agglomerations of the nanoparticles are seen due to the active nature of the particles to cluster and agglomerate.

The morphology of the particles differs slightly, as the silica has a spherical form, whilst the alumina is considered to have a nearly spherical shape. This is observable in the cluster formation difference of the particles. The cluster of silica particles can be seen to be more compact than the alumina. The particulate formation and observation of agglomerates correlate to similar Al_2O_3 and SiO_2 nanoparticles used within other studies (Cho et al., 2006; Conradi et al., 2014).

An EDX analysis was also performed on the nanoparticles and can be seen in Figure 23.

a.)

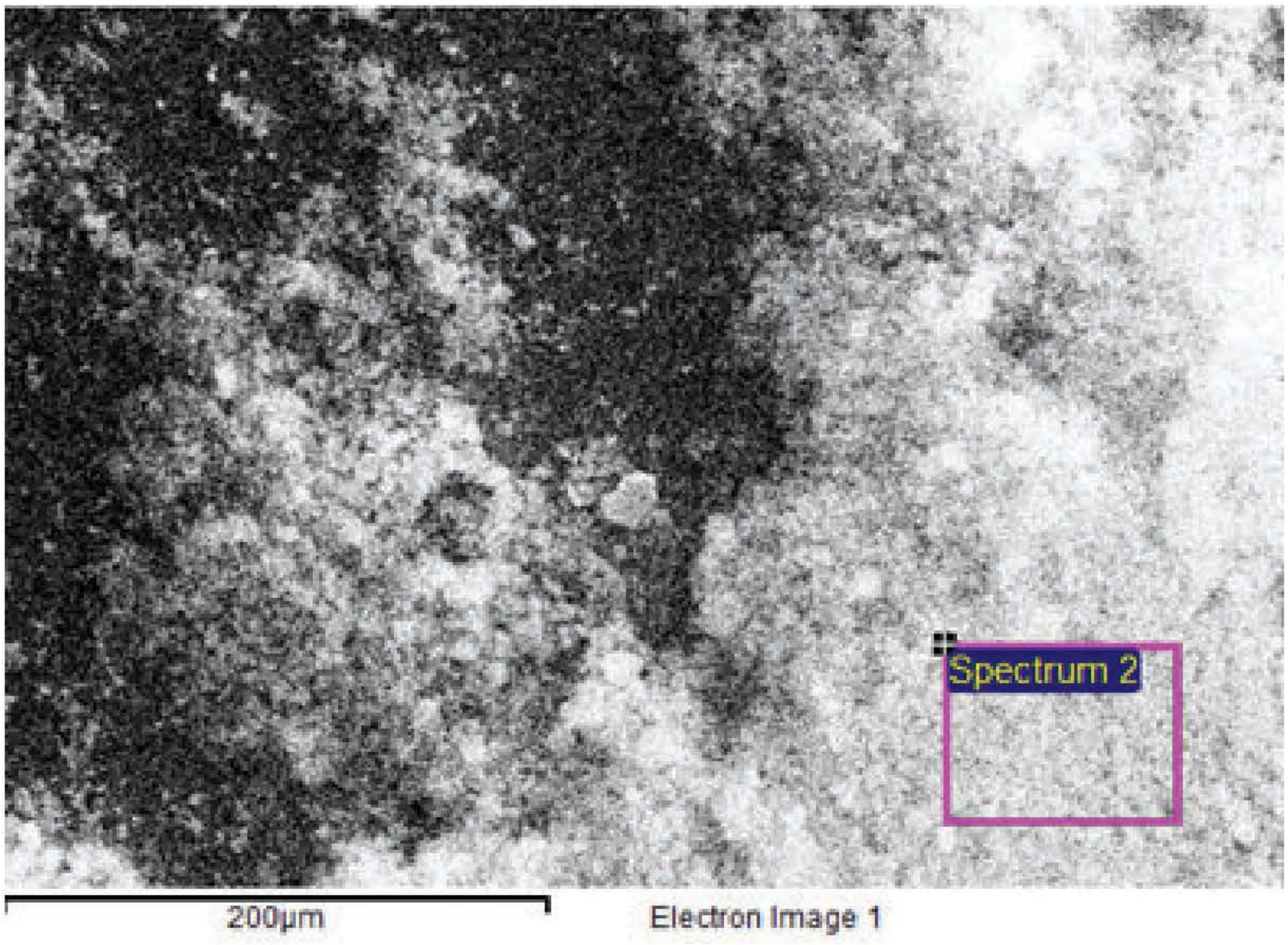

b.)

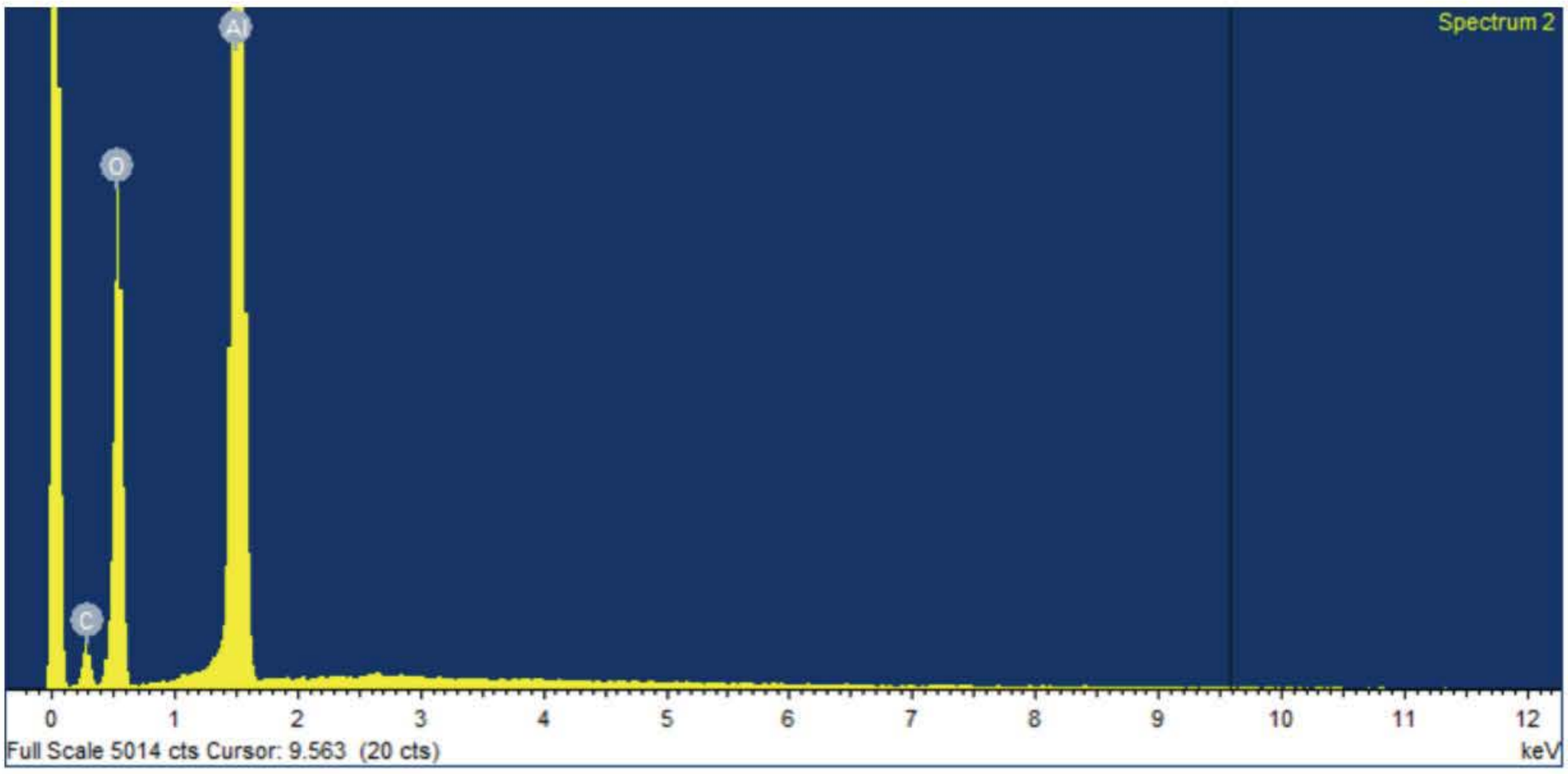

Figure 23: SEM image using Zeiss EVO LS10 of (a.) representing the location of EDX analysis (b.) of Al_2O_3 particles used to reinforce PE samples.

The EDX analysis of the Al_2O_3 particles exhibited the concentrations of elements Al, O, and C. The atomic concentrations consisted of 42 wt. % Al, 14 wt. % C and 44 wt. % O. The trace of C with the alumina is expected to be due the active adsorbent nature of alumina. The particles have a high

surface activity and are used as adsorbent and catalyst materials (Lee and Kang, 2013). The concentration of C, is relatively low in comparison to the presence of Al and O as demonstrated in Figure 23. The EDX analysis on SiO_2 particles is shown in Figure 24.

a.)

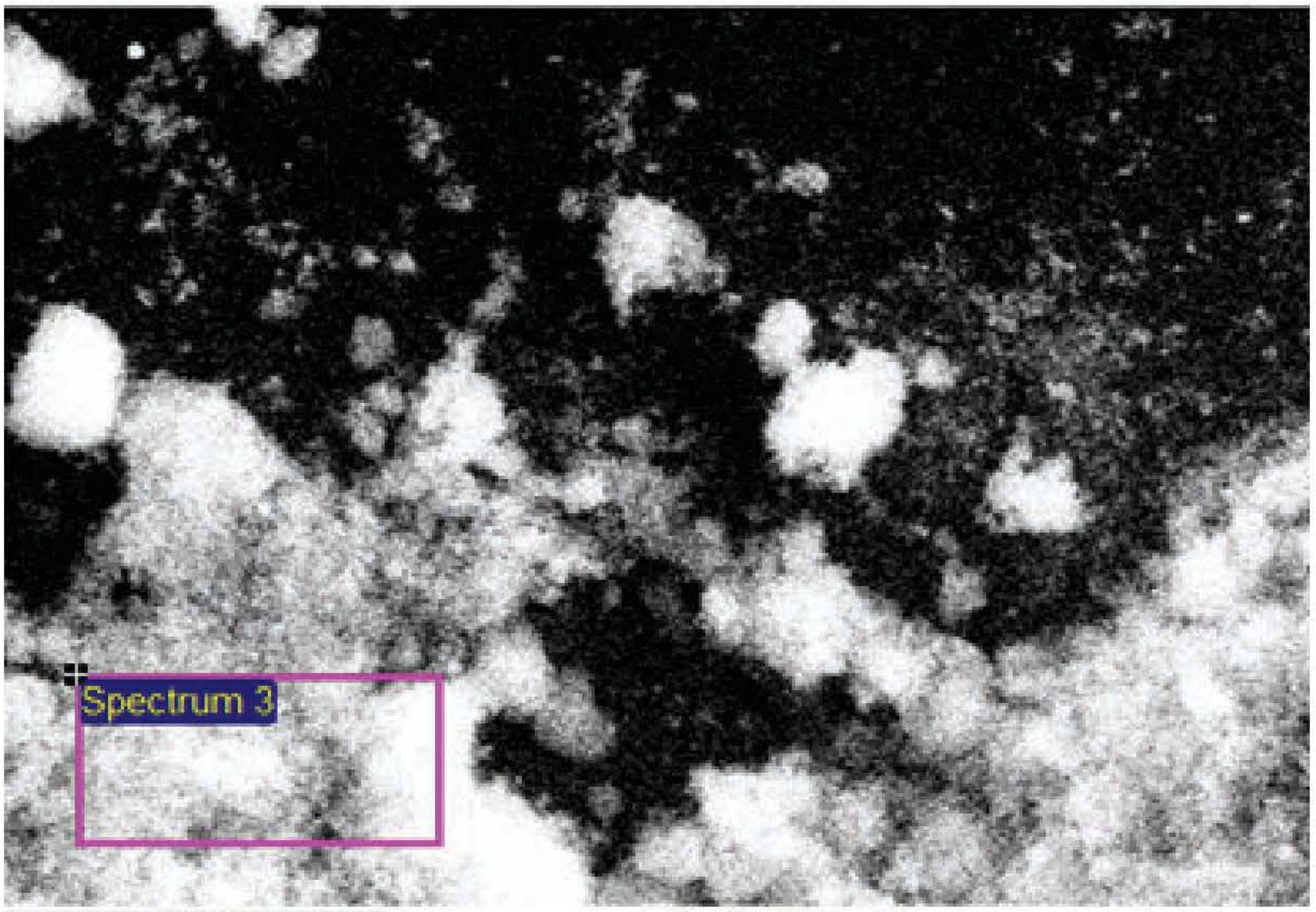

b.)

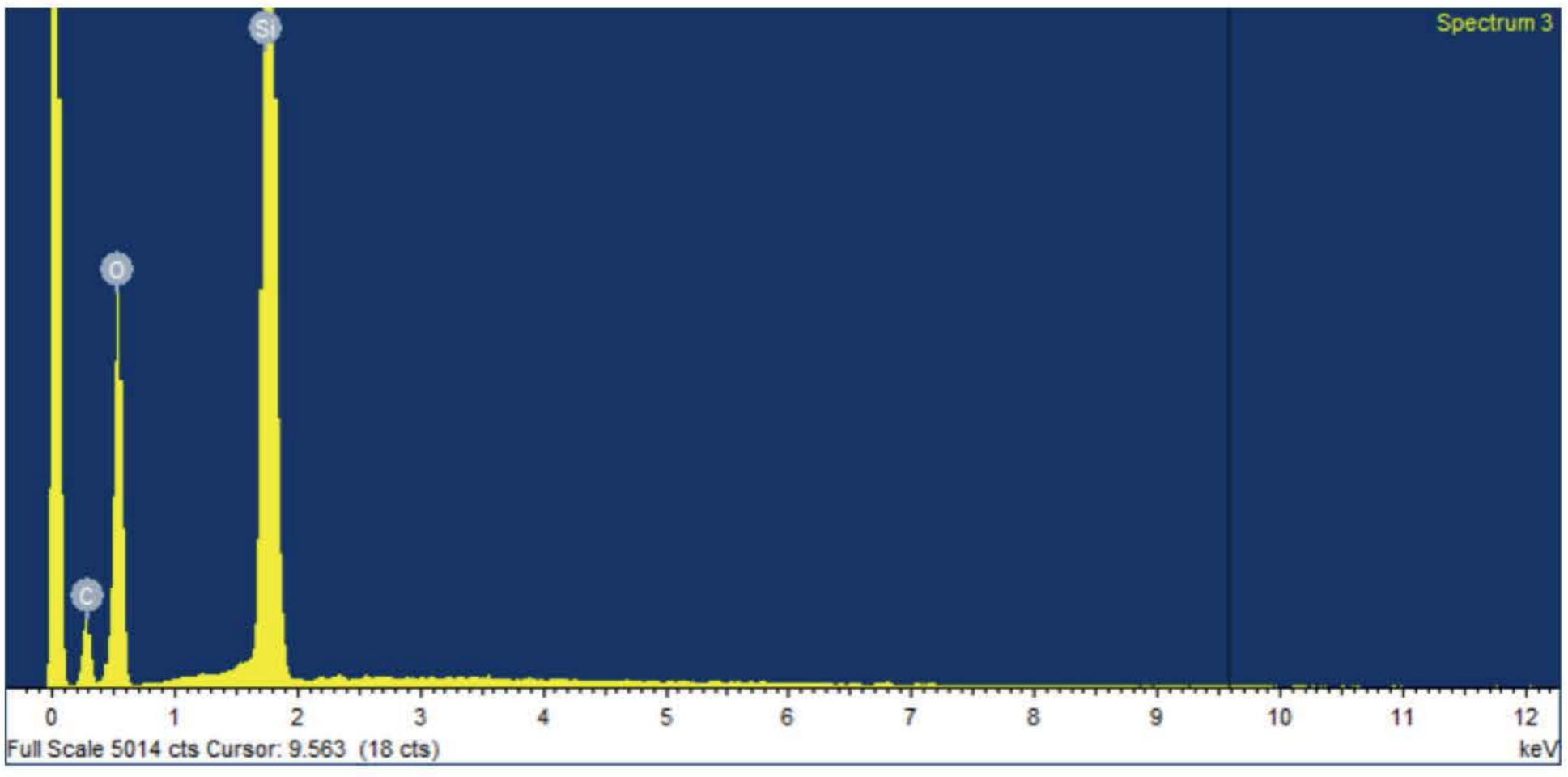

Figure 24: SEM image using Zeiss EVO LS10 of (a.) representing the location of EDX analysis (b.) of SiO_2 particles used to reinforce PE samples.

The EDX analysis on the SiO_2 particles exhibited the concentrations of elements of Si, O and C. The atomic concentrations consisted of 22 wt. % C, 44 wt. % O, and 34 wt. % Si. Similar with the Al_2O_3 particles shown in Figure 23, the SiO_2 particles shown in Figure 24, also exhibited a small traces of C. As demonstrated within literature (Lee and Kang, 2013), the adsorbent nature of the fillers is most likely the cause is demonstrating a peak at C. The concentration is relatively lower in comparison to the other elements.

The material surface morphologies are displayed in Figure 25. The filler reinforcements are visually recognisable for the two reinforcements.

a.)

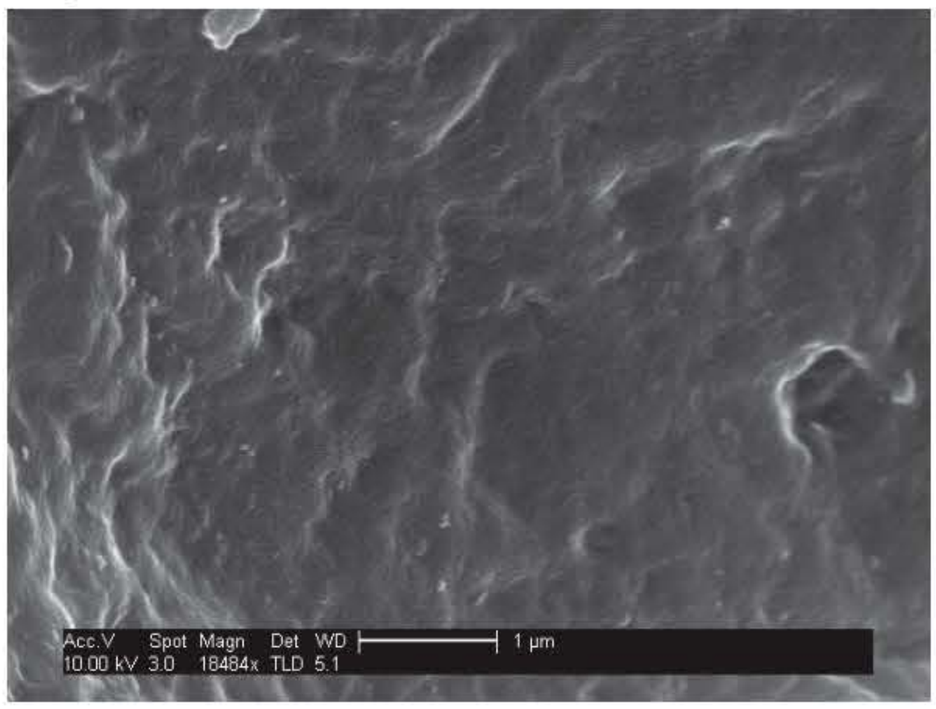

b.)

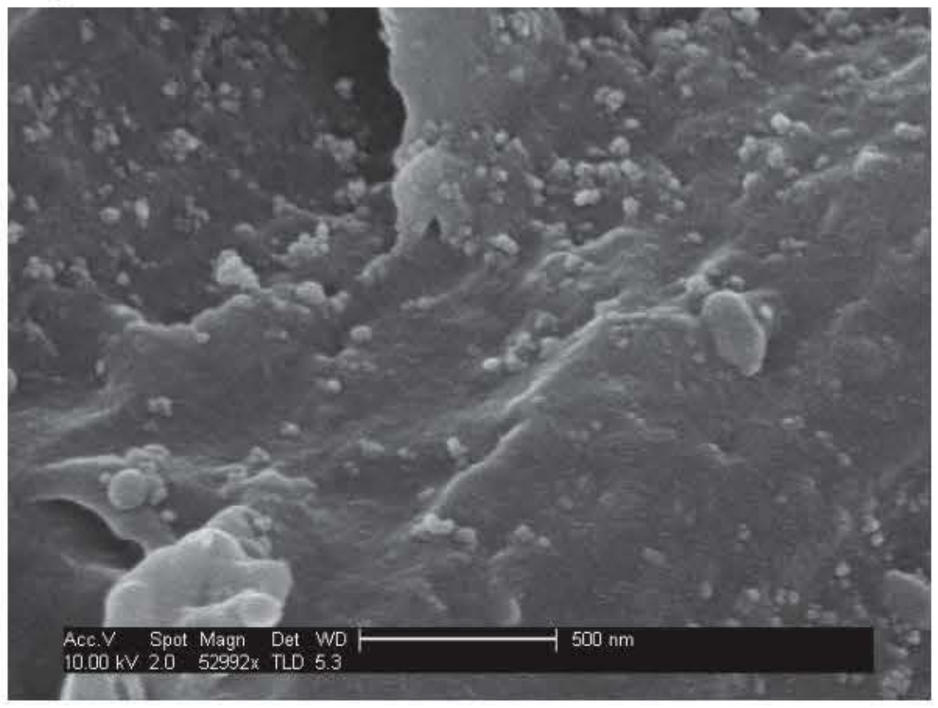

c.)

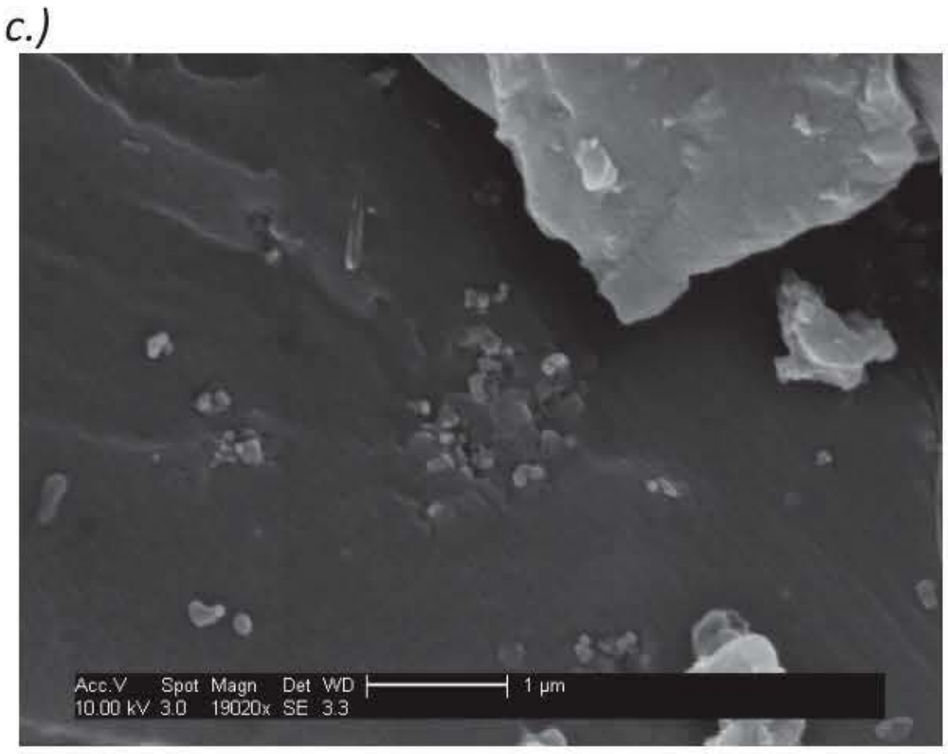

Figure 25: SEM images of the surfaces of manufactured samples a.) neat PE, b.) PE/Al_2O_3 2% c.) PE/SiO_2 2%.

The samples demonstrated in Figure 25 exhibit the introduction of the nanofillers on the surfaces of the PE-based materials carried out at SIRENA collaboration partners Cranfield University. The particles can be seen to be dispersed within the manufactured nanocomposites. A higher magnification of the PE/Al_2O_3 shows the particles in a better resolution than the PE/SiO_2 sample. The embedding of the particles show a clear surface morphology transformation. Nanoparticles can be identified on the

surface of the turns of every PE based samples. A smoother surface without any of the filler/matrix structures is observed. Although agglomerates of the fillers are distinguishable, the materials can be seen to have a good filler dispersion within the polyester matrix and correlate to similar surface changes observed in other studies (Allahverdi et al., 2012; Chen et al., 2005).

Epoxy Based Samples and Fillers

The epoxy-based composites and nanofillers used to reinforce the matrix are characterised using SEM and EDX. The SEM of CNT and CNF fillers is shown in Figure 26.

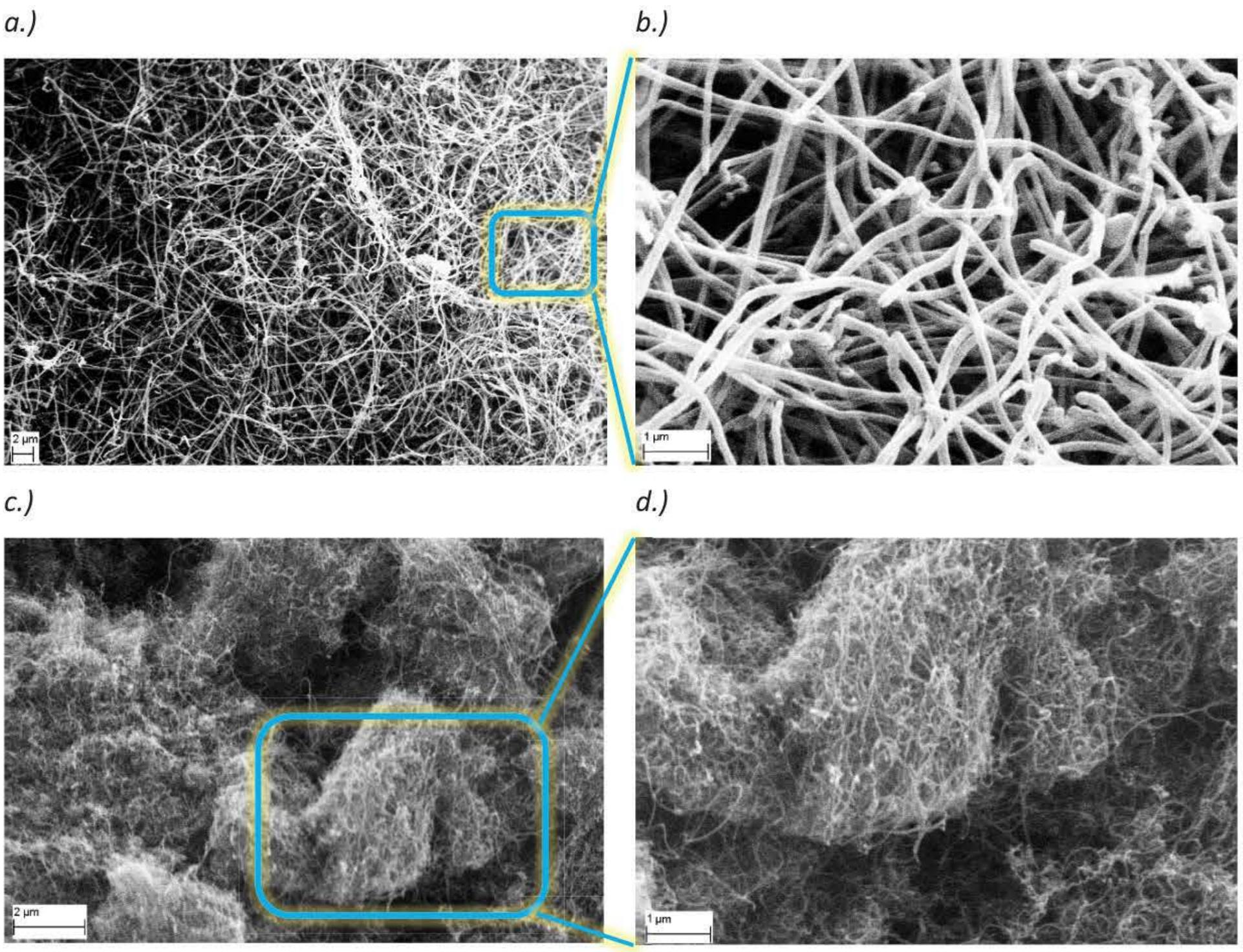

Figure 26: SEM images taken using Zeiss EVO LS10 of nanofillers used within EP-based samples. Images demonstrate two magnifications of the a.) and b.) CNF filler and c.) and d.) CNT filler.

The CNF particles clearly demonstrate their discontinuous fibrous structure in Figure 26 (a+b). The magnification of the fibres shows an average diameter of around 100 nm. The comparison of the CNFs to CNTs (Figure 26c and 26d) can be seen with some of the images being at the same magnification, and emphasising the dissimilarity in diameter of the fibres and tubes. At the resolution available and an average diameter between 10 nm to 15 nm, the CNTs are significantly smaller than the CNFs. The CNTs can also be seen to agglomerate more than the CNFs. Big clusters of the CNTs are observable in

Figure 26d. The structure and size of the particles correlate to similar studies on CNFs and CNTs (Kim et al., 2006; Zhuo et al., 2008; Gojny et al., 2004).

As with the other nanofillers, EDX analysis was carried out on the CNFs and is illustrated in Figure 27. Due to the resolution required on the SEM for EDX, the image is at a different magnitude to Figure 26.

a.)

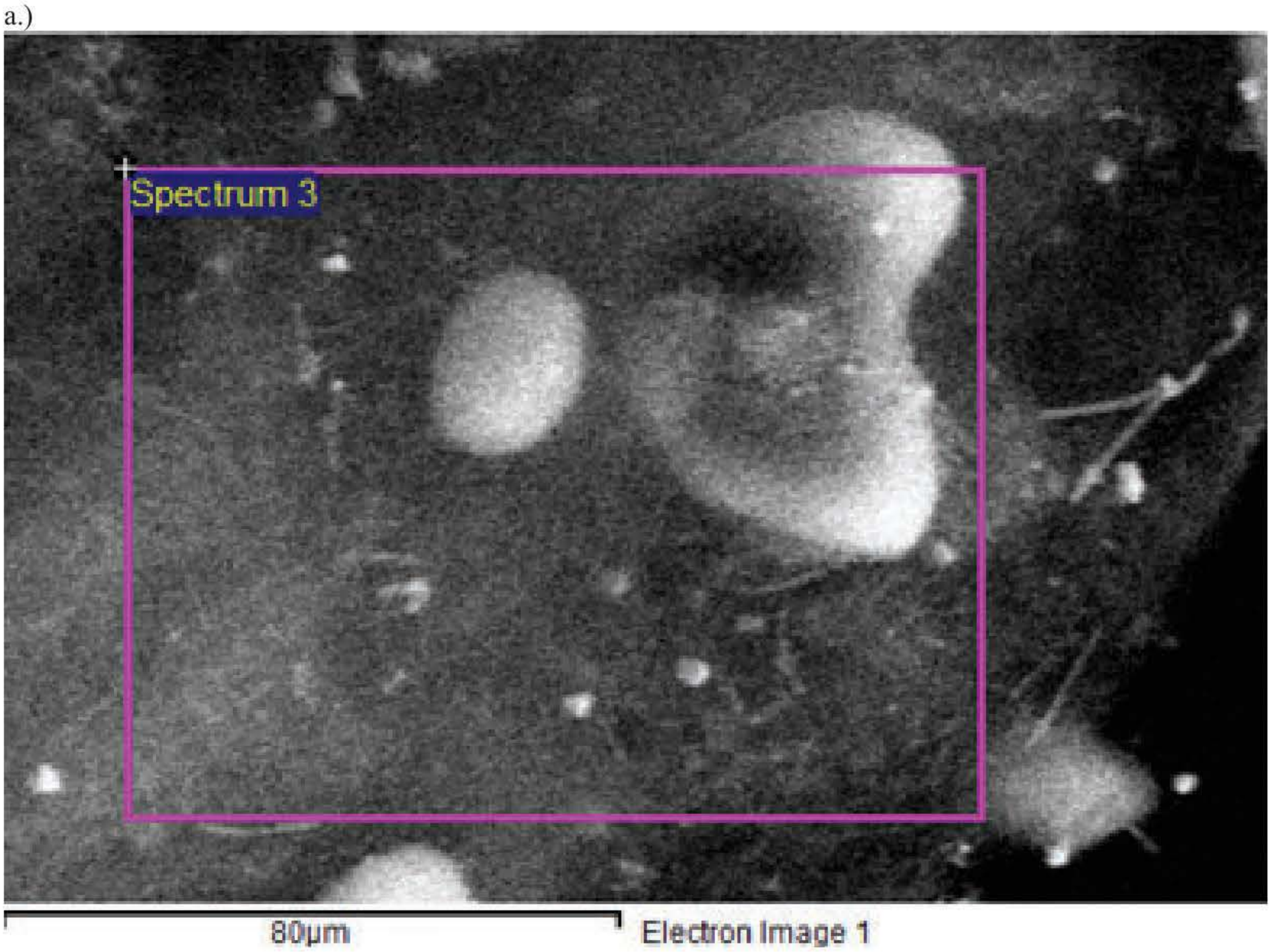

b.)

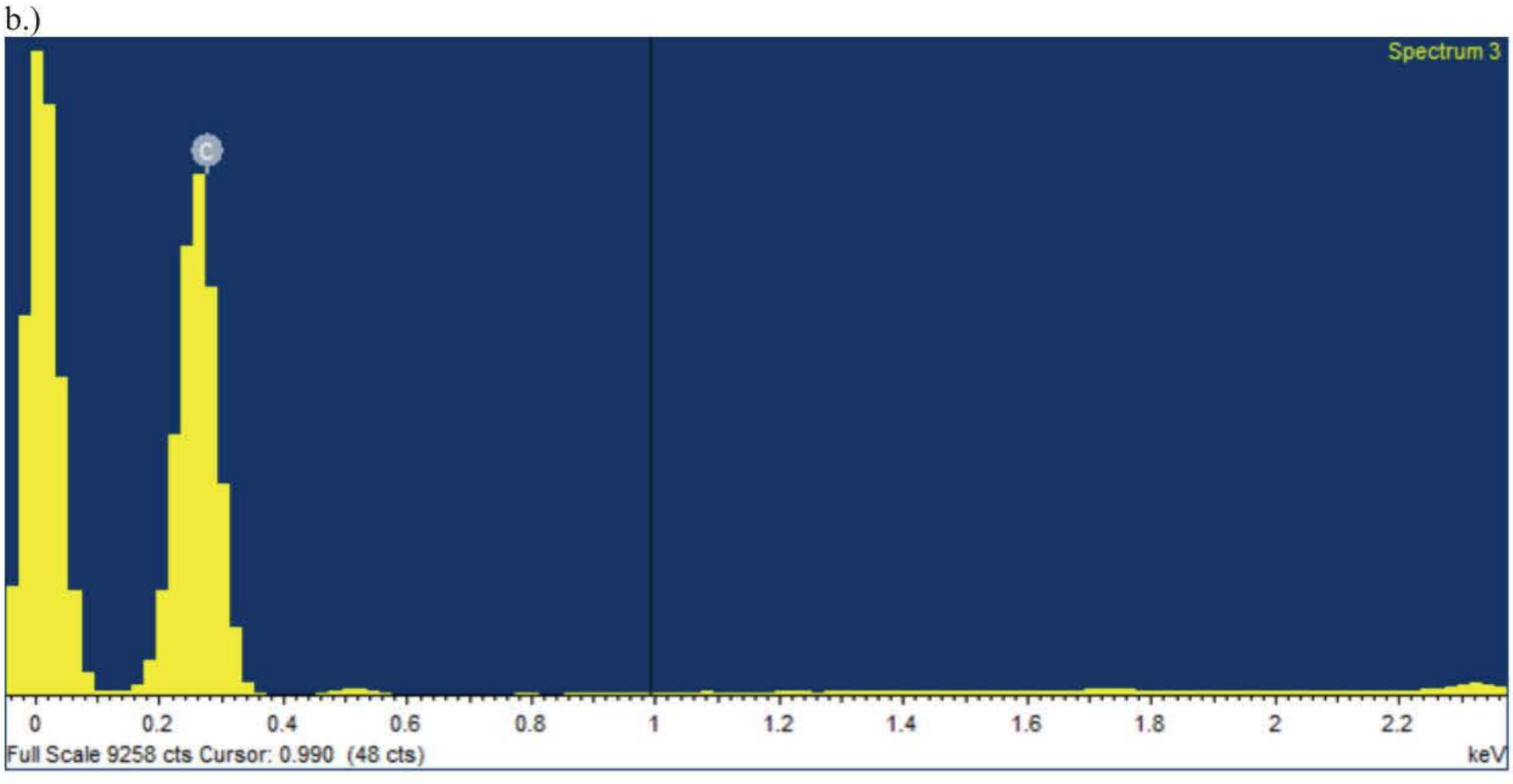

Figure 27: SEM image using Zeiss EVO LS10 of (a.) representing the location of EDX analysis (b.) of CNFs used to reinforce EP-based samples.

The EDX analysis of the CNFs confirm the composition of the fibres to be entirely out of C. The atomic concentration is therefore, 100 wt. % C. Figure 28 illustrates an EDX analysis on the CNTs.

a.)

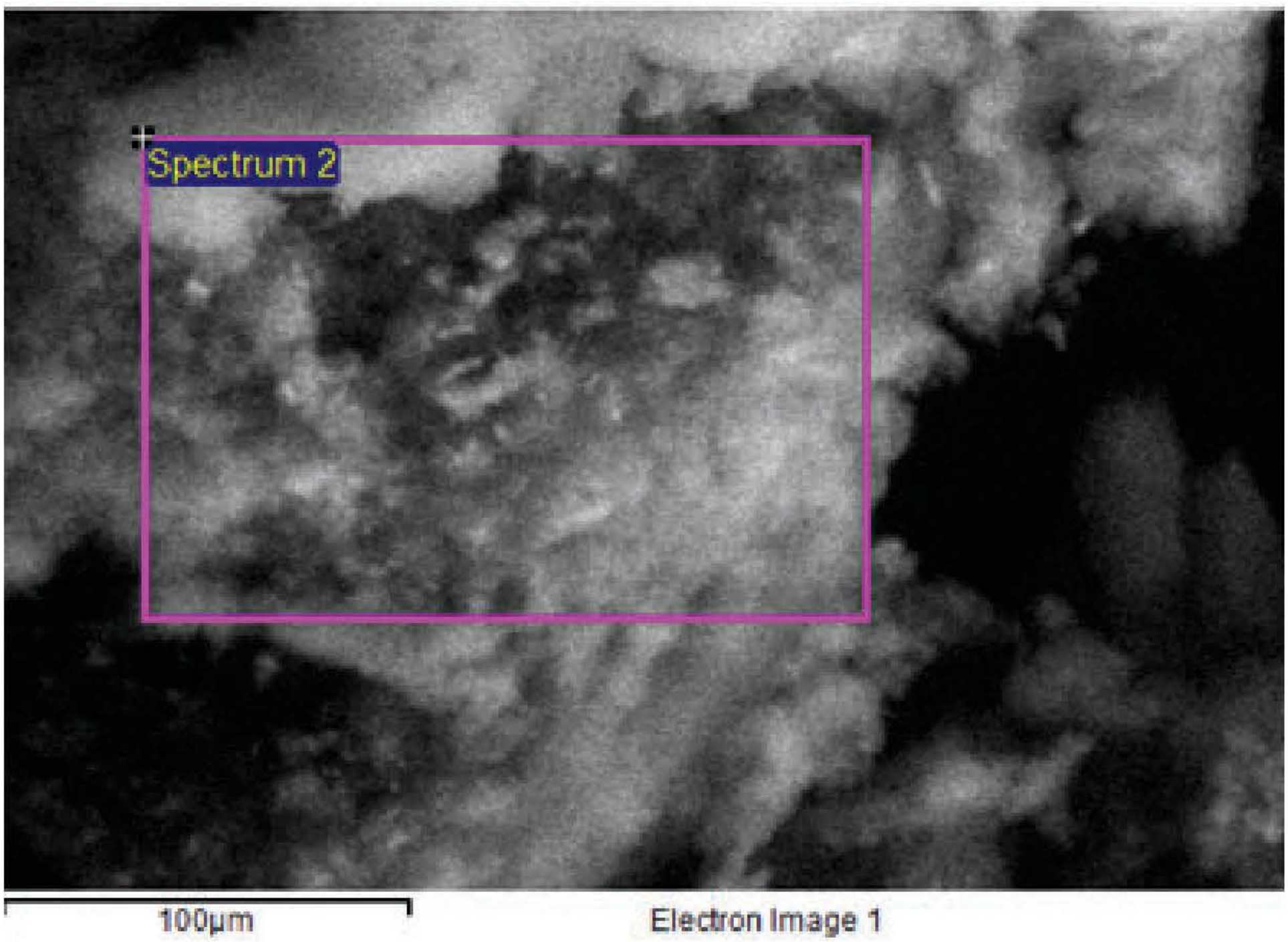

b.)

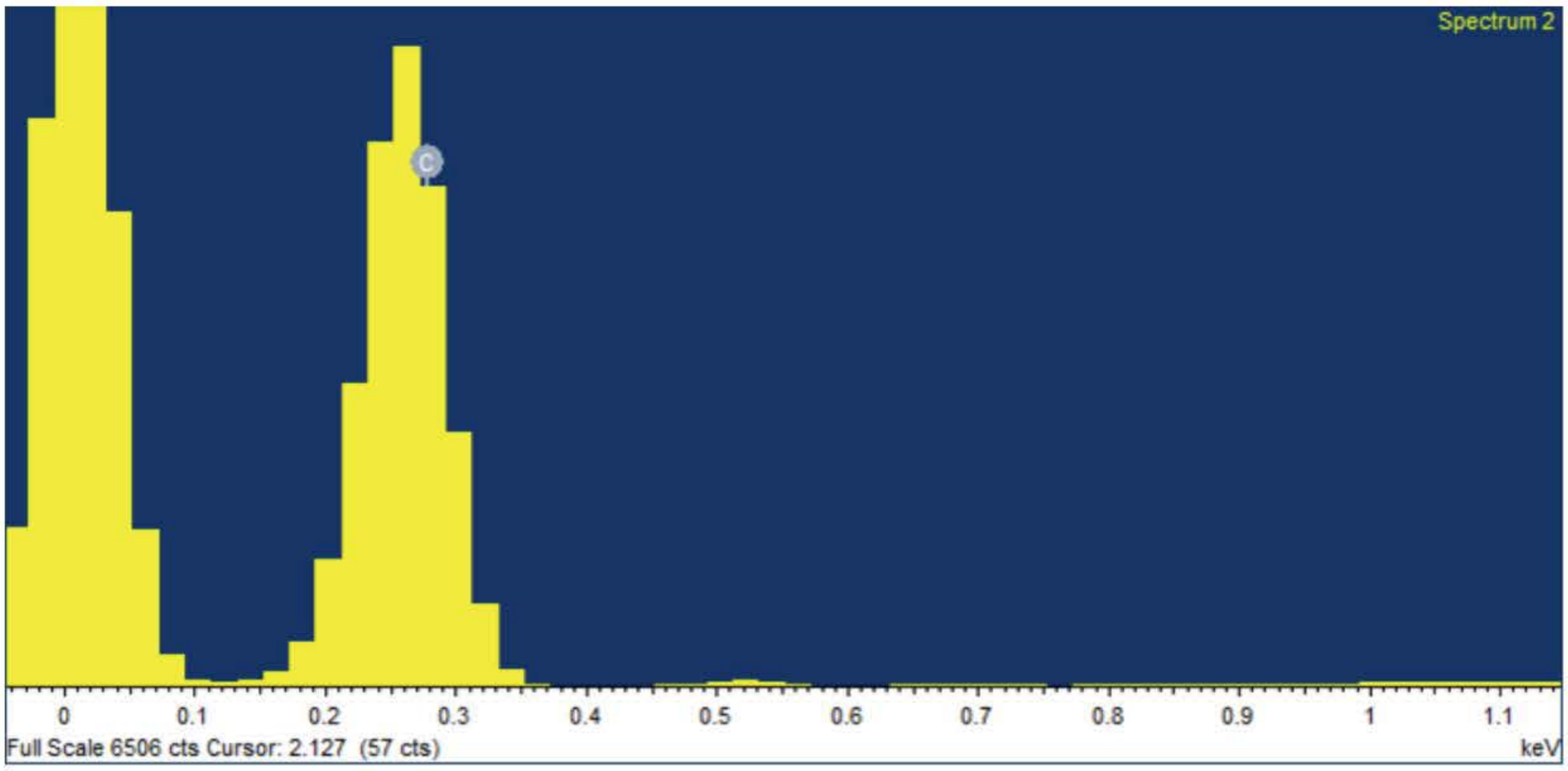

Figure 28: SEM image using Zeiss EVO LS10 of (a.) representing the location of EDX analysis (b.) of CNTs used to reinforce EP-based samples.

Similar to the CNF characterisation through EDX analysis, the CNTs demonstrated to be entirely composed of C. The atomic concentration is also given as 100 wt. % C.

Correspondingly, SEM analysis was carried out at SIRENA collaboration partners Cranfield University on the manufactured EP-based sampled, demonstrated in Figure 29.

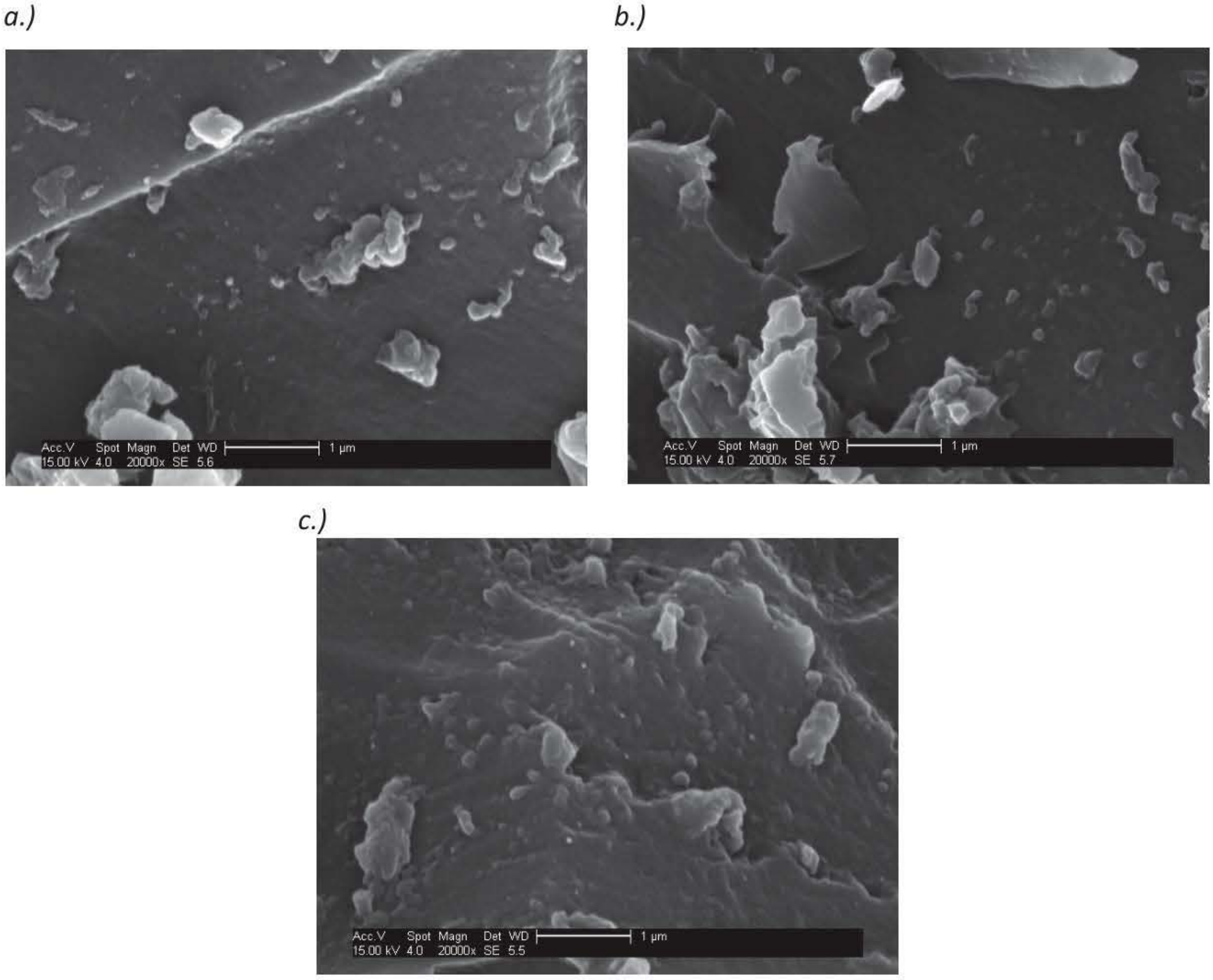

Figure 29: SEM images using FEI Quanta 200F of the surfaces of manufactured samples a.) neat EP, b.) EP/CNF 2% c.) EP/CNT 2%.

From the manufactured samples illustrated in Figure 29, nanoparticles and nanoparticle agglomerates can be noticed on the surfaces of all three EP-based samples. The SEM analysis was unable to identify the CNTs and CNFs on the surface of the materials. However, the surface morphology can be seen to have altered, with the introduction of the fillers. The fillers can be seen to have more particle agglomerates on the surface. The reinforced samples show particles visible on the surface to have more rugged edges and causing additional layers to the surface of the material.

Epoxy Carbon Fibre Based Samples and Filler

The EP reinforced with conventional micro-sized carbon fibre and GO composites and fillers used to reinforce the matrix are characterised using SEM and EDX. The SEM of GO filler is shown in Figure 30.

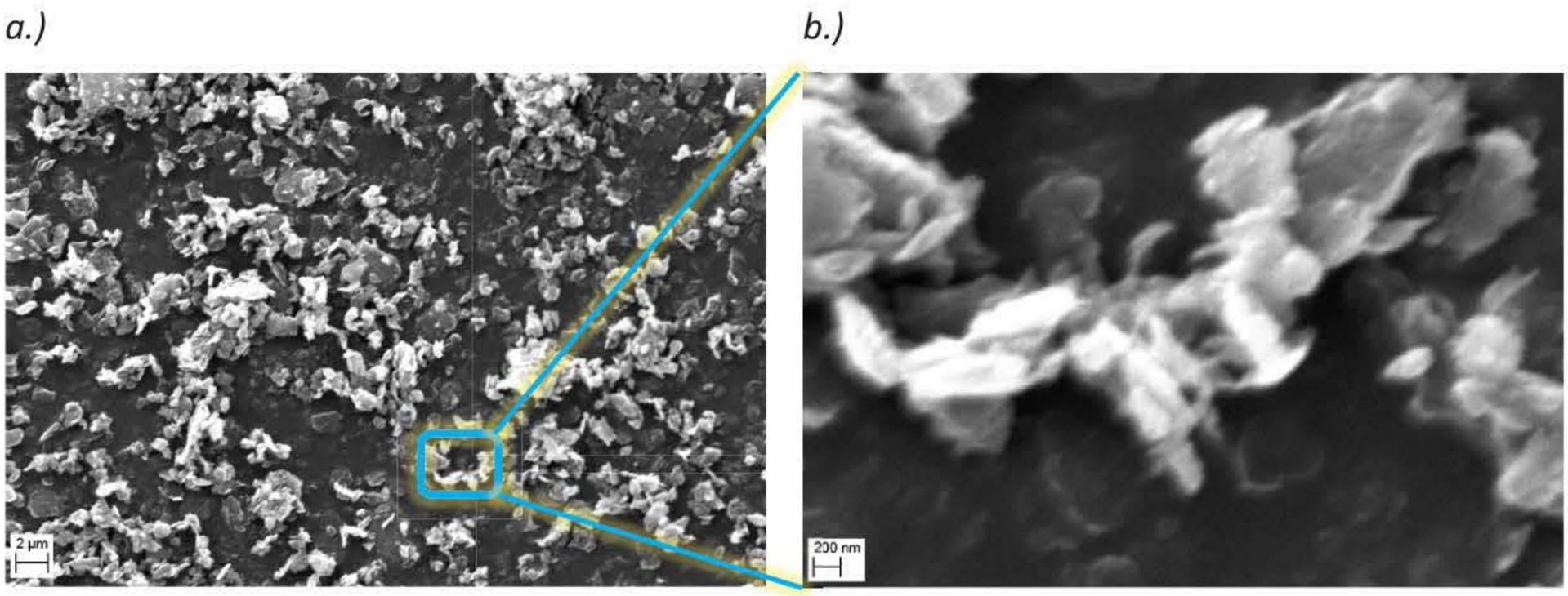

Figure 30: SEM images taken using Zeiss EVO LS10 of GO nanofiller used within EP/CF-based samples. Images demonstrate GO at a.) 6 kx and b.) 50 kx magnifications.

The GO fillers demonstrate the platelets and flake form expected with nano-range thicknesses. Agglomerations and different thicknesses are observed in Figure 30, showing individual platelets, or multiple agglomerated together. The particles are synthesised to have 15-20 layers thick, and therefore can be seen to have thicknesses of less than 200 nm as shown in Figure 30b. The limited resolution is unable to confirm particles with smaller dimensions, however Figure 30b does shown several separate platelets with a thickness clearly visibly lower than the 200 nm scale. The image correlates to studies on the use of GO particles (Zhu et al., 2010; Wan et al., 2014).

As with the other nanofillers, EDX analysis was carried out on the GO filler and is illustrated in Figure 31. The EDX analysis of the GO confirms the composition of the filler to have a composition of C and O. The atomic concentration demonstrated, 94.6 wt. % C and 5.40 wt. % O. Although the concentration is far smaller than that of C, the identification of O within the elements, relate to the reactive oxygen functional groups within GO that will render it a good candidate bond with the EP matrix (Dreyer et al., 2009). As expected, therefore, a majority presence of C was recognised in the elemental EDX analysis.

a.)

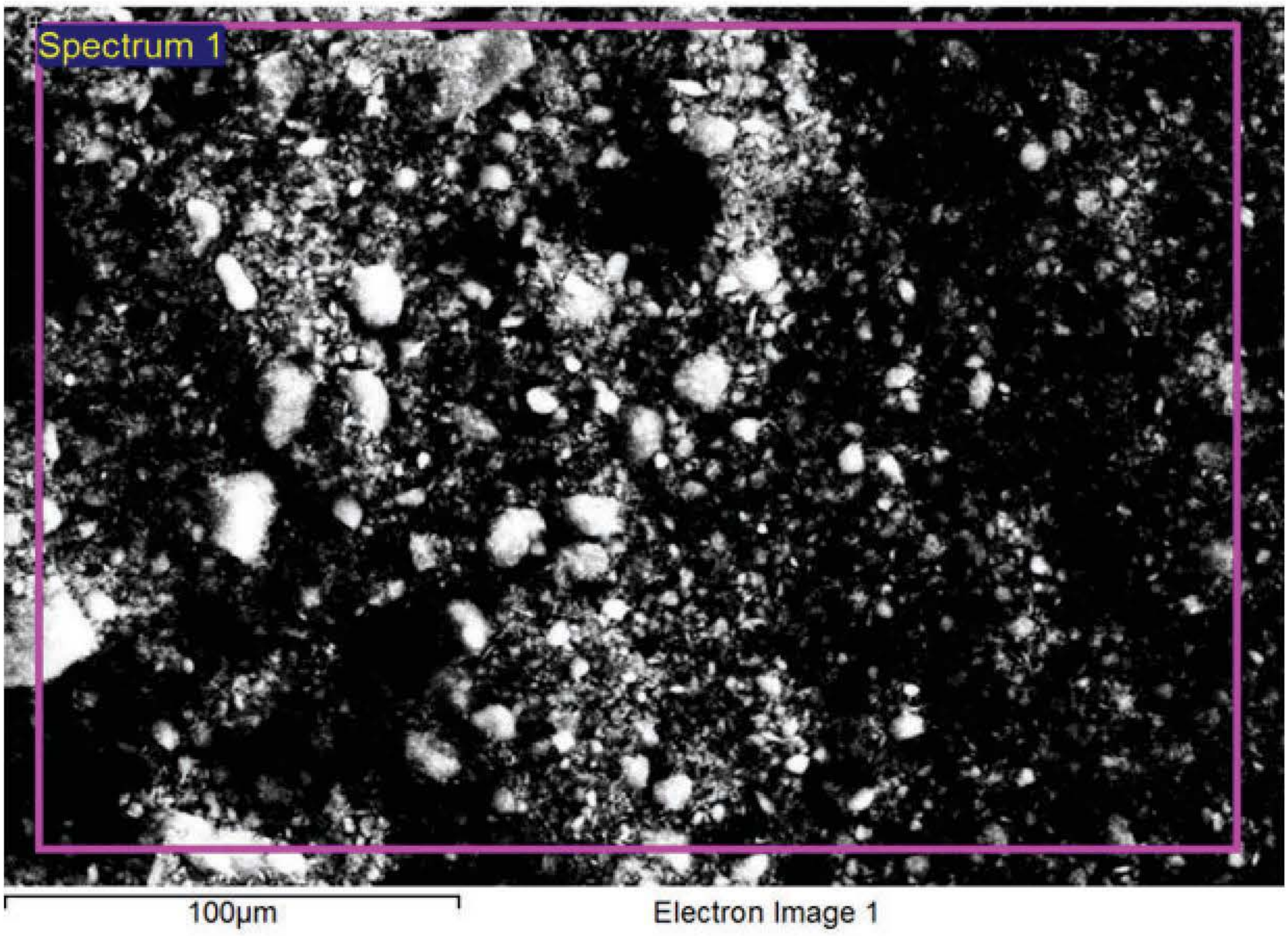

b.)

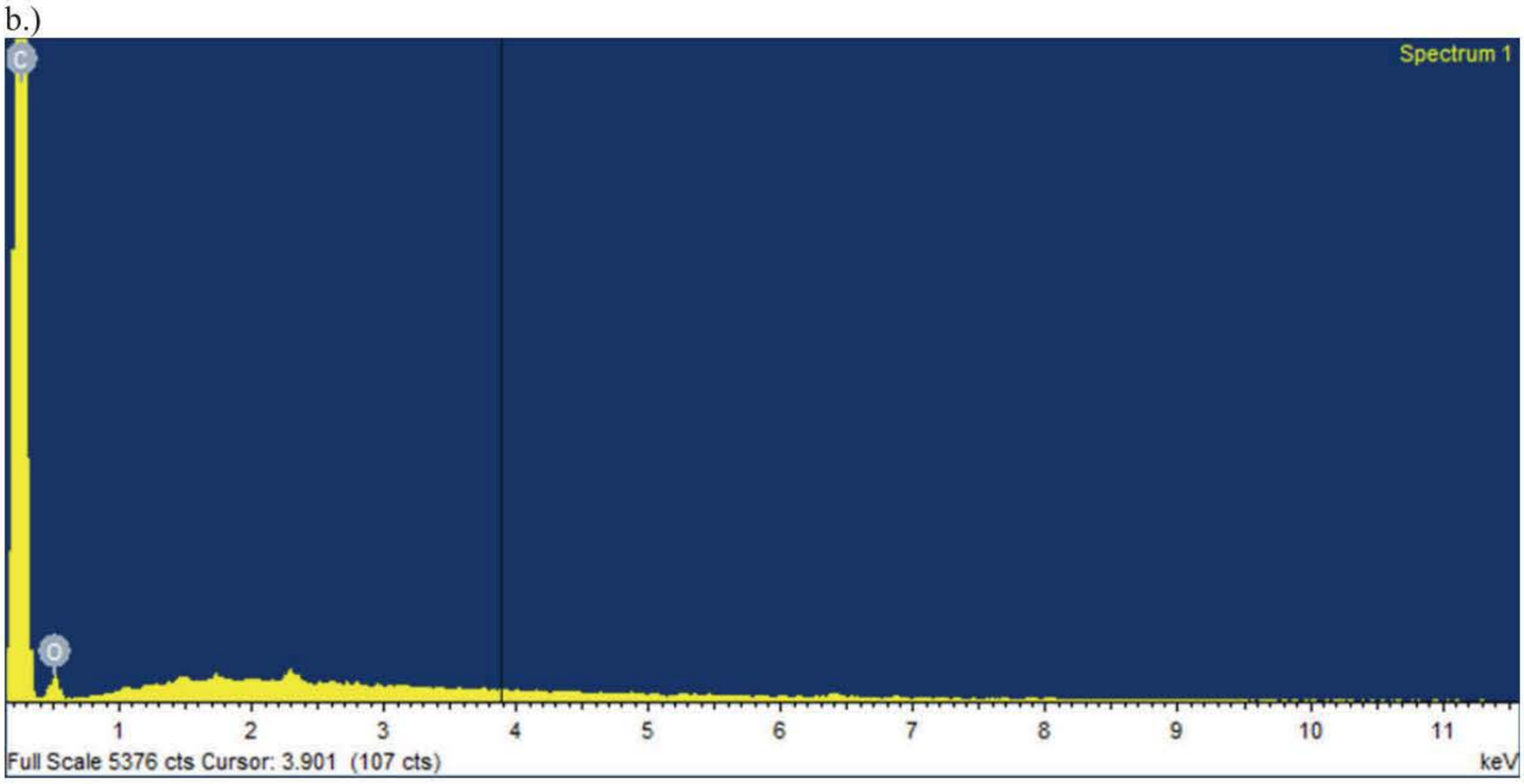

Figure 31: SEM image using Zeiss EVO LS10 of (a.) representing the location of EDX analysis (b.) of GO used to reinforce EP/CF-based samples.

Correspondingly, SEM analysis was carried out on the manufactured EP/CF-based samples, demonstrated in Figure 32.

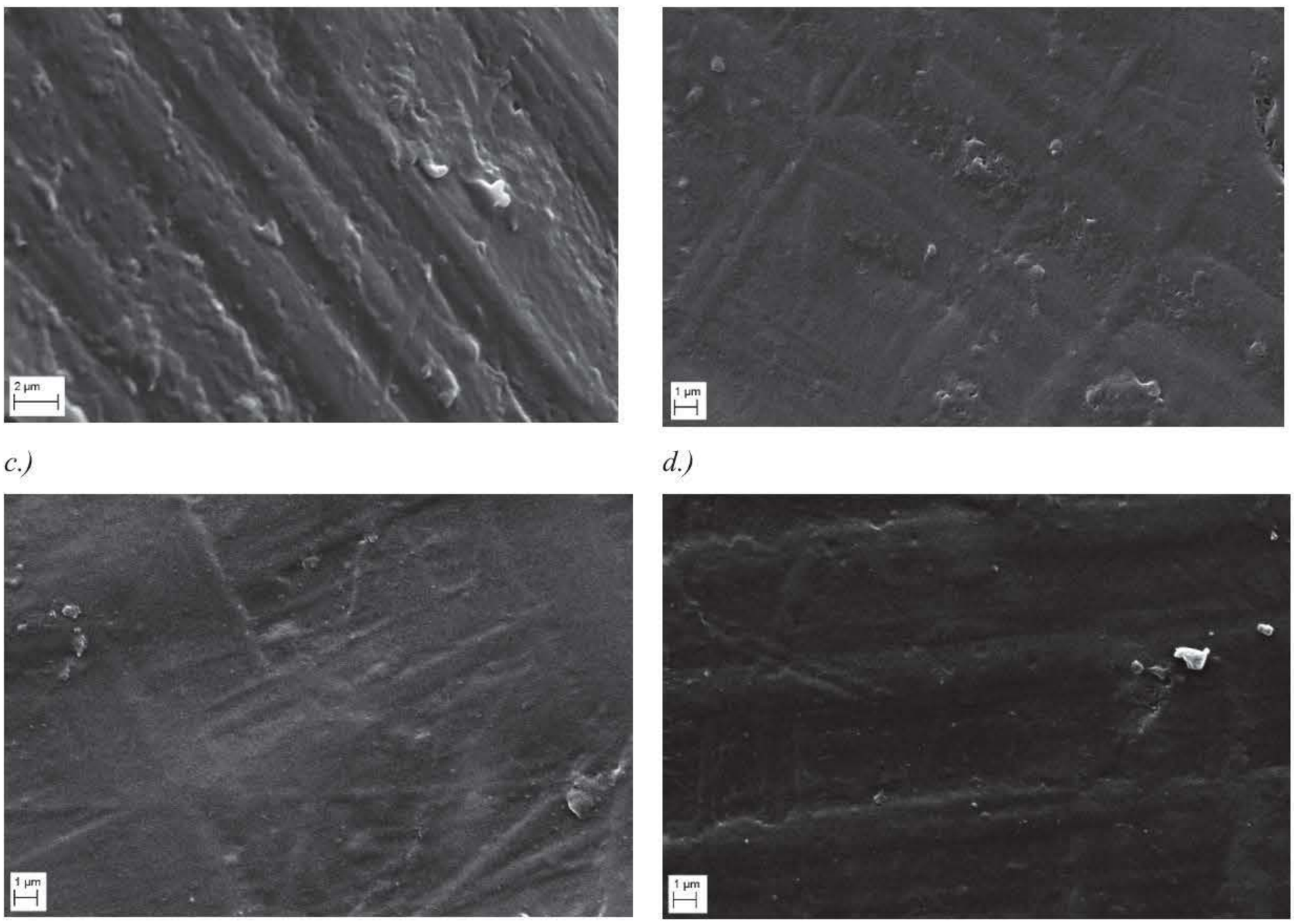

Figure 32: SEM images taken using Zeiss EVO LS10 of the surfaces of manufactured samples a.) neat EP/CF, b.) EP/CF/GO 0.05 wt.% c.) EP/CF/GO 0.1 wt.% and d.) EP/CF/GO 0.5 wt.%.

The microscopy on the surfaces demonstrate a clear change in surface morphology with the introduction of GO as a filler. In all images, the outline of the micron-sized carbon fibres are noticeably visible. With the magnification being quite significant, the images demonstrate the weave of the fibres in one direction. However, the EP/CF/GO 0.1 wt. % and EP/CF/GO 0.5 wt. % show several fibres out of the 90/90 twill weave. Several particles appearing as lumps are observable in all four samples. This is expected to be the EP matrix as it is seen in all four samples. The GO can be seen to create a smoother surface on the material, but individual GO particles and higher concentrations of GO particles are not evident in the images. This is again, due to the low weight concentration and the lack of identification of individual particles and change in surface is a common observation within literature (Shen et al., 2013; Wan et al., 2014).

3.3.2. FT-IR study

FT-IR analysis was also carried out on the samples to evaluate the differences with in incorporated nanofillers, as demonstrated for the PP-based samples in Figure 33.

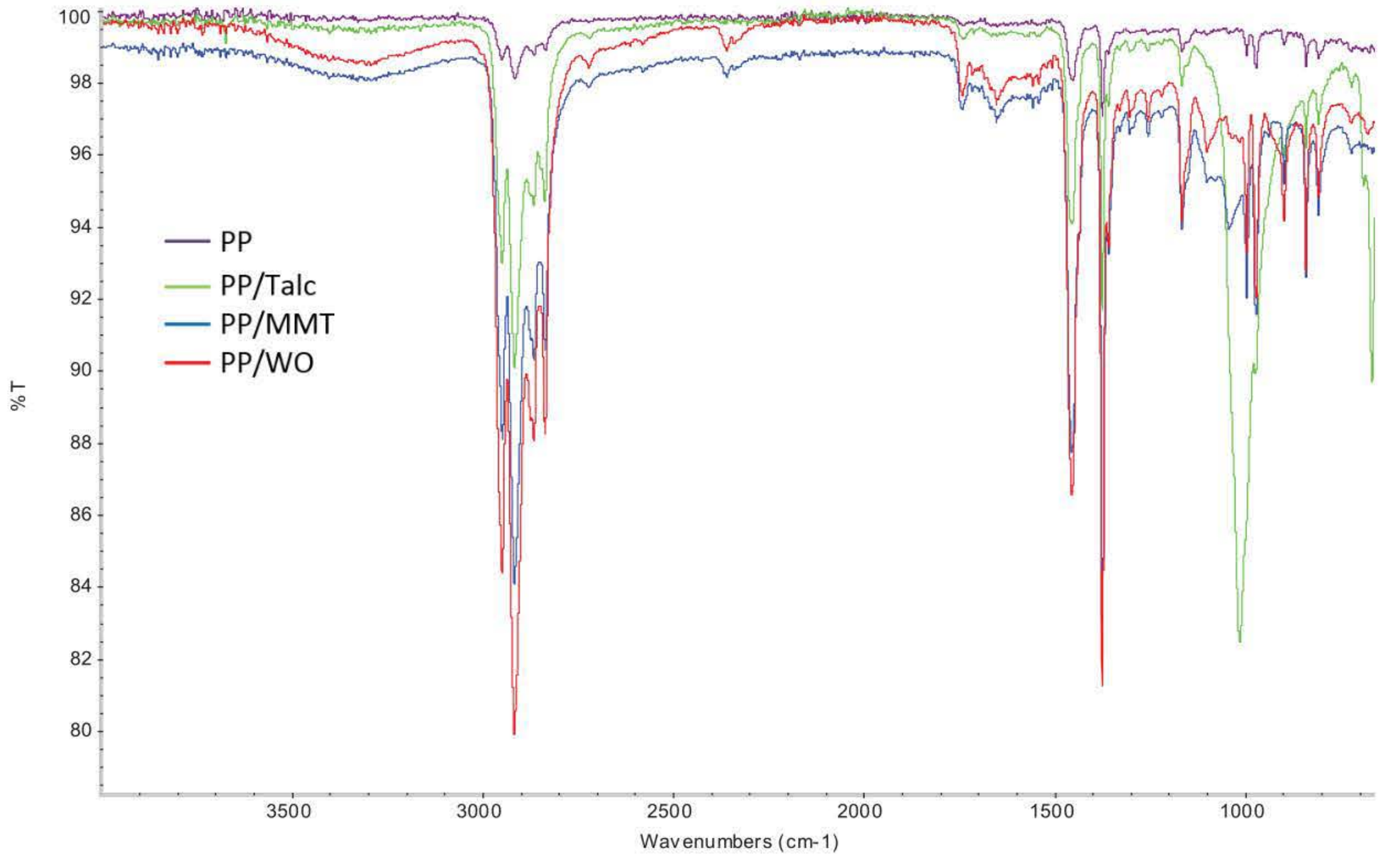

Figure 33: FT-IR spectrum analysis of manufactured PP based samples.

The introduction of the fillers can be seen to introduce new peaks into the FT-IR analysis compared to the neat PP sample. The similar wavelengths and largest peaks of all four samples depicts the PP, C_3H_6, molecule chain of carbon bonds in forms of a CH_3 asymmetric stretch, CH_3 asymmetric bend and CH_3 symmetric bend at approximately 2900cm^{-1}, 1460 cm^{-1} and 1370 cm^{-1} respectively (Paluszkiewicz et al., 2011). The chemical changes can then be distinguished and confirm the presence of the fillers with peaks introduced between 600 cm^{-1} to 1100 cm^{-1} for the PP/Talc, PP/WO and PP/MMT samples, such as the high peaks observed at approximately 1000 cm^{-1} assigned to CaO stretch, 950 cm^{-1} attributed to an Si-O stretch, and bending vibrations of Si–O bands at around 700 cm^{-1} (Beheri et al., 2013). Conversely, the small weight concentration of fillers show obscurity to differentiate between the fillers.

FT-IR analysis, illustrated in Figure 34, was carried out on the samples to obtain the infrared spectrum of absorption to characterise the PE-based materials.

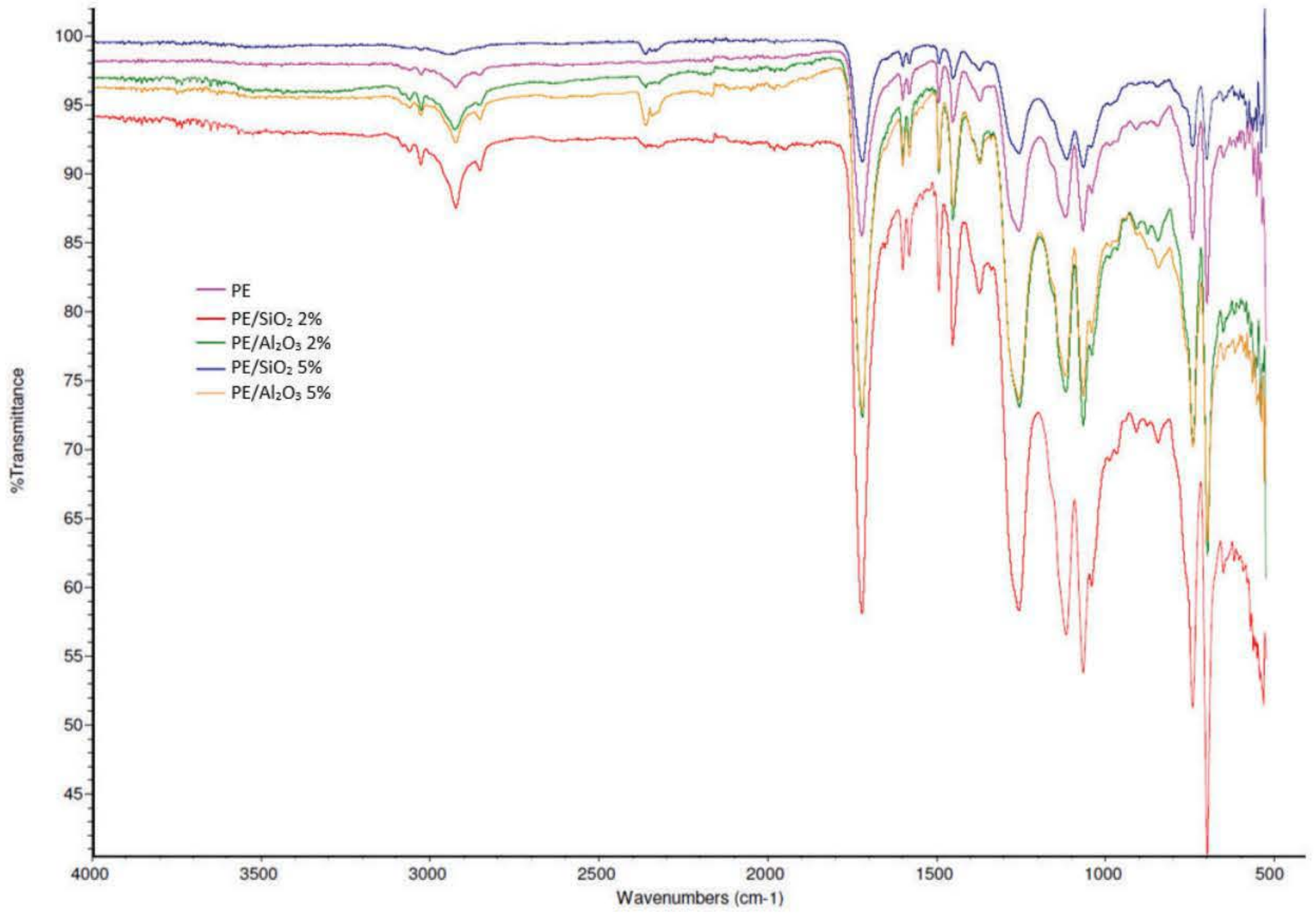

Figure 34*:* FT-IR spectrum analysis of manufactured PE based samples.

The use of the fillers and concentrations can be seen to have few differences on the FT-IR spectroscopy represented in Figure 34. All samples introduced numerous peaks below 1720cm^{-1} representing, as observed in literature, the spectrum of PE based materials (*Gubbels et al., 2013*). A peak at 1720 cm^{-1} is generally attributed to the formation of ester bonds characteristic for the C=O stretching vibrations. Peaks at 1448 cm^{-1} and 1380 cm^{-1} are assigned to CH_3 asymmetrical and CH_3 symmetrical bending vibrations respectively, whilst an aliphatic C-H stretch is observed at around 2900 cm^{-1} in polyester (Zhao et al., 2007). The only observable difference with the introduction of the reinforcements is a peak at 2360 cm^{-1}, which is a CO_2 asymmetric bond-stretching peak and normally attributed to the lab air and not the material samples, however, it has been reported as a characteristic peak of Al_2O_3 (Baskaran et al., 2011). The difference in peak sizes is due to the transmittance intensity. From the FT-IR analysis therefore, the spectra are unable to show the presence or difference between the samples, also likely due to the low weight concentrations.

FT-IR analysis, illustrated in Figure 35, was carried out on the samples to obtain the infrared spectrum of absorption to characterise the EP-based materials.

a.)

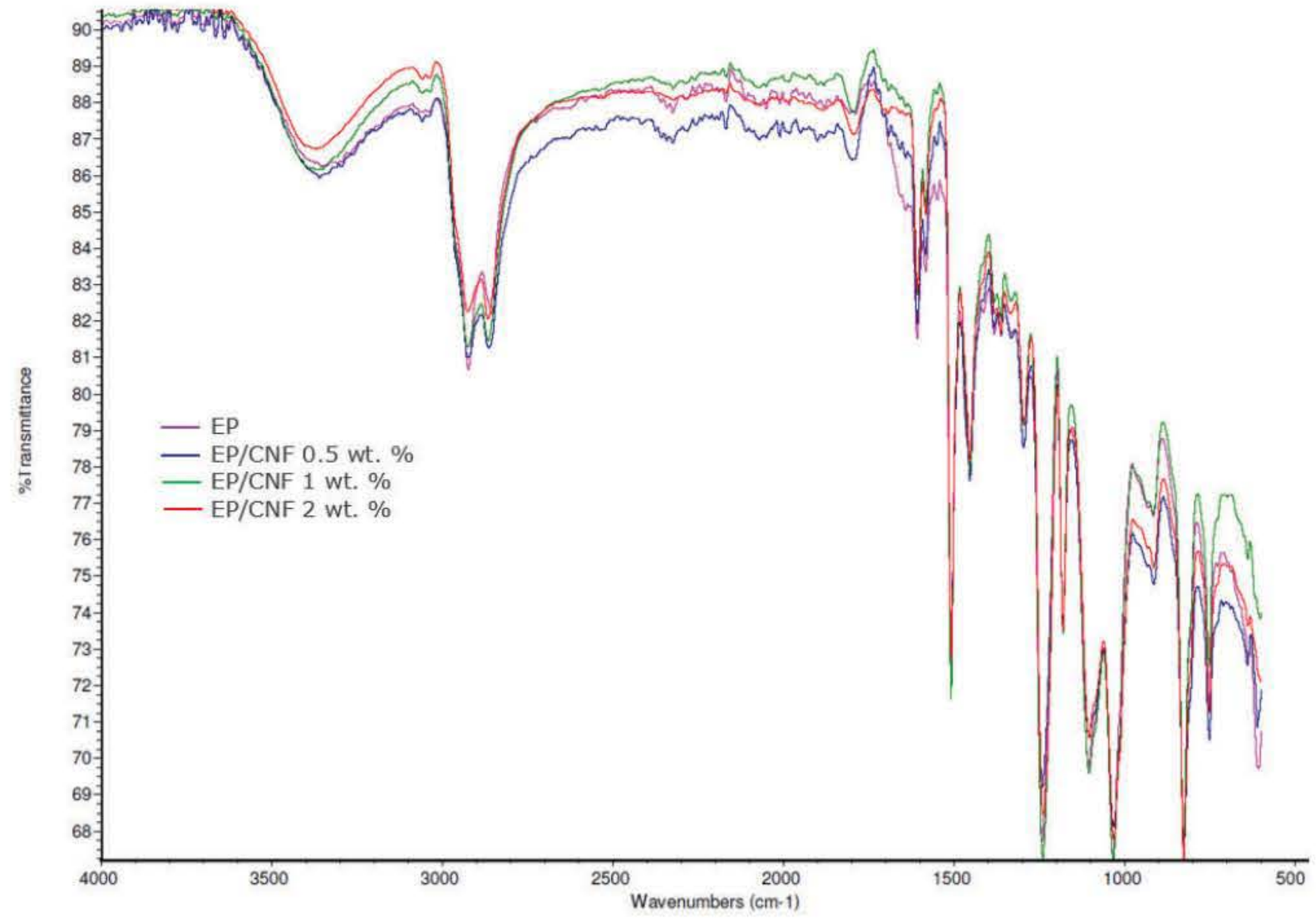

b.)

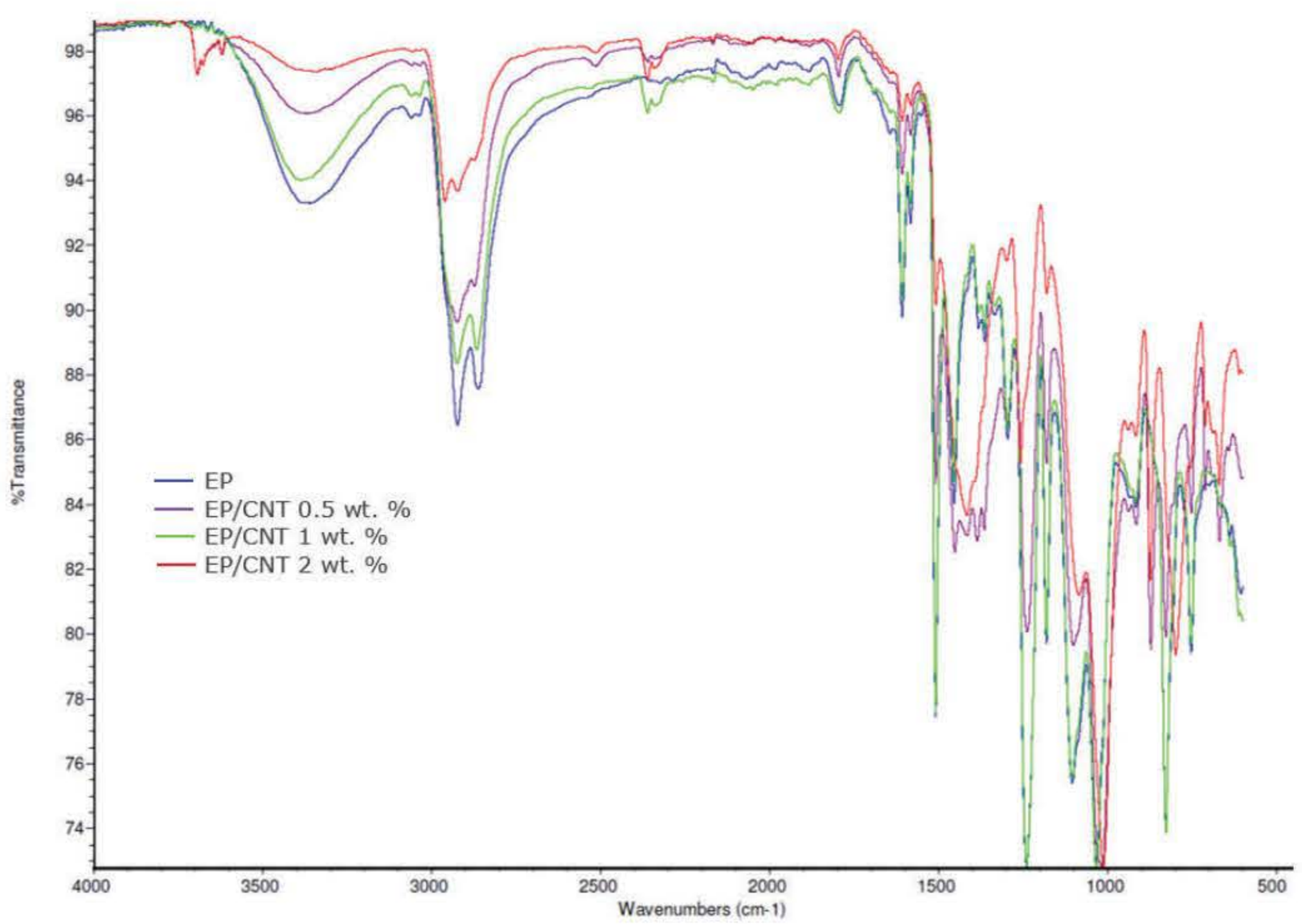

Figure 35*:* FT-IR spectrum analysis of manufactured EP based samples reinforced with a.) CNF filler and b.) CNT filler.

The introduction of the CNT and CNF fillers in the samples observed minimal influence on the FT-IR spectra. The intensity of the peaks observed to change, but the fillers do not appear to influence the spectra. As expected with epoxies, C–H stretching peaks at 1460 cm^{-1} and 1300 cm^{-1} are assigned to CH_3 asymmetrical bending and CH_3 symmetrical bending respectively, whilst aliphatic C-H stretch peaks are observed at around 2960 cm^{-1} in EP (May, 2018). A minor peak can be seen in the samples

at 1650 cm^{-1} which can be attributed to Stretching C=C of aromatic rings (May, 2018). A characteristic peak of epoxide rings appears at 829 cm^{-1} (Zheng et al., 2017) and other peaks located at wavelengths lower than 1500cm^{-1} are limited in comparison, however peaks located at 1247 cm^{-1} and 1024 cm^{-1} are assigned to C–O of epoxy groups and C–OH groups respectively (Pathak et al., 2016). The slight peaks observed for all samples around 3400 cm^{-1} originate from the stretching vibrations of –OH (Li et al., 2019). The minor shift in peak at 3600 cm^{-1} observed from the EP/CNT 2 wt. % sample is also attributed to stretching vibrations of –OH (Cui et al., 2013). Therefore, similar with the PP-based samples, the FT-IR analysis is unable to show the significant peak changes due to the low weight concentrations of the fillers.

FT-IR spectroscopy analysis, illustrated in Figure 36, was carried out on the samples to obtain the infrared spectrum of absorption to characterise the EP/CF-based materials.

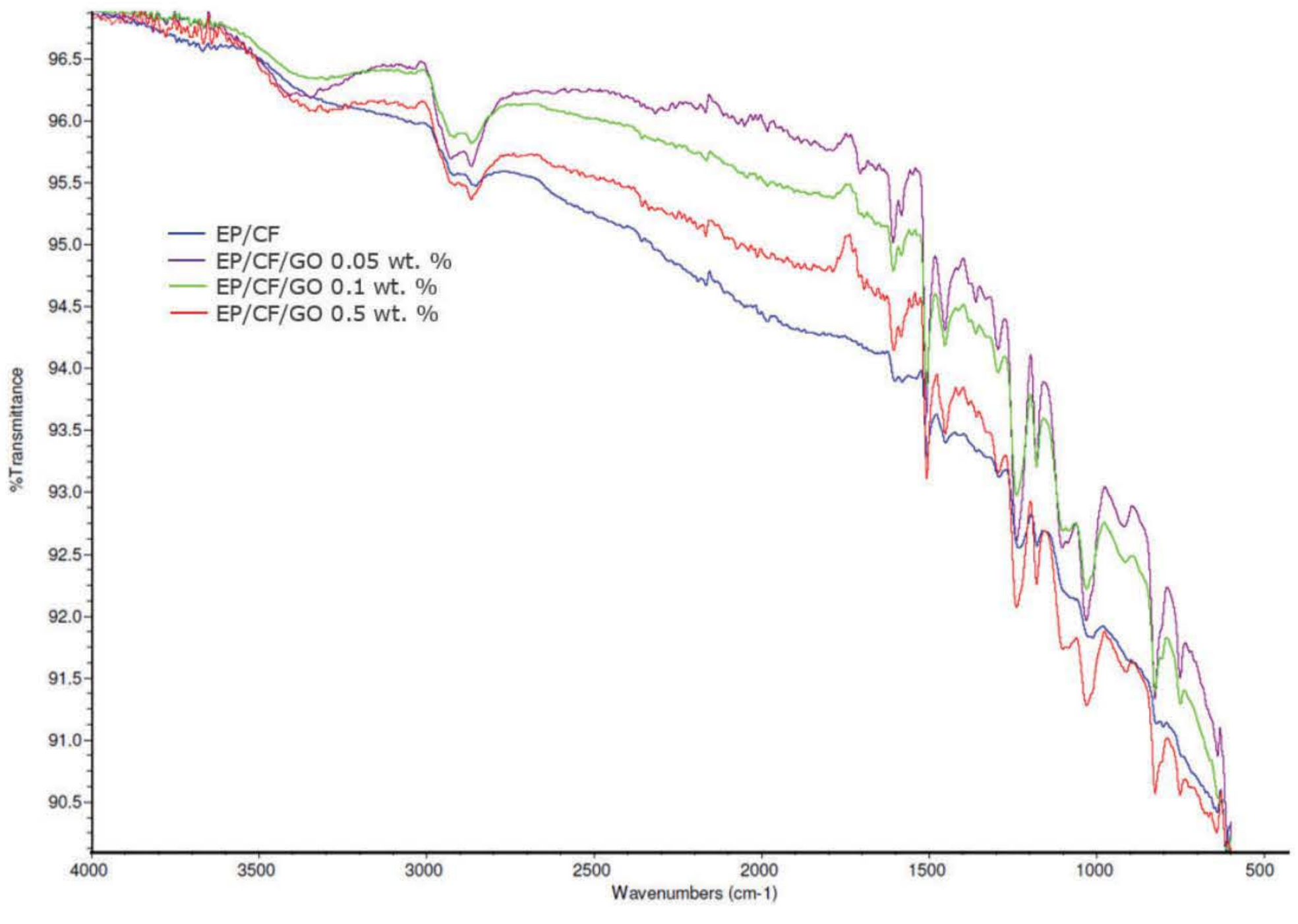

Figure 36: FT-IR spectrum analysis of manufactured EP/CF based samples reinforced with GO (EP/CF, EP/CF/GO 0.05 wt. %, EP/CF/GO 0.1 wt. % and EP/CF/GO 0.5 wt. %).

The incorporation of the GO fillers at different weight concentrations, observed few differences on the FT-IR spectroscopy, as shown in Figure 36. As expected and similar with the epoxies samples without CF, C–H stretching peaks at 1460 cm^{-1} and 1300 cm^{-1} are assigned to CH_3 asymmetrical bending and CH_3 symmetrical bending respectively, whilst aliphatic C-H stretch peaks are observed at

around 2960 cm^{-1} in EP (May, 2018). The slight peaks introduced around 3400 cm^{-1} originate from the stretching vibrations of –OH (Li et al., 2019). Peaks located at wavelengths lower than 1500cm^{-1} are limited in comparison, however peaks located at 1247 cm^{-1} and 1024 cm^{-1} are assigned to C–O of epoxy groups and C–OH groups respectively (Pathak et al., 2016). The most evident difference between the spectra is seen at 1651 cm^{-1} which is attributed to the shifting of carbonyl peak of GO as a result of H-bonding between GO and epoxy (Yang et al., 2013). The embedding of GO can therefore be seen to have a slight change in the spectra in comparison to the EP/CF sample.

3.3.3. Mechanical properties

Following the tensile testing standards of polymer matrix composite materials (ASTM D3039, 2019), the tensile properties of the materials are determined. Similarly, the flexural properties of the materials are determined from the standard for flexural properties of polymer matrix composite materials (ASTM D7264, 2019).

Polypropylene Based Samples and fillers

The averages (n=3) of the stress vs strain plots of the PP-based samples is displayed in Figure 37. The tensile stress vs strain plots of the repetitions on individual PP-based samples is included in Appendix D. The initial clear observation is the consistency in material behaviour from the neat PP samples relative to the reinforced samples. None of the samples observed to fracture and continued to extend. This is observed in the average PP plot, shown in Figure 37, not having any sudden drops in tensile stress. In contrast, the reinforced materials observed some fracture, or crack formation to cause a decrease in tensile stress. The total energy required to therefore fracture the materials, i.e. material toughness, can be seen to decrease with the use of additives as the area under the curve is larger for the neat PP sample due to no fracture point. Furthermore, all samples observed a similar corresponding ultimate tensile stress $\sigma_{Ultimate}$.

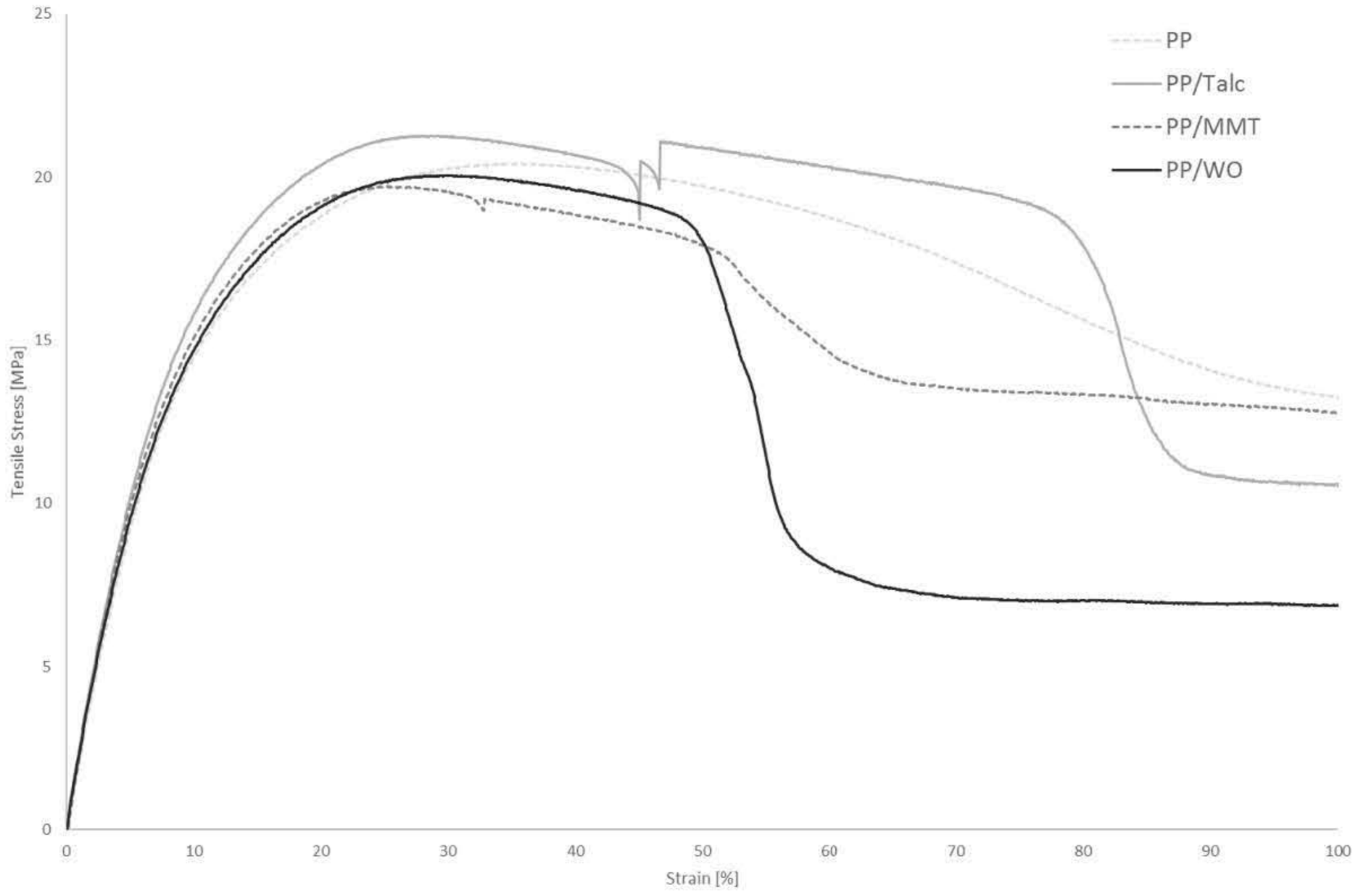

Figure 37: Stress vs strain curve averages from tensile tests on PP, PP/Talc, PP/MMT and PP/WO samples.

As expected with PP being a thermoplastic, the material observed ductile behaviour with a clear yield and plastic region (Shubhra et al., 2013). This is further demonstrated with a high percentage of elongation with strain values up to 100 % without fracture for the neat PP sample. The yield stress is seen to be consistent with all materials and followed closely by the ultimate tensile stress, $\sigma_{Ultimate}$. For this reason, the ultimate tensile stress is presented in the data summary Table 7 without the need of replication with determining the yield stress. Since the average stress vs strain plot will continue if a sample were to fracture and therefore not represent the mean ultimate tensile stress, the bar chart and numerical data presented in in Figure 38 and Table 7 respectively, are an adjusted representation to allow for this. The ultimate tensile strength and Young's modulus are determined and compared in Figure 38.

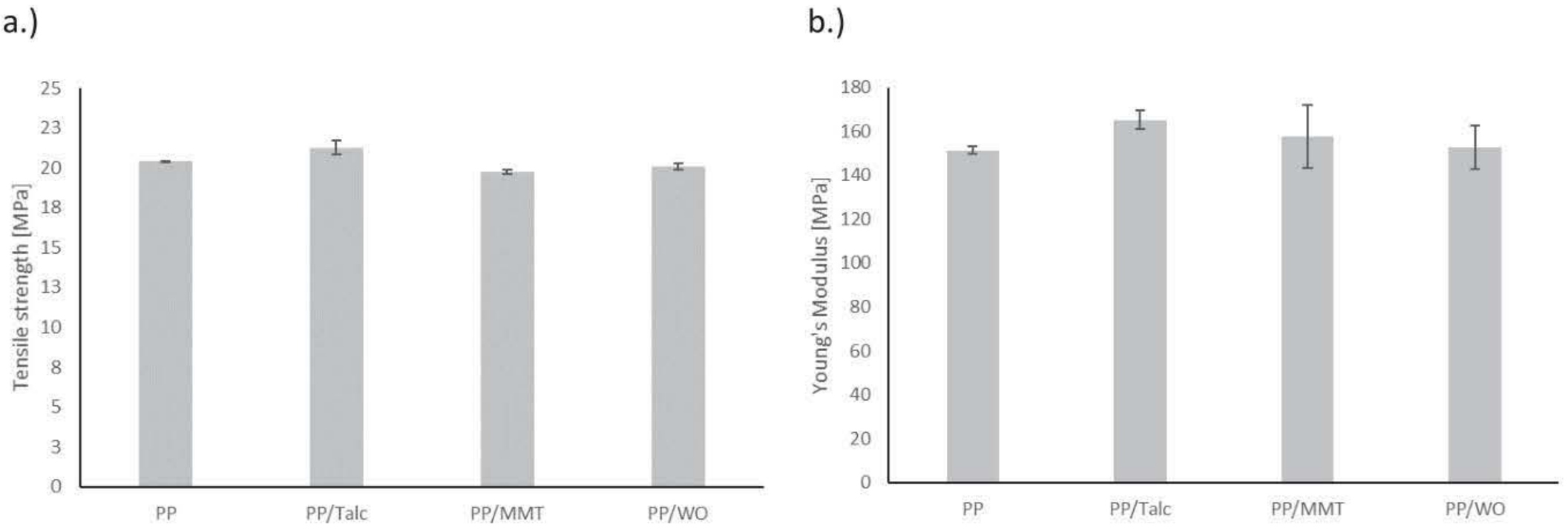

Figure 38: Comparison of mean values of PP-based samples of a.) tensile strength and b.) Young's Modulus

The comparison between the materials shows few differences between samples. The PP/Talc sample observed a marginal increase in tensile strength and Young's Modulus, whilst the PP/MMT and PP/WO observed a slight decrease. As is also highlighted in the numerical values of the tensile test data, represented in Table 7, all of the samples observed a slight increase in mean Young's Modulus but with higher standard deviations between samples. In contrast, the tensile strength only observed an increase for the PP/Talc sample and larger standard deviations between the reinforced samples. Whilst, the incorporation of fillers exhibited a slight effect on the Young's Modulus and tensile strength, the samples demonstrated more inconsistent material performance. This is also highlighted in CV values comparing PP/Talc (e.g. Young's Modulus CV = 22.0 MPa) to PP (Young's Modulus CV = 2.84 MPa).

In order to statistically analysis the effect of the fillers, and as mentioned previously, a t-test can be used to evaluate the two samples with a two samples t-test. This is also known as a two samples test of significance (DeCoursey, 2003). As explained, the samples are assessed by performing a hypothesis test between the two samples to identify if there is a statistically significant difference. If the t-score is not inward of the 90% interval, the sample means are not within the confidence interval and are therefore deemed statistically significantly different to one other. From the t-test between each sample and the PP sample, only the PP/Talc returned a statistically significant different for Young's Modulus ($P = 0.0203$). However, for the tensile strength, only the PP/MMT returned a statistically significant difference ($P = 0.00663$). The materials can therefore be seen to perform in a similar manner in relation to the modulus of elasticity and tensile strength. If the material were to exceed the yield stress and ultimate tensile strength, the reinforced samples would however show a significant decrease in elongation. This is a common phenomenon observed throughout literature (Lapcik et al., 2009; Weon and Sue et al., 2006; Dasari et al., 2004; Yousfi et al., 2013), where the use of fillers within PP has mostly shown to have a negative effect on the elongation. For example, although the use of

talc as a filler within PP has shown to improve tensile strength, it has also revealed to reduce the elongation from a similar 20 % (Yousfi et al., 2013) to a more substantial difference of reduction of 286 % (Weon and Sue, 2006). PP materials however are normally selected on tensile strength and Young's modulus (Shubhra et al., 2013).

Table 7: Summary and comparison of material properties collected from tensile tests on PP-based samples

Sample	Young's Modulus $E_{Young's} \pm s_{n-1}$: [MPa]	Percentage difference compared to PP	Tensile Strength: $\sigma_{Ultimate} \pm s_{n-1}$ [MPa]	Percentage difference compared to PP	Strain at Tensile Strength $\varepsilon_{Tensile}$ at $\sigma_{Ultimate}$	Percentage difference compared to PP
PP	151 ± 1.69	/	20.4 ± 0.043	/	0.35 ± 0.0020	/
PP/Talc	165 ± 4.20	9.13 %	21.3 ± 0.45	4.23 %	0.28 ± 0.0017	-26 %
PP/MMT	158 ± 14.35	4.09 %	19.7 ± 0.14	-3.38 %	0.26 ± 0.015	-19 %
PP/WO	153 ± 9.69	0.89 %	20.1 ± 0.29	-1.75 %	0.29 ± 0.0043	-16 %

When comparing more than two samples, the equality of means can also be tested all at once using analysis of variance F-test. This is a popular approach and is commonly known as the one-way Analysis of Variance (ANOVA). The ANOVA procedure evaluates a null hypothesis that the samples are the same and perform equally (Montgomery, 2001). ANOVA single factor analysis was performed to assess the variability in the Young's Modulus and the tensile strength means. For the Young's Modulus, the analysis returned statistically insignificant differences within the 4 samples (F value = 0.961 F critical value = 4.07) with a 45 % probability and therefore accepting a hypothesis that the samples displayed no difference. In contrast, for the tensile strength, the analysis returned statistically significant differences within the 4 samples (F value = 8.56, F critical value = 4.07) and a 0.7 % chance that the observation could have been observed due to random error alone and therefore rejecting a hypothesis that the samples displayed no difference. This is mainly due to the PP/MMT sample showing statistically significant difference in tensile strength in comparison to the PP sample.

The PP-based samples were also evaluated for flexural material properties. This was carried out with a 3-point flexural test as per the ASTM D7264M standard. The average (n= 3) stress vs strain plots for each PP-based composition is shown in Figure 39. The individual stress vs strain plots are presented in Appendix D.

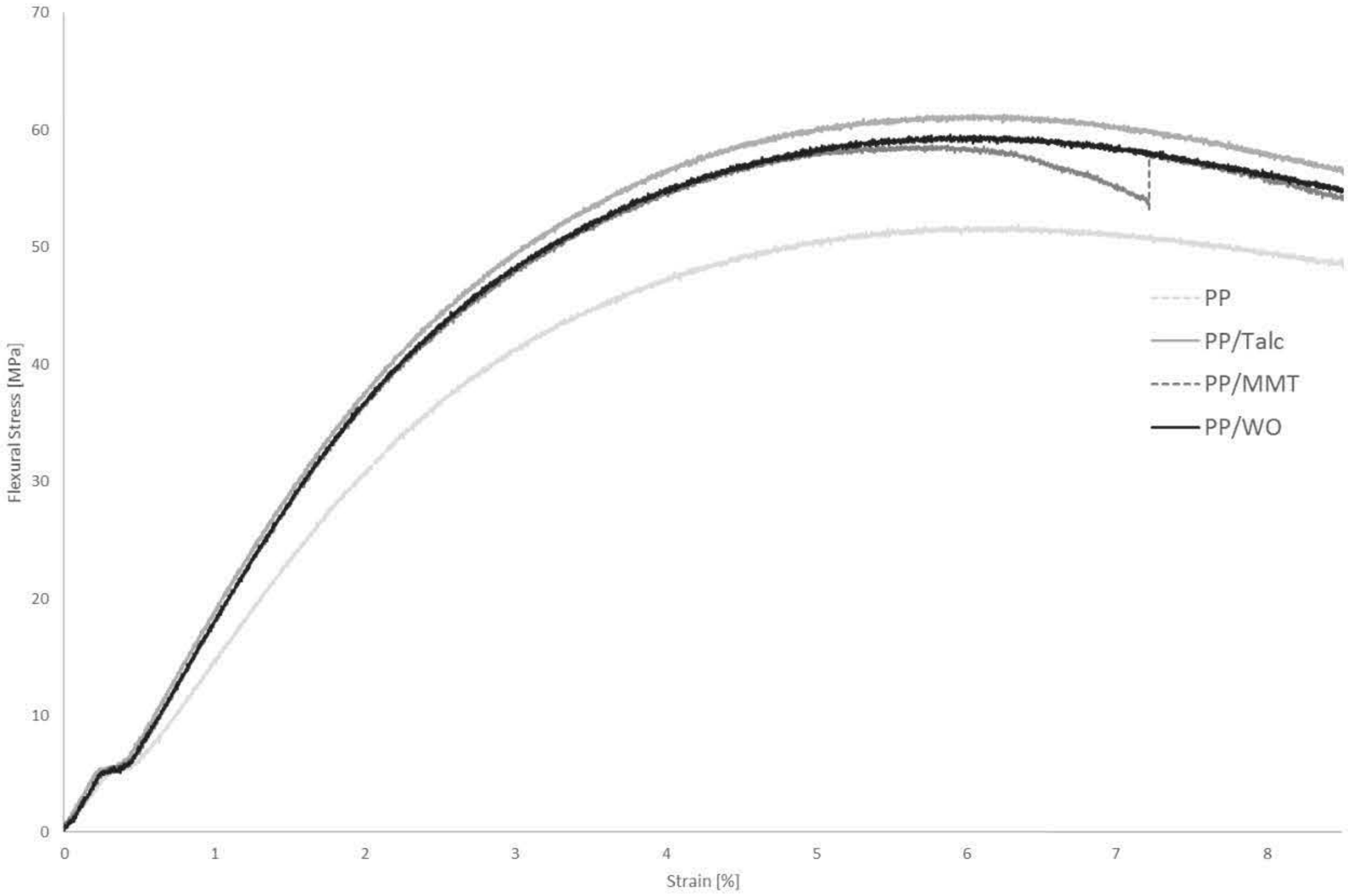

Figure 39: Stress vs strain curve averages from flexural 3-point bend tests on PP, PP/Talc, PP/MMT and PP/WO samples.

Similar to the tensile stress vs strain curve, an elastic region is observed prior to a yield and plastic portion of the curve. A small constant and flat stress is observed below 0.5% strain for all samples. This is due to the rollers compressing up against the fixture due to the load and is consistent with all samples. In contrast to the tensile material properties, all of the reinforced samples displayed evident improvement in flexural strength. Only one sample fractured before 8% strain which is also observed the drop of the PP/MMT average. This is also the cause in higher standard deviation in the PP/MMT data shown in Figure 40 and Table 8. As well as an increase in flexural strength, the flexural modulus can also be seen to increase for all reinforced samples. Although the PP/WO observed the highest flexural modulus, all reinforced samples showed over 28% increase. In comparison, the PP/Talc exhibited the highest flexural strength, whilst the PP/MMT and PP/WO displayed increases of 13% and 14.6 % over the PP sample respectively.

Statistical analysis was carried out on the samples. From the t-test between each sample and the PP sample, all of the reinforced samples returned a statistically significant difference for flexural modulus (PP/Talc P = 0.00930, PP/MMT P = 0.00686, PP/WO P = 0.00685). Similarly for the flexural strength, all of the samples also returned a statistically significant difference (PP/Talc P = 0.000122, PP/MMT P = 0.0129, PP/WO P = 0.00254). Furthermore, in a t-test between the PP/Talc and the two nanoparticle

reinforced samples, both the flexural modulus (PP/MMT P = 0.402, PP/WO P = 0.344) and flexural strength (PP/MMT P = 0.0836, PP/WO P = 0.0689) returned a statistically insignificant difference. The fillers can therefore be concluded as resulting in statistically insignificant differences to each other.

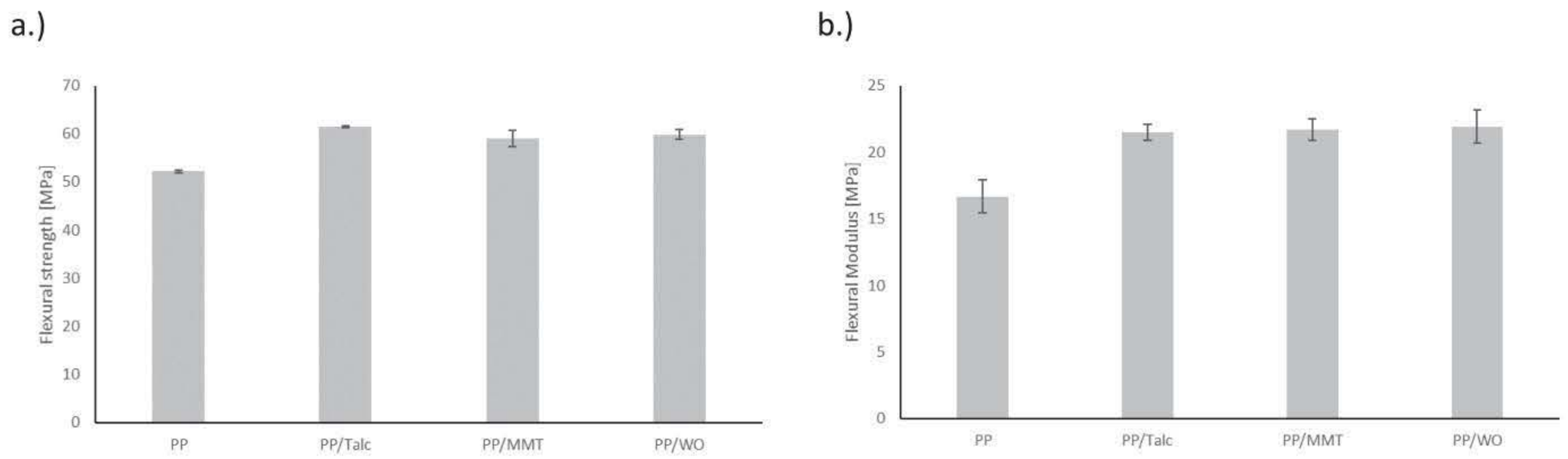

Figure 40: Comparison of mean values of PP-based samples of a.) flexural strength and b.) flexural Modulus

Table 8 : Summary and comparison of material properties collected from flexural tests on PP-based samples

Sample	Flexural Modulus $E^{Chord}_{Flexural}$ ± s_{n-1}: [MPa]	Percentage difference compared to PP	Flexural Strength: $\sigma_{Ultimate}$ ± s_{n-1} [MPa]	Percentage difference compared to PP	Strain at Flexural Strength $\varepsilon_{Flexural}$ at $\sigma_{Ultimate}$	Percentage difference compared to PP
PP	16.7 ± 1.27	/	52.2 ± 0.304	/	6.12 ± 0.328	/
PP/Talc	21.5 ± 0.612	28.8 %	61.5 ± 0.176	17.8 %	6.23 ± 0.0291	1.67 %
PP/MMT	21.7 ± 0.817	30.0 %	59.0 ± 1.67	13.0 %	5.81 ± 0.133	-5.05 %
PP/WO	21.9 ± 1.24	31.4 %	59.8 ± 1.01	14.6 %	6.00 ± 0.0622	-2.08 %

ANOVA single factor analysis was also performed to assess the variability between the flexural modulus and flexural strength means. For the flexural modulus, the analysis returned statistically significant differences within the 4 samples (F value = 12.1 F critical value = 4.07) and a 0.2 % chance that the observation could have been observed due to random error alone and therefore rejecting a hypothesis that the samples displayed no difference. Correspondingly for the flexural strength, the analysis returned statistically significant differences within the 4 samples (F value = 33.9, F critical value = 4.07) and a 0.0673 % chance that the observation could have been observed due to random error alone and therefore rejecting a hypothesis that the samples displayed no difference.

The increase in both flexural strength and flexural modulus with the use of MMT and WO is observed throughout literature. Selvakumar et al., (2010), reported an almost identical 13.1 % in flexural strength and 45.4 % increase in flexural modulus with 5 wt. % MMT added to PP. Other studies, such as Samal et al. (2008), reported a more significant 29.7 % increase in flexural strength and 161 % increase in flexural modulus with 5 wt. % MMT. The latter study was able to achieve the superior properties with particle functionalisation with alkyl ammonium. Correspondingly, a study by Chen et al. (2008) demonstrated a 20 % increase in flexural strength and a higher 88 % increase in flexural modulus with the use of WO as a filler in comparison to a virgin PP.

The introduction of the nanofillers can therefore be concluded to have observed minimal effect on the tensile properties in comparison to the reference PP and PP/Talc sample, as only the PP/MMT exhibited a statistically significant decrease with 3.38 % decrease in mean tensile strength. However, the PP/MMT and PP/WO exhibited statistically significant difference in improvement in flexural properties in comparison to the PP sample. As the materials were selected based on the use within the automotive industry, the use of nanofiller reinforcement in the PP is used to compare on the current standard PP/Talc sample. The use of the chosen nano reinforcement is to reduce the weight of the material, therefore the mechanical performance is only relevant when the material density is improved. The material density for the four materials is shown in Table 9.

Table 9*:* Material density values and comparison of PP-based samples.

Material	Density (gram/cm^3)	% of Density Reduction
PP	1.27	--
PP/Talc	1.02 (Reference value)	---
PP/WO	0.85	17
PP/MMT	0.84	18

Apart from the PP/MMT demonstrating a statistically significant decrease in tensile strength, the materials displayed a statistically significant increase in flexural properties and therefore can be ascertained to have similar flexural properties to that of the PP/Talc sample, as shown in Table 8. The material densities presented in Table 9, demonstrate the material weight improvement with the introduction of the nanofillers. With embedding 5 wt. % of WO in PP, the material achieved similar flexural properties as the reference PP/Talc sample, however, with a 17% density decrease. Therefore, a 17 % lighter material sample can be manufactured with the same mechanical performance which is a key factor in the automotive industry (Dasari et al., 2004). In comparison, the PP/MMT sample observed a similar 18% density decrease from the PP/Talc with similar flexural properties.

Polyester Based Samples and Fillers

The PE-based samples underwent a tensile test and the average plots (n=3) of the stress vs strain graph is shown in Figure 41. The tensile stress vs strain plots of the repetitions on individual PE-based samples is included in Appendix D. In comparison to the PP-based samples, the PE-based samples can immediately be seen to be less ductile with less elongation and more material fractures. The materials still have a plastic region after yielding but all samples fractured within 7 % strain.

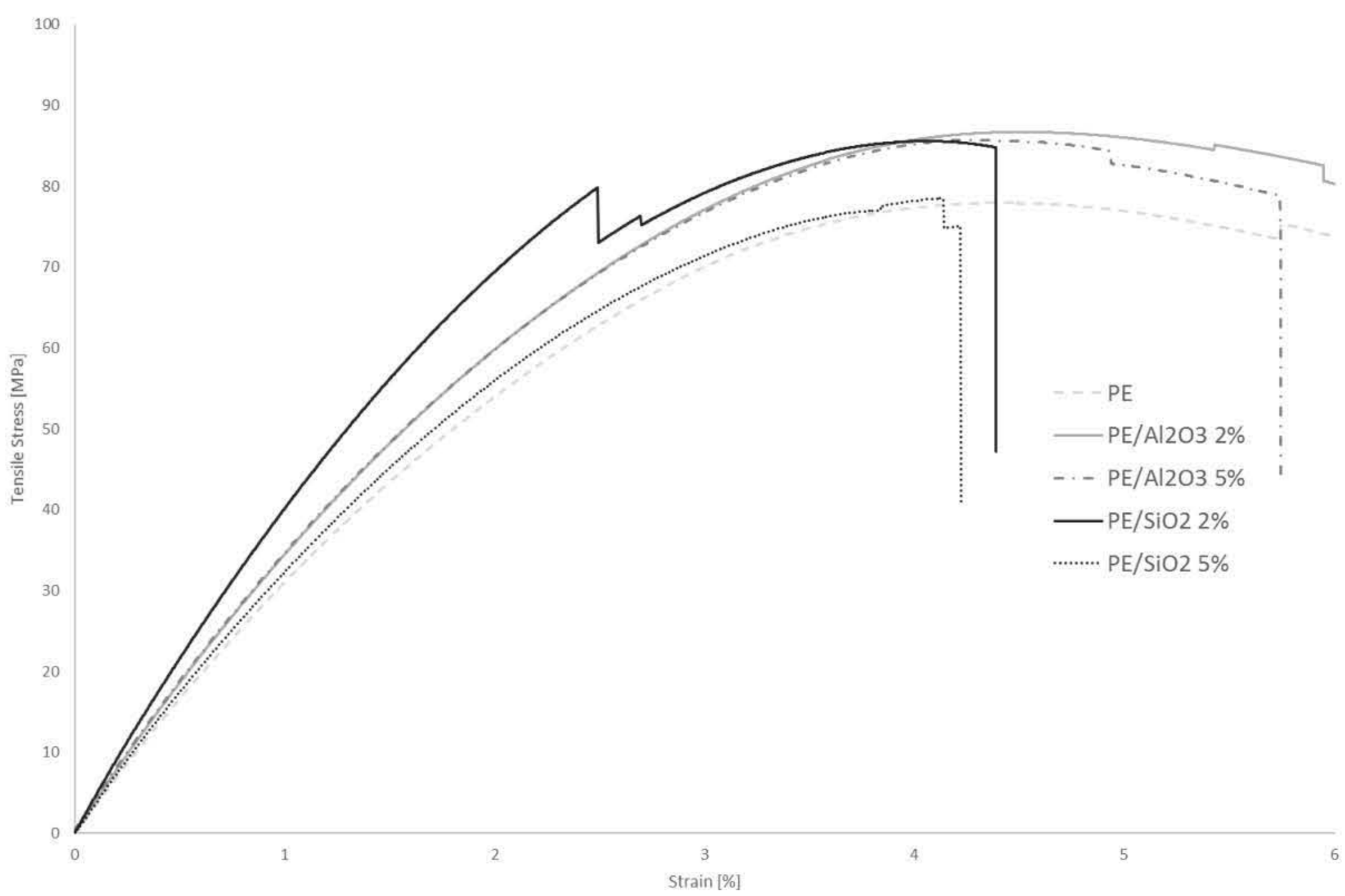

Figure 41: Stress vs strain curve averages from tensile tests on PE, PE/Al_2O_3 2 wt. %, PE/Al_2O_3 5 wt.%, PE/SiO_2 2 wt.% and PE/SiO_2 5 wt.% samples

As shown in Figure 41, PE/Al_2O_3 2 wt. %, PE/Al_2O_3 5 wt.% and PE/SiO_2 2 wt.% samples exhibited a visible increase in both Young's Modulus and tensile strength. However, apart from PP/Al_2O_3 2 wt.%, all of the reinforced samples also observed a reduction in elongation with reduced plastic regions and therefore earlier fractures.

Although the nanoparticles can be seen to improve the tensile properties, the particles can also be said to be affecting the elongation of the material. As shown in Figure 42 and Table 10, only the PE/SiO_2 5 wt.% did not show an increase in the tensile strength. One of the PE/SiO_2 5 wt.% samples fractured at a smaller strain value than the other two which has affected the standard deviation and higher CV ($\sigma_{Ultimate}$ CV = 43.2) compared to for example, the PE/Al_2O_3 2 wt. % sample ($\sigma_{Ultimate}$ CV = 0.221).

Statistical analysis was carried out on the samples. From the t-test between each sample and the PE sample, only the PE/SiO_2 2 wt.% returned a statistically significant difference for Young's Modulus (PE/Al_2O_3 2 wt. % P = 0.120, PE/Al_2O_3 5 wt.% P = 0.442, PE/SiO_2 2 wt.% P = 0.0473, and PE/SiO_2 5 wt.% P = 0.247). The analysis on the tensile strength, returned both PE/Al_2O_3 2 wt. % and PE/Al_2O_3 5 wt.% with a statistically significant difference (PE/Al_2O_3 2 wt. % P = 0.0336, PE/Al_2O_3 5 wt.% P = 0.0345, PE/SiO_2 2 wt.% P = 0.124, and PE/SiO_2 5 wt.% P = 0.493). Therefore, only the PE/SiO_2 5 wt.% observed no statistically significant difference in either Young's Modulus or tensile strength in comparison to the PE sample.

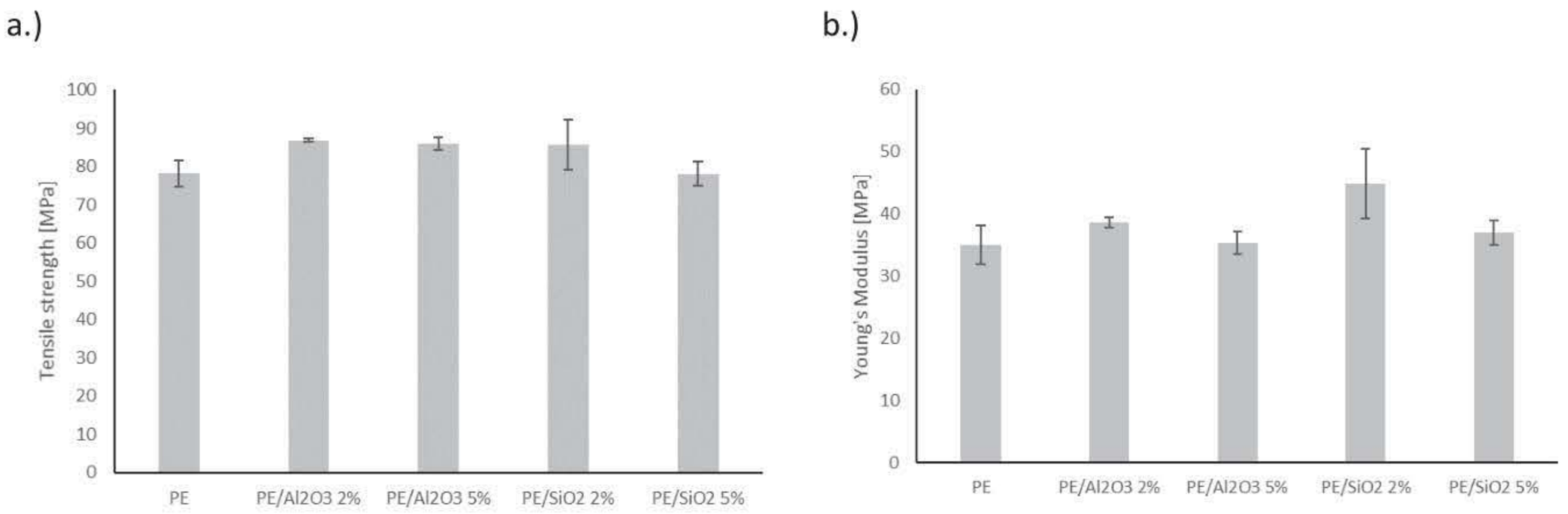

Figure 42: Comparison of mean values of PE-based samples of a.) tensile strength and b.) Young's Modulus

Table 10: Summary and comparison of material properties collected from tensile tests on PE-based samples

Sample	Young's Modulus $E_{Young's} \pm s_{n-1}$: [MPa]	Percentage difference compared to PE	Tensile Strength: $\sigma_{Ultimate} \pm s_{n-1}$ [MPa]	Percentage difference compared to PE	Strain at Tensile Strength $\varepsilon_{Tensile}$ at $\sigma_{Ultimate}$	Percentage difference compared to PE
PE	35.0 ± 3.16	/	78.1 ± 3.44	/	4.39 ± 0.235	/
PE/Al_2O_3 2 wt.%	38.6 ± 0.771	10.5 %	86.8 ± 0.422	11.2 %	4.51 ± 0.217	2.60 %
PE/Al_2O_3 5 wt.%	35.4 ± 1.78	1.16 %	85.8 ± 1.60	9.84 %	4.34 ± 0.0969	-1.3 %
PE/SiO_2 2 wt.%	44.9 ± 5.63	28.3 %	85.6 ± 6.57	9.57 %	3.09 ± 0.712	-29.7 %
PE/SiO_2 5 wt.%	37.0 ± 1.96	5.76 %	78.1 ± 3.09	-0.08 %	3.96 ± 0.257	-9.89 %

ANOVA single factor analysis was also performed to assess the variability between the Young's Modulus and tensile strength means. For the Young's Modulus, the analysis returned statistically significant differences within the 4 samples (F value = 3.50 F critical value = 3.48) and a 4.7 % chance

that the observation could have been observed due to random error alone and therefore rejecting a hypothesis that the samples displayed no difference. Correspondingly for the tensile strength, the analysis returned statistically insignificant differences within the 4 samples (F value = 2.88, F critical value = 3.48) and a 7 % chance that the observation could have been observed due to random error alone and therefore accepting a null hypothesis that the samples displayed no difference as it lies within the 0.05 confidence interval.

The PE-based samples were also evaluated for flexural material properties. This was carried out with a 3-point flexural test as per the ASTM D7264M standard. The average (n= 3) stress vs strain plots for each PE-based composition is shown in Figure 43. The individual stress vs strain plots are presented in Appendix D.

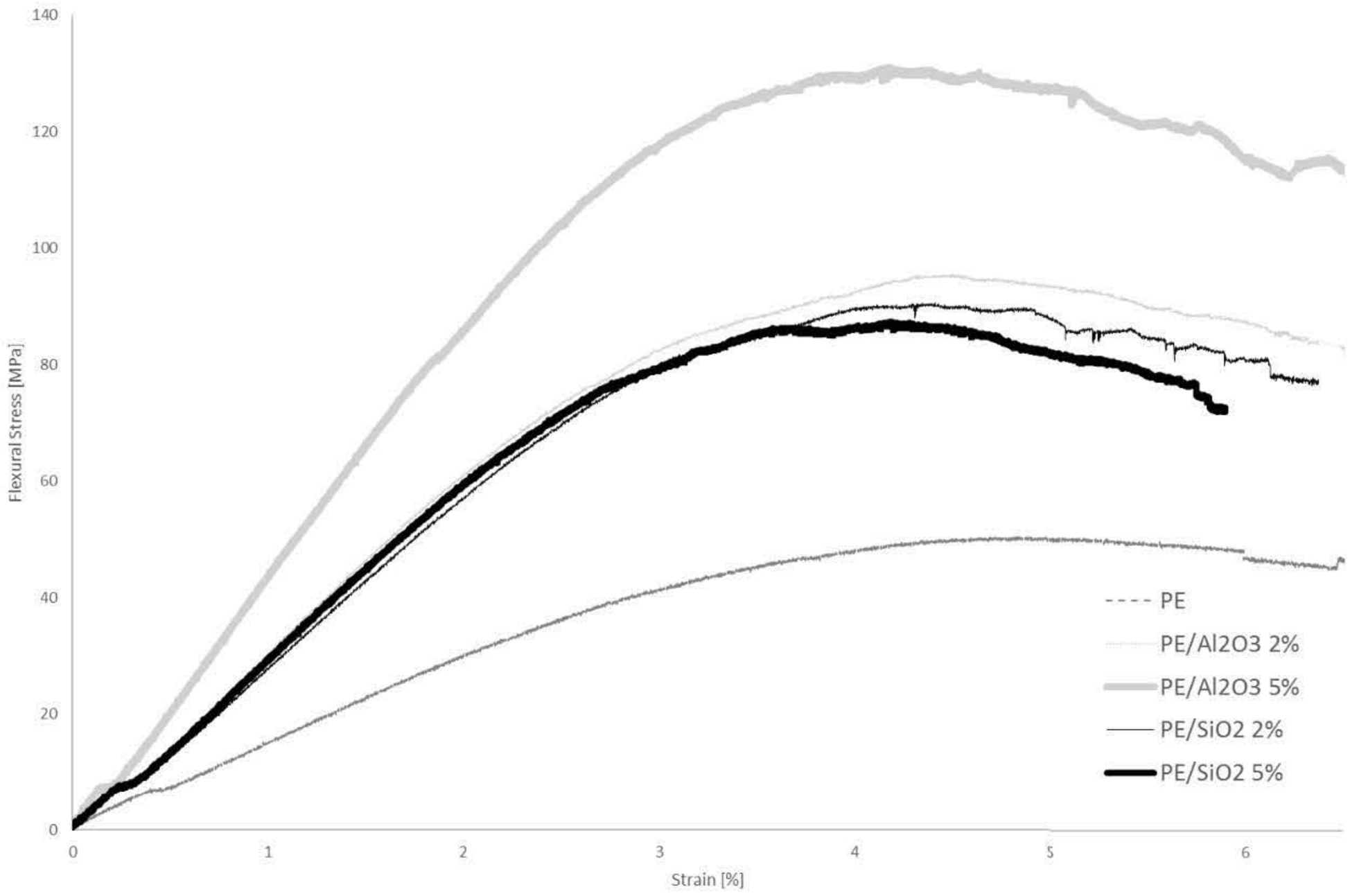

Figure 43: Stress vs strain curve averages from flexural 3-point bend tests PE, PE/Al_2O_3 2 wt. %, PE/Al_2O_3 5 wt.%, PE/SiO_2 2 wt.% and PE/SiO_2 5 wt.% samples

The reinforced PE samples observed a visible improvement in flexural properties. Parallel to the PP-based samples a small constant and flat stress is observed below 0.5% strain for all samples due to the rollers compressing up against the fixture due to the load and is consistent with all samples. The increase in flexural modulus and flexural strength observed a slight reduction in elongation. The material experiences similar elastic behaviour prior to a yield and can therefore be said to follow similar ductile material behaviour with no fracture prior to 6 % strain. The PE/Al_2O_3 5 wt.% illustrated

the highest flexural strength and flexural modulus. As can also be seen in Figure 44 and Table 11, both the PE/SiO_2 samples observed a similar increase in flexural strength and flexural modulus.

Another main difference observable in the plots shown in Figure 43, is the change in stability of stress after yielding and within the plastic region. Whilst the PE sample observed an almost constant strain after yielding and therefore exhibiting an almost Elastic-Perfectly Plastic (EPP) behaviour (Haddad, 2013), the reinforced samples demonstrated less linear behaviour in stress. These can consequently be attributed to the reinforcing fillers, as the behaviour is not observed with the neat PE samples. However, as with other polymers, this has little affect to the application as the material will be used within the yield strength and therefore also within the ultimate tensile strength.

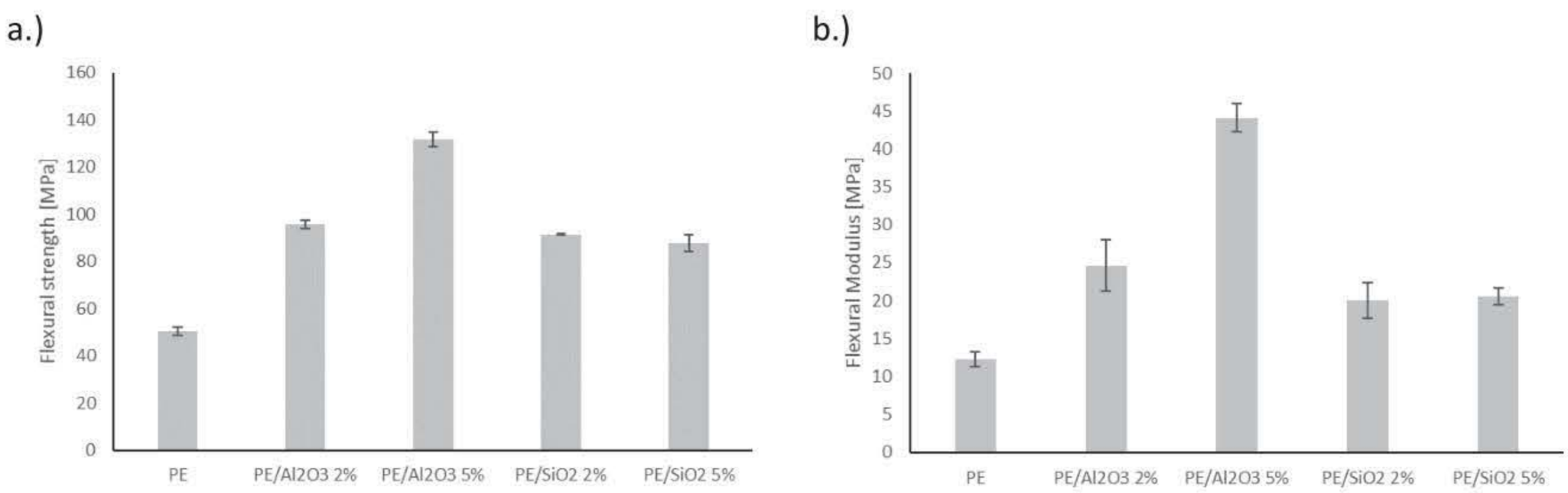

Figure 44: Comparison of mean values of PE-based samples of a.) flexural strength and b.) flexural modulus

Table 11: Summary and comparison of material properties collected from tensile tests on PE-based samples

Sample	Flexural Modulus $E^{Chord}_{Flexural}$ ± s_{n-1}: [MPa]	Percentage difference compared to PE	Flexural Strength: $\sigma_{Ultimate}$ ± s_{n-1} [MPa]	Percentage difference compared to PE	Strain at Flexural Strength $\varepsilon_{Flexural}$ at $\sigma_{Ultimate}$	Percentage difference compared to PE
PE	12.3 ± 0.965	/	50.5 ± 1.78	/	4.61 ± 0.394	/
PE/Al_2O_3 2 wt.%	24.6 ± 3.44	100 %	95.8 ± 1.82	89.6 %	4.39 ± 0.206	-4.76 %
PE/Al_2O_3 5 wt.%	44.1 ± 1.87	258 %	132 ± 3.05	161 %	4.23 ± 0.240	-8.36 %
PE/SiO_2 2 wt.%	20.0 ± 2.31	62.3 %	91.5 ± 0.395	81.1 %	4.55 ± 0.208	-1.41 %
PE/SiO_2 5 wt.%	20.6 ± 1.11	67.4 %	87.8 ± 3.56	73.8 %	4.27 ± 0.353	-7.42 %

Additional to the numerical values provided in Table 11, statistical analysis was carried out on the samples. From the t-test between each sample and the PE sample, all of the reinforced samples returned a statistically significant difference in flexural modulus (PE/Al_2O_3 2 wt. % P = 0.0147, PE/Al_2O_3 5 wt.% P = 0.000112, PE/SiO_2 2 wt.% P = 0.0142, and PE/SiO_2 5 wt.% P = 0.000728). The analysis on the flexural strength also returned all of the reinforced samples with a statistically significant difference (PE/Al_2O_3 2 wt. % P = 0.00000747, PE/Al_2O_3 5 wt.% P = 0.0000181, PE/SiO_2 2 wt.% P = 0.000287, and PE/SiO_2 5 wt.% P = 0.000514). Therefore all of the samples observed a statistically significant increase in both flexural modulus and flexural strength in comparison to the PE sample.

ANOVA single factor analysis was also performed to assess the variability between the flexural modulus and flexural strength means. For the flexural modulus, the analysis returned statistically significant differences within the 4 samples (F value = 62.0 F critical value = 3.48) and a 0.0000000507% chance that the observation could have been observed due to random error alone and therefore rejecting a hypothesis that the samples displayed no difference. Correspondingly for the flexural strength, the analysis returned statistically significant differences within the 4 samples (F value = 2.91, F critical value = 3.48) and a 2.68 x 10^{-12} % chance that the observation could have been observed due to random error alone and therefore rejecting a hypothesis that the samples displayed no difference.

In comparison to literature, studies have demonstrated nano alumina with an almost identical increase in tensile strength with 5 wt. % in comparison to neat PE with a 13.8 % increase (Baskaran et al., 2011). The same study reported a similar peak flexural strength increase with 5 wt. % nano alumina with an 11.2 % increase. Similarly, studies have concluded comparable conclusions with a peak mechanical performance at 2 wt. % and reducing in properties with further increases in weight concentration for SiO_2 (Rusmirovic et al., 2016; *Trinath et al., 2016*).

Epoxy reinforced with CNT fillers

The EP samples reinforced with CNTs underwent the same tensile test and the average plots (n=3) of the stress vs strain graph is shown in Figure 45. The tensile stress vs strain plots of the repetitions on individual samples is included in Appendix D.

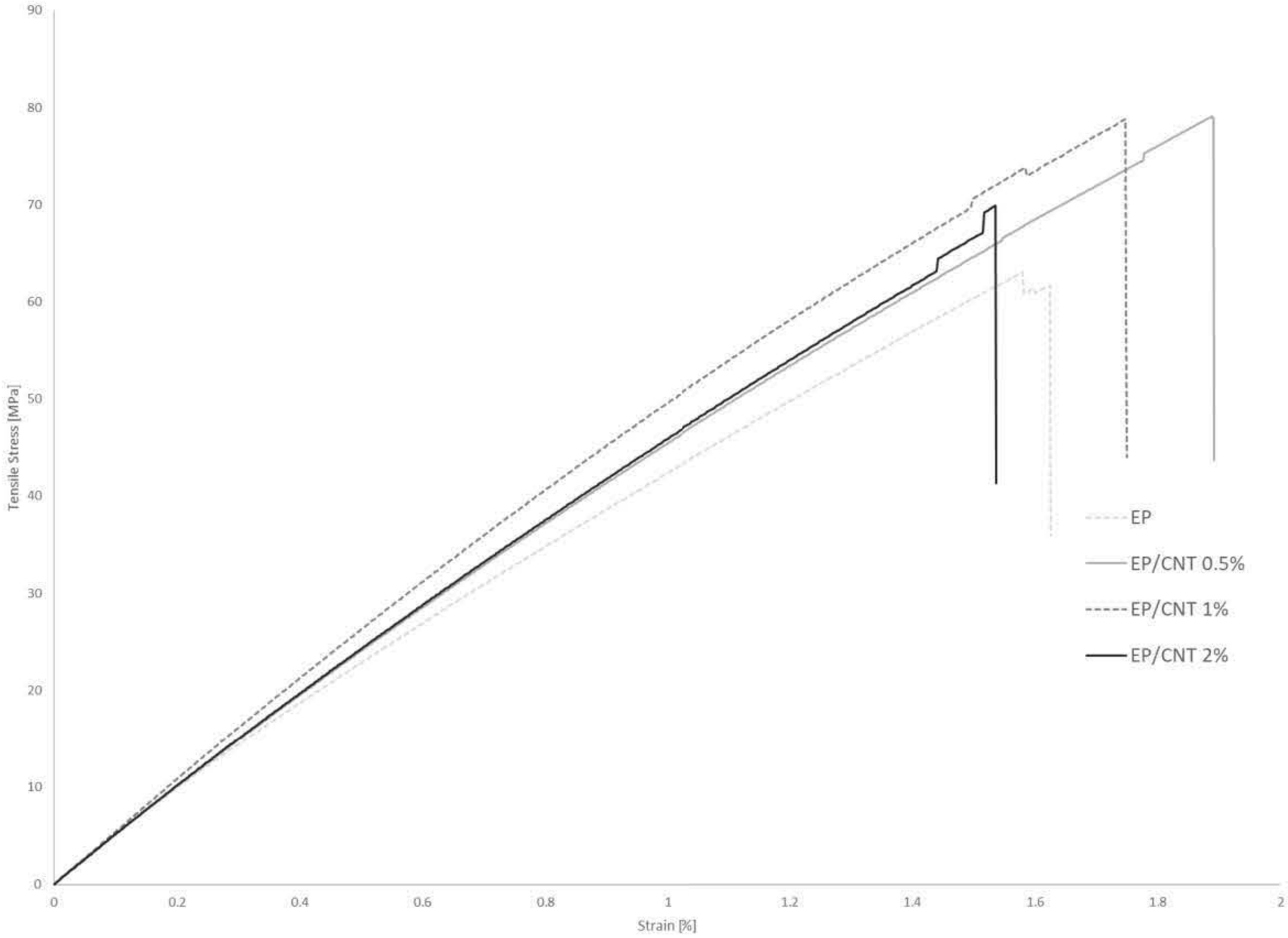

Figure 45: Stress vs strain curve averages from tensile tests on EP, EP/CNT 0.5 wt.%, EP/CNT 1 wt.% and EP/CNT 2 wt.%

In comparison to the PP-based and PE-based samples, the samples can immediately be seen to exhibit brittle material behaviour. The materials observed purely elastic regions prior to fracture, and therefore failure. The ultimate tensile strength is therefore also equivalent to the tensile stress at failure and there is no yielding of the material. The materials also observed a maximum elongation of 2 % strain. This behaviour is expected, as EP is a known to be a brittle thermosetting polymer (May, 2018). From the bar chart shown in Figure 46 and numerical data presented in Table 12, the introduction of the CNT filler can be seen to have the vaster effect on Young's Modulus in comparison to the tensile strength. The samples, e.g. for EP/CNT 0.5 wt.%, also observed much more consistent and lower variance in Young's Modulus (CV = 0.145 MPa) in comparison to the tensile strength (CV = 30.1 MPa). This is also evident with the standard deviation values included within Table 12 and Figure 46.

a.)

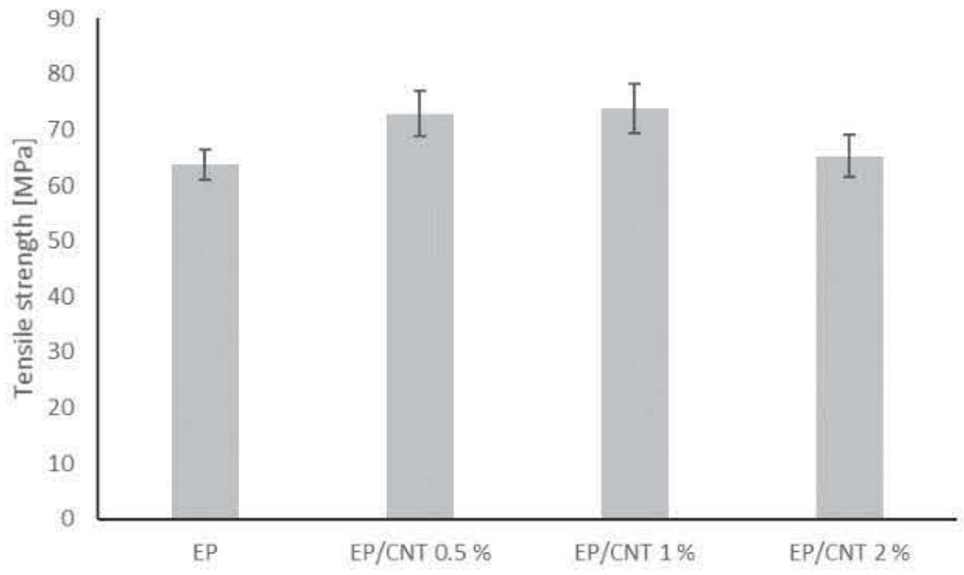

b.)

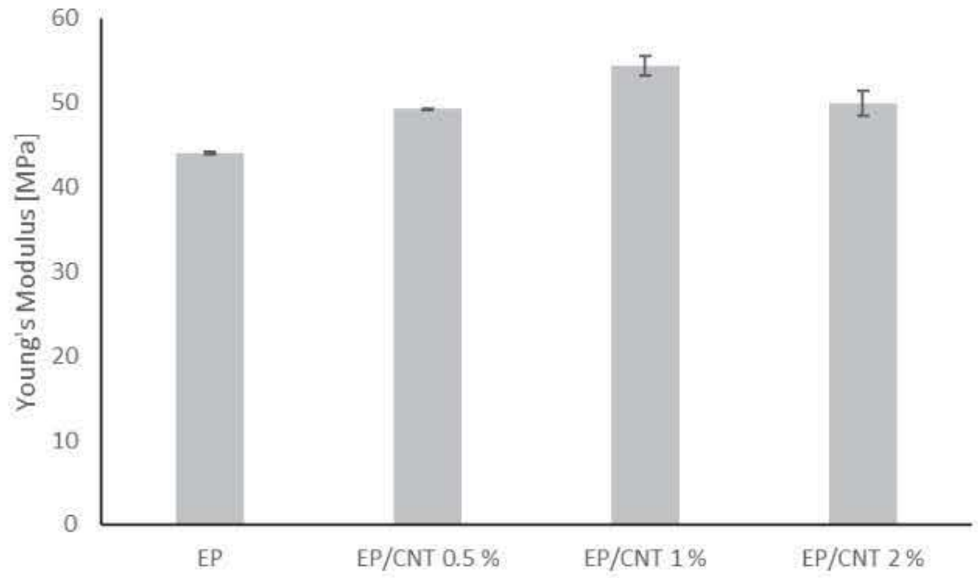

Figure 46: Comparison of mean values of EP-based samples reinforced with CNTs of a.) tensile strength and b.) Young's Modulus

Table 12: Summary and comparison of material properties collected from tensile tests on EP-based samples reinforced with CNTs

Sample	Young's Modulus $E_{Young's} \pm s_{n-1}$: [MPa]	Percentage difference compared to EP	Tensile Strength: $\sigma_{Ultimate} \pm s_{n-1}$ [MPa]	Percentage difference compared to EP	Strain at Tensile Strength $\varepsilon_{Tensile}$ at $\sigma_{Ultimate}$	Percentage difference compared to EP
EP	44.0 ± 0.213	/	63.8 ± 2.73	/	1.60 ± 0.0183	/
EP/CNT 0.5 wt.%	49.2 ± 0.0691	11.9 %	72.9 ± 4.06	14.4 %	1.74 ± 0.116	8.56 %
EP/CNT 1 wt. %	54.3 ± 1.13	23.5 %	73.9 ± 4.45	15.8 %	1.61 ± 0.104	0.51 %
EP/CNT 2 wt. %	49.9 ± 1.52	13.4 %	65.3 ± 3.73	2.36 %	1.50 ± 0.0412	-6.48 %

Statistical analysis was carried out on the samples. From the t-test between each sample and the EP sample, all of the samples returned a statistically significant difference for Young's Modulus (EP/CNT 0.5 wt.% P = 0.000168, EP/CNT 1 wt.% P = 0.00232, and EP/CNT 2 wt.% P = 0.0148). The analysis on the tensile strength, returned only the EP/CNT 1 wt.% with a statistically significant difference (EP/CNT 0.5 wt.% P = 0.0634, EP/CNT 1 wt.% P = 0.0320, and EP/CNT 2 wt.% P = 0.335). Therefore, although all of the samples observed a statistically significant increase in Young's Modulus, only the EP/CNT 1 wt.% observed a statistically significant increase in tensile strength.

ANOVA single factor analysis was also performed to assess the variability between the Young's Modulus and tensile strength means. For the Young's Modulus, the analysis returned statistically significant differences within the 4 samples (F value = 38.1, F critical value = 4.07) and a 0.00439 % chance that the observation could have been observed due to random error alone and therefore

rejecting a null hypothesis that the samples displayed no difference. Correspondingly for the tensile strength, the analysis returned statistically insignificant differences within the 4 samples (F value = 3.01, F critical value = 4.07) and a 9.47 % chance that the observation could have been observed due to random error alone and therefore accepting a null hypothesis that the samples displayed no difference as it lies within the 0.05 confidence interval.

The EP samples reinforced with CNT were also evaluated for flexural material properties. This was carried out with a 3-point flexural test as per the ASTM D7264M standard. The average (n= 3) stress vs strain plots for each composition is shown in Figure 47. The individual stress vs strain plots are presented in Appendix D.

Corresponding to the PP-based and PE-based samples a small constant and flat stress is observed below 0.5% strain for all samples due to the rollers compressing up against the fixture due to the load and is consistent with all samples. The stress can thereafter be seen to increase linearly in an elastic manner. Like the tensile behaviour, the samples did not observe any plastic region or yielding. The materials therefore observed brittle behaviour in relation to the stress vs strain curve. Noticeably, the materials also exhibited low strain values of only up to 2.5 % strain. The elongation therefore can be seen to be far less than the PP-based and PE-based samples. From the averages plot, the flexural stress demonstrated a visible increase with the reinforcing CNT concentrations. Although the EP/CNT 2 wt. % sample observed a similar elongation, the flexural stress is prominently higher, whereas the EP/CNT 0.5 wt. % and EP/CNT 1 wt. % both also observed a larger elongation as well as flexural strength.

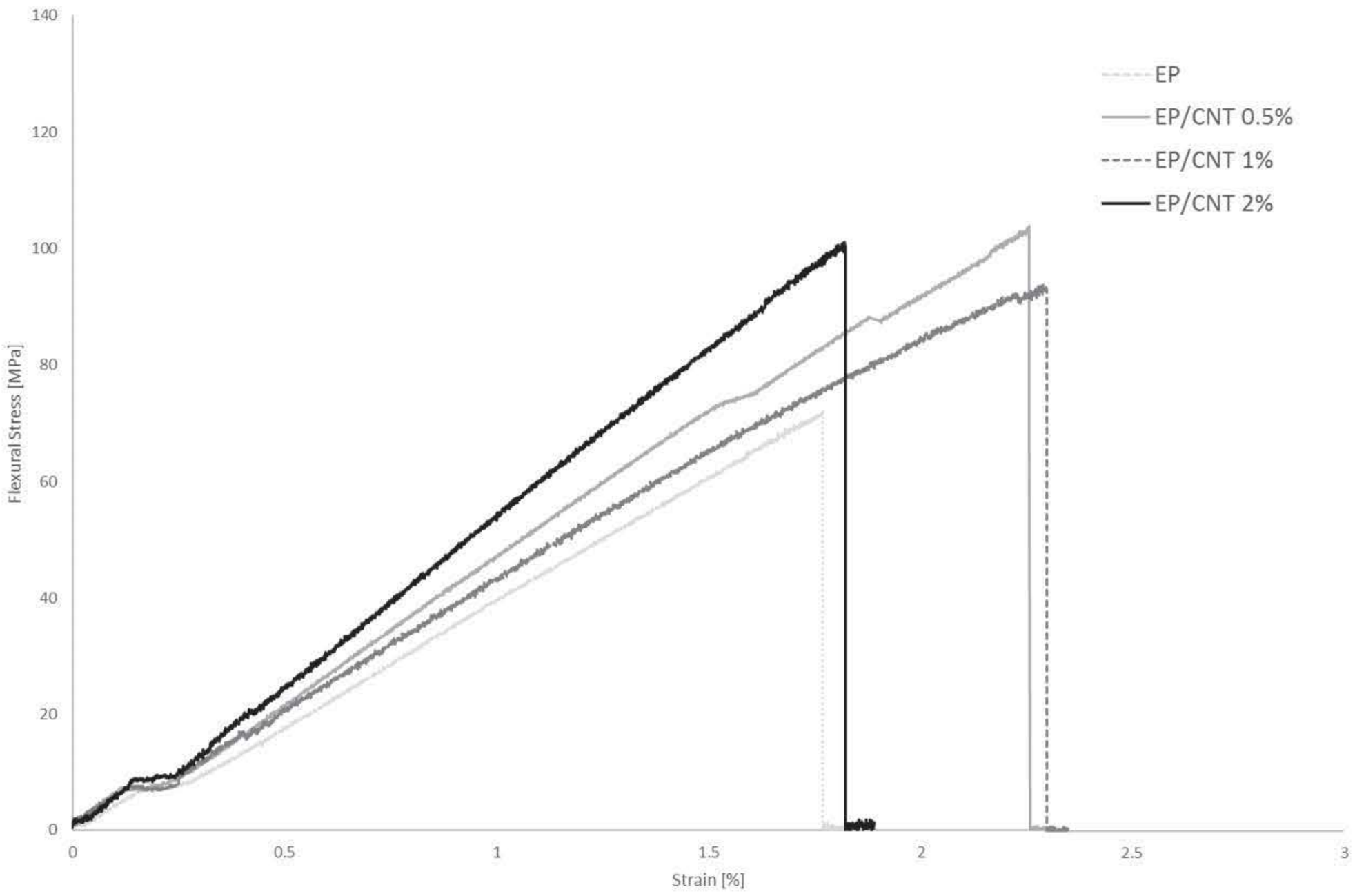

Figure 47: Stress vs strain curve averages from flexural 3-point bend tests on EP, EP/CNT 0.5 wt.%, EP/CNT 1 wt.% and EP/CNT 2 wt.%

The comparison of the numerical data presented in Table 13 and represented in bar charts in Figure 48, highlight the effect of CNTs on the flexural strength. All of the mean values observed a percentage increase in comparison to the neat EP sample. However, the samples also observed relatively high variation in performance in flexural strength e.g. observed for EP/CNT 2 wt. % sample (CV = 33.6 MPa).

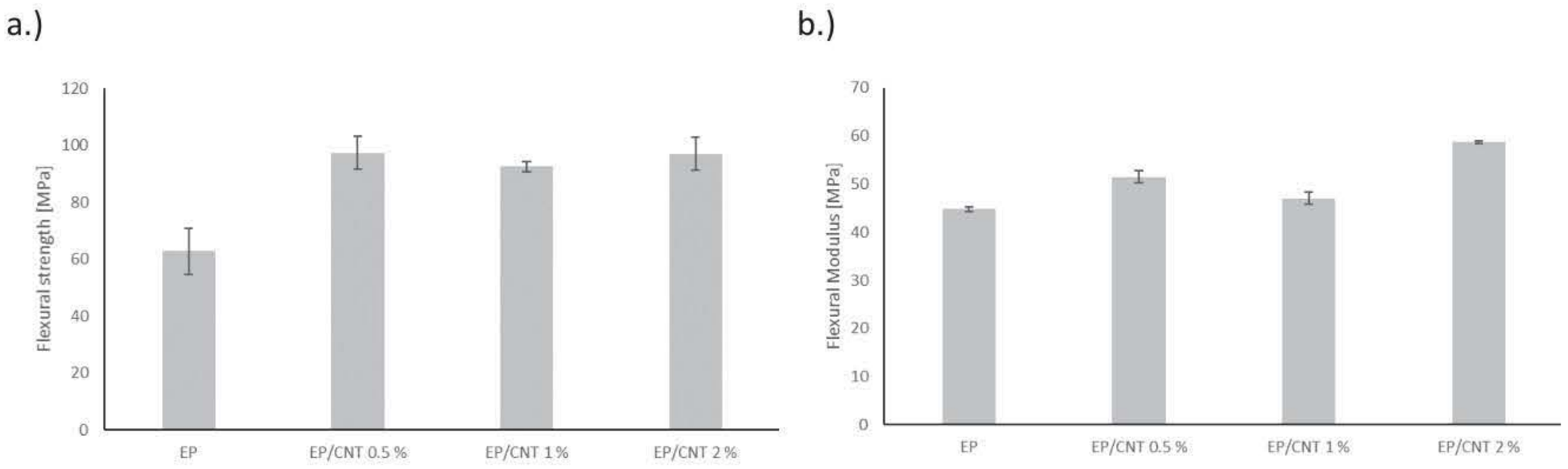

Figure 48: Comparison of mean values of EP-based samples reinforced with CNTs of a.) flexural strength and b.) flexural modulus

Table 13: Summary and comparison of material properties collected from flexural tests on EP-based samples reinforced with CNTs

Sample	Flexural Modulus $E_{Flexural}^{Chord}$ ± s_{n-1}: [MPa]	Percentage difference compared to EP	Flexural Strength: $\sigma_{Ultimate}$± s_{n-1} [MPa]	Percentage difference compared to EP	Strain at Flexural Strength $\varepsilon_{Flexural}$ at $\sigma_{Ultimate}$	Percentage difference compared to EP
EP	44.8 ± 0.422	/	62.8 ± 8.04	/	1.55 ± 0.191	/
EP/CNT 0.5 wt. %	51.5 ± 1.28	14.9 %	97.4 ± 5.77	55.0 %	2.08 ± 0.181	33.4 %
EP/CNT 1 wt. %	47.1 ± 1.34	5.09 %	92.5 ± 1.90	47.3 %	2.22 ± 0.0420	43.1 %
EP/CNT 2 wt. %	58.6 ± 0.225	31.0 %	97.1 ± 5.80	54.5 %	1.75 ± 0.0862	13.2 %

Additional to the numerical values provided in Table 13, statistical analysis was carried out on the samples. From the t-test between each sample and the EP neat sample, only the EP/CNT 1 wt.% sample returned a statistically insignificant difference in flexural modulus (EP/CNT 0.5 wt.% P = 0.00571, EP/CNT 1 wt.% P = 0.0639, and EP/CNT 2 wt.% P = 0.0000137). The analysis on the flexural strength returned all of the reinforced samples with a statistically significant difference (EP/CNT 0.5 wt.% P = 0.00502, EP/CNT 1 wt.% P = 0.0148, and EP/CNT 2 wt.% P = 0.00516). Therefore, the flexural modulus of the EP/CNT 1 wt.% sample is the only insignificant difference, with all of the other samples observing a statistically significant increase in flexural modulus and flexural strength in comparison to the EP sample.

ANOVA single factor analysis was also performed to assess the variability between the flexural modulus and flexural strength means. For the flexural modulus, the analysis returned statistically significant differences within the 4 samples (F value = 81.4 F critical value = 4.07) and a 2.46 x 10^{-8}% chance that the observation could have been observed due to random error alone and therefore rejecting a hypothesis that the samples displayed no difference. Correspondingly for the flexural strength, the analysis returned statistically significant differences within the 4 samples (F value = 16.3, F critical value = 4.07) and a 2.68 x 10^{-12} % chance that the observation could have been observed due to random error alone and therefore rejecting a hypothesis that the samples displayed no difference.

In comparison to literature, the increase in Young's Modulus corresponds to similar increases within literature, along with the statistically significant increase in tensile strength. The extend of the increase in strength with a maximum of 15.8% is lies in the middle of reported performance improvements with the introduction of CNTs at similar weight concentrations. A study by Wernik and Meguid (2014),

observed a 25 % increase in tensile strength attained at 1.5 wt. % CNT, whilst Chen et al. (2007) reported a 4.5% increase in tensile strength with 1 wt. % CNT. The differences can be attributed to the variation in CNTs (e.g. multiwalled or singe walled), polymer formulation, dispersion, aspect ratio, length of CNTs and alignment of CNTs into the matrix (Mittal et al., 2015).

Epoxy reinforced with CNF fillers

The EP samples reinforced with CNFs underwent the same tensile test and the average plots (n=3) of the stress vs strain graph is shown in Figure 49. The tensile stress vs strain plots of the repetitions on individual samples is included in Appendix D.

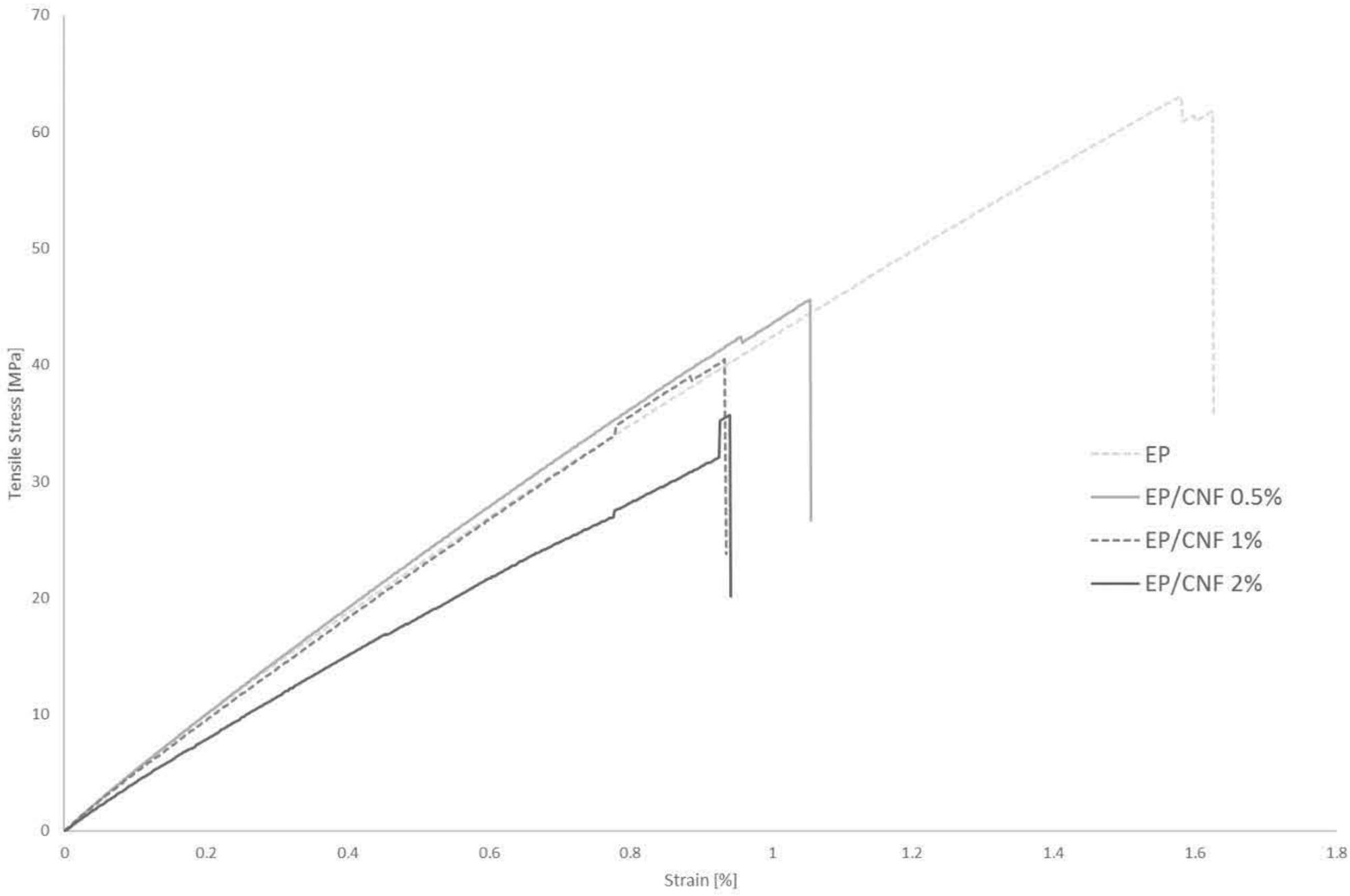

Figure 49: Stress vs strain curve averages from tensile tests on EP, EP/CNF 0.5 wt. %, EP/CNF 1 wt. % and EP/CNF 2 wt. %

From the comparison of the average stress vs strain plots, shown in Figure 49, the introduction of the CNFs can be visibly seen to decrease the tensile strength of the materials. All four materials observed brittle behaviour without a plastic region or a yield point. Furthermore, the increase in weight percentage of CNFs can also be seen to decrease the tensile strength further. With comparable modulus of elasticity, i.e. Young's Modulus, the virgin EP sample therefore also exhibited the longest elongation prior to fracture with almost double the elongation of the EP/CNF samples. The particles

can therefore be seen to have a negative impact on the tensile strength. This is further shown in the comparison bar chart in Figure 50 and numerical data presented in Table 14.

Not only did the use of CNF fillers decrease the tensile strength, but the deviation in performance also increased. The variance in tensile strength performance for the EP sample (CV = 3.72) is significantly lower than the EP/CNF 2 wt.% sample (CV = 16.1). This is also due to the lower tensile strength and therefore higher ratio of the standard deviation to the mean.

The lower concentration of CNFs can be seen to increase the Young's modulus in comparison to the virgin EP sample, followed by a decreasing trend with increase in weight percentage. The EP/CNF 2 wt. % displayed a visibly lower Young's Modulus compared to the EP sample.

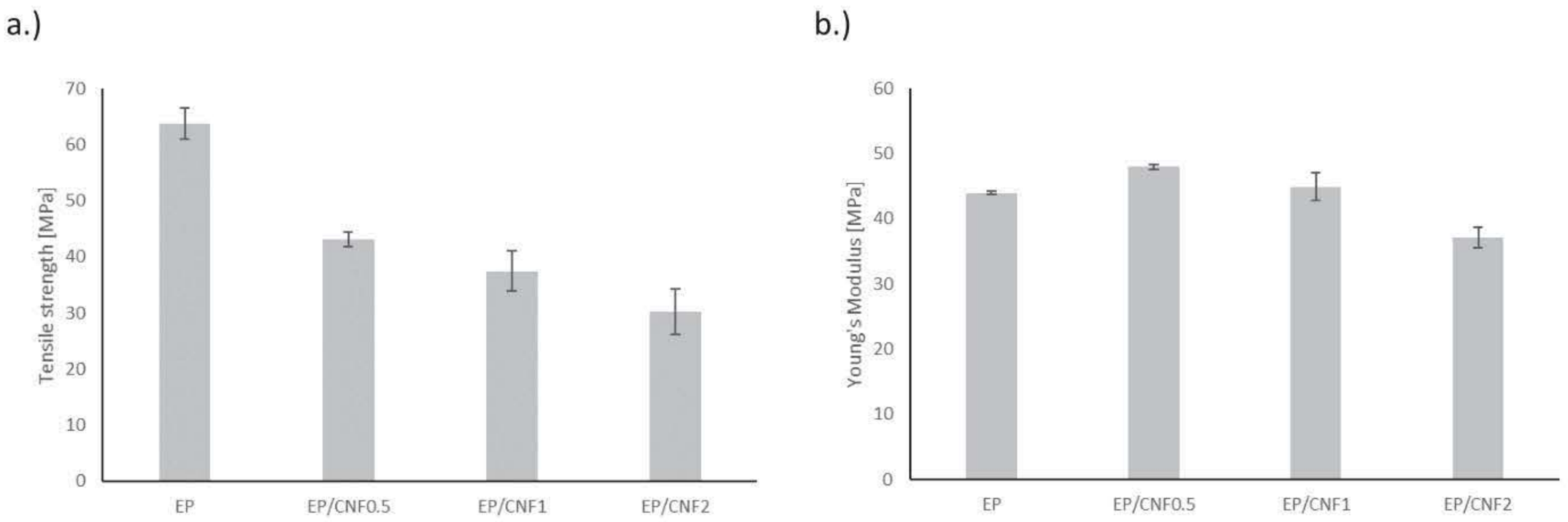

Figure 50: Comparison of mean values of EP-based samples reinforced with CNFs of a.) tensile strength and b.) Young's Modulus.

Table 14: Summary and comparison of material properties collected from tensile tests on EP-based samples reinforced with CNFs.

Sample	Young's Modulus $E_{Young's}$ ± s_{n-1}: [MPa]	Percentage difference compared to EP	Tensile Strength: $\sigma_{Ultimate}$± s_{n-1} [MPa]	Percentage difference compared to EP	Strain at Tensile Strength $\varepsilon_{Tensile}$ at $\sigma_{Ultimate}$	Percentage difference compared to EP
EP	44.0 ± 0.213	/	63.8 ± 2.73	/	1.60 ± 0.0183	/
EP/CNF 0.5 wt. %	48.0 ± 0.410	9.16 %	43.1 ± 1.30	-32.4 %	0.972 ± 0.0490	-39.3 %
EP/CNF 1 wt. %	44.9 ± 2.09	2.19 %	37.4 ± 3.60	-41.3 %	0.865 ± 0.0649	-46.0 %
EP/CNF 2 wt. %	37.1 ± 1.62	-15.6 %	30.2 ± 4.02	-52.6 %	0.880 ± 0.0742	-45.0 %

Statistical analysis was carried out on the samples. From the t-test between each sample and the EP sample, only the EP/CNF 1 wt.% did not return a statistically significant difference for Young's Modulus

(EP/CNF 0.5 wt.% P = 0.0162, EP/CNF 1 wt.% P = 0.291, and EP/CNF 2 wt.% P = 0.0126). The analysis on the tensile strength, returned all of the reinforced samples with a statistically significant difference (EP/CNF 0.5 wt.% P = 0.000711, EP/CNF 1 wt.% P = 0.000791, and EP/CNF 2 wt.% P = 0.000564). Therefore, whilst only the EP/CNF 1 wt.% returned a statistically insignificant change in Young's Modulus, all of the samples returned a statistically significant decrease in tensile strength.

ANOVA single factor analysis was also performed to assess the variability between the Young's Modulus and tensile strength means. For the Young's Modulus, the analysis returned statistically significant differences within the 4 samples (F value = 16.9, F critical value = 4.07) and a 0.0805 % chance that the observation could have been observed due to random error alone and therefore rejecting a null hypothesis that the samples displayed no difference. Correspondingly for the tensile strength, the analysis returned statistically significant differences within the 4 samples (F value = 41.0, F critical value = 4.07) and a 0.00333 % chance that the observation could have been observed due to random error alone and therefore rejecting a null hypothesis that the samples displayed no difference as it lies outside the 90% confidence interval.

The EP samples reinforced with CNFs were also evaluated for flexural material properties. This was carried out with a 3-point flexural test as per the ASTM D7264M standard. The average (n= 3) stress vs strain plots for each composition is shown in Figure 51. The individual stress vs strain plots are presented in Appendix D.

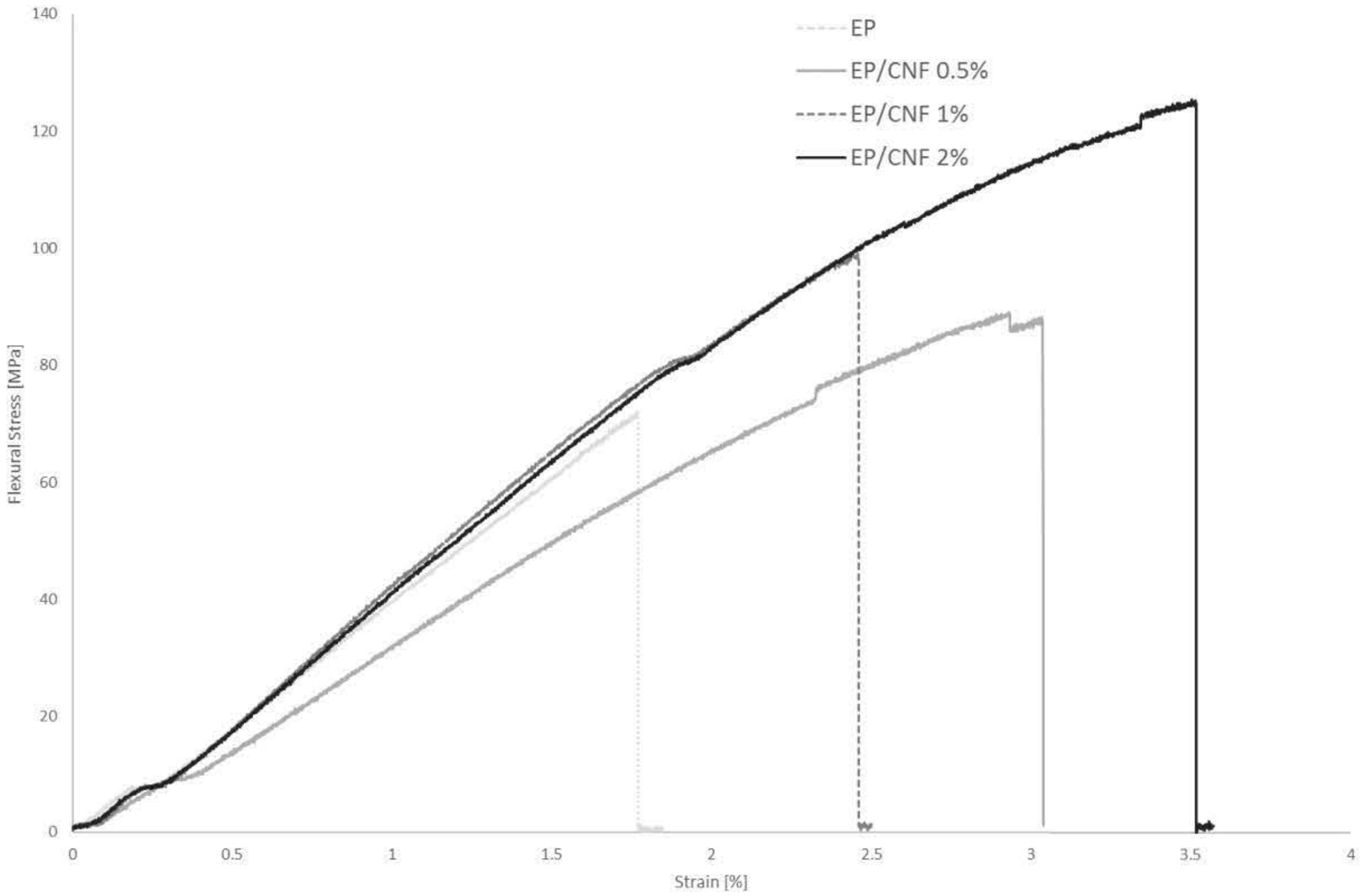

Figure 51: Stress vs strain curves from flexural 3-point bend tests on EP, EP/CNF 0.5 wt. %, EP/CNF 1 wt. % and EP/CNF 2 wt. % samples.

Corresponding to the PP-based and PE-based samples a small constant and flat stress is observed below 0.5% strain for all samples due to the rollers compressing up against the fixture due to the load and is consistent with all samples. The stress can thereafter be seen to increase linearly in an elastic manner. As with the tensile results, the samples did not observe any plastic region or yielding and therefore follow a more brittle material behaviour.

In comparison to the neat EP sample, the reinforced samples all observed a significant increase in elongation. Apart from the EP/CNF 0.5 wt.%, the EP/CNF 1 wt.% and EP/CNF 2 wt.% observed visible increase in flexural strength. From the average stress vs strain plots, shown in Figure 51, the EP/CNF 1 wt.% and EP/CNF 2 wt.% samples appear to exhibit similar Young' Modulus, however with an increase in tensile strength.

From the comparison in the bar chart shown in Figure 52 and numerical representation of the data presented in Table 15, a step increase with increase in CNF weight concentration is observed for the flexural strength. The Young's Modulus however does not show a correlating trend with increase in nanoparticle filler. The variation in sample property is also relatively high in relation to the tensile properties, with EP demonstrating the highest variation in flexural strength (CV = 64.6) and EP/CNF 1 wt. % with the lowest (CV = 13.2).

a.)

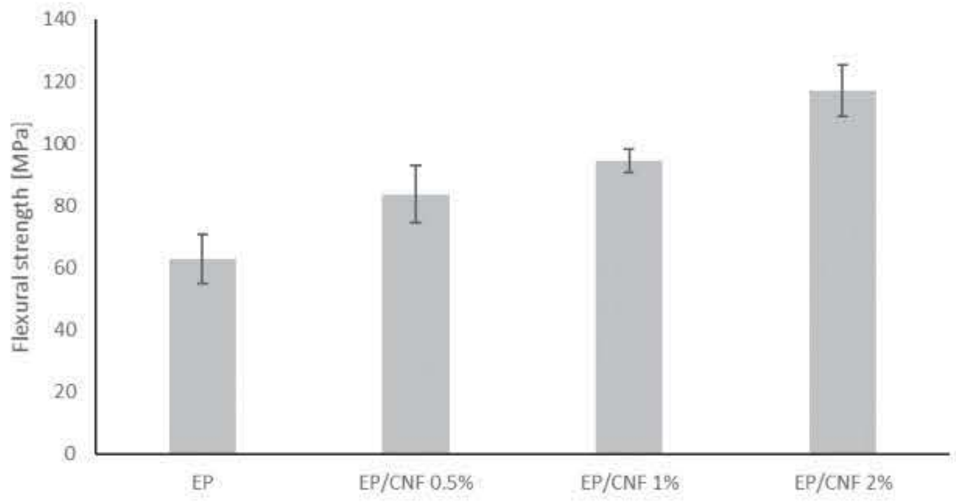

b.)

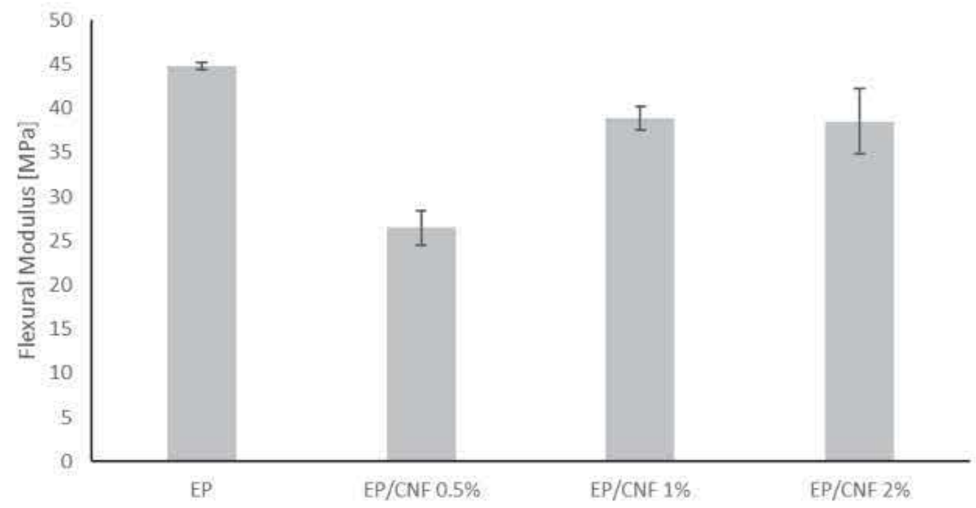

Figure 52: Comparison of mean values of EP-based samples reinforced with CNFs of a.) flexural strength and b.) flexural modulus.

Table 15: Summary and comparison of material properties collected from flexural tests on EP-based samples reinforced with CNFs.

Sample	Flexural Modulus $E_{Flexural}^{Chord}$ ± s_{n-1}: [MPa]	Percentage difference compared to EP	Flexural Strength: $\sigma_{Ultimate}$ ± s_{n-1} [MPa]	Percentage difference compared to EP	Strain at Flexural Strength $\varepsilon_{Flexural}$ at $\sigma_{Ultimate}$	Percentage difference compared to EP
EP	44.8 ± 0.422	/	62.8 ± 8.04	/	1.55 ± 0.191	/
EP/CNF 0.5 wt. %	26.4 ± 1.95	-35.8 %	83.6 ± 9.20	33.1 %	2.76 ± 0.312	78.2 %
EP/CNF 1 wt. %	38.9 ± 1.36	-5.55 %	94.4 ± 3.64	50.3 %	2.30 ± 0.120	48.2 %
EP/CNF 2 wt. %	38.5 ± 3.66	-6.51 %	117 ± 8.20	86.2 %	3.15 ± 0.392	103 %

Further to the numerical values provided in Table 13, statistical analysis was carried out on the samples. From the t-test between each sample and the EP neat sample, only the EP/CNF 2 wt.% sample returned a statistically insignificant difference in flexural modulus (EP/CNF 0.5 wt.% P = 0.00205, EP/CNF 1 wt.% P = 0.00932, and EP/CNF 2 wt.% P = 0.0673). The analysis on the flexural strength returned all of the reinforced samples with a statistically significant difference (EP/CNF 0.5 wt.% P = 0.0374, EP/CNF 1 wt.% P = 0.00888, and EP/CNF 2 wt.% P = 0.00132). Therefore, the flexural modulus of the EP/CNF 2 wt.% sample is the only insignificant difference, with all of the other samples observing a statistically significant increase in flexural modulus and flexural strength in comparison to the EP sample.

ANOVA single factor analysis was also performed to assess the variability between the flexural modulus and flexural strength means. For the flexural modulus, the analysis returned statistically significant differences within the 4 samples (F value = 24.7 F critical value = 4.07) and a 0.021% chance that the observation could have been observed due to random error alone and therefore rejecting a

hypothesis that the samples displayed no difference. Correspondingly for the flexural strength, the analysis returned statistically significant differences within the 4 samples (F value = 17.7, F critical value = 4.07) and a 0.0685 % chance that the observation could have been observed due to random error alone and therefore rejecting a hypothesis that the samples displayed no difference.

In addition to the mechanical performance, the EP, EP/CNF 2 wt. % and EP/CNT 2 wt. % samples underwent a surface electrical conductivity test (produced by Tecnalia) to demonstrate the influence of the CNFs and CNTs on electrical conductivity. The materials were tested in accordance the standard DC resistance or conductance testing of moderately conductive materials (ASTM D4496-13, 2013; ASTM D257-14, 2014) to evaluate the influence of CNTs and CNFs in surface and volume conductivity and are presented in Appendix D.

Epoxy Carbon Fibre reinforced with Graphene Oxide

The EP/CF samples reinforced with GO nanoparticles underwent the same tensile test and the average plots (n=3) of the stress vs strain graph is shown in Figure 53. The tensile stress vs strain plots of the repetitions on individual samples is included in Appendix D.

To add to the analysis, neat EP without the reinforcing micron-sized CF is also include within this section. Firstly, the use of CF can visible show a significant increase in both the tensile strength and Young's Modulus. All of the samples still observed brittle behaviour with purely elastic behaviour prior to fracture, and therefore no plastic deformation or yielding. The step drops observed in the samples represents where samples fractured, therefore affecting the average stress vs strain plot. The drops also highlight the differentiation in material performance, for example the EP/CF/GO 0.1 wt.% sample exhibiting two fractures quite substantially prior to the third. This is accounted for in the large standard deviation seen in Figure 54 and Table 16.

When represented in the bar chard, shown in Figure 54, the GO can be seen to exhibit a decrease in tensile strength in comparison to the EP/CF sample. However, the GO reinforced materials also observed significant variations in tensile strength. In comparison, the EP/CF/GO 0.05 wt.% sample exhibited a substantial increase in Young's Modulus. The EP/CF/GO 0.1 wt.% and EP/CF/GO 0.2 wt.% in contrast, showed opposing trends, with either a minor decrease or minor increase in Young's Modulus in comparison to the EP/CF sample. There is therefore no clear influence on the effect on the flexural modulus in relation to the weight concentration of GO.

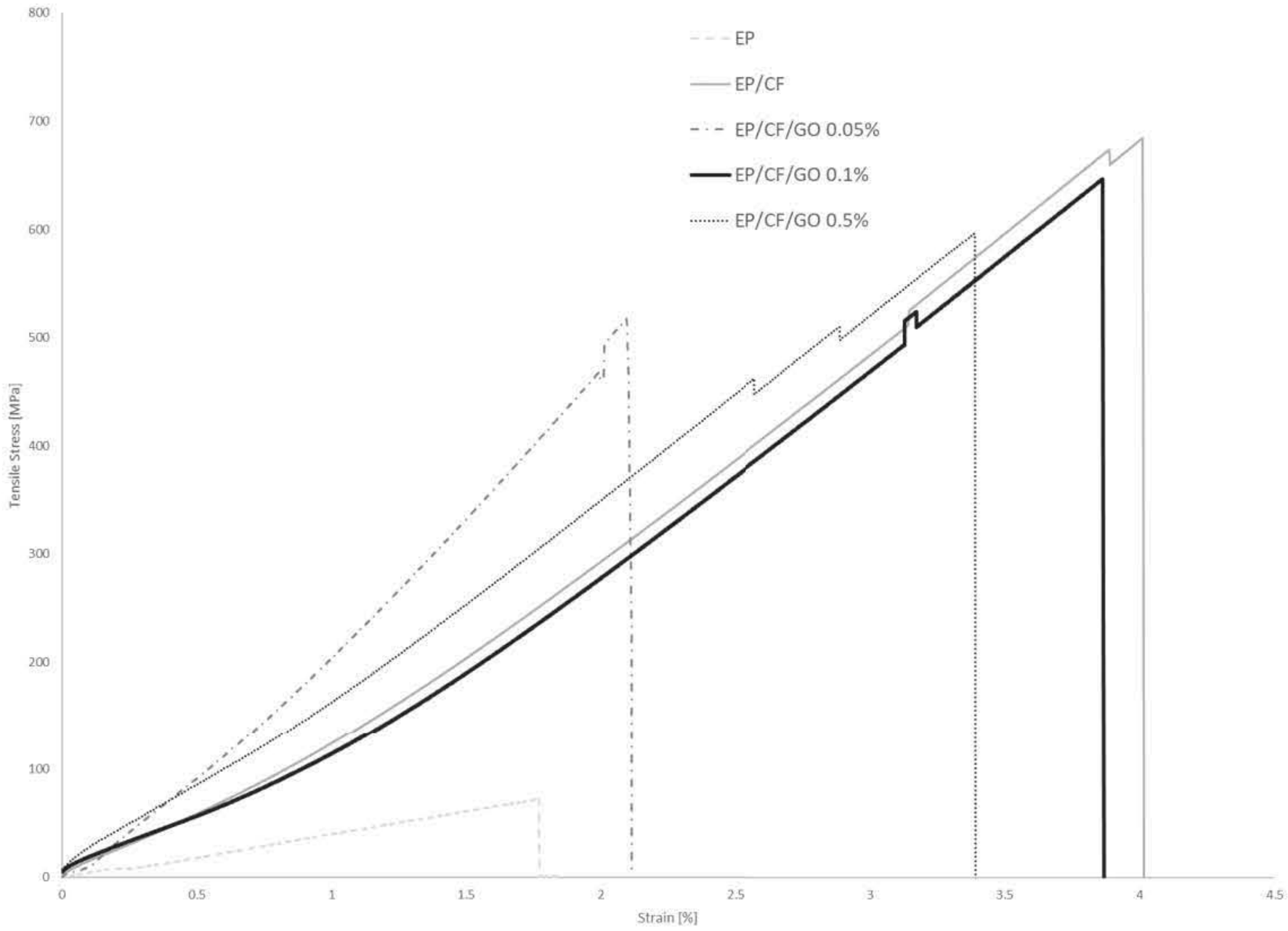

Figure 53: Stress vs strain curve averages from tensile tests on EP, EP/CF, EP/CF/GO 0.05 wt.%, EP/CF/GO 0.1 wt.% and EP/CF/GO 0.5 wt.% samples.

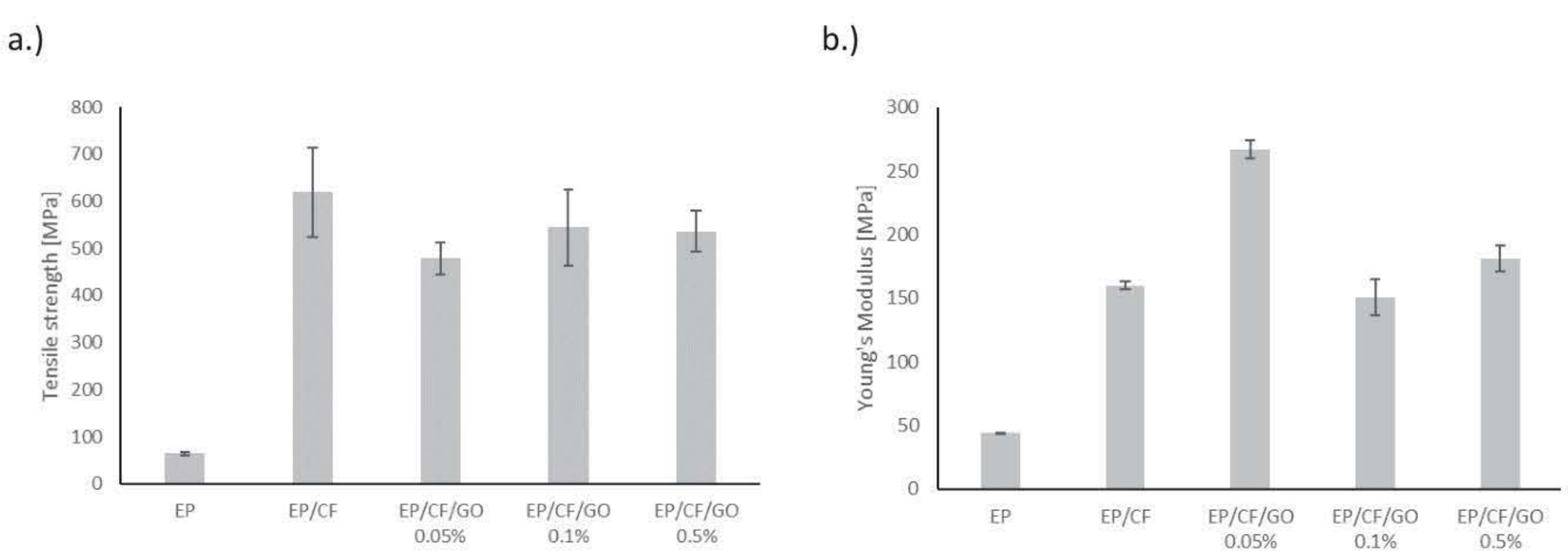

Figure 54: Comparison of mean values of EP/CF-based samples reinforced with GO of a.) tensile strength and b.) Young's Modulus.

Statistical analysis was carried out on the samples. A t-test with comparison to the EP will return a statistically significant difference for all samples for both tensile strength and Young's Modulus. Therefore, in a t-test between each sample and the EP/CF sample, only the EP/CF/GO 0.1 wt.% did not return a statistically significant difference for Young's Modulus (EP/CF/GO 0.05 wt.% $P = 0.0000567$, EP/CF/GO 0.1 wt.% $P = 0.240$, and EP/CF/GO 0.5 wt.% 2 wt.% $P = 0.0391$). The analysis on the tensile strength, returned all of the reinforced samples with a statistically insignificant difference (EP/CF/GO

0.05 wt.% P = 0.0814, EP/CF/GO 0.1 wt.% P = 0.222, and EP/CF/GO 0.5 wt.% 2 wt.% P = 0.175). This is attributed to the high deviation between samples. Therefore, whilst none of the samples returned a statistically significant difference in tensile strength, only the EP/CF/GO 0.1 wt.% did not return a statistically significant difference for Young's Modulus.

Table 16: Summary and comparison of material properties collected from tensile tests on EP/CF-based samples reinforced with GO.

Sample	Young's Modulus $E_{Young's} \pm s_{n-1}$: [MPa]	Percentage difference compared to EP	Tensile Strength: $\sigma_{Ultimate} \pm s_{n-1}$ [MPa]	Percentage difference compared to EP	Strain at Tensile Strength $\varepsilon_{Tensile}$ at $\sigma_{Ultimate}$	Percentage difference compared to EP
EP	44.0 ± 0.213	/	63.8 ± 2.73	/	1.60 ± 0.0183	/
EP/CF	160 ± 2.92	263 %	619 ± 94.9	870 %	2.88 ± 0.000500	80.2 %
EP/CF/GO 0.05 wt.%	267 ± 7.37	507 %	479 ± 34.0	651 %	2.03 ± 0.0445	27.0 %
EP/CF/GO 0.1 wt.%	151 ± 14.0	243 %	544 ± 80.8	753 %	3.39 ± 0.336	112 %
EP/CF/GO 0.5 wt.%	181 ± 10.2	312 %	536 ± 43.8	741 %	2.78 ± 0.149	73.7 %

ANOVA single factor analysis was also performed to assess the variability between the Young's Modulus and tensile strength means. For the Young's Modulus, the analysis returned statistically significant differences within the 4 samples (F value = 56.9, F critical value = 4.07) and a 9.67 x 10^{-4} % chance that the observation could have been observed due to random error alone and therefore rejecting a null hypothesis that the samples displayed no difference. Correspondingly for the tensile strength, the analysis returned statistically insignificant differences within the 4 samples (F value = 1.41, F critical value = 4.07) and a 30.9 % chance that the observation could have been observed due to random error alone and therefore accepting a null hypothesis that the samples displayed no difference as it lies within the 90% confidence interval.

The EP/CF samples reinforced with GO were also evaluated for flexural material properties. This was carried out with a 3-point flexural test as per the ASTM D7264M standard. The average (n= 3) stress vs strain plots for each composition is shown in Figure 55. The individual stress vs strain plots are presented in Appendix D.

As with the tensile data, the samples including CF showed a clear improvement in flexural strength and increase in flexural modulus in comparison to the neat EP sample. Relating the EP/CF sample with the EP/CF/GO reinforced samples, the samples are more comparative. As with the tensile properties,

the materials observed a purely elastic behaviour prior to a brittle failure without any yield or plastic region. The continuous brittle behaviour seen in all EP-based samples emphasises the influence the polymer has on the type of failure. The fillers can thereafter be seen to have a marginal increase or decrease in the flexural modulus and/or flexural strength. Noticeably within the EP/CF/GO samples, the EP/CF/GO 0.1 wt. % demonstrated a substantial decrease in elongation at failure. However, the flexural strength is comparable to that of the EP/CF/GO 0.5 wt. %.

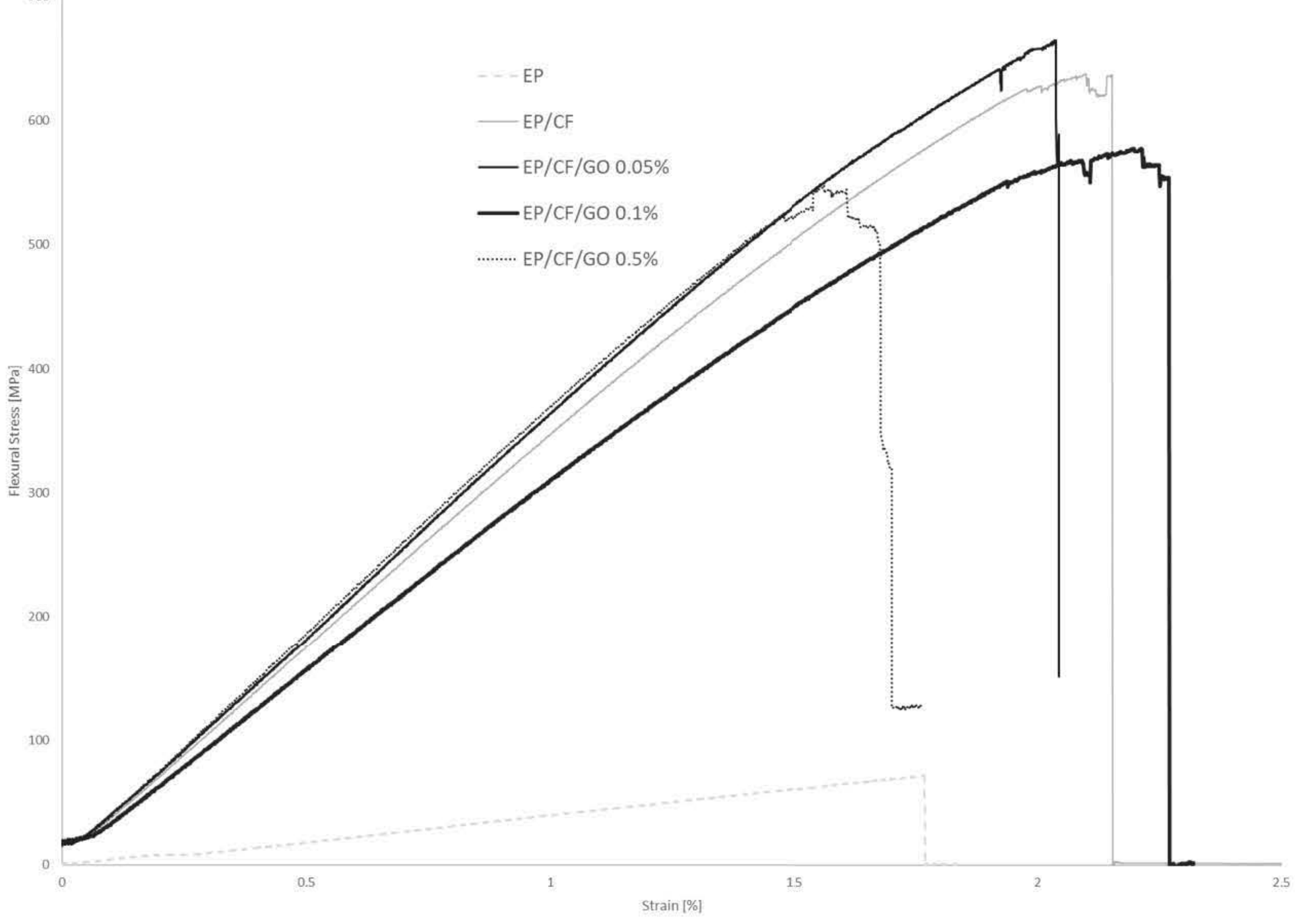

Figure 55: Stress vs strain curve averages from flexural 3-point bend tests on EP, EP/CF, EP/CF/GO 0.05 wt.%, EP/CF/GO 0.1 wt.% and EP/CF/GO 0.5 wt.% samples.

As with the previous samples, the average stress vs strain plot does not fully represent the mean flexural strength or flexural modulus as the plot will extend until the failure of the final sample. The numerical data presented in Table 17 and the bar chart shown in Figure 56, account for this. From the data shown in Table 17 and Figure 56, the EP/CF/GO 0.05 wt. % and EP/CF/GO 0.5 wt. % samples demonstrated a marginal increase in flexural modulus. In contrast, only the EP/CF/GO 0.05 wt. % sample exhibited a minor increase in flexural strength. In comparison to the neat EP sample (CV = 0.178), the variances of flexural modulus for the EP/CF (CV = 22.80), EP/CF/GO 0.05 wt. % (CV = 27.4 MPa), EP/CF/GO 0.1 wt. % (CV = 13.3 MPa) and EP/CF/GO 0.5 wt. % (CV = 54.7) are larger and therefore demonstrate a bigger deviation and less consistency in material property.

a.)

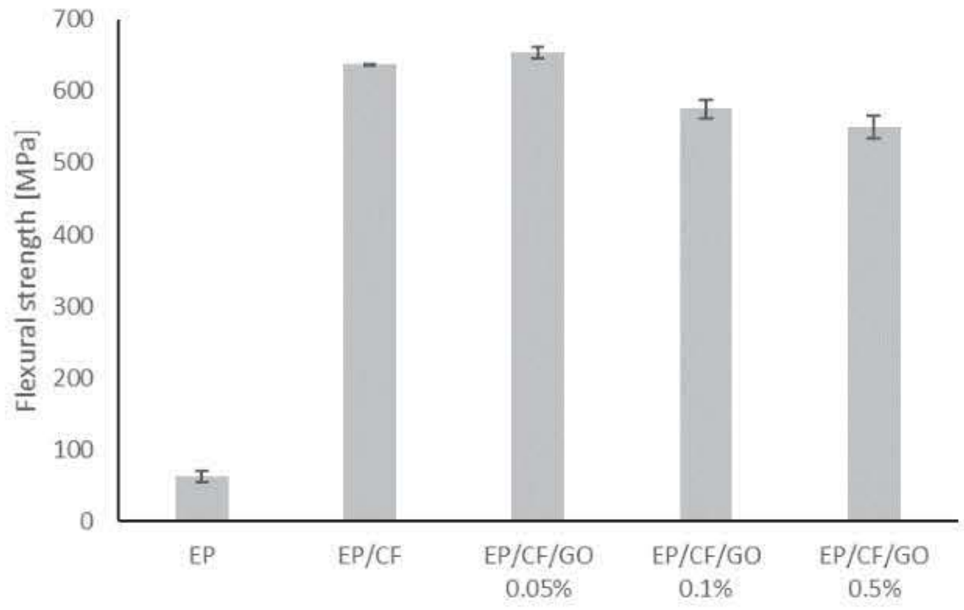

b.)

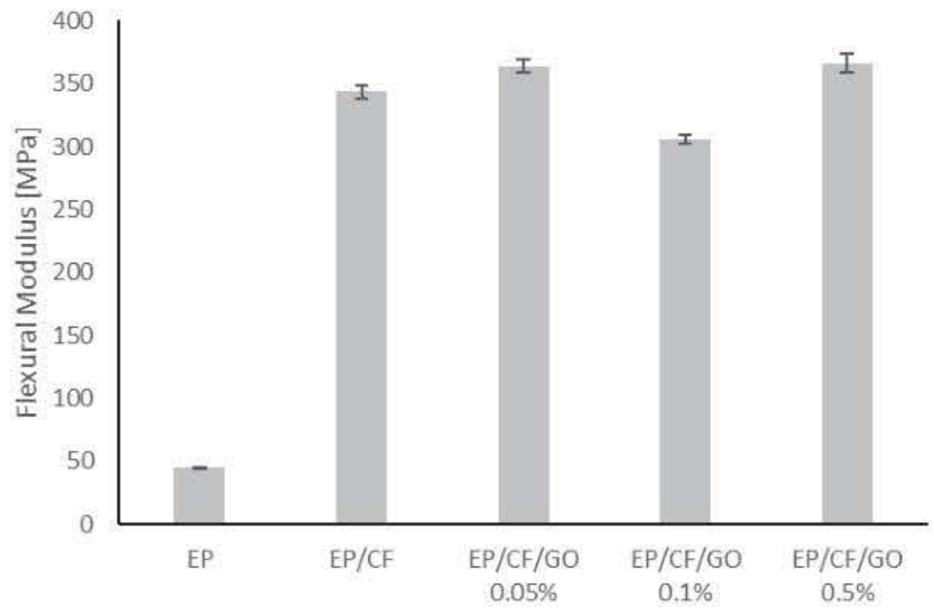

Figure 56: Comparison of mean values of EP/CF-based samples reinforced with GO of a.) flexural strength and b.) flexural modulus

Table 17: Summary and comparison of material properties collected from flexural tests on EP/CF-based samples reinforced with GO.

Sample	Flexural Modulus $E_{Flexural}^{Chord}$ ± s_{n-1}: [MPa]	Percentage difference compared to EP	Flexural Strength: $\sigma_{Ultimate}$± s_{n-1} [MPa]	Percentage difference compared to EP	Strain at Flexural Strength $\varepsilon_{Flexural}$ at $\sigma_{Ultimate}$	Percentage difference compared to EP
EP	44.8 ± 0.422	/	62.8 ± 8.04	/	1.55 ± 0.191	/
EP/CF	343 ± 4.78	666 %	638 ± 0.62	915 %	2.03 ± 0.0310	31.1 %
EP/CF/GO 0.05 wt.%	364 ± 5.23	712 %	653 ± 8.17	940 %	1.97 ± 0.0480	27.2 %
EP/CF/GO 0.1 wt.%	306 ± 3.65	583 %	575 ± 13.3	815 %	2.11 ± 0.0664	36.3 %
EP/CF/GO 0.5 wt.%	366 ± 7.40	717 %	549 ± 15.8	774 %	1.56 ± 0.0656	0.820 %

In additional to the numerical values provided in Table 17, statistical analysis was carried out on the samples. Similarly, as with the tensile properties, a t-test with comparison to the EP will return a statistically significant difference for all samples for both tensile strength and Young's Modulus. From the t-test between each sample and the EP/CF, all of the samples returned a statistically significant difference in flexural modulus (EP/CF/GO 0.05 wt.% P = 0.00784, EP/CF/GO 0.1 wt.% P = 0.000622, and EP/CF/GO 0.5 wt.% 2 wt.% P = 0.0142). The analysis on the flexural strength, only the EP/CF/GO 0.05 wt.% returned with a statistically insignificant difference (EP/CF/GO 0.05 wt.% P = 0.0575, EP/CF/GO 0.1 wt.% P = 0.0106, and EP/CF/GO 0.5 wt.% 2 wt.% P = 0.00765). Therefore, whilst the EP/CF/GO 0.05 wt.% returned with a statistically insignificant difference in flexural strength, the

inclusion of GO returned statistically significant differences in flexural modulus and flexural strength, both negative and positive.

ANOVA single factor analysis was also performed to assess the variability between the flexural modulus and flexural strength means. For the flexural modulus, the analysis returned statistically significant differences within the 4 samples (F value = 52.3, F critical value = 4.07) and a 0.001332% chance that the observation could have been observed due to random error alone and therefore rejecting a null hypothesis that the samples displayed no difference. Correspondingly for the flexural strength, the analysis returned statistically significant differences within the 4 samples (F value = 40.3, F critical value = 4.07) and a 0.00355 % chance that the observation could have been observed due to random error alone and therefore rejecting a null hypothesis that the samples displayed no difference.

3.4. Conclusion

The influence on mechanical properties of a variation in fillers within EP, EP/CF, PE and PP nanocomposites representing polymers with different applications were evaluated. Microscopy analysis demonstrated the nanofillers used within the polymers, followed by EDX and FT-IR analysis. The variation in nanoparticle size, shape and form were demonstrated, whilst also obtaining elemental and analytical data on the materials. Following this, the tensile and flexural properties of the materials are evaluated. The influence the fillers have on the material properties is gathered and presented. From the results, a variation in conclusions can be drawn for the separate materials.

The incorporation of reinforcing fillers within PP demonstrated to have little effect on the tensile properties, however, a statistically significant improvement in flexural properties. With PP/Talc taken as the reference in material performance for the automotive industry, the nanoparticle fillers can be ascertained to decrease the material density without significantly affecting the tensile and/or flexural properties. The material characterisation was unable to differentiate the incorporation of the nanofillers, this is however a common observation within literature due to the low concentrations used.

In comparison, the PE-based samples observed a less ductile behaviour than the PP samples and only the PE/SiO_2 5 wt.% observed no statistically significant difference in either Young's Modulus or tensile strength in comparison to the PE sample in tensile properties. The flexural properties exhibited that all reinforcing fillers improved both the flexural modulus and flexural strength in comparison to the PE sample. Although a change in surface is observable from the microscopy, the FT-IR was unable to differentiate the inclusion of the nanoparticles to the PE sample.

The EP reinforced with CNFs and CNTs displayed contrasting results. All of the EP-based samples displayed a purely elastic behaviour prior to fracture, i.e. no yield of plastic region. In comparison to the neat EP sample, only the flexural modulus of the EP/CNT 1 wt. % and EP/CNF 2 wt. % sample returned statistically insignificant difference in flexural properties. The tensile properties demonstrated similar results with only the EP/CNF 1 wt. % returning with a statistically insignificant difference for Young's Modulus and only the EP/CNT 0.5 wt.% and EP/CNT 2 wt.% observed a statistically insignificant difference in tensile strength.

The use of CF within EP exhibited a significant increase in both tensile and flexural properties in comparison to the neat EP. The incorporation of the GO nanofiller however, had contrasting influence on the material properties. Although, only the EP/CF/GO 0.1 wt. % returned a statistically insignificant difference for Young's Modulus, all of the GO reinforced samples returned a statistically insignificant difference in tensile strength. This is attributed to a large variation in material performance for both the EP/CF and Go reinforced samples. In contrast, all of the samples returned a statistically significant difference in flexural modulus, and only the EP/CF/GO 0.05 wt. % returned with a statistically insignificant difference in flexural strength. In addition, and similar with the other sample due to the low concentrations, the microscopy and FT-IR did not return clear evidence of the nanoparticles.

Comparing all of the polymers, the reference material can be seen to have the greatest influence in the tensile and flexural material property behaviour. The PP samples can be concluded to be highly ductile without many factures, whereas the PE samples did observe a small plastic region and consequently a less ductile material behaviour. In contrast, all of the EP-based samples, included the EP/CF based samples, observed a brittle failure with a purely elastic increase in stress with no evidence of a yield point prior to fracture and failure.

Each polymer and nanofiller demonstrated different correlation with influence on tensile and flexural properties. Nonetheless, a clear and notable correlation between the introduction of the nanofillers and material properties is established in the flexural strength. All but one sample, EP/CF/GO 0.05 wt. % returned a statistically significant result when compared to the sample without the nanoparticle reinforcement. Similarly, only two samples, EP/CNT 1 wt. % and EP/ CNF 2 wt. %, returned a statistically insignificant difference in flexural modulus. Correspondingly, the ANOVA single factor analysis performed to assess the variability between the means on each group of samples, rejected the null hypothesis that the samples displayed no difference for the flexural modulus and flexural strength for all samples.

Within the chapter, materials identified to include several potentially toxic nanoparticles within a variation of industry sectors that might undergo drilling within its life cycle were selected and mechanical properties evaluated. The influence of the nanofillers displayed contrasting effects on the tensile and flexural properties, as stated. The influence this will have on nanoparticle release when the materials undergo drilling, is therefore necessary to assess.

Chapter Four

Influence of MMT, WO and Talc on Nanoparticle Emissions from Polypropylene Based Nanocomposites during Automated Drilling

4.1 Introduction

Within this study, the effect on nanoparticle emissions during drilling on PP samples reinforced with three fillers is investigated. According to a report in 2018, PP is the most sought-after polymer type, representing 19.3% of all plastics demand within Europe (PlasticsEurope Market Research Group, 2018). The high consumer demand for the thermoplastic is mainly due to its simplicity in processing, lightweight, low cost and high recyclability (Liang et al., 2016). To improve the materials properties, PP is usually modified with inorganic fillers, such as talc (Lapcik et al., 2009; Weon and Sue., 2006), MMT (Selvakumar et al., 2010; Ghasemi et al., 2016), metallic powders (Esthappan et al., 2015; Shimpi et al., 2017), calcium carbonate (Payandehpeyman et al., 2017; Yong et al., 2011), glass fibres (Ashori et al., 2016; Luo et al., 2017), wood powder (AlMaadeed et al., 2012; Haque et al., 2019) and WO (Luyt et al., 2009; Ding et al., 2019). This chapter includes the use of talc, MMT and WO as mechanical reinforcements in PP composites as they are increasingly well-established fillers throughout literature.

Although the three fillers are established to improve material mechanical properties, these micro and nano-sized fillers have however shown potential cytotoxicity affects if exposed to and inhaled (Lordan et al., 2011; Maxim and McConnell, 2005; Maxim et al., 2014; Akhtar et al., 2014). Reviews of literature on the release and/or exposure of nanoparticles from ENMs have also concluded that high-energy processes, including drilling, have shown evidence of likelihood of nanoparticle release (Bainas et al., 2018; Debia et al., 2016; Froggett et al., 2014). As detailed within the Literature Review section 2.5.2, there is still an insufficient understanding on how these fillers effect the release of nanoparticles from

nanocomposite materials and the full risks associated to the emissions and nanoparticle exposure into the environment (Gendre et al., 2016; Njuguna et al., 2014). This chapter will therefore evaluate the influence of talc, WO and MMT on nanoparticle release from PP-based composites when under a simulated and controlled life cycle scenario: automated drilling process.

4.2 Experiments

4.2.1 Materials and Samples Manufacturing

The materials are manufactured at Tecnalia, Donostia (Spain), as described in section 3.2.1, and is incorporated here for aptness. A commercially available PP homopolymer (Moplen HP648T, Lyondell Basell Industries, Netherlands) was selected to represent the automotive industry. The reinforcements and concentrations chosen were 20 wt. % talcum as a common filler within industry and 5 wt. % WO (Harwoll 7ST5, Nordkalk, Finland) and 5 wt. % of MMT (Nanomer I30T, Nanocor Corporation, USA) as to enhance the mechanical performance properties (tensile and flexural). Neat samples of the PP were chosen to be used as reference materials as a comparison to evaluate the influence of the nanofillers. A Coperion ZSK 26 MEGAcompounder twin-screw extruder was used for homogenization of the nanocomposites. The extruded pellets of the materials were moulded by injection process by means of an Arburg All Rounder 270C-300-100 Injection Machine. Due to the diverse polarity nature of the polypropylene and the MMT and WO, a coupling agent (POLYBOND 3200 from ADDIVANT) was used to ensure adhesion between the nanofillers and the polymer.

4.2.2 Characterisation

To evaluate the samples manufactured, the materials were characterised through SEM, EDX and FT-IR. As explained in section 3.2.2, both a Zeiss EVO LS10 Variable Pressure Scanning Electron Microscope and an SEM/EDX (FEI Quanta 200F) with a beam current of 208 µA and voltage of 10 kV were used in the upcoming study and cross-checked using an electron probe microanalyser (EPMA) JEOL JXA-8621MX, with beam current of 30 nA and voltage of 15 kV. SEM samples of the materials were prepared using sputter coating of an ultra-thin coating of gold to minimize charging. The materials were further investigated using a NICOLET iS10, Thermo Scientific ATR-FT-IR. SEM, EDX and FT-IR of the materials prior to drilling are demonstrated in sections 3.3.1 and 3.3.2.

The materials were firstly investigated for mechanical properties. The effect of the nanofiller on the material mechanical performance are shown to demonstrate the original benefits and use to strengthen the materials. The materials underwent a flexural 3-point bend test in accordance with

ASTM D 7264/M flexural test (ASTM D7264M, 2015) and a standard ASTM D 3039/D tensile test (ASTM D3039, 2017). These results are included in section 3.3.3.

4.2.3 Automated Drilling Methodology

As highlighted within the literature review, in section 2.5 and 2.6., there is currently a lack of a harmonised method in testing nanocomposite materials for nanoparticle release during a variety of lifecycle scenarios, including drilling. A controllable and repeatable methodology is required to characterise and understand the release to be able to comprehend and/or prevent consequential toxicity of nanoparticles released from ENMs. Without any current standard methodology of quantifying the release of nanoparticles from mechanical drilling, a methodology is used to simulate mechanical drilling that allows direct measurement of nanoparticles emitted during drilling. A brief description of the methodology is included here with the full details, development and demonstration of repeatability of the automated drilling methodology included in Appendix A.

The methodology utilises a process related approach (as explained in literature review section 2.6. and categorised by Kuhlbusch et al. 2011). This process is designed to simulate mechanical drilling on nanocomposite materials and is continued work from the NEPHH project study (Sachse et al., 2012a; Sachse et al., 2012b). A crucial factor identified in the literature review for the methodology is to control the background particles to setup a controlled environment. Building on the NEPHH project, the chamber is capable of achieving a clean environment monitored using a CPC, importantly removing all background noise or interference on the measurement of number concentration and particle size distribution. The data collected is therefore a representation of the particles released solely from the material. Removing the background data allows for a depiction of any particles released from the materials which can be directly linked as an unconditional maximum exposure assessment (Kuhlbusch et al. 2011). As proposed in several studies, such as *Brouwer et al., (2012), Methner et al., (2010a), and Methner et al., (2010b)*, with a controlled testing setup and environment, only one parameter, material, is changed and investigated. This simplifies the issue of accounting for local background influences, as specified within the guidelines and reports by OECD ENV/JM/MONO (2017; 2019).

Once the chamber was cleared of any particles, the drilling studies were carried out by drilling across the width of the sample resulting in eight separate holes and bearing a time duration of 3 minutes of drilling, followed by 1 minute post-drilling. The eight holes drilled per sample were repeated three times to get an average of the particle number concentration and particle size distribution released.

Based on previous studies carried out on nanocomposite drilling (Sachse et al. 2012a, Sachse et al. 2012b; Bello et al. 2010; Irfan et al., 2013), a standard Dremel 4000 drilling tool with an industrial standard stainless steel 3.5mm twist drill bit was used at 10000 rpm with a feed rate of 78 mm/min. The setup uses an automated drilling assembly operated externally to the chamber to permit a repeatable and controlled environment within the chamber. The design drawing and apparatus setup is shown in Appendix A (Figure 130).

The closed steel chamber has dimensions of 740 mm x 550 mm x 590 mm, and therefore a total inner volume of 0.240 m^3. It is designed to assure a closed environment to simulate an appropriate volume around the drill and minimising electrostatic attraction to the surfaces. To quantify only the particles released from the sample, the chamber was initially cleared of particles through an inflow of clean air with the use of TSI 99.97 % retention HEPA Capsule Filters. A separate capsule was constructed around the drill with separate air flow to avoid any interference of the drilling fumes on the particle number concentration within the capsule. The nanoparticle release data with and without the chamber around the drill is presented in Appendix A. The clean air system using the HEPA Capsule filters and with the drill on, was capable of producing a particle number concentration reading within the chamber of 0 particles/cm^3 with false background counts <0.01 particles/cm^3, as measured using a TSI Environmental Condensation Particle Counter (CPC) model 3783 at a flow rate of 0.6 L/min, particle range of 7 - 3000 nm and concentration range of 0-10^6 particles/cm^3 and ± 10 % at 10^6 particles/cm^3. The level of background noise is therefore significantly within the ISO (ISO 14644-1, 2015) cleanroom standard for particles ≥0.1 µm of 10 particles/cm^3.

An outlet channel is placed adjacent to the test specimen for the nanoparticle release equipment readings. A standard IOM Inhalable Sampler for collection of inhalable particles was placed next the test specimen with a 2 L/min suction to attract and prevent particles from detaching away from the grid for post-test chemical analysis (Sanchez Jimenez et al., 2012). An additional sampling tray was positioned below the test specimen for collection of the deposited particles for further post-test analysis.

The scanning mobility particle sizer (SMPS) used for the study is a TSI 3080 Electrostatic Classifier utilizing a nano Differential Mobility Analyser (DMA) with 99 distinct particle diameters within a particle range of 4.61 -156.8 nm and a flow rate of 0.31 L/min. The principle of the Model 3080 Electrostatic Classifier with the DMA is based on the monotonic relationship between electrical mobility and particle size with singly charged particles. The aerosol particles go through a process of bipolar charging or “neutralization” and are then classified with the differential mobility analyser and then measured by a Condensation Particle Counter. The given particle size distribution is therefore

corresponding to the electrical mobility diameter. In addition, separate repeated runs were carried out using a Cambustion DMS50 Fast Particle Size Spectrometer with a 1 second sampling period, inlet flow rate of 6 L/min, with 34 distinct particle diameters of size range between 4.87 nm – 562.34 nm for the particle size distribution. The DMS50 utilizes a unipolar corona charger placing positive charges on each particle which are then classified along electrometer detectors based on mobility and hence particle size (*Cambustion DMS50 MKII, 2008*). The charge is conducted via an electrometer amplifier whose output indicates the flux of particles giving the particle concentration at that given particle size. Since the classification of particles according to their differing electrical mobility takes place in parallel (rather than in series as in the SMPS) the DMS50 can offer the faster sampled particle size distribution. This allowed for a size distribution every second compared to the SMPS of 45 s period (followed by 10 seconds for the classifier to regenerate to its initial voltage and 5 seconds to start the size distribution again) and therefore a faster representation of the particles being released from the sample during drilling. The SMPS uses the assumption of spherical particles. Hence, from the diameters of the particle size distribution measured, and the material density of the nanocomposites, the particle mass size distribution can be estimated.

Both Zeiss EVO LS10 Variable Pressure Scanning Electron Microscope and an SEM/EDX (FEI Quanta 200F) with a beam current of 208 µA and voltage of 10 kV were used for present study and cross-checked using an electron probe microanalyser (EPMA) JEOL JXA-8621MX, with beam current of 30 nA and voltage of 15 kV. SEM samples of the materials were prepared using sputter coating of an ultra-thin coating of gold to minimize charging. A sampling tray placed immediately below the drilling set up in the chamber was used to collect debris removed from the nanocomposites during the drilling operation.

4.3 Results & Discussion

4.3.1 Filler Effect on Particle Number Concentration

The four PP based samples underwent the automated drilling procedure described. Using the CPC, the particle number concentration was quantified in situ with a sampling rate of 1 second. An average of the repeated test (n = 3) for each sample is displayed in Figure 57.

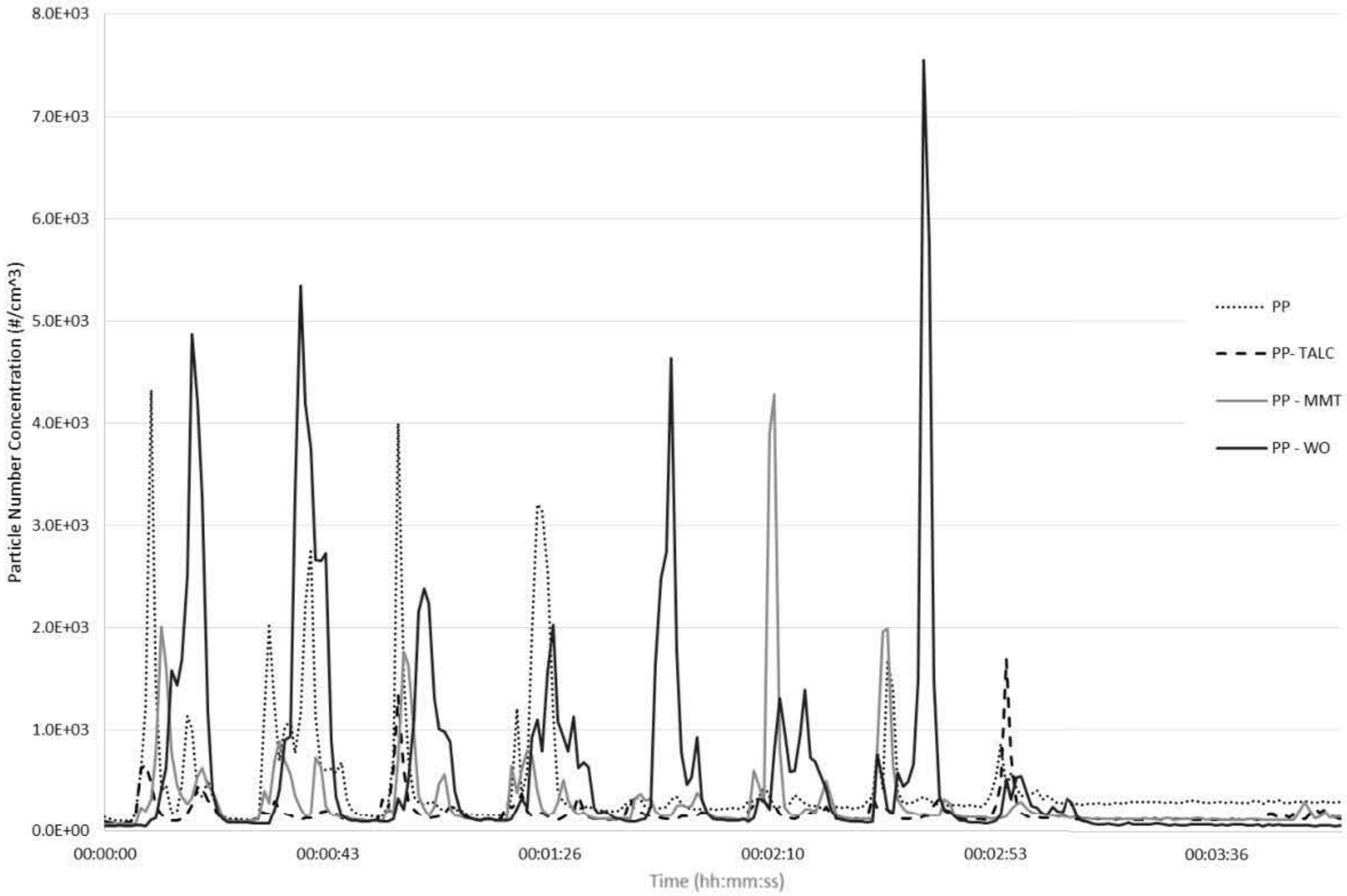

Figure 57*:* Particle number concentration averages of PP based nanocomposite samples during eight holes drilled within 3 minutes followed by 1 minute of no drilling as measured with the CPC (n=3 for each average).

The peaks observed in Figure 57 clearly exemplifies the eight holes drilled within the 3 minutes for the four PP based samples. On most of the peaks, the movement of the drill going in and out of the sample can also be perceived from peaks being faintly divided into two peaks. When the drill is out of the sample, the particle number concentration is seen to drop between each hole being drilled. The real-time data presents large concentration peaks introduced during the drilling process. A maximum value in terms of quantity of the particles being released at the time of drilling is obtained. The methodology is able to provide a comprehensive depiction of the particles released during the drilling before (anything within 1 second) dispersion and scattering within the chamber. The particle number concentration can then be observed to relatively stabilize during the 1 minute after the drilling has ended, but does not drop back to the initial 0 #/cm^3. Thus, the particles produced from the drilling remain airborne within the chamber environment. These two meaningful annotations therefore epitomise the release characteristics observed: peak particle number concentrations and remaining airborne concentration after 4 minutes of sampling.

When assessing the release of each material due to the drilling, the peak mean particle number concentrations introduced at the point of drilling can be used to provide confidence interval construction and hypothesis testing.

The PP/WO sample demonstrated the largest average peaks (9649 #/cm^3) across the eight holes drilled when compared to the PP (7546 #/cm^3), PP/Talc (960 #/cm^3) and PP/MMT (4354 #/cm^3). These numerical values are presented along with the inferential statistical confidence intervals in Table 18. The PP/WO sample displayed the only escalation in average peak particle number concentration due to the drilling in comparison to the neat PP sample. Whereas the PP/MMT exhibited a small reduction and the PP/Talc sample indicated the lowest peaks of all the samples.

Table 18*:* Inferential statistical representation of the particle number concentrations introduced at the peaks due to the drilling (n = 24 for each sample). Lower and upper limits represent the 90% confidence interval on a sampling t-distribution.

Sample	Mean: $\overline{\overline{X}}$ [#/cm^3]	Deviation: $S_{\overline{X}}$ [#/cm^3]	Minimum [#/cm^3]	Maximum [#/cm^3]	5% Lower limit of confidence interval [#/cm^3]	95% upper limit of confidence interval [#/cm^3]
PP	7.55 x 10^3	6.33 x 10^3	0.50 x 10^3	15.3 x 10^3	4.38 x 10^3	10.7 x 10^3
PP/Talc	0.96 x 10^3	0.93 x 10^3	0.32 x 10^3	3.02 x 10^3	0.50 x 10^3	1.43 x 10^3
PP/MMT	4.35 x 10^3	3.89 x 10^3	0.65 x 10^3	12.6 x 10^3	2.41 x 10^3	6.30 x 10^3
PP/WO	9.65 x 10^3	7.09 x 10^3	1.36 x 10^3	22.4 x 10^3	6.10 x 10^3	13.2 x 10^3

The inferential statistical analysis presented in Table 18 represents the differences between the peak particle number concentrations introduced from the 8 holes within the four minutes. The use of statistical analysis is reported throughout literature (Bainas et al., 2018). Efforts towards a harmonised method of assessing the release of nanoparticles from ENMs include the use of inferential statistics to evaluate if there is a statistically significant difference (i.e. evaluating if $P < 0.05$) from a formal test of arithmetic mean concentration being higher than background by at least three times the standard deviation of the background concentrations (OECD, 2015). As the background is cleared of any particles, this is evaluated using the neat PP sample. As can be seen in Table 18, the standard deviation and range for the mean peak particle number concentrations is considerably high. Therefore, the peak concentrations introduced due to the drilling can be concluded to still demonstrate a level of randomness and uncertainty. The calculated lower tail of 5% and upper tail of 95% give a representation of the data for a 90% confidence interval of a t-distribution. The two-sample t-test of significance was performed on each sample in comparison to the neat PP sample to identify any significant effect of the filler. The PP/Talc and PP/MMT displayed a statistically significant difference

in the mean peak particle number concentration (statistically significant decrease), whereas the PP/WO demonstrated to be within a 95% confidence interval of the PP sample (statistically insignificant). ANOVA single factor analysis was performed to assess the variability between the sample peak means introduced due to the filler. The analysis returned statistically significant differences within the 4 samples (F value = 4.34 and F critical value = 2.95) and a 1.24% chance that the observation could have been observed due to random error alone and therefore rejecting a hypothesis that the samples displayed no difference in peak particle number concentrations.

However, as shown in Figure 57 and accentuated in the bar chart in Figure 58, the PP/WO sample demonstrated to have the lowest average particle number concentration at the end of the four-minute sampling period (64 #/cm^3), and in contrast, the PP sample displayed the highest particle number concentration (372 #/cm^3).

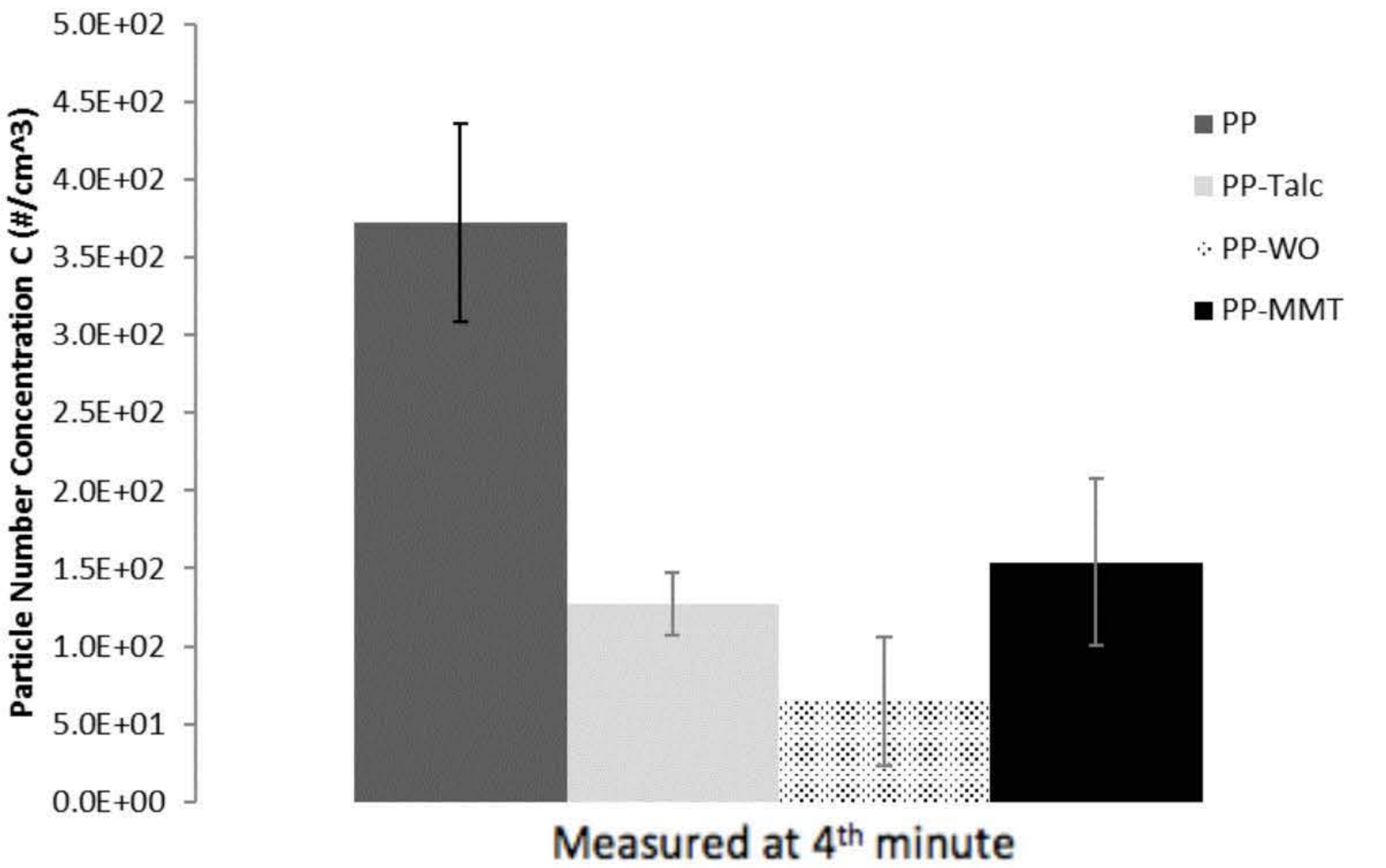

Figure 58*:* Particle number concentration recorded at 4th min (C, #/cm^3) for Polypropylene based samples as measured on the CPC (n=3 for each average).

The PP/Talc sample (127 #/cm^3) and PP/MMT sample (154 #/cm^3) remained in-between. Although, the PP/WO sample illustrated to have the highest peak value, peak average and total average over the entire four-minute sampling period (average over four-minutes: PP = 449 #/cm^3, PP/Talc = 183 #/cm^3, PP/MMT = 299 #/cm^3, PP/WO = 587 #/cm^3), the sample presented the lowest particle number concentration at the end of the four minutes.

The particles released from the PP/WO are therefore, perceived to deposit quicker than the three other samples. This conflicts with the nano-reinforced samples having a lower density to the PP or PP/talc sample (density given in Chapter 3). The lower particle number concentration after drilling is beneficial in relation to nanosafety and if considering materials following safety by design. The decrease in particle number concentration suggest reactive particles and either attracted to components within the chamber or agglomerating to larger particles the CPC is unable to pick up.

In relation to the average particle number concentration over the sampling period, PP/WO is the only sample that produced an increase in particles over the PP sample, with a 30 % increase, compared to the decrease of 59 % and 33 % from the PP/talc and PP/MMT samples respectively. The nano-filled samples therefore, exhibited a converse 33 % decrease (PP/MMT) or a 30 % increase (PP/WO) on the particle number concentration released over the PP sample. However, these sets of results prominently indicate that the matrix has a substantial contributing factor on the particle number concentration when comparing the PP samples with other polymers and the statistical significance results. A similar trend with a silicate nanofiller producing the most particles during drilling and the influencing factor of the PP is observed in the NEPHH project reported in *Irfan et al., 2013*.

4.3.2 Filler Effect on Particle Size Distribution

Simultaneous to the data gathered for the particle number concentration, the particle size distribution was quantified in situ using the SMPS and the DMS50. This provides a better understanding of the size of the particle number concentration seen in the Figure 57. An average of the four 1 minute sampling periods measured across the four minutes is represented in Figure 59.

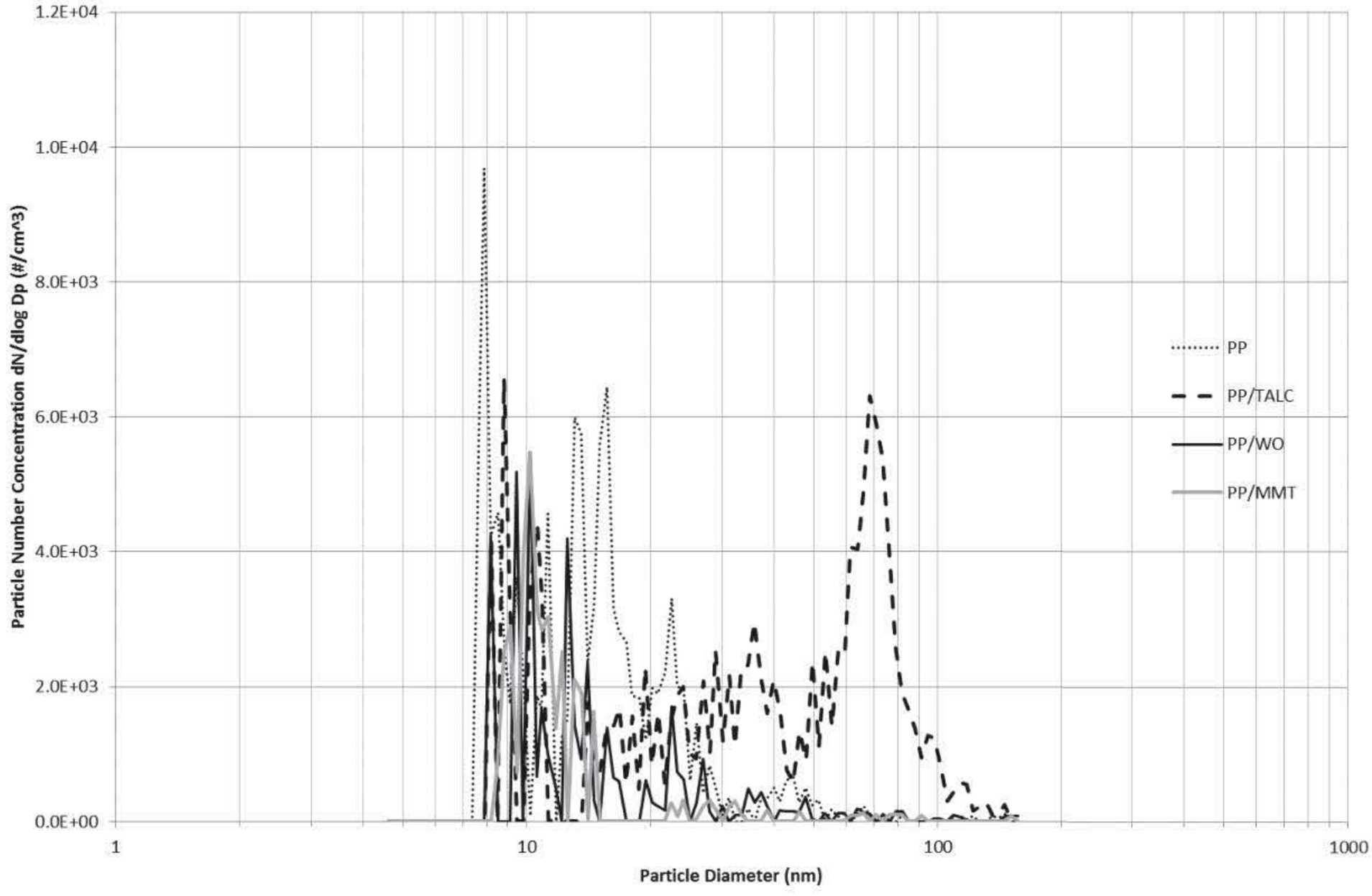

Figure 59*:* Average particle size distribution measured using SMPS of PP based nanocomposites (n=12 for each average).

From the plot portraying the average data across the four minutes and the three runs illustrated in Figure 59, the PP/Talc demonstrated the most evident difference in particle diameter release. All four samples exhibited a release between 7-20 nm, whilst the PP/Talc sample revealed an additional peak between 50-90 nm. The introduction of the nano-fillers, PP/WO and PP/MMT, can be determined to have minimal effect on the particle size distribution, whereas the micro-sized talc caused an observable nano-release characteristic. However, along with releasing a peak larger particle diameter, the sample released particles on the lower side of the distribution scale. The nature of the larger particle diameter introduced with the reinforcing talc is unknown and cannot be the independent talc particles as they are in the micro-size range. The filler can therefore instead indicate to alter the microstructure changing the release characteristics.

An alternative representation of the results can be displayed using the fraction of the total particle number concentration released on the y-scale. This is presented in Figure 60 and can present a more balanced distribution if there is a large discrepancy between the samples concentrations. This is not necessarily the case with the PP samples, as there is a relatively diminutive difference in particle number concentrations as presented in Figure 57.

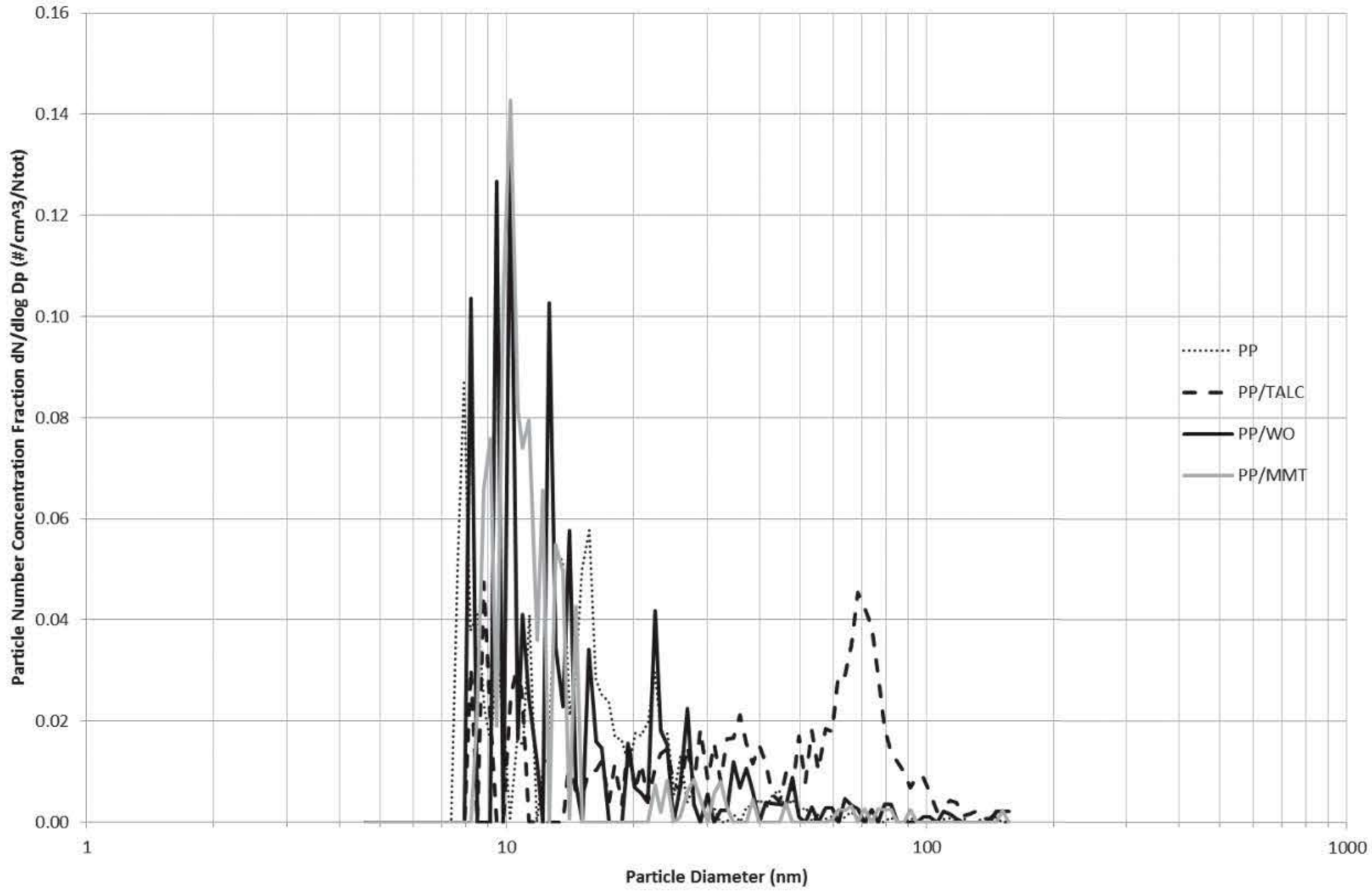

Figure 60*:* Average particle size distribution against fraction of total particle number concentration as measured using SMPS of PP-based nanocomposites (n=12 for each average).

The PP, PP/WO and PP/MMT samples demonstrated a substantial percentage of their particles in the 7 nm to 20 nm particle diameter range. Although the PP/Talc sample also released particles within this range, it only represents a portion of the released particles, as a higher percentage was observed larger than 20nm. Therefore, the PP, PP/WO and PP/MMT appeared to release a greater proportion of particles with smaller diameters compared to the PP/Talc sample. From the two illustrations alone in Figure 59 and Figure 60, there are no apparent differences between the PP, PP/WO and PP/MMT samples in particle size distribution.

In comparison to the SMPS, which has a sampling period of 1 minute, the DMS50 generates a size distribution every second. This provides a more live visual of the nanoparticles as they are being released from the material before the particles are dispersed within the chamber. A sample run of each sample is exhibited in Figure 61 and Figure 62.

a.)

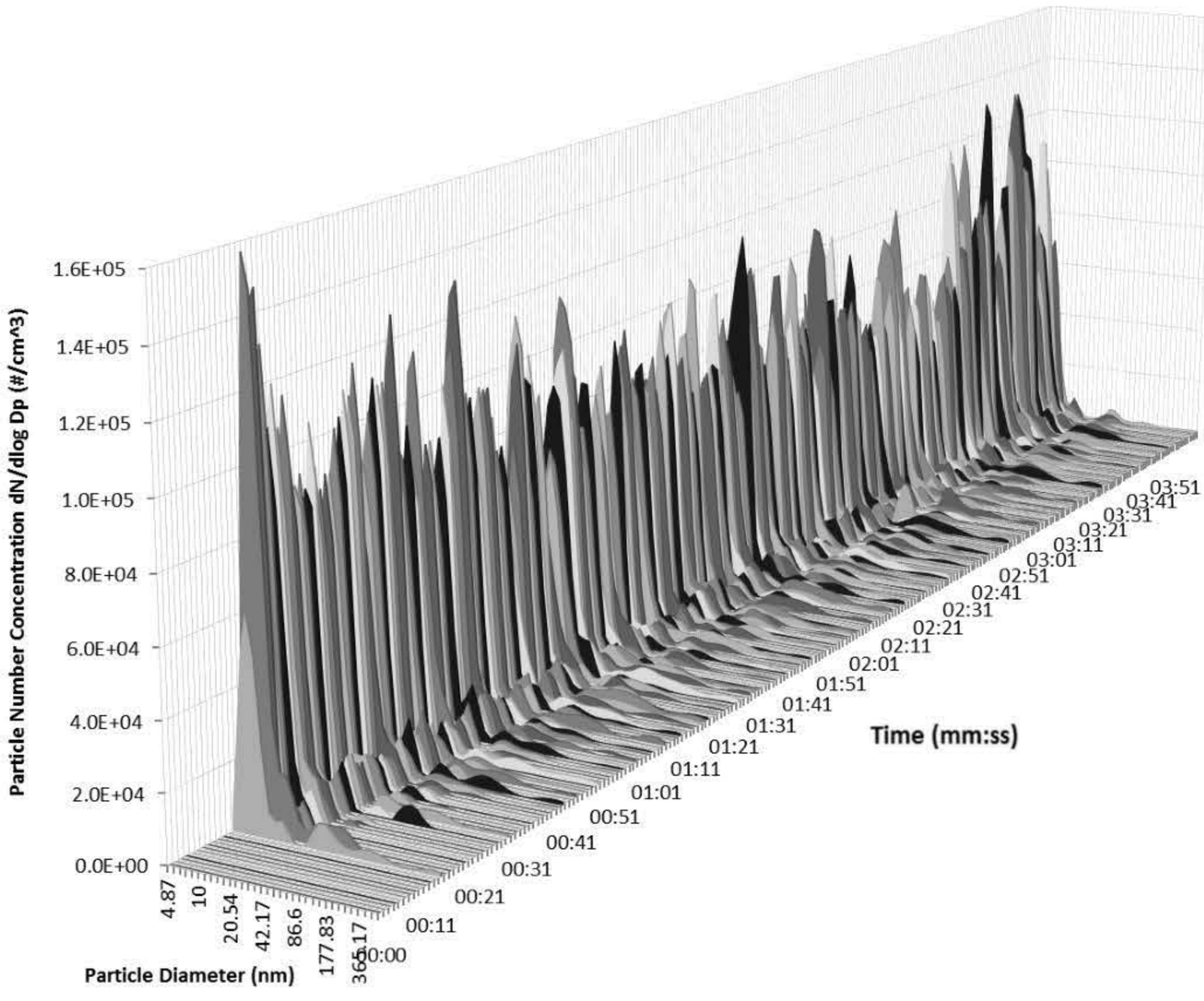

b.)

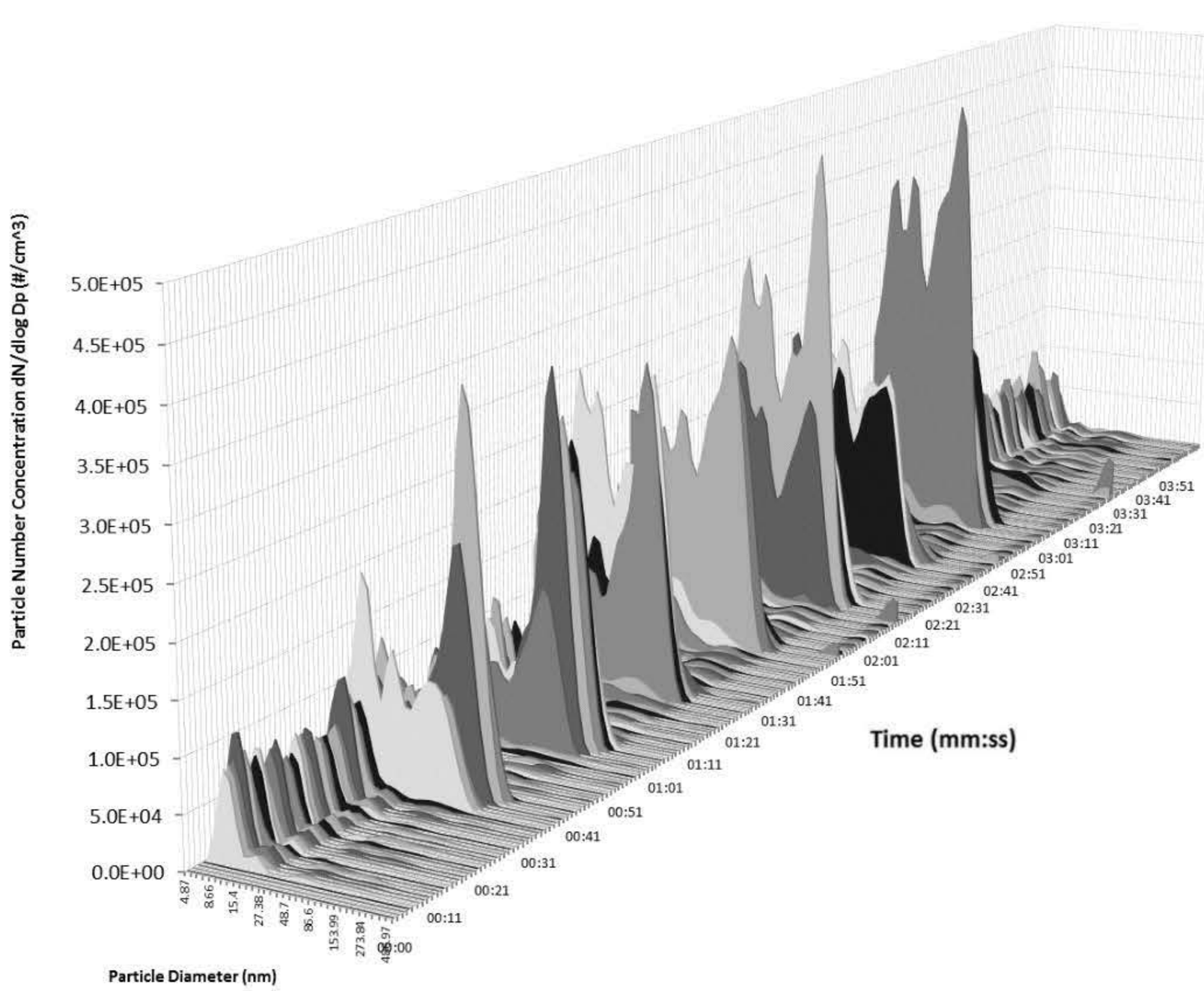

Figure 61*:* Particle size distribution over four minutes as measured on DMS50 of a.) neat PP sample and b.) PP/Talc sample.

a.)

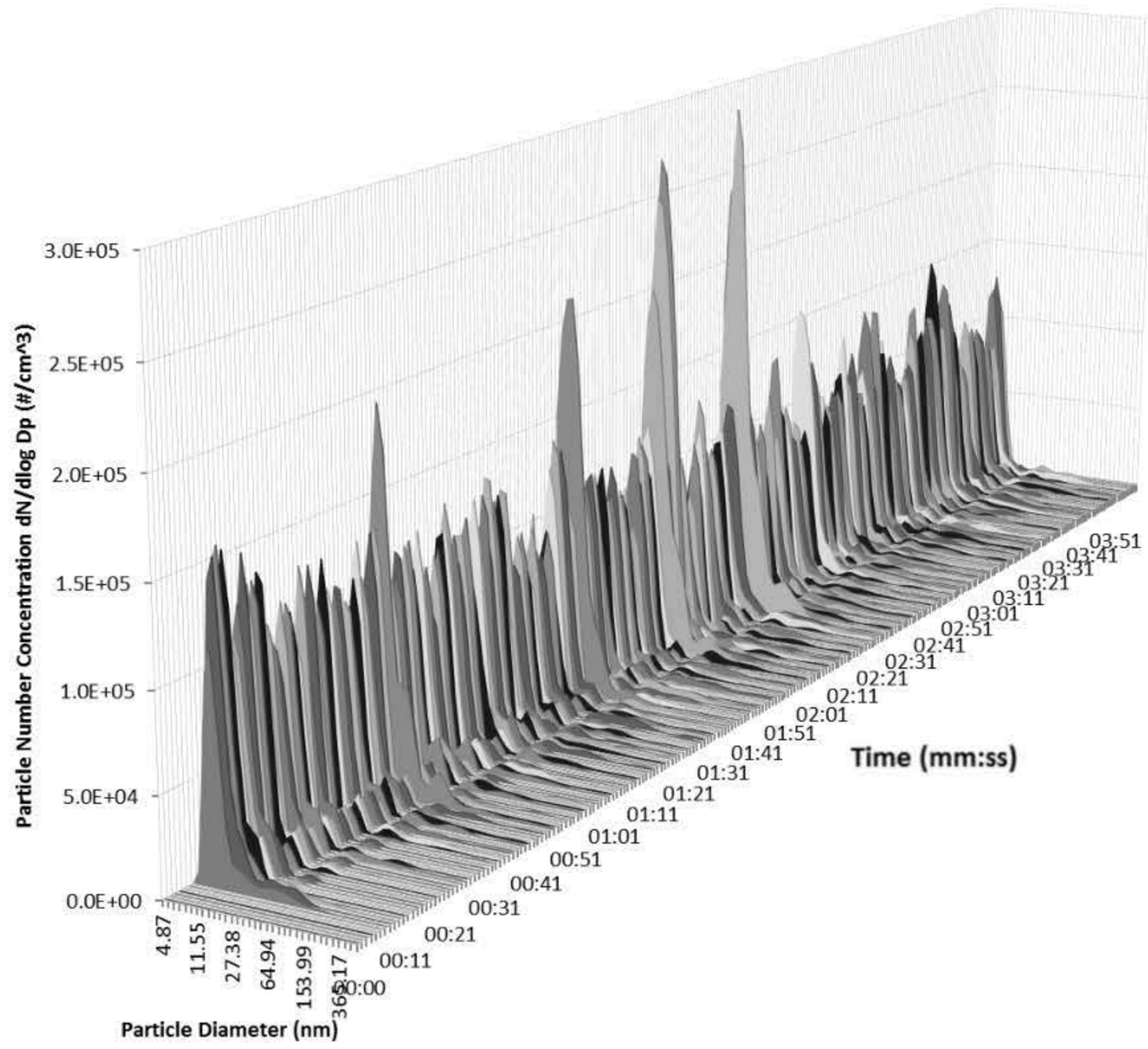

b.)

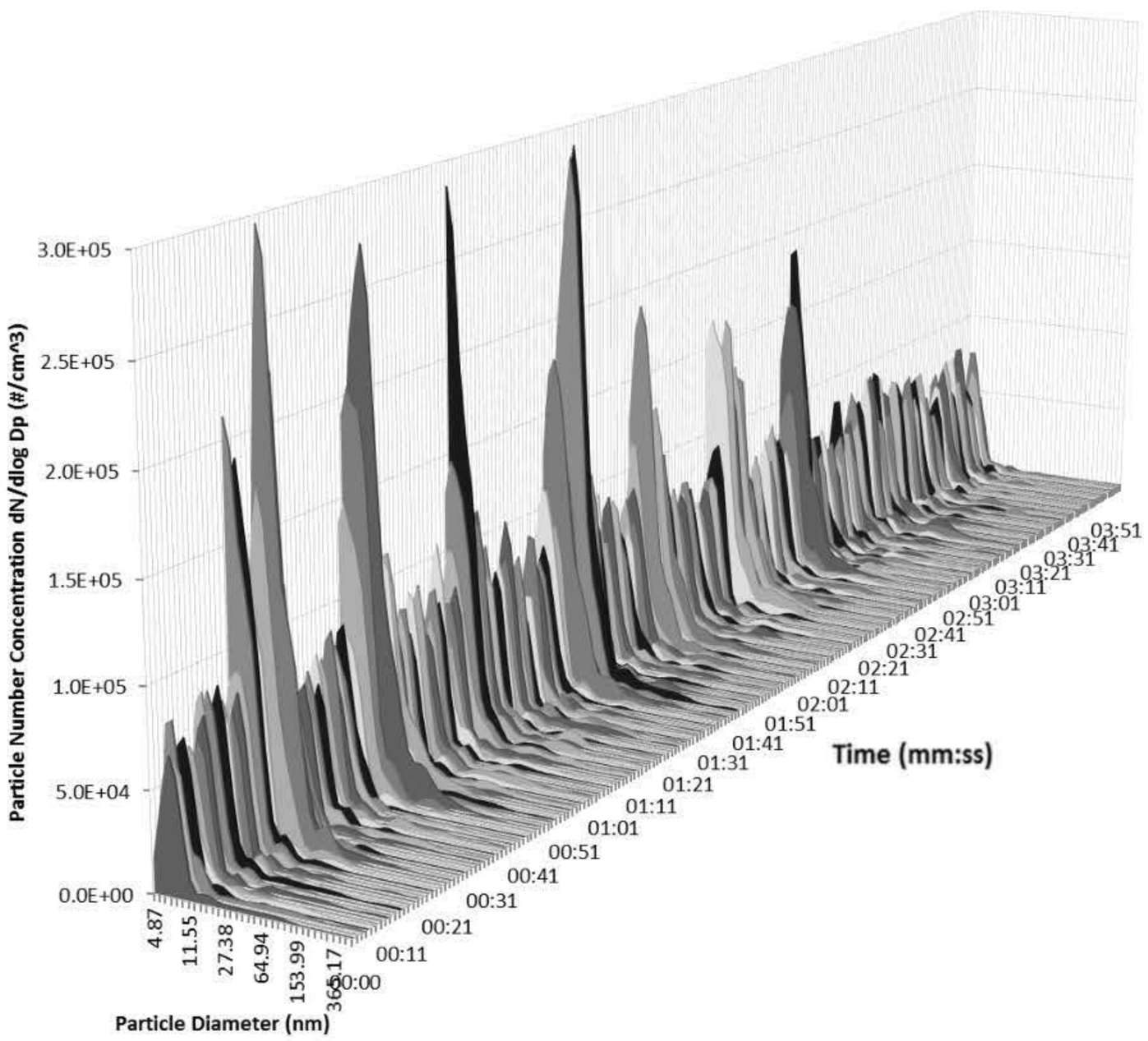

Figure 62*:* Particle size distribution over four minutes as measured on DMS50 of a.) PP/MMT sample, and b.) PP/WO sample.

Since a size distribution is generated every second, Figure 61 and Figure 62 illustrate the combination of the particle number concentration and its corresponding size distribution in a three-dimensional plot over the 4-minute sampling period. Like the CPC data, the drilling of the eight holes is perceivable with an initial introduction of particles for the first hole followed by 7 substantial peak concentration of particles emitted for the remaining holes. The size distributions between peaks and after drilling are less visible due to the high concentrations from the peaks. As indicated on the CPC data displayed in Figure 57, this highlights the vast particle concentrations produced at the time of drilling before the emissions disperse within the chamber and stabilise. Although the particles do stabilise and reduce in particle number concentration, a small percentage (<400 #/cm^3) remain airborne within the chamber environment. The PP/Talc sample observed the most apparent effect in particle size distribution introduced during the drilling. Although the PP, PP/WO and PP/MMT samples presented least distinct peaks due to the drilling, the particle size distribution corresponding. Furthermore, Figure 61 and Figure 62 demonstrate that the peaks of particles generated due to the drilling across the eight holes are relatively consistent in particle diameter for each sample. The size distributions released at the peaks and after drilling has finished are persistent and invariable. The particles can be observed not to change in distribution over time, eliminating the possibility of agglomeration or separation. Alternatively, the change in particle number concentration across the four minutes supports the CPC data indicating the high concentrations introduced followed by dispersion.

It is important to note that the data is taken from a separate run to the CPC and SMPS data due to the required increased inflow rate (6 L/min for the DMS50 compared to 0.6 L/min for the CPC) which is a possible cause for the increase in particle number concentrations relative to the CPC data represented in Figure 57.

To allow for a comprehensible comparison between the samples, a two-dimensional plot of the size distribution taken from the highest peak for each sample is displayed in Figure 63. The PP, PP/WO and PP/MMT samples revealed a substantial percentage of their particles between 5 nm to 20 nm particle diameter range. Therefore, the PP, PP/WO and PP/MMT appeared to release a greater proportion of particles with smaller diameters compared to the PP/Talc sample. Again, despite exhibiting a peak at a greater particle diameter, it must be noted that the PP/Talc sample released a high peak concentration of particles within the same diameters of other three PP-based samples. The data therefore suggests that the WO and MMT nano-sized reinforcements have little effect on the particle size distribution. The increase in particle number concentration seen in Figure 57 could also be associated to larger particle diameters as the CPC has a size range between 7 nm to 3000 nm.

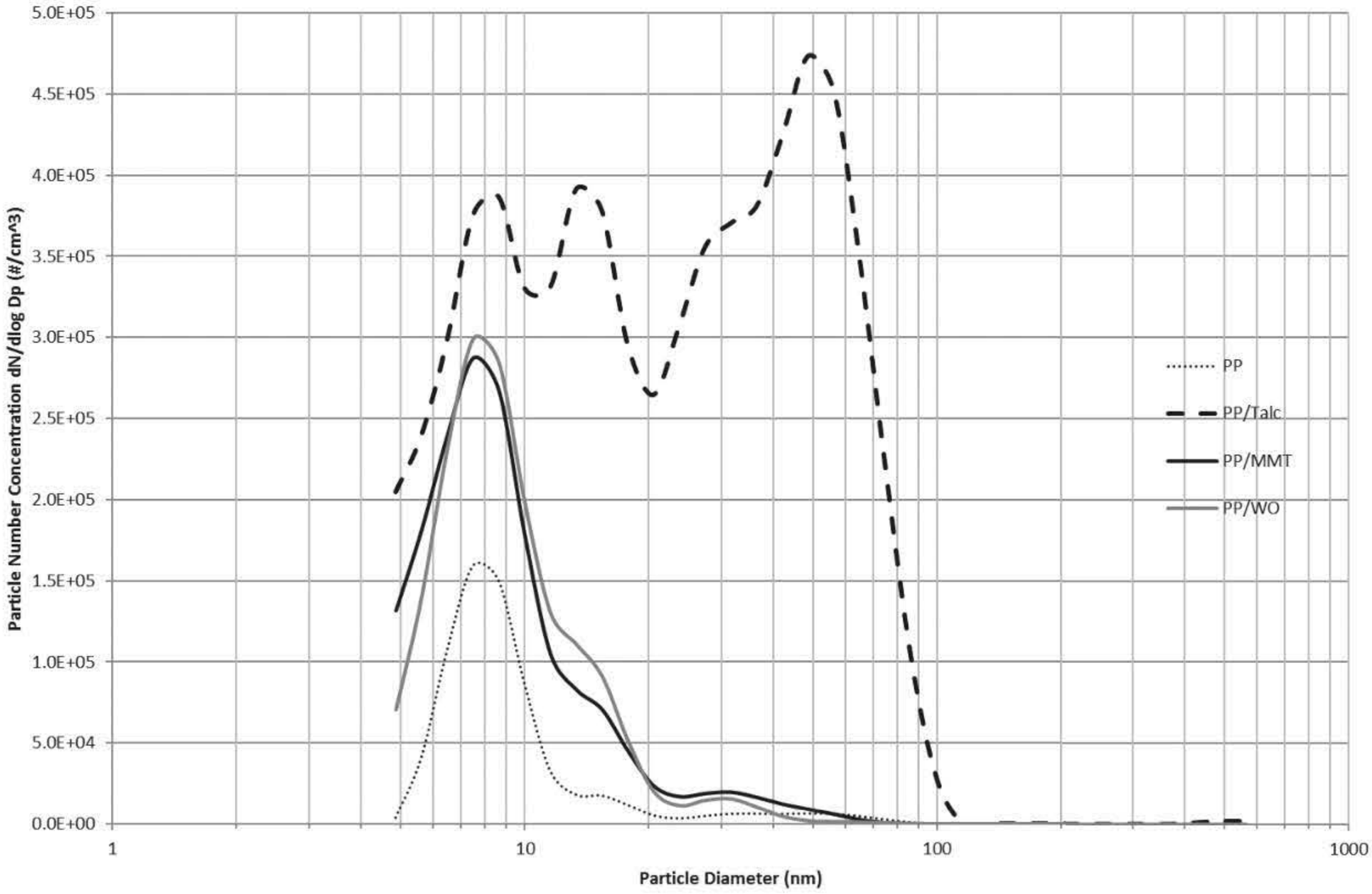

Figure 63*:* Particle size distribution average of peak number concentrations during 4-minute sampling period for PP based nanocomposite samples recorded on DMS50 (n= 24 for each average).

Comparable to the SMPS data, Figure 63 demonstrates that all samples released nanoparticles during the 4-minute sampling period, including the neat PP sample. None of the samples released particles between 115 nm to 562 nm. The data from the particle size distribution reveals that the particles released are highly influenced by the PP matrix. The nano-reinforcements of WO and MMT did not demonstrate any additional nano-sized peaks in the DMS50 or the SMPS results, and must therefore be agglomerating or adhering to the matrix. The talc reinforcement is the only filler showing an effect on the particle size distribution. This could also be due to the higher percentage of filler weight concentration.

The particle size distribution fraction in terms of total concentration, shown in Figure 64, emphasises the limited influence due to the nano-sized fillers, WO and MMT, and the effect of the talc filler.

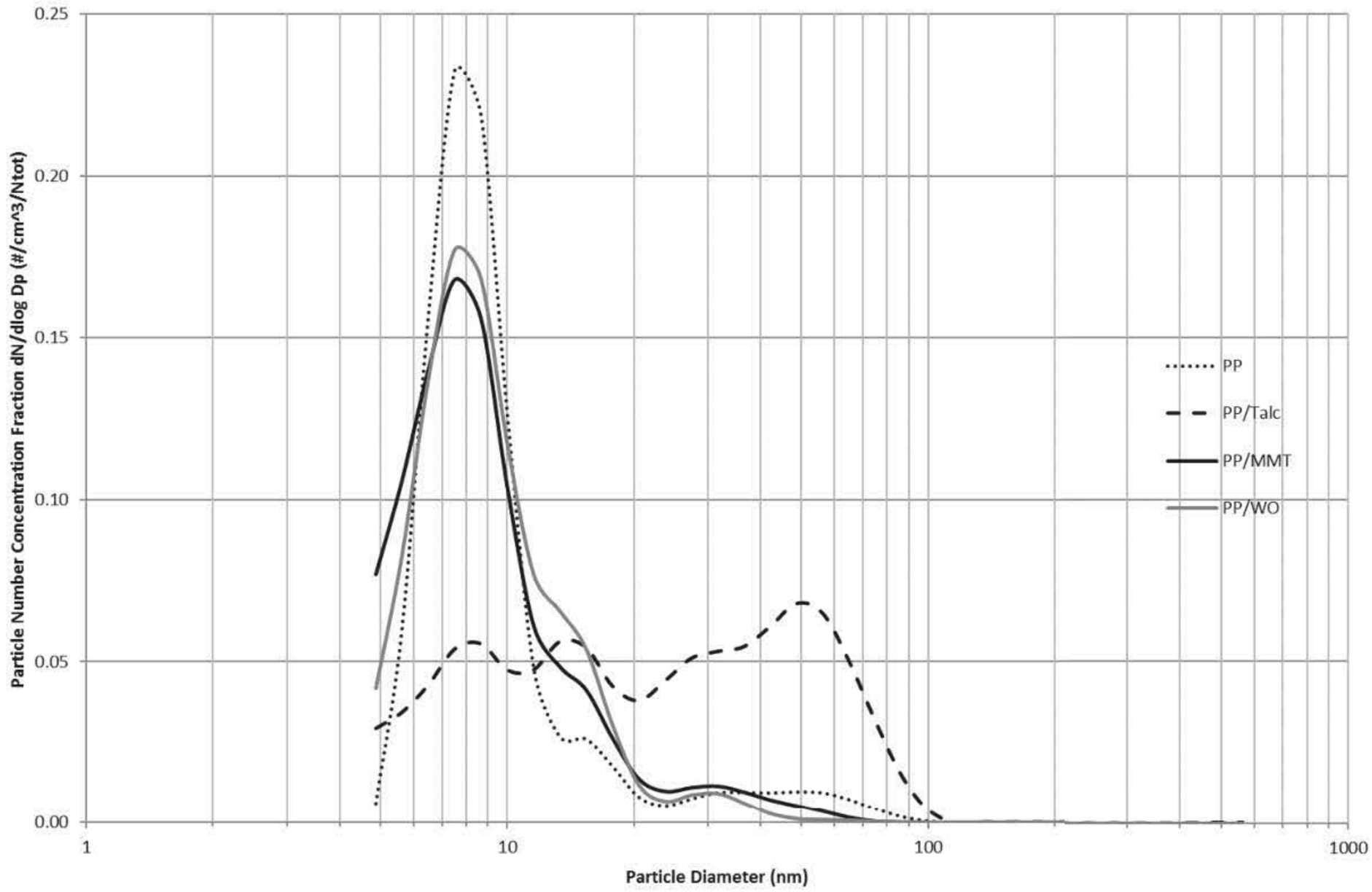

Figure 64*:* Peak particle size distribution against fraction of total particle number concentration as measured using DMS50 of Polypropylene-based nanocomposites (n= 24 for each average).

The PP, PP/MMT and PP/WO samples show almost identical proportions of the particles released to be below 20 nm. Whereas, the PP/Talc displayed a correlative release up to 100 nm. The fraction plot of particle size distribution can provide an independent visualisation of the filler effect irrespective of the influence of particle number concentration differences. Occupational limits dealing with nanoparticle exposures mostly establish concentrations limits within a justified particle size range, however, the fraction can be used when comparing the material performance. Figure 64 gives an evident representation of the effect on material release-ability changes due to the use of talc as a reinforcement.

A direct comparison of the particle number concentration fraction as recorded on the SMPS and DMS50 is presented in Figure 65. As stated, in comparison to the SMPS which has a sampling period of 1 minute, the DMS50 generates a size distribution every second. The comparison between the two instruments demonstrates a slight variation in particle size distribution. The two instruments both exhibited no peak measurements above 100 nm. The majority of the particles released from the PP, PP/MMT and PP/WO samples are seen to be less than 20 nm in both instruments. However, the DMS50 was able to detect more particles at diameters less than 8 nm. The fraction of particle number concentrations also differ quite significantly. The PP/Talc sample displayed a peak particle number

concentration between 50 to 80 nm in both instruments. Despite this, the SMPS did not demonstrate the peak particle number concentration fractions as the DMS50 between 20 nm to 60 nm for the PP/Talc sample.

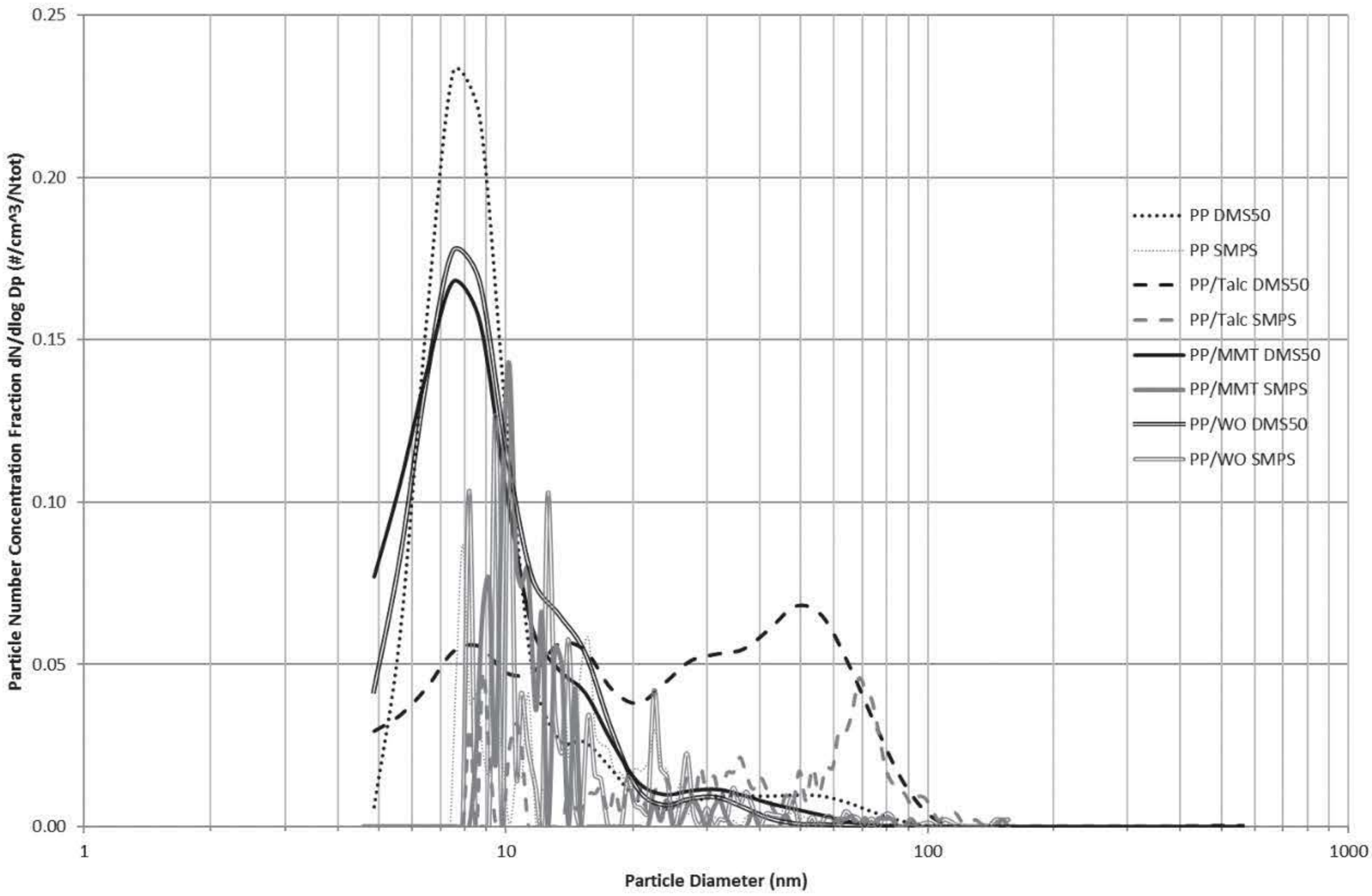

Figure 65: Comparison between peak particle size distribution against fraction of total particle number concentration as measured using DMS50 and SMPS of Polypropylene-based nanocomposites (n= 24 for each average).

The instrument and sampling time can therefore be seen to have a slight influence on the particle size distribution. This can be attributed to the sampling time and required flow rate. This therefore must be taken into consideration when evaluating the particle size distribution and has been reported as a challenge within comparing data throughout literature (*Hameri et al., 2002; Kuhlbusch et al., 2011; Hornsby & Pryor, 2014*).

4.3.3 Particle Mass Concentration

Since the drilling was conducted within a clean environment, all the particles measured with the instrumentation can be expected to be from the nanocomposite material. Therefore, since the SMPS functions on the measuring principle of spherical particles, using the particle size distribution measured, the mass can also be calculated. Particle mass concentration is considered another vital parameter to consider when assessing exposure to nanoparticles. Assuming the known density of the

individual materials to remain constant, the particle mass concentration can be estimated. Using the diameter and density of the material, the particle mass concentration is illustrated in Figure 66. The assumed constant material density for the three nanocomposites are: PP = 1.27 g/cm^3, PP/Talc = 1.02 g/cm^3, PP/MMT = 0.84 g/cm^3, and PP/WO = 0.85 g/cm^3.

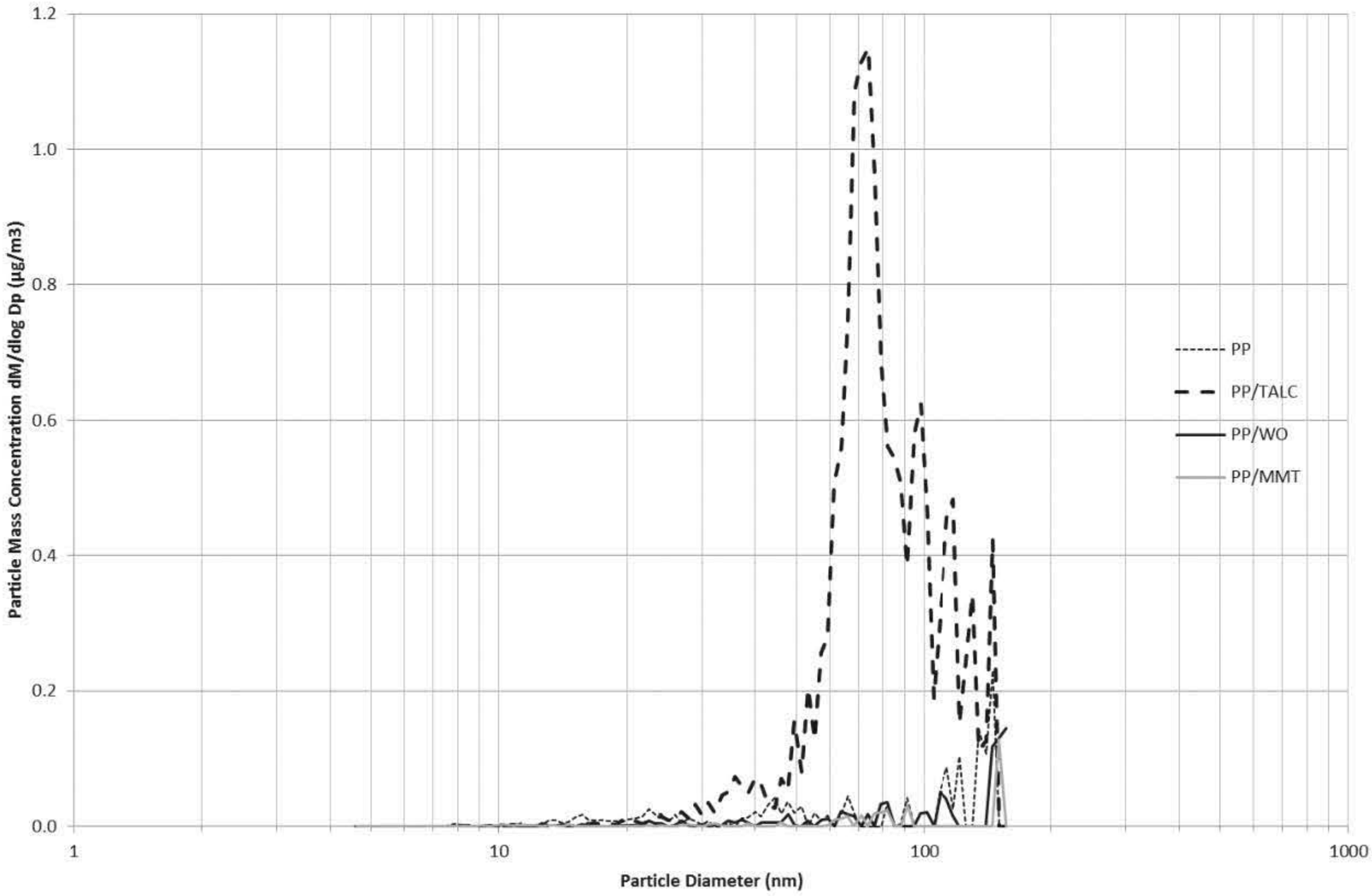

Figure 66*:* Particle mass distribution calculated from SMPS data for the polypropylene based samples (n= 12 for each average).

The particle diameters with high particle number concentrations observed in the SMPS results, on Figure 59, have adjusted due to the consequent mass increase of larger particles. The low mass of particles measuring less than 20 nm in diameter produce almost no evident peak. The plot is swayed entirely by the larger particle diameters observed from the release of the PP/Talc sample. The previously unobservable peak above 100 nm for the PP, PP/MMT and PP/WO highlights the influence of particle diameter on mass concentration. The high particle number concentration peaks observed below 20 nm have little impact on the particle mass concentration.

The results demonstrate the importance of the varied parameters and instruments required to present the entire picture of particles released from the material. From Figure 66, the PP/Talc sample can be seen to release a significantly higher total particle mass concentration of 15.27 µg/m^3 in the measured size range of the SMPS of 4.61 nm to 156.8 nm, compared to the other samples (PP = 1.49

$\mu g/m^3$, PP/MMT = 0.85 $\mu g/m^3$ and PP/WO = 0.33 $\mu g/m^3$). This represents a 925% increase in mass concentration from the PP sample within the SMPS size range.

Since the CPC can measure a larger particle size range, an alternative mass concentration is valuable to quantify the release. Using the particle number concentration measurement at the end of the four-minute sampling period, and the calculated total quantity of mass drilled, an estimation of the concentration of particles/mass drilled can be acquired and is presented in Figure 67. This is calculated using the particle number concentration of the CPC (size range: 7 nm to 3000 nm), material density values and equivalent of mass drilled based on hole size and number of holes.

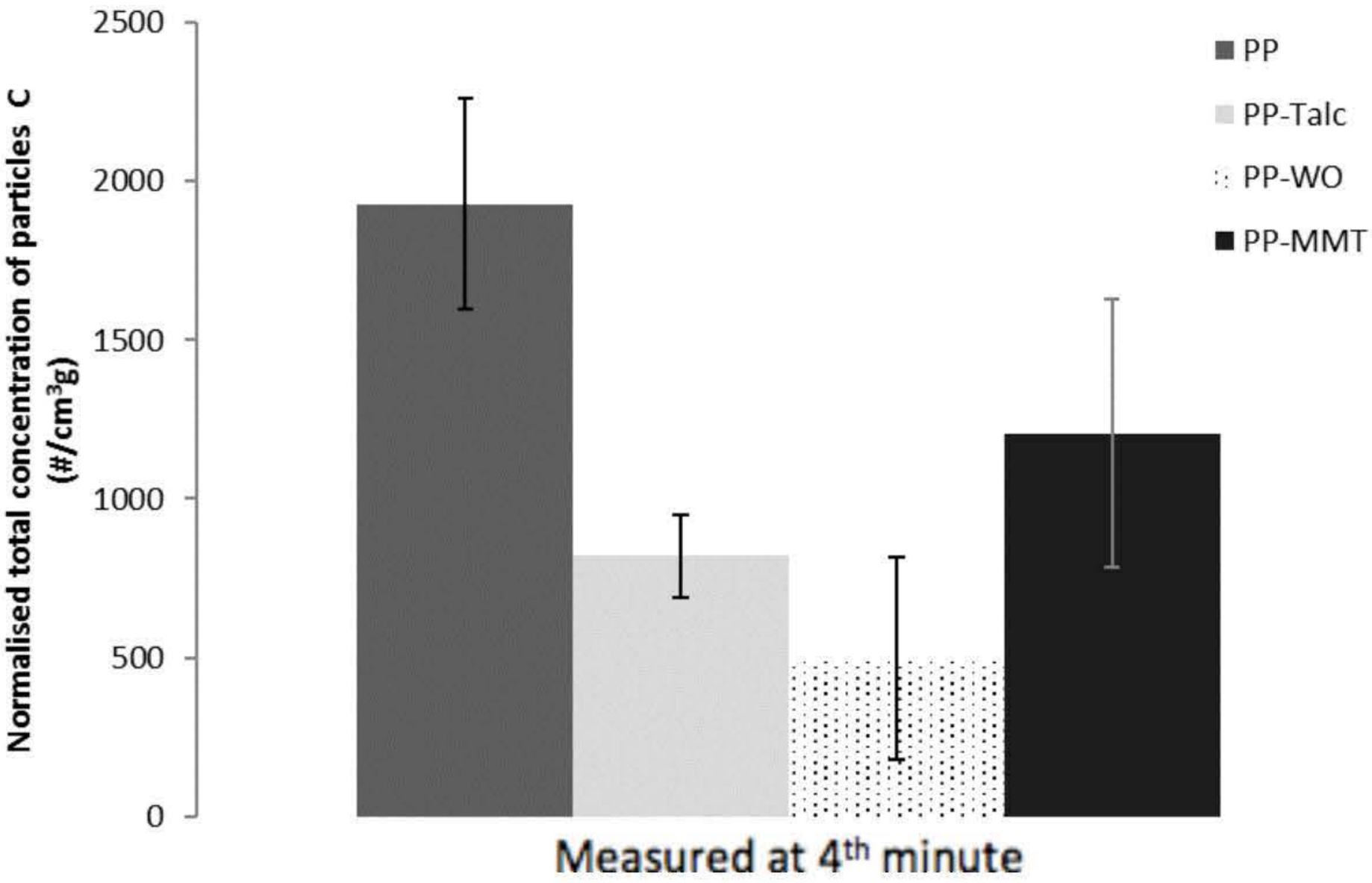

Figure 67*:* Normalised total concentration of particles (C divided by estimated drilled mass) recorded at 4th min for Polypropylene samples (n=3 for each average).

Although the PP/Talc sample displayed the highest particle mass concentration from the SMPS data, the PP sample displayed the highest concentration of particles to estimated total mass drilled from the CPC data after four minutes. The bar chart demonstrates that even with the highest density and equivalent normalisation of the data to the mass drilled, the PP sample still generates a substantial increase in particle number concentration. The lower densities of the PP/WO and PP/MMT samples cause a smaller diminution in difference from the PP sample in the normalised data (PP = 1929 $\#/cm^3g_{drilled}$, PP/Talc = 821 $\#/cm^3g_{drilled}$, PP/MMT = 1206 $\#/cm^3g_{drilled}$, and PP/WO = 499 $\#/cm^3g_{drilled}$).

Figure 67 also indicates that the PP, PP/WO and PP/MMT samples must have released a considerable proportion of the released particles outside of the SMPS range of 4.61nm to 156.8 nm, and therefore in the CPC range of 7 nm to 3000 nm.

The particle mass concentration is a vital parameter required when evaluating the nanoparticle release. The data identifies important differences from the findings in the influence of the filler in particle number concentration and particle size distributions.

4.3.4 Assessment of Deposited Particles

The particle number concentration, size distribution and mass concentration are valuable release quantification methods but lack in the characterisation. Therefore, particles were collected within the test chamber to characterize the particle measurements on the CPC and SMPS. The quantification data identified the release of nano-sized particles, but the nature and morphology of the particles is unknown. It is relevant to attempt to classify the particles as the composites consist of more than one constituent. Nanotoxicity studies have found the exposure to only certain nanoparticles to cause toxicological effects to humans (as per the definition of a composite).

The studies on the PP samples presents SEM images of the released nanoparticles using characterisation equipment mentioned in section 3.2.2 and Appendix A. Figure 68 illustrates a particle collected on the standardised IOM filter placed within the chamber and near the drilling on the PP/MMT sample. The filter is aimed at collecting airborne particles released around the sample during drilling.

From the image alone, the chemical nature of the particle cannot be understood. The instrumentation was unable to perform an EDX analysis on the particle due to insufficient material. However, the image indicates a nanoparticle embedded within a larger particle. This could conceivably be a montmorillonite particle embedded within the polypropylene. Using the same aerosol sample collection method described in the Characterisation section 4.2.2., Figure 69 illustrates an SEM image of particles collected from the PP/WO drilling samples.

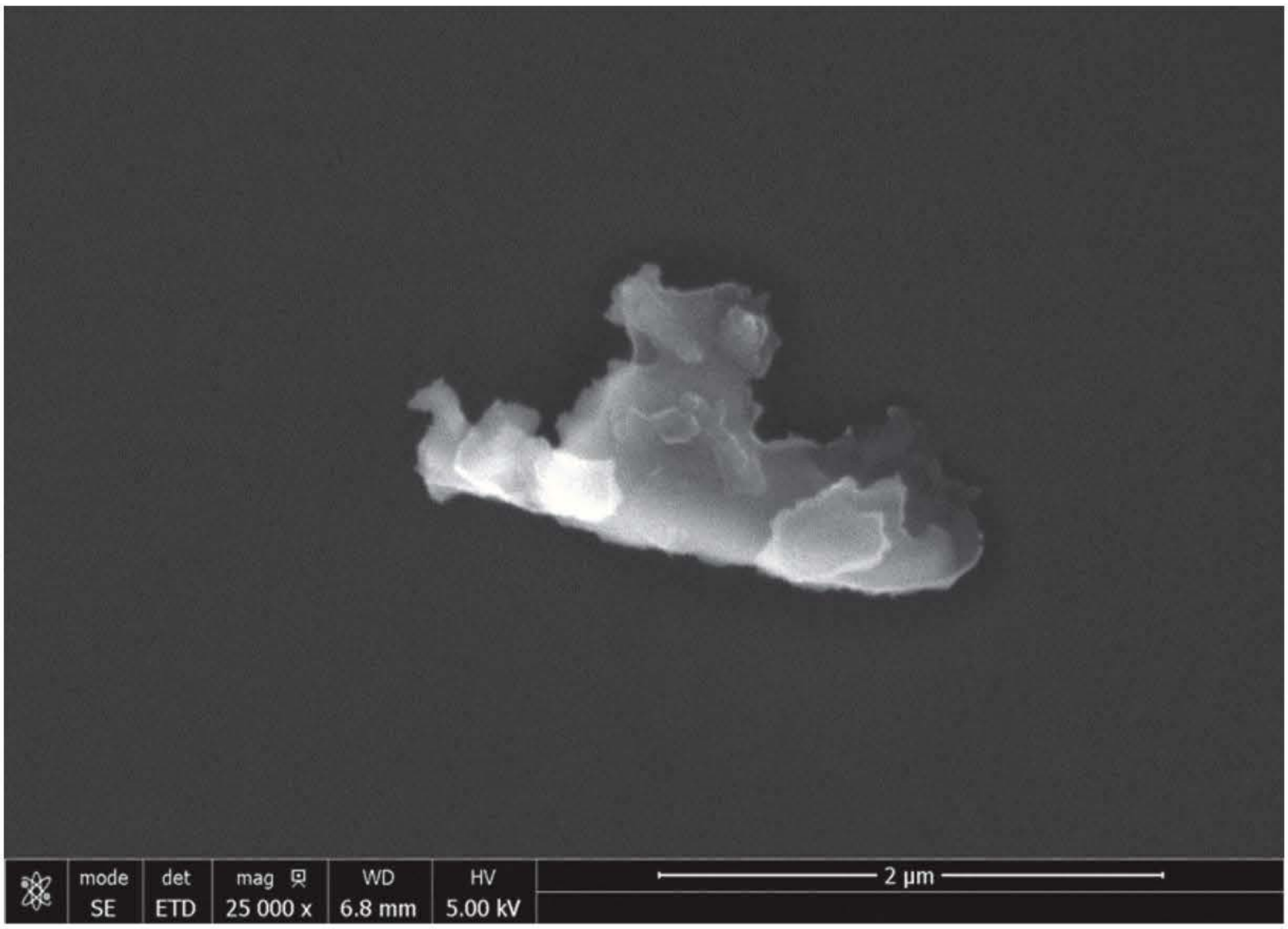

Figure 68*:* SEM image of sample collected on filter during drilling on PP/MMT sample.

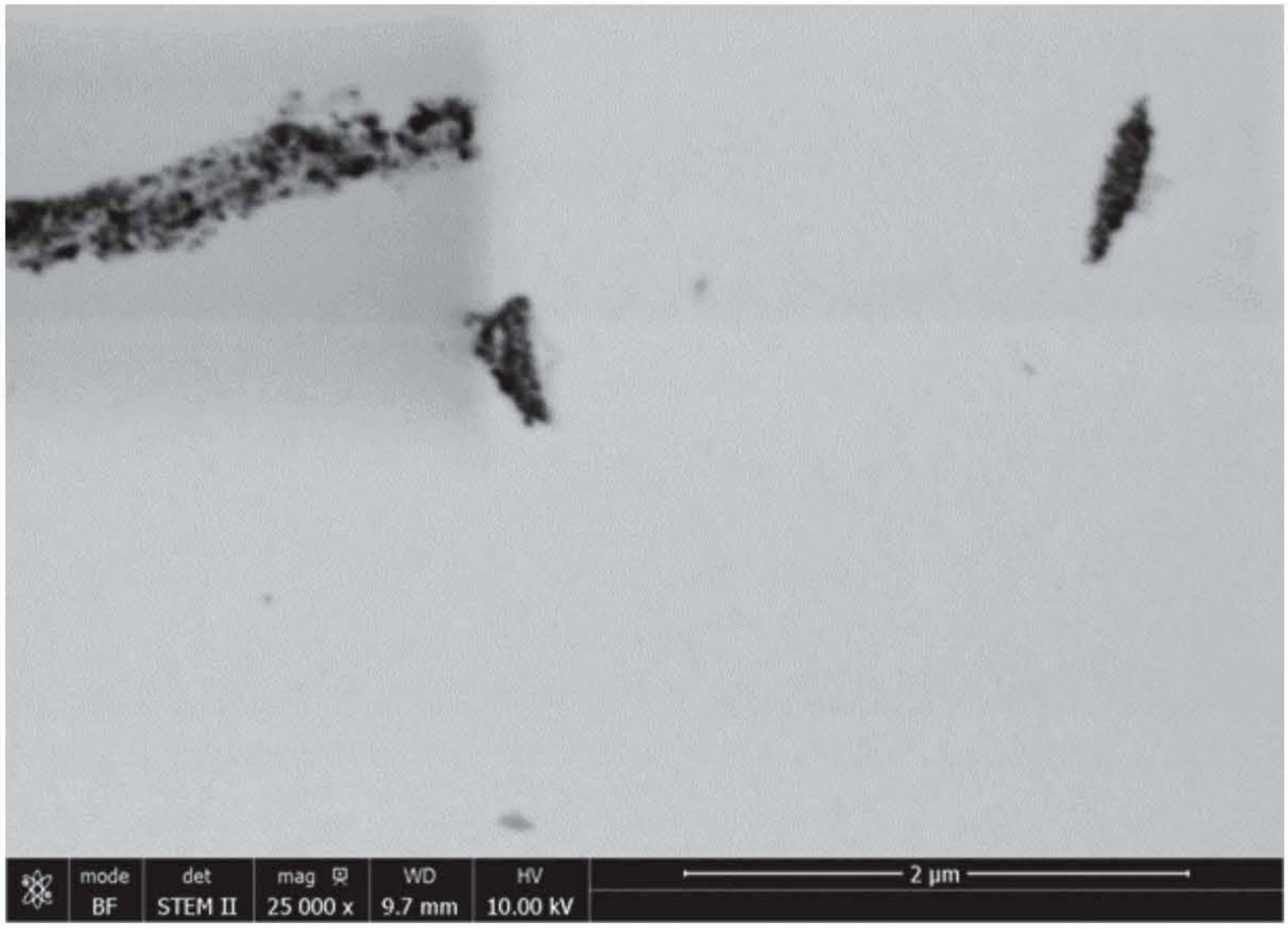

Figure 69*:* SEM image of sample collected on filter during drilling on PP/WO sample.

An agglomeration of nanoparticles is visible in Figure 69. However, like the particles collected on the filter within the chamber, due to the insufficient material content, and EDX was unable to be performed on the nanoparticles. With a 2 L/min suction to attract and prevent particles from detaching away from the grid for post-test chemical analysis, the filter was unable to obtain sufficient material. This could be due to the limited time of drilling and recommended short-term exposure sampling period (usually min of 15min of the IOM filter sampler) but could relate to the particles and/or number of particles produced. To have a chemical composition of the particles released, analysis was instead carried out on the particles collected on the sampling tray which was placed below the testing sample. Due to the placement directly under the drilling, a considerable quantity of particles were collected. Two SEM images of the particles collected in the sampling tray during the drilling on the PP/WO sample are illustrated in

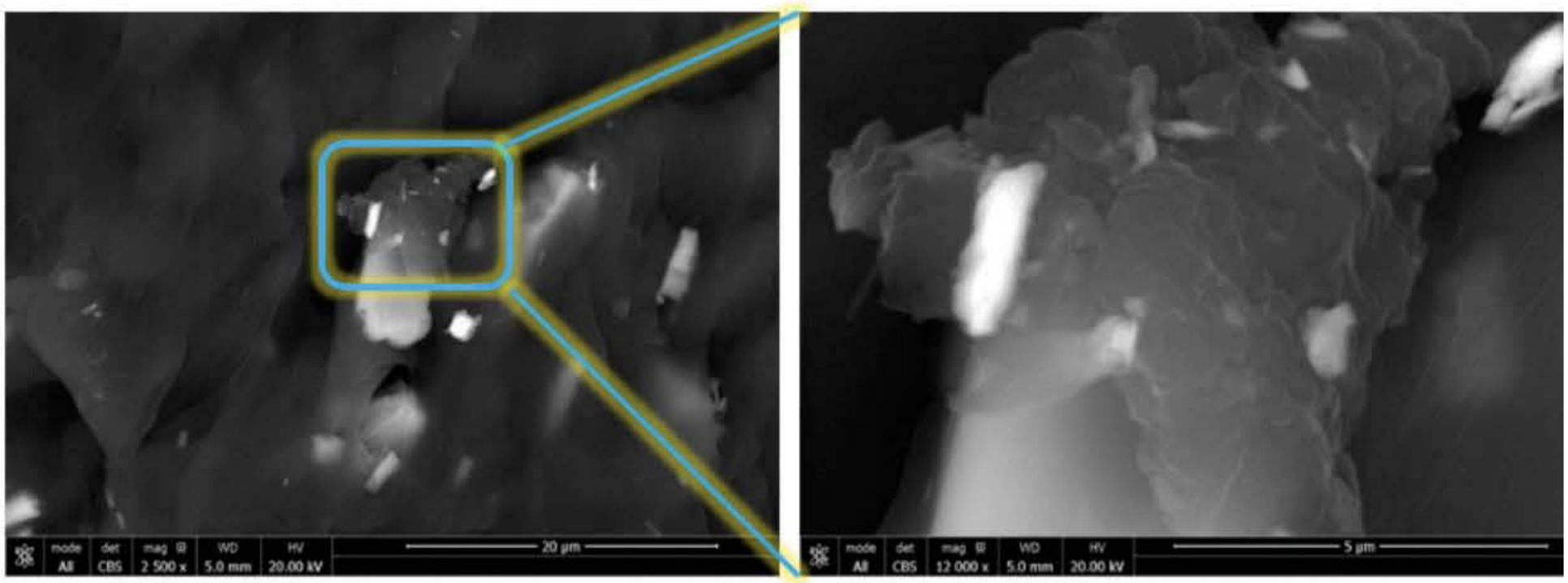

Figure 70*:* Magnified SEM image of particles collected in sampling tray during drilling on PP/WO sample.

The WO particles can be seen to be embedded within the matrix in the two figures. The filler particles appear brighter in both the images with additional nanoparticles being more evident in the magnified image in Figure 69. This sample analysis provides evidence of the particles remaining embedded within the PP matrix. Although a distinction between some particle surfaces can be made, no independent filler particle was identified in the PP/WO, PP/MMT or PP/Talc samples. It is important to note however, that these are the particles collected in the tray placed underneath the drilling. The particles collected therefore are considered "deposited" particles in comparison to the airborne particle readings of the CPC, SMPS and DMS50 data. The nature of the particles collected in the tray would therefore assumed to be larger and heavier as they do not remain airborne.

As can be seen, more material is present than the particles collected in Figure 69, allowing for an EDX analysis to be carried out. Therefore, selecting five distinct points including locations where filler particles are perceived as shown in Figure 71, an EDX analysis was carried out.

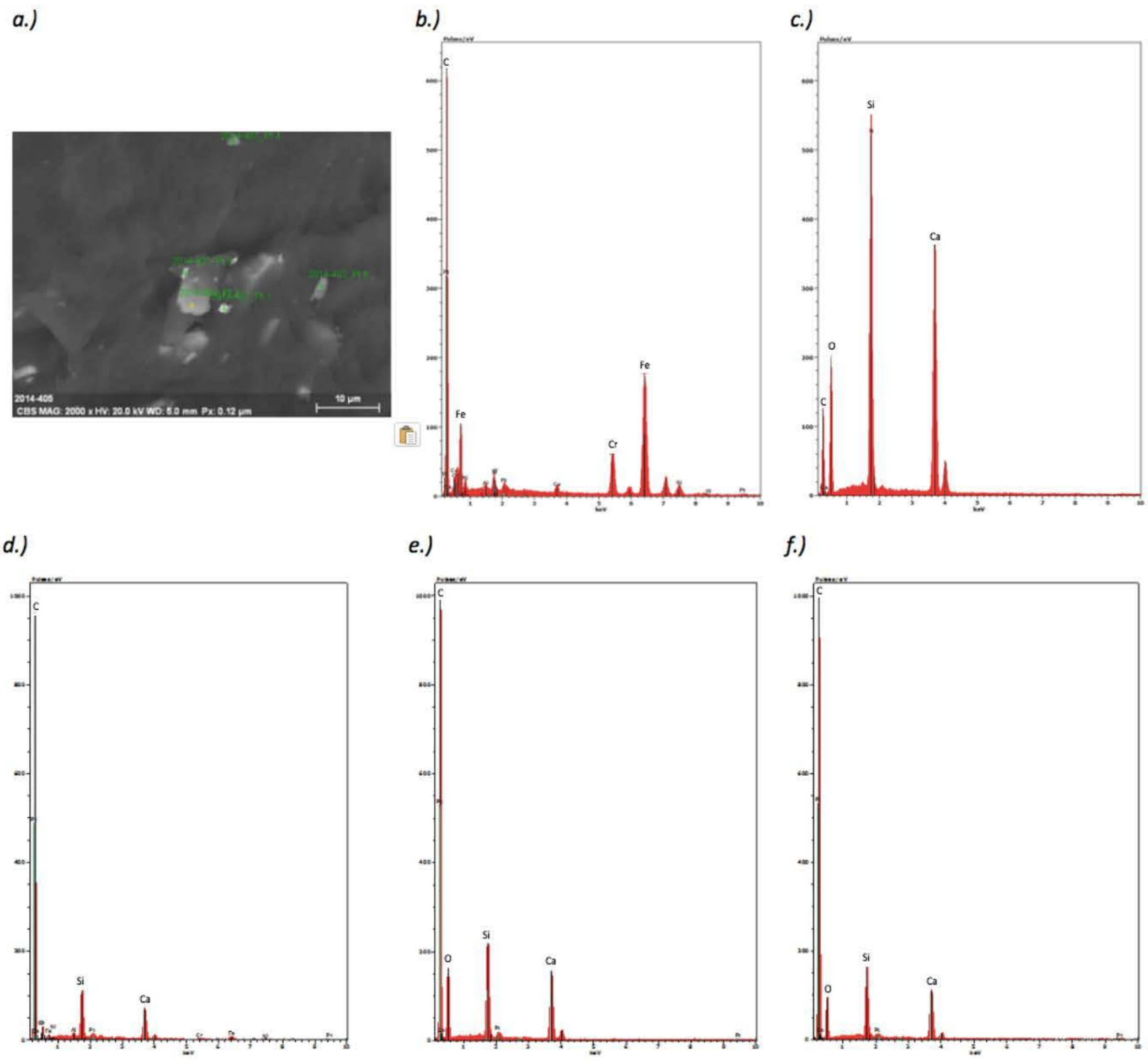

Figure 71*:* Analysis of the particles collected in sample tray from drilling on PP/WO sample through a.) SEM image of analysis and retrospective locations of EDX analysis on b.) point 1, c.) point 2, d.) point 3, e.) point 4 and f.) point 5.

From the EDX analysis, the WO particles were detected at location points 2-5 shown in Figure 71. The elemental analysis detected particles of Ca, Si and O which make up the composition of the WO filler. Large quantities of C were observed in most of the points as this is the PP matrix. Additionally, the analysis was also able to detect constituents of Fe at point 1. The origin of the iron is unknown as it is not a principal element of the nanocomposite. However, it may have been introduced from the drill

bit (stainless steel) or even during the manufacturing process (PP hardener, POLYBOND 3200 from ADDIVANT).

Furthermore, FT-IR spectroscopy was performed on the samples in order to evaluate any internal chemical bond change in the material. The FT-IR comparison of the materials before and after the drilling (termed dust as this was carried by collaboration partners at Cranfield University) are presented in Figure 72.

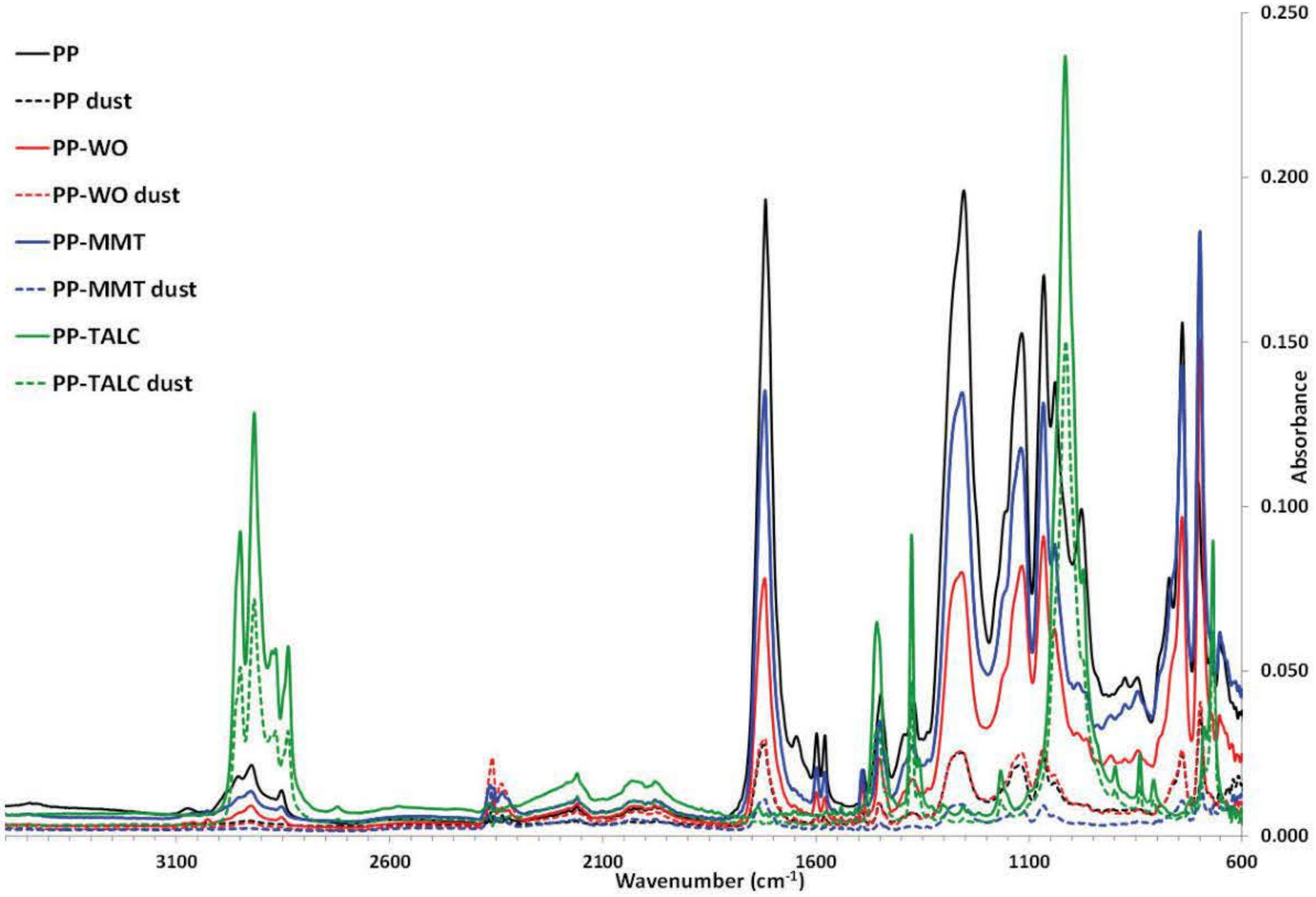

Figure 72*:* FT-IR spectroscopy comparison of particles collected after drilling and pre-drilled materials of PP-based samples.

The spectra observed in Figure 72, show that the collected material perceived no significant changes in molecular structure due to the drilling. As shown, the peaks for all samples can be seen to not differ from the pre-drilled samples. No difference is therefore detected. Hence, no independent fillers were identified with the measurements. It is important to note that this is carried out on the collected particles due to the required minimum amount of material necessary in order to perform an FT-IR. Insufficient material was collected on the filter and Nano aerosol sampler to perform an FT-IR. As the fillers are within the nano-range, the FT-IR would be unable to isolate and identify the nanofillers. Therefore, the FT-IR is useful in assessing any internal micro structure change within the material. Within the capacity of the instrument, the data reveals that the drilling caused no distinguishable changes to the material.

The FT-IR, SEM and EDX analysis of the particles collected in the sampling tray placed underneath the drilling confirms the detection and embedding of the nanoparticles within the matrix. Similar results were observed with the PP/Talc and PP/MMT samples. However, no independent nanoparticles were found within the collected samples and methods used.

In relation to the quantification data, the characterisation results support the findings that the release is substantially matrix associated. As no independent fillers could be identified, the change in release quantity due to the addition of the fillers is more quantity linked instead of release of filler particles. The addition of the fillers to the material does not appear to introduce or remove a certain particle, but instead has an influence on the concentration of particles released.

4.4 Conclusion

The automated drilling process demonstrates a nanoparticle release testing methodology permitting a direct measurement of nanoparticle emissions into a clean chamber environment without any background interference. The methodology presents real-time nanoparticle release quantification from a material life-cycle scenario, drilling. Emission measurements are taken using a condensation particle counter (CPC), scanning mobility particle sizer (SMPS) and DMS50 Fast Particulate Size Spectrometer (FMPS). This provides the particle number concentration, size distribution and mass concentration of particles released. Additional to this, the particles are analysed ex-situ for material characterization.

The methodology demonstrated an investigation into the influence of talc, MMT and WO on the nanoparticle release during drilling. The PP/Talc and PP/WO reinforced composites are both the first demonstrations of nanoparticle release within available literature and compared to PP/MMT and neat PP. The data presented reveal minor difference in nanoparticle release between the four PP-based samples. All four samples exposed a concentration of nanoparticles introduced due to the drilling into the chamber environment. The nanofillers (WO and MMT) demonstrated both an increase and decrease in nanoparticle release, but no visible difference in particle size distribution. The higher concentration of talc as a filler had the biggest effect on particle size distribution compared to the other PP based samples.

The data found that the size distribution and particle number concentration alone don’t give the full account of the release. Although large quantities of particles are observed lower than 20 nm, the particle mass concentration reveals significant releases at higher particle diameters due to the increased mass of larger particles. Many exposure limits are given in particle mass concentrations

which would render these values important, but still don't represent the entire circumstances of the release characteristics and quantification. The instruments alone do not reveal enough to represent the entire release characteristics. The data demonstrates that the varied aspects quantifying the release are all needed as they revealed alternative effects of the fillers. Nonetheless, the characterisation findings support the overall results from the CPC, SMPS and DMS50 in that the matrix has the most influence over the particle release during drilling. Only deposited particles with filler embedding or protruding fillers were identified in the microscopy analysis. Therefore, since all samples revealed nanoparticle release, and whilst the nanofillers demonstrated a minor effect on the particle number concentration, the data suggests the PP matrix is attributed as the most influential cause of the release.

Chapter Five

Effect of Nano Silica and Nano Alumina on Nanoparticle Release from Polyester Based Nanocomposites due to Automated Drilling

5.1. Introduction

This chapter investigates the effect of embedding nano silica (SiO_2) and nano alumina (Al_2O_3) in PE-based nanocomposites on nanoparticle release during automated drilling. As mentioned within the material properties in Chapter Three, PE is a widely used thermoset as emphasised in a report on the use within industry expecting the industry to surpass $14.5 billion by 2024 at a compound annual growth rate of 7.5 % (Graphical Research, 2018). Nano fillers have shown to further enhance the beneficial properties of PE through the incorporation of SiO_2 (Zhao et al., 2016; Rusmirović et al., 2016), Al_2O_3 (Ribeiro et al., 2015; Rajesh et al., 2014), halloysite (Saharudin et al., 2016; Lin et al., 2017) and TiO_2 (Gaminian & Majid, 2015; Patel & Dhanola, 2016) as a selected few examples. This study includes the embedding of Al_2O_3 and SiO_2 within PE-based nanocomposites. With small weight concentrations of the nanoparticles the materials have proven improved mechanical properties and are subsequently being recognised within industry. Two separate reports estimated the global market size of nano silica to be 3348 kilo tonnes in 2015 (Market Research Report, 2017) and the global high purity alumina market size to be over 20 kilo tonnes in 2015 (Market Research Report, 2016).

The introduction of the nano-sized and SiO_2 into the workplace institutes conceivable health risks when release into the environment is concerned. Literature has vastly reported on toxicity effects of SiO_2 such as increasing oxidative stress, pro-inflammatory responses, silicosis, chronic obstructive pulmonary disease (COPD) and pulmonary tuberculosis (Calvert et al., 2003; Lin et al., 2006; Eom & Choi, 2009; Park & Park, 2009; Kaewamatawong et al., 2006; Rabolli et al.,2010). Equally, Al_2O_3 is being investigated for toxicity with studies having shown nano Al_2O_3 to cause cellular toxicity, increase in

oxidative stress, increase the lactate dehydrogenase level in the blood, and induced the development of a pathological lesion in the liver and kidneys (Alshatwi et al., 2013; Park et al., 2015; Zhang et al., 2013; Zhang et al., 2011). Hence, nano Al_2O_3 and SiO_2 particles are generally agreed upon throughout literature that to have shown toxic effects. Reviews of literature on the release and/or exposure of nanoparticles from ENMs have also concluded that high-energy processes, including drilling, have shown evidence of likelihood of nanoparticle release (Basinas et al., 2018; Debia et al., 2016; Froggett et al., 2014). Therefore, this chapter will evaluate the effect of two weight concentrations of nano Al_2O_3 and SiO_2 particles have on the release from PE-based nanocomposite due to drilling.

5.2. Experiment

The PE-based samples were selected and manufactured as discussed in Chapter Three. Two nanocomposite fillers, SiO_2 and Al_2O_3, were used to reinforce the material and will be compared to the neat PE. Two material weight concentrations of 2 wt. % and 5 wt. % of the nanofillers were manufactured to investigate the effect of filler weight concentration. The materials morphology, structure and composition are demonstrated in section 3.3.1 and 3.3.2.

To evaluate the samples manufactured, the materials were characterised through SEM, EDX and FT-IR. The characterisation equipment used within this study is detailed in section 4.2.2.

The materials were firstly investigated for mechanical properties. The effect of the nanofiller on the material mechanical performance are shown to demonstrate the original benefits and use to strengthen the materials. The materials underwent a flexural 3-point bend test in accordance with ASTM D 7264/M flexural test (ASTM D7264M, 2015) and a standard ASTM D 3039/D tensile test (ASTM D3039, 2017). These results are included in section 3.3.3.

The samples underwent the exact same drilling described in section 4.2.3 with further details of the methodology also available in Appendix A. A standard Dremel 4000 drilling tool with an industrial standard stainless steel 3.5mm twist drill bit was used at 10000 rpm with a feed rate of 78 mm/min.

Once the chamber was cleared of any particles, the drilling studies were carried out by drilling across the width of the sample resulting in eight separate holes and bearing a time duration of 3 minutes of drilling, followed by 1 minute post-drilling. The eight holes drilled per sample were repeated three times to get an average of the particle number concentration and particle size distribution released.

The nanoparticle release is quantified through a CPC, SMPS, DMS50, A standard IOM Inhalable Sampler, XRF, SEM and EDX. More information on the equipment used within this study is detailed in section 4.2.2.

5.3. Results

5.3.1 Filler Effect on Particle Number Concentration

The PE nanocomposite samples underwent the replicated drilling setup as described. In comparison to the neat PE sample, the introduction of the SiO_2 and Al_2O_3 nanofillers were classified to have a significant effect on the nanoparticle release during drilling operation. An image of the number of visible particles generated is displayed in Figure 73.

Figure 73*:* Post completion of mechanical drilling process on a virgin PE sample.

The averages of the particle number concentration released from the three samples is shown in Figure 74. As with the data from the PP-based results, the peaks in Figure 74 exemplified across the three minutes clearly highlight the 8 holes being drilled. Visible on most of the peaks, the movement of the

drill entering and withdrawing the sample can also be seen from peaks being faintly divided into two parts each. The drilling can be seen to release a substantial quantity of nanoparticles for all three samples. When the drill bit is out of the sample, the particle concentration is seen to drop between each hole being drilled. The mechanical drilling can therefore be seen to generate a substantial quantity of nanoparticles into the environment, which then quickly disperse inside the chamber. The particle number concentration was perceived to relatively stabilize during the 1 minute of recorded data after the drilling was completed, but remained at considerably higher particle number concentration than before drilling had started. Thus, the nanoparticles released during drilling remained airborne and can be expected to disperse throughout the chamber (however there is no other sampling point to support this and is not pertinent for the process related approach followed).

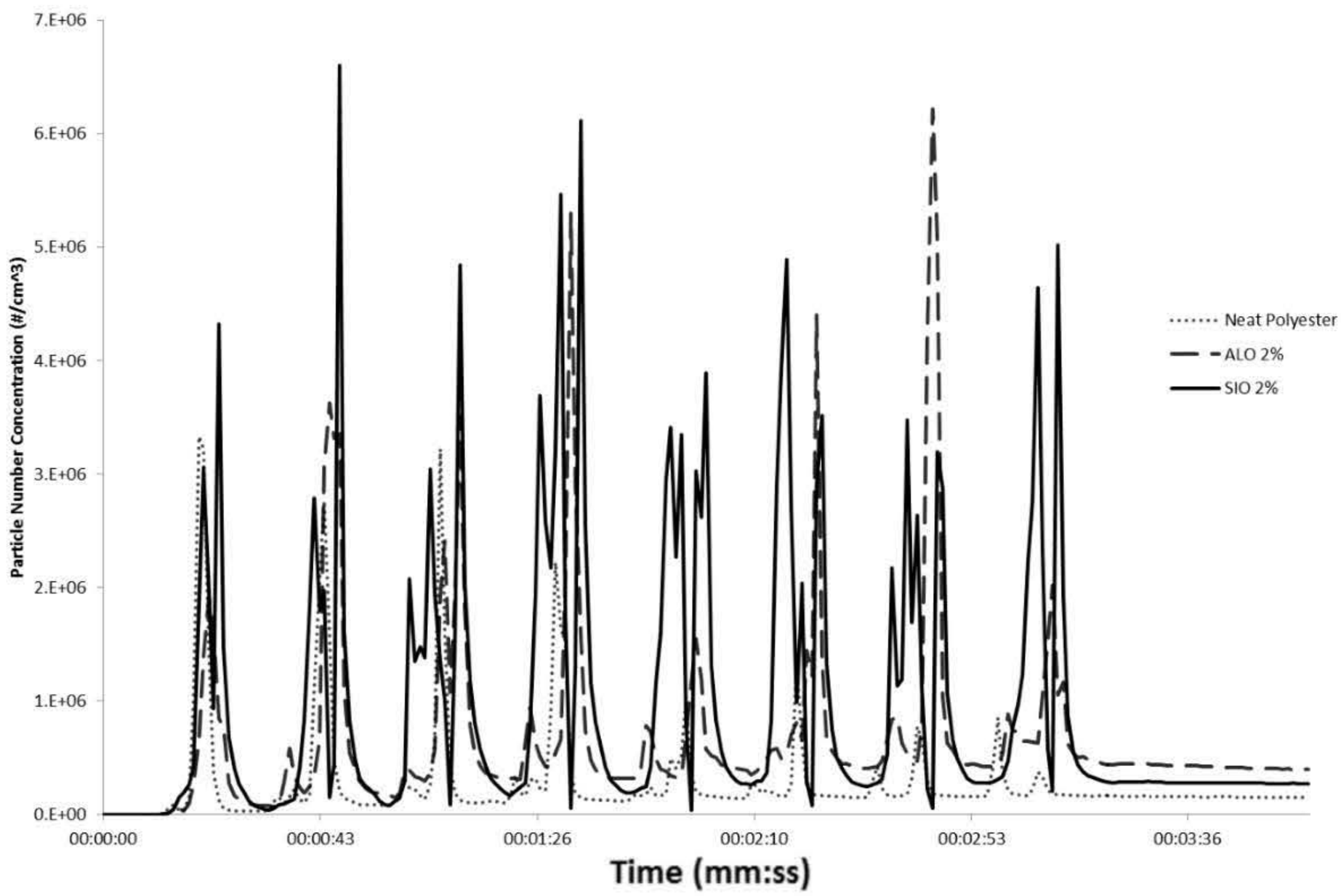

Figure 74*:* Particle number concentration averages of polyester-based nanocomposites recorded using the CPC (n=3 for each average).

Over the eight holes, the two nanofilled polyester sample averages demonstrated higher nanoparticle peaks (PE/SiO_2 nanocomposites $6.6x10^6$ #/cm^3, PE/Al_2O_3 nanocomposites $6.2x10^6$ #/cm^3) than the neat PE sample ($3.3x10^6$ #/cm^3). The results clearly demonstrate the immediate release of nanoparticles from the samples during drilling. At the 4th minute, once drilling was concluded, the results traits are in accordance with *Sachse et al. (2012*) in which PE/SiO_2 nanocomposites demonstrated a significant increase, with 56 times the nano-emissions than the pristine polyester

samples. However, in *Sachse et al., (2012*) the background noise was not accounted for, and highlighted the limitation and challenge to compare particle number concentrations as no common methodology has been used in the past that allows for a repeatable experiment, mainly due to the inability to conceal background influence and noise. Previous studies have also used various machining techniques, dissimilar composite materials and the influencing background particle number concentrations. Hence this current study eliminates all the background noise in the measurements allowing for a more comparable set of data between studies.

The nanofillers demonstrated an increase in particle number concentration. Between the PE/SiO_2 and PE/Al_2O_3, the PE/SiO_2 nanocomposites recorded a higher average concentration during the three minutes of drilling. However, the PE/Al_2O_3 nanocomposites demonstrated a slightly higher particle number concentration during the 1 minute following the drilling conclusion. Although a higher concentration of particles was emitted from the PE/SiO_2 nanocomposites during the drilling, the particles from the aluminium oxide PE/Al_2O_3 nanocomposites remained airborne for longer and displayed a 22 % higher particle number concentration following the conclusion of the drilling (PE/Al_2O_3 = 4.3 x 10^5 #/cm^3, PE/SiO_2 = 3.52 x 10^5 #/cm^3). Across the entire 4 minutes, the aluminium oxide produced a 136% increase in particle number concentration compared to the neat polyester, as shown in Figure 74. The silicon dioxide sample produced a further 228 % increase compared to the neat polyester, also shown in Figure 74. The nanofillers can therefore be seen to have a substantial escalation in the particle number concentration throughout the entire 4 minutes for particles ranged 7 nm to 3000 nm.

The use of nano-silica and nano-alumina is established to improve the mechanical properties of the PE. Nevertheless, a small addition of the nanofillers provided significant influence on the release material composition. Although, the Al_2O_3 reinforced sample presented the greatest flexural strength over the SiO_2 and neat PE samples, the sample released the medium peak nanoparticle concentration number. The Al_2O_3 reinforced sample exposed a different release composition to the two other samples, as it had the highest quantity of remaining airborne particles after the drilling had finished (PE = 2.1 x 10^5 #/cm^3, PE/Al_2O_3 = 4.3 x 10^5 #/cm^3, PE/SiO_2 = 3.52 x 10^5 #/cm^3). Therefore, along with the quantity of nanoparticles released, the data represented from the CPC, as shown in Figure 74, also indicate to the particle characteristics due to the disparate rapidity of dispersion and particle deposition.

Two distinct concentrations of the reinforced samples were fabricated in order to investigate the effect of the nano-filler weight percentage on nanoparticle release during drilling. Figure 75 illustrates the influence for the Al_2O_3 reinforced PE sample. The data in Figure 75 displays the increase of Al_2O_3

nano-filler demonstrated a miniature difference in the particle number concentration. The increased concentration of the 5 wt. % exhibited a 33 % increase in particle number concentration during the peaks (2 wt. % Al_2O_3 at $3.6x10^6$ #/cm^3 and 5 wt. % Al_2O_3 at $4.7x10^6$ #/cm^3) and at the conclusion of the drilling during the 1-minute post drilling (2 wt. % Al_2O_3 at $4.0x10^5$ #/cm^3 and 5 wt. % Al_2O_3 at $4.7x10^5$ #/cm^3). The concentration at the end of the 4 minutes of the 5 wt. % alumina sample represented a 19 % increase in particle number concentration from the 2 wt. % alumina sample.

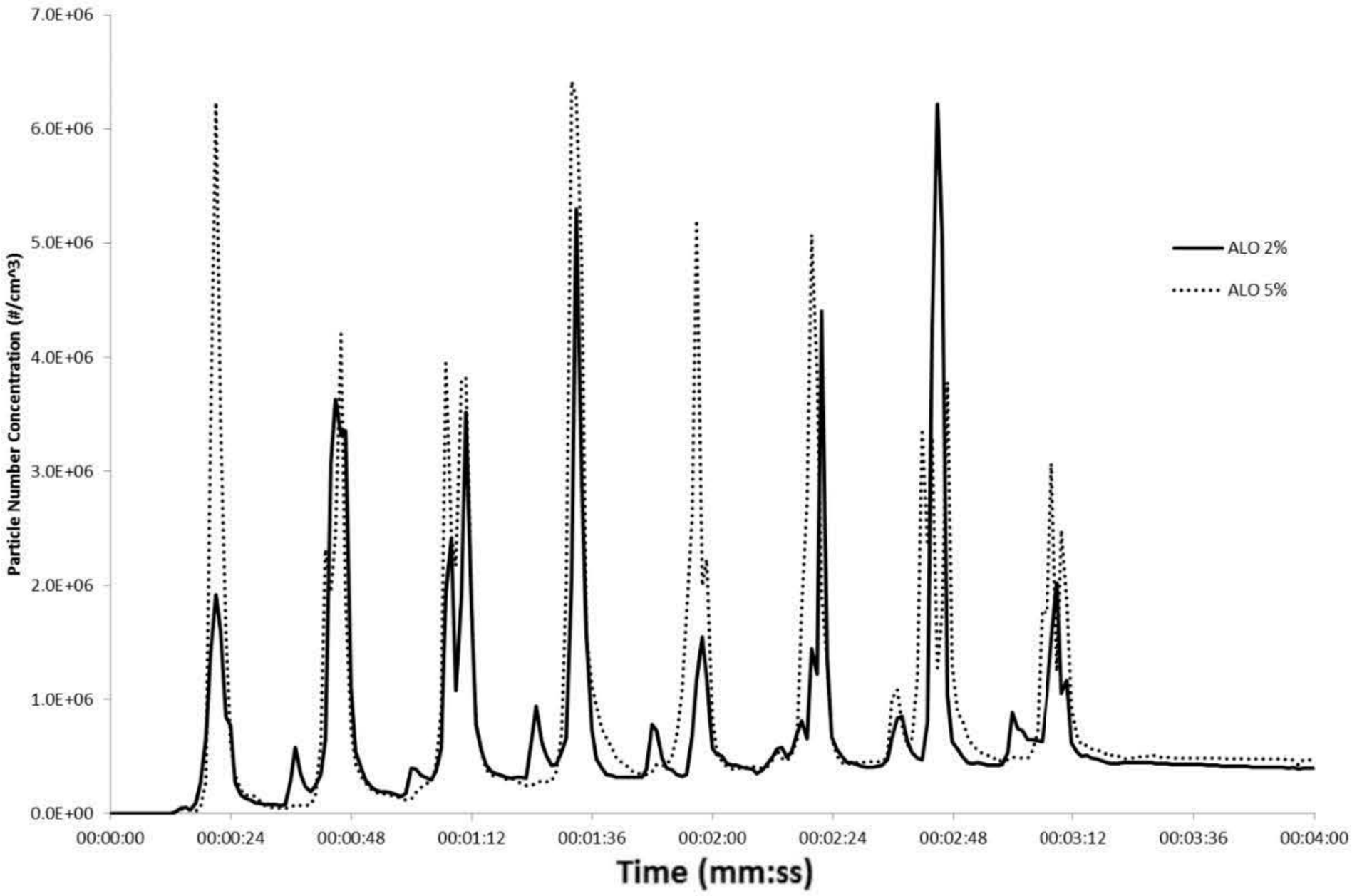

Figure 75*:* Average particle number concentration of 2 wt. % Al_2O_3 and 5 wt. % Al_2O_3 reinforced PE nanocomposites recorded on CPC (n=3 for each average).

The influence on the particle number concentration can be correlated to material properties to evaluate the effect of mechanical properties on release, as well as potentially designing materials to reduce the risk of release of potentially toxic particles, whilst still attaining material performance. This

correlation between the material's mechanical performance and nanoparticle release is essential when considering materials through concepts of safety by design.

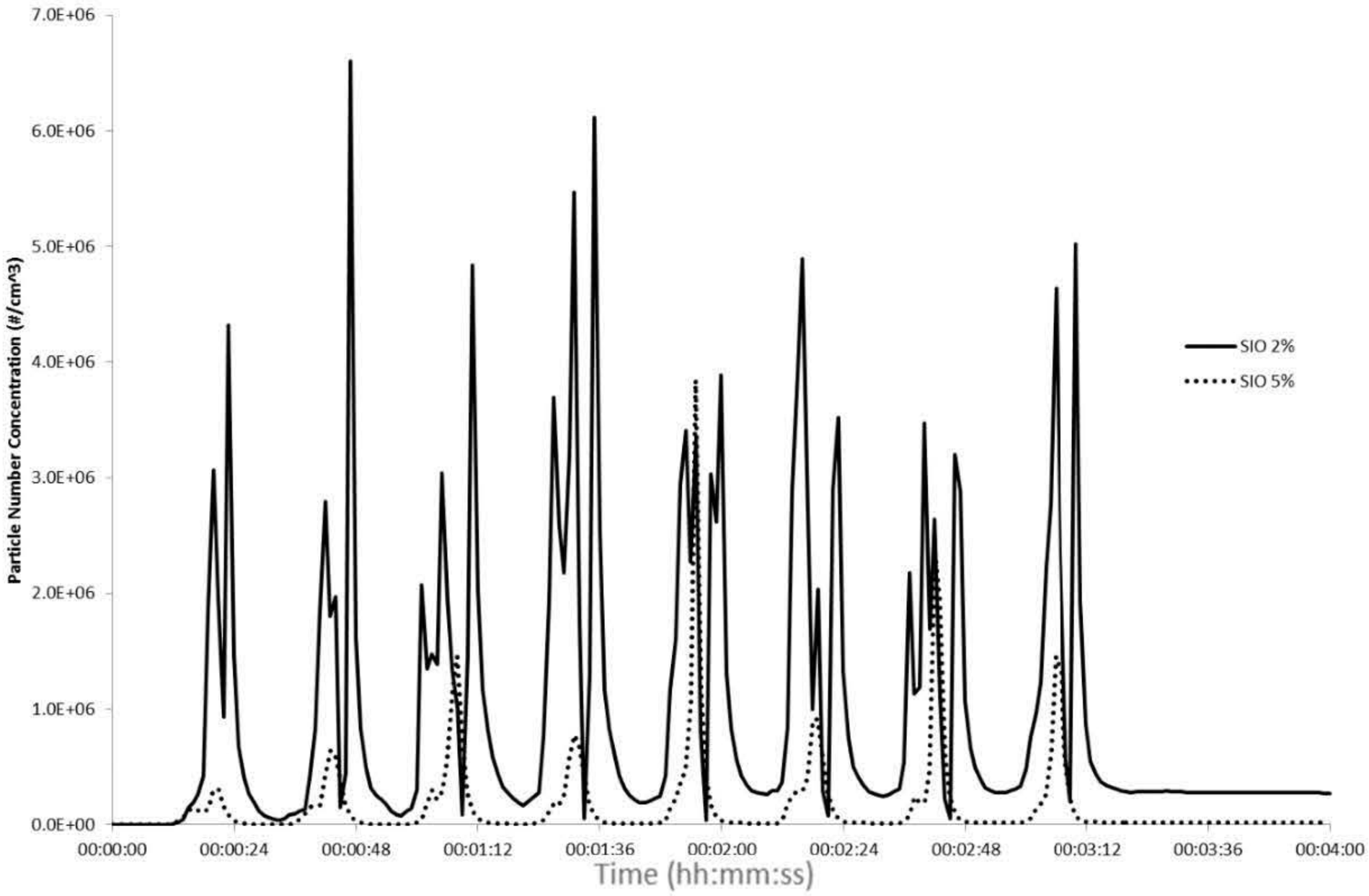

Figure 76*:* Average particle number concentration of 2 wt. % SiO_2 and 5 wt. % SiO_2 reinforced polyester nanocomposites as recorded on CPC (n=3 for each average).

The comparison of two concentrations of the PE/SiO_2 nanocomposites was also carried out. The particle number concentration release from the SiO_2 samples, shown on Figure 76, can be seen to have an inverse correlation on the nanoparticle release compared to the alumina nanofiller, shown in Figure 75. The increase to 5 wt. % of the SiO_2 filler displayed an average decrease of 70 % of nanoparticles introduced across the eight peaks of particles released. Furthermore, an average 94 % decrease of particle number concentration was observed at the end of the 4-minute sampling period for the 5 wt. % SiO_2 sample.

With an increase in nanoparticles embedded within the material, one would expect a resulting increase in nanoparticle release due to the presence of more nanoparticles. However, the increase in nano-silica may have further molecular effects to the structure of the material, such as reforming the embedding and bonding of the nanoparticles to the nanocomposite or bonding/agglomeration variations which may cause the release of larger micro-sized particles. This may be the cause for the contrasting influences in results between the nanosilica and nanoalumina reinforced samples. Based on this study, a rise in nanoparticle filler wt. % content in the matrix may either augment or reduce

the quantity of nanoparticles released. The corresponding result on particle number concentration released is therefore more dependent on the matrix-filler bonding and consequent material structure, instead of solely the quantity of nanofiller weight percentage embedded within.

Table 19*:* Inferential statistical representation of the particle number concentrations introduced at the peaks due to the drilling on polyester-based samples (n = 24 for each sample). Lower and upper limits represent the 90% confidence interval on a sampling t-distribution. (Note: CPC limit of 9.99 × 10^6 #/cm^3 and the mean peaks with the greater than symbol therefore represent a lower bound value that include the saturated peaks.)

Sample	Mean: $\bar{\bar{X}}$ [#/cm^3]	Deviation: $S_{\bar{X}}$ [#/cm^3]	Minimum [#/cm^3]	Maximum [#/cm^3]	5% Lower limit of confidence interval [#/cm^3]	95% upper limit of confidence interval [#/cm^3]
PE	3.97 x 10^6	2.54 x 10^6	1.19 x 10^6	8.88 x 10^6	2.70 x 10^6	5.24 x 10^6
PE/ Al_2O_3 2%	6.35 x 10^6	2.16 x 10^6	2.78 x 10^6	9.66 x 10^6	5.26 x 10^6	7.43 x 10^6
PE/ Al_2O_3 5%	>8.52 x 10^6	>1.03 x 10^6	7.27 x 10^6	>9.99 x 10^6	8.00 x 10^6	9.03 x 10^6
PE/ SiO_2 2%	>8.15 x 10^6	>1.21 x 10^6	6.45 x 10^6	>9.99 x 10^6	7.55 x 10^6	8.76 x 10^6
PE/ SiO_2 5%	2.97 x 10^6	2.91 x 10^6	5.61 x 10^6	9.61 x 10^6	1.51 x 10^6	4.42 x 10^6

Table 19 displays the statistical analysis carried out on the peak particle number concentrations of the samples. The mean peak values are influenced and confined by the saturated CPC measurement capability (i.e. 1 × 10^7#/cm^3) and are therefore only a lower bound representation for the PE/ Al_2O_3 5% and PE/ SiO_2 2% samples. Respectively, the data from Table 8 represents the statistical differences between the peak concentrations introduced due to drilling. The calculated lower tail of 5% and upper tail of 95% give a representation of the data for a 90% confidence interval of a t-distribution. This highlights the disparities between the peak particle number concentrations and therefore, a statistically significant difference with the introduction of nanofillers on release in comparison to the neat polyester. A two sample t-test of significance of each sample mean and deviation to the neat polyester sample returned statistically significant differences for all samples except for the PE/SiO_2 5% which demonstrated to be within a 95% confidence interval of the PE sample (statistically insignificant). Equally, the increase in nanofiller weight concentration demonstrated a statistically

significant difference in comparison to the lower weight concentration for both SiO_2 and Al_2O_3. ANOVA single factor analysis was performed to assess the variability between the sample peak means introduced due to the filler. The analysis returned statistically significant differences within the 5 samples (F value = 9.68 F critical value = 2.64) and a 0.22% chance that the observation could have been observed due to random error alone and therefore rejecting a hypothesis that the samples displayed no difference.

Further to the statistical analysis carried out in Table 19, a bar chart illustrated in Figure 77 accentuates the difference in particle number concentration at the end of the four minute sampling period and the potential for manufacturing materials through safety by design concepts.

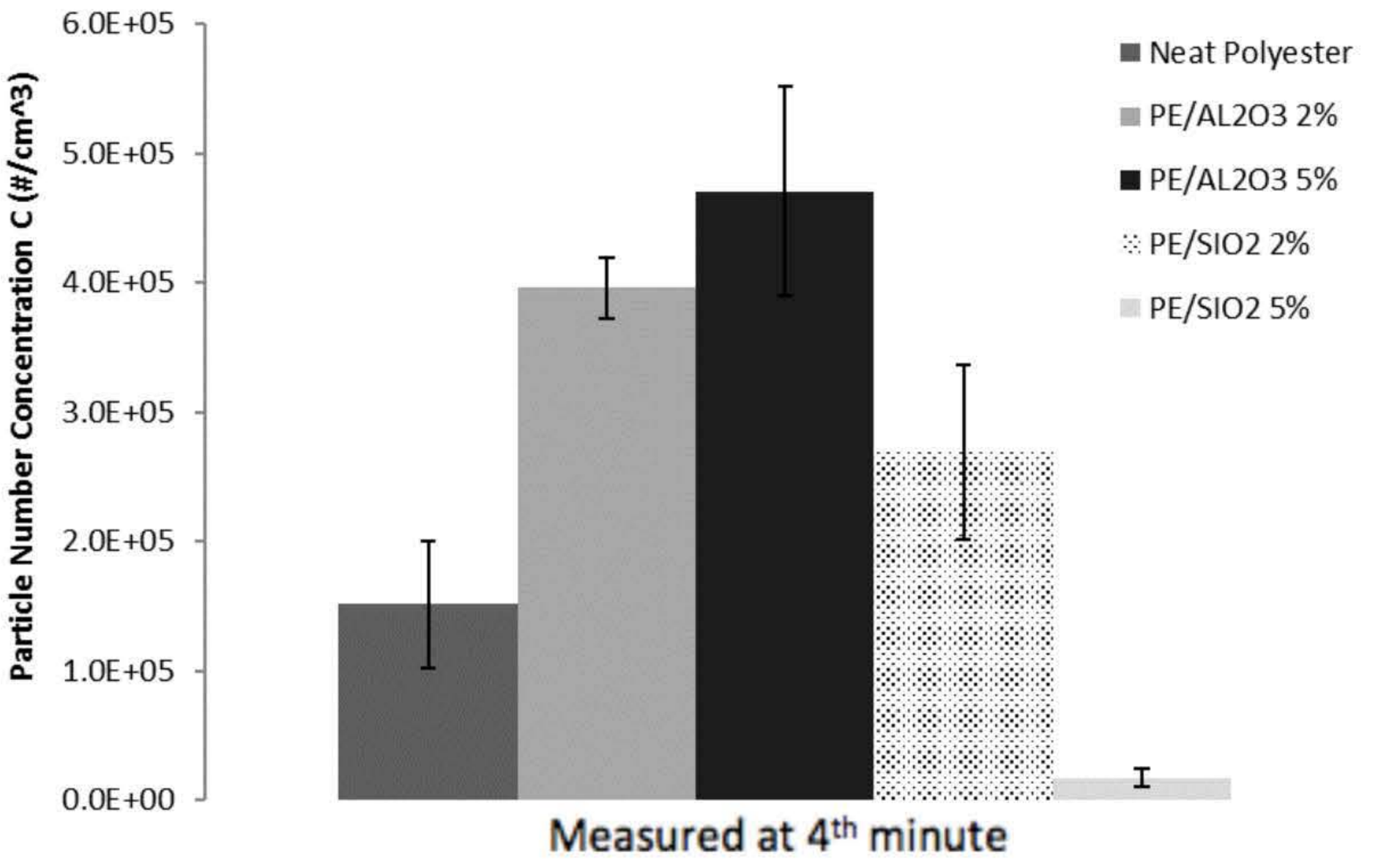

Figure 77*:* Total concentration of particles recorded at 4th min (C, particles/cm^3) for Polyester based samples as measured on the CPC (n=3 for each average).

As shown in Figure 77, the PE/Al_2O_3 sample displayed the highest particle number concentration at the end of the four minutes for both filler concentrations. This difference to the mean peak particle number concentration, suggests that the filler can be seen to influence the time to deposit as well as the number of particles released. Furthermore, the concentration at the end of the 4 minutes of the 5 wt. % alumina sample represented a 19% increase in particle number concentration from the 2 wt. % alumina sample.

In comparison, the introduction of the SiO_2 filler has both an increase and decrease effect on the particle number concentration. An average 94 % decrease of particle number concentration was

observed at the end of the 4-minute sampling period for the 5 wt. % nanosilica sample (and therefore consequently a material that suggests could be useful through safety by design concepts) in comparison to the 2 wt. % sample. The PE/ SiO_2 is the only sample to observe a decrease in particle number concentration at the end of the four minutes from the neat PE sample.

As seen in the graphical representation over the four minutes in Figure 74, although a higher concentration of particles was emitted from the PE/SiO_2 2 wt. % nanocomposites during the drilling, the particles from the aluminium oxide PE/Al_2O_3 2 wt. % nanocomposites remained airborne for longer and displayed a 22% higher particle number concentration following the conclusion of the drilling (PE/Al_2O_3 2 wt. % = 4.3 x 10^5 #/cm^3, PE/SiO_2 2 wt. % = 3.52 x 10^5 #/cm^3).

5.3.2 Filler effect on Particle Size Distribution

With a sampling period of 1 minute, an average of the 4 data sets from the SMPS across the 4 minutes for each repeated sample is displayed in Figure 78. The particle size distribution data illustrates little contrast between the three samples in the sizes of the nanoparticles released. However, the data accentuates the large particle number concentration disparity between the samples as shown in the CPC data in *Figure 74*. The larger particle number concentration released from the silicon dioxide sample is clearly visible over the aluminium oxide and neat polyester samples. Nonetheless, two of the peak size distributions are indicated to be around the same particle diameters.

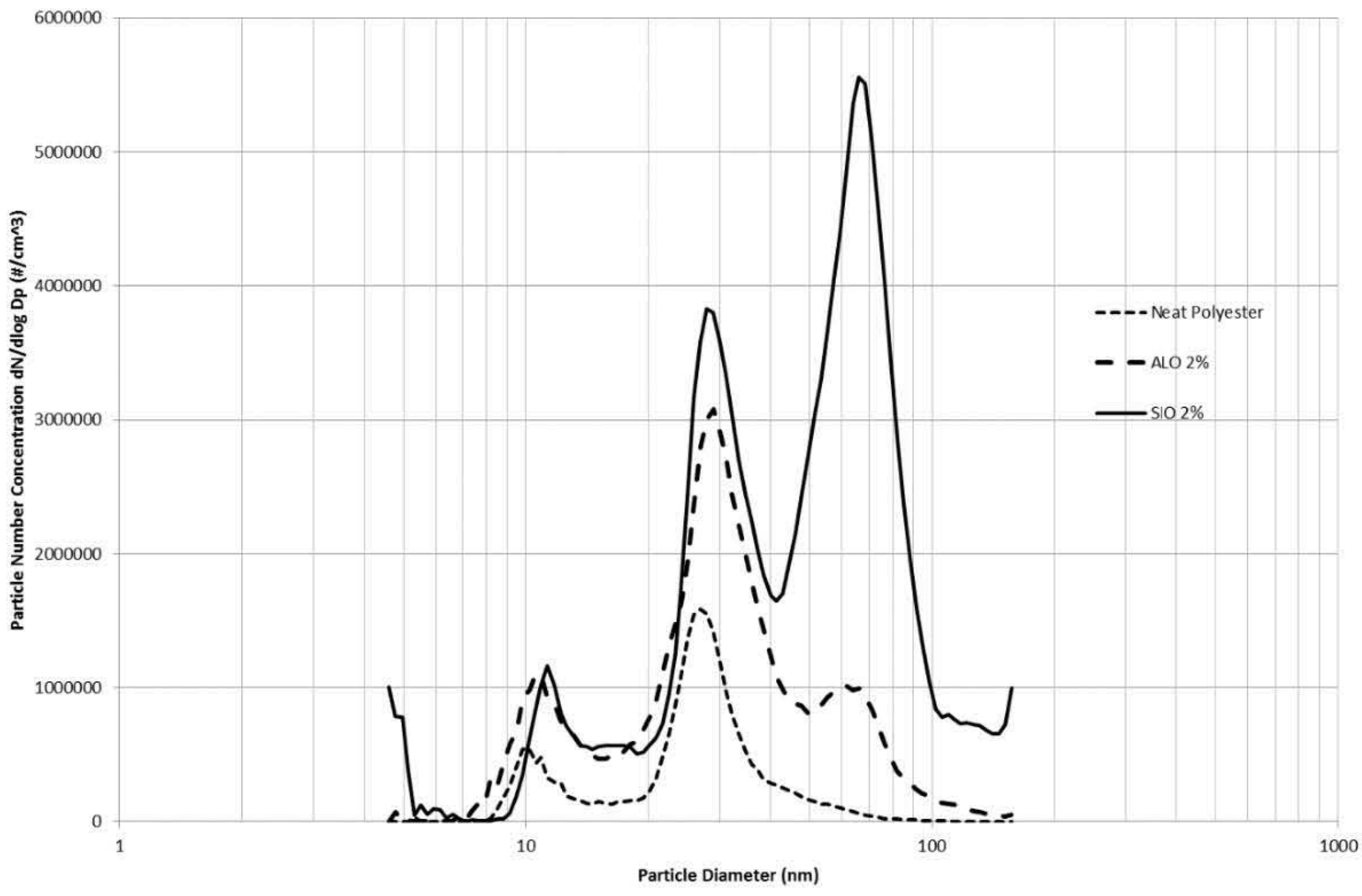

Figure 78*:* Average particle size distribution measure using SMPS of polyester-based nanocomposites (n=12 for each average).

All three samples displayed particle number concentration peaks at 10 nm and 30 nm. The nano-filled samples revealed a third peak between 60nm to 70nm. The nanofillers can therefore be apparent to introduce a concentration of larger sized nanoparticles. In one previous study (*Sachse et al., 2012*), that investigated the effect of nano-silica on nanoparticle release reported that a principal peak release at 30 nm particle diameter at the highest concentration of release within a particle size range of 5.6 nm to 1083 nm. The further two diameter peaks seen in the size distributions in Figure 78 were not reported. The third peak at 60-70 nm may therefore be as a result of polymer matrix-filler embedment since a different matrix has been used in the present study. A comparison between the

two studies suggests that the matrix has a meaningful influence on the size of the nanoparticles released. Although not nano sized in origin, the matrix polymer released identifiable nanoparticles as shown in the particle size distribution in *Sachse et al. (2012)* and Figure 78, and as shown in the CPC data in Figure 74.

The effect of weight percentage of nanofiller on nanoparticle release was also investigated. The two concentrations of alumina demonstrated that an increase to 5 wt. % from 2 wt. % displayed an increase in particle number concentration. A comparison of the two particle size distributions is shown in Figure 79.

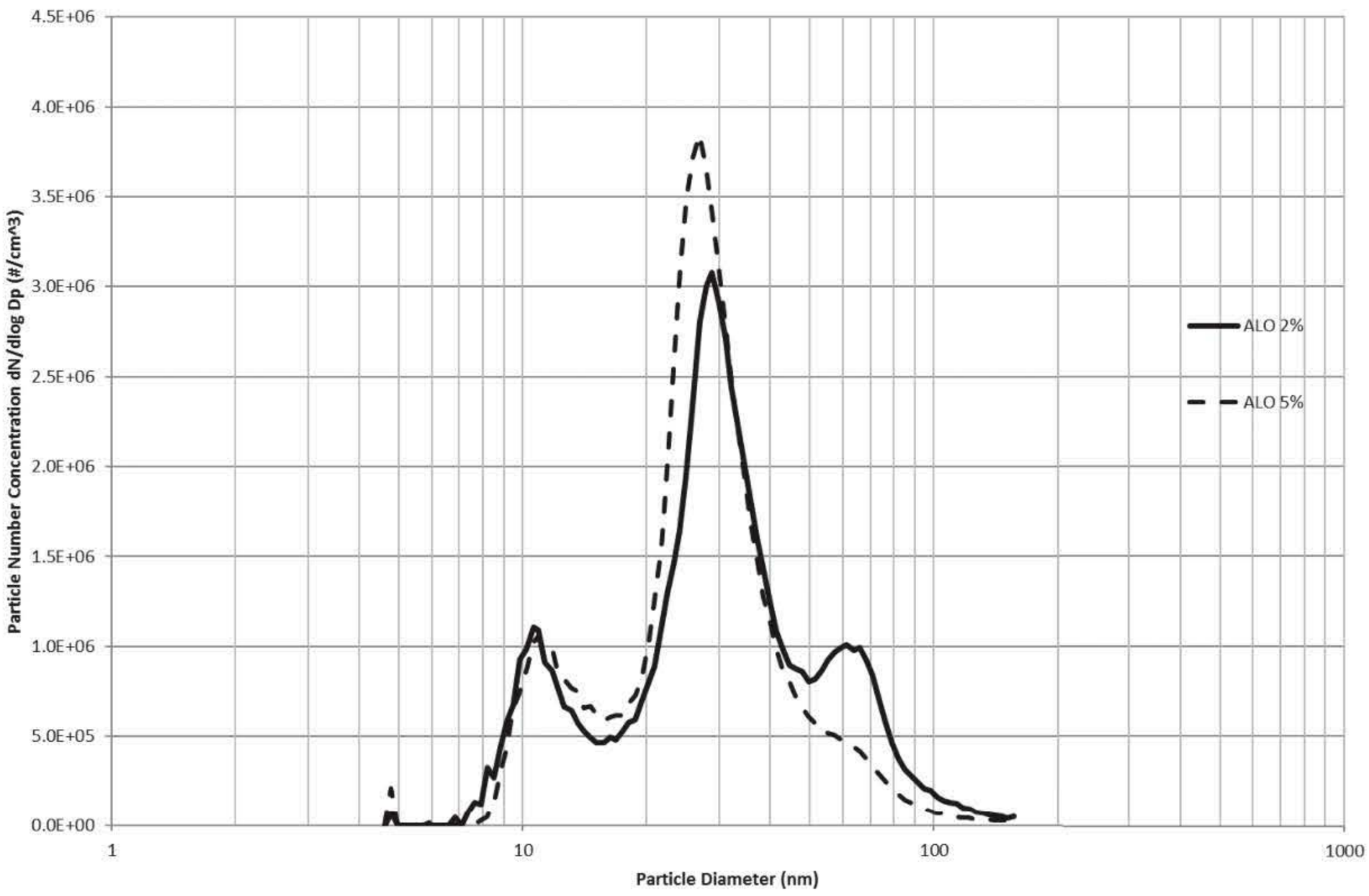

Figure 79*:* Average particle size distributions collected on SMPS of 2 wt. % Al_2O_3 and 5 wt. % Al_2O_3 reinforced polyester nanocomposite samples (n=12 for each average).

The two samples demonstrated similar particle size distributions. Both samples presented peaks at 10nm and 30nm. A third peak at 60nm is more visible for the 2 wt. % sample than a diminished peak for 5 wt. % sample. The largest quantity of particles for both samples was witnessed to be around 30nm. However, PE/Al_2O_3 (5 wt.%) nanocomposites released a 25 % greater average of particle number concentration at this particle diameter compared to the 2 wt. % sample as shown in Figure 79.

When linking to the SMPS data, the increase in particle number concentration observed in the CPC data, shown in Figure *75*, can be understood to be due to the increase of particles around 30 nm. Given that the average particle size of the nanoalumina is less than 50 nm, the peak observed may be the release of the independent nanofillers. The increase in weight percentage concentration of the nanofiller indicates to be increasing the release of liberated nanofiller.

The concentration of the alumina nanofiller has an effect on the particle number concentration and corresponding particle size distributions. The similar performance in mechanical properties between the 2 wt. % and the 5 wt. % silica reinforcement, demonstrated a decrease in particle number concentration of the potentially hazardous 30 nm particle diameter range. When considering the fabrication of alumina reinforced materials through safety by design, the particle number concentration release and corresponding size distributions are two parameters to consider minimalizing nanotoxicological risks. The comparison of the two filler weight percentage concentrations is illustrated in Figure 80.

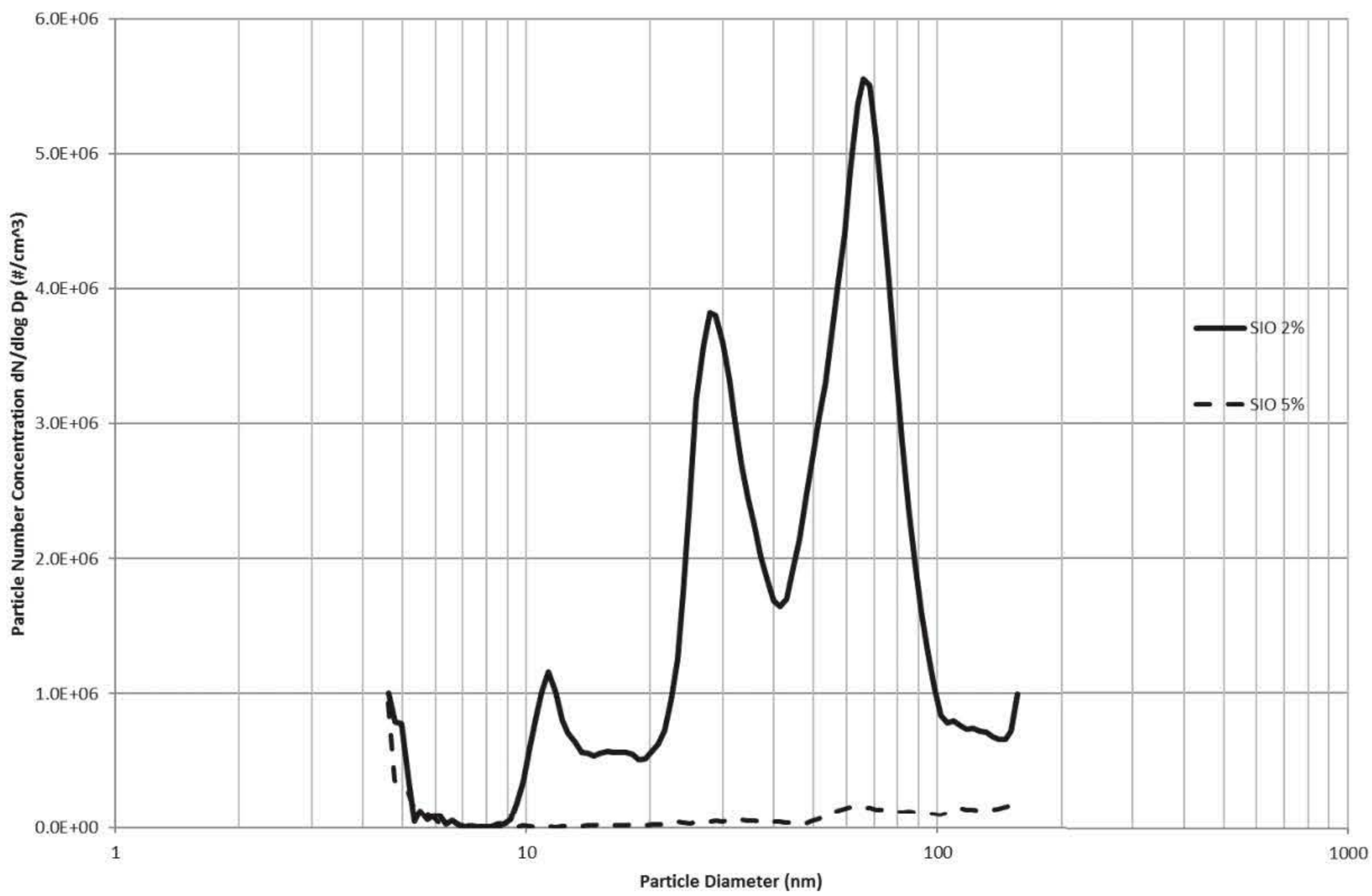

Figure 80*:* Average particle size distributions collected on SMPS of 2 wt. % SiO_2 and 5 wt. % SiO_2 reinforced polyester nanocomposite samples (n=12 for each average).

If taking into consideration, exposure to particle number concentration alone as a nanotoxicology factor, the nanosilica demonstrated that the increased weight percentage displays a reduced risk in

contrast to the alumina nanofiller results shown in Figure 79. A reduced particle number concentration can be presupposed to have a direct reduction in exposure to the nanoparticles. However, the sample exhibited a high concentration of nanoparticles at the lower end of the spectrum, at 5 nm. These factors in relation to the mechanical properties, could provide a potential opportunity when fabricating materials through safety by design concepts.

Further to the data collected on the SMPS, data was also gathered on the DMS50 for the particle size distribution. Three dimensional plots shown in Figure 81 and Figure 82 illustrate the combination of the particle number concentration and its corresponding size distribution throughout the four minutes. This constructs an instantaneous and direct representation of the particle size distribution released from the material before dispersion within the chamber. The size distribution across the eight holes drilled is represented for the neat PE, PE/Al_2O_3 2 wt. % and PE/SiO_2 2 wt. % samples. It is important to note that the data is taken from a separate run to the CPC and SMPS data due to the required increased inflow rate.

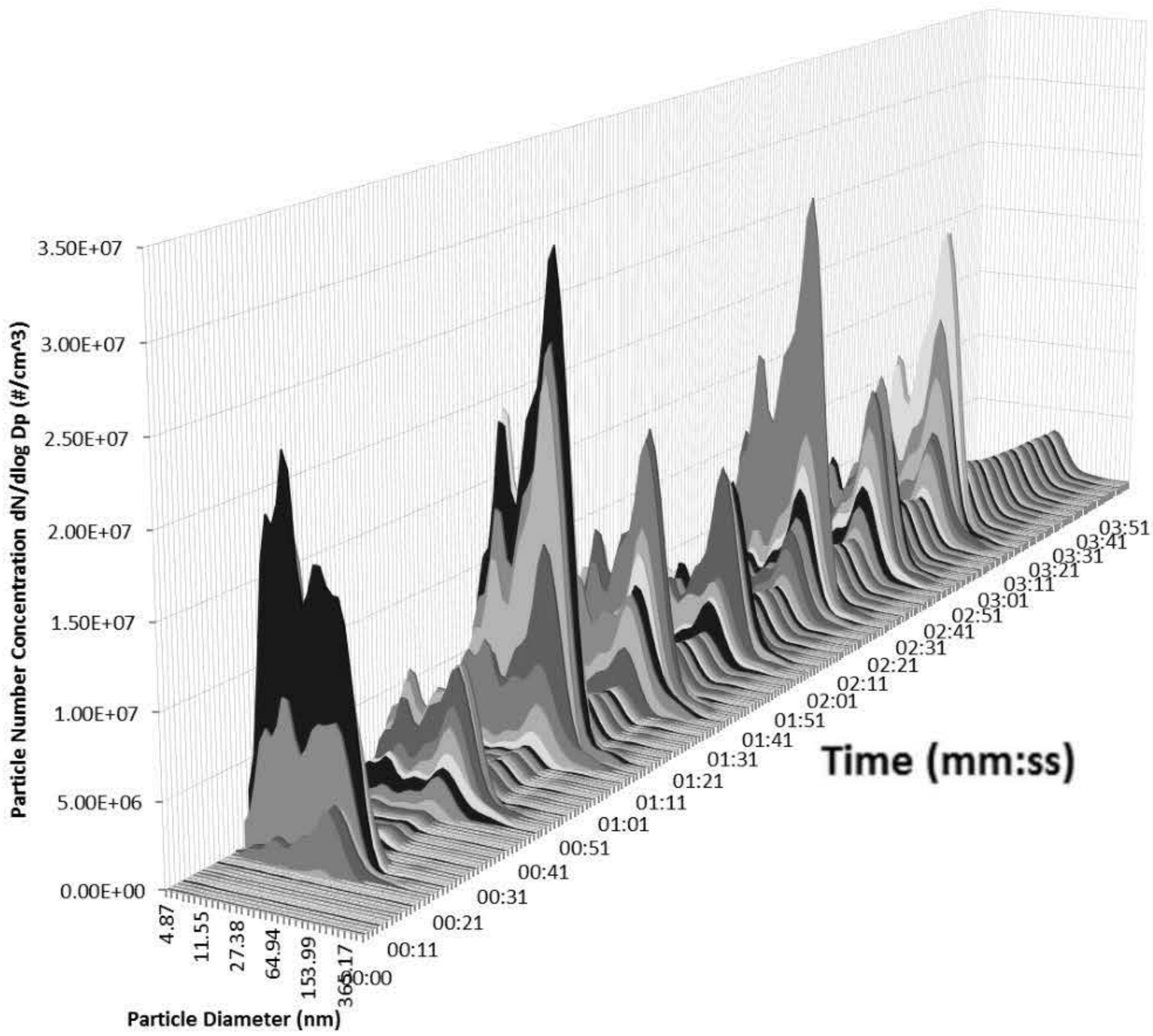

Figure 81*:* Particle size distribution over four minutes as measured on DMS50 of neat PE sample.

a.)

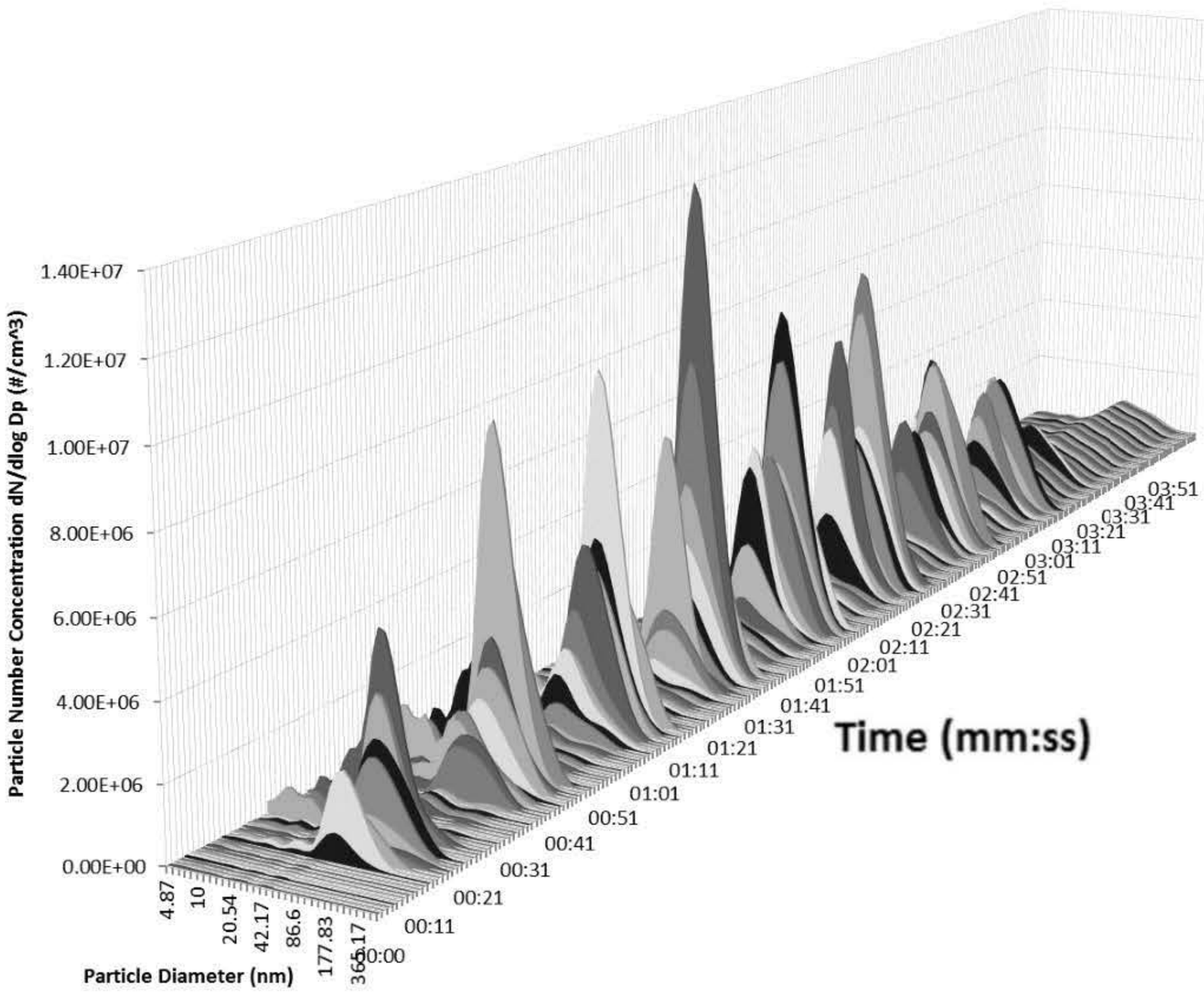

b.)

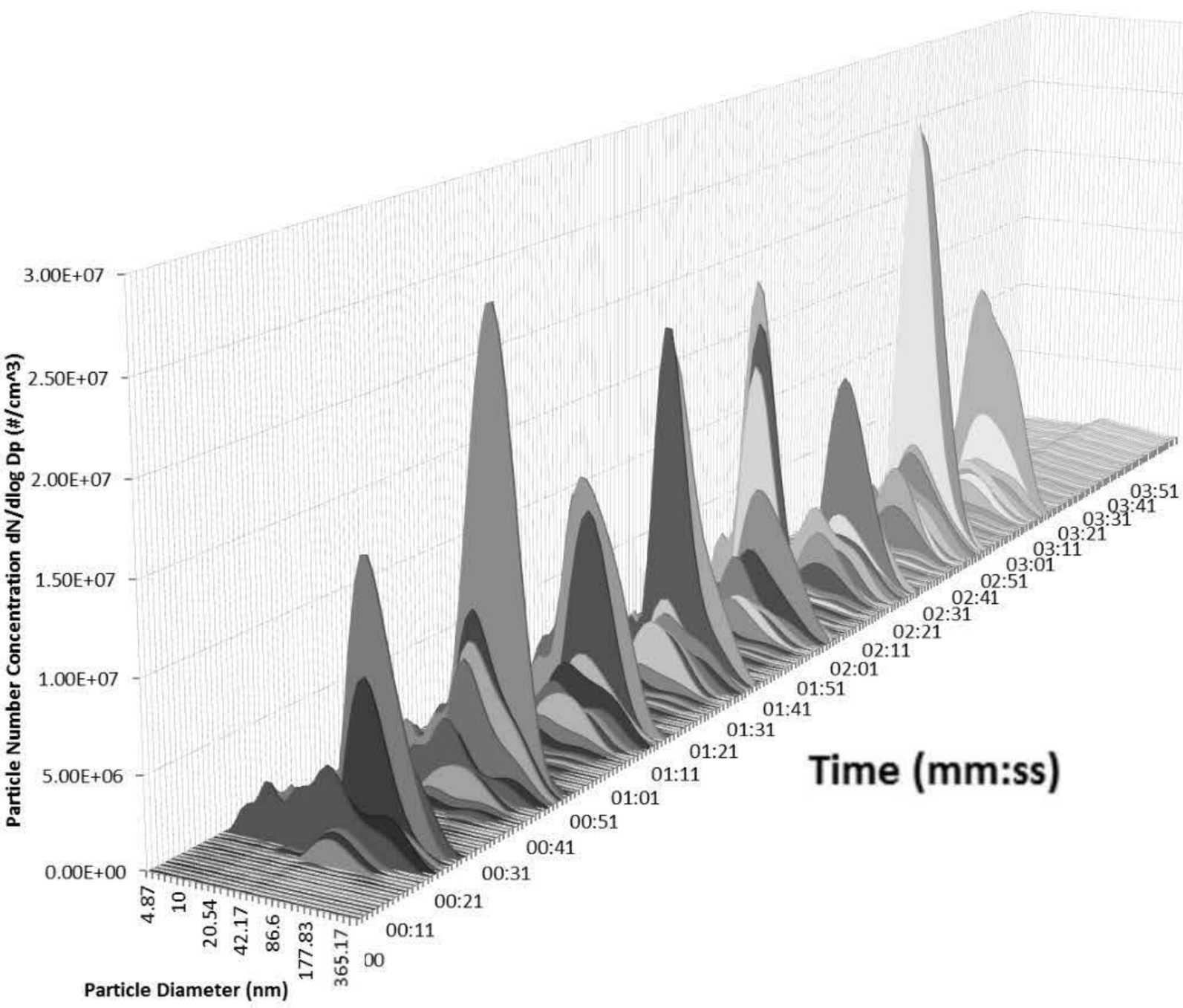

Figure 82*:* Particle size distribution over four minutes as measured on DMS50 of a.) PE/Al_2O_3 2 wt. % sample and b.) PE/SiO_2 2 wt. % sample.

The peak concentrations introduced from the 8 holes drilled in one test run can be visibly distinguished by the peaks. The size distributions between peaks and after drilling are less visible due to the high concentrations from the peaks. The peaks detectable in the size distributions across the eight holes are relatively consistent in particle diameter. However, as with the CPC data shown in Figure 74, the peaks are less consistent in particle number concentration. This could be attributed to the difference in inflow rate necessary for the two instruments and the sensitivity therewith associated, as the DMS50 requires a 6 L/min flow rate compared to 0.6 L/min flow rate for the CPC. For instance, the peak particle number concentration induced by the eight holes on the silicon dioxide sample shown in Figure 82 has a standard deviation of $52x10^5$ #/cm^3 which equates to a variation coefficient of 27%.

The peak particle number distributions for the three samples are of most interest to investigate the real-time size distribution being released from the materials at the moment of drilling. This gives a representation of all the particles released at the time of drilling minimalizing effects of dispersion and agglomeration. Figure 83 illustrates a two-dimensional plot of the size distribution taken from the highest peak for the PE/ Al_2O_3 2 wt. % and the PE/SiO_2 2 wt. %. The neat PE can be seen to have two peaks across the size distribution axis, whereas the aluminium oxide and silicon dioxide samples displayed one peak only at a relatively large particle diameter.

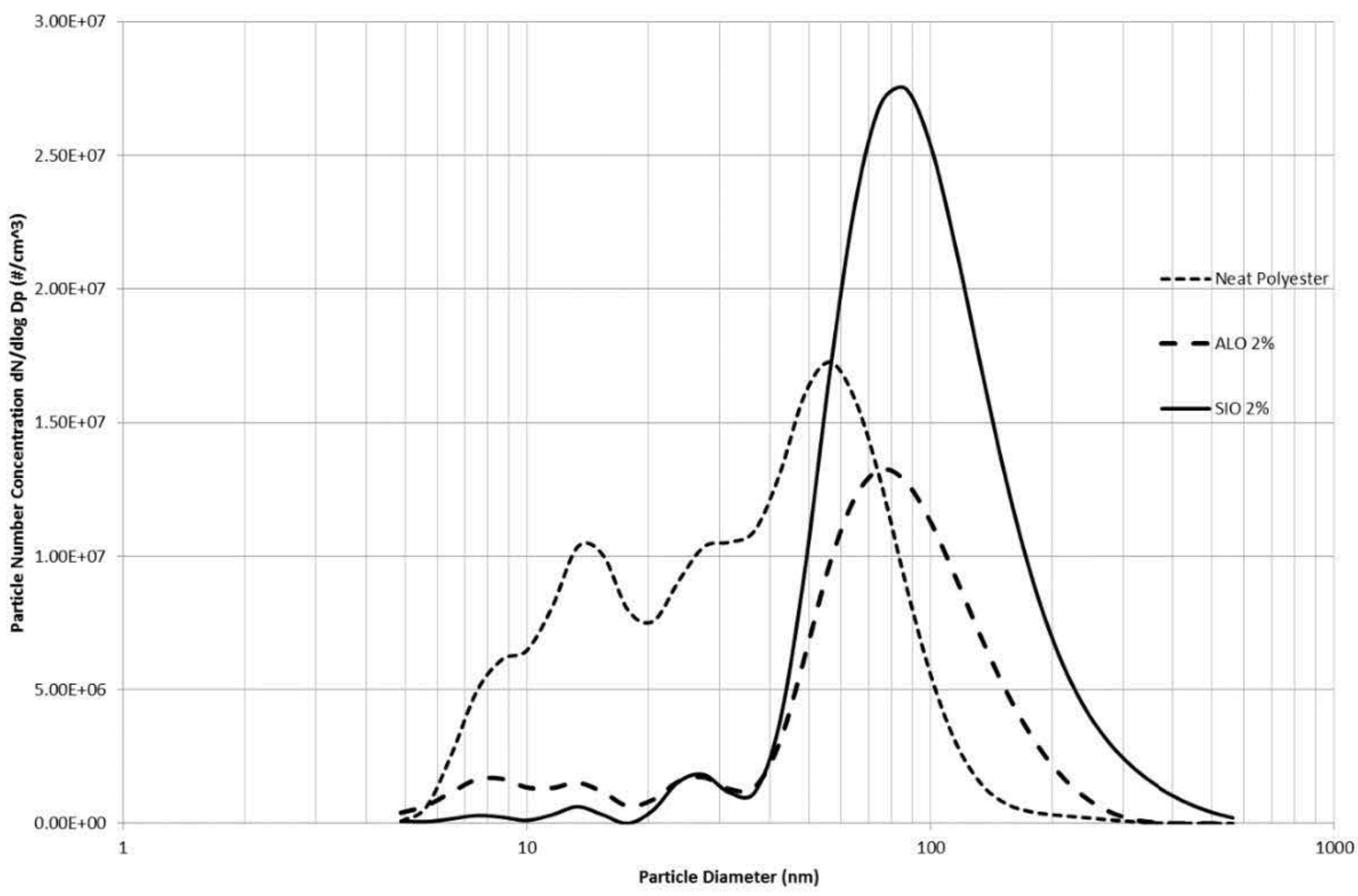

Figure 83*:* Particle size distribution of peak concentrations within 4 minutes drilling of polyester-based nanocomposite samples recorded on DMS50.

Differentiating from the nanofilled samples, the neat PE has a second peak within 10-20 nm particle diameter. The plot indicates the neat PE sample emitted a substantial group of particles smaller than those emitted from the aluminium oxide and silicon dioxide samples. It should be noted that this correlation conflicts with the results displayed from the SMPS. This may be related to the accuracies, sampling period and time resolution difference between the SMPS and DMS50 and should be a focus for future works. Studies have experienced similar issues as *Njuguna & Sachse (2014)* documented the limitations and deficiencies of current nano-sized aerosol measurement techniques.

From the DMS50 data shown in Figure 83, a larger percentage of the particles emitted from the PE/Al_2O_3 sample are in the smaller range of particle diameters compared to the PE/ SiO_2 sample. The PE/Al_2O_3 sample is seen to have a similar particle diameter peak to the silicon dioxide sample, but also a higher concentration within the smaller particle diameters. Conversely the PE/SiO_2 nanocomposites produced few particles around the 10 nm range, but a larger peak towards 100 nm. When correlated to the CPC data on Figure 74, this could be associated with the increase in particles during the post-drilling phase from the aluminium oxide sample compared to the silicon dioxide sample.

It should be noted that the analysis on the average particle size distribution during drilling and the 4^{th} min post drilling from both the SMPS and DMS50 show conflicting results. The DMS50 results for all three samples showed an unchanged peak in particle diameters during the drilling and during the 4^{th} minute with a lower particle number concentration. Therefore, no shift in size distribution was seen from the particles emitted during the DMS50 run, removing the prospect of agglomeration of the airborne particles over the 4 minutes. Considering the DMS50 data, if particle agglomeration were to happen it would have to occur instantaneously.

The SMPS data compared to the data from the DMS50 presents peak changes in particle size distributions. The individual plots for the SMPS data and the DMS50 data for the neat polyester displayed only a change in magnitude between the averages and 4^{th} minute drilling read on each instrument. However, the particle diameter of the peaks between the two instruments differs. The disparate peaks seen on the two instruments introduce important deductions and effectiveness of instrumentations required for real-time data. Although the two instruments both use electrical mobility measurements to classify the particle size distribution, the difference in sampling period could be the source of the varied results in real-time measurements during drilling.

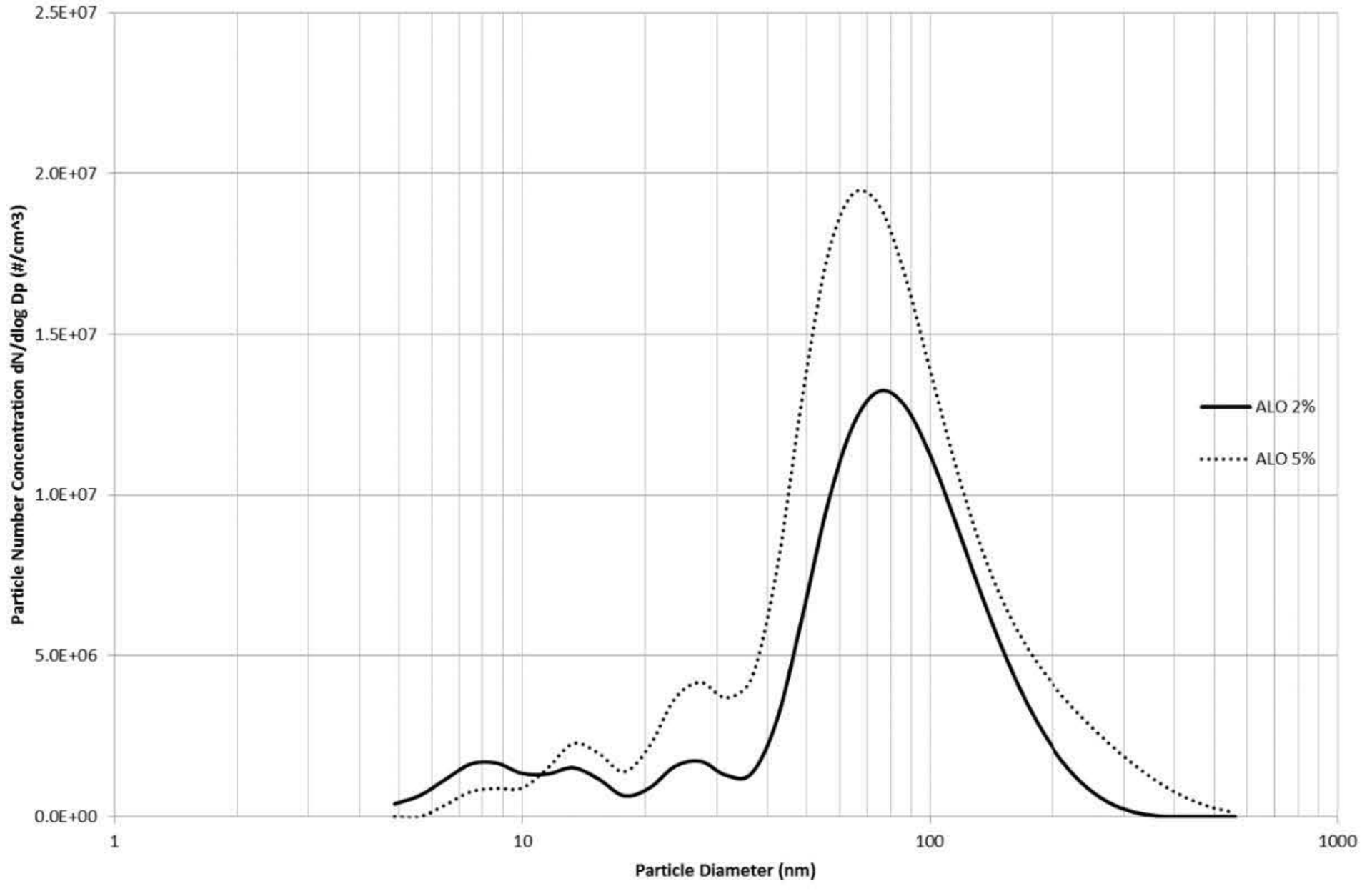

Figure 84*:* Peak particle size distribution of 2 wt. % Al_2O_3 and 5 wt. % Al_2O_3 reinforced polyester nanocomposite samples recorded on DMS50.

Additional to the comparison between the nanofillers and neat PE, two different weight concentrations of the separate nanofillers were examined, shown in Figure 84. The change in filler weight concentration shows a slight divergence in particle size distribution and a shift towards a higher particle number concentration. The increase in filler showed to evidently increase the particle number concentration, supporting the CPC (shown in Figure 75), and the SMPS data (shown in Figure 79). The augmented concentration of nano-alumina displayed peaks at similar particle diameters but remained at higher particle number concentrations compared to the 2 wt. % sample. The exception is for particle diameter of smaller than 10 nm, where the 2 wt. % sample presented a minimal higher particle number concentration than the 5 wt. % sample. The peak particle diameter released from the 5 wt. % alumina sample at a diameter of 65 nm ($1.94x\ 10^7$ #/cm^3) exhibited an increase of 47 % from the peak particle diameter released from the 2 wt. % alumina at a diameter of 75 nm (1.32×10^7 #/cm^3). The peak concentration diameters conflict with the SMPS data, but support the increasing effect of particle number concentration release with increasing nano-alumina content.

The comparison and effect of two weight concentrations of the nano-silica was carried out and illustrated in Figure 85.

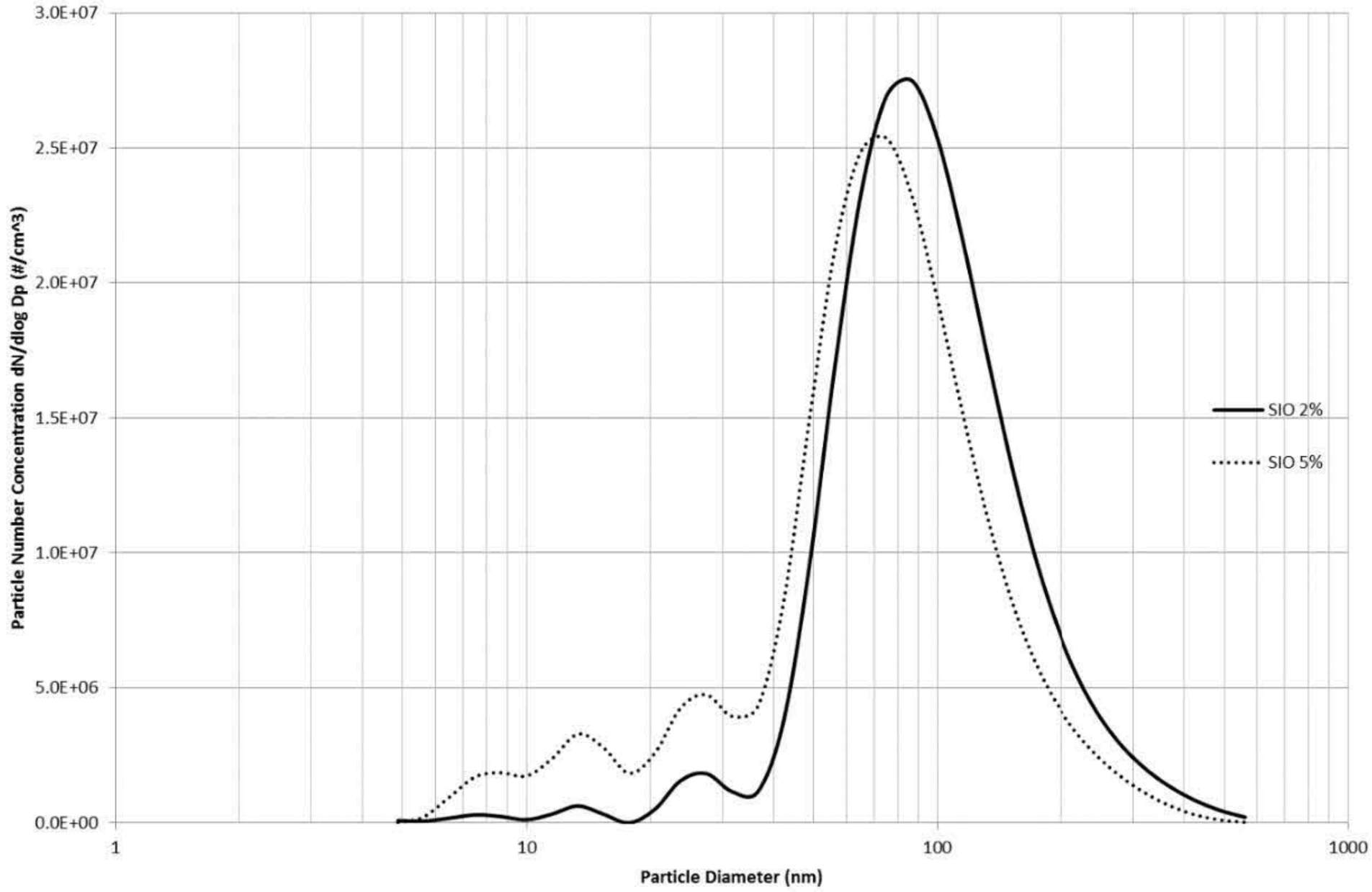

Figure 85*:* Peak particle size distribution of 2 wt. % against 5 wt. % nano-silica reinforced samples recorded on DMS50.

From Figure 85, the increase in weight concentration shows a shift in the plot indicating a reduction of particle number concentration above 70 nm, and increase in the particle number concentration released below 70nm. The peak concentration of the 5 wt. % at a diameter of 75 nm (2.54×10^7 #/cm^3) demonstrated a decrease of 8 % from the peak concentration of the 2 wt. % at a diameter of 87 nm (2.75×10^7 #/cm^3). However inversely, the peak visible at 28 nm illustrated an average particle number concentration of 4.75×10^6 #/cm^3 for the 5 wt. % sample, an increase of 160 % from the 1.82×10^6 #/cm^3 for the 2 wt. % sample. The total particle number concentration released at the lower particle diameters is significantly lower than at 70nm, but the augmented weight percentage had a moderate increasing effect on particle diameters less than 70nm.

Although the CPC data (shown in Figure 76) presented a decreasing effect of release of particle number concentration along with the SMPS (shown in Figure 80) for the higher weight percentage, the DMS50 data revealed an average increase in particle number concentration for particles smaller than 70 nm. When considering fabricating nano-silica reinforced polyester composites through the safety by design strategy, a further assessment of the quantity and range of particle diameters could be evaluated for minimising the nanoparticle emissions and exposure even further. In terms of total particle number concentration of nanoparticles released, the 2 wt. % reinforced silica sample still

demonstrated the adverse of the two samples, but with a reduced percentage of nanoparticles on the lower end of diameter spectrum.

As with the SMPS data, the DMS50 supports the contrasting effect of increasing the nano-alumina or nano-silica weight percentage in the PE. The results demonstrated that with an increase in nanofiller weight concentration the particle size distribution will not merely intensify at certain peaks, but will shift the curve to the release of different particle size diameters. The particle size distribution is therefore not directly interrelated to the release of the independent nanofillers, but the matrix-filler bonding and molecular material structure formed with the nanofiller concentration.

5.3.3 Filler Effect on Mass Size Distribution

Since the drilling was conducted within a clean environment, all of the particles measured with the instrumentation is perceived to be from the nanocomposite material. Therefore, since the SMPS functions on the measuring principle of spherical particles, using the particle size distribution measured, the mass can also be calculated. Particle mass concentration is considered another vital parameter to consider when assessing exposure to nanoparticles. Assuming the known density of the individual materials to remain constant, the particle mass concentration can be estimated. Using the diameter and density of the material, the particle mass concentration is illustrated in Figure 86**.** The assumed constant material density for the three nanocomposites are: PE = 1.24 g/cm^3, PE/Al_2O_3 2 wt. % = 1.29 g/cm^3 and PE/SiO_2 2 wt. % = 1.23 g/cm^3.

The particle diameters with high particle number concentrations observed in the SMPS results in Figure *78*, have adjusted due to the consequent mass increase of larger particles. The low mass of particles measuring less than 40 nm in diameter produce almost no evident peak. The plot is swayed entirely by the larger particle diameters observed from the release of the PE/SiO_2 sample. A substantial peak at 70 nm of over 1000 µg/m^3 is observed for the PE/SiO_2 sample. A huge peak between 100 nm to 156 nm reaches 2470 µg/m^3 for the PE/SiO_2 sample. These large peaks release from the PE/SiO_2 sample almost diminish the peak mass concentrations released from the PE and PE/Al_2O_3 sample. Is should be noted however that the PE sample released its largest peak of 22 µg/m^3 at 23 nm and the PE/Al_2O_3 sample at 203 µg/m^3 at 71 nm. These mass concentrations are still considerably more than the mass concentrations observed from the PP based samples presented in Chapter Four.

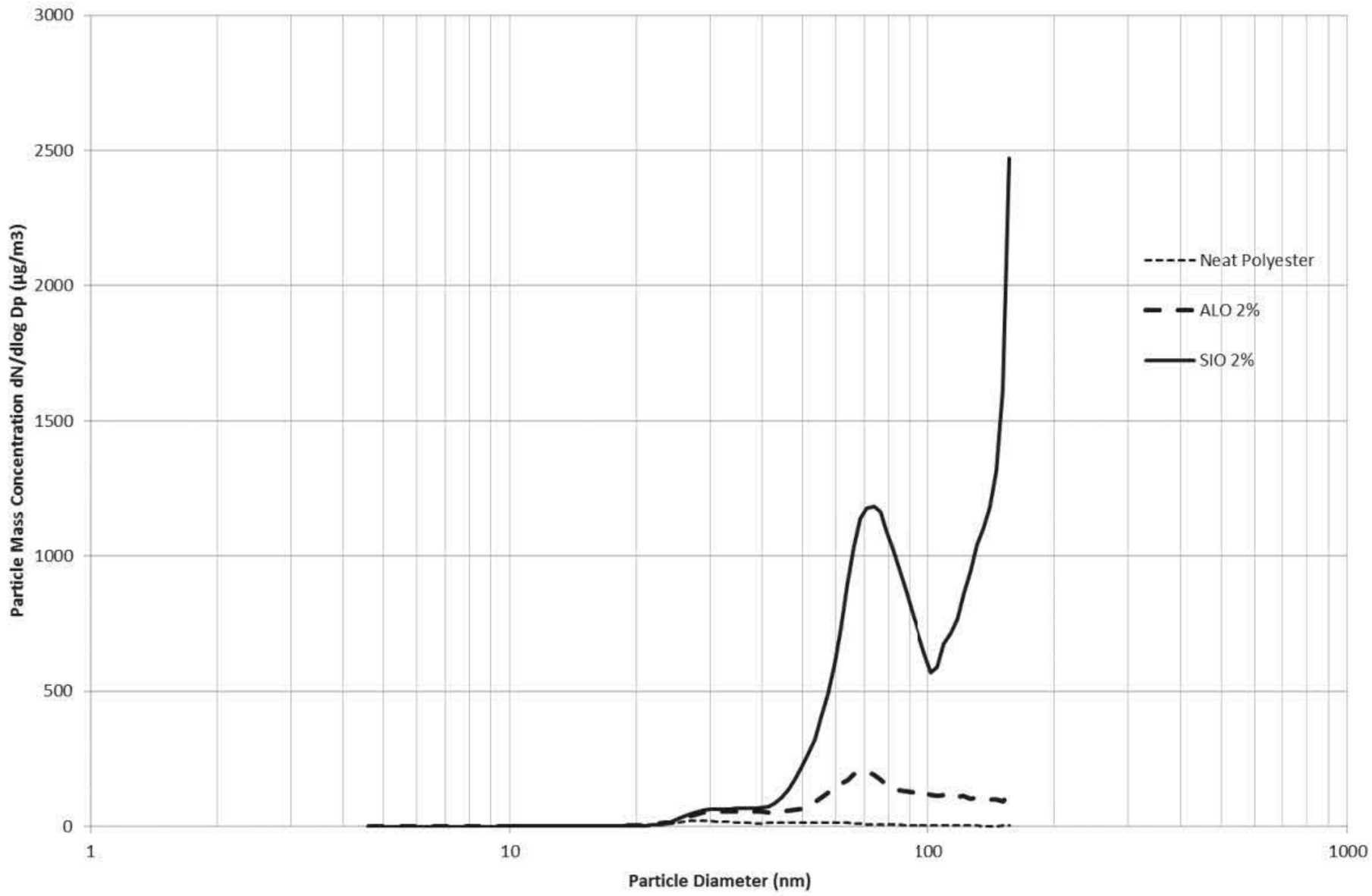

Figure 86*:* Particle mass distribution calculated from SMPS data for the PE based samples (n= 12 for each average).

The substantial increase in particle mass concentration released from the PE/SiO_2 sample can be highlighted if the total mass concentrations are compared for the measured size range of the SMPS of 4.61 nm to 156.8 nm. The total particle mass concentration represented in Figure 86 for the PE/SiO_2 sample is 30980 µg/m^3 signifying a 5439 % increase from the neat PE sample (total mass concentration PE = 559 µg/m^3 and PE/Al_2O_3 = 5286 µg/m^3).

Since the CPC can measure a larger particle size range, an alternative mass concentration is valuable to quantify the release. Using the particle number concentration measurement at the end of the four-minute sampling period, and the calculated total quantity of mass drilled, an estimation of the concentration of particles/mass drilled can be acquired and is presented in Figure 87**.** This is calculated using the particle number concentration of the CPC (size range: 7 nm to 3000 nm), material density values and equivalent of mass drilled based on hole size and number of holes.

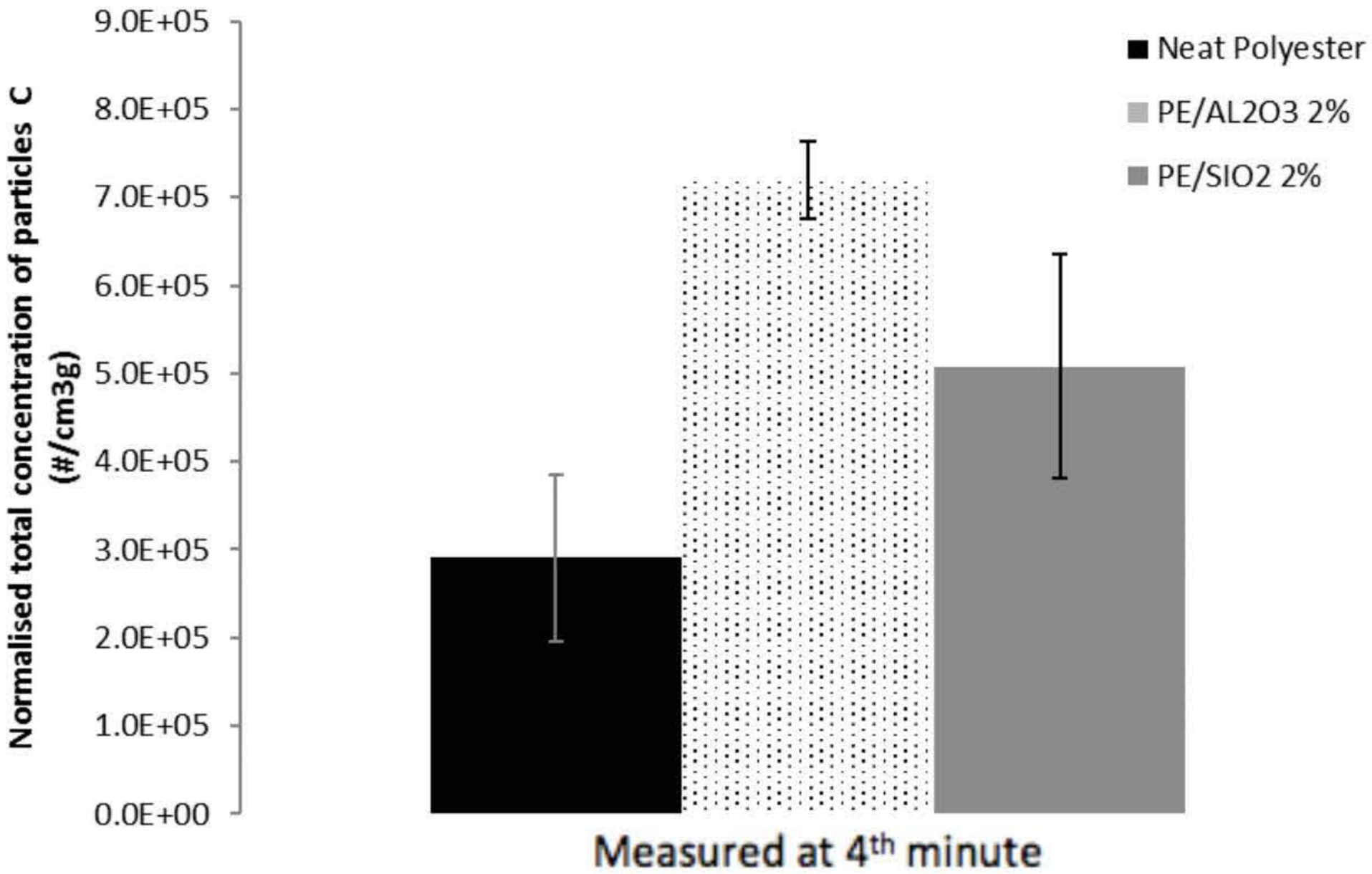

Figure 87*:* Normalised total concentration of particles (C divided by estimated drilled mass) recorded at 4th min for Polyester samples (n= 3 for each average).

The number of particles to mass drilled ratio also presents the PE/AL_2O_3 sample with the highest particle release over the neat PE and PE/SiO_2 samples. Although the PE/SiO_2 sample has a large standard deviation which crosses the standard deviation of the neat PE sample, the PE/SiO_2 sample observed a higher average of normalised particles released. Since the samples have similar material densities, the normalised data is similar to the particle number concentration presented in Figure 77. The PE sample released the lowest normalised data (PE = 290640 #/$cm^3g_{drilled}$, PE/AL_2O_3 2 wt. % = 720000 #/$cm^3g_{drilled}$, and PE/SiO_2 2 wt. % = 507547 #/$cm^3g_{drilled}$).

The particle mass concentration is a vital parameter required when evaluating the nanoparticle release. The data identifies important differences from the findings in the effect of the filler in particle number concentration and particle size distributions.

5.3.4 Assessment of Deposited Particles

The airborne particles during the drilling process of PE/ Al_2O_3 nanocomposites were collected using the Aerosol Nano Sampler and further studied using SEM. Figure 88 represents the SEM images of the characterised debris captured by the Aerosol Nano Sampler that indicate the agglomerations and clusters of nanoparticles formed on the spirals produced by the drill bit during the drilling process.

However, the Aerosol Nano Sampler proved to be insufficient in collecting enough quantity of in situ drilling cutting debris and we were unable to conduct further studies on the airborne debris at this stage. This may be attributed to the fact that the Nano Aerosol Sampler was connected to the same chamber outlet as the CPC, SMPS and DMS50 and the majority of nanoparticles released were drawn to the equipment instead of the Nano Aerosol Sampler. Future studies should focus on this area, particularly in developing a better methodology for capturing airborne particles and more so to establish if independent Al_2O_3 particles can be captured from the release of PE/ Al_2O_3 nanocomposites during the drilling process.

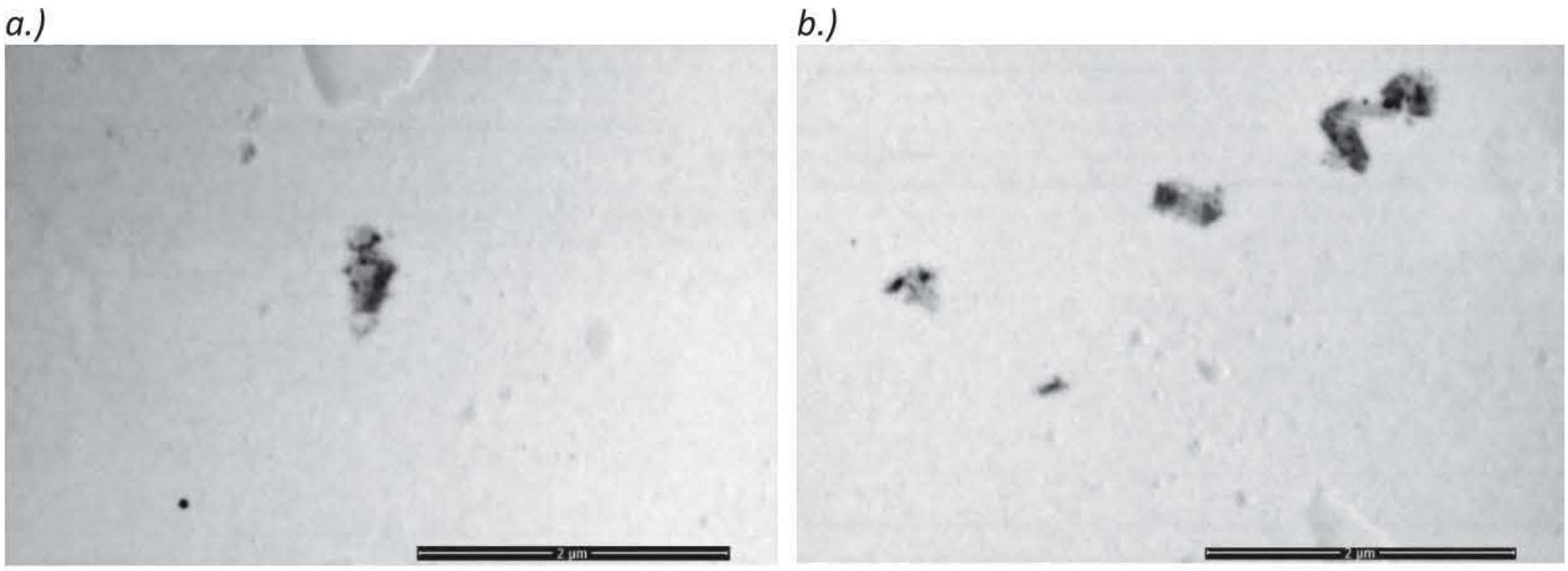

Figure 88*:* SEM image of nanoparticles collected on the Nano Aerosol Sampler from a.) PE/Al_2O_3 2 wt. % sample, and b.) cluster of nanoparticles released from PE/Al_2O_3 5 wt.% sample.

The debris and particles deposited on the sampling tray were studied using SEM and XRD techniques. The SEM image of the particles collected from the PE/Al_2O_3 5 wt.% nanocomposites and PE/SiO_2 5 wt.% nanocomposites is displayed in Figure 89. The rough surface morphology and layered architecture on the debris created by the drilling pressure is illustrated, as it cut through the PE/ Al_2O_3 nanocomposite. However, the stacks on the cuttings created remained intact displaying a strong interfacial bonding and elastic strength despite the drilling conditions such as high rotational pressure of the drill bit, temperature changes and shear stress. As shown, no loose debris or particles were observed during microscopy studies. A clear distinction between the surface morphology can be observed in that significant number of nanoscale sized particles appears on the surface of the drilling fragments collected from PE/Al_2O_3 5 wt.% nanocomposites, whereas large layered fragments

dominate the PE/SiO_2 5 wt. % nanocomposites. In both cases, however, there are a significant number of nano-sized particles that can be observed as result of the drilling progress.

a.)

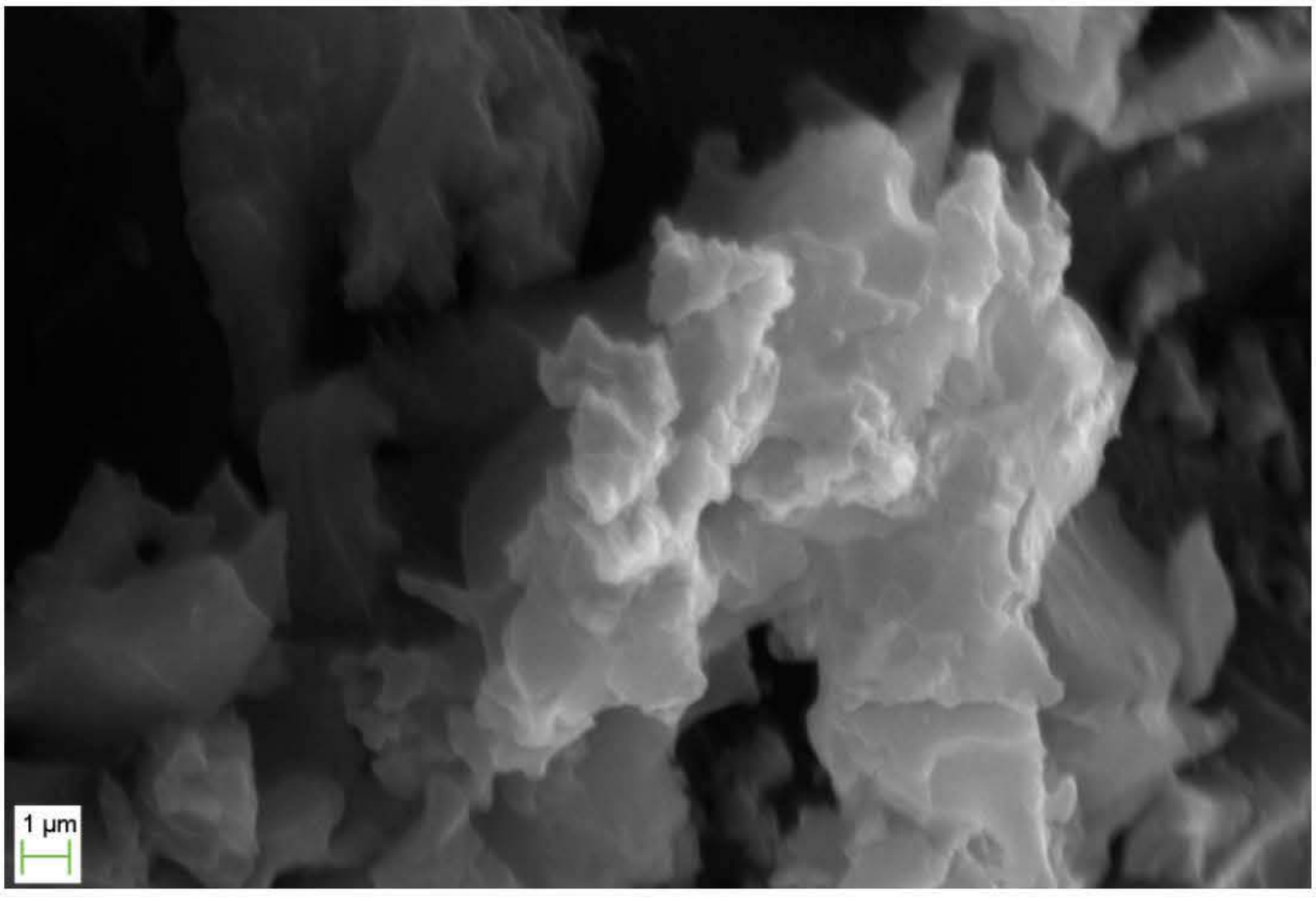

b.)

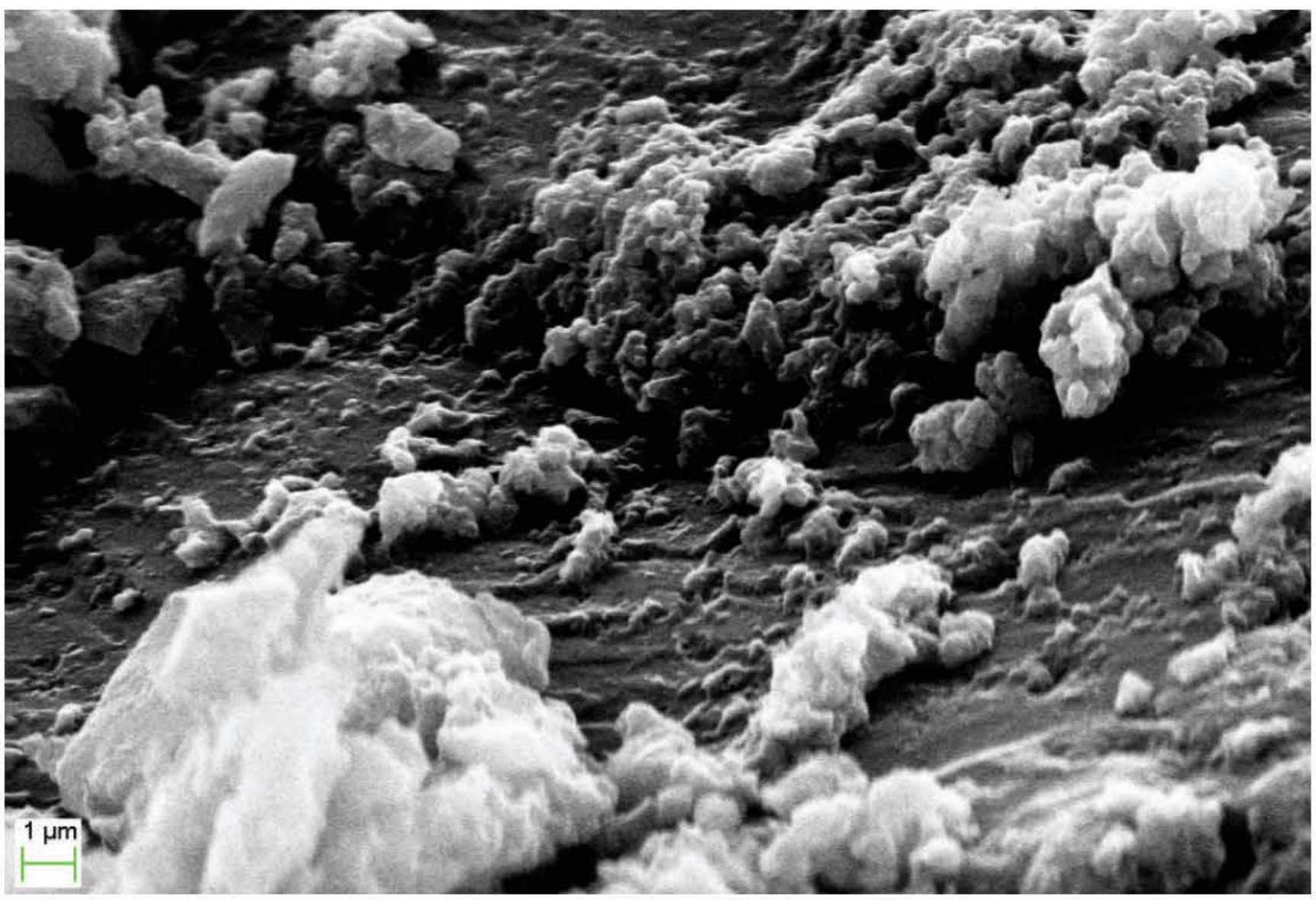

Figure 89*:* SEM image of material collected on sampling tray from a.) PE/Al_2O_3 5 wt.% and b.) PE/SiO_2 5 wt. % nanocomposites.

PE/SiO_2 nanocomposites shows a different surface morphology following the drilling operation as shown in Figure 89. It appears that the significant number of micro-scale structures were formed and deposited with nanoscale particles lying loose on the microstructural debris deposited. It can be concluded that during the drilling operation, the drill bit not only cuts off the materials but also fractures the drilled surfaces instead of the peeling and high elasticity strength evidenced in the PE/ Al_2O_3 nanocomposites. This can be associated with increase in stiffness as a result of SiO_2 in PE nanocomposites as expected. Furthermore, although a smoother surface texture on the material was observed, spherical or close to spherical nanoparticles can be observed in Figure 89 either as loose particles or as clusters from debris deposited from PE/SiO_2 nanocomposites drilling operation indicating a evidence of SiO_2 nanoparticles on the surface structure.

Table 20*:* XRF analysis illustrating elements found in PE, PE/ Al_2O_3 2 wt. % and PE / SiO_2 2 wt. %.

	NA	Mg	Al	Si	P	S	Ti	V	Cr	Mn	Fe	As	Se	Mo	Cd
PE	<1.2	<0.7	<0.7	<0.5	<0.15	<0.8	<0.1	<0.1	<0.1	<0.1	<0.6	<0.1	<0.15	<0.3	<0.5
PE/ Al_2O_3	<1.2	<0.7	<0.7	<0.5	<0.15	<0.8	<0.1	<0.1	<0.1	<0.1	0.77	<0.1	<0.15	<0.3	<0.5
PE / SiO_2	<1.2	<0.7	<0.7	2.94	<0.15	<0.8	<0.1	<0.1	<0.1	<0.1	<0.6	<0.1	<0.15	<0.3	<0.5

Table 20 shows the chemical composition of the samples recorded from XRF analysis. It is important to note that the filters used to analyse the collected particles contain K, Ca, Ni, Cu, Zn, Y, and Pb (and therefore not reported). As a polymer functionalised by ester groups, the neat polyester samples did not contain any of the XRF elements. The silicon dioxide sample showed a small quantity of silicon demonstrating that the nanofiller was embedded within the collected debris. The aluminium oxide sample did not show signs of aluminium but instead appeared to contain a minor quantity of iron which is suspected to be from the hardener used for the material fabrication as it contains a small quantity of iron.

As with the PP-based samples, FT-IR spectroscopy was performed on the samples in order to evaluate any internal chemical bond change in the material. The FT-IR comparison of the materials before and after the drilling (termed dust as this was carried by collaboration partners at Cranfield University) are presented in Figure 90 for the neat Polyester, and PE/SiO_2 2 wt. % and PE/Al_2O_3 2 wt. % samples.

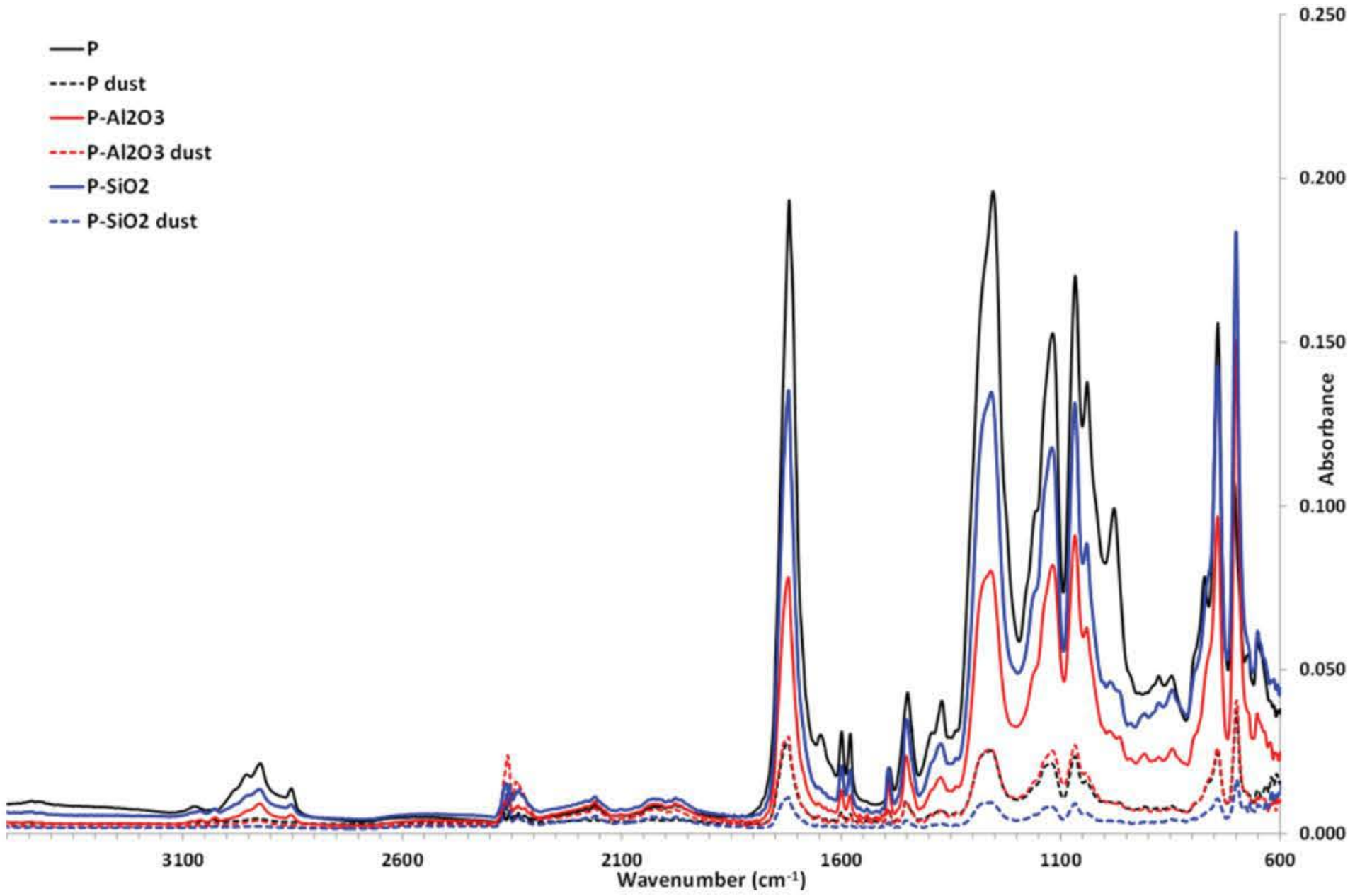

Figure 90: FT-IR analysis of pre-drilled polyester samples compared to dust particles collected after drilling.

From the spectrums shown in Figure 90, the samples can be observed to show no internal chemical change due to the drilling. The peaks comparison before and after drilling, show no shift for all the samples. Due to the capabilities and limitations of the instrument, the FT-IR spectrum is unable to identify independent nanofillers due to the minimal required material. The analysis is only capable of giving a representation of the internal chemical bond change of a larger matrix-embedded particle. The data is also a representation of the deposited particles collected within the chamber, and not the measured airborne particles through the particle quantification instruments.

5.4. Conclusion

Three polyester based nanocomposites were fabricated with two different nanofillers. All samples tested, including the neat polyester, revealed that nanoparticles were generated and released from the sample during the drilling process. Across the entire 4 minutes of simultaneous drilling and particles measurement, the reinforced aluminium oxide and the silicon dioxide samples produced an increase of 136 % and 228 % respectively in particle number concentration compared to the neat polyester.

The different concentrations of nanofiller displayed inverse results with the alumina releasing an increase in nanoparticles with the 5 wt. % reinforced sample, whereas the silica revealed a decreasing effect in nanoparticles released. This data leads to the potential of tailoring the material for a reduction of nanoparticle release and as a concept of safety by design. Since the materials with different filler concentration demonstrated similar properties, the data establishes the possibility of development towards linking the particle release to reducing the possible particle exposure yet keeping the material properties for functionality. Through this concept, materials can be manufactured to using safety by design concepts by reducing the nanoparticle release from the material. Through the understanding of the filler-matrix interfacial bonding, the release characteristics can minimise the release of potentially toxic nanoparticles and subsequently reducing exposure to the potentially toxic nanofillers.

The particle emissions for the materials studied demonstrated that the nano-filled polyester nanocomposites produced a substantial escalation in particle number concentration and therefore have a detrimental effect on nanoparticle release during drilling. This is most sizeable when the mass concentration of the particles released was considered, with the silica causing a 5439% increase in total particle mass concentration compared to the PE sample.

The significant difference between the three materials and filler concentrations provide significant data that should be considered for exposure purposes when undergoing a similar scenario of drilling. The DMS50 presented explicit results that indicated that the neat polyester emitted a smaller range of particles (>20nm) compared to the two nanofilled PE nanocomposites. As the smaller particle diameter peak is not seen in the release in the two nano-filled samples, there is no evidence that the nanofillers are released from the matrix and it is apparent that the nanofillers are adhering to and embedded within the polyester matrix. The correlation between increase in nanoparticle reinforcement weight percentage and nanoparticle release can be seen between the PE/SiO_2 and PE/Al_2O_3 nanocomposite samples. The two nanofillers displayed almost an inverse correlation with the higher weight percentage of nanofiller. The SEM, XRD and XRF analysis supports the real-time findings as there was no evidence of the nanofillers independent of the polyester matrix.

Chapter Six

Assessment of Nanoparticles Release into the Environment during Drilling of Carbon Nanotubes/ Epoxy and Carbon Nanofibres/ Epoxy Nanocomposites

6.1 Introduction

The aim of this study is to investigate the influence of CNTs and CNFs on nanoparticle release from embedding within EP industrial nanocomposites during drilling. A report on the CNT global market forecasts a compound annual growth rate of 20.6 % during the period 2016-2022 with an expected value of $ 3.8 billion by 2022 (Allied Market Research, 2016). A similar report from a different publisher, estimates the global EP resin market to be $ 10.6 billion by 2023 with a slower compound annual growth rate of 5.24 % during 2017-2023 (Cooked Research Reports, 2017). As covered in the literature review, EP can be reinforced or modified with several nanofillers, such as CNFs (Ahmadi et al., 2015; Shokrieh et al., 2014), CNTs (Yue et al., 2014; Gardea et al., 2014), GO (Zhang et al., 2017; Abdullah & Ansari, 2015), graphene (Chandrasekaran et al., 2014; Ahmadi-Moghadam et al., 2015) as a selective few. CNTs and CNFs are two nanofillers currently already established and growing within various industries, including the aeronautical and automotive industries. This chapter will include the incorporation of CNTs and CNFs within EP.

Despite the beneficial material properties of CNTs and CNFs, the nanofillers have shown conceivable health risks and toxicity to humans and the environment. Studies have validated that certain concentrations of CNT exposure has shown to induce cytotoxicity and apoptosis (*Wang et al., 2011; Bottini et al., 2006*), genotoxicity (*Patlolla et al., 2010; Guo et al., 2011*), systemic immune function alterations (*Mitchell et al., 2007*) and pulmonary damage, inflammation and granuloma lesions (*Chou*

et al., 2008; Porter et al., 2010; Poland et al., 2008). Reviews of literature on the release and/or exposure of nanoparticles from ENMs have also concluded that high-energy processes, including drilling, have shown evidence of likelihood of nanoparticle release (Basinas et al., 2018; Debia et al., 2016; Froggett et al., 2014). As detailed within the Literature Review section 2.5.2, there is still an insufficient understanding on how these fillers effect the release of nanoparticles from nanocomposite materials and the full risks associated to the emissions and nanoparticle exposure into the environment (Gendre et al., 2016; Njuguna et al., 2014). This chapter will therefore evaluate the influence of CNTs and CNFs on nanoparticle release from EP-based composites when under a simulated and controlled life cycle scenario: automated drilling process.

6.2 Experiment

The EP-based samples were selected and manufactured as discussed in Chapter Three. Two composite fillers, CNFs and CNTs, were used to reinforce the material and will be compared to the neat EP. Whilst different weight concentrations were evaluated for mechanical properties, the most common in literature and industry, 2 wt. % of the nanofillers were chosen to investigate the effect of the fillers on nanoparticle release during drilling. The materials morphology, structure and composition are demonstrated in section 3.3.1 and 3.3.2.

To evaluate the samples manufactured, the materials were characterised through SEM, EDX and FT-IR. The characterisation equipment used within this study is detailed in section 4.2.2.

The materials were firstly investigated for mechanical properties. The effect of the nanofiller on the material mechanical performance are shown to demonstrate the original benefits and use to strengthen the materials. The materials underwent a flexural 3-point bend test in accordance with ASTM D 7264/M flexural test (ASTM D7264M, 2015) and a standard ASTM D 3039/D tensile test (ASTM D3039, 2017). These results are included in section 3.3.3.

The samples underwent the exact same drilling procedure described in section 4.2.3 with further details of the methodology also available in Appendix A. A standard Dremel 4000 drilling tool with an industrial standard stainless steel 3.5mm twist drill bit was used at 10000 rpm with a feed rate of 78 mm/min.

Once the chamber was cleared of any particles, the drilling studies were carried out by drilling across the width of the sample resulting in eight separate holes and bearing a time duration of 3 minutes of drilling, followed by 1 minute post-drilling. The eight holes drilled per sample were repeated three times to get an average of the particle number concentration and particle size distribution released.

The nanoparticle release is quantified through a CPC, SMPS, DMS50, A standard IOM Inhalable Sampler, XRF, SEM and EDX. More information on the equipment used within this study is detailed in section 4.2.2.

6.3 Results & Discussion

6.3.1 Filler Effect on Particle Number Concentration

The EP based nanocomposite samples underwent the replicated drilling setup. In comparison to the neat EP sample, the introduction of CNTs and CNFs significantly influence the nanoparticle release from the drilling process.

A graphical representation of the CPC particle number concentration averages from the repeated runs on the samples is displayed in Figure 91. Equivalent to the PP and PE based samples, across the duration of 4 minutes, 8 peaks exemplify the 8 holes drilled before the 1 minute of post drilling. For each individual hole, the peak concentration introduced into the chamber is observed to be split into two, revealing the drill entering and withdrawing the sample. Importantly, all three of the samples can be seen to introduce a high concentration of nanoparticles into the chamber, including the neat epoxy sample. Upon completion of the drilling of 8 holes, the concentration relatively stabilize for the final 1 minute of data sampling. Similarly, the concentration remains relatively linear between each hole being drilled. The mechanical drilling therefore generate a substantial quantity of nanoparticles into the environment, which then quickly disperse, but remain airborne.

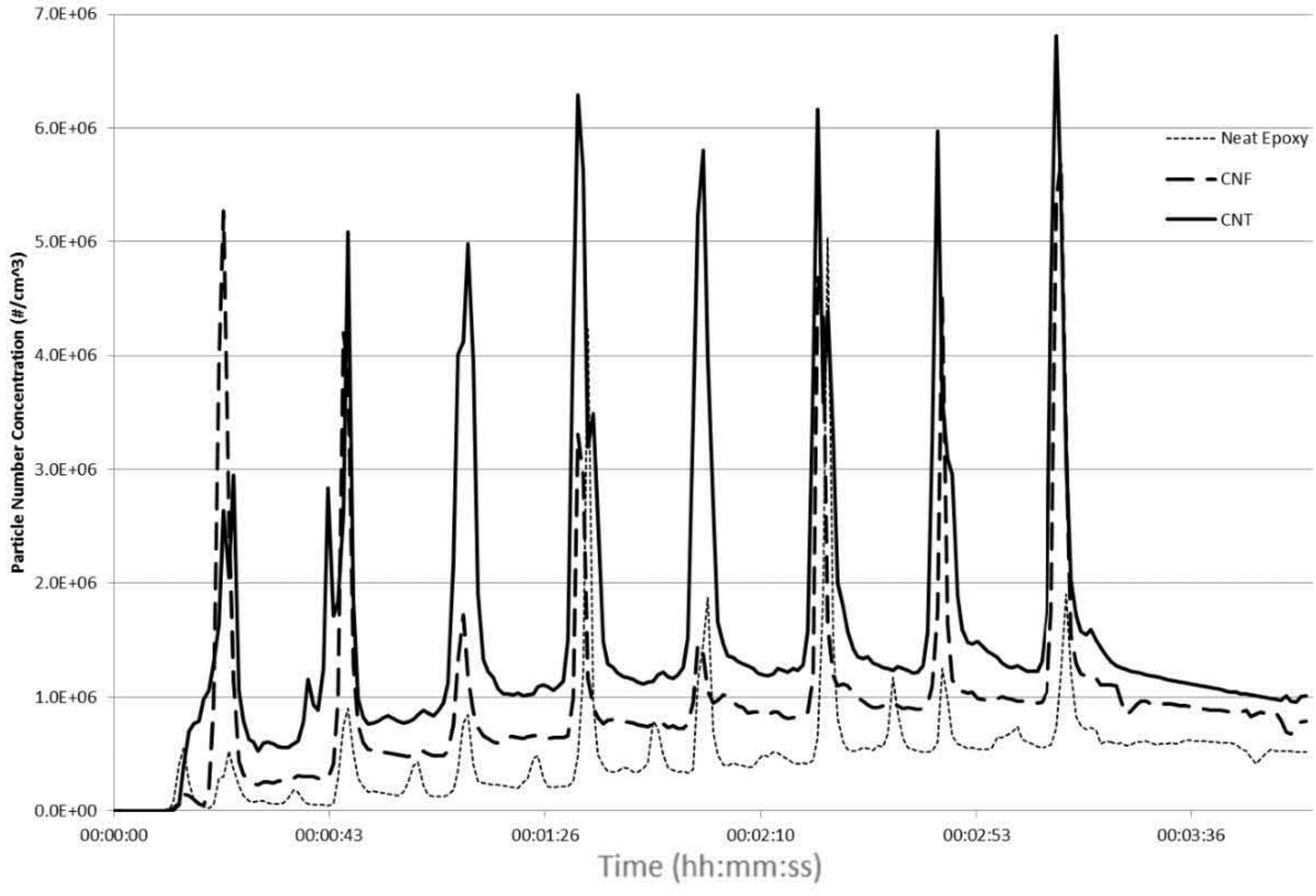

Figure 91*:* Particle number concentration averages of nanoparticles introduced from epoxy-based samples measured using CPC (n=3 for each average).

The substantial particle number concentration from the EP-based samples surpassed the CPC concentration limit of 1 x10^7 #cm^{-3} on numerous instances. During the first drilling run of the neat EP, the emissions exceeded this limit on two occasions. The EP/CNF and EP/CNT samples both surpassed the limit on three occasions. The averages plot in Figure 91 illustrate the two nano-reinforced samples to evidently produce a more consistently high peak towards the limit of the CPC compared to the neat EP sample. The averages of the three samples clearly illustrate the augmenting effect of the carbon nano-fillers on the particle number concentration. The neat EP sample exhibited a concentration lower than the reinforced samples for virtually the entire four minutes. The EP/CNF sample produced noticeably higher concentration in relation to the neat epoxy, but lower than the EP/CNT sample. Whilst producing the highest concentration and peaks during the drilling, the CNT sample furthermore demonstrated the highest concentration at the end of the four minute examining period. The high number concentration introduced during the drilling indicates to disperse within the chamber but crucially remain airborne. The EP/CNT sample presented a particle number concentration remaining above 1x 10^6 #/cm^3 even after the drilling and 1 minute post drilling was concluded. Additionally, as holes were drilled on the EP/CNT, the relatively stable concentration between holes increased for the

three repeated samples. This advocates the induction and augmenting effect drilling has on nanoparticles from the samples.

Table 21*:* Inferential statistical representation of the particle number concentrations introduced at the peaks due to the drilling on epoxy-based samples (n = 24 for each sample). Lower and upper limits represent the 90% confidence interval on a sampling t-distribution (Note: CPC limit of 9.99 × 10^6 #/cm^3 and the mean peaks therefore represent a lower bound value that include the saturated peaks).

Sample	Mean: $\bar{\bar{X}}$ [#/cm^3]	Deviation: $S_{\bar{X}}$ [#/cm^3]	Minimum [#/cm^3]	Maximum [#/cm^3]	5% Lower limit of confidence interval [#/cm^3]	95% upper limit of confidence interval [#/cm^3]
EP	>4.06 x 10^6	>3.87 x 10^6	0.81 x 10^6	>9.99 x 10^6	2.12 x 10^6	5.99 x 10^6
EP/CNT	>8.56 x 10^6	>3.44 x 10^6	6.61x 10^6	>9.99x 10^6	7.98 x 10^6	9.15 x 10^6
EP/CNF	>7.59 x 10^6	>1.17 x 10^6	1.62 x 10^6	>9.99 x 10^6	5.87 x 10^6	9.31 x 10^6

Table 21 displays the statistical analysis carried out on the peak particle number concentrations of the samples. As with the PE-based samples, the mean peak values are influenced and confined by the saturated CPC measurement capability (i.e. 1 × 10^7#/cm^3) and are therefore only a lower bound representation. The calculated lower tail of 5% and upper tail of 95% give a representation of the data for a 90% confidence interval of a t-distribution. This highlights the disparities between the peak particle number concentrations and therefore, a statistically significant difference with the introduction of nanofillers on release in comparison to the neat epoxy. A two sample t-test of significance of each sample mean and deviation to the neat epoxy sample returned statistically significant differences for all samples (outside the 95% confidence interval). ANOVA single factor analysis was performed to assess the variability between the sample peak means introduced due to the fillers. The analysis returned statistically significant differences within the 3 samples (F value = 4.80 F critical value = 3.47) and a 1.92% chance that the observation could have been observed due to random error alone and therefore rejecting a hypothesis that the samples displayed no difference.

Since all three samples exceeded the maximum of the CPC of 1x 10^7 #/cm^3, the samples produced the same peak particle number concentration in the numerical data representation in Table 21. The mean

peak values are influenced and confined by the saturated CPC measurements (twice for EP and three times for the EP/CNT and EP/CNF samples) and are therefore only a lower bound representation. The high standard deviation and range demonstrate a level of randomness and uncertainty in the peak releases. Taking the saturated values into consideration, the EP/CNT and EP/CNF samples demonstrated a clear increase in particle number concentration during drilling peaks, between drilling and across the entire 4 minutes of sampling. From the numerical values, the EP/CNT reinforced sample exhibited the uppermost mean value over the 4 min of 1.48 x 10^6 #/cm^3 introduced into the chamber due to drilling. Furthermore, also demonstrated in Figure 92, the EP/CNT sample demonstrated the largest concentration after 4 minutes of sampling (1.01 x 10^6 #/cm^3). In relation to the neat epoxy, the EP/CNF and EP/CNT produced an increase of nanoparticles of 102 % and 227 % in average over the 4 minutes when excluding the saturated values. Therefore, the carbon nanofillers studied can be seen to increase the emitted particle number concentration recorded.

A graphical comparison of the average particle concentration measured at the end of the four-minute sampling period is presented in Figure 92.

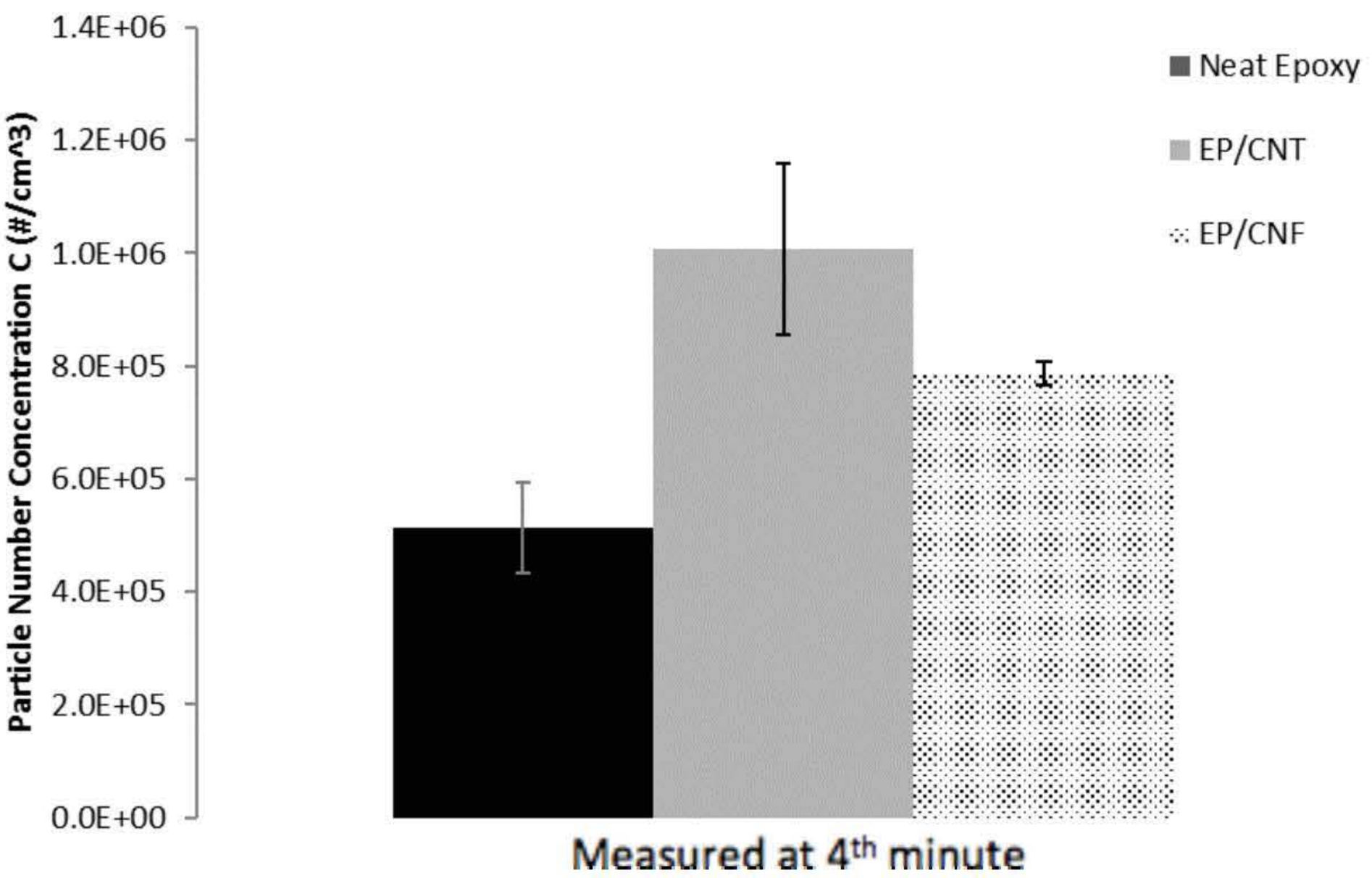

Figure 92*:* Total concentration of particles recorded at 4th min (C, particles/cm^3) for epoxy based samples as measured on the CPC (n=3 for each average).

The total particle number concentration measured at the end of the sampling period is beneficial to evaluate the effect of the filler on the rapidity of depositing and dispersion within the chamber. The

difference in particle concentration at the time of release due to the holes and concentration at the end of the sampling period presents an indication into these properties. The EP/CNT sample observed a 96 % increase measured at the 4th min from the neat EP sample in comparison to the 211 % increase over the previous four minutes (EP/CNF displayed a 53 % increase from the neat EP measured at the 4th minute). This suggests both the EP/CNT and EP/CNF samples display a quicker dispersion/depositing properties in relation to the neat EP sample, even though the neat EP sample has a higher material density.

6.3.2 Filler Effect on Particle Size Distribution

With a sampling period of 1 minute, an average of the 4 data sets from the SMPS across the 4 minutes for each sample is displayed in Figure 93. The three samples exhibited two distinct peaks on the SMPS. The smaller peak for the samples occurred at around 10 nm, and a larger particle diameter peak between 20-30 nm. The size distribution data illustrates minimal effect of the carbon nanofillers on the epoxy sample. The reinforced samples displayed an increasing effect on the particle number concentration although little difference in particle size distribution was observed. Nonetheless, two of the peak size distributions are indicated to be around the same particle diameters.

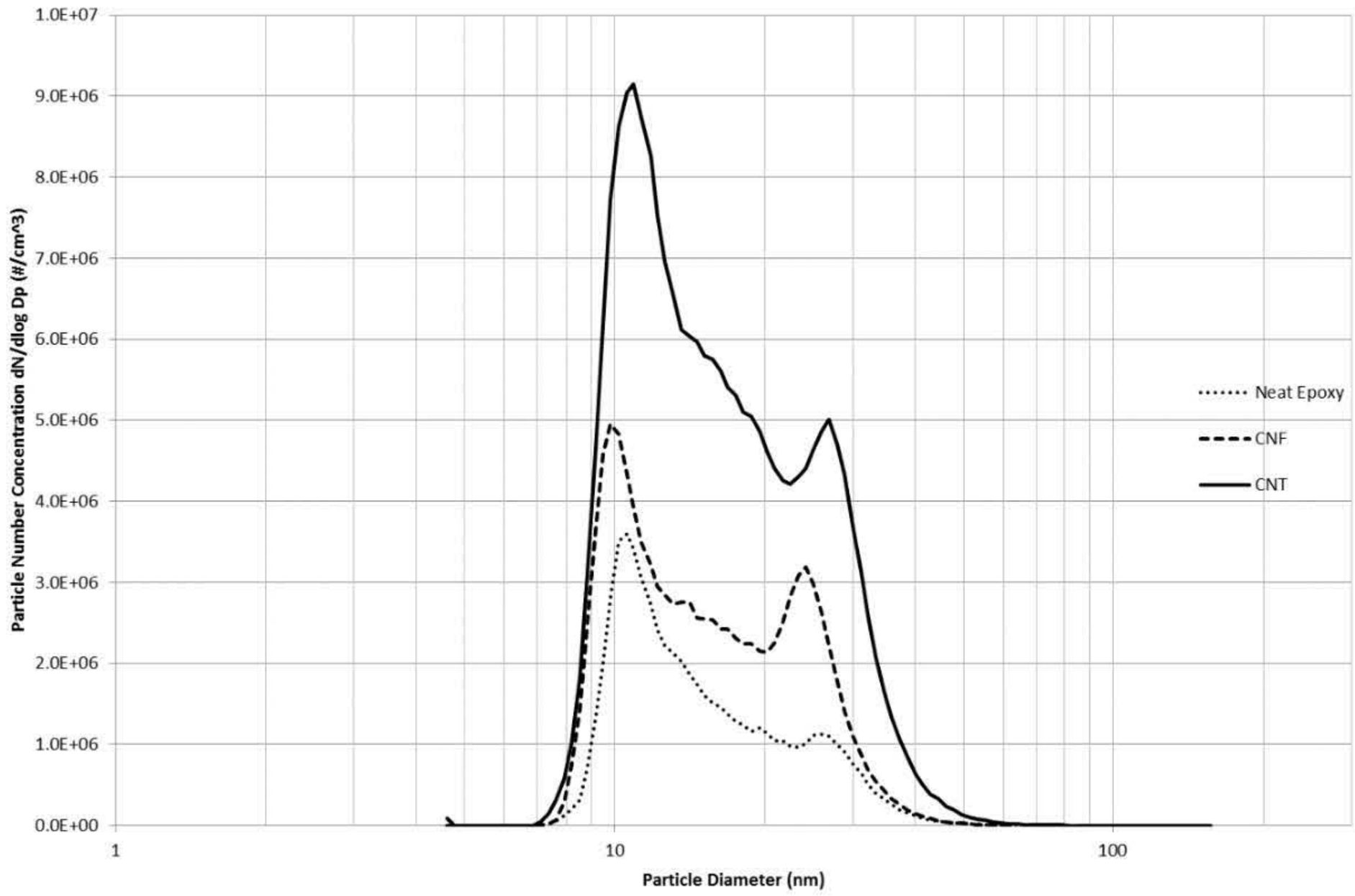

Figure 93*:* Average particle size distribution measured using SMPS of Epoxy-based nanocomposites (n=12 for each average).

Since the increase in particle number concentration is at the same particle diameter indicates that the particles are matrix associated, and not the nanofillers independently. Any independent carbon nanofillers or matrix-filler embedding released from the samples would be expected to demonstrate a different peak in particle diameter from the neat epoxy sample. Evidenced from the SMPS data alone, the addition of the CNTs and CNFs can be established to effect the material particle number concentration, but is assumed not to release the fillers independently from the matrix or sample. Since the CNTs have a diameter of 10 nm to 15 nm, the increased concentration observed at 10 nm in Figure 93 may lead to the suspicion that this could be caused by independent CNT. However, for this assumption to be true, the peak would not be expected for the EP/CNF or EP sample e.g. CNF has 100 nm diameter.

Further to the data collected on the SMPS, separate data was gathered on the DMS50 for the size distribution at each second and is displayed in a 3-D plot as shown for the three samples in Figure 94 and Figure 95 (Note: data is taken from a separate run to the CPC and SMPS data due to the required increased inflow rate).

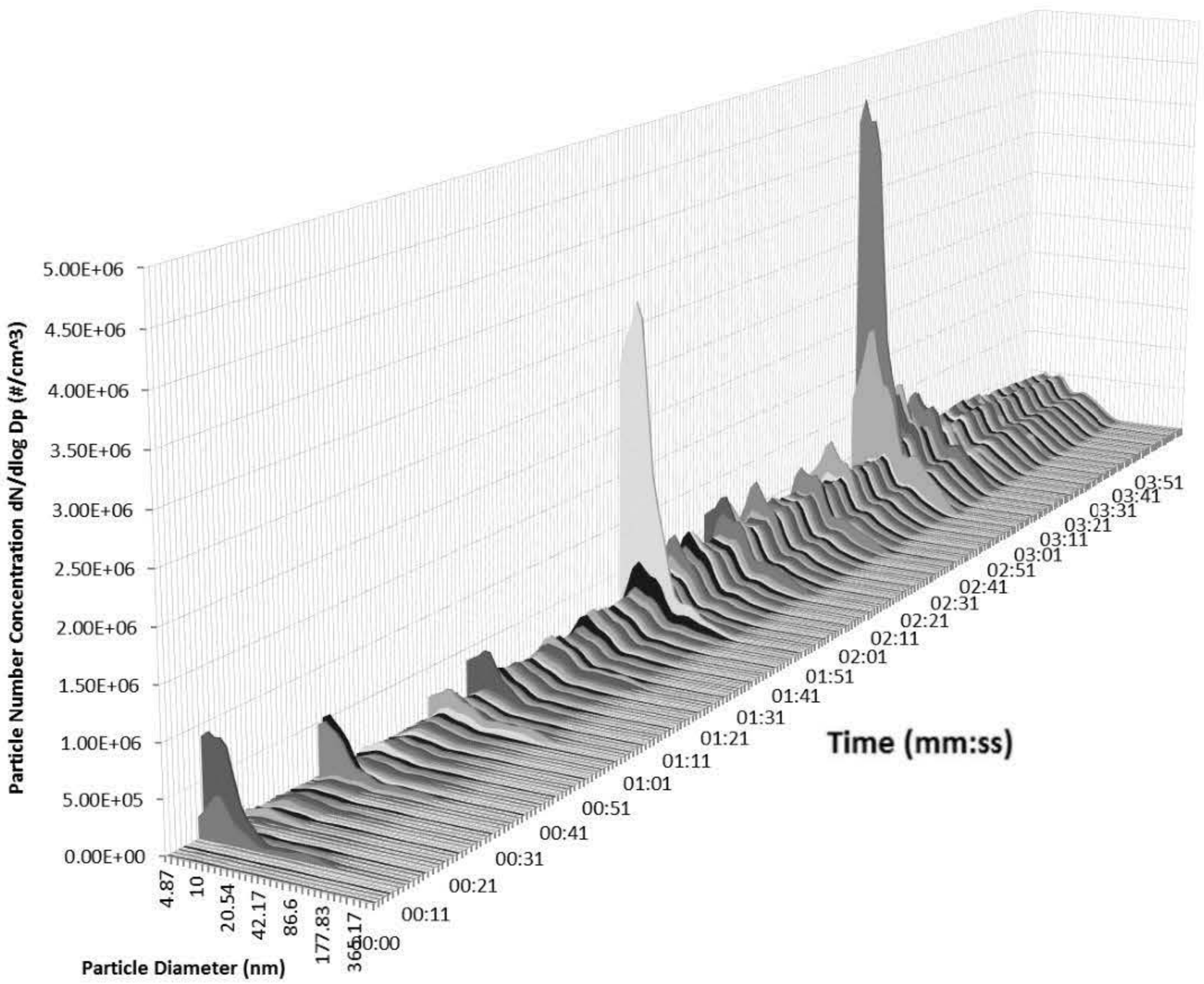

Figure 94: Size distribution recorded on DMS50 during 4 minutes for EP sample.

a.)

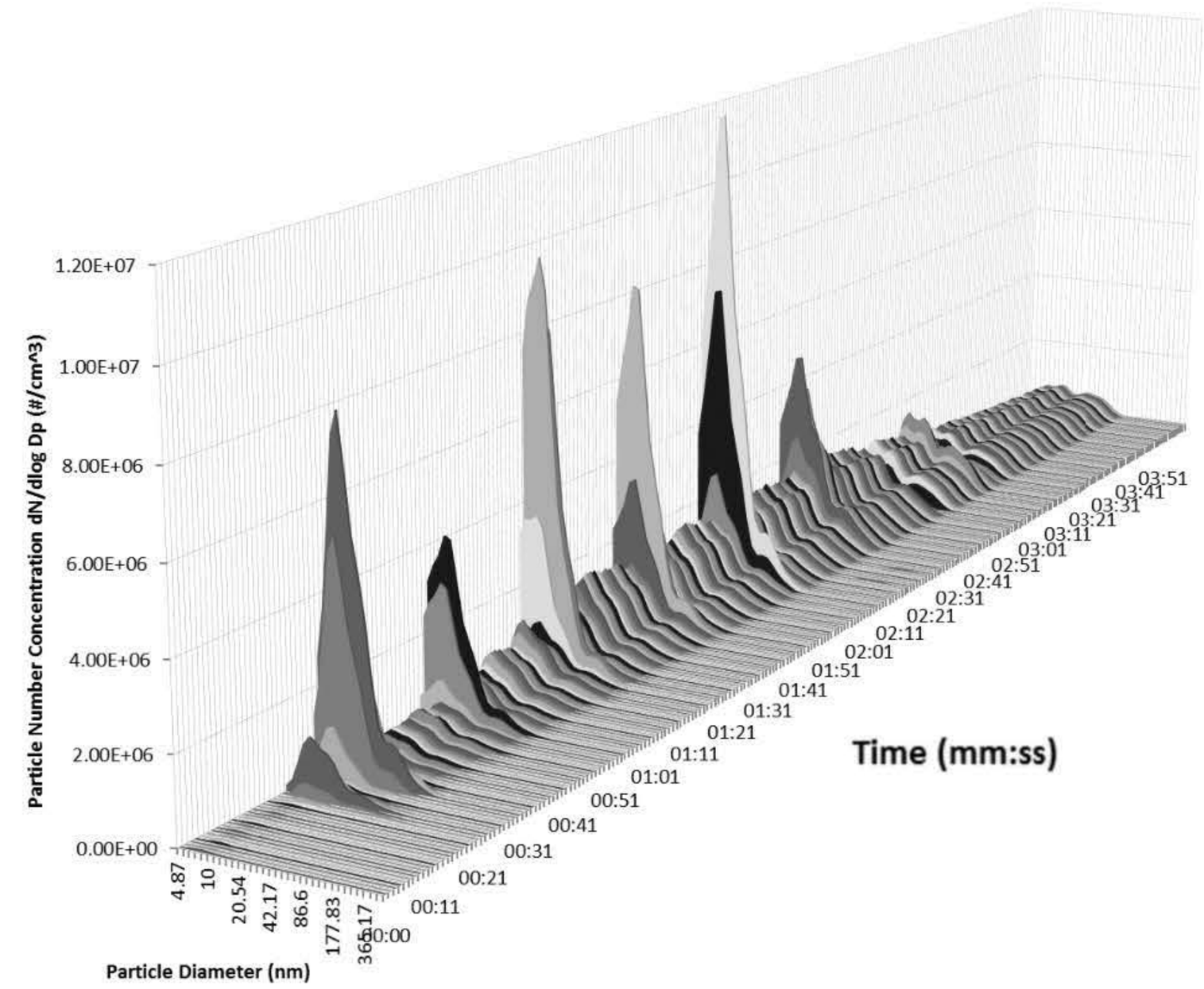

b.)

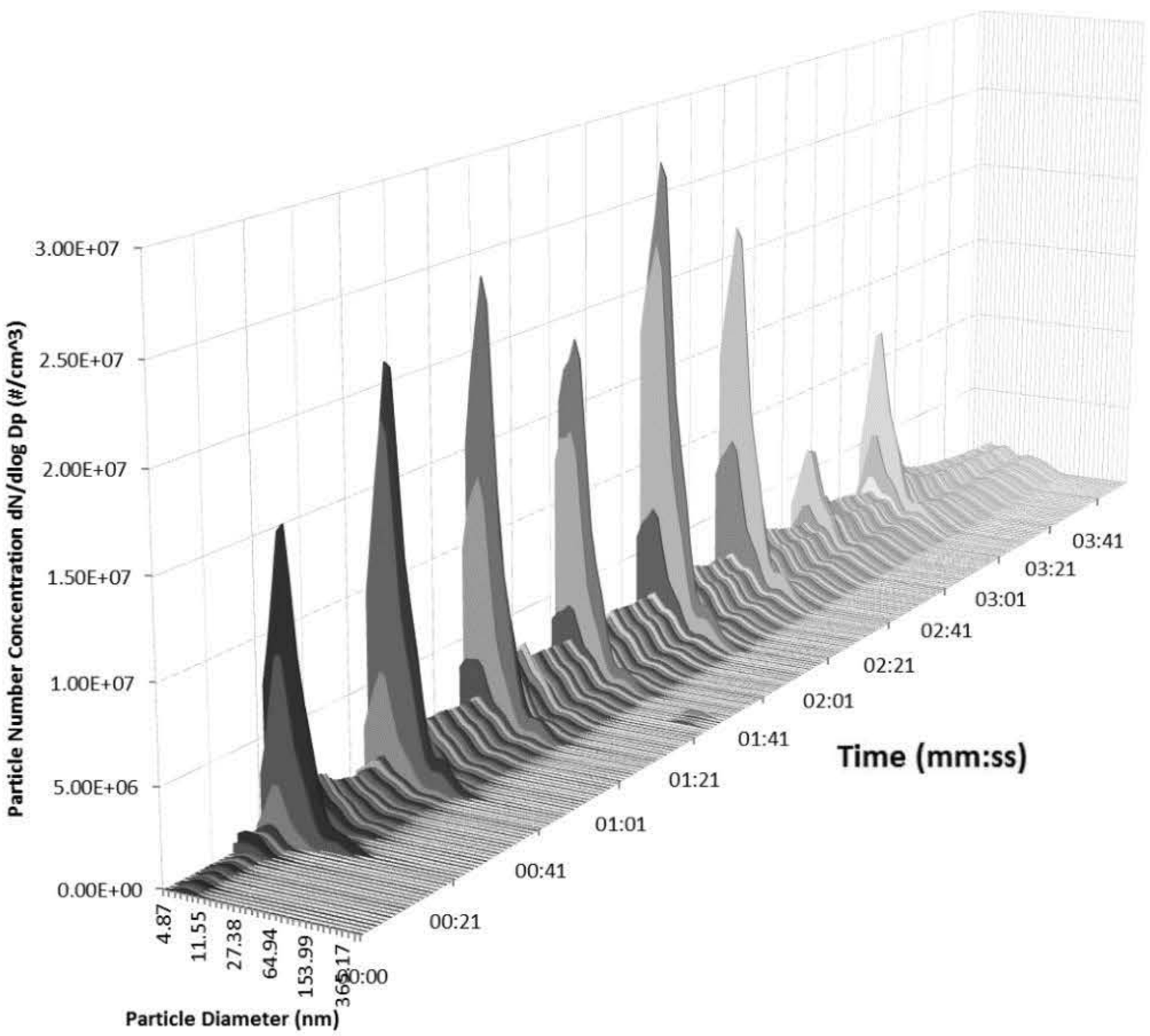

Figure 95*:* Size distribution recorded on DMS50 during 4 minutes for a.) *EP/CNF sample and b*.) EP/CNT sample.

As with the CPC data shown in Figure 91, the eight peak particle number concentrations introduced due to the drilling are visibly notable in the DMS50 data in Figure 94 and Figure 95. Due to the high escalation of particles introduced during the 5th and 8th hole for the neat EP sample, the peaks introduced from the other 7 holes are less perceivable. Similarly, the final two holes drilled in the EP/CNT sample revealed a reduced peak values in comparison with the previously drilled 6 holes on the same sample. The relatively constant concentration between each peak is seen to increase after each hole being drilled up until the 7th hole followed by a minimal decrease in concentration perceived during the 1-minute post-drilling. A less consistent peak particle number concentration was observed for samples as the EP/CNF sample displayed a standard deviation of 3.19 x10^{6} #/cm^{3} and coefficient of variation of 48 %. The EP/CNT sample demonstrated a standard deviation of 6.21 x10^{6} #/cm^{3} and coefficient of variation of 34 %, whereas the CPC data observed a standard deviation of 1.09 x10^{6} #/cm^{3} and coefficient of variation of 13 %. This could be associated to variability of the different size ranges, with the smaller size range of 4.87 nm to 562.34 nm compared to the CPC size range of 7 nm to 3000 nm.

Although the concentration is seen to be inconsistent, the particle size distribution at the peak particle number concentrations during the drilling of each hole are seen to be consistent. Similar to the SMPS data shown in Figure 93, no particles are measured above 40 nm for the duration of the 4-minute sampling time. No change in size distribution from the peaks to the constant concentrations removes the prospect of agglomeration (below 562 nm) of particles within the chamber after the 1 second sampling time. Considering the DMS50 data, if particle agglomeration were to happen it would have to occur instantaneously. The particles are however seen to rapidly disperse within the chamber.

The almost instantaneous particle size distribution permits an analysis on the peak concentrations at the moment of drilling. Figure 95 illustrates a two-dimensional particle size distribution plot of the largest peaks released from the three samples. A similar size distribution at distinctively different number concentrations is observed.

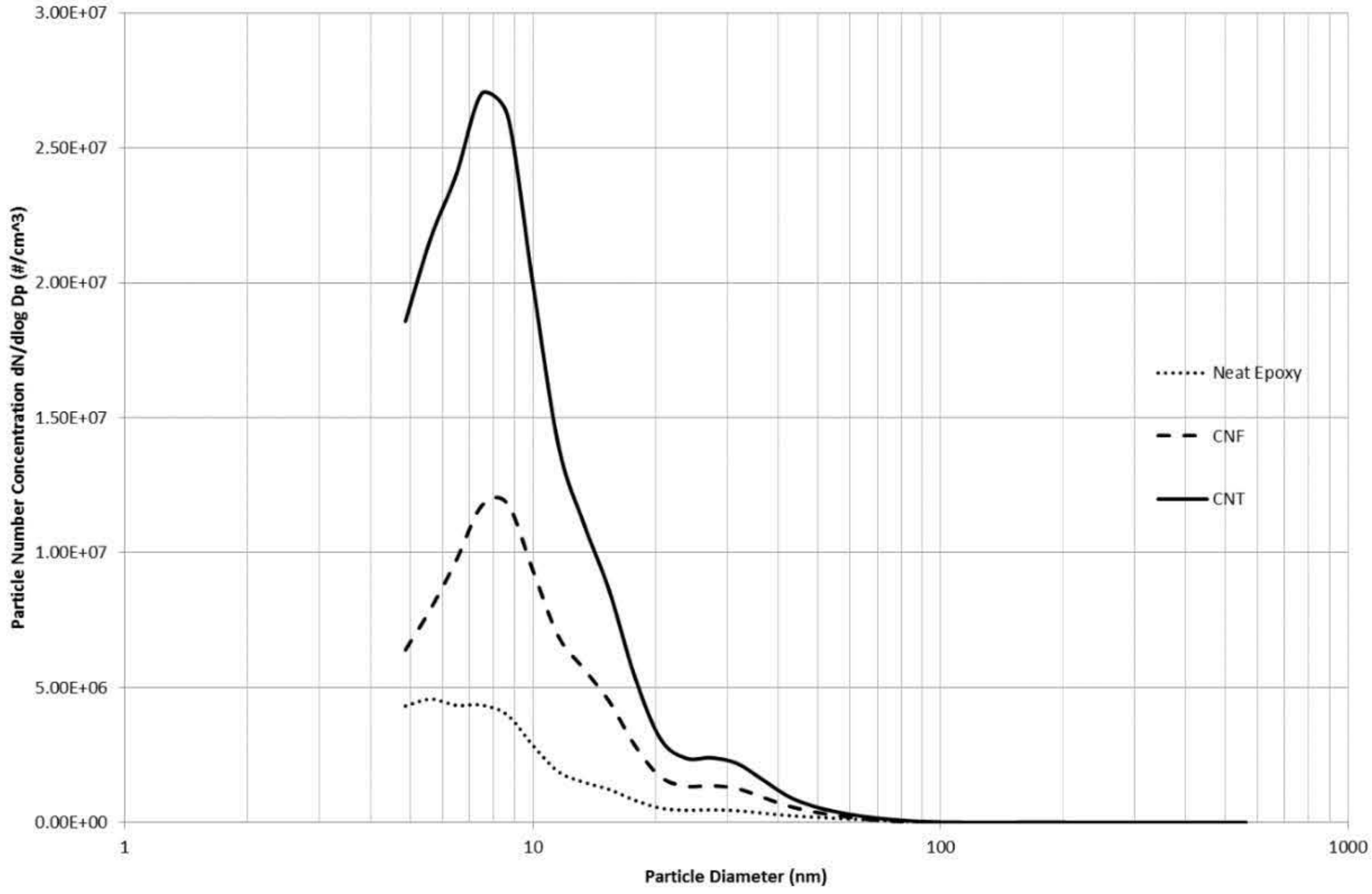

Figure 96*:* Peak particle size distribution within the 4 minutes sampling of the epoxy-based samples recorded on DMS50.

A common peak between 7-9 nm for the three samples can be seen to be released during the drilling. As with the CPC and SMPS data shown in Figure 91 and Figure 93 respectively, the two nano-filled samples released a considerably higher number concentration. All three instruments used to quantify the released particles (CPC, SMPS & DMS50) demonstrate a harmonised increase in particle number concentration with the introduction of the CNTs and CNFs. The EP/CNT produced the highest concentration in all three instruments.

In contrast, the presence of the carbon nano-fillers can be seen to have a limited effect on the particle size distribution. All three of the samples displayed a peak concentration of released particles below 10 nm. But the size distribution of the nano reinforced samples can be seen to be relatively similar to the neat epoxy. In comparison to the SMPS average over the 4minutes, the size distribution on the DMS50 sampled at 1 second is disparate as only one peak is visible. However, both plots indicate that none of the samples emitted any particles above 50 nm. The second peak in particle diameter in the particle size distribution from the SMPS data was not recorded on the DMS50. This disparate peaks seen on the two instruments introduce debateable deductions and effectiveness of instrumentations required for real-time data. Studies in the literature have experienced similar issues as reported and already highlighted by Njuguna and Sachse (2014) who documented the limitations and deficiencies

of current nano-sized aerosol measurement techniques. Although the two instruments both use electrical mobility measurements to classify the particle size distribution, the difference in sampling period could be the source of the varied results in real-time measurements during drilling. In summary, the SMPS data revealed minor differences on the particle size distribution compared to DMS50. Although the evidently greater particle number concentrations, the same particle diameters indicate a matrix association. A similar conclusion can be drawn from the DMS50 data. However, the two instruments displayed similar small diameters in the particle size distributions with a high percentage of the particles within 6 nm to 20 nm, and no significant concentration larger than 70 nm. The fillers therefore had minor effect on the particle size distribution.

6.3.3 Filler Effect on Mass Size Distribution

Since the drilling was conducted within a clean environment, all of the particles measured with on the instrumentation is from the nanocomposite material. With the use of the SMPS and the known density of the individual nanocomposites, the particle mass concentration can therefore be estimated. The data utilises the diameter of the particles measured using the SMPS. The constant material density for the three nanocomposites are: EP= 1.24 g/cm^3, EP/CNT = 1.20 g/cm^3 and EP/CNF= 1.14 g/cm^3.

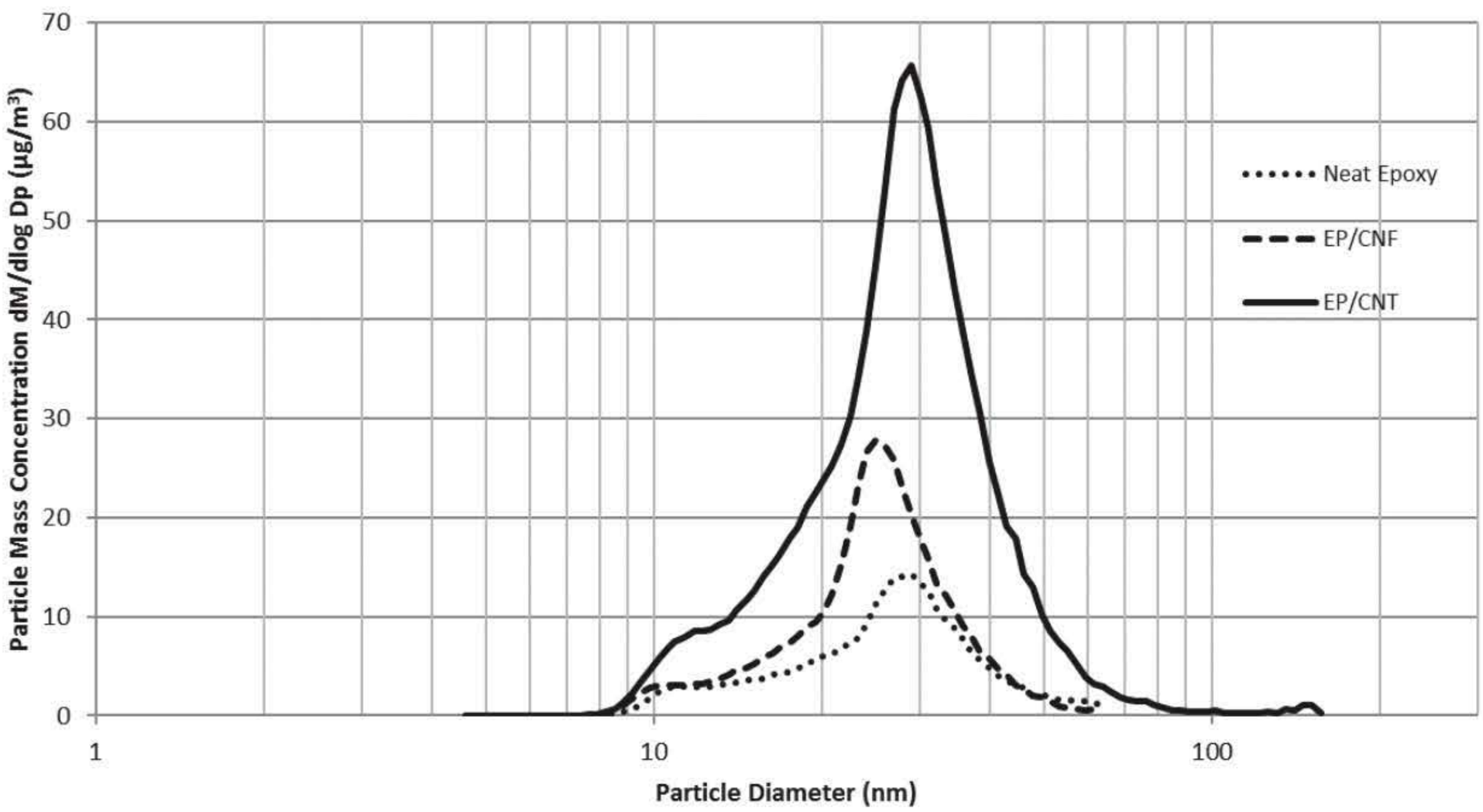

Figure 97*:* Particle mass concentration average over 4 minutes of epoxy based nanocomposites determined from SMPS (n= 12 for each average).

The average mass concentration across the 4-minute sampling period for different particle size diameters is illustrated in Figure 97. The particle diameters with high particle number concentrations

observed in the SMPS results in Figure 93 have adjusted due to the consequent mass increase of larger particles. Figure 97 displays a peak particle mass concentration at the same particle diameter for the three samples at around 30 nm. As with the particle number concentration and particle size distribution, the carbon nanofillers still clearly demonstrate an augmenting effect in concentration, with the EP/CNT sample revealing the highest particle mass concentration between the three samples.

Various governing institutes have developed maximum exposure limits when concerning release of hazardous materials. The United States federal agency responsible for occupational related injuries and illness, the National Institute for Occupational Safety and Health (NIOSH), have published a report on the hazard and exposure assessment on CNTs and CNFs (*NIOSH, 2013*). From the risk assessment conducted, NIOSH published recommended exposure limits (RELs) in relation to CNTs. The estimated exposure concentration dosage associated with a 10 % risk of adverse lung effects and above background for a slight or mild lung effects (grade 2 or higher) was given a maximum likelihood estimate of 1 to 44 μg / m^3 during an estimated working lifetime exposure concentration (8-hr TWA). The averages presented in Figure 97 clearly exceed the exposure limit values recommended by NIOSH. However, the recommendation does relate to a direct release of only CNTs; whereas, the data presented in Figure 96 represents the CNTs embedded within the epoxy matrix and a substantial amount of the matrix as shown in the neat EP curve. However, the difference and 330 % increase from neat epoxy to EP/CNT in total particle mass concentration observed on Figure 96 is still above the recommended amount.

Since the CPC can measure a larger particle size range, an alternative mass concentration is valuable to quantify the release. Using the particle number concentration measurement at the end of the four-minute sampling period, and the calculated total quantity of mass drilled, an estimation of the concentration of particles/mass drilled can be acquired and is presented in Figure 98. This is calculated using the particle number concentration of the CPC (size range: 7 nm to 3000 nm), material density values and equivalent of mass drilled based on hole size and number of holes.

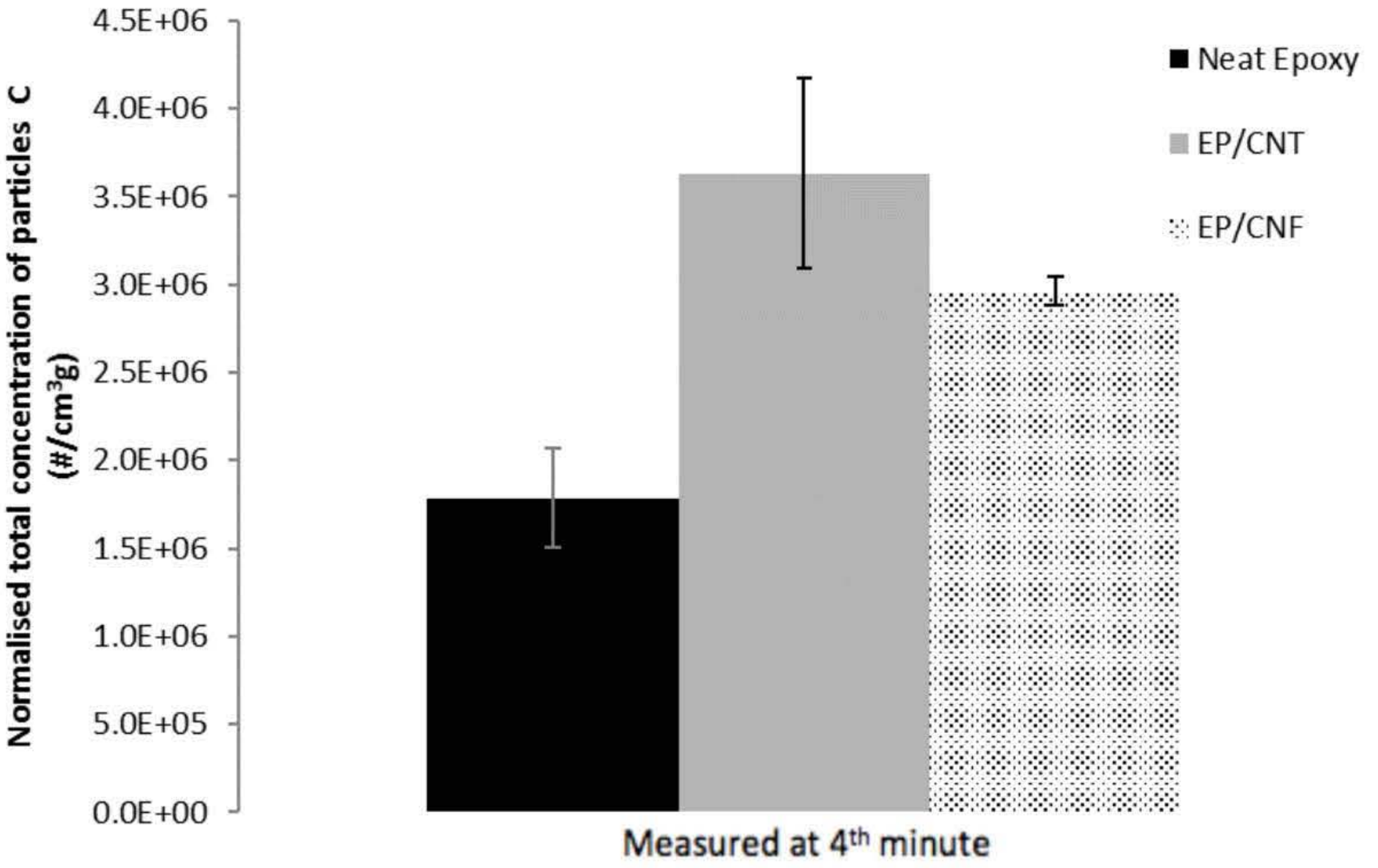

Figure 98*:* Normalised total concentration of particles (C divided by estimated drilled mass) recorded at 4th min for Epoxy based samples (n= 3 for each average).

The number of particles to mass drilled ratio also presents the EP/CNT sample with the highest particle release over the neat EP and EP/CNF samples. The EP/CNF sample observed a substantial increase from the neat EP sample with a 66% increase, and the EP/CNT sample with a 103% increase in normalised total concentration. Figure 97 demonstrates that with the material density in consideration and comparison to the particle number concentration at 4 minutes illustrated in Figure 92, the reinforced samples displayed a further increase in particle concentration in relation to the neat EP sample. The particle mass concentration is a vital parameter required when evaluating the nanoparticle release. The data identifies important differences and support the findings in the effect of the filler in particle number concentration and particle size distributions (EP = 1785805 $\#/cm^3g_{drilled}$, EP/CNT = 3630443 $\#/cm^3g_{drilled}$, and EP/CNF = 2963075 $\#/cm^3g_{drilled}$).

6.3.4 Assessment of Deposited Particles

Debris collected in the chamber as described in the methodology was analysed using an SEM. An SEM image of the neat epoxy, EP/CNF and EP/CNT samples are displayed in Figure 99.

a.) b.) c.)

Figure 99*:* SEM images of collected debris from sampling tray within chamber of a.) Neat Epoxy b.) EP/CNF and c.) EP/CNT samples.

The SEM images on Figure 99 illustrate the material surfaces with a scale of 10 µm. The SEM limitation was unable to identify free standing CNTs or CNFs, but dissimilarity between the materials can be seen. An EDX study was also performed on the samples and as expected, due to the nature of the epoxy matrix a high concentration of carbon was detected. The surfaces demonstrated different textures and morphologies revealing the material release variances. Diverse agglomerations of matrix fragments covered in nanoparticles are observed across the three materials. Critically, no independent CNTs or CNFs were established.

Equally to the other materials within this project, FT-IR analysis was performed on the pre-drilled and dust particles (termed dust as this was carried by collaboration partners at Cranfield University) from epoxy based samples and is displayed in Figure 100. The analysis is carried out on the particles collected within the sampling tray placed directly below the drilling.

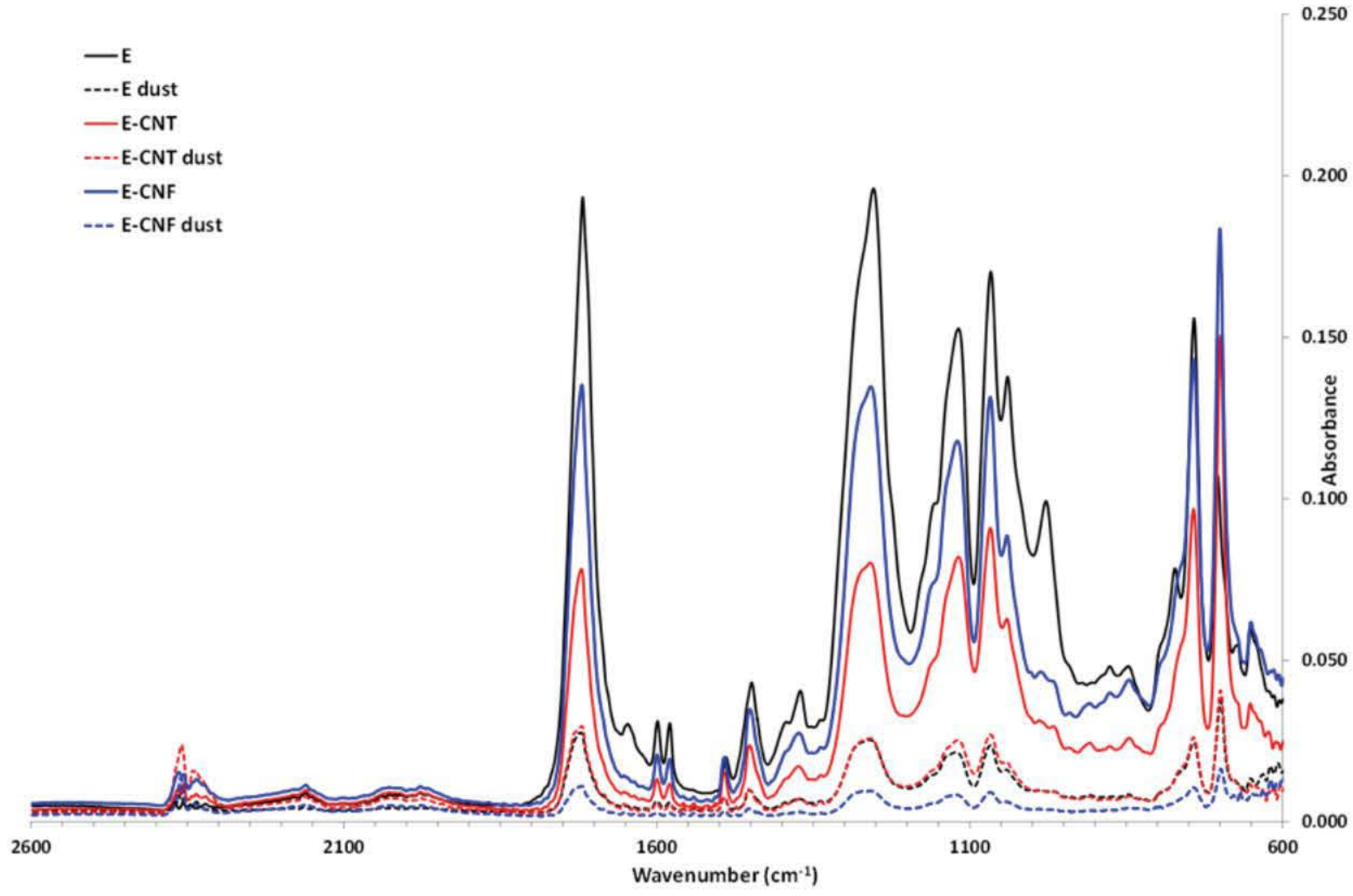

Figure 100*:* FT-IR analysis of pre-drilled epoxy samples compared to dust particles collected after the drilling.

The spectra observed no difference between the materials before and after the drilling. The material therefore displayed no internal chemical change due to the drilling. Due to the capabilities and limitations of the instrument, the FT-IR spectrum is unable to identify independent nanofillers due to the minimal required material. The analysis is only capable of giving a representation of the internal chemical bond change of a larger matrix-embedded particle. The data is also a representation of the deposited particles collected within the chamber, and not the measured airborne particles through the particle quantification instruments.

6.4 Conclusion

Three EP based nanocomposites were fabricated with two different carbon nanofillers (CNTs and CNFs). From the manufactured and mechanically tested samples, the neat epoxy with reinforced 2 wt.% CNFs and 2 wt.% CNTs were investigated for nanoparticle release during drilling. The samples tested, including the neat epoxy, revealed that nanoparticles were generated and released from the sample during the drilling process. It was observed that all three samples emitted significant concentrations which surpassed the limits of the CPC instrument on several occasions during the drilling. In comparison to the neat epoxy sample, the EP/CNF and EP/CNT samples produced an

increase of 93 % and 211 % respectively in average particle number concentration across the 4 minutes. The two sample t-test of significance of each sample mean and deviation to the neat epoxy sample returned statistically significant differences for all samples in the particle number concentration. Similar with the mechanical properties observed for the materials, a significant proportion of the nanoparticle release can be seen to be related to the polymer matrix. However, although the matrix can be attributed to having the biggest influence on the nanoparticle release, the nanoparticle fillers still observed a statistically significant influence on the particle number concentration. It is therefore crucial to consider the polymer and filler concentrations when evaluating the nanoparticle release.

The SMPS data displayed little influence of the fillers on the particle size distribution. The CNT and CNF reinforced samples presented similar peaks compared to the neat epoxy sample. However, the particle number concentration was evidently greater in the nano-filled samples even in the SMPS data. The carbon fillers therefore had an increasing effect on the particle number concentration. The DMS50 data highlighted the increasing effect of the carbon nano-fillers on particle number concentration even further. The two instruments displayed similar small diameters in the particle size distributions with a high percentage of the particles within 6-20 nm, and no significant concentration larger than 70 nm.

Furthermore, the particle mass concentration revealed a release substantially above the NIOSH recommended exposure limits when working with CNTs and CNFs, as well as different dispersion/depositing properties. Nonetheless, the data includes release of the epoxy matrix and revealed no evidence of independently free standing CNTs or CNFs in the microscopy analysis of the deposited particles.

Chapter Seven

Investigation of the Influence of Graphene Oxide on Nanoparticle Release during Drilling from Carbon Fibre Reinforced Epoxy Hybrid Nanocomposites

7.1 Introduction

The aim of this study is to investigate the influence GO has on nanoparticle release from EP/CF hybrid composites during drilling. EP is one of the most utilised thermosets within polymers, with an estimated global EP resin market to be $10.6 billion by 2023 at a compound annual growth rate of 5.24% during 2017-2023 (Cooked Research Reports, 2017). A separate report on global fibre reinforced composites forecasts a compound annual growth rate of 8.20% during 2018-2024 (Zio Market Research, 2018). The use of carbon nanofillers to improve interfacial bonding between CFs and the polymer matrix is widely demonstrated in literature with fillers such as GO (Hung et al., 2019; Zhang et al., 2016), RGO (Shin et al., 2012), graphene (Wang and Cai, 2019; Gangineni et al., 2019), carbon black (Srivastava et al., 2017), and silver nanoparticles (Tang et al., 2017). This chapter includes three weight concentrations of GO as nanofillers within EP/CF hybrid composite materials as highlighted fillers within literature.

As well as demonstrating beneficial material properties, GO has also been demonstrated potential cytotoxicity affects (Akhavan et al., 2012; Matesanz et al., 2013; Seabra et al., 2014; Lalwani et al., 2016; Kang et al., 2017). As EP/CF composite materials are currently mostly used within the automotive and aeronautical industry (Zio Market Research, 2018), the materials will undergo drilling during assembly and manufacturing stages. As evident within sever studies, composite materials with nanoparticles have shown potential release of the nanoparticles (Basinas et al., 2018; Debia et al.,

2016; Froggett et al., 2014). This chapter will therefore investigate the influence of the GO nanoparticles on the nanoparticle release during the identified release scenario, drilling.

7.2 Experiment

The EP/CF-based samples were selected and manufactured as discussed in Chapter Three. GO nanoparticles were used to reinforce the material and will be compared to the neat EP/CF. Three material weight concentrations of 0.05 wt.%, 0.1 wt.% and 0.5 wt.% of the nanofillers were manufactured to investigate the effect of filler weight concentration. The materials morphology, structure and composition are demonstrated in section 3.3.1 and 3.3.2.

To evaluate the samples manufactured, the materials were characterised through SEM, EDX and FT-IR. The characterisation equipment used within this study is detailed in section 4.2.2.

The materials were firstly investigated for mechanical properties. The effect of the nanofiller on the material mechanical performance are shown to demonstrate the original benefits and use to strengthen the materials. The materials underwent a flexural 3-point bend test in accordance with ASTM D 7264/M flexural test (ASTM D7264M, 2015) and a standard ASTM D 3039/D tensile test (ASTM D3039, 2017). These results are included in section 3.3.3.

The samples underwent the exact same drilling described in section 4.2.3 with further details of the methodology also available in Appendix A. A standard Dremel 4000 drilling tool with an industrial standard stainless steel 3.5mm twist drill bit was used at 10000 rpm with a feed rate of 78 mm/min.

Once the chamber was cleared of any particles, the drilling studies were carried out by drilling across the width of the sample resulting in eight separate holes and bearing a time duration of 3 minutes of drilling, followed by 1 minute post-drilling. The eight holes drilled per sample were repeated three times to get an average of the particle number concentration and particle size distribution released.

The nanoparticle release is quantified through a CPC, SMPS, DMS50, A standard IOM Inhalable Sampler, XRF, SEM and EDX. More information on the equipment used within this study is detailed in section 4.2.2.

7.3 Results & Discussion

7.3.1 Filler Effect on Particle Number Concentration

The GO reinforced EP/CF samples underwent the repeated drilling and the particle number concentration was measured during the testing. A graphical representation of the CPC particle number concentration averages from the repeated runs on the samples is displayed in Figure 101. Similar to previous samples, the 8 holes drilled are clearly evident within the particle number concentration over the 4 minutes of data sampling. Eight peaks represent the eight holes drilled, followed by one minute on no drilling and the concentration stabilises. Similarly, the concentration returns to similar values between each hole being drilled. The mechanical drilling therefore generates a substantial quantity of nanoparticles, which then quickly disperse, but remain airborne within the chamber (evident through stable concentration). From the comparison between the EP/CF sample to the reinforced samples with GO, any disparity between the samples is not clearly apparent.

The peaks concentrations of release during drilling are spread across two peaks which can be associated to the drill bit entering and the withdrawal of the drill bit from the material. Unlike the other materials tested, the withdrawal of the drill bit can clearly be evident of producing the higher particle number concentration. Within the averages, only the first hole of the EP/CF samples displayed a higher particle number concentration from the drill bit entering the material than during the withdrawal. As this was not observed with the EP-based samples, the cause can therefore be associated to the CF as it is apparent in all EP/CF samples. The high yield and tensile strength of the CF combined with the larger filler size, is seen to restrict the release of the material during the drill bit entering the material. However, the introduction of GO into the samples at the three different weight concentrations did not demonstrate any noticeable difference to the profile of the relase during entering or withdrawing the drill bit.

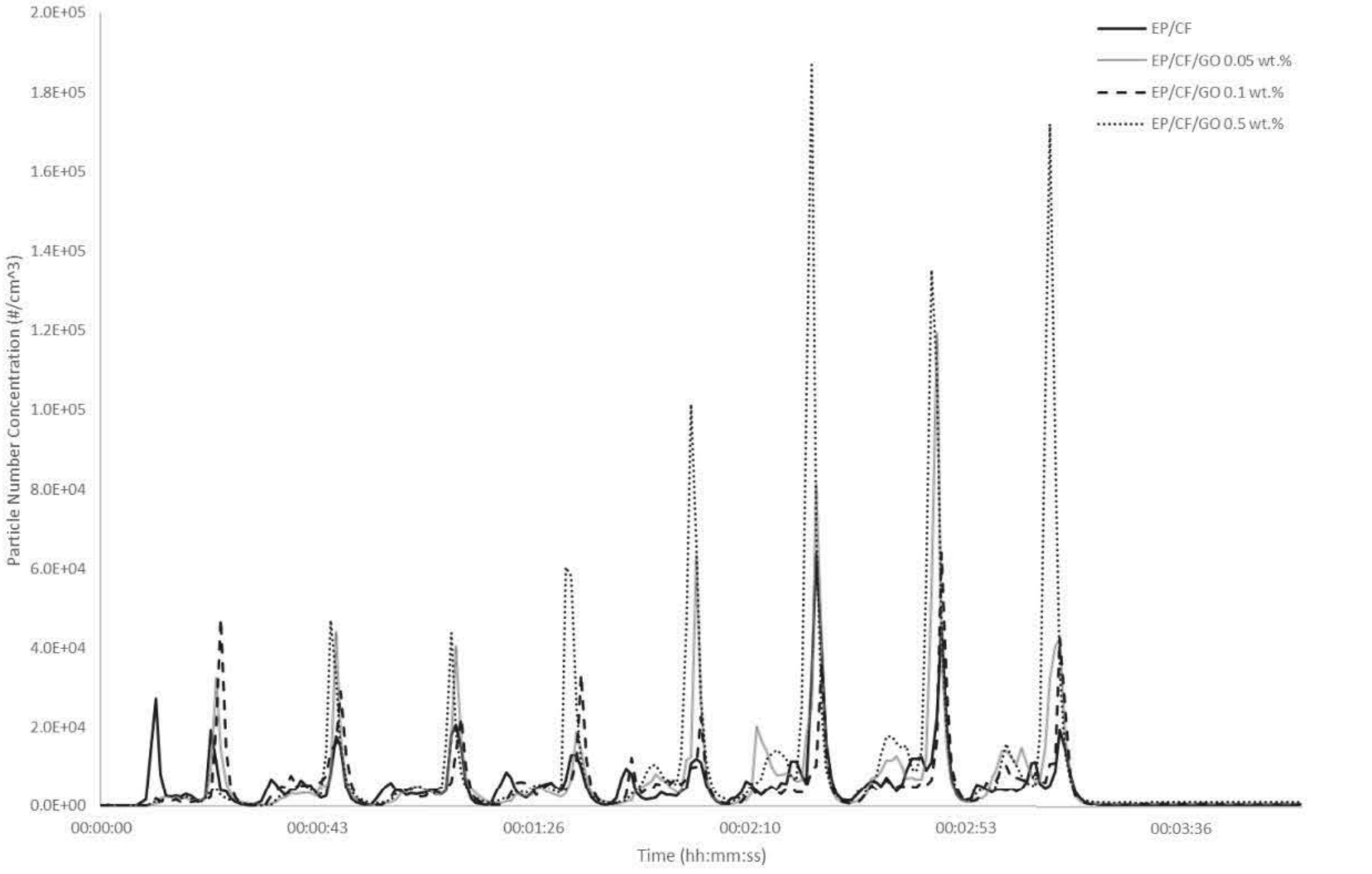

Figure 101*:* Particle number concentration averages of nanoparticles introduced from EP/CF-based samples reinforced with GO and measured using CPC (n=3 for each average).

The data demonstrates that even the samples without the reinforcement of GO nanoparticles, released a substantial particle number concentrations during drilling. The EP/CF sample without any nanoparticles, observed a peak particle number concentrations comparable to the samples reinforced with the GO nanoparticles. However, from the average profiles, the EP/CF/GO 0.5 wt. % sample can be seen to have observed the highest peaks. These also can be seen to slowly increase in size over the eight holes, with the exception of the seventh hole. This would suggest the more holes being drilled, also increases the particle number concentration peak size. This however is not observed in any of the other samples. Furthermore, this was not observed within any of the release profiles of the individual runs from the other samples either. The GO therefore at 0.5 wt. % can be seen to show an increasing trend with more holes drilled, which is not evident with lower weight concentrations.

Whilst the 0.5 wt. % GO can be understood to increase the peak particle number concentrations released during drilling (with a 243 % increase in mean particle number concentration), the two other GO weight contrations have contrasting effects. The peaks introduced from the EP/CF/GO 0.1 wt. % followed a comparable profile to the peaks from the EP/CF samples, whereas the EP/CF/GO 0.05 wt. % can be seen to have released some slightly higher peak concentrations. A numerical and statistical representation of the data from all samples is shown in Table 22.

Table 22*:* Inferential statistical representation of the particle number concentrations introduced at the peaks due to the drilling on EP/CF-based samples reinforced with GO (n = 24 for each sample). Lower and upper limits represent the 90% confidence interval on a sampling t-distribution.

Sample	Mean: $\overline{\overline{X}}$ [#/cm^3]	Deviation: $S_{\overline{X}}$ [#/cm^3]	Minimum [#/cm^3]	Maximum [#/cm^3]	5% Lower limit of confidence interval [#/cm^3]	95% upper limit of confidence interval [#/cm^3]
EP/CF	2.74 x 10^4	1.81 x 10^4	1.21 x 10^4	6.38 x 10^4	1.84 x 10^4	3.65 x 10^4
EP/CF/GO 0.05 wt. %	5.44 x 10^4	3.30 x 10^4	1.42 x 10^4	11.9 x 10^4	3.79 x 10^4	7.09 x 10^4
EP/CF/GO 0.1 wt. %	3.72 x 10^4	1.39 x 10^4	2.26 x 10^4	6.40 x 10^4	3.03 x 10^4	4.42 x 10^4
EP/CF/GO 0.5 wt. %	9.39 x 10^4	6.59 x 10^4	4.29 x 10^3	18.7 x 10^4	6.10 x 10^4	12.7 x 10^4

Table 22 displays the statistical analysis carried out on the peak particle number concentrations of the samples. In comparison to EP-based samples without CF reinforcement, the peak particle number concentrations can be seen to be significantly lower. Importantly, the data avoided the saturation point of the CPC measurement capability (i.e. 1×10^7#/cm^3), unlike the EP-based samples without CF. The calculated lower tail of 5% and upper tail of 95 % give a representation of the data for a 90 % confidence interval of a t-distribution. This highlights the disparities between the peak particle number concentrations and therefore, a statistically significant difference with the introduction of GO on release in comparison to the EP/CF. A two sample t-test of significance of each sample mean and deviation to the neat EP/CF sample returned statistically significant differences for all concentrations of GO (outside the 95% confidence interval). ANOVA single factor analysis was performed to assess the variability between the sample peak means introduced due to the fillers. The analysis returned statistically significant differences within the 4 samples (F value = 4.63 F critical value = 2.95) and a 0.946% chance that the observation could have been observed due to random error alone and therefore rejecting a hypothesis that the samples displayed no difference.

It is important to note that although the statistical analysis returned a statistically significant difference with the introduction of the GO, this does not embrace the extend of the difference. From the data represented in both Table 22 and Figure 101, the incorporation can be seen to have a minor influence in the increase in particle number concentration. With the comparison of the samples, the EP/CF/GO 0.5 wt. % demonstrated a clear increase in all aspects of the particle number concentration.

Whereas, the 0.05 wt. % and 0.1 wt. % displayed a more minor increase in peak particle number concentration values. As with all other samples, the statistical analysis does consider the high standard deviation and range demonstrated and therefore includes the level of randomness and variability in the peaks released.

From the numerical values, the EP/CF/GO 0.5 wt. % reinforced sample exhibited the uppermost mean value over the 4 min with 1.07 x 10^4 #/cm^3 introduced into the chamber during drilling. In relation to the EP/CF, the EP/CF/GO 0.05 wt. % and EP/CF/GO 0.1 wt.% produced a difference in nanoparticle concentration of 31.9 % and -1.17 % in average over the 4 minutes. Therefore, although the EP/CF/GO 0.05 wt. % and EP/CF/GO 0.5 wt. % observed an increase in particle number concentration over the 4 minutes, the EP/CF/GO 0.1 wt. % demonstrated a slight decrease.

Furthermore, to correlate the increasing weight concentration of GO on nanoparticle release, no statistical model can be created. This is due to an increase in concentration with 0.5 wt. % GO followed by a decrease from the 0.1 wt. % GO, and finally a larger increase from the 0.5 wt. % sample. The correlation therefore does not follow a trend or correlation between weight concentration and particle number concentration released. However, the performance in nanoparticle release correlates closer to the performance in mechanical material properties. The 0.1 wt. % demonstrated the lowest Young's Modulus and flexural modulus of the GO reinforced samples. Therefore, the nanoparticle release can be seen to relate to mechanical factors, as opposed to a simple correlation to nanoparticle weight concentration embedded within the material.

Whilst producing the highest concentration and peaks during the drilling, the EP/CF/GO 0.5 wt. % sample also demonstrated the highest concentration at the end of the four minute sampling period. The high number concentration introduced during the drilling indicates to disperse within the chamber but crucially remain airborne. The EP/CF/GO 0.5 wt. % sample presented a particle number concentration remaining above 1.2 x 10^3 #/cm^3 even after the drilling and 1 minute post drilling was concluded. The graphical representation of the average particle number concentration measured at the end of the four-minute sampling period is presented in Figure 102.

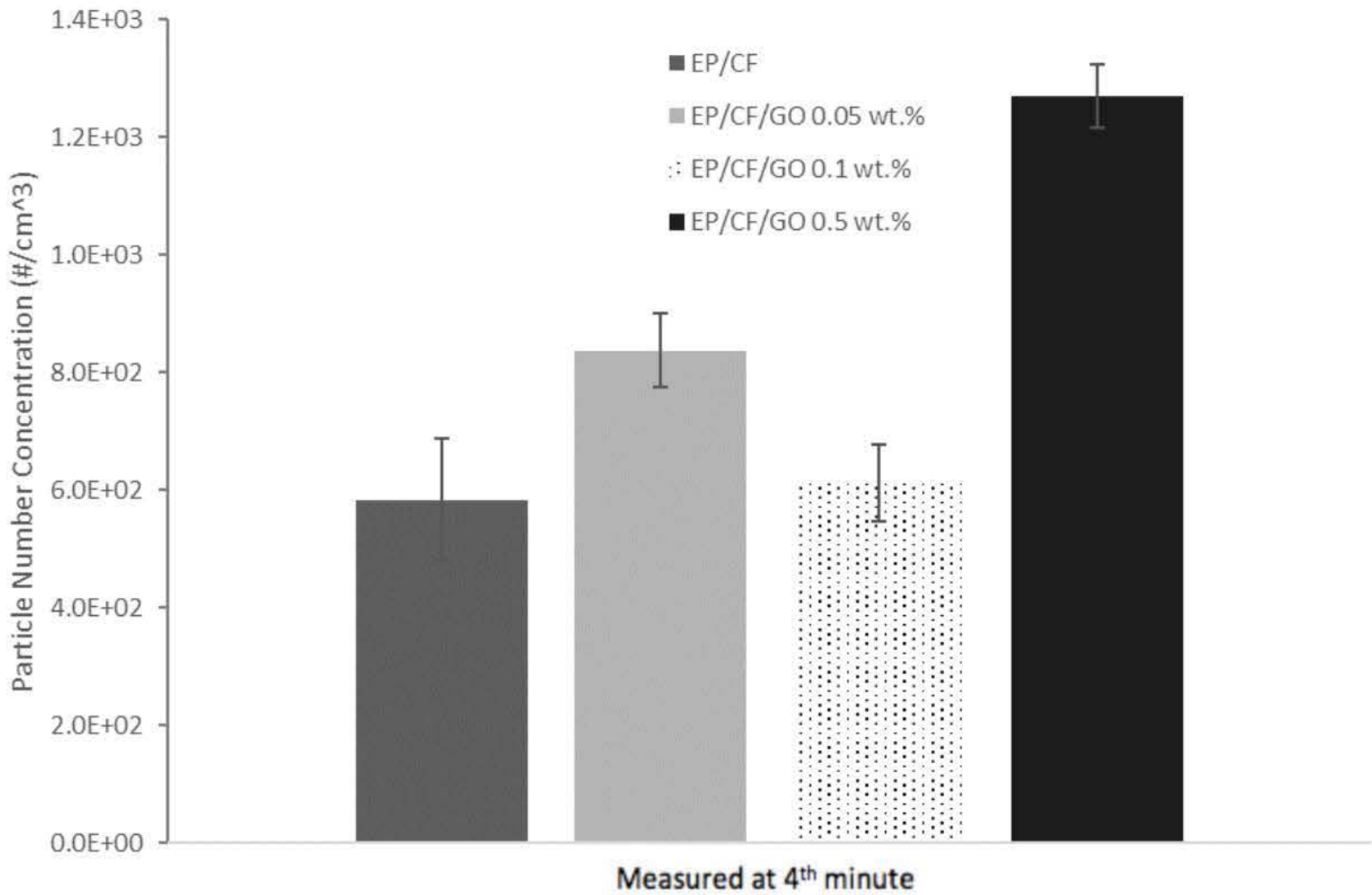

Figure 102*:* Particle number concentration recorded at 4th min (#/cm^3) for EP/CF based samples reinforced with GO as measured on the CPC (n=3 for each average).

The total particle number concentration measured at the end of the sampling period is beneficial to evaluate the effect of the filler on the rapidity of depositing and dispersion within the chamber. The difference in particle concentration at the time of release due to the holes and concentration at the end of the sampling period presents an indication into these properties. The EP/CF/GO 0.5 wt. % sample observed a 118% increase measured at the 4th min from the EP/CF sample in comparison to the 112% increase over the previous four minutes (EP/CF/GO 0.05 wt. % increase of 43.5 % and EP/CF/GO 0.1 wt. % increase of 4.85 % increase from the EP/CF sample measured at the 4th minute). The difference at the 4th minute being similar to that measured over the four minutes demonstrate the deposition rate during the 1-minute post drilling is similar between all samples. Therefore, as well as demonstrating the highest peak particle number concertation released during drilling, the particles released from the EP/CF/GO 0.5 wt. % do not deposit any quicker and remain airborne to observe the highest particle number concentration post drilling.

7.3.2 Filler Effect on Particle Size Distribution

With a sampling period of 1 minute, an average of the 4 data sets from the SMPS across the 4 minutes for each sample is displayed in Figure 103. From the distribution, the EP/CF/GO 0.5 wt. % can be seen

to have the most substantial effect on the particle size distribution. Two large peaks are observed on the limits of the SMPS between 4 to 6 nm and 80 to 100 nm particle diameters. All the other samples observed smaller peaks, and at different particle diameters. The size distribution illustrates minimal effect with the introduction of GO nanofillers at 0.05 wt. % and 0.1 wt. % in comparison to the EP/CF sample. Excluding the EP/CF/GO 0.5 wt. %, the size distribution can be seen to be relatively scatter across the 100 nm spectrum. Slight increases are observed at 18 nm and between 40 to 50 nm, but these are still unparalleled to the peaks observed from the EP/CF/GO 0.5 wt. % sample.

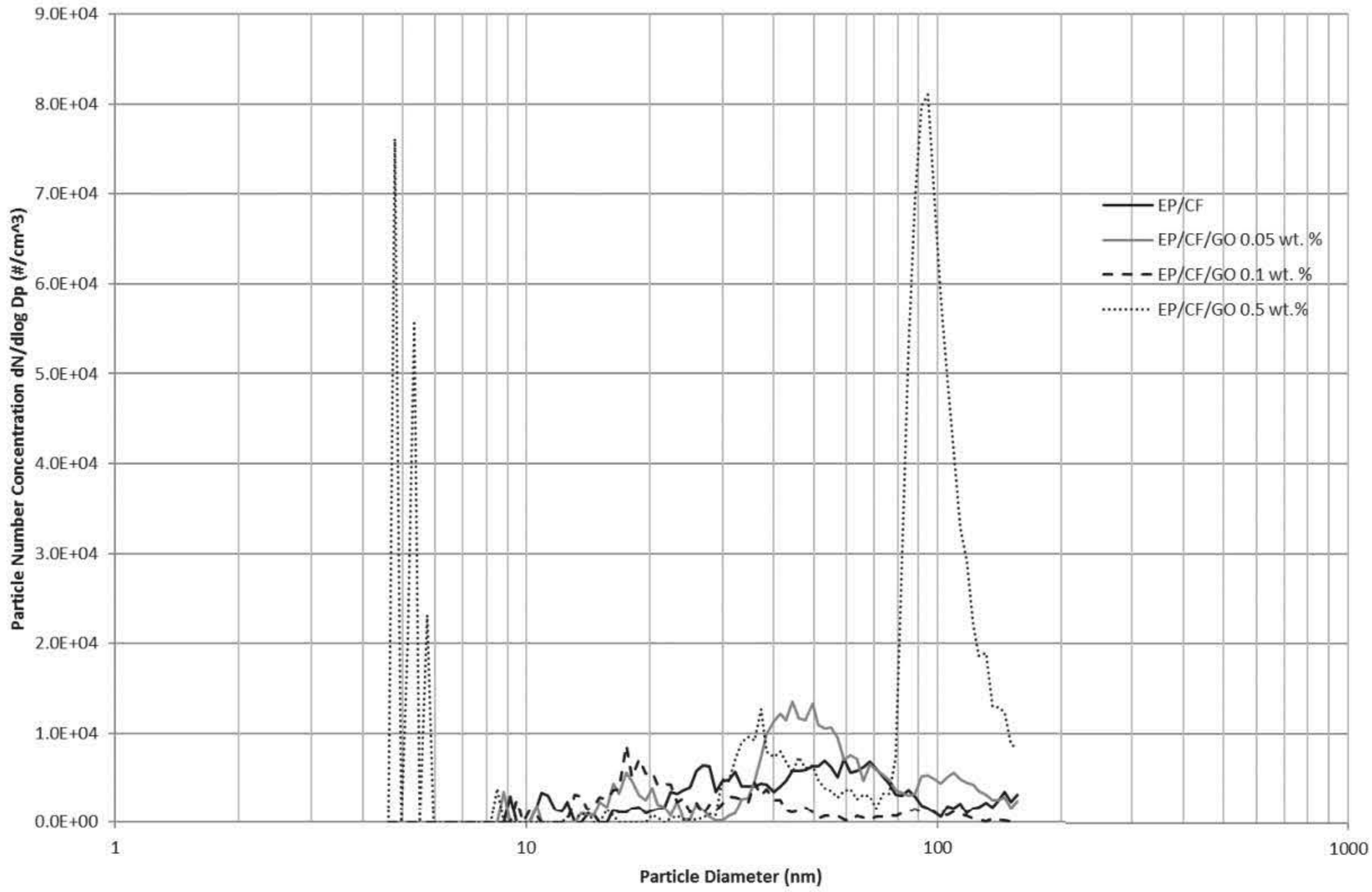

Figure 103*:* Average particle size distribution measured using SMPS of EP/CF-based nanocomposites reinforced with GO (n=12 for each average).

The peaks observed below 6 nm from the EP/CF/GO 0.5 wt. % are quite significant in magnitude and substance. The GO embedded within the EP/CF consists of 15 to 20 sheet flakes which will therefore have a thickness of up to 20 nm. Each GO sheet can have a thickness of around 1 nm (796034 Sigma Aldrich). Drilling creates shear forces within the material which can therefore be related to possible separation of the layers due to the drilling. Furthermore, the EP/CF sample without any nanofiller did not exhibit any release peaks at these diameters. It is possible therefore, that the peaks observed below 6 nm could be associated to the GO fillers. However, this cannot be confirmed without identification of the independent GO fillers and peaks at the original thicknesses of the GO would be expected at around 20 nm.

The peak observed around 100 nm does not correlate to either individual fillers. The CF fibres have a thickness within the micron-range and were not apparent in the particle size distribution of the EP/CF sample. Any independent CF or matrix-filler (EP and CF) embedding released from the samples would be expected within the EP/CF sample. The peak could instead be associated to either agglomerations of the GO nanoparticles or GO embedded within the matrix. However, both would also be expected within the other GO reinforced samples, unless the higher weight concentration is likely to increase the separation of the GO from the CF. Nonetheless, the EP/CF/GO 0.5 wt. % can be concluded to have influenced the particle size distribution quite significantly. In comparison however, the EP/CF/GO 0.05 wt. % and EP/CF/Go 0.1 wt. % observed minimal influence on the particle size distribution in contrast to the EP/CF sample.

Further to the data collected on the SMPS, separate data was gathered on the DMS50 for the size distribution at each second and is displayed in a 3-D plot as shown for the four samples in Figure 104, Figure 105 and Figure 106 (Note: data is taken from a separate run to the CPC and SMPS data due to the required increased inflow rate).

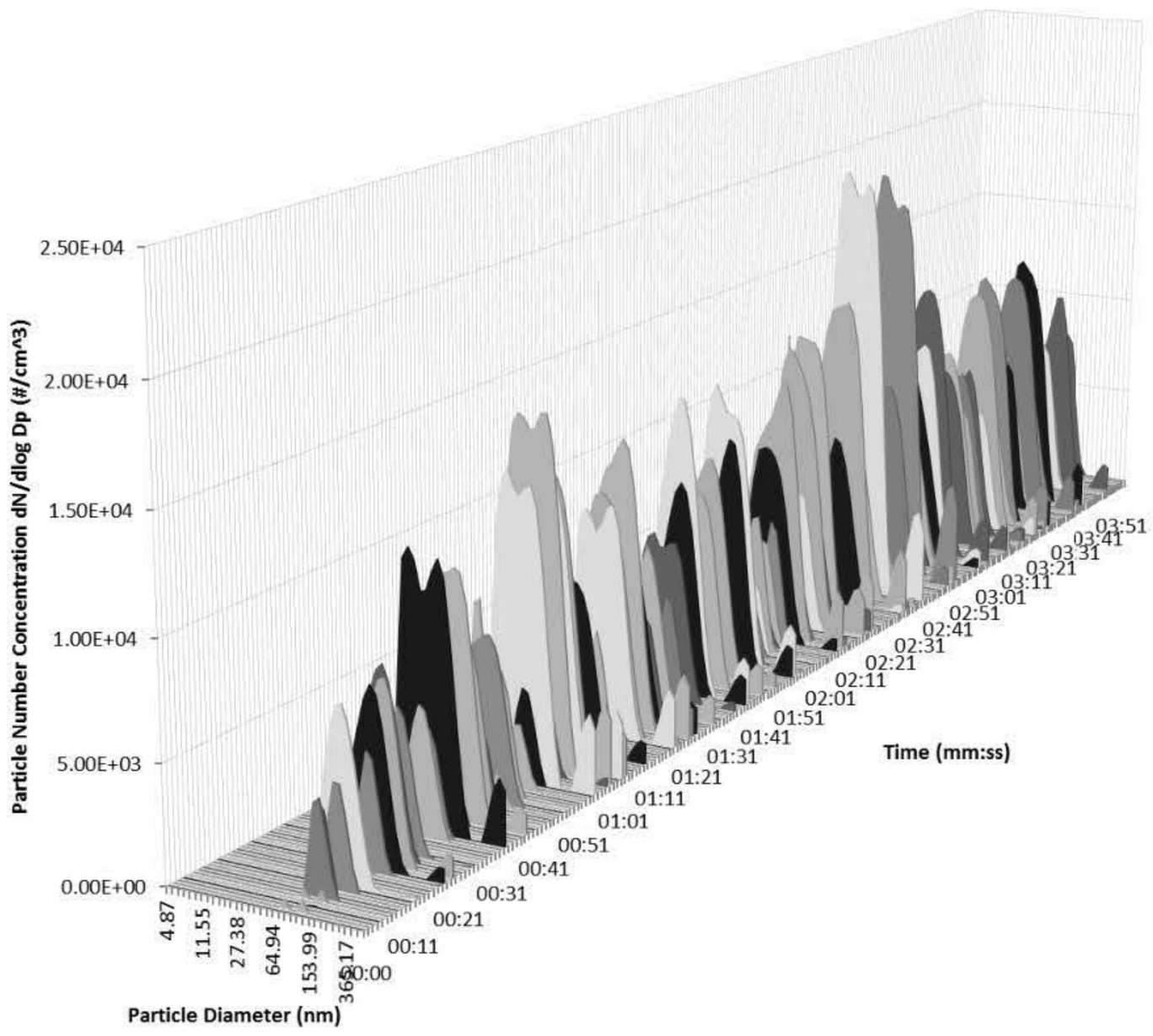

Figure 104: Particle size distribution recorded on the DMS50 during 4 minutes from the EP/CF sample.

a.)

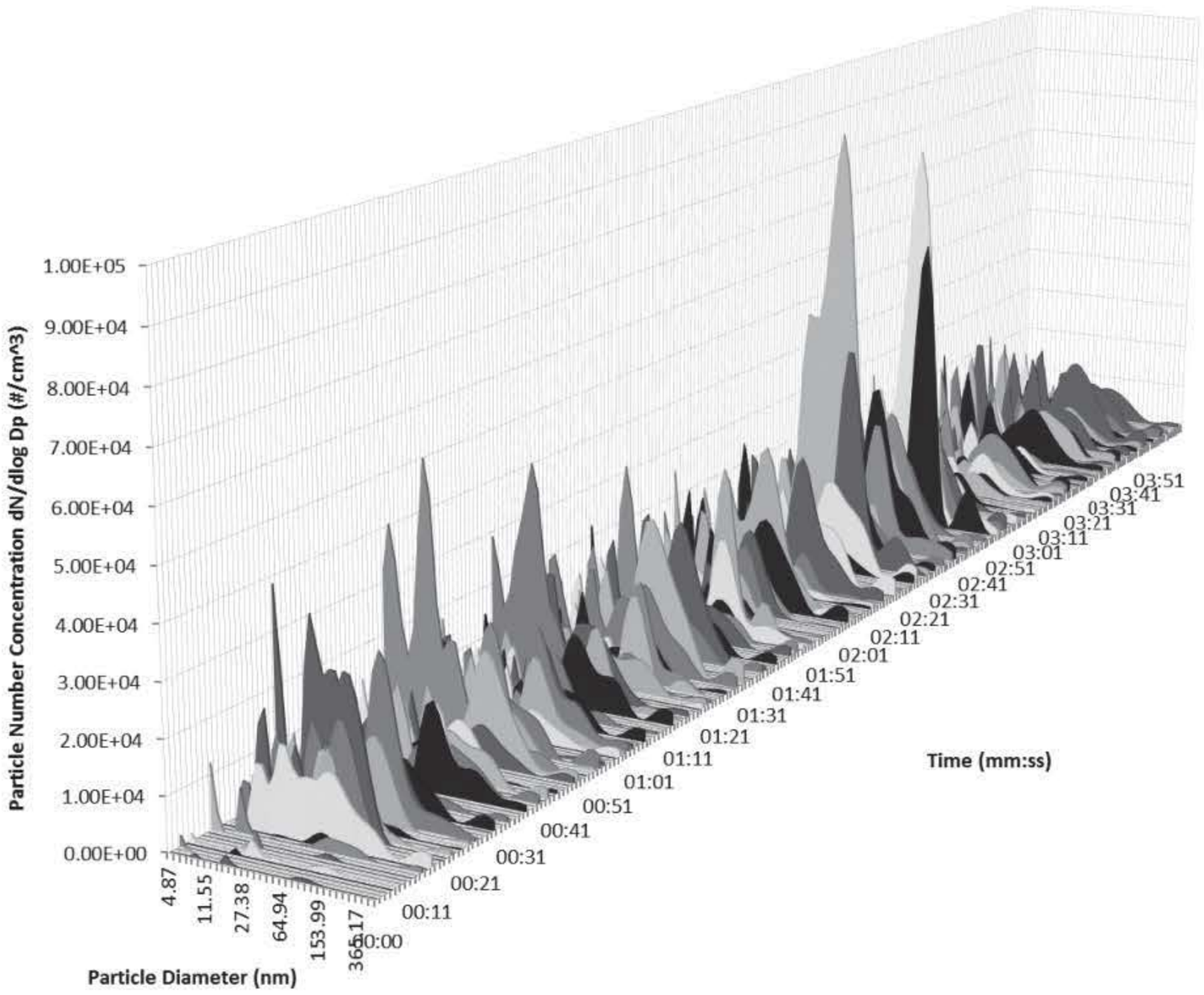

b.)

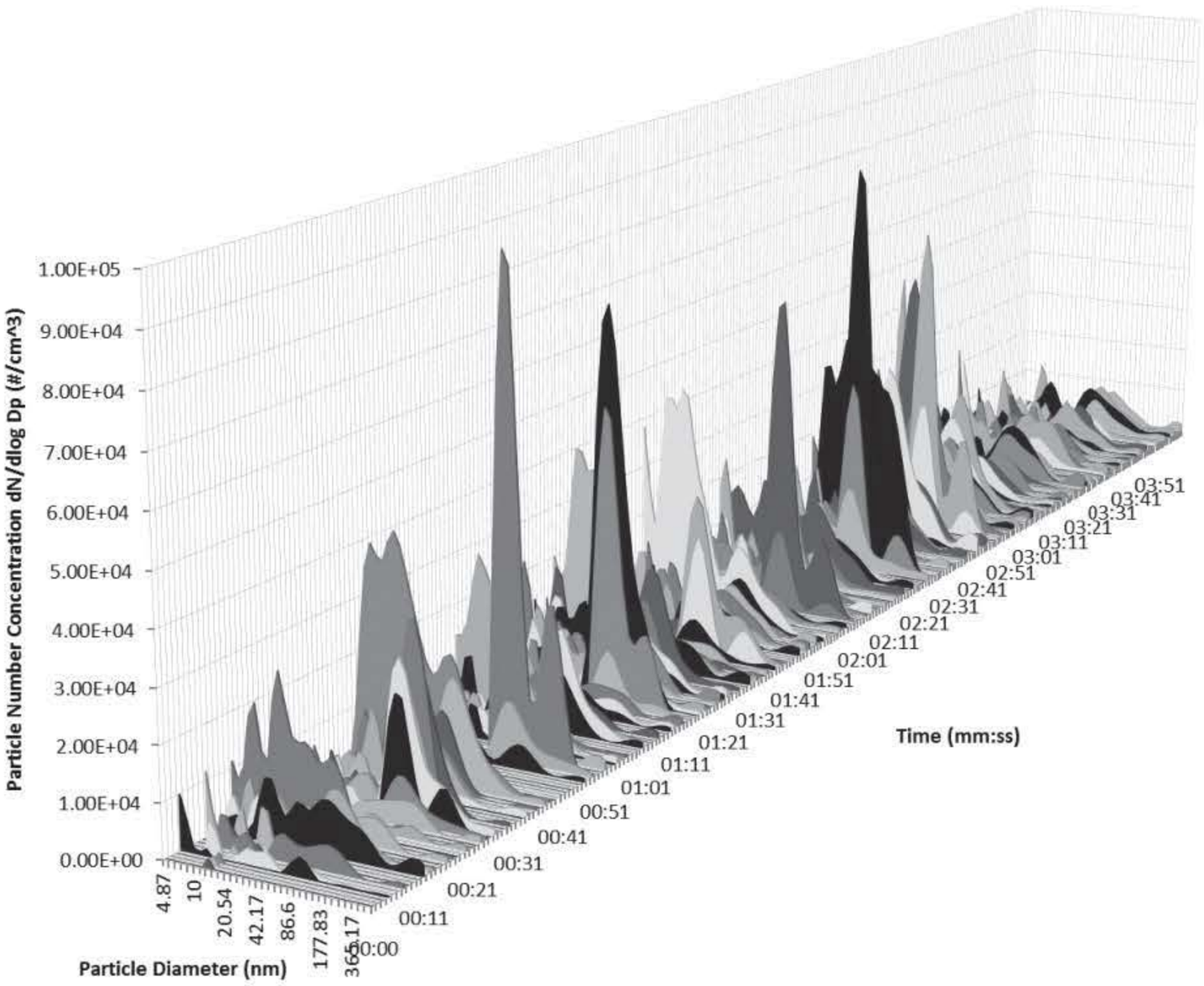

Figure 105*:* Particle size distribution recorded on the DMS50 during 4 minutes from the a.) EP/CF/GO 0.05 wt. % sample and b.) EP/CF/GO 0.1 wt. % sample.

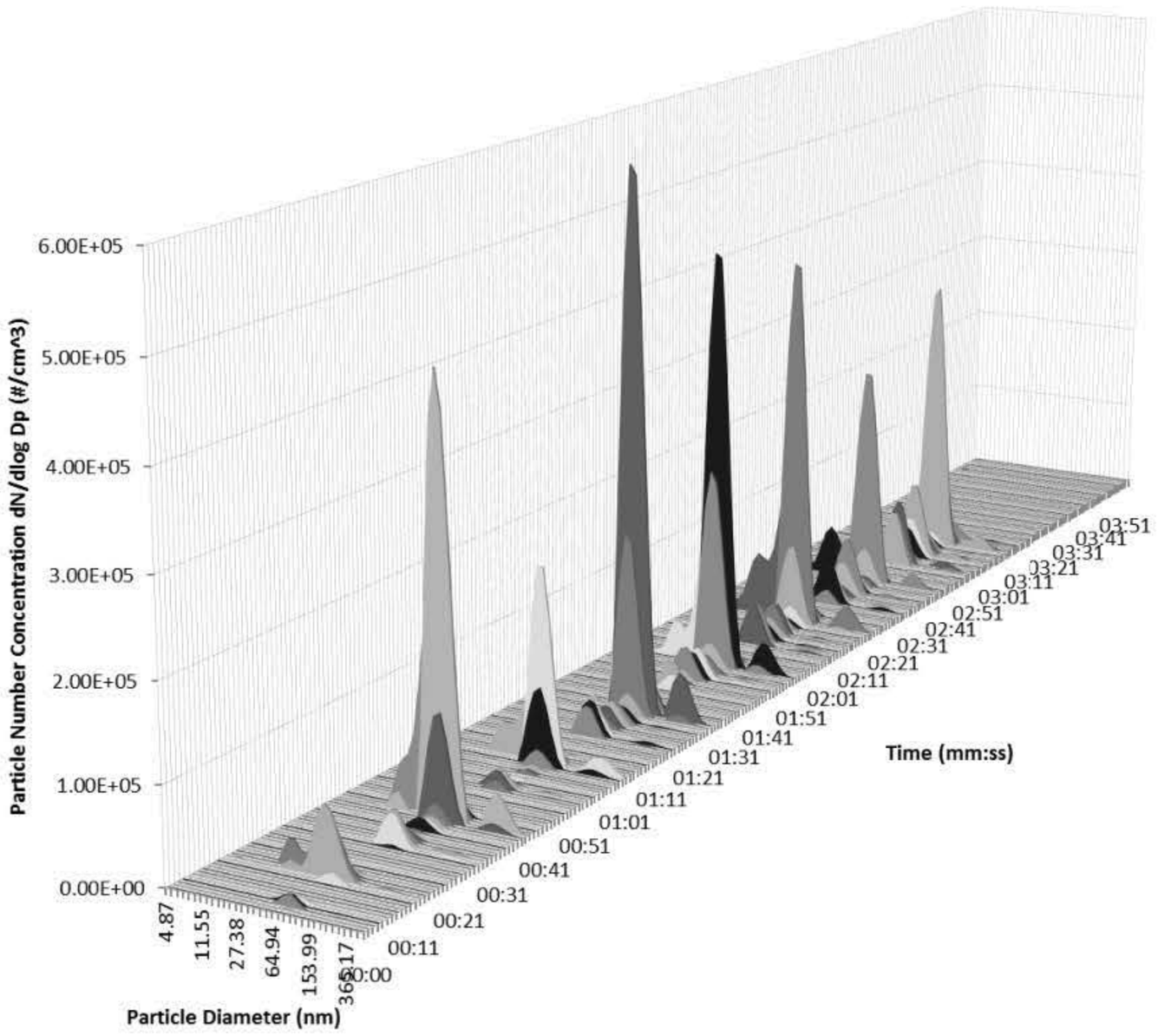

Figure 106: Particle size distribution recorded on the DMS50 during 4 minutes from the EP/CF/GO 0.5 wt. % sample.

As demonstrated in the CPC data previously shown in Figure 101, the DMS50 data displays the peaks introduced during drilling across the first three minutes, followed by the post-drilling minute with reduced particle number concentrations. The eight peaks represent the eight holes drilled. This is apparent in all of the samples reinforced with GO, however, less obvious and more challenging to detect in the EP/CF sample DMS50 data. The EP/CF sample displayed an increase in particle number concentration once drilling started, followed by a continued high concentration once drilling was complete. Due to the relatively low particle number concentrations, the peaks during drilling are less apparent. In contrast, due to the high escalation in particles from the EP/CF/GO 0.5 wt. % sample during drilling, the particle size distribution is not clearly evident in the one-minute post-drilling. Similarly, this is also witnessed from the concentrations between drilling. In comparison, the EP/CF/GO 0.05 wt. % and EP/CF/GO 0.1 wt. % displayed an in-between profile, with most holes drilled evident, but with high relative concentrations between drilling and during the fourth sampling minute. The difference between the samples is similar to the CPC data, where the EP/CF/GO 0.5 wt. % sample exhibited the highest particle number concentration which is conveyed into the DMS50 data. Lower peak concentrations are observed for the other samples, with relatively lower concentrations after drilling. As a result, the DMS50 data concurs with the CPC data on the influence of the GO on particle number concentration.

Noticeable within all samples, and as demonstrated in the CPC data, the peak particle number concentrations introduced during the drilling are relatively inconsistent followed by a more stable and consistent post-drilling concentration. Although the particle size distributions introduced during the peaks from drilling are different between samples, the distributions are relatively consistent within each sample. The particle size distributions can therefore be associated to the material, as opposed to any factor related to the continuation of the drilling such as the particles present, or the number of holes already been drilled by the drill bit. A two-dimensional plot of the average particle size distribution introduced at the peaks due to drilling will therefore be representative of the eight holes drilled for each sample, and is presented in Figure 107.

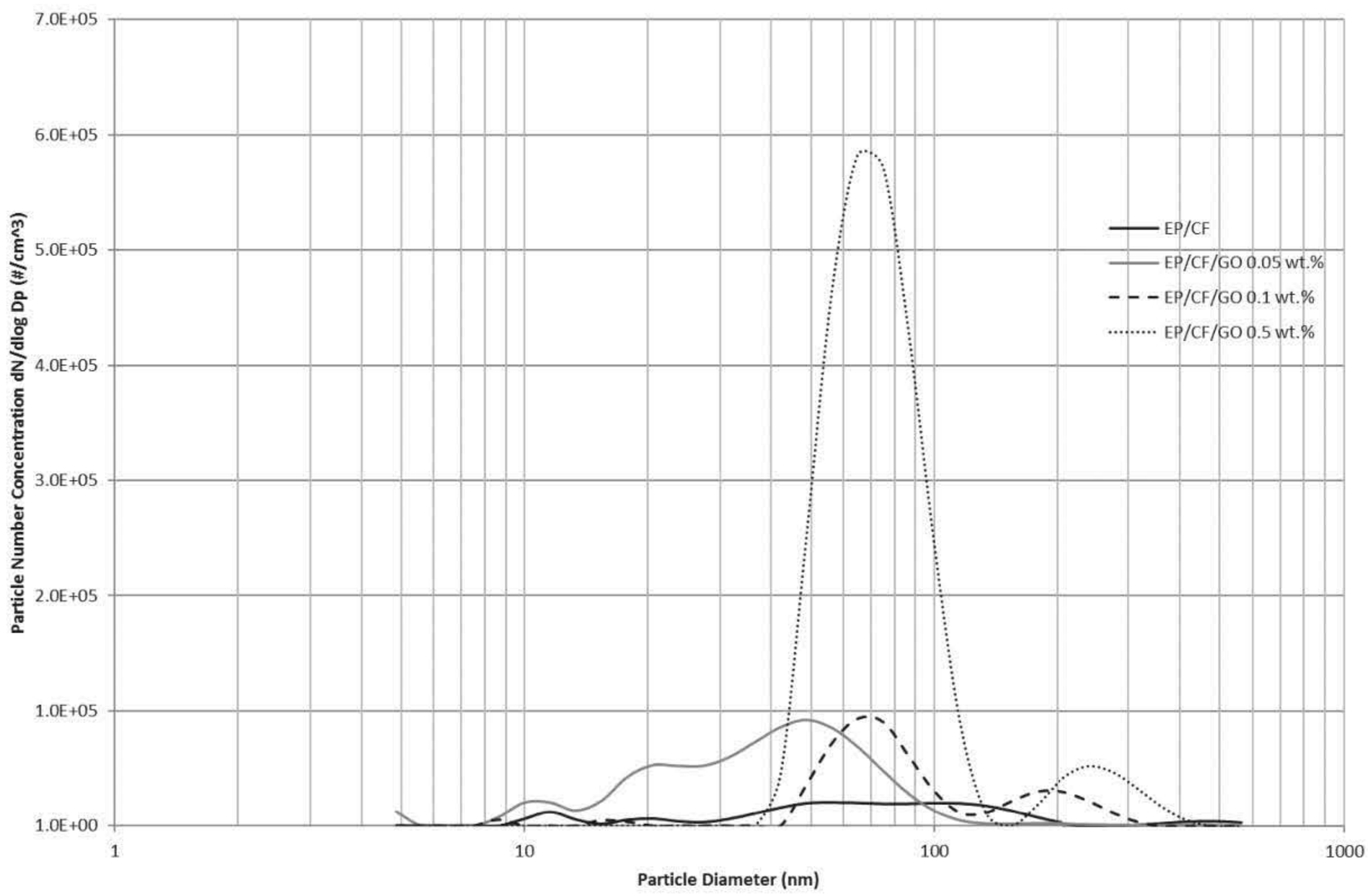

Figure 107*:* Peak particle size distribution within the 4 minutes sampling of the EP/CF-based samples reinforced with GO recorded on DMS50.

The four samples displayed contrasting results in particle size distribution released at the moment of drilling. Although demonstrating different peak sizes, a relative high proportion of the size distribution from the four samples is ascertained to be between a 40 to 100 nm particle diameter. Whilst the EP/CF sample did not display a discrete sharp peak, all other samples revealed the highest peak within this same size range. This is however, the one similar element visible in the four samples. The sample without any GO nanoparticles, observed a broad range of particle diameters. Similarly, the peaks exhibited from the EP/CF/GO 0.05 wt. % were split across a 10 to 70 nm particle diameter. In contrast,

the EP/CF/GO 0.5 wt. % displayed two peaks, one between 40 to 100 nm and one between 150 to 400 nm particle diameter.

In comparison to the SMPS data of the particle size distribution, the broad range and variation in particle diameter for the EP/CF, EP/CF/GO 0.05 wt. % and EP/CF/GO 0.1 wt. % samples are in moderate agreement with the DMS50 data. The peak observed at around 100 nm from EP/CF/GO 0.5 wt. % sample is somewhat similar to the SMPS data, however, the DMS50 did not display a peak for the sample at lower concentrations. Similar to the data presented in previous chapters, the disparate peaks seen on the two instruments introduce debateable deductions and limited effectiveness of instrumentations required for real-time data. Nonetheless, the data from the DMS50 demonstrated no evidence of independent nano-sized GO fillers within any of the particle size distributions for the GO reinforced samples. With almost no peak apparent less than 10 nm particle diameter, the suggestion of GO layers separation due to the drilling shear forces is not evident in the DMS50 data. However, the GO can be seen to increase the particle number concentration between 40 to 100 nm. The source of the increase is due to the higher particle number concentration observed in the GO reinforced samples. However, due to the particle size diameters these cannot be associated to independent nanofillers, and instead either agglomerations or matrix-filler embedded particles. Nonetheless, all three instruments used to quantify the released particles (CPC, SMPS & DMS50) demonstrate a harmonised maximum increase in particle number concentration from the EP/CF/GO 0.5 wt. % sample.

7.3.3 The Filler Effect on Mass Size Distribution

Since the drilling was conducted without any interference from background particles, all of the particles measured on the instrumentation are from the nanocomposite material. With the use of the SMPS and the known density of the individual nanocomposites, the particle mass concentration can therefore be estimated. The data utilises the diameter of the particles measured using the SMPS. The constant material density for the three nanocomposites are: EP/CF= 1.59 g/cm^3, EP/CF/GO 0.05 wt.% = 1.59 g/cm^3, EP/CF/GO 0.05 wt.% = 1.59 g/cm^3 and EP/CF/GO 0.5 wt.% = 1.57 g/cm^3. The average mass concentration across the 4-minute sampling period for different particle size diameters is illustrated in Figure 108.

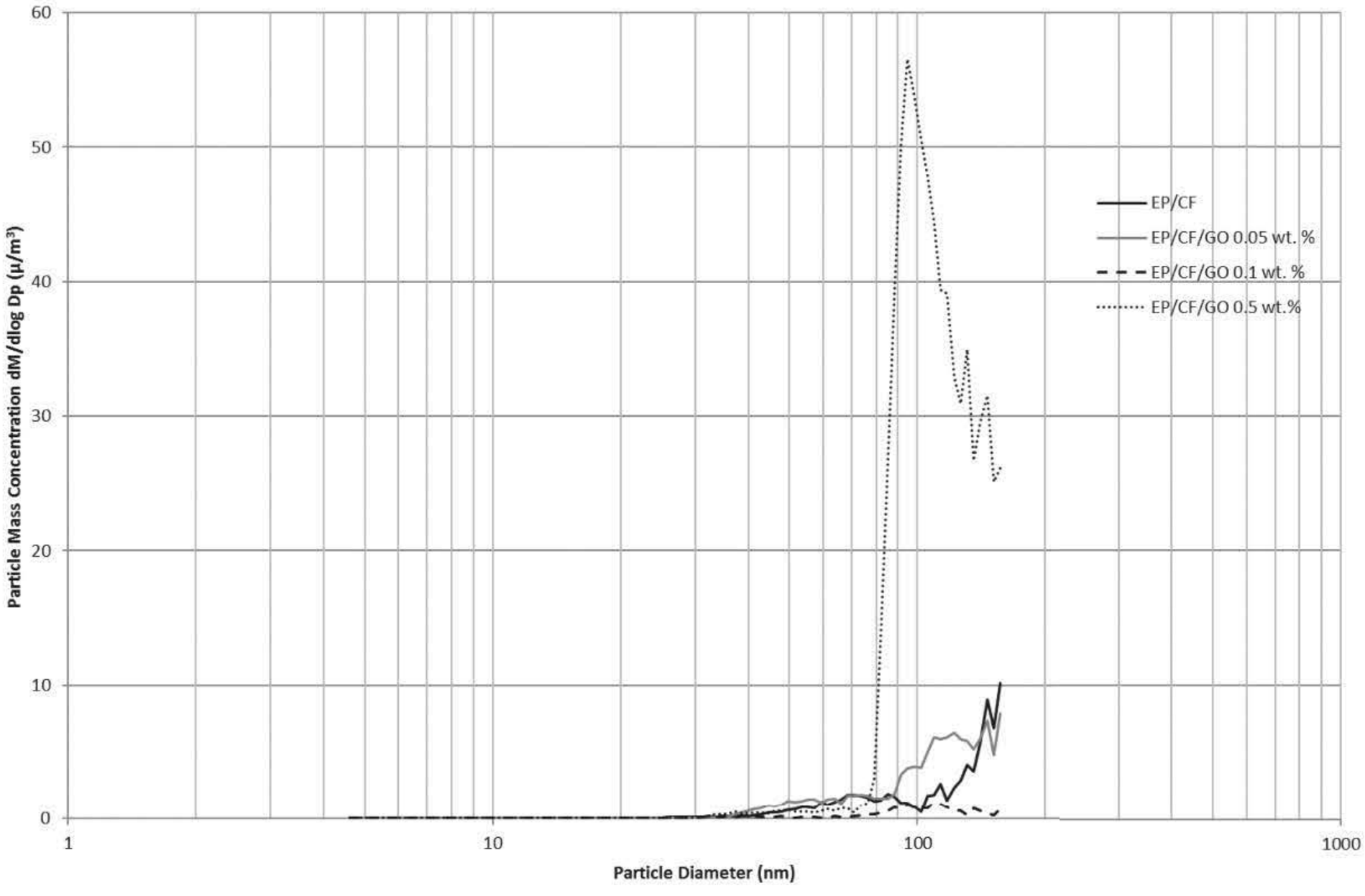

Figure 108*:* Particle mass concentration average over 4 minutes of EP/CF based nanocomposites reinforced with GO determined from SMPS (n=12 for each average).

As with the previous particle mass concentration distributions plotted within this thesis, the particle diameters with high particle number concentrations observed in the SMPS results have adjusted due to the consequent mass increase of larger particles. Almost no significant peak was perceived below 50 nm. All of the samples consequently displayed an increase in particle mass concentration in diameters larger than 50 nm up until the SMPS limit of approximately 157 nm. As with the particle size distribution, the EP/CF/GO 0.5 wt. % demonstrated the largest peak at around 100 nm. The remaining samples can be seen to observe similar relative peaks between 50 nm to 157 nm. The EP/CF/GO 0.05 wt. % and EP/CF sample displayed a similar increasing profile in particle mass concentration over 100 nm. As with the particle number concentration and particle size distribution, the EP/CF/GO 0.5 wt. % clearly demonstrated an augmenting effect in concentration, with similar mass concentrations for the remaining EP/CF, EP/CF/GO 0.05 wt. % and EP/CF/GO 0.1 wt. % samples.

Since the CPC can measure a larger particle size range, an alternative mass concentration is valuable to quantify the release. Using the particle number concentration measurement at the end of the four-minute sampling period, and the calculated total quantity of mass drilled, an estimation of the concentration of particles/mass drilled can be acquired and is presented in Figure 109. This is

calculated using the particle number concentration of the CPC (size range: 7 nm to 3000 nm), material density values and equivalent of mass drilled based on hole size and number of holes.

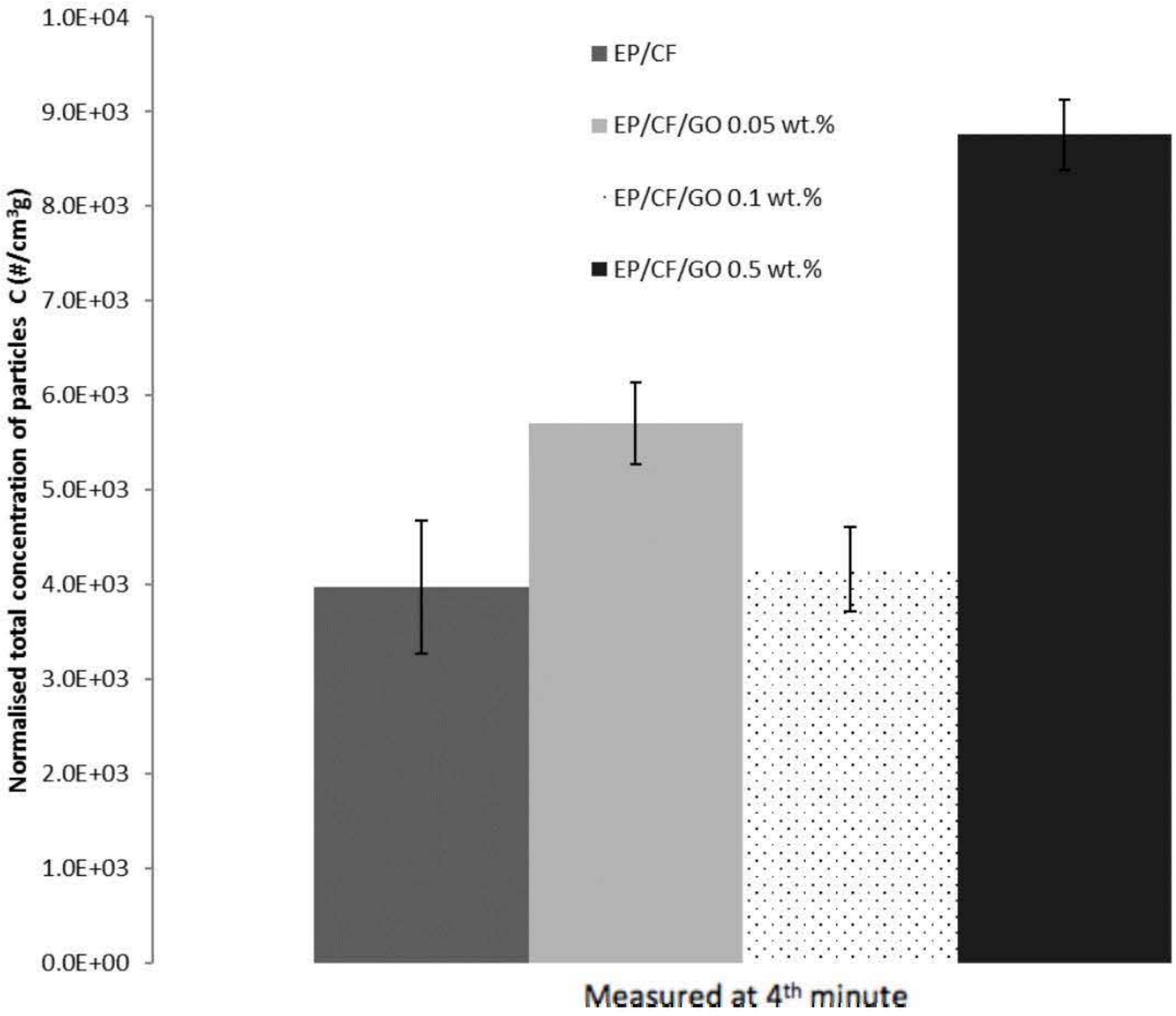

Figure 109*:* Normalised total concentration of particles (C divided by estimated drilled mass) recorded at 4th min for EP/CF based samples reinforced with GO (n=3 for each average).

The number of particles to mass drilled ratio also presents the EP/CF/GO 0.5 wt.% sample with the highest particle release over the EP/CF and other GO reinforced samples (EP/CF = 3974 #/$cm^3g_{drilled}$, EP/CF/GO 0.05 wt.% = 5702 #/$cm^3g_{drilled}$, EP/CF/GO 0.1 wt.% = 4167 #/$cm^3g_{drilled}$, and EP/CF/GO 0.5 wt.% = 8758 #/$cm^3g_{drilled}$). Since the density of the EP/CF/GO 0.05 wt.% and EP/CF/GO 0.1 wt.% sample did not change sufficiently to be measured with the addition of the GO, the correlation to the EP/CF sample is the same as the particle number concentration previously presented. However, the slight decrease in density in the EP/CF/GO 0.5 wt.% sample, means the sample observed a 118 % increase in normalised total concentration over the EP/CF sample.

As discussed within the literature review, the particle mass concentration is an important parameter when evaluating the release or exposure to nanoparticles. The data identifies important differences and supports the findings on the effect of the filler on particle number concentration and particle size

distributions. The GO at lower weight concentrations can be seen to have minimal effect on the release, whereas the EP/CF/GO 0.5 wt. % sample displayed a significant difference in comparison to the EP/CF sample.

7.3.4 Assessment of Deposited Particles

The debris collected in the chamber as described in the methodology was analysed using an SEM. An SEM image of the the debris for each sample is displayed in Figure 111. A larger magnification of the dust collected in the sampling placed underneath the drilling is shown in Figure 110.

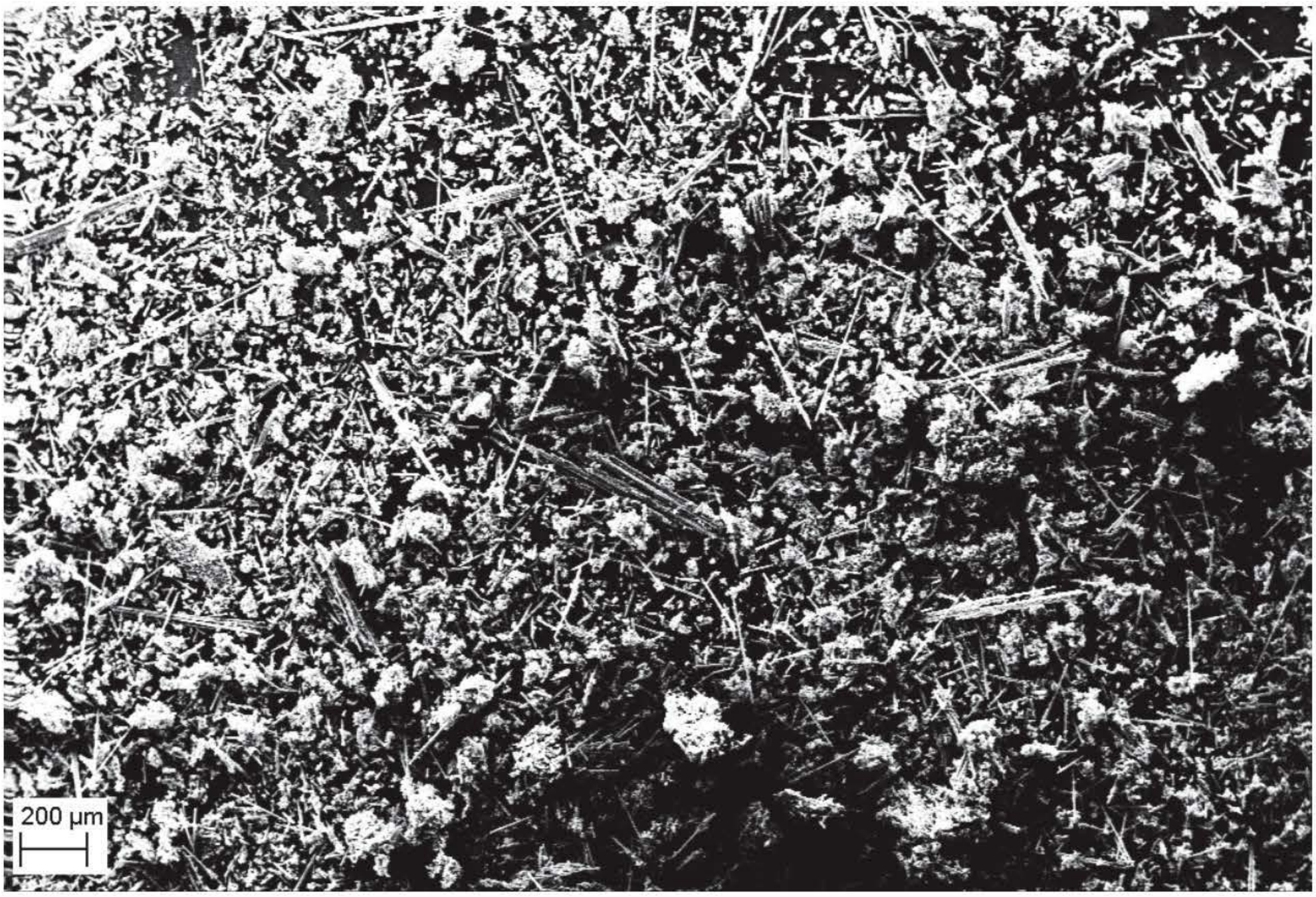

Figure 110: Deposited particles collected in sampling tray placed directly below drilling from EP/CF/GO 0.5 wt. % sample.

The deposited particles collected illustrate a large variation such as particles, agglomerates and independent fibres and matrix. The image has a relatively distant magnification which allows to display the micro-sized CFs and particle aggregation at a mirco level. The nanoparticles are therefore not distinguisable and are shown in Figure 111.

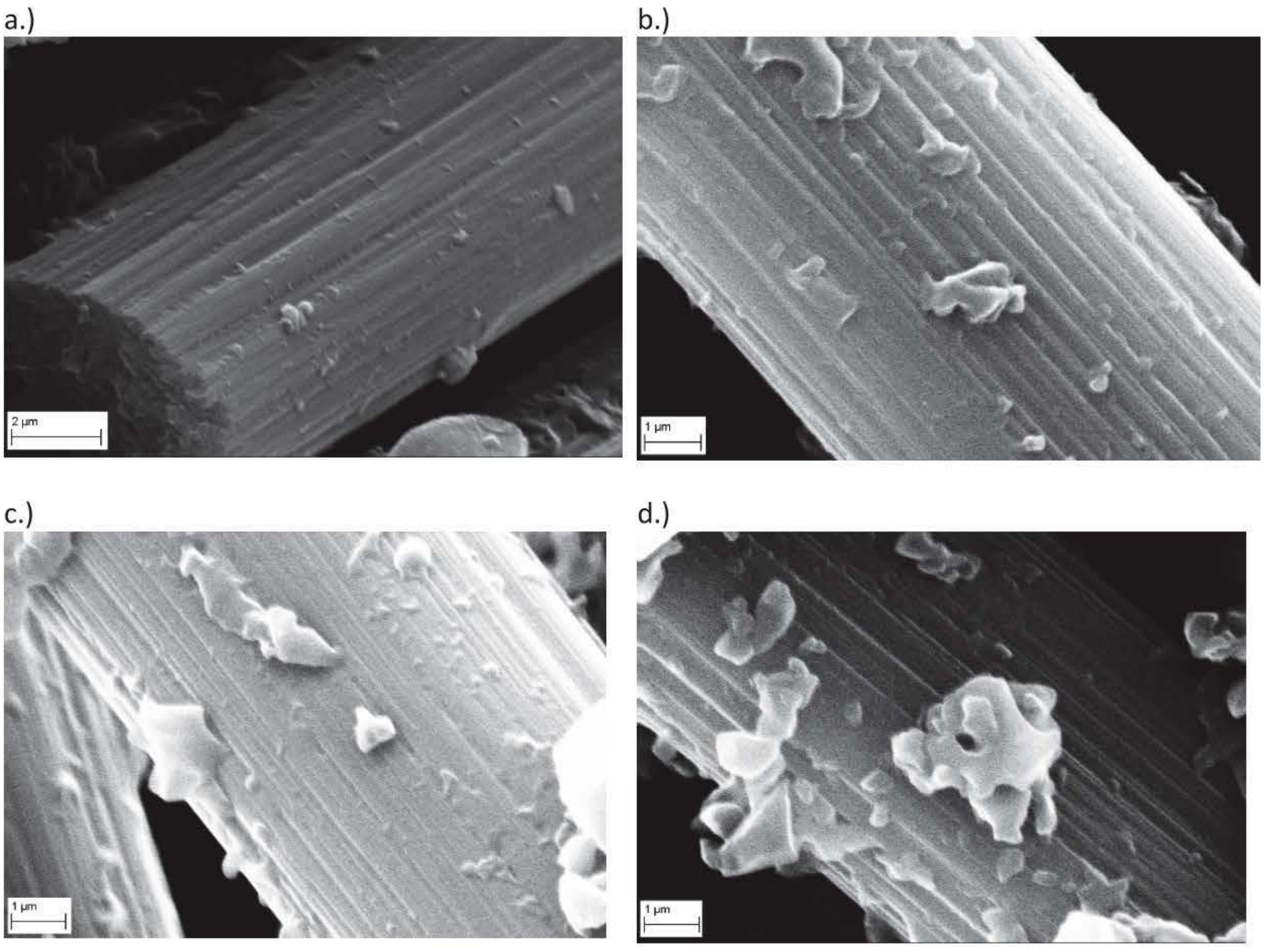

Figure 111: SEM images of deposited particles collected in sampling tray from drilling on a.) EP/CF sample, b.) EP/CF/GO 0.05 wt. % sample, c.) EP/CF/GO 0.1 wt. % sample and d.) EP/CF/GO 0.5 wt. % sample.

Within the micrscopy analysis of all the GO reinforced samples, no independent GO nanoparticles were identified. The GO reinforced samples instead were seen to demonstrate an increase in particles embedded or adhered to the surface of the CFs as can be seen in Figure 111. The neat EP/CF sample displayed significantly fewer particles attached onto the independent fibres identified within the deposited particles. The few particles attached onto the CF shown in Figure 111 a. can be attributed to the EP as no GO has been added. The GO reinforced samples however, demonstrated visibly more particles on the surface of the CFs. This can be attributed to either the GO particles and/ or EP. As demonstrated within literature and discussed within the literatuer review, GO particles are seen to improve the interfacial bonding between the CF and EP. The microscopy images of the surface of the carbon fibres with attached particles of GO and EP are in accordance with similar findings to other recent studies that have embedded GO within EP/CF samples(Luo et al., 2017; Li et al., 2019). The deposited particles therefore observed no identifable independent GO nanoparticles, and instead, were seen to increase the particles bonding to the surface of the CFs.

As can be seen in both Figure 110 and Figure 111, the majority of the nanopraticle emissions are seen to be in a fibrous form with the addition of the GO embedded or attached. The microscopy findings therefore highlight a limitation with the aerosol quantification measurements due to assuming all particles are spherical. The measurement of the particle number concentration of the CPC by creating a vapour from a working fluid (water) onto the particles to allow them to go through the nucleation via condensation to be optically counted, assumes all particles are spherical. Since the CPC measures the number of particles, this should have little affect on the particle number concentration, however may affect the particle size distribution as this also requires a CPC. The instrument assumptions on spherical particles might therefore be seen to have a slight influence on the particle size distribution if only one side of the particle is optically counted for fibres which have a signficant difference in length compared to the diameter. This therefore must be taken into consideration and a limitation of the instrumentation when evaluating the particle size distribution and has been reported as a challenge within comparing data throughout literature (Hameri et al., 2002).

The findings within deposited particles therefore, do not aid in identifying the source of the observation in increase in the particle size distribution and particle mass distributions at 100 nm. The deposited particles do not provide evidence of independent GO nanoparticles released from the embedding within the nanocomposite materials. The data however is a representation of the deposited particles collected within the sampling tray, and not the measured airborne particles through the particle quantification instruments. Within the deposited particles, the release indicates to be matrix or CF orientated with GO embedded or adhered to the surface.

7.4 Conclusion

Four EP/CF based composites were manufactured with three variations in weight concentrations of GO; 0.05 wt. %, 0.1 wt. % and 0.5 wt. %. The influence of three GO nanoparticle weight concentrations has on nanoparticle release during drilling was investigated. As with the other materials investigated within this thesis, all samples demonstrated nanoparticle release, including the neat EP/CF sample without any GO nanoparticles. Although a two sample t-test of significance of each sample mean and deviation to the neat EP/CF sample returned statistically significant differences for all concentrations of GO (outside the 95% confidence interval), the inclusion of 0.05 wt. % and 0.1 wt. % GO nanoparticles demonstrated minimal effect on nanoparticle release. However, the EP/CF/GO 0.5 wt. % demonstrated a 243 % increase in mean peak particle number concentration introduced during drilling. Similarly, at the end of the four-minute sampling period, the EP/CF/GO 0.5 wt. % sample observed a 118 % increase in comparison to the EP/CF sample. However, the minor increases observed

for the lower weight concentrations of GO reinforced samples, do not substantiate an increase in particle number concentration with an increase in GO nanoparticles (EP/CF/GO 0.05 wt. % increase of 43.5 % and EP/CF/GO 0.1 wt. % increase of 4.85 % increase from the EP/CF sample measured at the 4th minute). Nonetheless, the statistical analysis returned a statistically significant difference with the introduction of GO nanoparticles within the nanocomposites on nanoparticle release during drilling.

The particle size distribution illustrated minimal effect with the introduction of GO nanofillers at 0.05 wt. % and 0.1 wt. % in comparison to the EP/CF sample. As with the particle number concentration, the EP/CF/GO 0.5 wt. % can be concluded to have influenced the particle size distribution quite significantly. However, due to the particle size diameters the peaks cannot be associated to independent GO nanofillers, and instead either agglomerations or matrix-filler embedded particles.

The particle mass distribution displayed similar findings, with the EP/CF/GO 0.5 wt. % sample demonstrating a significant difference in comparison to all other samples. All of the samples displayed an increase in particle mass concentration in diameters larger than 50 nm up until the SMPS diameter limit of approximately 157 nm. The EP/CF/GO 0.5 wt. % sample peak particle mass concentration is observed at similar diameters as the EP/CF sample, and can therefore be understood to not alter the particle diameter, but instead, influence the particle mass concentration. This correlation indicates the release to be associated to the EP/CF as opposed to independent GO fillers. Correspondingly, the assessment on the deposited particles displayed no evidence of independent GO nanoparticles. The GO reinforced samples were instead seen to demonstrate an increase in particles embedded or adhered to the surface of the CFs.

Therefore, although the EP/CF/GO 0.5 wt.% sample displayed an influence on the particle number concentration, particle size distribution and particle mass distribution, no significant evidence leads to independent GO nanoparticles to be released. Nonetheless, all three instruments used to quantify the airborne released particles (CPC, SMPS & DMS50) exhibited a harmonised increase in particle number concentration from the EP/CF/GO 0.5 wt. % sample in comparison to all other samples.

Chapter Eight

Overall Discussion

8.1. Introduction

The investigation into the different materials have shown different conclusions for the infleunce of the nanofillers on nanoparticle release during drilling. The aim of this chapter is to correlate, evaluate and discuss the results. Prior to this study, and as highlighted within the literature review, there was limited knowledge on the influence nanofillers have on nanoparticle release from nanocomposites during drilling. Literature has reported that processes of high-energy input on nanocomposite materials have provided evidence that inhalation exposure occurs (Basinas et al., 2018; Debia et al., 2016). The findings from the literature review demonstrate that although remarkable progress has been made in understanding the influence of nanoparticles on nanocomposite properties and release of nanoparticles, the review also highlights the urgent need for continued development and more data. This chapter provides on overall discussion on the materials investigated within this thesis.

8.2. Influence of Filler

A comparison of all the nanocomposite materials studied within this thesis found significant differences with the introduction of the nanoparticle reinforcement. Depending on the polymer, filler and weight concentration, the nanoparticle fillers displayed both an increase and decrease on the particle number concentration in comparison to the sample without nanoparticle reinforcement. In some instances, statistical analysis on the results reject a hypothesis that the samples displayed no difference in peak particle number concentration, and therefore can be concluded to have an effect on the nanoparticle release. A comparison of the particle number concentrations measured at 4 minutes for all of the samples tested in illustrated in Figure 112.

Due to the substantial differences in particle number concentrations, the PP-based samples and EP/CF based samples are barely visible. The EP-based samples can be seen to release the highest concentration of nanoparticles. A more suitable comparison to evaluate the influence of nanoparticles in reference to the neat polymer is shown in Figure 113. Although samples, such as the PP/Talc and

PP/MMT, displayed a statistically significant difference in the mean particle number concentration in relation to the neat PP (statistically significant decreases), neither of the differences are evident in Figure 112.

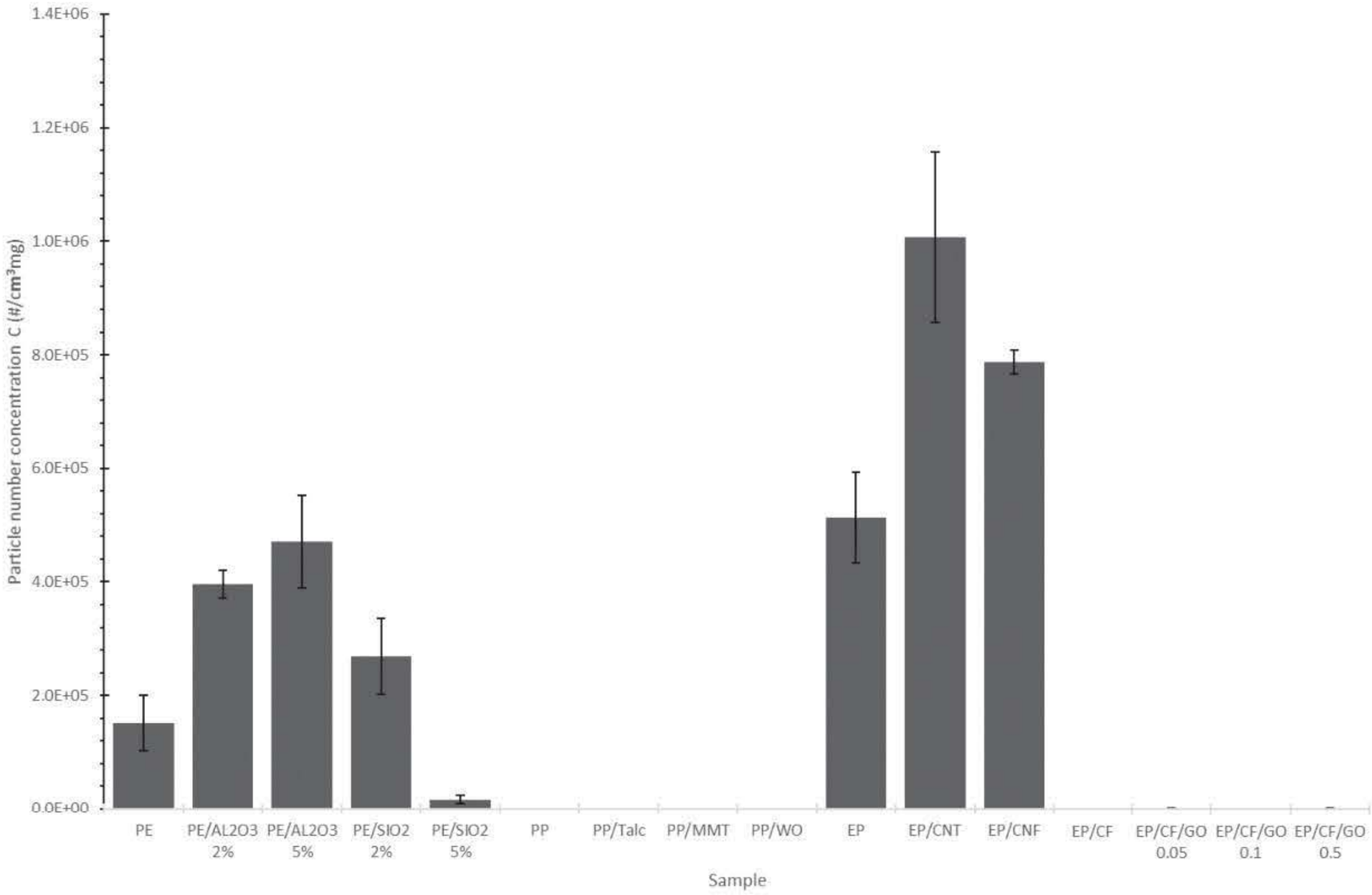

Figure 112*:* Comparison of average particle number concentration measured at the 4th minute with CPC for all nanocomposite samples (n = 3 for each average).

The percentage increase in comparison to the reference polymer, shown in Figure 113, demonstrate the influence the nanoparticle fillers have on particle number concentrations. From the twelve samples investigated with the incorporation of nanofillers, ten demonstrated a statistically significant difference in a two-sample t-test of significance of each sample mean and deviation to the reference sample (test of 95% confidence interval). The results therefore demonstrate, of the samples investigated on the influence of nanoparticles within nanocomposite materials on nanoparticle release during drilling, 83 % exhibited a statistically significant influence on average particle number concentration. Eight out of twelve nanocomposites (67%) displayed a statistically significant increase, and two (17%) displayed a statistically significant decrease in the particle number concentration release during drilling in comparison to the reference materials without nanoparticles.

The nano-sized Al_2O_3 reinforcement within polyester nanocomposites observed to have the biggest influence on particle number concentration, with a 211 % and 162 % increase exhibited from the PE/Al_2O_3 5 wt. % and PE/Al_2O_3 2 wt. % respectively.

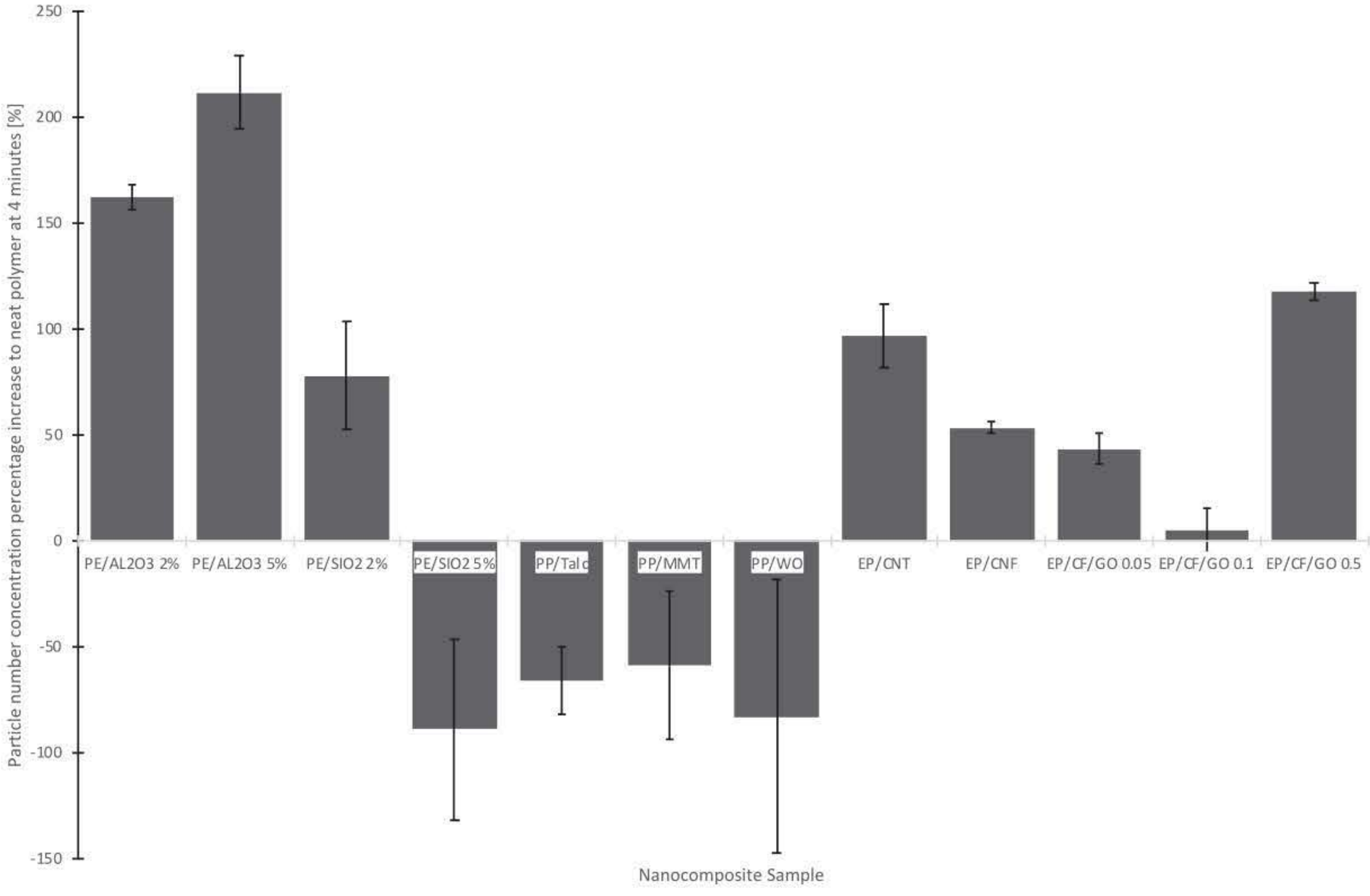

Figure 113*:* Comparison of nanocomposite percentage increase in particle number concentration measured at 4th minute in relation to neat polymer measured with the CPC (n = 3 for each average).

The low concentrations observed from the PP-based samples, revealed a high standard deviation within samples, and therefore also demonstrated similar percentage decreases in comparison to the neat PP (PP/Talc = 66 %, PP/MMT = 59 %, PP/WO = 83 % decrease). In contrast, the carbon nanofillers within EP observed a statistically significant increase on the EP matrix (EP/CNT = 96 % and EP/CNF = 53 % increase). Whereas, the PE based samples observed dissimilar trends due to the reinforcement concentrations (PE/SiO_2 2 wt. % = 78 % increase, PE/SiO_2 5 wt. % = 89 % decrease). The different weight concentrations of GO within EP/CF samples, reveal that there is no direct correlation between weight concentration within the nanocomposite and influence on particle number concentration. The samples displayed an increase in particle number concentration with 0.5 wt. % and 0.05 wt. % GO, but minimal effect with 0.1 wt. % GO (EP/CF/GO 0.05 wt. % = 43 % increase, EP/CF/GO 0.1 wt. % = 5 % increase, and EP/CF/GO 0.5 wt. % = 118 % increase).

In view of the fact that the GO reinforced samples demonstrated the filler weight concentration within the nanocomposite alone does not correlate to the influence particle number concentration (i.e. increase in weight concentration does not demonstrate an equivalent increase in particle number concentration), the influence on particle number concentration can be compared with the influence on mechanical properties. With all other parameters unchanged, the only change in parameter is the

nanocomposite composition. The comparison between the influences of reinforcement fillers with the neat PP is shown in Figure 114.

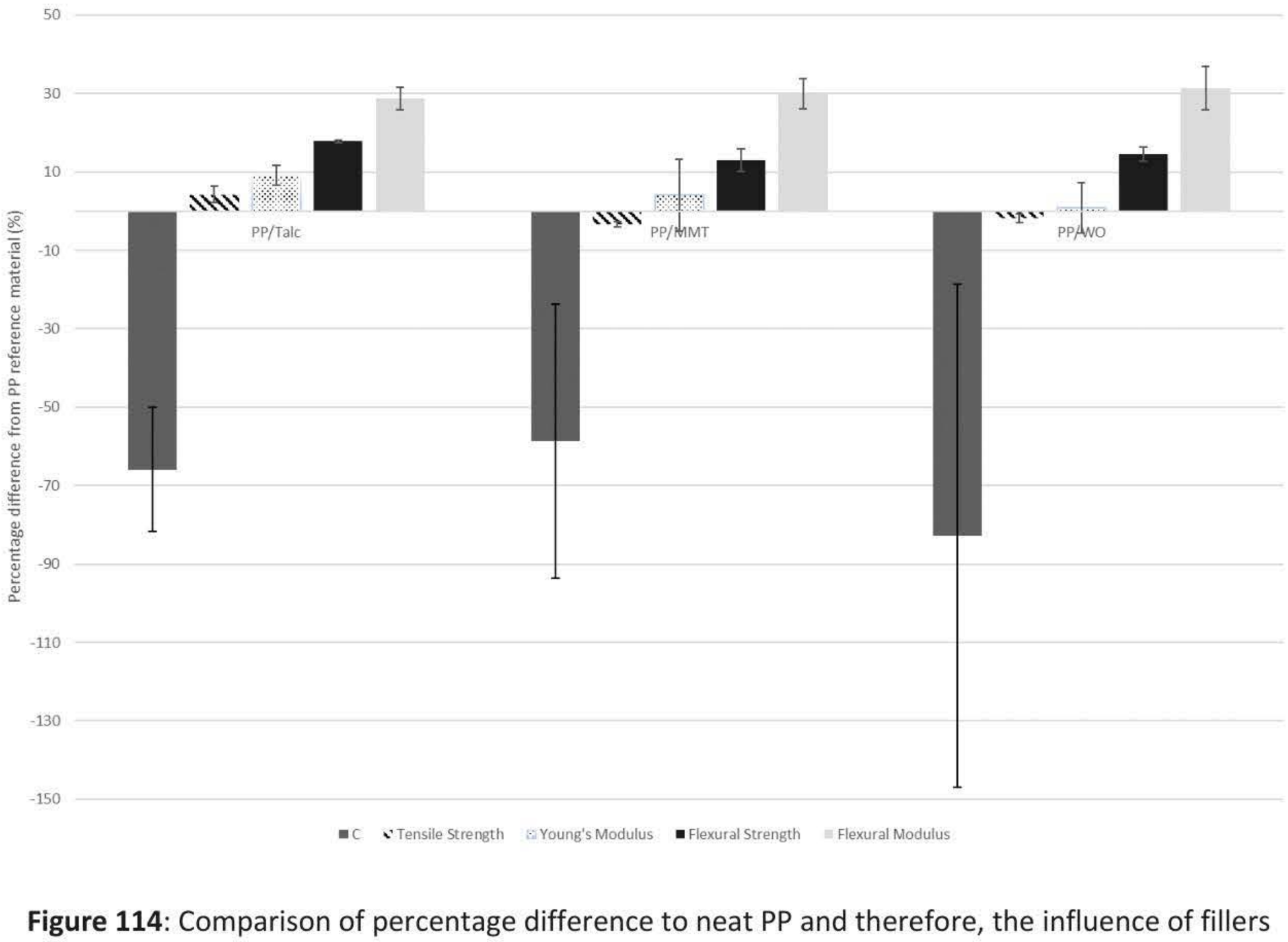

Figure 114: Comparison of percentage difference to neat PP and therefore, the influence of fillers within PP-based samples on particle number concentration (C), tensile strength, Young's Modulus, flexural strength and flexural modulus (Note high standard deviations are observed due to the combined deviations of each sample and neat PP).

The influence of the fillers on mechanical properties can be seen to be relatively less than the influence on particle number concentration. The use of reinforcing fillers within PP demonstrated to have little effect on the tensile properties, however, a statistically significant improvement in flexural properties and a statistically significant difference in particle number concentration for the PP/Talc and PP/MMT. The two nanofillers are layered silicates and known to have an octahedral substituted structure (Selvakumar et al., 2010). Talc on the other hand has a platy or layered structure of two silica tetrahedral fused to an edge-shared octahedral sheet of magnesium hydroxide (Hadal et al., 2004). The octahedral substituted structure in the nanofiller is known to be challenging in interacting with polymer matrices (Selvakumar et al., 2010), due to the inorganic filler having a polar surface, and was therefore mixed with a coupling agent (Polybond 3200 from ADDIVANT) to ensure adhesion between the fillers and the PP. The coupling agent works to improve the interfacial adhesion between the layered silicates and the PP. The adhesion between WO and PP is a particular topic of research within

literature, attempting to create strong bonds between the acicular forms with PP. In a study by (Svab et al., 2005), the correlation between adhesion parameters of PP and WO is calculated, based on surface free energies of pure components and the contact angle method and mechanical properties of the corresponding composites. The study highlights how strong interactions in the composites were found with high surface free energy WO lead into the improved tensile properties of the composite material. The strong adhesion in the PP/WO composites is reflected with higher yield stress and tensile strength at break, but in lower elongation at break (Svab et al., 2005). The tensile properties achieved within this study, did not demonstrate an increase in properties, rather a statistically insignificant change but with a decrease in density. However, the flexural properties demonstrated a statistically significant increase in comparison to the virgin PP sample and attaining similar properties to the PP/Talc sample. The PP/WO increase in material properties also observed the highest mean particle number concentration in the release, however the sample also observed the largest standard deviation and subsequently returned to not shown a statistically significant difference in comparison to the neat PP.

Achieving the material properties is correlated to achieving good interfacial adhesion and associated to intercalated structures of the nanofillers within the polymer crystal lattice and exfoliated filler structures within the material (Selvakumar et al., 2010; Weon and Sue, 2006). Literature has reported on where exfoliation has shown to increase stiffness of the nanocomposite with increasing clay content, the impact strength and tensile ductility have shown a decrease (Tjong, 2006, Park & Jana, 2003). The mixing of the nanofillers within the PP and failure to identify the fillers on the surface can be reasoned with the intercalation within the polymer lattice. Furthermore, the low weight concentration has shown to be challenging to identify within literature (Luyt et al., 2009; Dev et al., 2015; Dasari et al., 2004). As mentioned within Chapter Three, studies also demonstrated similar influence in material properties with the use of the nanofillers (Selvakumar et al., 2010; Samal et al., 2008; Chen et al., 2008). The improved flexural properties can therefore be attributed to the successful bonding between the nanofillers, but with minimal effect on the tensile properties. The only association between the mechanical properties and release however, is with an increase in flexural properties, a decrease in particle number concentration was observed for the PP based samples.

This is the first study to compare the nanoparticles release of MMT, talc and WO together within PP during drilling. However, the decrease in particle number concentration with the introduction of MMT within polyamide was also observed in nanoparticle release studies during drilling by *Irfan et al. (2013) and Sachse et al (2012b*). Both studies used 5 wt. % of MMT, which therefore support the findings within this thesis. Whilst the fillers can be concluded to have an influence in decreasing the release during drilling, the material properties do not shown a direct correlation to the nanoparticle release.

To support the findings within this project, the PP based samples were tested for particle emissions from machining in collaboration with another project funded by CSIRO (Commonwealth Scientific and Industrial Research Organisation) in Australia and Nanosafety Stream of the Advanced Materials Transformational Capability Platform (AMTCP). The findings of this report are published in *Schutz JA, (2015)*.

The methodology used in *Schutz JA (2015)*, used a hermetically sealed aerosol test environment with a stream of test gas (nitrogen) to entrain the airborne particles for detection. This method requires a significantly large area and expense to measure the released particles. The particle concentration and size was measured using an Optical Particle Sizer (OPS, TSI Model 3330, 16 channels from 0.3 µm to 10 µm) and a CPC (CPC, TSI Model 3007, 1 channel, 0.01 µm to 1.0 µm). An Aciera F3 Universal Mill with 10 mm mill-cutter at 1250 RPM was used to machine 5 cm long section of the PP samples. Contrasting to this methodology used within this project, the methodology in Schutz JA (2015) quantifies the release over a background noise.

Figure 115 illustrates the results from the report. The results are expressed in a diverse style due to the use of alternative nanoparticle quantification equipment and methodology. The particle size distribution is demonstrated in the contour plots on the leftward side of the figure. The representation denotes the same 3D plots from the DMS50 data presented in section 4.3.2 with the particle size distribution measured across the sampling time. The concentrations are graded to a colour scale (see legend) as a function of time (abscissa) and particle diameter (ordinate). The figure also represents the particle concentration changes over time from the CPC data, comparable to the results presented in section 4.3.1.

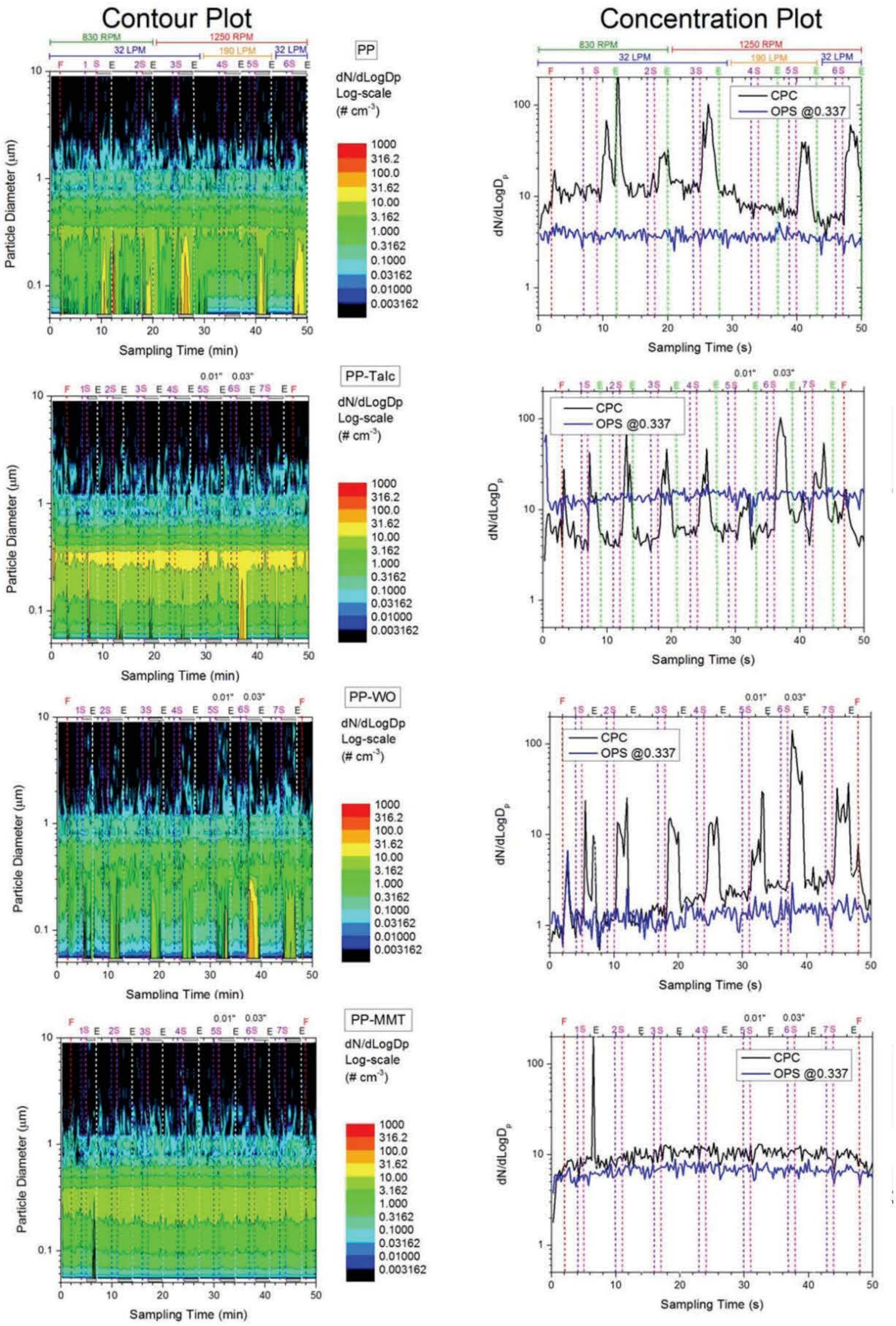

Figure 115*:* Airborne particle release generated from milling of PP based samples (Schutz JA, 2015)

The report found that all samples, excluding the PP-MMT sample to clearly demonstrate correlated increase for particles smaller than a 300 nm diameter and minimal differences for particles larger than 300 nm. The specific detector limitations of the equipment used provide a limited comparison between the particle size distributions. Nonetheless the findings within the article on the particle size distributions support the findings within this thesis. The DMS50 was capable of measuring particles within the size range of 4.87 nm – 562.34 nm. The results indicate no influence in particles larger than 100 nm. And both the SMPS and DMS50 results established particles released and differences below 100 nm, including the PP-MMT sample.

In relation to the particle number concentration, *Schutz JA (2015)* reported the PP-MMT sample exhibited no evidence of detectable airborne release above the particle background noise. From Figure 115, the samples can be seen to release particle peaks in the 100 #/cm^3 range. The report summarised the findings in order of particle number concentrations (where two larger than symbols represent more substantial difference) as:

PP-MMT << PP-Talc < PP < PP-WO

The conclusions on the particle number concentration results are diverse from the measurements at the 4th minute represented in Figure *114* (PP/WO < PP/Talc < PP/MMT << PP). However, a comparison to the findings from the peak particle number concentrations introduced from the materials shows similar findings (PP/Talc < PP/MMT < PP < PP/WO). From the peak particle number concentrations measured on the CPC data as presented in Table 18 in section 4.3.1., the PP/Talc released the lowest peak, followed by PP/MMT, PP, and the PP/WO releasing the highest peak particle number concentration. It is important to note that comparing the two studies highlights the need for a standardised methodology in evaluating nanoparticle release due to a variation in background, method and sampling size ranges in the equipment used. However, the findings of the nano-reinforced samples in comparison demonstrated equivalent conclusions in relation to the neat PP sample, with the PP/WO producing an increase in particle number concentration and the PP/MMT demonstrating a decrease in peak particle number concentration. Nonetheless the relative unison of results on the influence of nanofillers on nanoparticle release from the same set of samples testifies a level of consistency in the methodologies used. The method used within this thesis is able to provide the particle number concentration without background interference and an expanded analysis of the release of particles from the samples during drilling. The limitations found in other studies and specifically to the data collected for Figure 115, are addressed in the design and allow for an investigation into the particles release without having to consider the influence of background particles.

As with the discussion on the PP-based samples, the influence of the nanoparticles used within the PE on particle number concentration and mechanical properties is shown in Figure 116.

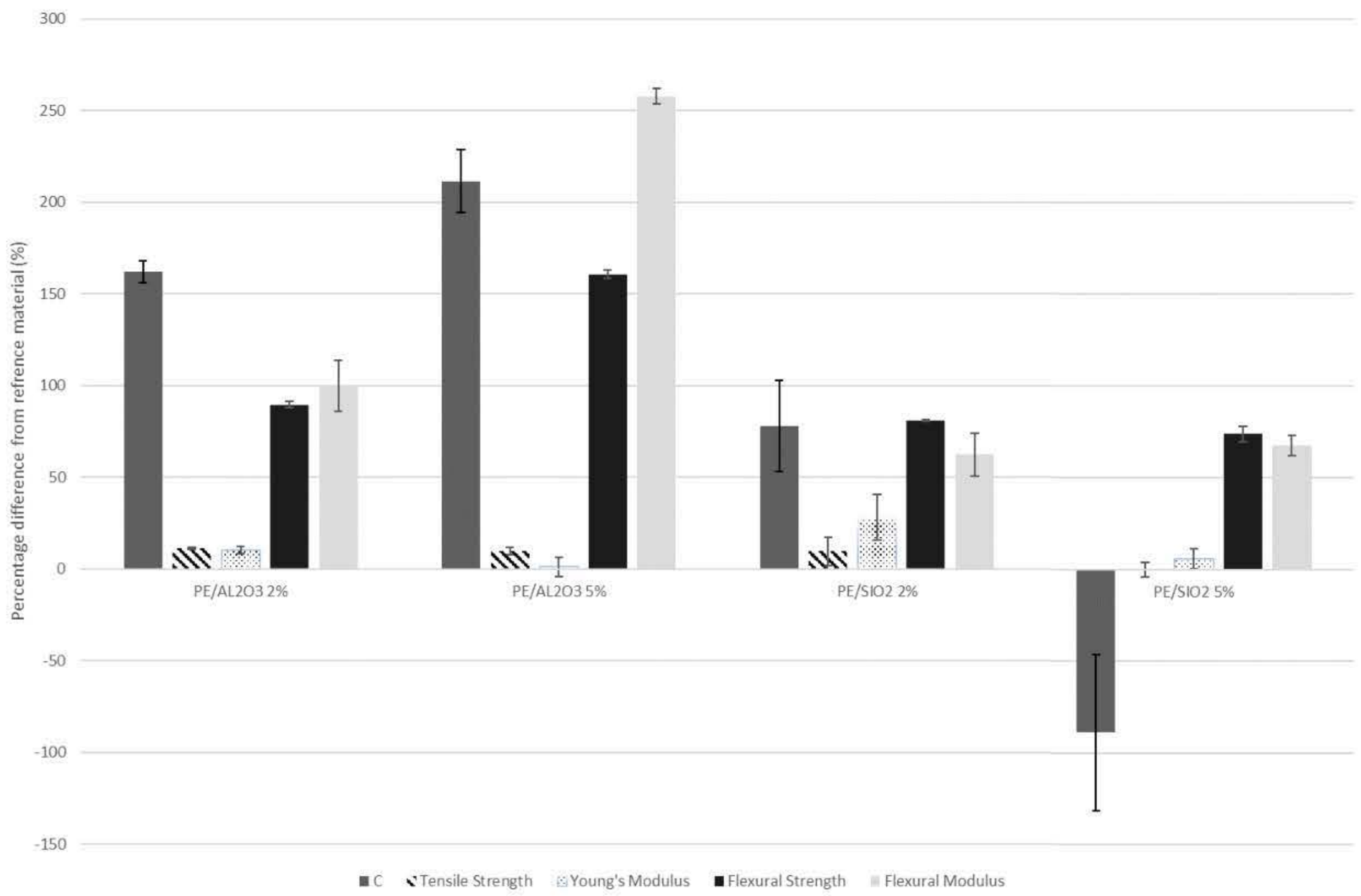

Figure 116: Comparison of percentage difference to neat PE and therefore, the influence of fillers within PE-based samples on particle number concentration (C), tensile strength, Young's Modulus, flexural strength and flexural modulus (Note high standard deviations are observed due to the combined deviations of each sample and neat PE).

The nano-sized fillers used to modify the PE-based samples exhibited a comparable minimal influence on the tensile properties, but a more substantial increase in flexural properties. The Al_2O_3 exhibited a statistically significant increase in tensile strength whereas, the SiO_2 demonstrated an increase in tensile modulus. Both nano fillers displayed a statistically significant increase in flexural properties, with the Al_2O_3 at 5 wt. % demonstrating the highest improvement. The mechanical properties agree with literature as studies have demonstrated more than 5 wt. % alumina is needed to see reduction in mechanical properties due to the start of agglomeration of particles in the matrix (Baskeran et al., 2011).The increase in mechanical properties however does not directly correlate to the influence on nanoparticle release.

The influence on mechanical properties due to the fillers is associated to the interfacial adhesion between the Al_2O_3 or SiO_2 nanoparticles and strong filler/PE cross-linking (Ribeiro et al., 2015). SiO_2 nanoparticles tend to be more hydrophilic which can explain the minimal influence in tensile properties and lower improvement in flexural properties. Studies have found similar conclusions with a peak mechanical performance at 2 wt. % and reduction in properties with further increases in weight concentration for SiO_2 (Rusmirovic et al., 2016; *Trinath et al., 2016*). Incorporating more than 3 wt. % of SiO_2 observed to cause formation of aggregates and agglomerates creating defects in the cross-linked between polymer-nanofiller. This is associated to the nature of the functional groups present on the surface of the SiO_2 and PE chain providing a high intensity π, π-stacking attractive interaction. The minimal influence on mechanical properties with higher than 2 wt. % SiO_2 weight concentrations, correlates to a decrease in particle number concentration in the release. A relationship is therefore to some extent, evident. An increase in flexural properties from 2 wt. % to 5 wt. % Al_2O_3 demonstrated an increase in particle number concentration. Although there is a decrease in mechanical properties from the Al_2O_3 to the SiO_2 samples which demonstrate a decrease in particle number concentration, this is not confirmed if taken into comparison with the neat PE sample. The samples therefore do not show a direct correlation between particle release and tensile and flexural properties.

The decrease in particle number concentration observed for the PE/SiO_2 5 wt. % sample indicates a slight modification in the reinforcement quantity, will affect the release characteristics. Although the PE/SiO_2 2 wt. % and PE/SiO_2 5 wt. % observed similar mechanical properties, the two samples differ significantly in particle number concentration. This trend opens a new concept to tailoring the material to reduce the nanoparticle release without significant influence on the material properties and is subsequently an opportunity to act as a safety by design concept.

The particle number concentration from the EP-based samples was compared to the mechanical properties and is shown in Figure 117. The CNTs exhibited a more significant improvement in flexural properties over tensile properties. The EP/CNT 2 wt. % sample displayed a statistically significant increase in Young's Modulus, flexural strength and flexural modulus. The results correlate to a statistically significant increase in particle number concentration in the release during drilling.

CNTs are a relatively new allotropy of carbon, composed of extremely thin hollow cylinder which individually have shown extraordinary properties. The filler is constructed of purely carbon atoms linked in hexagonal shapes, with each carbon atom covalently bonded to three other carbon atoms (*Ajayan et al., 2001*). The strength of the nano fillers is reported due to this extremely strong molecular interaction and chemically bonding with sp^2 bonds. Similar to other nano particles, the fillers tend to rope together via van der Waal forces and agglomerate. A homogenous dispersion and alignment

inhibit agglomerations and provides better load transfer to the CNTs and away from the weaker polymer matrix (Velasco-Santos et al., 2003). There are several other causes which are attributed to the variation in material properties with similar weight concentrations. Mittal et al. (2015) reported an extensive review in which carbon nano fillers are appraised to identify the correlation between the filler and material properties. The report concluded that along with the difference in polymer and nanofiller, factors demonstrated to affect the material properties include: dispersion, aspect ratio, length of CNTs and alignment of CNTs into the matrix (Mittal et al., 2015). The increase in material properties can therefore be attributed to a successful dispersion of the CNTs within the EP which consequently exhibited an increase in particle number concentration.

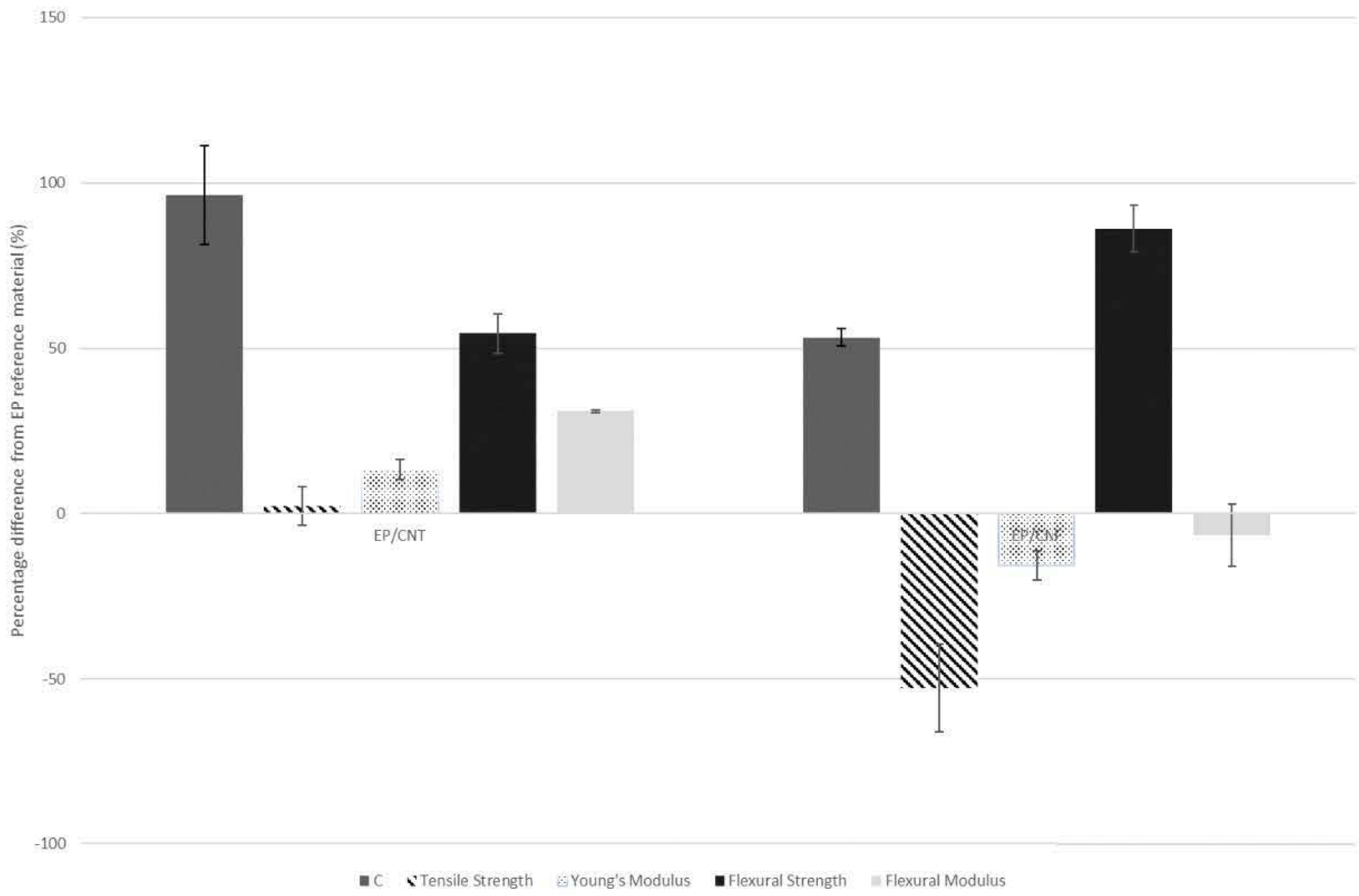

Figure 117: Comparison of percentage difference to neat EP and therefore, the influence of fillers within EP-based samples on particle number concentration (C), tensile strength, Young's Modulus, flexural strength and flexural modulus (Note high standard deviations are observed due to the combined deviations of each sample and neat EP).

In contrast, the incorporation of CNFs within the EP-nanocomposite observed a statistically significant decrease in tensile strength. However, a statistically significant increase in flexural strength was also observed. The decrease in material properties in tensile strength is generally conflicting with literature, such as Zhu et al. (2010) which demonstrated an increase in tensile strength up to 1 wt. % CNF, or a study by Zhou et al., (2007) reporting a 17.4 % tensile strength increase with 2 wt. % CNF in

comparison to neat EP. However, more literature is reported on the increase in flexural strength such as: a study by Zhu et al. (2010) having demonstrated a 12.6 % improvement in flexural properties with 0.1 wt. % CNFs, a 10 % increase in flexural strength with 0.25 wt. % CNFs (Shokrieh et al., 2014), or a 49 % increase in flexural modulus with 1 wt. % CNFs (Bal, 2010) in comparison to neat EP samples. The property improvement is attributed to the covalent bonding between CNFs and the EP between the functional groups on the wall of CNFs and epoxide groups (Zhu et al., 2010). The covalent bonding thus restricts the mobility of the main chain of the EP resin by the adhesive interfacial forces between the filler and matrix. The larger decrease in strength in comparison to Young's modulus indicates the CNFs are forming less elastic interfacial layer between the CNFs and matrix, which is more sensitive to tensile loading over flexural loading which is also illustrated in the decrease in elongation at break. This can be correlated into effecting the nanoparticle release, and a source of the small increase in comparison to the CNT sample. However, in comparison to the neat EP, the material properties do not show a correlation with the particle number concentration. Although both samples displayed an increase in flexural strength and particle number concentration, the higher increase in flexural strength observed from the EP/CNF sample demonstrated a lower increase in particle number concentration. The influence on release can therefore not be concluded to correlate to the influence in mechanical properties investigated.

The mechanical properties and particle number concentrations were correlated for the EP/CF/GO samples and are presented in Figure 118.

The use of GO as a nanofiller displayed conflicting effects on the mechanical properties and particle number concentration from the EP/CF hybrid composites. The EP/CF/GO 0.05 wt. % sample displayed the most significant improvement in mechanical properties with a statistically significant increase in flexural strength, flexural modulus and Young's Modulus in comparison to the EP/CF sample. This resulted in a statistically significant increase in particle number concentration, but lower than the increase introduced from the EP/CF/GO 0.5 wt. % sample. The 0.1 wt. % GO observed a decrease in all mechanical properties, whilst the 0.5 wt. % GO displayed a statistically significant increase in both Young's and flexural modulus, but a decrease in related strengths. These results contrast to several studies that show an increase in mechanical properties with low weight concentrations of GO and a decrease from after a threshold quantity. A study by Pathak et al. (2016), found the peak mechanical performance at 0.3 wt. % GO with a clear decrement in properties from 0.4 wt. % GO. In contrast, a study by Hung et al., (2019) observed maximum flexural properties at 0.5 wt. % GO, followed by a decline. However, no studies were found to have reported on the mechanical properties with concentrations lower than 0.1 wt. % GO added to EP/CF and is therefore the first reporting of such.

Similarly, no studies have reported on the release of GO from EP/CF hybrid composites and is therefore also the first reporting of such.

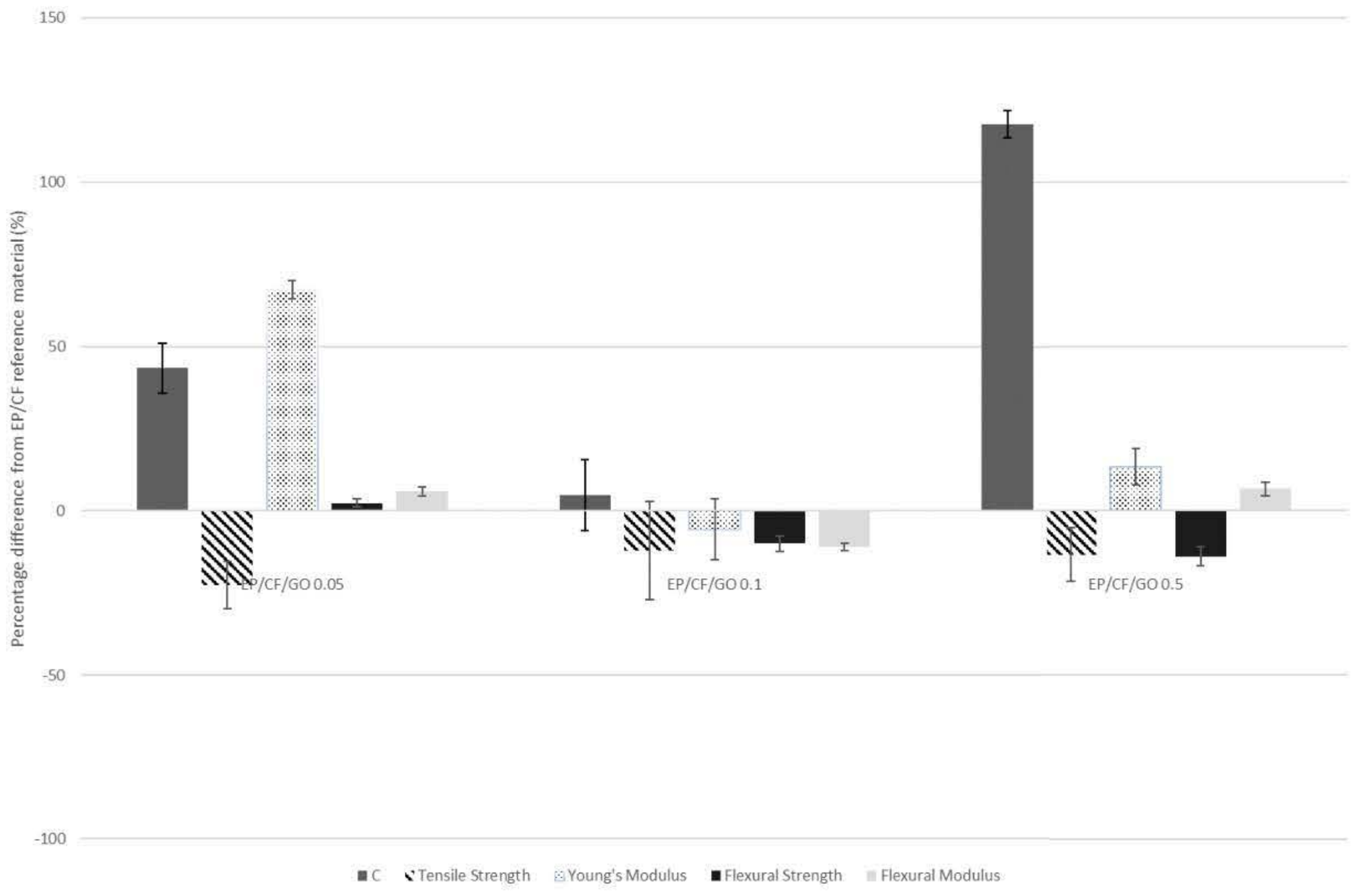

Figure 118: Comparison of percentage difference to the reference EP/CF and therefore, the influence of fillers within EP/CF-based samples on particle number concentration (C), tensile strength, Young's Modulus, flexural strength and flexural modulus (Note high standard deviations are observed due to the combined deviations of each sample and reference EP/CF).

Among literature, the improvement to the bonding between the CF and polymers has shown that oxidative treatments or particles that can generate –OH (observed in FT-IR study in Chapter Three) or –COOH groups on the fibre surface will act as coupling or bonding agents (Wu et al., 2015). GO can effectively enhance the interfacial adhesion as the sp^2 structure of the GO is prone to attach onto the surface of the CF by π-π stacking interaction (Deng et al., 2016). The improved bonding and interfacial adhesion between the matrix, GO and CF allows for an optimisation in stress transfer between the softer matrix of the polymer phase, to the CF (Hung et al., 2017). The limit of GO content is said to be at the point where GO initiates to bond with the hardener and hence prevent the interface between the epoxy and hardener. The cross-linking therefore is reduced, resulting in weaker interfacial interaction (Pathak et al., 2016). The peak concentration was not evident in either the material properties or nanoparticle release. The 0.1 wt. % GO sample demonstrated the least influence on mechanical properties and also nanoparticle release. However, improvement in mechanical

properties observed from the 0.05 wt. % and 0.5 wt. % GO samples did not show a correlation to the particle number concentration increase. Therefore, although the GO nanoparticles can be seen to influence the particle number concentration and mechanical properties, no correlation between weight concentration and the subsequent mechanical properties or nanoparticle release are evident.

As discussed within the literature review, there is currently no method of accurately predicting the mechanical performance and nanoparticle inclusion within nanocomposite materials. Attempts at modelling the correlation between nanoparticle filler and mechanical properties have led to several simplified theories such as the Halpin-Tsai composite theory (Mallick, 2007), Mori-Tanaka average stress theory (Odegard et al., 2005), and work by Zare (2016) as a selected few. Work by Pukansky and Voros (1995 and 2002) developed a semi-quantitative model to evaluate the interfacial adhesion between nanoparticles, such as SiO_2 and polymer matrixes. The model proposes a method to quantify the interfacial strength related to the volume fraction of particles, stress in the matrix, stress in the particles and a proportionality constant "k" (Bray et al., 2013). The model works on the hypothesis of being able to use reported magnitudes of k, which is limited for most nanomaterials entirely dependent on the interphase region, and various assumptions, such as no voids present or plastic void growth prior to fracture. Other attempts at specific nanoparticle filler/matrix combinations such as work by Zhang et al. (Zhang et al., 2006) for SiO_2 and epoxy, have demonstrated some predictions, but unable to support their hypothesis with experimental evidence (Bray et al., 2013; Domun et al., 2015). A review of modelling or attributing theoretical equations to nanocomposite materials by Hu et al. (2010) concluded that despite progress in the past decade, models are limited and the field faces several challenges in developing solution strategies. A later review by Armbrister et al. (2015) had a similar conclusion, stating that from the available literature, numerous complexities still arise when comparing any composite theory to experimental data.

Similarly, and as discussed within the literature review, only six few studies have evaluated the influence of nanoparticles on nanoparticle release during drilling (Bello et al., 2010; Sachse et al., 2012a, b; Irfan et al., 2013; Gendre et al., 2015; Ding et al., 2017). All of the studies observed nanoparticle release and have highlighted the potential hazard and exposure to humans which needs to be understood. From study by Bello et a. (2010) that investigated a comparison between drilling and cutting on the same nanocomposites, drilling demonstrated the higher quantity of nanoparticle release. The effect of filler/polymer and filler concentration on nanoparticle release during machining is yet to be understood. The findings within this thesis provide data on the influence of the various nanocomposite materials. As with the conclusions within literature on the influence of nanoparticles on nanocomposite material properties (Hu et al.,2010; Armbrister et al.,2015), the correlation between nanoparticle and effect on nanoparticle release is challenging. The results are in unison with

multiple reports or reviews in the complexity in nanoparticle release data from the nanoparticle fillers. A quote from an article by Hankin and Read (2016), appropriate to the findings within this study, however relating to the current knowledge of risks associated with nanotechnology, stated "research conducted to date has shown the potential risks of nanotechnologies to be associated with a high degree of complexity and uncertainty, with no clear-cut cause-and-effect relationship".

Although there is currently no predictive model on the release of nanoparticles from nanocomposite during drilling, the closest literature is on the production of emissions from drilling on metals (e.g. Songmene et al., 2011; Songmene et al., 2015; Niknam et al., 2014). The life of a drill tool is of extreme interest within the machining of metals, and the formation of chips has been linked to the type of drilling tool. Studies have therefore attempted to correlate the emissions produced from drilling on metals. The study by Songmene et al. (2011) attempted to evaluate the effect on material brittleness on chip formation from aluminium during drilling. The authors also concluded a reasonably broad statement that the chip/dust depends on material brittleness and cutting conditions. The study highlights the particle formation process through two main steps which depend on the material workpiece. The first step occurs during the material separation (i.e. drilling forces exceeding fracture forces), and step two occurs when the chip slides on the tool rake face. This correlates to the drilling peaks observed within this study to be split into two separate peaks. The study also reported the fracture of the material to be highly associated to the brittleness of the material. A brittle material will cause chip formation by brittle fracture, with very small chip contact length. The authors also indicate that the contact between the drill bit and irregular chip surface, caused by the brittle fracture, can break up particles from the internal chip surface. In contrast, in more ductile materials, the chip is formed by micro-segments that undergo a local work hardening due to the contact roughness of the drill bit tool. The hardened small part is then separated by a local brittle fracture. The nanoparticles used within this study had minimal influence on the brittleness and ductility of the materials in comparison to the reference material without the fillers. Although the nanoparticles observed to have an influence on some of the material properties, overall no significant influence on the brittleness of the material was observed.

However, the data and correlation between the nanofiller concentration, nanoparticle release and mechanical properties may be used when improving materials safer by design. It follows that the means for hazard reduction whilst simultaneously obtaining the necessary mechanical performance is a growing challenge and an opportunity likewise in nanocomposite materials manufacturing. The reduction in nanoparticle number concentration can be used towards developing less hazardous particles released from silica reinforced composites. A minor increase or decrease in nanofiller may

end up reducing the nanoparticle release hazard, without having a significant effect on mechanical properties if Safer by Design principles are followed during material development. This principle leads to the potential of tailoring the material for a reduction of nanoparticle release and thus the possibility of development towards linking the particle release to reducing the particle exposure yet keeping the material properties for function.

This fits to a key concept which was found within literature, and is an alternative approach to handling the nanotoxicity of materials, by tailoring materials through safety by design (*Njuguna et al., 2014;* Lynch et al., 2016; Hjorth et al., 2017). Another study by *Reijnders (2009*) identified this principle when considering various options at hazard reduction for nanosilica reinforced nanocomposites. Understanding the release characteristics of the materials and reducing the hazard can potentially improve the safe use of nanocomposites. Through this concept, materials can be manufactured to following safety by design strategies by minimising the nanoparticle release. Through the physio-chemical studies and understanding of the filler-matrix interfacial bonding, the release characteristics can minimise the nanoparticle release, and subsequent exposure to potentially toxic nanofillers whilst simultaneously maintaining mechanical and electrical properties.

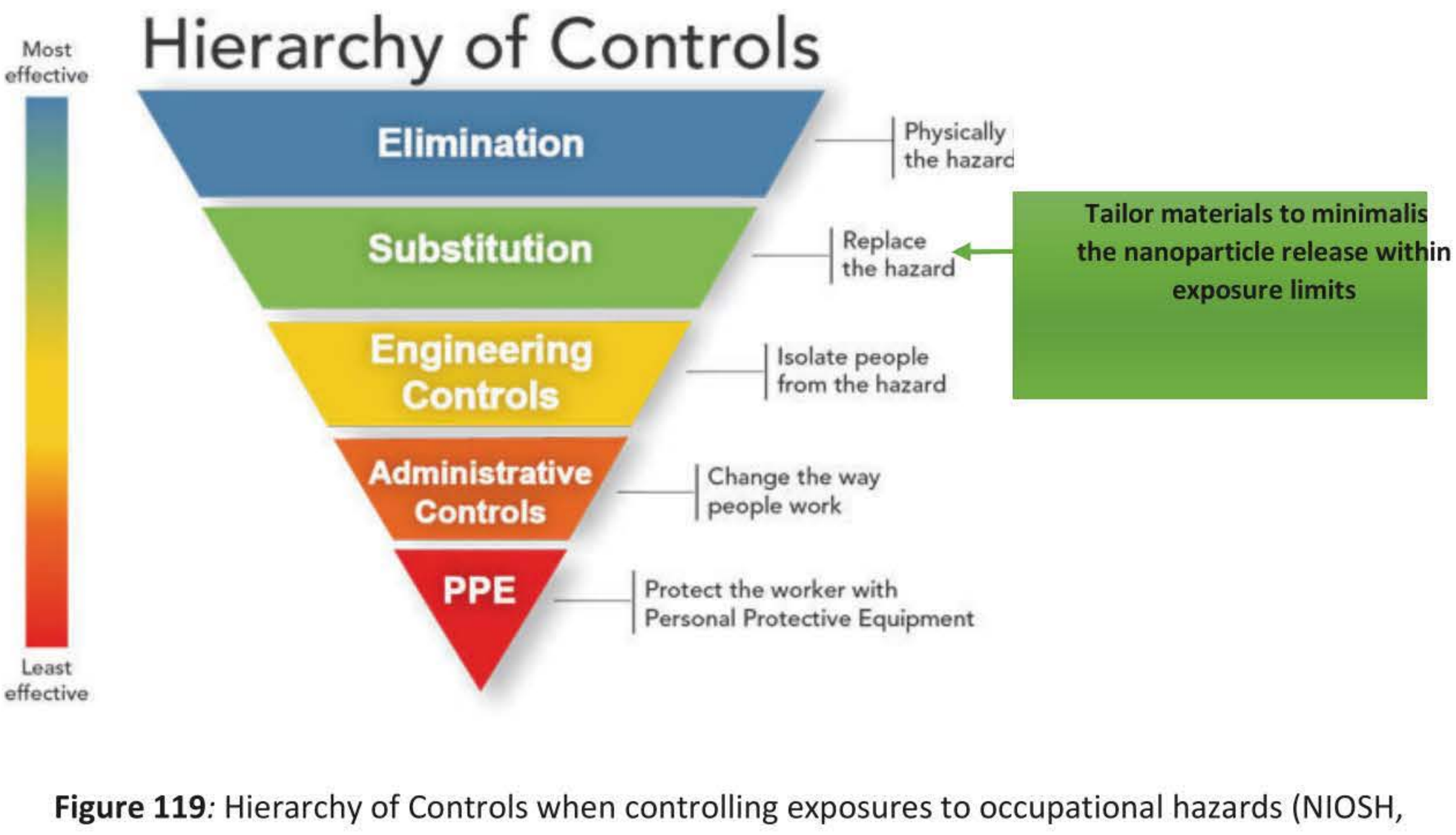

Figure 119*:* Hierarchy of Controls when controlling exposures to occupational hazards (NIOSH, 2016).

When the occupational exposure to hazardous materials is concerned, a hierarchy of controls developed by NIOSH as displayed in Figure 119 (*Niosh, 2016*). Once a hazard, in this case the release of nanoparticles, the controls are assessed in order from most effective and protective, to least effective. The hierarchy is implemented to develop occupational safe systems, where risk of illness or

injury is substantially reduced. The substitution stage would potentially be applied prior to the current controls provided by various governing bodies and institutes (e.g. *NIOSH, 2013; EU-OSHA, 2009; ISO/TS 12901-2, 2014; CEN/TC 352, 2016; OECD, 2017; ASTM E2535, 2018; BSI PD 6699, 2007; WHO, 2017).*

Since the use of nanoparticles is manipulated to improve the material properties within lightweight applications, the first platform of eliminating the hazard is difficult to implement. However, the tailoring of the materials without influencing the material properties observed within this thesis would provide an opportunity to replace the materials with similar mechanical performance but demonstrating a reduced nanoparticle release. The data set and correlation between the nanofiller concentration, nanoparticle release and mechanical properties observed for the PE-based samples, may be used to improve the materials through safety by design concepts. It follows that the means for hazard reduction whilst simultaneously obtaining the necessary mechanical performance is a growing challenge and an opportunity in nanocomposite materials manufacturing (*Njuguna et al. 2014*).

8.3. Influence of Matrix

The nanoparticle release data demonstrated throughout this thesis highlighted that the majority of the release characteristics indicated to be dependent on the material polymer. A comparison between all four reference polymer matrices studied within this thesis indicates significant differences in the particle number concentration introduced. Depending on the polymer and filler, the nanoparticle fillers displayed both an increase and decrease on the particle number concentration in comparison to the neat polymer by a factor of up to 250 %. The comparison between the reference materials however, demonstrated differences by a factor of up to 53674% (PP compared to EP). The comparison between the reference matrices particle number concentration and mechanical properties is shown in Table 23.

Table 23: Comparison between reference polymer material properties and particle number concentration in descending order of highest particle number concentration to lowest.

	Flexural Modulus $E_{Flexural}^{Chord}$ ± s_{n-1}: [MPa]	Flexural Strength: $\sigma_{Ultimate}$± s_{n-1} [MPa]	Strain at Flexural Strength $\varepsilon_{Flexural}$ at $\sigma_{Ultimate}$	Young's Modulus $E_{Young's}$ ± s_{n-1}: [MPa]	Tensile Strength: $\sigma_{Ultimate}$± s_{n-1} [MPa]	Strain at Tensile Strength $\varepsilon_{Tensile}$ at $\sigma_{Ultimate}$	Peak Particle Number Concentration Mean: $\bar{\bar{x}}$ [#/cm³]
EP	44.8 ± 0.422	62.8 ± 8.04	1.55 ± 0.191	44.0 ± 0.213	63.8 ± 2.73	1.60 ± 0.0183	>4.06 x 10^6
PE	12.3 ± 0.965	50.5 ± 1.78	4.61 ± 0.394	35.0 ± 3.16	78.1 ± 3.44	4.39 ± 0.235	3.97 x 10^6
EP/CF	343 ± 4.78	638 ± 0.62	2.03 ± 0.0310	160 ± 2.92	619 ± 94.9	2.88 ± 0.000500	2.74 x 10^4
PP	16.7 ± 1.27	52.2 ± 0.304	6.12 ± 0.328	151 ± 1.69	20.4 ± 0.043	0.35 ± 0.0020	7.55 x 10^3

As can be seen, the EP sample revealed to release the highest concentration of nanoparticles, with the PP sample producing the least. The introduction of CF within the EP to form the micro-sized reinforced composite, demonstrated to reduce the particle number concentration below that of the PE sample. A comparison between the trend in particle number concentration and the mechanical properties shown in Table 23, do not demonstrate a clear correlation but instead an association to the Young's Modulus. Evaluating the material brittleness and ductility (i.e. correlation to point of failure and plasticity observed) from the mechanical properties presented in section 3.3., also shows a close association to the nanoparticle release. The chip formation from drilling is due to the interaction between the drill and material at the microstructure level (Sheikh-Ahmad, 2009). Therefore, the material plasticity deformation and failure properties are to be associated with the characteristics of nanoparticle release. The thermoplastic and more ductile properties of the PP show a much lower particle number concentration than the brittle thermosets of EP, EP/CF and PE. The high energy release when subject to stress of the brittle materials can be seen to cause a significantly higher particle number concentration. The ductility of the material can therefore be seen to indicate an influence on the nanoparticle release. This is similar to the findings in the studies on drilling on metallic materials (e.g. Songmene et al., 2011; Songmene et al., 2015; Niknam et al., 2014).

As shown in the comparison on the influence of fillers on particle number concentration between the different polymers, the data suggests the majority of the release characteristics to be dependent on the polymer matrix. And a comparison between all four reference polymer matrices indicates significant differences in the emitted particle number concentration following drilling. A comparison of the Young's Modulus similarly shows a vast difference between the samples. The EP and PE samples have similar, lower Young's Modulus compared to that of the EP/CF and PP samples, which translate into respective higher and lower particle number concentrations. Figure 120 shows all of the samples'

released particle number concentration over Young's modulus, from which a relationship is evident over large ranges instead of minor effects shown by the introduction of the nanoparticles.

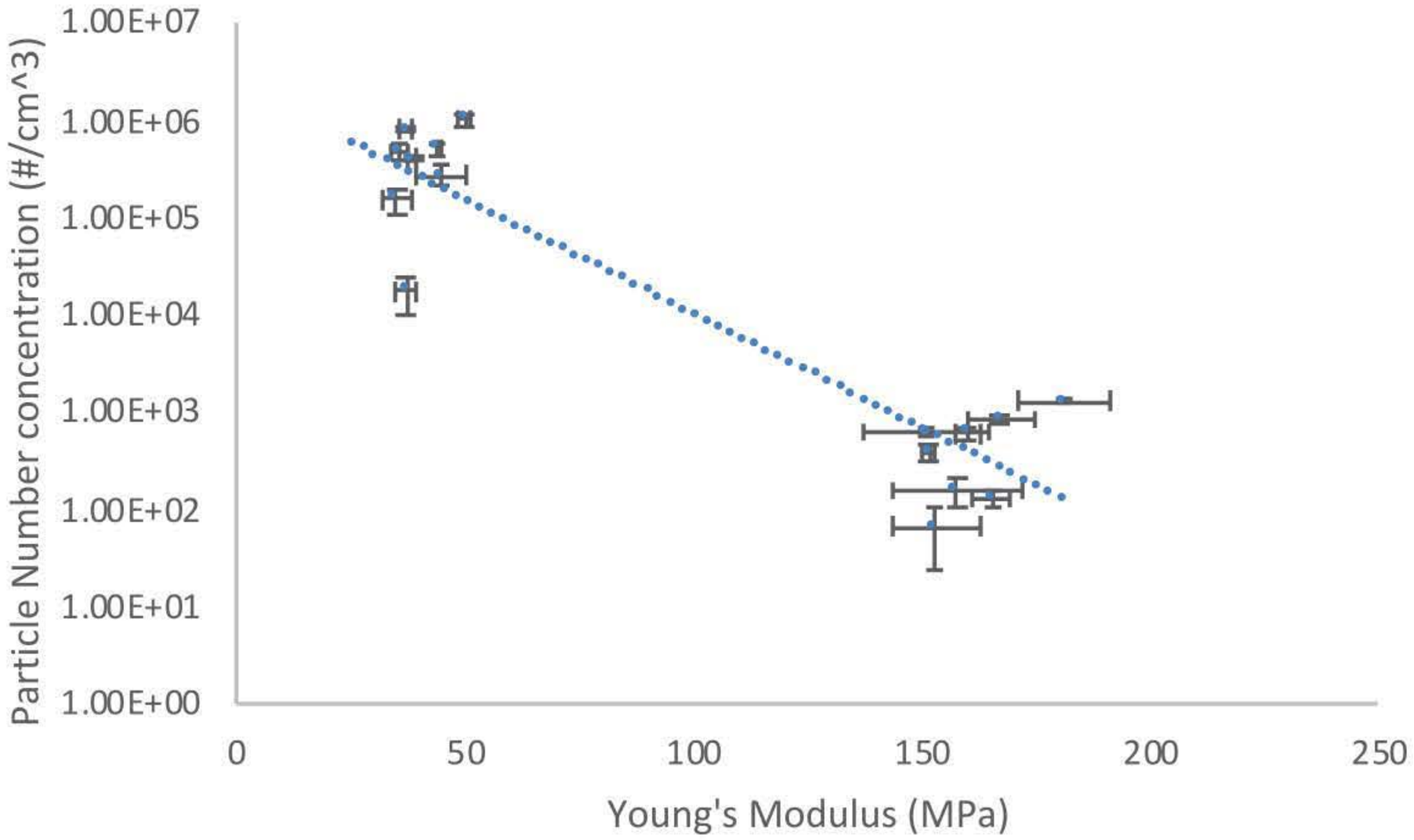

Figure 120: Comparison of particle number concentration and Young's modulus of nanocomposite samples investigated. Numerical values are given in Table 2. Trend line is drawn to demonstrate the decreasing effect in particle number concentration observed with increasing Young's Modulus.

The correlation between the nanoparticle release and Young's modulus could help explain observations in other studies on nanoparticle release. For example, polyurethane with SiO_2 in Ding et al. (2017) compared to polyamide with SiO_2 in Sachse et al. (2012) showed a higher particle number concentration by a factor of 1000. Polyurethane notably has reported lower Young's modulus compared to polyamide. Similarly, with reported concentrations of 1.4×10^6 #/cm^3 from polyamide in Sachse et al. (2012), would be in the same region as the EP-based results observed in this thesis. The two materials have also reported very similar Young's modulus (Songmene et al., 2011). Polyurethane has a lower Young's modulus than any material tested in this thesis and observed release of 10^9 #/cm^3, also above levels seen in this thesis.

Furthermore, the material plasticity deformation and failure properties, which predict when undergoing a critical energy input that has to overcome the local stress, are to be associated with the characteristics of nanoparticle release. The thermoplastic and more ductile PP show a much lower emitted particle number concentration than the brittle thermosets of EP, EP/CF and PE. The high energy release when subject to stress of the brittle materials can be seen to cause a significantly higher

particle number concentration. The ductility of the material can therefore be a predictor of the nanoparticle release. This is similar to the findings in the studies on drilling of metallic materials [Songmene et al.2015; Niknam et al., 2014; Wohlleben et al., 2011).

The Young's Modulus, brittleness and ductility differences between the materials is also evident in the peak shape profiles observed in the CPC data. The more brittle and lower Young's Modulus materials are seen to have a more evident separation of the drill bit going into the withdrawing from the sample with a concentration drop in-between. Instead, as is mainly evident in the EP/CF samples, less of a drop whilst the drill is going through the sample is observed for the materials with a higher Young's Modulus. A comparison of the particle number concentrations is shown in Figure 121, represented on a logarithmic scale in order to make all samples visible on one graph.

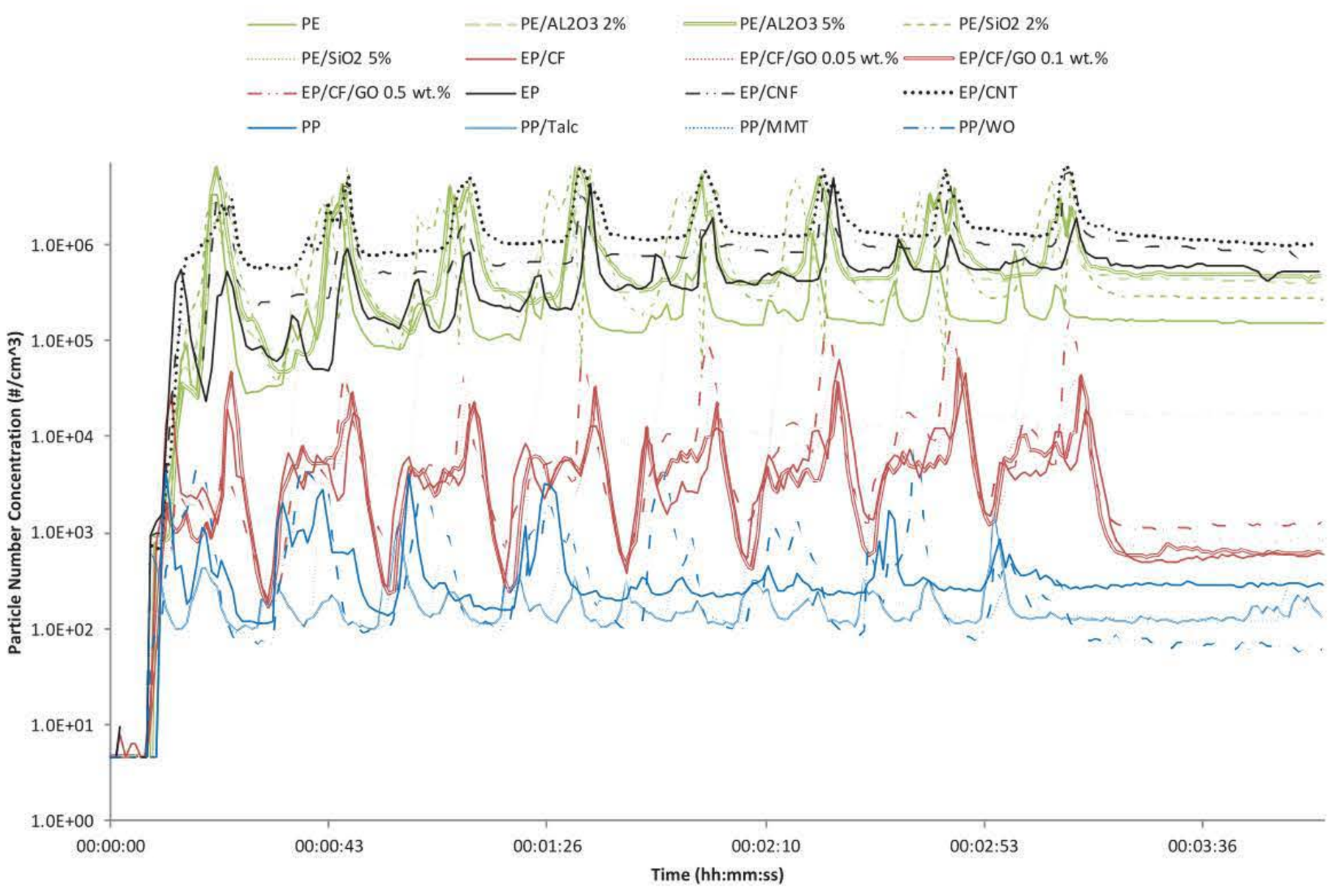

Figure 121: Particle number concentration averages of nanoparticles introduced from all nanocomposite samples (measured using CPC).

The profile of the release can therefore be said to be mostly dictated by the polymer matrix and larger filler weight concentration (if present). This is most evident with the EP and EP/CF based samples, where the introduction of CF is observed to visibly both decrease the particle number concentration and alter the profile of the release peaks during drilling. The larger peak being visible with the withdrawal of the drill bit tool in the EP/CF samples is not evident in the EP-based samples. The introduction of CF can therefore both limit the release during the drill bit entry contact and also overall

reduce the particle number concentration. The content of CF within the samples is significantly high, representing 60 % of the weight, and will also be harder to reduce into the nanoparticle size range due to its high yield and tensile strength. The peak particle number concentration is therefore substantially reduced from the EP-based samples but could however observe more micron-sized particles instead outside of the CPC size range. It is also important to note that the particle number concentration is entirely composed of the polymer.

Although the introduction of the nanoparticles at the varied weight concentrations within this study have shown an effect on the particle release in comparison to the neat polymer, the basic profile of the release did not observed a significant change (unlike the EP-based samples in comparison to the EP/CF based sample). Therefore, whilst the nanoparticles might have an effect on the nanoparticle release, the substantial profile of the release is dictated by the polymer and larger filler weight concentrations. This is similar to the mechanical properties. The tensile and flexural properties of the materials are highly dictated by the original polymer and larger filler concentrations. The introduction of CF into the EP demonstrated an extensive increase in tensile and flexural strength over the EP sample, with only minor changes with the incorporation of the nanofillers. The minor influences on nanoparticle release with the introduction of nanoparticles therefore indicate to be matrix orientated.

As discussed within the literature review, although some studies have demonstrated no increased toxicity (e.g. Wohlleben et al., 2011; Wohlleben et al., 2013, Saber et al., 2012; Saber et al., 2012, Schlagenhauf et al., 2015), there is still a lack of understanding whether most embedded nanoparticles within the matrix are toxic as they have not been investigated due to the complexity and variations in material phases (Froggett et al., 2014; Debia et al., 2016). The toxicity studies previously reported within this thesis report the understanding and toxicity of only the individual nanoparticles as opposed to a matrix/filler combination. Additionally, the identification of release of the embedded hazardous nanoparticles must also be linked to the exposure of the released particles for toxicological assessments (*Kuhlbusch et al., 2011*). As with particles exposed to human cells through inhalation, and ingestion, literature has reported it to be necessary to study each nanoparticle individually to fully understand the toxicity effects (*Crosera et al., 2009; Hristozov et al., 2012*).

Therefore, as with the mechanical properties which have been seen to drive the use of nanoparticles incorporation within industrial materials, the nanoparticles have contrasting relatively minor, yet still statistically significant, influence on the nanoparticle release.

In comparison to the other polymers investigated within this thesis and as the polymer has a significant effect on the particle number concentration, the particle size distributions observed similar dependency on the matrix. The use of the fillers introduced minor shifts in peaks with the introduction

of the diameters. The comparison of the particle size distributions of the SMPS and DMS50 showed contrasts in the particle characteristics released. This disparate peaks seen on the two instruments introduce debateable deductions and effectiveness of instrumentations required for real-time data. Although the two instruments both use electrical mobility measurements to classify the particle size distribution, the difference in sampling period could be the source of the varied results in real-time measurements during drilling. The data therefore demonstrates that, when possible, the use of multiple calibrated and sensitive measuring equipment is required when assessing the nanoparticle release. Due to the highly reactive nature of nanoparticles, the use of different measuring techniques and sampling periods to give a better understanding of the release.

A factor to also consider on the particle size distribution techniques available at the moment, are that the equipment works on the assumption that the particles shape is spherical, which is usually not the case. This might have a significant influence on the materials that included fibres, as they have a substantial difference in length compared to the diameter (as highlighted in the previous chapter). However, due to this assumption and using the material density, the mass size distribution was attainable. The polymer-related peaks observed to have the most influence on the data gathered from the nanocomposite fillers. However, the nanofillers still observed statistically significant influence on mass concentrations in comparison to the neat polymers.

Another limitation and important consideration are the differences between the particle size distributions measured using the SMPS and DMS50. Since the classification of particles according to their differing electrical mobility takes place in parallel (rather than in series as in the SMPS), the DMS50 is able to offer the faster sampled particle size distribution. This allowed for a size distribution every second compared to the SMPS TSI model 3080 of 1-minute period and therefore an accurate representation of the particles being released from the sample in a given time and more appropriate for this short-duration dynamic process. Whilst similarities are seen between the results, a direct comparison of the particle number concentration fraction between the SMPS and DMS50 demonstrated a slight variation in particle size distribution. This can be attributed to the sampling time and required flow rate. This therefore must be taken into consideration when evaluating the particle size distribution and has been reported as a challenge within comparing data throughout literature (Hameri et al., 2002; Kuhlbusch et al., 2011; Hornsby & Pryor, 2014).

Furthermore, the data presented within this thesis is a representation of release from a process related approach (as explained in literature review section 2.6. and categorised by Kuhlbusch et al. 2011). The methodology used a clean environment through the removal of all background interference. The data collected is therefore a representation of the particles released solely from the

material. Removing the background data allows for a depiction of any particles released from the materials which can be directly linked as an unconditional maximum exposure assessment (Kuhlbusch et al. 2011). The findings presented within this study therefore is data representing a maximum potential release from the process and may differ from an actual work place scenario. As previously discussed, the results represent a worst-case scenario of potential nanoparticle release from the materials. The removal of any background particles provides a clean environment to be able to evaluate the full release from the investigated materials. Particle background interference will differ in all lab environments and could influence/affect the particles release. The data provided allows for a comparison and evaluation of the material with and without the nanoparticle fillers and can be used to identify if release is likely. The full extent of exposure or intensity in a workplace scenario could potentially differ and should therefore be evaluated. The results therefore represent the potential release of the fillers and do not represent the exposure. As discussed within Basinas et al. (2018), the identification of potential release is necessary in relation to the materials and given scenario. Other exposure determinants that may be important, such as personal behaviour, experience, maintenance of hoods/ventilations, as well as housekeeping practices will need to be considered when using the data to determine any exposure controls.

Chapter Nine

Conclusion & Future Work

The overarching aim of this thesis is to investigate the influence of various nanoparticles, utilized within industrial polymer nanocomposites, on nanoparticle emissions during drilling. To achieve this within this thesis, the influence of nanoparticles on nanoparticle emissions on four reference polymers has been investigated. The study utilised an automated drilling methodology with only the material as the varying parameter to evaluate the nanoparticle release from the nanocomposite materials. A variety of nanocomposite materials representing industry sectors were identified and manufactured. Nanoparticles which have been identified within literature as potentially being toxic as well as providing mechanical reinforcement were chosen based on the application and newly introduced materials within industry. Within the industrial applications, the materials could all undergo drilling during assembly stages of the material lifecycle. It is therefore necessary to assess the influence of the nanoparticles within the materials for nanoparticle release during drilling.

Within the scope of this thesis, the literature review ascertained that although various test guidelines and reports on exposure assessments have made remarkable progress and are available to assist in carrying out an adequate approach on some exposure assessments, there is currently no available standard or harmonised method in assessment of nanomaterial release during machining. A need for a standardised methodology that can be repeated and controlled to give consistent results is necessary. Based on the findings within the literature review, the methodology used within this thesis followed on from previous studies with an automated drilling assembly and removal of all background noise in the measurements allowing for a process related assessment of the nanoparticle emissions during drilling. The automated drilling methodology was evaluated to minimise influence from all factors apart from the change in material. The data collected from the methodology therefore is a representation of the particles released solely from the material during drilling. The results from the

PP based nanocomposites were compared to a different methodology which evaluated the release from the same set of materials and demonstrated similar findings for the nano-reinforced PP samples in comparison to the virgin PP sample.

The four sets of nanocomposite materials (PP based, PE based, EP based and EP/CF based samples) were subsequently investigated for the influence of the nanoparticle fillers on particle number concentration, particle size distribution, mass size distribution and material structure and morphology during drilling and correlated to the tensile and flexural properties. The study found the following conclusions:

- Each polymer and nanofiller combination demonstrated different correlation with influence on tensile and flexural properties. Nonetheless, all but one of the samples demonstrated an improvement in the flexural strength with the introduction of the nanofillers. Only the EP/CF/GO 0.05 wt. % sample returned a statistically insignificant result in flexural strength when compared to the sample without the nanoparticle reinforcement. Although some nanofillers observed to have an influence on the material properties, the reference material can be seen to have the greatest influence on the tensile and flexural material property behaviour.
- All of the materials, including the neat polymers released airborne nanoparticles. Moreover, the matrix type was found to be the biggest influence on the nanoparticle release when comparing all of the nanocomposite materials. The virgin PP observed the lowest nanoparticle concentrations, whilst the epoxy demonstrated the highest. Both sets of the PE and EP samples demonstrated to exceed the saturated CPC particle number concentration of 9.99×10^6 #/cm^3. The data for these samples is therefore a lower bound representation of the release.
- The introduction of the nanofillers demonstrated to have an influence on the nanoparticle release during drilling. The different nanofillers had different effects, both positive and negative, on the release properties from the materials, and can therefore be concluded to have an influence on the nanoparticle release. Of the samples investigated on the influence of nanoparticles within nanocomposite materials on nanoparticle release during drilling, 83% exhibited a statistically significant influence on the average particle number concentration. 67% of the total nanocomposites investigated displayed a statistically significant increase, and 17% displayed a statistically significant decrease in the particle number concentration release during drilling in comparison to the reference materials without nanoparticles.
- The PP based samples exhibited statistically significant influences with a 33% decrease (PP/MMT) or a 30% increase (PP/WO) on average particle number concentration released in

comparison to the neat PP sample. Although there are minor influences on the nanoparticle release, the data suggests the PP matrix is the most influential cause of the release. Whereas, in comparison to the virgin EP sample, the EP/CNF and EP/CNT samples also observed statistically significant influences demonstrating an increase of 93 % and 211 % respectively in average particle number concentration across the 4 minutes. Similarly, the introduction of GO within EP/CF demonstrated an influence in particle number concentration with the EP/CF/GO 0.5 wt. % sample observing a statistically significant influence and a 118 % increase in comparison to the EP/CF sample (EP/CF/GO 0.05 wt. % increase of 43.5 % and EP/CF/GO 0.1 wt. % increase of 4.85 %).

- Different concentrations of nanofiller displayed inverse results within the PE and EP/CF based samples. The PE/Al_2O_3 observed an increase in nanoparticle release with an increase from 2 wt. % to 5 wt. % reinforced sample, whereas the PE/SiO_2 revealed a decreasing effect in nanoparticle release with the same increase in weight concentration. This data set and correlation between the nanofiller concentration, nanoparticle release and mechanical properties may be used when improving materials and has potential to act as a concept of safety by design.
- The data indicated that the size distribution and particle number concentration alone do not give a full account of the release. Although large quantities of particles are observed at small particle diameters, the particle mass concentration reveals significant releases at higher particle diameters due to the increased mass of larger particles. Many exposure limits due to toxicological studies are given in particle mass concentrations. Significantly, data from the particle mass concentration from the EP/CNF and EP/CNT samples revealed concentration increases to be a substantial amount above the NIOSH recommended exposure limits when working with CNTs and CNFs.
- Despite the nanoparticle reinforced samples displaying differences in comparison to the neat polymers, no evidence in the microscopy studies was found of the independent nanofillers being released from the matrix. It is apparent therefore, that either, the nanofillers are adhering to and embedded within the polymer matrix, or, the current method used for post characterisation is unable to identify the individual airborne nanofillers. However, the microscopy results are limited due to challenges in collecting sufficient material to perform an EDX analysis required to identify any independent fillers.
- The link between the release and mechanical properties observed an association with the influence of the nanoparticles within the materials. A significant correlation between the polymer Young's modulus and nanoparticle release was observed. The fracture mechanics of

requiring higher stresses to deform or overcome the local stresses and materials bonds with higher Young's Modulus correlates to a lower particle number concentration released. With this novel understanding of the relation between material properties and nanoparticle release, certain materials could be selected for specific applications with improved human and environmental safety in mind. However, numerous complexities still arise with the addition of nanoparticles within nanocomposite materials as the evidence is less clear on minor influences on mechanical properties. The comparison between matrices highlighted that the majority of the release characteristics indicated to be dependent on the material polymer. Furthermore, the more brittle the material, the higher the particle number concentration, as demonstrated with a 53674% increase when comparing the more ductile PP thermoplastic to the brittle EP thermoset. The findings are therefore in unison with similar conclusions within literature, that numerous complexities still arise with the addition of nanoparticles within nanocomposite materials and should be evaluated on a case-by-case basis.

Furthermore, the effects on particle number concentration was seen to be the foremost influence on the particle size distribution and particle mass distribution. Most materials demonstrated peaks at similar particle diameters but at higher particle number or mass concentrations. Therefore, as emphasised within literature, it is vital that the particle number concentration is assessed. However, the data from the particle size distributions and the mass distributions accentuate that the particle number concentration alone is not sufficient to quantify the nanoparticle release. Thereafter, since the neat polymers release nanoparticles, it is important to analyse any shift in particle size distribution if an increase in particle number concentration is observed. However, the data observed within this thesis has shown that the particle size distribution is highly influenced by the matrix, also as no independent nanofillers were identifiable in the post-test analysis. This does not conclude that the nanofillers were not separated from the matrix, as some of the data observed in the SMPS and DMS50 suggests otherwise with peak diameters observed at nanofiller diameters for a few samples. The particle size distribution alone will therefore, not be sufficient in evaluating the nanoparticle release from the materials. Therefore, although the nanofillers are concluded to have demonstrated an influence on the nanoparticle release during drilling, the materials demonstrated a level of complexity with no clear cause and effect relationship.

Future Work

- The elimination of the background noise for precise measurements has permitted this analysis on the nanocomposite materials. Future studies should work on the continued demonstration

and verification of the methodology developed in order to work towards a standardised testing method as is highlighted as necessary within literature. Improvements to the methodology design could allow for a more flexible setup to be adaptable to other mechanical processes such as cutting, milling, grinding etc. Furthermore, as demonstrated within the wide data presented, there is still a need to develop the current guidelines to standardised testing parameters (such as particle size distribution, mass distribution, chemical compositions, surface area etc.) which will cover the necessary exposure and toxicological aspects and towards bridging the gap between nanoparticle quantification and nanotoxicity.

- Literature has found conflicting results in the identification of free standing nanoparticles in the microscopy characterisation. This study observed significant increases in particle number concentration with the introduction of the nanoparticles, as well as increases at relevant nanoparticle diameters in the size distribution, but was unable to identify independent and free standing nanoparticles (due to insufficient material collected on filter). Further studies should explore and evaluate improvements in the the capture and characterisation of the airborne nanoparticles measured. Currently, the airborne particles are demonstrating and indicating that the nanoparticle fillers are being released, but are unable to be verified in the characterisation studies (as mentioned, due to both instrument limitations and potentially quantity of particles released). This would also link in to the limitations of the instrumentation, such as the assumption of spherical particles from the SMPS, particle size range, saturation limits and the level of randomness and uncertainty evident in the high standard deviation and range of peaks observed. The limitations have been discussed within this thesis, and are most apparent in the statistical analysis. Further studies might therefore verify the instrumentation limitations and findings where these uncertainties are.
- Investigations into further concentrations of nanoparticle fillers in order to provide more data on the filler-matrix relationship to be able to understand and manufacture materials through concepts of safety by design. Materials with similar material properties but with a reduction in potentially toxic nanoparticles released, provide a potential approach towards minimising the exposure risk when occupational exposure is concerned. A construction of a database and work towards mathematical models to depict the relation between the matrix and filler concentration to nanoparticle release is required to optimise the safety by design approach. The understanding of the release characteristics whilst maintaining the material properties will provide safety by design tools that can be implemented at the early stages of the nanocomposite development process.

- Further investigation into the toxicity and safety of embedded nanoparticles is required. All of the samples considered within this thesis observed substantial release of nanoparticles, including the neat polymers. Although no independent nanoparticles of the fillers were identified in the microscopy analysis, increases in concentrations were observed with the reinforced nanocomposites. Therefore, although toxicity and exposure limits have been quantified for certain individual nanoparticles (such as CNTs and CNFs), there is currently no full understanding or exposure standards relating to the limits of the embedded nanoparticles within a polymer matrix.
- The correlation between the Young's Modulus, brittleness and ductility is a novel understanding between material properties and nanoparticle release, with beneficial use if certain materials could be selected for specific applications with improved human and environmental safety in mind. This correlation between the properties and nanoparticle release should be investigated further with more materials with both, similar properties to verify the findings, as well as dissimilar properties to investigate the relationship further (e.g. higher and lower Young's Modulus, more or less brittle etc.).

This study has demonstrated that the nanoparticle release of nanofiller reinforced polymers should be considered. All of the samples revealed dissimilar nanoparticle release characteristics during the automated drilling, and it is therefore necessary to investigate each filler and matrix combination individually prior to making a judgement on the material release characteristics. The differences and high quantities of nanoparticles introduced due to the reinforcing filler of some nanocomposites, such as the EP/CNF and EP/CNT samples, accentuate the need for a standardised test regime and further assessments of the influence of nanoparticles on nanoparticle release from nanocomposite materials during drilling.

References

ABDULLAH, S.I. and ANSARI, M., 2015. Mechanical properties of graphene oxide (GO)/epoxy composites. *Hbrc Journal,* 11(2), pp. 151-156

ABRAO, A.M. et al., 2007. Drilling of fiber reinforced plastics: A review. *Journal of Materials Processing Technology,* 186(1-3), pp. 1-7

ACGIH, 1996. *Threshold Limit Values for Chemical Substances and Physical Agents and Biological Exposure Indices.* Cincinnati, Ohio: American Conference of Governmental Industrial Hygienists.

AEROSPACE TECHNOLOGY INSTITUTE, September 2018. *Composite Material Applications in Aerospace.* Cranfield, UK: ATI.

AHMADI, M., MASOOMI, M. and SAFI, S., 2015. Mechanical property characterization of carbon nanofiber/epoxy nanocomposites reinforced by GMA-grafted UHMWPE fibers. *Composites Part B: Engineering,* 83, pp. 43-49

AHMADI-MOGHADAM, B. et al., 2015. Effect of functionalization of graphene nanoplatelets on the mechanical response of graphene/epoxy composites. *Materials & Design (1980-2015),* 66, pp. 142-149

AHN, K. et al., 2017. Development of international standard on nano aerosol generation for inhalation toxicology study. *Toxicol.Open Access,* 3(127), pp. 2476-2067

AITKEN, R.J. et al., 2008. A multidisciplinary approach to the identification of reference materials for engineered nanoparticle toxicology. *Nanotoxicology,* 2(2), pp. 71-78

AJAYAN, P.M., SCHADLER, L.S. and BRAUN, P.V., 2006. *Nanocomposite science and technology.* John Wiley & Sons.

AJAYAN, P.M. and ZHOU, O.Z., 2001. Applications of carbon nanotubes. *Carbon nanotubes.* Springer. pp. 391-425

AJAYAN, P.M. et al., 1994. Aligned carbon nanotube arrays formed by cutting a polymer resin--nanotube composite. *Science (New York, N.Y.),* 265(5176), pp. 1212-1214

AKHAVAN, O., GHADERI, E. and AKHAVAN, A., 2012. Size-dependent genotoxicity of graphene nanoplatelets in human stem cells. *Biomaterials,* 33(32), pp. 8017-8025

ALIAN, A., KUNDALWAL, S. and MEGUID, S., 2015. Interfacial and mechanical properties of epoxy nanocomposites using different multiscale modeling schemes. *Composite Structures,* 131, pp. 545-555

AL-KATTAN, A. et al., 2013. Release of TiO 2 from paints containing pigment-TiO 2 or nano-TiO 2 by weathering. *Environmental Science: Processes & Impacts,* 15(12), pp. 2186-2193

ALLAHVERDI, A. et al., 2012. The effect of nanosilica on mechanical, thermal and morphological properties of epoxy coating. *Progress in Organic Coatings,* 75(4), pp. 543-548

ALLIED MARKET RESEARCH, December, 2016. *Epoxy Resin Market by Type (DGBEA, DGBEF, Novolac, Aliphatic, Glycidylamine, and Others), by Physical Form (Solid, Liquid, and Solution), by Application (Paints & Coatings, Adhesives, Composites, and electronic encapsulation & others), and by End user (Building & Construction, Transportation, General Industrial, Consumer Goods, Wind Power, Aerospace, and Marine & Others) - Global Opportunity Analysis and Industry Forecast, 2014-2022.* Portland, USA: Allied Market Research, Sahu, Yashwant;.

ALLIED MARKET RESEARCH, September 2016. *Carbon Nanotubes Market to Reach $3,812 Million, Globally, by 2022.* Portland, USA: Allied Market Research, Yashwant Singh Sahu.

ALMAADEED, M.A. et al., 2012. Date palm wood flour/glass fibre reinforced hybrid composites of recycled polypropylene: Mechanical and thermal properties. *Materials & Design,* 42, pp. 289-294

ALSHATWI, A.A. et al., 2013. Aluminium oxide nanoparticles induce mitochondrial-mediated oxidative stress and alter the expression of antioxidant enzymes in human mesenchymal stem cells. *Food Additives & Contaminants: Part A,* 30(1), pp. 1-10

AMEUR, M. et al., 2017. Machinability analysis of dry drilling of carbon/epoxy composites: cases of exit delamination and cylindricity error. *The International Journal of Advanced Manufacturing Technology,* 88(9-12), pp. 2557-2571

ARASH, B., WANG, Q. and VARADAN, V., 2014. Mechanical properties of carbon nanotube/polymer composites. *Scientific reports,* 4, pp. srep06479

ARMBRISTER, C.E., OKOLI, O.I. and SHANBHAG, S., 2015. Micromechanics predictions for two-phased nanocomposites and three-phased multiscale composites: a review. *Journal of Reinforced Plastics and Composites,* 34(8), pp. 605-623

ASCHBERGER, K. et al., 2010. Review of carbon nanotubes toxicity and exposure—Appraisal of human health risk assessment based on open literature. *Critical reviews in toxicology,* 40(9), pp. 759-790

ASHORI, A., MENBARI, S. and BAHRAMI, R., 2016. Mechanical and thermo-mechanical properties of short carbon fiber reinforced polypropylene composites using exfoliated graphene nanoplatelets coating. *Journal of Industrial and Engineering Chemistry,* 38, pp. 37-42

ASHORI, A., RAHMANI, H. and BAHRAMI, R., 2015. Preparation and characterization of functionalized graphene oxide/carbon fiber/epoxy nanocomposites. *Polymer Testing,* 48, pp. 82-88

ASHRAFI, B. et al., 2011. Enhancement of mechanical performance of epoxy/carbon fiber laminate composites using single-walled carbon nanotubes. *Composites Science and Technology,* 71(13), pp. 1569-1578

ASTM D 4060, 2007. *Standard Test Method for Abrasion Resistance of Organic Coatings by the Taber Abraser.* Pennsylvania, USA: American Society for Testing and Materials.

ASTM E2535, 2018. *Standard Guide for Handling Unbound Engineered Nanoscale Particles in Occupational Settings.* Pennsylvania, USA: American Society for Testing and Materials.

ASTM, D., 2015. *Standard Test Method for Rubber Property—Durometer Hardness.* West Conshohocken, PA: ASTM International.

ASTM, D., 2014. *Standard Test Methods for DC Resistance or Conductance of Insulating Materials.* West Conshohocken, PA: ASTM International.

ASTM, D., 2017. *Standard Test Method for Tensile Properties of Polymer Matrix Composite Materials.* West Conshohocken, PA: ASTM International.

ASTM, D., 2013. *Standard Test Method for D-C Resistance or Conductance of Moderately Conductive Materials.* West Conshohocken, PA: ASTM International.

ASTM, D., 2015. *Standard Test Method for Flexural Properties of Polymer Matrix Composite Materials.* West Conshohocken, PA: ASTM International.

AWAD, W.H. et al., 2009. Material properties of nanoclay PVC composites. *Polymer,* 50(8), pp. 1857-1867

AYATOLLAHI, M. et al., 2011. Effect of multi-walled carbon nanotube aspect ratio on mechanical and electrical properties of epoxy-based nanocomposites. *Polymer Testing,* 30(5), pp. 548-556

AZEEZ, A.A. et al., 2013. Epoxy clay nanocomposites–processing, properties and applications: A review. *Composites Part B: Engineering,* 45(1), pp. 308-320

BAALOUSHA, M. and LEAD, J.R., 2013. Nanoparticle dispersity in toxicology. *Nature nanotechnology,* 8(5), pp. 308-309

BAKER, M. et al., 2002. Evaluating the microstructure and performance of nanocomposite PVD TiAlBN coatings. *Surface and Coatings Technology,* 151, pp. 338-343

BAL, S., 2010. Experimental study of mechanical and electrical properties of carbon nanofiber/epoxy composites. *Materials & Design (1980-2015),* 31(5), pp. 2406-2413

BANIASSADI, M. et al., 2011. Mechanical and thermal behavior of nanoclay based polymer nanocomposites using statistical homogenization approach. *Composites Science and Technology,* 71(16), pp. 1930-1935

BAO, C. et al., 2011. In situ preparation of functionalized graphene oxide/epoxy nanocomposites with effective reinforcements. *Journal of Materials Chemistry,* 21(35), pp. 13290-13298

BARBERO, E.J., 2010. *Introduction to composite materials design.* CRC press.

BASINAS, I., JIMÉNEZ, A.S., GALEA, K.S., TONGEREN, M.V. AND HURLEY, F., 2018. A systematic review of the routes and forms of exposure to engineered nanomaterials. *Annals of work exposures and health*, 62(6), pp.639-662.

BASKARAN, R., SAROJADEVI, M. and VIJAYAKUMAR, C., 2011. Unsaturated polyester nanocomposites filled with nano alumina. *Journal of Materials Science,* 46(14), pp. 4864-4871

BASTÚS, N.G. and PUNTES, V., 2018. Nanosafety: towards safer nanoparticles by design. *Current medicinal chemistry,* 25(35), pp. 4587-4601

BCC RESEARCH, June 2018. *Nanocomposites, Nanoparticles, Nanoclays and Nanotubes: Global Markets to 2022.* Wellesley, USA: BCC Research.

BCC RESEARCH and MCWILLIAMS, A., 2014. *Global markets for nanocomposites, nanoparticles, nanoclays, and nanotubes.* [online] Available from: http://www.bccresearch.com/market-research/nanotechnology/nanocomposites-market-nan021f.html [Accessed 09/01 2015]

BECKER, O., VARLEY, R. and SIMON, G., 2002. Morphology, thermal relaxations and mechanical properties of layered silicate nanocomposites based upon high-functionality epoxy resins. *Polymer,* 43(16), pp. 4365-4373

BEHERI, H.H., MOHAMED, K.R. and EL-BASSYOUNI, G.T., 2013. Mechanical and microstructure of reinforced hydroxyapatite/calcium silicate nano-composites materials. *Materials & Design,* 44, pp. 461-468

BELLO, D., WARDLE, B.L., YAMAMOTO, N., DEVILLORIA, R.G. and HALLOCK, M., 2009. Exposures to Nanoscale Particles and Fibers During Handling, Processing, and Machining of Nanocomposites and Nanoengineered Composites Reinforced with Aligned Carbon Nanotubes. *17th International conference on composite materials (ICCM) proceedings, Edinburgh, Scotland.*

BELLO, D. et al., 2010. Characterization of exposures to nanoscale particles and fibers during solid core drilling of hybrid carbon nanotube advanced composites. *International journal of occupational and environmental health,* 16(4), pp. 434-450

BERGIN, I.L. and WITZMANN, F.A., 2013. Nanoparticle toxicity by the gastrointestinal route: evidence and knowledge gaps. *International journal of biomedical nanoscience and nanotechnology,* 3(1-2), pp. 10.1504/IJBNN.2013.054515

BHATTACHARYYA, S., SALVETAT, J. and SABOUNGI, M., 2006. Reinforcement of semicrystalline polymers with collagen-modified single walled carbon nanotubes. *Applied Physics Letters,* 88(23), pp. 233119

BLAKE, R. et al., 2004. A generic organometallic approach toward ultra-strong carbon nanotube polymer composites. *Journal of the American Chemical Society,* 126(33), pp. 10226-10227

BORREGO, L. et al., 2014. Fatigue behaviour of glass fibre reinforced epoxy composites enhanced with nanoparticles. *Composites Part B: Engineering,* 62, pp. 65-72

BORTZ, D.R., HERAS, E.G. and MARTIN-GULLON, I., 2011. Impressive fatigue life and fracture toughness improvements in graphene oxide/epoxy composites. *Macromolecules,* 45(1), pp. 238-245

BOTTINI, M. et al., 2006. Multi-walled carbon nanotubes induce T lymphocyte apoptosis. *Toxicology letters,* 160(2), pp. 121-126

BOUILLARD, J.X. et al., 2013. Nanosafety by design: risks from nanocomposite/nanowaste combustion. *Journal of nanoparticle research,* 15(4), pp. 1519

BOURBIGOT, S. and DUQUESNE, S., 2007. Fire retardant polymers: recent developments and opportunities. *Journal of Materials Chemistry,* 17(22), pp. 2283-2300

BRAY, D. et al., 2013. The modelling of the toughening of epoxy polymers via silica nanoparticles: the effects of volume fraction and particle size. *Polymer,* 54(26), pp. 7022-7032

BREUER, U.P., 2016. *Commercial aircraft composite technology.* Springer.

BROUWER, D. et al., 2009. From workplace air measurement results toward estimates of exposure? Development of a strategy to assess exposure to manufactured nano-objects. *Journal of Nanoparticle Research,* 11(8), pp. 1867

BROUWER, D. et al., 2012. Harmonization of measurement strategies for exposure to manufactured nano-objects; report of a workshop. *The Annals of Occupational Hygiene,* 56(1), pp. 1-9

BROWN, J.S. et al., 2013. Thoracic and respirable particle definitions for human health risk assessment. *Particle and fibre toxicology,* 10(1), pp. 12

BSI PD 6699, 2007. *Nanotechnologies – Part 2: Guide to safe handling and disposal of manufactured nanomaterials.* UK: British Standards Institution.

BURAK KAYBAL, H. et al., 2019. Evaluation of boron nitride nanoparticles on delamination in drilling carbon fiber epoxy nanocomposite materials. *Journal of Composite Materials,* , pp. 0021998319860245

CALVERT, G.M. et al., 2003. Occupational silica exposure and risk of various diseases: an analysis using death certificates from 27 states of the United States. *Occupational and environmental medicine,* 60(2), pp. 122-129

CAMBUSTION DMS50 MKII, 2008. *DMS50 Fast Aersol Size Spectrometer.*

CAMPBELL, F.C., 2010. *Structural composite materials.* ASM international.

CANTOR, B., GRANT, P. and JOHNSTON, C., 2008. *Automotive engineering: lightweight, functional, and novel materials.* CRC Press.

CASTRANOVA, V., SCHULTE, P.A. and ZUMWALDE, R.D., 2012. Occupational nanosafety considerations for carbon nanotubes and carbon nanofibers. *Accounts of Chemical Research,* 46(3), pp. 642-649

ÇELIK, Y.H., KILICKAP, E. and KOÇYIĞIT, N., 2019. Evaluation of drilling performances of nanocomposites reinforced with graphene and graphene oxide. *The International Journal of Advanced Manufacturing Technology,* 100(9-12), pp. 2371-2385

CEN (EUROPEAN COMMITTEE FOR STANDARDIZATION), 1993. *Workplace atmospheres-size fraction definitions for measurement of airborne particles.* (Report No. BS EN 481:1993). London, Egnalnd: British Standards Institute.

CEN/TC 352, 2016. *Nanotechnologies - Guidance for the responsible development of nanotechnologies.* Brussels, Belgium: European Committee for Standardization.

CENA, L.G. and PETERS, T.M., 2011. Characterization and control of airborne particles emitted during production of epoxy/carbon nanotube nanocomposites. *Journal of occupational and environmental hygiene,* 8(2), pp. 86-92

CHANDRASEKARAN, S. et al., 2014. Fracture toughness and failure mechanism of graphene based epoxy composites. *Composites Science and Technology,* 97, pp. 90-99

CHANGIZI, F. and HADDAD, A., 2015. Strength properties of soft clay treated with mixture of nano-SiO2 and recycled polyester fiber. *Journal of Rock Mechanics and Geotechnical Engineering,* 7(4), pp. 367-378

CHAPMAN, R. and MULVANEY, P., 2001. Electro-optical shifts in silver nanoparticle films. *Chemical physics letters,* 349(5), pp. 358-362

CHAWLA, K.K., 2012. *Composite materials: science and engineering.* Springer Science & Business Media.

CHE, D. et al., 2014. Machining of carbon fiber reinforced plastics/polymers: a literature review. *Journal of Manufacturing Science and Engineering,* 136(3), pp. 034001

CHEN, B. et al., 2008. A critical appraisal of polymer–clay nanocomposites. *Chemical Society Reviews,* 37(3), pp. 568-594

CHEN, L., PANG, X. and YU, Z., 2007. Study on polycarbonate/multi-walled carbon nanotubes composite produced by melt processing. *Materials Science and Engineering: A,* 457(1-2), pp. 287-291

CHEN, L., WONG, S. and PISHARATH, S., 2003. Fracture properties of nanoclay-filled polypropylene. *Journal of Applied Polymer Science,* 88(14), pp. 3298-3305

CHEN, M. et al., 2008. Effects of interfacial adhesion on properties of polypropylene/wollastonite composites. *Journal of Applied Polymer Science,* 107(3), pp. 1718-1723

CHEN, N. et al., 2004. Effect of nano-CaCO3 on mechanical properties of PVC and PVC/Blendex blend. *Polymer Testing,* 23(2), pp. 169-174

CHEN, X. et al., 2003. In situ polymerization and characterization of polyester-based polyurethane/nano-silica composites. *Polymer International,* 52(6), pp. 993-998

CHEN, Y. et al., 2005. Structure and properties of polyurethane/nanosilica composites. *Journal of Applied Polymer Science,* 95(5), pp. 1032-1039

CHERAGHIAN, G. et al., 2018. Effect of a novel clay/silica nanocomposite on water-based drilling fluids: Improvements in rheological and filtration properties. *Colloids and Surfaces A: Physicochemical and Engineering Aspects,* 555, pp. 339-350

CHO, J., JOSHI, M. and SUN, C., 2006. Effect of inclusion size on mechanical properties of polymeric composites with micro and nano particles. *Composites Science and Technology,* 66(13), pp. 1941-1952

CHOI, Y. et al., 2005. Mechanical and physical properties of epoxy composites reinforced by vapor grown carbon nanofibers. *Carbon,* 43(10), pp. 2199-2208

CHOU, C. et al., 2008. Single-walled carbon nanotubes can induce pulmonary injury in mouse model. *Nano Letters,* 8(2), pp. 437-445

CHRISTENSEN, R.M., 2012. *Mechanics of composite materials.* Courier Corporation.

CINAUSERO, N. et al., 2008. *Fire retardancy of polymers: new strategies and mechanisms.* Royal Society of Chemistry.

CLARK, K. et al., 2012. Limitations and information needs for engineered nanomaterial-specific exposure estimation and scenarios: recommendations for improved reporting practices. *Journal of Nanoparticle Research,* 14(9), pp. 970

COLLINGS, N., RONGCHAI, K. and SYMONDS, J., 2014. A condensation particle counter insensitive to volatile particles. *Journal of Aerosol Science,* 73, pp. 27-38

CONRADI, M. et al., 2014. Mechanical and anticorrosion properties of nanosilica-filled epoxy-resin composite coatings. *Applied Surface Science,* 292, pp. 432-437

COOKED RESEARCH REPORTS, October, 2017. *Epoxy Resin Market Research Report- Forecast to 2023.* India: Market Research Future.

CROSERA, M. et al., 2009. Nanoparticle dermal absorption and toxicity: a review of the literature. *International archives of occupational and environmental health,* 82(9), pp. 1043-1055

CUI, L. et al., 2013. Functionalization of multi-wall carbon nanotubes to reduce the coefficient of the friction and improve the wear resistance of multi-wall carbon nanotube/epoxy composites. *Carbon,* 54, pp. 277-282

DANIEL, I.M. et al., 1994. *Engineering mechanics of composite materials.* Oxford university press New York.

DASARI, A., ROHRMANN, J. and MISRA, R., 2004. On the scratch deformation of micrometric wollastonite reinforced polypropylene composites. *Materials Science and Engineering: A,* 364(1-2), pp. 357-369

DAVIM, J.P. and REIS, P., 2003. Study of delamination in drilling carbon fiber reinforced plastics (CFRP) using design experiments. *Composite structures,* 59(4), pp. 481-487

DE VOLDER, M.F. et al., 2013. Carbon nanotubes: present and future commercial applications. *Science (New York, N.Y.),* 339(6119), pp. 535-539

DEBIA, M. et al., 2016. A systematic review of reported exposure to engineered nanomaterials. *Annals of Occupational Hygiene,* 60(8), pp. 916-935

DECOURSEY, W., 2003. *Statistics and probability for engineering applications.* Elsevier.

DELORME, M.P. et al., 2012. Ninety-day inhalation toxicity study with a vapor grown carbon nanofiber in rats. *Toxicological sciences : an official journal of the Society of Toxicology,* 128(2), pp. 449-460

DELVA, L. et al., 2014. The effect of multiple extrusions on the properties of montmorillonite filled polypropylene. *Polymers,* 6(12), pp. 2912-2927

DENG, C. et al., 2016. Influence of surface properties of graphene oxide/carbon fiber hybrid fiber by oxidative treatments combined with electrophoretic deposition. *Surface and Interface Analysis,* 48(4), pp. 212-217

DEY, V. et al., 2015. Mechanical properties of micro and sub-micron wollastonite fibers in cementitious composites. *Construction and Building Materials,* 82, pp. 351-359

DING, Q. et al., 2019. Effect of hybrid wollastonite with different nucleation and morphology on the crystallization and mechanical properties of polypropylene. *Polymer Composites,* 40(S1), pp. E638-E646

DING, Q. et al., 2013. Preparation and characterization of wollastonite with a β-nucleating surface and its filled isotactic polypropylene composites. *Journal of Materials Science,* 48(15), pp. 5225-5235

DOMUN, N. et al., 2015. Improving the fracture toughness and the strength of epoxy using nanomaterials–a review of the current status. *Nanoscale,* 7(23), pp. 10294-10329

DONG, C. and DAVIES, I.J., 2015. Flexural strength of bidirectional hybrid epoxy composites reinforced by E glass and T700S carbon fibres. *Composites Part B: Engineering,* 72, pp. 65-71

DREYER, D.R. et al., 2010. The chemistry of graphene oxide. *Chemical Society Reviews,* 39(1), pp. 228-240

EOM, H. and CHOI, J., 2009. Oxidative stress of silica nanoparticles in human bronchial epithelial cell, Beas-2B. *Toxicology in Vitro,* 23(7), pp. 1326-1332

ESTHAPPAN, S.K., NAIR, A.B. and JOSEPH, R., 2015. Effect of crystallite size of zinc oxide on the mechanical, thermal and flow properties of polypropylene/zinc oxide nanocomposites. *Composites Part B: Engineering,* 69, pp. 145-153

EU-OSHA, 2009. *Workplace exposure to nanoparticles.* European Agency for Safety and Health at Work.

FALK, A. et al., 2016. Research roadmap for nanosafety-Part III: Closer to the market (CTTM).

FEICHT, P. et al., 2017. Systematic evaluation of different types of graphene oxide in respect to variations in their in-plane modulus. *Carbon,* 114, pp. 700-705

FEITO, N. et al., 2018. Experimental and numerical analysis of step drill bit performance when drilling woven CFRPs. *Composite Structures,* 184, pp. 1147-1155

FROGGETT, S.J. et al., 2014. A review and perspective of existing research on the release of nanomaterials from solid nanocomposites. *Particle and fibre toxicology,* 11(1), pp. 1

FROHLICH, E., 2012. The role of surface charge in cellular uptake and cytotoxicity of medical nanoparticles. *International journal of nanomedicine,* 7, pp. 5577-5591

FU, P.P. et al., 2014. Mechanisms of nanotoxicity: generation of reactive oxygen species. *Journal of Food and Drug Analysis,* 22(1), pp. 64-75

GAMINIAN, H. and MONTAZER, M., 2015. Enhanced self-cleaning properties on polyester fabric under visible light through single-step synthesis of cuprous oxide doped nano-TiO2. *Photochemistry and photobiology,* 91(5), pp. 1078-1087

GANGINENI, P.K. et al., 2019. Mechanical behavior of Graphene decorated carbon fiber reinforced polymer composites: An assessment of the influence of functional groups. *Composites Part A: Applied Science and Manufacturing,* 122, pp. 36-44

GANTAYAT, S., ROUT, D. and SWAIN, S.K., 2018. Carbon Nanomaterial–Reinforced Epoxy Composites: A Review. *Polymer-Plastics Technology and Engineering,* 57(1), pp. 1-16

GARDEA, F. and LAGOUDAS, D.C., 2014. Characterization of electrical and thermal properties of carbon nanotube/epoxy composites. *Composites Part B: Engineering,* 56, pp. 611-620

GAY, D., 2014. *Composite materials: design and applications.* CRC press.

GENDRE, L., RODRIGUEZ, V.M., ABHYANKAR, H., BLACKBURN, K. and BRIGHTON, J., 2015. Measurement of Nanoparticles Release during Drilling of Polymer Nanocomposites. *Journal of Physics: Conference Series.* IOP Publishing. pp. 012027

GENG, D. et al., 2019. Delamination formation, evaluation and suppression during drilling of composite laminates: A review. *Composite Structures,*

GEORGOPANOS, P. et al., 2017. Improvement of mechanical properties by a polydopamine interface in highly filled hierarchical composites of titanium dioxide particles and poly (vinyl butyral). *Composites Science and Technology,* 146, pp. 73-82

GHASEMI, F.A. et al., 2016. Optimization of mechanical properties of polypropylene/talc/graphene composites using response surface methodology. *Polymer Testing,* 53, pp. 283-292

GIRIFALCO, L., HODAK, M. and LEE, R.S., 2000. Carbon nanotubes, buckyballs, ropes, and a universal graphitic potential. *Physical Review B,* 62(19), pp. 13104

GLOBAL MARKET INSIGHTS, June 2018. *Carbon Nanotubes Market Size By Product (Single-Walled Carbon Nanotubes, Multi-Walled Carbon Nanotubes), By Application (Polymers, Energy, Electrical &*

Electronics), Industry Analysis Report, Regional Outlook (U.S., Canada, Germany, UK, France, Spain, Italy, Russia, China, Japan, India, Australia, Indonesia, Malaysia, Brazil, Mexico, GCC, South Africa), Growth Potential, Price Trends, Competitive Market Share & Forecast, 2018 – 2024. Delaware, USA: Kiran Pulidindi, Hemant Pandey.

GNACH, A. et al., 2015. Upconverting nanoparticles: assessing the toxicity. *Chemical Society Reviews,* 44(6), pp. 1561-1584

GÖHLER, D., NOGOWSKI, A., FIALA, P. and STINTZ, M., 2013. Nanoparticle release from nanocomposites due to mechanical treatment at two stages of the life-cycle. *Journal of Physics: Conference Series.* IOP Publishing. pp. 012045

GOJNY, F. et al., 2004. Carbon nanotube-reinforced epoxy-composites: enhanced stiffness and fracture toughness at low nanotube content. *Composites Science and Technology,* 64(15), pp. 2363-2371

GOMEZ, V. et al., 2014. Comparison of dust release from epoxy and paint nanocomposites and conventional products during sanding and sawing. *The Annals of Occupational Hygiene,* 58(8), pp. 983-994

GOPINATH, A., KUMAR, M.S. and ELAYAPERUMAL, A., 2014. Experimental investigations on mechanical properties of jute fiber reinforced composites with polyester and epoxy resin matrices. *Procedia Engineering,* 97, pp. 2052-2063

GORHAM, J.M. et al., 2012. Photo-induced surface transformations of silica nanocomposites. *Surface and Interface Analysis,* 44(13), pp. 1572-1581

GÖRNER, P. and FABRIÈS, J., 1996. Industrial aerosol measurement according to the new sampling conventions. *Occupational Hygiene,* 3(6), pp. 361-376

GOWDA, B.U. et al., 2015. Optimization of process parameters in drilling of epoxy Si3N4 composite material. *Materials Today: Proceedings,* 2(4-5), pp. 2852-2861

GRAPHICAL RESEARCH, November, 2018. *Unsaturated Polyester Resin (UPR) Market By End-Use (Building & Construction, Artificial Stones, Pipes & Tanks, Transport, Electrical, Marine), By Product (Isopthalic, Orthopthalic, DCPD), Industry Size, Share, Growth Trends & Forecast, 2018 – 2024.* India: Graphical Research Report.

GRIFFITHS, B., 2013. *A350 & A400M wing spars: A study in contrasts* . [online] Available from: http://www.compositesworld.com/articles/a350-a400m-wing-spars-a-study-in-contrasts [Accessed 03/11 2016]

GUADAGNO, L. et al., 2011. Effect of functionalization on the thermo-mechanical and electrical behavior of multi-wall carbon nanotube/epoxy composites. *Carbon,* 49(6), pp. 1919-1930

GUBBELS, E., JASINSKA-WALC, L. and KONING, C., 2013. Synthesis and characterization of novel renewable polyesters based on 2, 5-furandicarboxylic acid and 2, 3-butanediol. *Journal of Polymer Science Part A: Polymer Chemistry,* 51(4), pp. 890-898

GUO, Y. et al., 2011. Cytotoxic and genotoxic effects of multi-wall carbon nanotubes on human umbilical vein endothelial cells in vitro. *Mutation Research/Genetic Toxicology and Environmental Mutagenesis,* 721(2), pp. 184-191

GUPTA, R.K., KENNEL, E. and KIM, K., 2009. *Polymer nanocomposites handbook.* CRC press.

HADAL, R. et al., 2004. Effect of wollastonite and talc on the micromechanisms of tensile deformation in polypropylene composites. *Materials Science and Engineering: A,* 372(1-2), pp. 296-315

HADDAD, Y.M., 2013. *Mechanical Behaviour of Engineering Materials: Volume 2: Dynamic Loading and Intelligent Material Systems.* Springer Science & Business Media.

HADDEN, C.M. et al., 2015. Mechanical properties of graphene nanoplatelet/carbon fiber/epoxy hybrid composites: Multiscale modeling and experiments. *Carbon,* 95, pp. 100-112

HÄMERI, K. et al., 2002. The particle detection efficiency of the TSI-3007 condensation particle counter. *Journal of Aerosol Science,* 33(10), pp. 1463-1469

HANKIN, S.M. and READ, S.A., 2016. Governance of Nanotechnology: Context, Principles and Challenges. Managing Risk in Nanotechnology. Springer. pp. 29-49

HAQUE, M.M. et al., 2019. Melt-viscosity and mechanical behaviour of polypropylene (PP)/wood flour composites: Effect of pulverization of wood flour with and without water. *Advanced Industrial and Engineering Polymer Research,* 2(1), pp. 42-50

HARPER, S., WOHLLEBEN, W., DOA, M., NOWACK, B., CLANCY, S., CANADY, R. and MAYNARD, A., 2015. Measuring nanomaterial release from carbon nanotube composites: review of the state of the science. *Journal of Physics: Conference Series.* IOP Publishing. pp. 012026

HE, H. et al., 1998. A new structural model for graphite oxide. *Chemical physics letters,* 287(1), pp. 53-56

HE, P. et al., 2016. Preparation of multiscale graphene oxide-carbon fabric and its effect on mechanical properties of hierarchical epoxy resin composite. *Polymer Composites,* 37(5), pp. 1515-1522

HO-CHENG, H. and DHARAN, C., 1990. Delamination during drilling in composite laminates. *Journal of Engineering for Industry(Transactions of the ASME),* 112(3), pp. 236-239

HOCHENG, H. and PUW, H., 1993. Machinability of fiber-reinforced thermoplastics in drilling. *Journal of engineering materials and technology,* 115(1), pp. 146-149

HOCHENG, H. andTSAO, C., 2001. Analysis of delamination in drilling composite materials using step drill. *18th Conference Mechanical Engineering, Taipei, Taiwan.* pp. 895-900

HOCHENG, H. and TSAO, C., 2003. Comprehensive analysis of delamination in drilling of composite materials with various drill bits. *Journal of Materials Processing Technology,* 140(1-3), pp. 335-339

HO-CHENG, H. and TSAO, C., 2003. Analysis of delamination in drilling composite materials using core drill. *Australian Journal of Mechanical Engineering,* 1(1), pp. 49-53

HORNSBY, K. and PRYOR, S., 2014. A laboratory comparison of real-time measurement methods for 10–100-nm particle size distributions. *Aerosol Science and Technology,* 48(5), pp. 571-582

HRISTOZOV, D.R. et al., 2012. Risk assessment of engineered nanomaterials: a review of available data and approaches from a regulatory perspective. *Nanotoxicology,* 6(8), pp. 880-898

HSIEH, T. et al., 2010. The toughness of epoxy polymers and fibre composites modified with rubber microparticles and silica nanoparticles. *Journal of Materials Science,* 45(5), pp. 1193-1210

HSU, L. and CHEIN, H., 2007. Evaluation of nanoparticle emission for TiO 2 nanopowder coating materials. *Journal of Nanoparticle Research,* 9(1), pp. 157-163

HU, H., ONYEBUEKE, L. and ABATAN, A., 2010. Characterizing and modeling mechanical properties of nanocomposites-review and evaluation. *Journal of minerals and materials characterization and engineering,* 9(04), pp. 275

HUFENBACH, W. et al., 2007. Optimization of the rivet joints of the CFRP composite material and aluminium alloy. *Journal of Achievements in Materials and Manufacturing Engineering,* 20(1-2), pp. 119-122

HULL, D. and CLYNE, T., 1996. *An introduction to composite materials.* Cambridge university press.

HUNG, P. et al., 2019. Effect of graphene oxide concentration on flexural properties of CFRP at low temperature. *Carbon,*

HUNG, P. et al., 2018. Surface modification of carbon fibre using graphene–related materials for multifunctional composites. *Composites Part B: Engineering,* 133, pp. 240-257

HYER, M.W. and WHITE, S.R., 2009. *Stress analysis of fiber-reinforced composite materials.* DEStech Publications, Inc.

IRFAN, A. et al., 2013. Assessment of nanoparticle release from polyamide 6-and polypropylene-silicon composites and cytotoxicity in human lung A549 cells. *Journal of Inorganic and Organometallic Polymers and Materials,* 23(4), pp. 861-870

ISO, 1995. *Air Quality - Particle size fraction definitions for health-related sampling.* (ISO Standard 7708). Geneva, Switzerland: International Organization for Standardization.

ISO 14644-1:2015, 2015. *ISO 14644-1:2015 Cleanrooms and Associated Controlled Environments.* International Organisation for Standardization.

ISO TS 80004-2:2015, 2015. ISO/TS 80004-2:2015, Nanotechnologies -- Vocabulary -- Part 2: Nano-objects. *International Organisation for Standardization,* 1

ISO, 1., 2010. *Plastics Determination of Flexural Properties.* Switzerland: International Standard Organisation.

ISO, 5., 2012. *Plastics — Determination of tensile properties — Part 1: General principles.* Switzerland: International Standard Organisation.

ISO, T.8., 2015. ISO/TS 80004-2:2015, Nanotechnologies -- Vocabulary -- Part 2: Nano-objects. *International Organisation for Standardization,* 1

ISO/TS 12901-2, 2014. *Nanotechnologies — Occupational risk management applied to engineered nanomaterials — Part 2: Use of the control banding approach.* Geneva, Switzerland: International Organization for Standardization.

IUTA et al., 2011. *Tiered approach to an exposure measurement and assessment of nanoscale aerosols released from engineered nanomaterials in workplace operations.*

JACOBSEN, N.R. et al., 2008. Genotoxicity, cytotoxicity, and reactive oxygen species induced by single-walled carbon nanotubes and C60 fullerenes in the FE1-Muta™ Mouse lung epithelial cells. *Environmental and molecular mutagenesis,* 49(6), pp. 476-487

JENKINS, P. et al., 2019. Influence of Reduced Graphene Oxide on Epoxy/Carbon Fiber Reinforced Hybrid Composite: Flexural and Shear Properties under Varying Temperature Conditions. *Advanced Engineering Materials*, 21(6), pp. 1800614

JIANG, S. et al., 2016. Multiscale graphene oxide–carbon fiber reinforcements for advanced polyurethane composites. *Composites Part A: Applied Science and Manufacturing,* 87, pp. 1-9

JOHNSTON, H.J. et al., 2010a. A critical review of the biological mechanisms underlying the in vivo and in vitro toxicity of carbon nanotubes: The contribution of physico-chemical characteristics. *Nanotoxicology,* 4(2), pp. 207-246

JOHNSTON, H.J. et al., 2010b. A review of the in vivo and in vitro toxicity of silver and gold particulates: particle attributes and biological mechanisms responsible for the observed toxicity. *Critical reviews in toxicology,* 40(4), pp. 328-346

JONES, R.M., 2014. *Mechanics of composite materials.* CRC press.

KAEWAMATAWONG, T. et al., 2006. Acute and subacute pulmonary toxicity of low dose of ultrafine colloidal silica particles in mice after intratracheal instillation. *Toxicologic pathology,* 34(7), pp. 958-965

KAFI, A. et al., 2014. Effect of surface functionality of PAN-based carbon fibres on the mechanical performance of carbon/epoxy composites. *Composites Science and Technology,* 94, pp. 89-95

KAHN, D., 2015. *Attacking Problems in Logarithms and Exponential Functions .* New York: Dover Publications.

KAMPEERAPAPPUN, P. et al., 2007. Preparation of cassava starch/montmorillonite composite film. *Carbohydrate Polymers,* 67(2), pp. 155-163

KANG, Y. et al., 2017. Graphene oxide and reduced graphene oxide induced neural pheochromocytoma-derived PC12 cell lines apoptosis and cell cycle alterations via the ERK signaling pathways. *International journal of nanomedicine,* 12, pp. 5501-5510

KARATAŞ, M.A. and GÖKKAYA, H., 2018. A review on machinability of carbon fiber reinforced polymer (CFRP) and glass fiber reinforced polymer (GFRP) composite materials. *Defence Technology,* 14(4), pp. 318-326

KARLSSON, H.L. et al., 2009. Size-dependent toxicity of metal oxide particles—a comparison between nano-and micrometer size. *Toxicology letters,* 188(2), pp. 112-118

KHARE, R. and BOSE, S., 2005. Carbon nanotube based composites-a review. *Journal of minerals and Materials Characterization and Engineering,* 4(01), pp. 31

KIM, H. et al., 2004. Charge transport properties of composites of multiwalled carbon nanotube with metal catalyst and polymer: application to electromagnetic interference shielding. *Current Applied Physics,* 4(6), pp. 577-580

KIM, J. and MAI, Y., 1998. *Engineered interfaces in fiber reinforced composites.* Elsevier.

KIM, J.A. et al., 2006. Effects of surface modification on rheological and mechanical properties of CNT/epoxy composites. *Carbon,* 44(10), pp. 1898-1905

KISIN, E. et al., 2011. Genotoxicity of carbon nanofibers: are they potentially more or less dangerous than carbon nanotubes or asbestos? *Toxicology and applied pharmacology,* 252(1), pp. 1-10

KOBAYASHI, N., IZUMI, H. and MORIMOTO, Y., 2017. Review of toxicity studies of carbon nanotubes. *Journal of occupational health,* , pp. 17-0089-RA

KOO, J.H., 2016. *Fundamentals, properties, and applications of polymer nanocomposites.* Cambridge University Press.

KOPLEV, A., LYSTRUP, A. and VORM, T., 1983. The cutting process, chips, and cutting forces in machining CFRP. *Composites,* 14(4), pp. 371-376

KOTAL, M. and BHOWMICK, A.K., 2015. Polymer nanocomposites from modified clays: Recent advances and challenges. *Progress in Polymer Science,* 51, pp. 127-187

KRUG, H.F., 2014. Nanosafety research—are we on the right track? *Angewandte Chemie International Edition,* 53(46), pp. 12304-12319

KULKARNI, P., BARON, P.A. and WILLEKE, K., 2011. *Aerosol measurement: principles, techniques, and applications.* John Wiley & Sons.

KULKARNI, R. et al., 2019. Taguchi Analysis of the Thrust Force and Delamination in Drilling of Glass Fiber Reinforced Epoxy/Clay Nanocomposites. *Journal of Polymer & Composites,* 2(2), pp. 14-23

KUMAR, D. and SINGH, K., 2019. Investigation of delamination and surface quality of machined holes in drilling of multiwalled carbon nanotube doped epoxy/carbon fiber reinforced polymer nanocomposite. *Proceedings of the Institution of Mechanical Engineers, Part L: Journal of Materials: Design and Applications,* 233(4), pp. 647-663

KUMAR, S.K. et al., 2017. 50th anniversary perspective: are polymer nanocomposites practical for applications? *Macromolecules,* 50(3), pp. 714-731

LACHAUD, F. et al., 2001. Drilling of composite structures. *Composite structures,* 52(3-4), pp. 511-516

LADANI, R.B. et al., 2015. Improving the toughness and electrical conductivity of epoxy nanocomposites by using aligned carbon nanofibres. *Composites Science and Technology,* 117, pp. 146-158

LALWANI, G. et al., 2016. Toxicology of graphene-based nanomaterials. *Advanced Drug Delivery Reviews,* 105, pp. 109-144

LANDEL, R.F. and NIELSEN, L.E., 1993. *Mechanical properties of polymers and composites.* Crc Press.

LAPCIK JR, L., JINDROVA, P. and LAPCIKOVA, B., 2009. Effect of Talc Filler Content on Poly (Propylene) Composite Mechanical Properties. *Engineering Against Fracture.* Springer. pp. 73-80

LEAVEY, A. et al., 2013. Comparison of measured particle lung-deposited surface area concentrations by an Aerotrak 9000 using size distribution measurements for a range of combustion aerosols. *Aerosol Science and Technology,* 47(9), pp. 966-978

LEE, J.W. and KANG, Y.T., 2013. CO2 absorption enhancement by Al2O3 nanoparticles in NaCl aqueous solution. *Energy,* 53, pp. 206-211

LEE, S.K. et al., 2010. Flame retardant epoxy complex produced by addition of montmorillonite and carbon nanotube. *Journal of Industrial and Engineering Chemistry,* 16(6), pp. 891-895

LESZCZYŃSKA, A. et al., 2007. Polymer/montmorillonite nanocomposites with improved thermal properties: Part II. Thermal stability of montmorillonite nanocomposites based on different polymeric matrixes. *Thermochimica Acta,* 454(1), pp. 1-22

LI, K., QIU, R. and LIU, W., 2015. Improvement of interfacial adhesion in natural plant fiber-reinforced unsaturated polyester composites: A critical review. *Reviews of Adhesion and Adhesives,* 3(1), pp. 98-120

LI, L. et al., 2019. Improving the interfacial properties of carbon fiber–epoxy resin composites with a graphene-modified sizing agent. *Journal of Applied Polymer Science,* 136(9), pp. 47122

LI, N. et al., 2015. Drilling delamination and thermal damage of carbon nanotube/carbon fiber reinforced epoxy composites processed by microwave curing. *International Journal of Machine Tools and Manufacture,* 97, pp. 11-17

LIANG, J. et al., 2016. Tensile properties of graphene nano-platelets reinforced polypropylene composites. *Composites Part B: Engineering,* 95, pp. 166-171

LIANG, Y. and PEARSON, R., 2009. Toughening mechanisms in epoxy–silica nanocomposites (ESNs). *Polymer,* 50(20), pp. 4895-4905

LIN, J. et al., 2017. In-situ fabrication of halloysite nanotubes/silica nano hybrid and its application in unsaturated polyester resin. *Applied Surface Science,* 407, pp. 130-136

LIN, S. et al., 2018. Nanomaterials Safer-by-Design: An Environmental Safety Perspective. *Advanced Materials,* 30(17), pp. 1705691

LIN, W. et al., 2006. In vitro toxicity of silica nanoparticles in human lung cancer cells. *Toxicology and applied pharmacology,* 217(3), pp. 252-259

LIN, Y. et al., 2011. Effects of coating amount and particle concentration on the impact toughness of polypropylene/CaCO3 nanocomposites. *European polymer journal,* 47(3), pp. 294-304

LINDBERG, H.K. et al., 2009. Genotoxicity of nanomaterials: DNA damage and micronuclei induced by carbon nanotubes and graphite nanofibres in human bronchial epithelial cells in vitro. *Toxicology letters,* 186(3), pp. 166-173

LIU, D., TANG, Y. and CONG, W., 2012. A review of mechanical drilling for composite laminates. *Composite structures,* 94(4), pp. 1265-1279

LIU, L. et al., 2007. Tensile mechanics of electrospun multiwalled nanotube/poly (methyl methacrylate) nanofibers. *Advanced Materials,* 19(9), pp. 1228-1233

LIU, S. et al., 2018. A review of extending performance of epoxy resins using carbon nanomaterials. *Composites Part B: Engineering,* 136, pp. 197-214

LIU, W., HOA, S.V. and PUGH, M., 2005. Fracture toughness and water uptake of high-performance epoxy/nanoclay nanocomposites. *Composites Science and Technology,* 65(15), pp. 2364-2373

LIU, Y. et al., 2012. Understanding the toxicity of carbon nanotubes. *Accounts of Chemical Research,* 46(3), pp. 702-713

LIUFU, S., XIAO, H. and LI, Y., 2005. Thermal analysis and degradation mechanism of polyacrylate/ZnO nanocomposites. *Polymer Degradation and Stability,* 87(1), pp. 103-110

LO, L. et al., 2012. Evaluation of Engineering Controls in a Manufacturing Facility Producing Carbon Nanotube-Based Products; EPHB-356-13a; US Department of Health and Human Services. *Public Health Service, Centers for Disease Control and Prevention: Cincinnati, OH, USA,*

LORDAN, S., KENNEDY, J.E. and HIGGINBOTHAM, C.L., 2011. Cytotoxic effects induced by unmodified and organically modified nanoclays in the human hepatic HepG2 cell line. *Journal of applied toxicology,* 31(1), pp. 27-35

LORENZ, C. et al., 2012. Characterization of silver release from commercially available functional (nano) textiles. *Chemosphere,* 89(7), pp. 817-824

LOVE, S.A. et al., 2012. Assessing nanoparticle toxicity. *Annual review of analytical chemistry,* 5, pp. 181-205

LUCINTEL, December 2018. *Polypropylene Compound Market Report: Trends, Forecast and Competitive Analysis.* Texas, USA: Research and Markets.

LUO, G. et al., 2017. Coupling effects of glass fiber treatment and matrix modification on the interfacial microstructures and the enhanced mechanical properties of glass fiber/polypropylene composites. *Composites Part B: Engineering,* 111, pp. 190-199

LUO, J. and DANIEL, I.M., 2003. Characterization and modeling of mechanical behavior of polymer/clay nanocomposites. *Composites Science and Technology,* 63(11), pp. 1607-1616

LUO, W. et al., 2014. Interface enhancement of glass fiber/unsaturated polyester resin composites with nano-silica treated using silane coupling agent. *Wuhan University Journal of Natural Sciences,* 19(1), pp. 34-40

LUO, Y. et al., 2017. Fabrication of a three-dimensional reinforcement via grafting epoxy functionalized graphene oxide onto carbon fibers. *Materials Letters,* 209, pp. 463-466

LUYT, A. et al., 2009. Morphology, mechanical and thermal properties of composites of polypropylene and nanostructured wollastonite filler. *Polymer Testing,* 28(3), pp. 348-356

LYNCH, I., 2014. *Compendium of Projects in the European NanoSafety Cluster: 2014 Edition.* Birmingham, UK: NanoSafety Cluster.

LYNCH, I., 2015. *Compendium of Projects in the European NanoSafety Cluster: 2015 Edition.* Birmingham, UK: NanoSafety Cluster.

LYNCH, I., 2016. *Compendium of Projects in the European NanoSafety Cluster: 2016 Edition.* Birmingham, UK: NanoSafety Cluster.

LYNCH, I., WEISS, C. and VALSAMI-JONES, E., 2014. A strategy for grouping of nanomaterials based on key physico-chemical descriptors as a basis for safer-by-design NMs. *Nano Today,* 9(3), pp. 266-270

MA, J. et al., 2008. Effect of inorganic nanoparticles on mechanical property, fracture toughness and toughening mechanism of two epoxy systems. *Polymer,* 49(16), pp. 3510-3523

MADANI, S.Y., MANDEL, A. and SEIFALIAN, A.M., 2013. A concise review of carbon nanotube's toxicology. *Nano Reviews & Experiments,* 4

MAGREZ, A. et al., 2006. Cellular toxicity of carbon-based nanomaterials. *Nano letters,* 6(6), pp. 1121-1125

MAI, Y. and YU, Z., 2006. *Polymer nanocomposites.* Woodhead publishing.

MALLICK, P.K., 2007. *Fiber-reinforced composites: materials, manufacturing, and design.* CRC press.

MANALO, A.C. et al., 2015. Effects of alkali treatment and elevated temperature on the mechanical properties of bamboo fibre–polyester composites. *Composites Part B: Engineering,* 80, pp. 73-83

MARKET RESEARCH REPORT, April 2017. *NanoSilica Market Analysis, By Product (P Type, S Type, and Type III), By Application (Rubber, Healthcare, Food, Coatings, Plastics, Concrete, Gypsum, Battery, Electronics, Cosmetics), And Segment Forecasts, 2018 - 2025.* San Francisco, USA: Market Research Report.

MARKET RESEARCH REPORT, August 2016. *High Purity Alumina Market Analysis By Product (4N, 5N, 6N), By Application (Light Emitting Diodes, Semiconductors, Phosphor, Sapphire) And Segment Forecasts To 2024.* San Francisco, USA: Market Research Report.

MARQUIS, D.M., GUILLAUME, E. and CHIVAS-JOLY, C., 2011. Properties of nanofillers in polymer. *Nanocomposites and Polymers with Analytical Methods.* Intech.

MATESANZ, M. et al., 2013. The effects of graphene oxide nanosheets localized on F-actin filaments on cell-cycle alterations. *Biomaterials,* 34(5), pp. 1562-1569

MATHEW, J., JOY, J. and GEORGE, S.C., 2018. Potential applications of nanotechnology in transportation: A review. *Journal of King Saud University-Science,*

MAXIM, L.D. and MCCONNELL, E., 2005. A review of the toxicology and epidemiology of wollastonite. *Inhalation toxicology,* 17(9), pp. 451-466

MAXIM, L.D. et al., 2014. Wollastonite toxicity: an update. *Inhalation toxicology,* 26(2), pp. 95-112

MAY, C., 2018. *Epoxy resins: chemistry and technology.* Routledge.

MAYNARD, A.D. and AITKEN, R.J., 2007. Assessing exposure to airborne nanomaterials: current abilities and future requirements. *Nanotoxicology,* 1(1), pp. 26-41

MAZZUCKELLI, L.F. et al., 2007. Identification and characterization of potential sources of worker exposure to carbon nanofibers during polymer composite laboratory operations. *Journal of occupational and environmental hygiene,* 4(12), pp. D125-D130

MCALLISTER, M.J. et al., 2007. Single sheet functionalized graphene by oxidation and thermal expansion of graphite. *Chemistry of materials,* 19(18), pp. 4396-4404

MCELWAIN, S.E. et al., 2008. Effect of particle size on the wear resistance of alumina-filled PTFE micro-and nanocomposites. *Tribology Transactions,* 51(3), pp. 247-253

METHNER, M., CRAWFORD, C. and GERACI, C., 2012. Evaluation of the potential airborne release of carbon nanofibers during the preparation, grinding, and cutting of epoxy-based nanocomposite material. *Journal of occupational and environmental hygiene,* 9(5), pp. 308-318

METHNER, M. et al., 2010. Nanoparticle emission assessment technique (NEAT) for the identification and measurement of potential inhalation exposure to engineered nanomaterials—Part B: Results from 12 field studies. *Journal of occupational and environmental hygiene,* 7(3), pp. 163-176

METHNER, M., HODSON, L. and GERACI, C., 2010. Nanoparticle emission assessment technique (NEAT) for the identification and measurement of potential inhalation exposure to engineered nanomaterials—Part A. *Journal of occupational and environmental hygiene,* 7(3), pp. 127-132

MIHALACHE, R. et al., 2017. Occupational exposure limits for manufactured nanomaterials, a systematic review. *Nanotoxicology,* 11(1), pp. 7-19

MITCHELL, L.A. et al., 2007. Pulmonary and systemic immune response to inhaled multiwalled carbon nanotubes. *Toxicological sciences : an official journal of the Society of Toxicology,* 100(1), pp. 203-214

MITTAL, G. et al., 2015. A review on carbon nanotubes and graphene as fillers in reinforced polymer nanocomposites. *Journal of Industrial and Engineering Chemistry,* 21, pp. 11-25

MOHAN, V.B. et al., 2018. Graphene-based materials and their composites: a review on production, applications and product limitations. *Composites Part B: Engineering,* 142, pp. 200-220

MONTGOMERY, D., 2001. *Engineering Statistics.* 2nd Edition ed. New York: Wiley.

MOREAU, J.L. et al., 2012. Long-term mechanical durability of dental nanocomposites containing amorphous calcium phosphate nanoparticles. *Journal of Biomedical Materials Research Part B: Applied Biomaterials,* 100(5), pp. 1264-1273

MOROSE, G., 2010. The 5 principles of "design for safer nanotechnology". *Journal of Cleaner Production,* 18(3), pp. 285-289

MOTZKUS, C., CHIVAS-JOLY, C., GUILLAUME, E., DUCOURTIEUX, S., SARAGOZA, L., LESENECHAL, D. and MACE, T., 2011. Characterization of aerosol emitted by the combustion of nanocomposites. *Journal of Physics: Conference Series.* IOP Publishing. pp. 012020

MURRAY, A.R. et al., 2012. Factoring-in agglomeration of carbon nanotubes and nanofibers for better prediction of their toxicity versus asbestos. *Particle and fibre toxicology,* 9(1), pp. 1

NANOPORTAL, 2015. *Development of common approaches to the risk assessment of nanomaterials.* [online] Available from: http://nanoportal.gc.ca/default.asp?lang=En&n=9073BB1A-1&offset=3&toc=hide#_ftn7 [Accessed 08/31/ 2017]

NANOSAFER, 2017. *NanoSafer control-banding and risk management tool.* [online] Available from: http://www.nanosafer.org/ [Accessed 08/31/ 2017]

NGUYEN, T. et al., 2012. Characterization of surface accumulation and release of nanosilica during irradiation of polymer nanocomposites by ultraviolet light. *Journal of nanoscience and nanotechnology,* 12(8), pp. 6202-6215

NGUYEN, T. et al., 2017. Impact of UV irradiation on multiwall carbon nanotubes in nanocomposites: Formation of entangled surface layer and mechanisms of release resistance. *Carbon,* 116, pp. 191-200

NIH, 2017. *Hazardous substances data bank (HSDB).* [online] Available from: https://toxnet.nlm.nih.gov/cgi-bin/sis/htmlgen?HSDB [Accessed 08/31/ 2017]

NIKNAM, S.A., KHETTABI, R. and SONGMENE, V., 2014. Machinability and machining of titanium alloys: a review. *Machining of titanium alloys.* Springer. pp. 1-30

NIOSH, 2013. *Current Intelligence Bulletin 65: Occupational Exposure to Carbon Nanotubes and Nanofibers.* US Department of Health and Human Services, Centers for Disease Control, National Institute for Occupational safety and Health.

NIOSH, 2016. *The national institute for occupational safety and health - hierarchy of controls.* [online] Available from: https://www.cdc.gov/niosh/topics/hierarchy/default.html [Accessed 10/10 October 2018]

NJUGUNA, J. et al., 2014. Nanomaterials, nanofillers, and nanocomposites: types and properties. *Health and Environmental Safety of Nanomaterials: Polymer Nancomposites and Other Materials Containing Nanoparticles,* , pp. 1-27

NJUGUNA, J. et al., 2009. Opportunities and environmental health challenges facing integration of polymer nanocomposites: technologies for automotive applications. *International Journal of Applied Polymers and Technologies,* 1, pp. 2-3

NJUGUNA, J., PIELICHOWSKI, K. and FAN, J., 2012. Polymer nanocomposites for aerospace applications. *Adv.Polymer Nanocomposites: Types Appl.,*

NJUGUNA, J., PIELICHOWSKI, K. and DESAI, S., 2008. Nanofiller-reinforced polymer nanocomposites. *Polymers for Advanced Technologies,* 19(8), pp. 947-959

NJUGUNA, J. and SACHSE, S., 2014. Measurement and sampling techniques for characterization of airborne nanoparticles released from nano-enhanced products. *Health and Environmental Safety of Nanomaterials.Polymer Nancomposites and Other Materials Containing Nanoparticles.,* , pp. 78-111

NJUGUNA, J. and PIELICHOWSKI, K., 2003. Polymer nanocomposites for aerospace applications: properties. *Advanced Engineering Materials,* 5(11), pp. 769-778

NSC, 2016. *2016 Edition of the Nanosafety Cluster Compendium of projects.* NanoSafety Cluster.

OBERDÖRSTER, G. et al., 2015. Inhalation exposure to carbon nanotubes (CNT) and carbon nanofibers (CNF): Methodology and dosimetry. *Journal of Toxicology and Environmental Health, Part B,* 18(3-4), pp. 121-212

OBERDORSTER, G., OBERDORSTER, E. and OBERDORSTER, J., 2005. Nanotoxicology: an emerging discipline evolving from studies of ultrafine particles. *Environmental health perspectives,* 113(7), pp. 823-839

ODEGARD, G., CLANCY, T. and GATES, T., 2005. Modeling of the mechanical properties of nanoparticle/polymer composites. *Polymer,* 46(2), pp. 553-562

OECD, 2017. *Consumer And Environmental Exposure To Manufactured Nanomaterials Information used to characterize exposures: Analysis of a Survey.* Paris, France: Organisation for Economic Co-operation and Development.

OECD ENV/JM/MONO, 2009. *Emission Assessment For The Identification Of Sources And Release Of Airborne Manufactured Nanomaterials In The Workplace: Compilation Of Existing Guidance.* Paris: Organisation for Economic Co-operation and Development.

OECD ENV/JM/MONO, 2009. *Preliminary Review of OECD Test Guidelines for their Applicability to Manufactured Nanomaterials.* Paris: Organisation for Economic Co-operation and Development.

OECD ENV/JM/MONO, 2012. *Guidance on Sample Preparation and Dosimetry for the Safety Testing of Manufactured Nanomaterials.* Paris: Organisation for Economic Co-operation and Development.

OECD ENV/JM/MONO, 2015. *Harmonized tiered approach to measure and assess the potential exposure to airborne emissions of engineered nano-objects and their agglomerates and aggregates at workplaces.* Paris: Organisation for Economic Co-operation and Development.

OECD ENV/JM/MONO, 2019. *Physical-Chemical Decision Framework To Inform Decisions For Risk Assessment Of Manufactured Nanomaterials.* Paris: Organisation for Economic Co-operation and Development.

OGURA, I., KOTAKE, M., SHIGETA, M., UEJIMA, M., SAITO, K., HASHIMOTO, N. and KISHIMOTO, A., 2013. Potential release of carbon nanotubes from their composites during grinding. *Journal of Physics: Conference Series.* IOP Publishing. pp. 012049

OKADA, A. et al., 1988. *Composite material and process for manufacturing same, U.S. Patent No. 4,739,007. Washington, DC: U.S. Patent and Trademark Office.*

ONO-OGASAWARA, M., TAKAYA, M., KUBOTA, H., SHINOHARA, Y., KODA, S., AKIBA, E., TSURUOKA, S. and MYOJO, T., 2013. Approach to the exposure assessment of MWCNT by considering size distribution and oxidation temperature of elemental carbon. *Journal of Physics: Conference Series.* IOP Publishing. pp. 012004

PALUSZKIEWICZ, C. et al., 2011. FT-IR study of montmorillonite–chitosan nanocomposite materials. *Spectrochimica Acta Part A: Molecular and Biomolecular Spectroscopy,* 79(4), pp. 784-788

PANCHAGNULA, K.K. and PALANIYANDI, K., 2018. Drilling on fiber reinforced polymer/nanopolymer composite laminates: a review. *Journal of materials research and technology,* 7(2), pp. 180-189

PARK, E. and PARK, K., 2009. Oxidative stress and pro-inflammatory responses induced by silica nanoparticles in vivo and in vitro. *Toxicology letters,* 184(1), pp. 18-25

PARK, E. et al., 2015. A 13-week repeated-dose oral toxicity and bioaccumulation of aluminum oxide nanoparticles in mice. *Archives of Toxicology,* 89(3), pp. 371-379

PARK, J.H. and JANA, S.C., 2003. The relationship between nano-and micro-structures and mechanical properties in PMMA–epoxy–nanoclay composites. *Polymer,* 44(7), pp. 2091-2100

PARK, M.V. et al., 2011. The effect of particle size on the cytotoxicity, inflammation, developmental toxicity and genotoxicity of silver nanoparticles. *Biomaterials,* 32(36), pp. 9810-9817

PARK, S. et al., 2008. Graphene oxide papers modified by divalent ions—enhancing mechanical properties via chemical cross-linking. *ACS nano,* 2(3), pp. 572-578

PASRICHA, A. et al., 2012. Comparative study of leaching of silver nanoparticles from fabric and effective effluent treatment. *Journal of Environmental Sciences,* 24(5), pp. 852-859

PASZKIEWICZ, S. et al., 2012. Electrical conductivity of poly (ethylene terephthalate)/expanded graphite nanocomposites prepared by in situ polymerization. *Journal of Polymer Science Part B: Polymer Physics,* 50(23), pp. 1645-1652

PATEL, V.K. and DHANOLA, A., 2016. Influence of CaCO3, Al2O3, and TiO2 microfillers on physico-mechanical properties of Luffa cylindrica/polyester composites. *Engineering Science and Technology, an International Journal,* 19(2), pp. 676-683

PATHAK, A.K. et al., 2016. Improved mechanical properties of carbon fiber/graphene oxide-epoxy hybrid composites. *Composites Science and Technology,* 135, pp. 28-38

PATLOLLA, A., KNIGHTEN, B. and TCHOUNWOU, P., 2010. Multi-walled carbon nanotubes induce cytotoxicity, genotoxicity and apoptosis in normal human dermal fibroblast cells. *Ethnicity & disease,* 20(1 Suppl 1), pp. S1-65-72

PAUL, D.R. and ROBESON, L.M., 2008. Polymer nanotechnology: nanocomposites. *Polymer,* 49(15), pp. 3187-3204

PAYANDEHPEYMAN, J., MAJZOOBI, G. and BAGHERI, R., 2017. Experimental and analytical investigations into the effects of inorganic filler on the polypropylene nanocomposite microhardness. *Journal of Thermoplastic Composite Materials,* 30(11), pp. 1484-1502

PICCINNO, F. et al., 2012. Industrial production quantities and uses of ten engineered nanomaterials in Europe and the world. *Journal of Nanoparticle Research,* 14(9), pp. 1-11

PIELICHOWSKI, K. and NJUGUNA, J., 2005. *Thermal degradation of polymeric materials.* iSmithers Rapra Publishing.

PIELICHOWSKI, K., NJUGUNA, J. and MICHAŁOWSKI, S., 2014. Recent developments of foamed polymer/layered silicates nanocomposites. *Handbook of Polymernanocomposites. Processing, Performance and Application.* Springer. pp. 453-479

PLASTICSEUROPE MARKET RESEARCH GROUP, 2018. *Plastics – the Facts 2018. An analysis of European plastics production, demand and waste data.* Belgium: PlasticsEurope.

PLUEDDEMANN, E.P., 2016. *Interfaces in Polymer Matrix Composites: Composite Materials.* Elsevier.

POLAND, C.A. et al., 2008. Carbon nanotubes introduced into the abdominal cavity of mice show asbestos-like pathogenicity in a pilot study. *Nature nanotechnology,* 3(7), pp. 423-428

PORTER, D.W. et al., 2010. Mouse pulmonary dose-and time course-responses induced by exposure to multi-walled carbon nanotubes. *Toxicology,* 269(2), pp. 136-147

POVEDA, R.L. and GUPTA, N., 2016. *Carbon nanofiber reinforced polymer composites.* Springer.

PRASHANTHA, K. et al., 2009. Masterbatch-based multi-walled carbon nanotube filled polypropylene nanocomposites: Assessment of rheological and mechanical properties. *Composites Science and Technology,* 69(11), pp. 1756-1763

QIN, W. et al., 2015. Mechanical and electrical properties of carbon fiber composites with incorporation of graphene nanoplatelets at the fiber–matrix interphase. *Composites Part B: Engineering,* 69, pp. 335-341

RABOLLI, V. et al., 2010. Influence of size, surface area and microporosity on the in vitro cytotoxic activity of amorphous silica nanoparticles in different cell types. *Nanotoxicology,* 4(3), pp. 307-318

RADER, D.J., 1990. Momentum slip correction factor for small particles in nine common gases. *Journal of Aerosol Science,* 21(2), pp. 161-168

RAFIEE, M.A., 2011. *Graphene-based composite materials. Rensselaer Polytechnic Institute: Troy, NY, USA.*

RAJAKUMAR, I.P.T., HARIHARAN, P. and SRIKANTH, I., 2013. A study on monitoring the drilling of polymeric nanocomposite laminates using acoustic emission. *Journal of Composite Materials,* 47(14), pp. 1773-1784

RAJESH, S. et al., 2014. Analysis of Mechanical Behavior of Glass Fibre/Al2O3-SiC Reinforced Polymer composites. *Procedia Engineering,* 97, pp. 598-606

RASMUSSEN, K. et al., 2016. Review of achievements of the OECD Working Party on Manufactured Nanomaterials' Testing and Assessment Programme. From exploratory testing to test guidelines. *Regulatory Toxicology and Pharmacology,* 74, pp. 147-160

RAY, S.S. and OKAMOTO, M., 2003. Polymer/layered silicate nanocomposites: a review from preparation to processing. *Progress in polymer science,* 28(11), pp. 1539-1641

REACH, 2017. *Regulation on Registration, Evaluation, Authorization and Restriction of Chemical.* Commission Regulation (EU) 2017/999: European Union.

REDDY, J.N. and MIRAVETE, A., 2018. *Practical analysis of composite laminates.* CRC press.

RIBEIRO, M., SOUSA, S. and NÓVOA, P., 2015. An investigation on fire and flexural mechanical behaviors of nano and micro polyester composites filled with SiO2 and Al2O3 particles. *Materials Today: Proceedings,* 2(1), pp. 8-19

RUSMIROVIĆ, J. et al., 2016. High performance unsaturated polyester based nanocomposites: Effect of vinyl modified nanosilica on mechanical properties. *Express Polymer Letters,* 10(2),

SABA, N. et al., 2016. A review on dynamic mechanical properties of natural fibre reinforced polymer composites. *Construction and Building Materials,* 106, pp. 149-159

SABER, A.T. et al., 2012. Inflammatory and genotoxic effects of sanding dust generated from nanoparticle-containing paints and lacquers. *Nanotoxicology,* 6(7), pp. 776-788

SACHSE, S., SILVA, F., IRFAN, A., ZHU, H., PIELICHOWSKI, K., LESZCZYNSKA, A., BLAZQUEZ, M., KAZMINA, O., KUZMENKO, O. and NJUGUNA, J., 2012. Physical characteristics of nanoparticles emitted during drilling of silica based polyamide 6 nanocomposites. *IOP Conference Series: Materials Science and Engineering.* IOP Publishing. pp. 012012

SACHSE, S., SILVA, F., IRFAN, A., ZHU, H., PIELICHOWSKI, K., LESZCZYNSKA, A., BLAZQUEZ, M., KAZMINA, O., KUZMENKO, O. and NJUGUNA, J., 2012a. Physical characteristics of nanoparticles emitted during drilling of silica based polyamide 6 nanocomposites. *IOP Conference Series: Materials Science and Engineering.* IOP Publishing. pp. 012012

SACHSE, S. et al., 2012b. The effect of nanoclay on dust generation during drilling of PA6 nanocomposites. *Journal of Nanomaterials,* 2012, pp. 26

SADEGHALVAAD, M. and SABBAGHI, S., 2015. The effect of the TiO2/polyacrylamide nanocomposite on water-based drilling fluid properties. *Powder Technology,* 272, pp. 113-119

SAHARUDIN, M.S. et al., 2016. The degradation of mechanical properties in polymer nano-composites exposed to liquid media–a review. *RSC Advances,* 6(2), pp. 1076-1089

SAMAL, S.K., NAYAK, S.K. and MOHANTY, S., 2008. Polypropylene nanocomposites: effect of organo-modified layered silicates on mechanical, thermal & morphological performance. *Journal of Thermoplastic Composite Materials,* 21(3), pp. 243-263

SANCHEZ JIMENEZ, A., VAN TONGEREN, M. and AITKEN, R., 2012. Guidance for collection of inhalable and respirable Ni dust. *IOM report,* , pp. 538-0000

SCHLAGENHAUF, L. et al., 2012. Release of carbon nanotubes from an epoxy-based nanocomposite during an abrasion process. *Environmental science & technology,* 46(13), pp. 7366-7372

SCHUTZ JA, 2015. *Particle Emissions from Machining of Polypropylene Composites* Australia: CSIRO.

SELVAKUMAR, V., PALANIKUMAR, K. and PALANIVELU, K., 2010. Studies on mechanical characterization of polypropylene/Na -MMT nanocomposites. *Journal of Minerals and Materials Characterization and Engineering,* 9(08), pp. 671

SEN, S. et al., 2007. Chain conformations and bound-layer correlations in polymer nanocomposites. *Physical Review Letters,* 98(12), pp. 128302

SHAO, ed. 2008. *Mathematical Statistics.* Second Edition ed. New York: Springer.

SHEN, X. et al., 2013. Significantly modified tribological performance of epoxy nanocomposites at very low graphene oxide content. *Polymer,* 54(3), pp. 1234-1242

SHEN, X. et al., 2014. Tribological performance of carbon nanotube–graphene oxide hybrid/epoxy composites. *Composites Part B: Engineering,* 57, pp. 120-125

SHIMPI, N., SHIROLE, S. and MISHRA, S., 2017. Polypropylene/nTiO2 nanocomposites using melt mixing and its investigation on mechanical and thermal properties. *Polymer Composites,* 38(7), pp. 1273-1279

SHIN, M.K. et al., 2012. Synergistic toughening of composite fibres by self-alignment of reduced graphene oxide and carbon nanotubes. *Nature communications,* 3, pp. 650

SHOKRIEH, M.M., SAEEDI, A. and CHITSAZZADEH, M., 2013. Mechanical properties of multi-walled carbon nanotube/polyester nanocomposites. *Journal of Nanostructure in Chemistry,* 3(1), pp. 1-5

SHOKRIEH, M. et al., 2014. Flexural fatigue behavior of synthesized graphene/carbon-nanofiber/epoxy hybrid nanocomposites. *Materials & Design (1980-2015),* 62, pp. 401-408

SHUBHRA, Q.T., ALAM, A. and QUAIYYUM, M., 2013. Mechanical properties of polypropylene composites: A review. *Journal of Thermoplastic Composite Materials,* 26(3), pp. 362-391

SKAKALOVA, V., DETTLAFF-WEGLIKOWSKA, U. and ROTH, S., 2005. Electrical and mechanical properties of nanocomposites of single wall carbon nanotubes with PMMA. *Synthetic Metals,* 152(1-3), pp. 349-352

SONGMENE, V. et al., 2011. Machining and machinability of aluminum alloys. *Alum.Alloys Theory Appl,*

SONGMENE, V. et al., 2015. Nanoparticle measurement, control and characterization: procedure applied to machining and mechanical friction.

SOUTAR, C.A. et al., 2000. Epidemiological evidence on the carcinogenicity of silica: factors in scientific judgement. *The Annals of Occupational Hygiene,* 44(1), pp. 3-14

SPITALSKY, Z. et al., 2010. Carbon nanotube–polymer composites: chemistry, processing, mechanical and electrical properties. *Progress in polymer science,* 35(3), pp. 357-401

SRIVASTAVA, V.K. et al., 2017. Effect of nanomaterial on mode I and mode II interlaminar fracture toughness of woven carbon fabric reinforced polymer composites. *Engineering Fracture Mechanics,* 180, pp. 73-86

STAROST, K., et al., 2017. Environmental Particle Emissions due to Automated Drilling of Polypropylene Composites and Nanocomposites Reinforced with Talc, Montmorillonite and Wollastonite. *IOP Conference Series: Materials Science and Engineering*. IOP Publishing. pp. 012011

STAROST, K. et al., 2017. Assessment of nanoparticles release into the environment during drilling of carbon nanotubes/epoxy and carbon nanofibres/epoxy nanocomposites. *Journal of hazardous materials*, 340, pp. 57-66

STAROST, K. et al., 2017. The effect of nanosilica (SiO2) and nanoalumina (Al2O3) reinforced polyester nanocomposites on aerosol nanoparticle emissions into the environment during automated drilling. *Aerosol Science and Technology*, 51(9), pp.1035-1046.

STAROST, K. and NJUGUNA, J., 2014. A review on the effect of mechanical drilling on polymer nanocomposites. *IOP Conference Series: Materials Science and Engineering*. IOP Publishing. pp. 012031

STAROST, K. and NJUGUNA, J., 2020. The Influence of Graphene Oxide on Nanoparticle Emissions during Drilling of Graphene/Epoxy Carbon-Fiber Reinforced Engineered Nanomaterials. Atmosphere, 11(6), pp. 573

STONE, V. et al., 2010. Nanomaterials for environmental studies: classification, reference material issues, and strategies for physico-chemical characterisation. *Science of the total environment,* 408(7), pp. 1745-1754

ŠVAB, I., MUSIL, V. and LESKOVAC, M., 2005. The adhesion phenomena in polypropylene/wollastonite composites. *Acta Chim.Slov,* 52, pp. 264-271

TAGLIAFERRI, V., CAPRINO, G. and DITERLIZZI, A., 1990. Effect of drilling parameters on the finish and mechanical properties of GFRP composites. *International Journal of Machine Tools and Manufacture,* 30(1), pp. 77-84

TAKAYA, M. et al., 2012. Evaluation of exposure risk in the weaving process of MWCNT-coated yarn with real-time particle concentration measurements and characterization of dust particles. *Industrial health,* , pp. 1201290120-1201290120

TAN, C., AZMI, A. and MUHAMMAD, N., 2016. Delamination and surface roughness analyses in drilling hybrid carbon/glass composite. *Materials and Manufacturing Processes,* 31(10), pp. 1366-1376

TANG, C. et al., 2017. Silver nanoparticles-loaded activated carbon fibers using chitosan as binding agent: Preparation, mechanism, and their antibacterial activity. *Applied Surface Science,* 394, pp. 457-465

TETI, R., 2002. Machining of composite materials. *CIRP Annals,* 51(2), pp. 611-634

TJONG, S.C., 2006. Structural and mechanical properties of polymer nanocomposites. *Materials Science and Engineering: R: Reports,* 53(3), pp. 73-197

TRINATH, K. and RAMANJANEYULU, G., 2016. Mechanical characteristics of micro and Nano Silica, ZnO and chitin powder filled unsaturated polyester composites. *Indian J Sci Technol,* 9(S1), pp. 1-5

TSAI, S., 2018. *Introduction to composite materials.* Routledge.

TSI CPC-003-A4, 2014. *TSI Fundamentals of condensation Particle counters (CPC) and Scanning mobility particle sizer (SMPS) spectrometers.* TSI Incorporated.

TSI P/N 1933792, 2009. *Series 3080, Electrostatic Classifiers, Operation and Service Manual.* TSI Incorporated.

URDL, K. et al., 2017. Self-healing of densely crosslinked thermoset polymers—a critical review. *Progress in Organic Coatings,* 104, pp. 232-249

VAIA, R.A. and WAGNER, H.D., 2004. Framework for nanocomposites. *Materials today,* 7(11), pp. 32-37

VARSOU, D. et al., 2019. A safe-by-design tool for functionalised nanomaterials through the Enalos Nanoinformatics Cloud platform. *Nanoscale Advances,* 1(2), pp. 706-718

VASILIEV, V. and MOROZOV, E.V., 2013. *Advanced mechanics of composite materials and structural elements.* Newnes.

VEGA-VILLA, K.R. et al., 2008. Clinical toxicities of nanocarrier systems. *Advanced Drug Delivery Reviews,* 60(8), pp. 929-938

VELASCO-SANTOS, C. et al., 2003. Improvement of thermal and mechanical properties of carbon nanotube composites through chemical functionalization. *Chemistry of materials,* 15(23), pp. 4470-4475

VISAKH, P. and YOSHIHIKO, A., 2015. *Flame retardants: Polymer blends, composites and nanocomposites.* Springer.

VON GOETZ, N. et al., 2013. Migration of Ag-and TiO2-(Nano) particles from textiles into artificial sweat under physical stress: experiments and exposure modeling. *Environmental science & technology,* 47(17), pp. 9979-9987

VORBAU, M., HILLEMANN, L. and STINTZ, M., 2009. Method for the characterization of the abrasion induced nanoparticle release into air from surface coatings. *Journal of Aerosol Science,* 40(3), pp. 209-217

VÖRÖS, G. and PUKÁNSZKY, B., 1995. Stress distribution in particulate filled composites and its effect on micromechanical deformation. *Journal of Materials Science,* 30(16), pp. 4171-4178

VÖRÖS, G. and PUKÁNSZKY, B., 2002. Prediction of the yield stress of composites containing particles with an interlayer of changing properties. *Composites Part A: Applied Science and Manufacturing,* 33(10), pp. 1317-1322

WAN, Y. et al., 2014. Grafting of epoxy chains onto graphene oxide for epoxy composites with improved mechanical and thermal properties. *Carbon,* 69, pp. 467-480

WANG, F. and CAI, X., 2019. Improvement of mechanical properties and thermal conductivity of carbon fiber laminated composites through depositing graphene nanoplatelets on fibers. *Journal of Materials Science,* 54(5), pp. 3847-3862

WANG, J. et al., 2011. Cytotoxicity of single-walled carbon nanotubes on PC12 cells. *Toxicology in vitro,* 25(1), pp. 242-250

WANG, L. et al., 2010. Mechanical properties and microstructure of polyetheretherketone–hydroxyapatite nanocomposite materials. *Materials Letters,* 64(20), pp. 2201-2204

WANG, Z., GU, P. and ZHANG, Z., 2010. Indentation and scratch behavior of nano-SiO 2/polycarbonate composite coating at the micro/nano-scale. *Wear,* 269(1), pp. 21-25

WARHEIT, D.B., REED, K.L. and DELORME, M.P., 2013. Subchronic inhalation of carbon nanofibers: No apparent cross-talk between local pulmonary and cardiovascular/systemic responses. *Carbon,* 62, pp. 165-176

WATSON, G., STAROST, K., BARI, P., FAISAL, N., MISHRA, S. and NJUGUNA, J., 2017. Tensile and Flexural Properties of Hybrid Graphene Oxide/Epoxy Carbon Fibre Reinforced Composites. *IOP Conference Series: Materials Science and Engineering*. IOP Publishing. pp. 012009

WEON, J. and SUE, H., 2006. Mechanical properties of talc-and CaCO 3-reinforced high-crystallinity polypropylene composites. *Journal of Materials Science,* 41(8), pp. 2291-2300

WERNIK, J. and MEGUID, S., 2014. On the mechanical characterization of carbon nanotube reinforced epoxy adhesives. *Materials & Design,* 59, pp. 19-32

WETZEL, B., HAUPERT, F. and ZHANG, M.Q., 2003. Epoxy nanocomposites with high mechanical and tribological performance. *Composites Science and Technology,* 63(14), pp. 2055-2067

WIEDENSOHLER, A. et al., 2012. Mobility particle size spectrometers: harmonization of technical standards and data structure to facilitate high quality long-term observations of atmospheric particle number size distributions. *Atmospheric Measurement Techniques,* 5, pp. 657-685

WITSCHGER, O., 1999. *Sampling of Airborne Dusts in Workplace Atmospheres.* (3rd European ALARA Network Workshop). Neuherberg, Germany: ALARA Network.

WORLD HEALTH ORGANIZATION, 2017. *WHO guidelines on protecting workers from potential risks of manufactured nanomaterials.* World Health Organization.

WU, G. et al., 2015. Interfacially reinforced methylphenylsilicone resin composites by chemically grafting multiwall carbon nanotubes onto carbon fibers. *Composites Part B: Engineering,* 82, pp. 50-58

WU, Q. et al., 2010. Study of fire retardant behavior of carbon nanotube membranes and carbon nanofiber paper in carbon fiber reinforced epoxy composites. *Carbon,* 48(6), pp. 1799-1806

XIA, Z., 2016. *Biomimetic principles and design of advanced engineering materials.* John Wiley & Sons.

XIE, J., BAYOUMI, A. and ZBIB, H., 1996. A study on shear banding in chip formation of orthogonal machining. *International Journal of Machine Tools and Manufacture,* 36(7), pp. 835-847

XU, J., MKADDEM, A. and EL MANSORI, M., 2016. Recent advances in drilling hybrid FRP/Ti composite: a state-of-the-art review. *Composite Structures,* 135, pp. 316-338

YANG, P. et al., 2013. Effect of hydrogen bonds on the modulus of bulk polybenzoxazines in the glassy state. *Physical Chemistry Chemical Physics,* 15(37), pp. 15333-15338

YANG, Z. et al., 2010. A review of nanoparticle functionality and toxicity on the central nervous system. *Journal of the Royal Society Interface,* 7(suppl_4), pp. S411-S422

YOONESSI, M. et al., 2014. Carbon nanotube epoxy nanocomposites: the effects of interfacial modifications on the dynamic mechanical properties of the nanocomposites. *ACS applied materials & interfaces,* 6(19), pp. 16621-16630

YOUSFI, M. et al., 2013. Use of new synthetic talc as reinforcing nanofillers for polypropylene and polyamide 6 systems: thermal and mechanical properties. *Journal of colloid and interface science,* 403, pp. 29-42

YUE, L. et al., 2014. Epoxy composites with carbon nanotubes and graphene nanoplatelets–Dispersion and synergy effects. *Carbon,* 78, pp. 268-278

ZANNA, S. et al., 2010. Ageing of plasma-mediated coatings with embedded silver nanoparticles on stainless steel: An XPS and ToF-SIMS investigation. *Applied Surface Science,* 256(22), pp. 6499-6505

ZARE, Y., 2016. Study of nanoparticles aggregation/agglomeration in polymer particulate nanocomposites by mechanical properties. *Composites Part A: Applied Science and Manufacturing,* 84, pp. 158-164

ZHANG, H. et al., 2015. Improved fracture toughness and integrated damage sensing capability by spray coated CNTs on carbon fibre prepreg. *Composites Part A: Applied Science and Manufacturing,* 70, pp. 102-110

ZHANG, H. et al., 2006. Property improvements of in situ epoxy nanocomposites with reduced interparticle distance at high nanosilica content. *Acta Materialia,* 54(7), pp. 1833-1842

ZHANG, R. et al., 2016. Directly grafting graphene oxide onto carbon fiber and the effect on the mechanical properties of carbon fiber composites. *Materials & Design,* 93, pp. 364-369

ZHANG, Y., RHEE, K.Y. and PARK, S., 2017. Nanodiamond nanocluster-decorated graphene oxide/epoxy nanocomposites with enhanced mechanical behavior and thermal stability. *Composites Part B: Engineering,* 114, pp. 111-120

ZHANG, Q. et al., 2013. Lysosomes involved in the cellular toxicity of nano-alumina: combined effects of particle size and chemical composition. *Journal of Biological Regulators and Homeostatic Agents,* 27(2), pp. 365-375

ZHANG, Q.L. et al., 2011. In vivo toxicity of nano-alumina on mice neurobehavioral profiles and the potential mechanisms. *International Journal of Immunopathology and Pharmacology,* 24(1 Suppl), pp. 23S-29S

ZHAO, X. et al., 2004. Smallest carbon nanotube is 3 Å in diameter. *Physical Review Letters,* 92(12), pp. 125502

ZHAO, Y. et al., 2007. Synthesis and characterization of ZnS/hyperbranched polyester nanocomposite and its optical properties. *Polymer,* 48(10), pp. 2853-2859

ZHAO, Y. et al., 2016. Mechanical, thermal and tribological properties of polyimide/nano-SiO2 composites synthesized using an in-situ polymerization. *Tribology International,* 103, pp. 599-608

ZHENG, N. et al., 2017. Improvement of interlaminar fracture toughness in carbon fiber/epoxy composites with carbon nanotubes/polysulfone interleaves. *Composites Science and Technology,* 140, pp. 8-15

ZHENG, S., PASCAULT, J. and WILLIAMS, R., 2010. Epoxy polymers: new materials and innovations. *Pascault, JP, Williams, RJJ, Eds,*

ZHOU, K. et al., 2015. MoS2 nanolayers grown on carbon nanotubes: an advanced reinforcement for epoxy composites. *ACS applied materials & interfaces,* 7(11), pp. 6070-6081

ZHOU, S. et al., 2003. Effect of nanosilica on the properties of polyester-based polyurethane. *Journal of Applied Polymer Science,* 88(1), pp. 189-193

ZHOU, Y., PERVIN, F. and JEELANI, S., 2007. Effect vapor grown carbon nanofiber on thermal and mechanical properties of epoxy. *Journal of Materials Science,* 42(17), pp. 7544-7553

ZHOU, Y. et al., 2008. Improvement in mechanical properties of carbon fabric–epoxy composite using carbon nanofibers. *Journal of Materials Processing Technology,* 198(1-3), pp. 445-453

ZHU, J. et al., 2010. In situ stabilized carbon nanofiber (CNF) reinforced epoxy nanocomposites. *Journal of Materials Chemistry,* 20(23), pp. 4937-4948

ZHU, Y. et al., 2010. Graphene and graphene oxide: synthesis, properties, and applications. *Advanced Materials,* 22(35), pp. 3906-3924

ZION MARKET RESEARCH, October 2018. *Fiber Reinforced Composites (FRC) Market by Product (Short Fiber-Reinforced Composites and Long Fiber/Continuous Reinforced Composites), by Fiber Type (Glass, Carbon, and Aramid), by Matrix (Polymer Matrix, Metal Matrix, and Non-metal Matrix) by End-user (Automotive, Building & Construction, Aerospace, Electrical & Electronics, Marine, Sports & Leisure, and Other End-User Industries): Global Industry Perspective, Comprehensive Analysis and Forecast, 2017 – 2024.* India: Zion Market Research.

ZITOUNE, R. and COLLOMBET, F., 2007. Numerical prediction of the thrust force responsible of delamination during the drilling of the long-fibre composite structures. *Composites Part A: Applied Science and Manufacturing,* 38(3), pp. 858-866

ZITOUNE, R., KRISHNARAJ, V. and COLLOMBET, F., 2010. Study of drilling of composite material and aluminium stack. *Composite Structures,* 92(5), pp. 1246-1255

ZOU, H., WU, S. and SHEN, J., 2008. Polymer/silica nanocomposites: preparation, characterization, properties, and applications. *Chem.Rev,* 108(9), pp. 3893-3957

Scientific Contributions

1. Journal Papers

Starost K, Frijns E, Van Laer J, Faisal N, Egizabal A, Elizextea C, Nelissen I, Blazquez M, Njuguna J. The effect of nanosilica (SiO_2) and nanoalumina (Al_2O_3) reinforced polyester nanocomposites on aerosol nanoparticle emissions into the environment during automated drilling. *Aerosol Science and Technology*. Vol. 51, Iss. 9, 2017.

Starost K., Frijns E., Van Laer J., Faisal N., Egizabal A., Elizextea C., Blazquez, M. & Njuguna J.: Assessment of Nanoparticles Release into the Environment during Drilling of Carbon Nanotubes/ Epoxy and Carbon Nanofibres/Epoxy Nanocomposites, *Journal of Hazardous Materials,* 2017; 340: pp 57-66.

Jenkins, P., Siddique, S., Khan, S., Usman, A., Starost, K., MacPherson, A., Bari, P., Mishra, S. and Njuguna, J.: Influence of Reduced Graphene Oxide on Epoxy/Carbon Fiber-Reinforced Hybrid Composite: Flexural and Shear Properties under Varying Temperature Conditions. *Advanced Engineering Materials*; 2019, p.1800614.

Starost K, Frijns E, Van Laer J, Faisal N, Egizabal A, Elizextea C, Nelissen I, Blazquez M, Njuguna J. A Study on the Nanoparticle Emissions into Environment During Mechanical Drilling of Polyester, Polypropylene and Epoxy Nanocomposite Materials. *Environmental Science: Nano*. Submitted April 2020.

Starost K, and Njuguna J. The Influence of Graphene Oxide on Nanoparticle Emissions during Drilling of Graphene/Epoxy Carbon-Fiber Reinforced Engineered Nanomaterials. *Atmosphere*, 11(6), pp. 573

2. Conference Papers and Oral Presentations

Starost K, Frijns E, Laer JV, Faisal N, Egizabal A, Elizextea C, Nelissen I, Blazquez M, Njuguna J. Environmental Particle Emissions due to Automated Drilling of Polypropylene Composites and Nanocomposites Reinforced with Talc, Montmorillonite and Wollastonite. In IOP Conference Series: Materials Science and Engineering 2017 May (Vol. 195, No. 1, p. 012011). IOP Publishing.

Watson G, Starost K, Bari P, Faisal N, Mishra S, Njuguna J. Tensile and Flexural Properties of Hybrid Graphene Oxide/Epoxy Carbon Fibre Reinforced Composites. InIOP Conference Series: Materials Science and Engineering 2017 May (Vol. 195, No. 1, p. 012009). IOP Publishing.

Starost K, Njuguna J. A review on the effect of mechanical drilling on polymer nanocomposites. InIOP Conference Series: Materials Science and Engineering 2014 (Vol. 64, No. 1, p. 012031). IOP Publishing.

Starost K., Frijns E., Van Laer J., Faisal N., Egizabal A., Elizextea C., Nelissen I., Blazquez, M. & Njuguna J.: The Effect of Drilling on Nanoparticles Release from Silica and Alumina Reinforced Polyester Nanocomposites, *7th International Symposium on Nanotechnology, Occupational and Environmental Health*, South Africa, 19-22nd October 2015 (Oral Presentation)

Starost K., Frijns E., Van Laer J., Faisal N., Egizabal A., Elizextea C., Nelissen I., Blazquez, M. & Njuguna J.: The Effect of Talc, Montmorillonite (MMT) and Wollastonite (WO) on Nanoparticle Release due to Mechanical Drilling from Polypropylene (PP) Composites, Nanostruc 2016, Aberdeen, 12-15th September 2016 (Oral Presentation)

P. Jenkins, S. Ingram, S. Khan, K. Starost, P. Bari, S. Mishra, J. Njuguna: Flexural and Shear Properties of Reduced Graphene Oxide/Epoxy Reinforced Carbon Fibre Hybrid Composites, Euromat 2017, Thessaloniki, Greece, September 17-22nd , 2017 (Oral presentation)

3. Poster Presentations

Starost K., Faisal N., Njuguna J.: Nano Particle Release and Emission from Nanoreinforced Polymer Nanocomposites: A case Study on Drilling Process, *Nanostruc 2014*, Madrid, 20-21 May 2014.

Starost K., Frijns E., Van Laer J., Faisal N., Nelissen I., Njuguna J.: Nanoparticle Release During Drilling of Gaphene/Epoxy/Fibre Reinforced Nanocomposites, *QualityNano Conference and Training Workshop*, Crete, Greece, 15-17th July 2015

Frijns E., Verstraelen S., Nelissen I., Starost K., Njuguna J.: FP7 QualityNano Transnational Access case studies at VITO's exposure assessment facility, *Nano in Belgium Workshop*, Brussels, Belgium, 22nd October 2015

Watson G, Starost K, Bari P, Faisal N, Mishra S, Njuguna J.: Tensile and Flexural Properties of Hybrid Graphene Oxide/Epoxy Carbon Fibre Reinforced Composites. *Nanostruc 2016*, Aberdeen, 12-15th September 2016.

Blazquez M, Marchante V, Gendre L, Starost K, Njuguna J, Schutz J, Egizabal A, Elizetxea C, Cajaraville M P,: On the pathway towards the standardization for exposure assessment throughout life cycle of nanocomposites, SETAC Europe 29th Annual Meeting, Helsinki, Finland, May 26th – 30th, 2019

4. Book Chapters

Starost K, and Njuguna J. Measurement and sampling techniques for characterization of airborne nanoparticles released from nano-enhanced products. Health and Environmental Safety of Nanomaterials, Elsevier, Submitted April 2020.

Starost K, and Njuguna J. Health and Safety Arising from Machining Polymer Nanocomposites, New Horizon of Nano Fillers and Their Enhanced Nanocomposites, Elsevier, Submitted April 2020.

5. Award

Best Poster Award at the 3rd International Conference on Structural Nano Composites, 12-15th September 2016.

Appendix A -

Automated Drilling Methodology: Design & Development

Introduction

There is currently a lack of a harmonised method in testing nanocomposite materials for nanoparticle release during a variety of lifecycle scenarios, including drilling, as highlighted within the literature review in Chapter Two. A controllable and repeatable methodology is required to characterise and understand the exposure to avoid and moderate the potential toxicity of nanoparticles released from nanocomposite materials. In accordance with and following several guidelines and reports on exposure assessment approaches (OECD ENV/JM/MONO, 2012; OECD ENV/JM/MONO, 2019; OECD ENV/JM/MONO 2017), this chapter will go through the design and development stages of the testing methodology before being used to evaluate the nanoparticle release from the PP, PE, EP/CF and EP samples.

Several studies, such as *Brouwer et al., 2012*, and *Methner et al., 2010a, b*, have produced suggestive strategies towards a harmonized testing procedure that would allow for repeatable and controllable investigations across three parameters: testing methods, materials and environments. Therefore, the intention of this study is to develop a method that considers a comparable set of data output that can be used to evaluate the effect of only one changing parameter independent of the other two parameters. To achieve this, the chamber is evaluated to remove or minimise the influence from any other factor. The chamber is developed through testing of polyamide-based composite samples.

Nanocomposite Drilling Methodology

The methodology utilizes a process related approach (as explained in literature review section 2.6. and categorised by Kuhlbusch et al. 2011). This process is designed to simulate mechanical drilling on nanocomposite materials and is continued work from the NEPHH project study (Sachse et al., 2012a; Sachse et al., 2012b). A crucial factor identified in the literature review for the methodology is to control the background particles to setup a controlled environment. Building on the NEPHH project, the chamber is capable of achieving a clean environment monitored using a CPC, importantly removing all background noise or interference on the measurement of number concentration and particle size distribution. The data collected is therefore a representation of the particles released solely from the material. Removing the background data allows for a depiction of any particles

released from the materials which can be directly linked as an unconditional maximum exposure assessment (Kuhlbusch et al. 2011). As proposed per several studies, such as *Brouwer et al., 2012*, *Methner et al., 2010a, and Methner et al., 2010b*, with a controlled testing setup and environment, only one parameter, material, is changed and investigated. This simplifies the issue of accounting for local background influences, as specified within the guidelines and reports by OECD ENV/JM/MONO (2017; 2019).

Therefore, to remove the influencing background noise as discussed in the Literature Review, a purpose-built controlled test chamber was designed and developed to allow for the direct measurements of nanoparticles emitted during drilling from the material. Building on other drilling release studies, (Sachse et al., 2012a; Sachse et al., 2012b), the chamber must achieve a completely clean environment to allow for a controllable and repeatable methodology. This approach differs from the Nanoparticle Emission Assessment Technique (NEAT) which investigates the nanoparticle release related to background data (*Methner et al., 2010a, b)* instead of a clean environment. The data collected within this design setup will therefore be a representation of the particles released solely from the material, excluding any background interference. Removal of the background data allows for a complete understanding of any particles released from the materials which can be directly linked as an unconditional maximum exposure assessment. Additionally, from the methodology designed and as a deliverable of the SIRENA project, a *Best Practice Manual for the Simulation of the Release of Nanomaterials from Polymer Nanocomposite Products* was established on the basis of the experience gained during the development stages and can be found in Appendix B. This will be further discussed in the discussion section of this thesis.

Instrumentation

The methodology developed is designed to be able to use a variety of measurement characteristics depending on the study aims, material and available devices. The outlet channel can be linked up to numerous external instruments to quantify and characterise the release. For the development and studies carried out throughout this thesis an established set of instrumentation was selected.

The particle number concentration is gathered using a TSI Environmental Particle Counter Model 3783 which employs proven Condensation Particle Counter (CPC) technology. A flow rate of 0.6 L/min, particle range of 7 nm to 3000 nm and concentration range of 0-10^6 particles/cm^3 with false background counts <0.01 particles/cm^3 and ±10% at 10^6 particles/cm^3.

The scanning mobility particle sizer (SMPS) used for the study is a TSI 3080 Electrostatic Classifier utilizing a nano Differential Mobility Analyser (DMA) with 99 distinct particle diameters within a

particle range of 4.61 -156.8 nm and a flow rate of 0.31 L/min. The data collected from the SMPS produces a representation of the particle size distribution over a 45s period followed by 10s for the classifier to regenerate to its initial voltage and 5s to start the size distribution again. This gives a 1 minute sampling period.

In addition, separate repeated runs were carried out using a Cambustion DMS50 Fast Particle Size Spectrometer with a 1 second sampling period, inlet flow rate of 6 L/min, with 34 distinct particle diameters of size range between 4.87 nm – 562.34 nm for the particle size distribution. This allows for a size distribution every second compared to the SMPS of 45s period but requiring a different flow rate.

Particles released (drill cuttings) or deposited from the drilling process were captured using the sampling tray placed immediately below the drilling set up in the chamber as shown in Figure 132. The particles were then analysed using the characterisation equipment mentioned section 4.2.2. Figure 122 shows the final setup of the chamber and measuring equipment used throughout these studies.

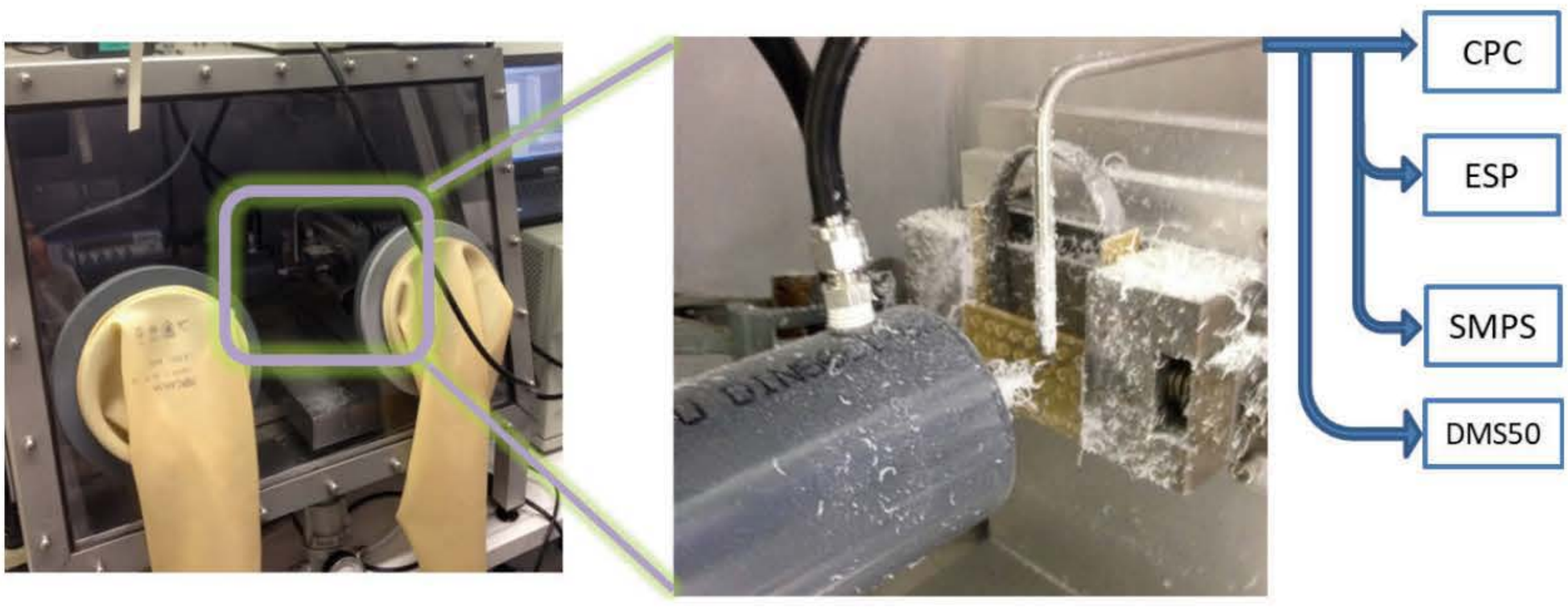

Figure 122: Chamber (Left) used for enclosure of drilling setup (centre) for the characterization of the nanoparticles released (right) from the chosen nanocomposites. The aerosol flow sampling is collected through the probe and with either: simultaneous use of CPC, ESP and SMPS, or DMS50. The high flow rate required for the DMS50 necessitates it is connected independently without any other aerosol measurement instrument. The CPC, ESP and SMPS are connected jointly through a 3-way flow splitter.

The setup is designed to meet the recommendations for measurement and data analysis introduced in a paper attempting to harmonize measurement strategies for exposure to manufactured nano-objects (*Brouwer et al., 2012*). Studies have evaluated and as documented by *Hornsby & Pryor (2014*) the limitations and deficiencies of current nano-sized aerosol measurement techniques, and how they

may differ to actual lung-deposited particles (*Leavey et al., 2013*). However, the chamber design allows for the use of any instrumentation through the sampling probe if nanoparticle aerosol measurement techniques are to be improved.

Statistical Analysis

Statistical analysis is carried out on all of the data from the varied equipment to evaluate the statistical significance of the variable under consideration. The data set collected from the instruments represent a sample of the release characteristics from the materials and process. It is therefore necessary to deduce properties of an underlying probability distribution to give the statistical inference. The data analysis through statistical inference provides a deduction of the representative probability density function. The analysis takes the errors and deviation into account to give the statistical significance of the variation in results. This is particularly essential when comparing two or more samples with a varying parameter (e.g. material content).

A direct comparison between samples can be obtained using inferences on the sample mean particle number concentration. When assessing the release of each material due to the drilling, the peak mean particle number concentrations introduced at the point of drilling can be used to provide confidence interval construction and hypothesis testing. These are two fundamental techniques of statistical inference (*Shao, 2008*). A commonly used statistical analysis and given that the data collected is a sample valuation of the full release with unknown population variance, the estimated mean, standard deviations and variance can be projected in a t-distribution. From the distribution, a confidence interval can be constructed giving an inference of a chosen confidence interval of the population mean will lie in (from sample collected). The calculation carried out to identify the 90% confidence interval for the peak particle number concentration is as follows (*DeCoursey, 2003*):

$$\textit{Confidence limits} = \bar{x} \pm t\left(\frac{s}{\sqrt{n}}\right) \qquad \text{- } \textbf{\textit{Equation A.1}}$$

$\bar{x}$ = mean peak particle number concentration: $\bar{x} = \frac{x_1 + \cdots + x_n}{n}$

s = standard error (standard deviation) where variance: $s^2 = \frac{1}{n-1}\sum_{i=1}^{n}(x_i - \bar{x})^2$

n = sample size

t = t-score value for 90% confidence interval = 1.645

The calculated confidence intervals will provide the upper and lower limit values of a 90% confidence the mean of peak concentration will sit within. This deduction provides the inference about one sample mean. The t-test can also be used to evaluate the two samples with a two samples t-test. This is also called a two samples test of significance. The samples are assessed by performing a hypothesis test between the two samples to identify if there is a statistically significant difference. The description of the method used for the test is displayed in Equation A.2 and A.3.

$$t = \frac{\bar{x}_1 - \bar{x}_2}{\sigma_{\bar{x}-\bar{x}}} \quad \text{- } \textbf{\textit{Equation A.2}}$$

Where:
$\bar{x}_1$= mean peak particle number concentration of first sample
$\bar{x}_2$= mean peak particle number concentration of second sample
The mean of the difference between samples means will be zero: $\mu_{\bar{x}-\bar{x}} = 0$
$\sigma_{\bar{x}-\bar{x}}$ = standard error defined by the mean of difference equal to zero

$$\sigma_{\bar{x}-\bar{x}} = \sqrt{\frac{(n_1 - 1){s_1}^2 + (n_2 - 1){s_2}^2}{n_1 + n_2 - 2}} \sqrt{\frac{n_1 + n_2}{n_1 n_2}} \quad \text{- } \textbf{\textit{Equation A.3}}$$

The t-score is referred with the critical values of a t-distribution to see if it lies within a 90% confidence interval. If the t–score is within the 90% confidence interval critical values, the t-test is classified as statistically insignificant and demonstrated possibility of no change. If the t-score is not inward of the 90% interval, the sample means are not within the confidence interval and are therefore deemed statistically significantly different to one other.

The t-test can be performed to assess the differences between any additional samples. However, when dealing with more than two samples, the equality of means can be tested all at once using analysis of variance F-test. This is a popular approach and is commonly known as the one-way Analysis of Variance (ANOVA). The ANOVA procedure evaluates a null hypothesis that the samples are the same and perform equally (*Montgomery, 2001*).

Principally, one-way ANOVA compares the amount of variation between the samples with the amount of variation within the samples as shown in Equation A. 4.

$$F = \frac{variance\ between\ samples}{variance\ within\ samples} \quad \text{- } \textbf{\textit{Equation A.4}}$$

Where:

Total sum of squares (TSS) = $\sum x_i^2 - n\bar{x}^2$

Variance between samples = $\frac{sum\ of\ squares\ between\ (SSB)}{degrees\ of\ freedom} = \frac{\sum n_s(\overline{x_s}-\bar{x})^2}{k-1}$

Variance within samples = $\frac{sum\ of\ squares\ within\ (SSW)}{degrees\ of\ freedom\ from\ each\ of\ k} = \frac{\mathrm{TSS}-\mathrm{SSB}}{n-k}$

$$= \frac{\sum x_i^2 - n\bar{x}^2 - \sum n_s(\overline{x_s}-\bar{x})^2}{n-k}$$

$\overline{x_s}$= mean for given sample
n_s= number of cases in given sample
k = number of samples

The calculation returns an F-ratio which is compared to the critical values from an F-score table to identify the exact significance level and whether or not to accept the null hypothesis of no difference. If found true, the result indicates that the sample means (accounting standard deviations and errors) have a probability of being equal to each other. If the hypothesis is rejected, the materials can be regarded significantly different. The approach returns the probability that the observation could have been due to random error alone on top of accepting or rejecting the hypothesis that the samples displayed a difference. As a universal method of statistically evaluating the variance between results, several software tools are available such as MS Excel which is used to execute this analysis.

This data analysis provides a statistical comparison between the materials. The hypothesis testing measures the probability that a relationship between the data is caused by the change in material and not random chance. The confidence intervals inference the range the mean value will be with a confidence interval of 90%. When measuring the effect of a change in parameter, as with material filler, this analysis is essential.

Design Development and Background Removal

The literature review was able to identify the necessary design considerations required to achieve a controllable and repeatable setup for the assessment of nanoparticle release. The following design specifications were considered to be necessary:

- Elimination of background interference through a clean environment.
- Removal of any background particles introduced due to the process source i.e. from the drill bit.
- Repeatable, consistent and controlled mechanical process.
- A sampling probe positioned at the location of mechanical process for a process related approach on the nanoparticles release.
- A variety of nanoparticle characterisation and quantification instrumentation techniques for both live data and post analysis, to represent particle attributes linked to toxicity.

Therefore, with these design specifications in consideration, a closed stainless-steel chamber with dimensions of 740 mm x 550 mm x 590 mm, and therefore a total inner volume of 0.240m^3, is used to assure a closed environment to simulate an appropriate volume around the drill and additionally, minimising electrostatic attraction to the surfaces. An outlet channel is placed adjacent to the test specimen for the nanoparticle release equipment readings and therefore representing a process-

related approach. The outlet channel can be connected to a variety of instrumentation. In this case it is connected to a CPC, DMS50 and SMPS.

Figure 123*:* CPC reading of particle number concentration within chamber demonstrating ability to achieve 0 #/cm^3 with inflow of clean air through HEPA Capsule Filters

For the removal of any particles airborne and to quantify only the particles released from the sample, the chamber was initially cleared of particles through an inflow of clean air with the use of TSI 99.97% retention HEPA Capsule Filters. Figure 123 demonstrates the ability within the setup and the reading on CPC required before any tests are carried out.

The initial clearing stage of the chamber with clean air through the HEPA Capsule Filters from 5 test runs is presented in Figure 124 and Figure 125. Due to the initial high number of particles (representing a normal environment), both a linear and logarithmic scale are required to represent the data. The inflow of clean air can be seen to have an exponential decay in particle number concentration. The representation of the data on a logarithmic scale, shown in Figure 125 confirms this until the concentration reaches around 100 #/cm^3. The removal of the final particles within the chamber demonstrated a higher fluctuation within the plot, but still follow the exponential decay. Additionally, the slight leap observed at 13 min for Run 2 is expected to be due to either particles separating from a surface or particles passing through the HEPA Capsule Filters. Either possibility, this only had a minor affect with a slight increase in time to remove all the particles.

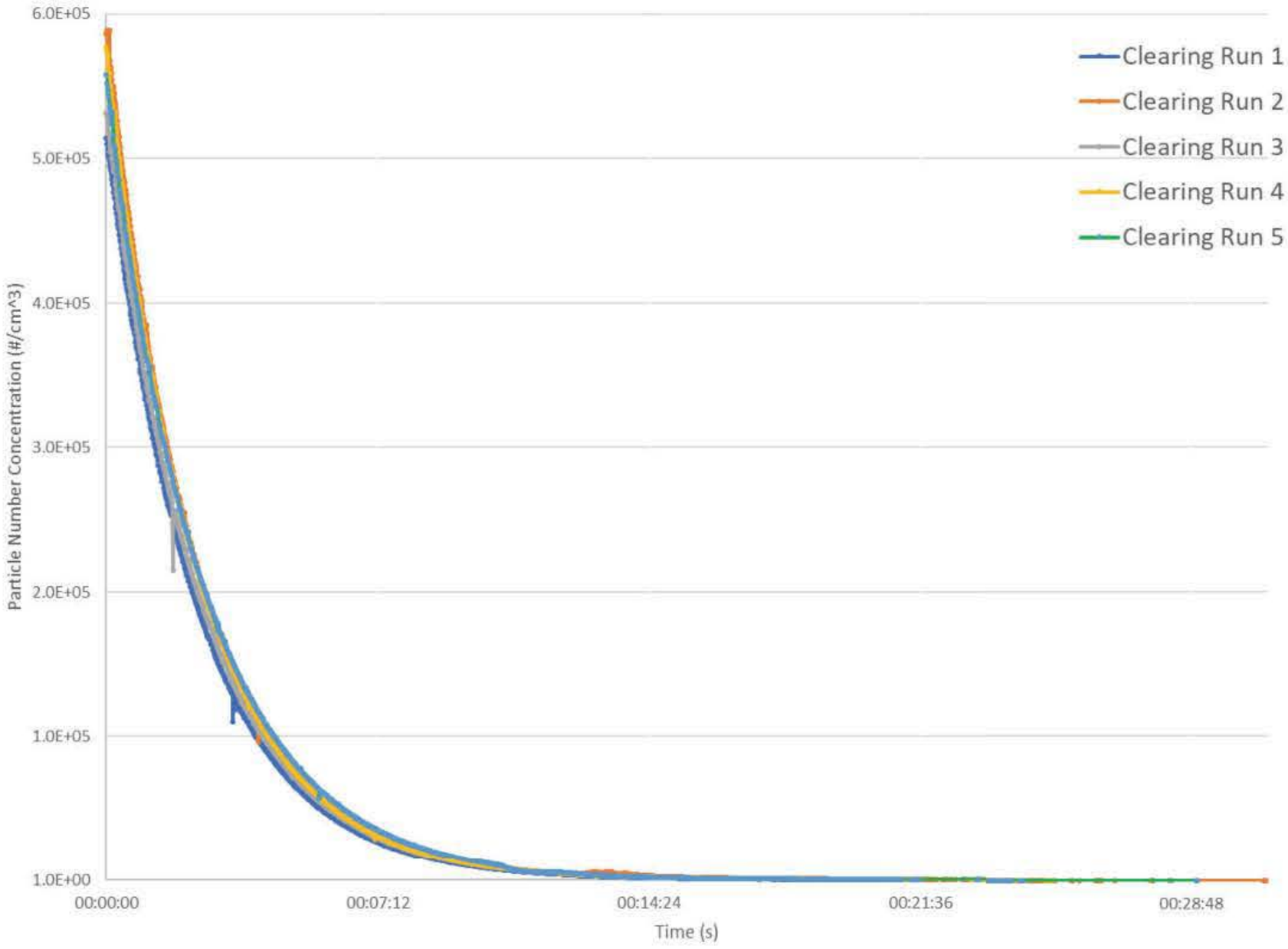

Figure 124: Particle number concentration measured within chamber during clearing of air through HEPA Capsule Filters

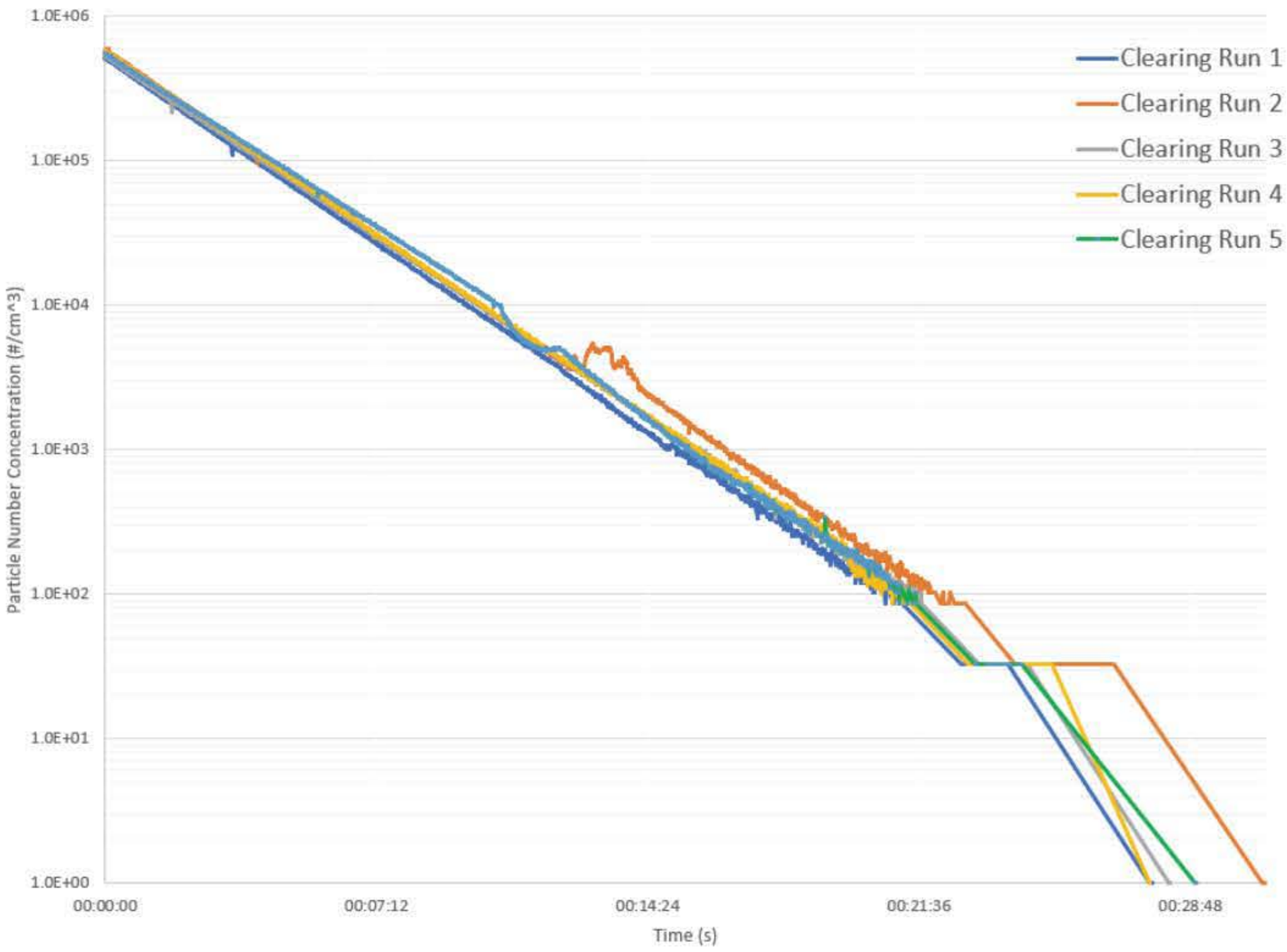

Figure 125: Logarithmic scale of Particle number concentration measured within chamber during clearing of air through HEPA Capsule Filters

The numerical values are also represented in table format, shown in Table 24, to summarise the differences between runs. The 5 runs established a mean, $\bar{\bar{X}}$, of 28:42 minutes and a standard deviation, $S_{\bar{X}}$, of 1:07 minutes when removing initial particle number concentrations ranging from 514000 #/cm^3 to 586000 #/cm^3. Therefore, when material tests are carried out, an estimated 28:42 minutes are needed as a minimum between each test to allow for a clean environment. Furthermore, due to the clearly visible exponential function of the decay in particle number concentration, an exponential equation representing the curve is generated using a first-order exponential function of a quantity *N* as follows:

$$N\,(t) = N_o e^{-\lambda t} \qquad \textit{Equation A.5}$$

where N_o is the initial value (at t = 0), and e^x is the exponential function for the changing time, *t*, and decay constant, λ (Kahn, 2015). As shown in Table 24, similar trendline equations represent the decay, with identical decay constants for Runs 1 to Run 4, and a minimal change for Run 5. The data therefore showed a consistently similar decay in particle number concentration.

Table 24: Numerical representation of the particle number concentration measured within chamber during clearing of air through HEPA Capsule Filters, where *N* is decrease in particle number concentration and *t* is the change in time.

	Initial Particle Number Concentration [#/cm^3]	Time to 0 #/cm^3 [minutes:seconds]	Trendline equation
Run 1	514000	27:47	$N = 514850e^{-0.007t}$
Run 2	586000	27:43	$N = 586000e^{-0.007t}$
Run 3	532000	28:17	$N = 532000e^{-0.007t}$
Run 4	577000	28:58	$N = 577000e^{-0.007t}$
Run 5	558000	30:47	$N = 558000e^{-0.006t}$

The chamber inlet and outlet were used when flushing the chamber with clean air to obtain the clean environment. As demonstrated, the clean air system using the HEPA Capsule filters is therefore capable of producing a particle number concentration reading within the chamber of 0 #/cm^3 with false background counts <0.01 #/cm^3, as monitored using the CPC. The level of background noise is therefore well within the ISO Cleanrooms and Associated Controlled Environments standard for particles ≥0.1 µm of 10 #/cm^3 (*ISO 14644-1:2015, 2015*).

As mentioned in available literature, the mechanical process has shown to have an effect on the particles within the chamber. Studies such as Irfan et al. (2013), Bello et al. (2010), found that the drill was generating additional particles into the test chamber. Therefore, in order to have a controlled environment with no influencing background on the particles released from the materials, the

particles produced from the drill itself are to be removed. Furthermore, to ensure a repeatable and replicable methodology, the drill is placed on an automated assembly operated via an external computer that controlled the feed rate in the x-axis, while the sample was moved in the z-axis to allow for multiple holes to be drilled.

Once the background was cleared of all particles, the drill and automated assembly were evaluated for influence on the background environment. Held at a clean environment for 1 minute, the drill and automated assembly were switched on for 4 minutes without drilling on a material, with a drilling speed of 17500 RPM, feed rate of 78mm/min, and drill bit diameter of 3.5mm. A Dremel 4000 drilling tool with an industrial standard stainless-steel twist drill bit was used. The effect on particle number concentration when the drill was operated is shown in Figure 126 and Figure 127. As acknowledged and documented within literature, the drill was found to produce an immediate effect on the particle number concentration. Therefore, a separate capsule/chamber was constructed around the drill with separate air flow to avoid any interference of the drilling fumes on the particle number concentration within the chamber.

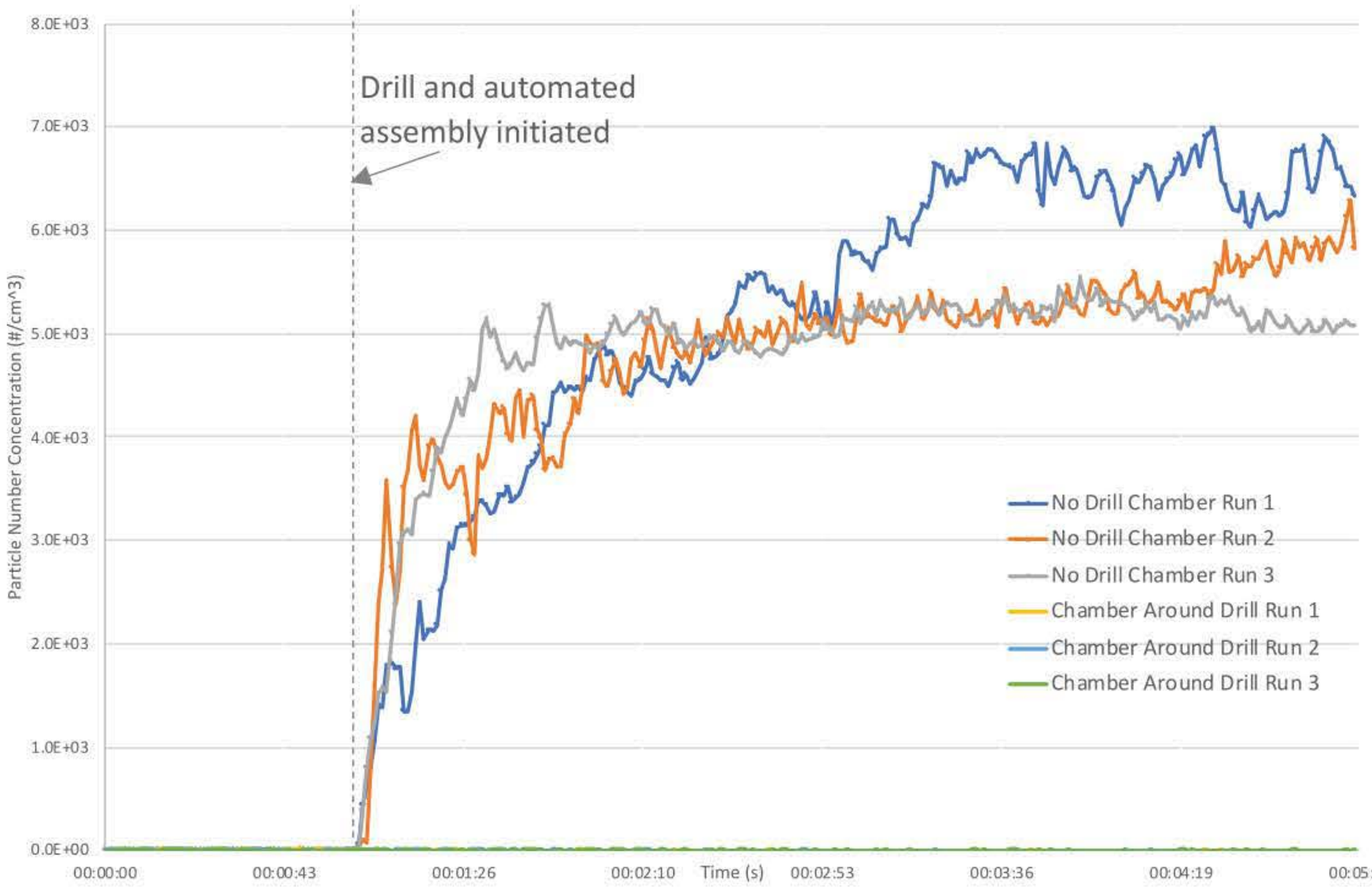

Figure 126: Particle number concentration comparison of drill with and without chamber.

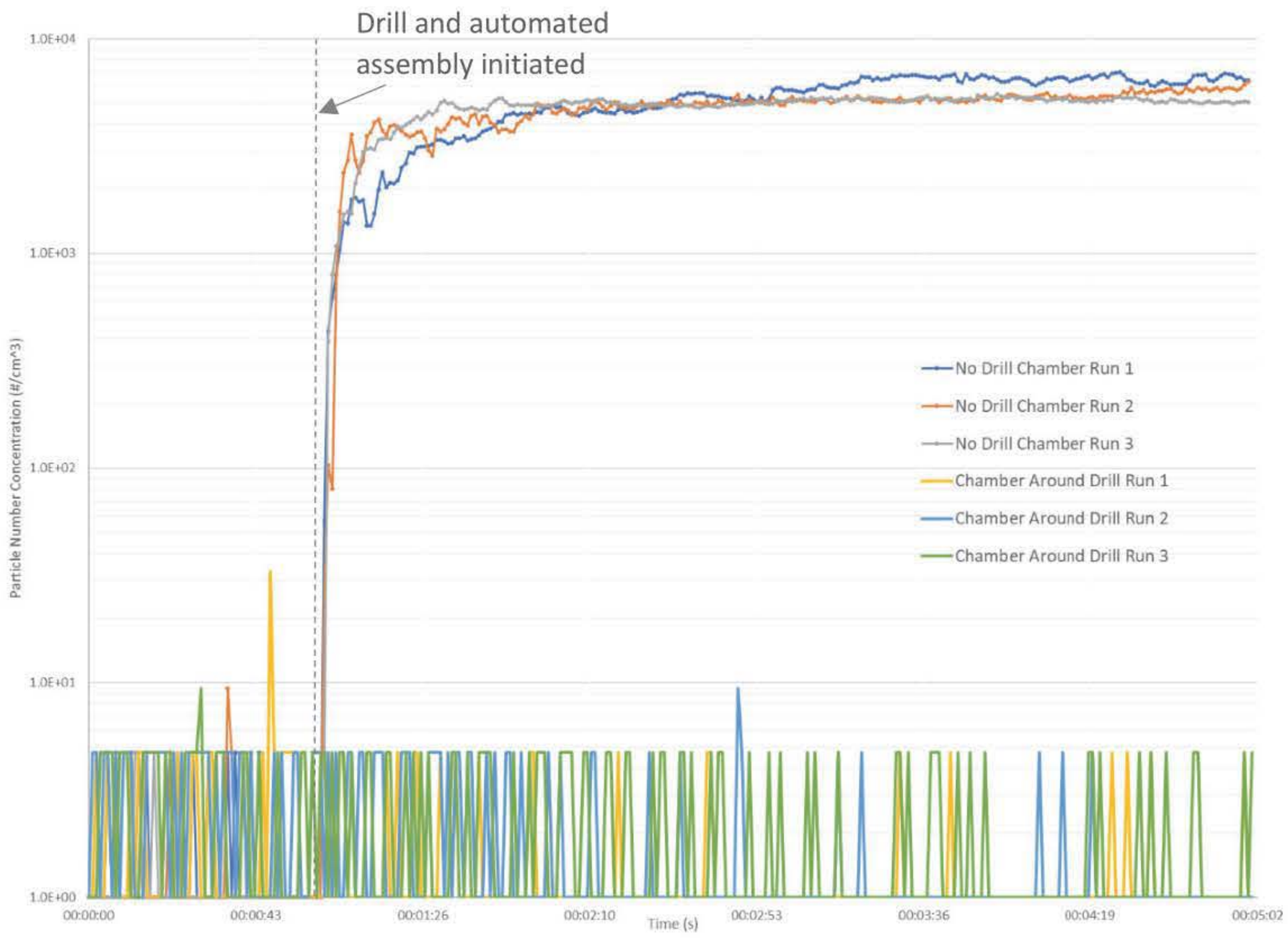

Figure 127: Particle number concentration comparison of drill with and without chamber on logarithmic scale.

The introduction of the chamber around the drill successfully removed any influence on the particle number concentration when the drill was switched on. The logarithmic representation of the data, shown in Figure 127, demonstrates the low concentration fluctuate between 0 #/cm^3 to 5 #/cm^3. Peaks seen before the start of the drill are while the concentration fluctuates with similar number of particles, which are negligible. The numerical and statistical representation of the particles introduced due to the drill and assembly with and without the chamber are presented in Table 25 and Table 26.

The calculated lower tail of 5% and upper tail of 95% give a representation of the data for a 90% confidence interval of a t-distribution. This statistically highlights the disparities between the particle number concentrations after 1 minute and therefore, substantiate a statistically significant difference with the introduction of chamber around the drill in comparison to no chamber. A two-sample t-test of significance of the two setups mean and deviations after 1 minute returned statistically significant differences with the introduction of the chamber around the drill.

Table 25: Numerical representation of the particle number concentrations introduced due to drill and assembly with and without chamber around the drill.

	Maximum Particle Number Concentration [#/cm^3]	Mean Particle Number Concentration Before 1 minute [#/cm^3]	Mean Particle Number Concentration After 1 minute [#/cm^3]	Final Particle Number Concentration at 4 minutes [#/cm^3]
No Drill Chamber Run 1	6.99×10^3	0.851	5.23×10^3	6.42×10^3
No Drill Chamber Run 2	6.29×10^3	0.387	4.83×10^3	6.29×10^3
No Drill Chamber Run 3	5.54×10^3	0.541	4.83×10^3	5.08×10^3
Chamber around Drill Run 1	33.0	2.24	0.411	0.00
Chamber around Drill Run 2	9.44	2.71	0.783	0.00
Chamber around Drill Run 3	9.44	2.40	1.35	4.72

Table 26: Inferential statistical representation of the particle number concentrations introduced due to drill and assembly with and without chamber around the drill. Lower and upper limits represent the 90% confidence interval on a sampling t-distribution.

	Mean [n=240] after 1 minute: $\overline{\overline{X}}$ [#/cm^3]	Deviation after 1 minute: $S_{\overline{X}}$ [#/cm^3]	Minimum [#/cm^3]	Maximum [#/cm^3]	5% Lower limit of confidence interval [#/cm^3]	95% upper limit of confidence interval [#/cm^3]
No Drill Chamber	4.96×10^3	1.07×10^3	4.72	6.99×10^3	4.86×10^3	5.06×10^3
Chamber around Drill	0.842	1.06	0	33.0	0.750	0.939

ANOVA single factor analysis was performed to assess the variability between the means during the last 4 minutes and therefore particles introduced due to the drill and assembly functioning. The analysis also returned statistically significant differences within the 2 setups (F value = 4727 F critical value = 3.86) and a 5.8×10^{-251}% chance that the observation could have been observed due to random error alone and therefore rejecting a hypothesis that the chamber around the drill has no difference.

The drill and assembly clearly produce an increase in particle number concentration when switched on and without the chamber around the drill. Fumes generated from the drill are the main cause of the surge and produce an increase up to 6.99×10^3 #/cm^3. These levels of particles are still below the level observed at the initial particle number concentration within the lab (shown in Table 24, ranging

from 5.14 x 10^5 #/cm^3 to 5.86 x 10^5 #/cm^3) but will still have a significant influence on the particle number concentration when drilling on the materials. Therefore, the chamber around the drill was introduced and can evidently be seen to completely remove the particles generated from the drill. Furthermore, the average particle number concentration was shown to have a 90% confidence interval of just 0.1891 #/cm^3 and stay below 1 #/cm^3, maintaining the clean environment achieved before the drill is started.

To further substantiate the importance of removing the particles generated from the drill, the particle size distribution provides a more complete understanding of the particles introduced. The CPC data of particle number concentration in Figure 126 and Figure 127 shows an introduction of particles between particle range of 7 nm to 3000 nm and concentration range of 0-10^6 #/cm^3 with false background counts <0.01 #/cm^3 and ±10% at 10^6 #/cm^3. Therefore, a particle size distribution would also identify if any of the generated particles are within the range of material nanoparticles which are to be evaluated. The particle size distribution recorded during "No drill chamber run 1" is shown in Figure 128.

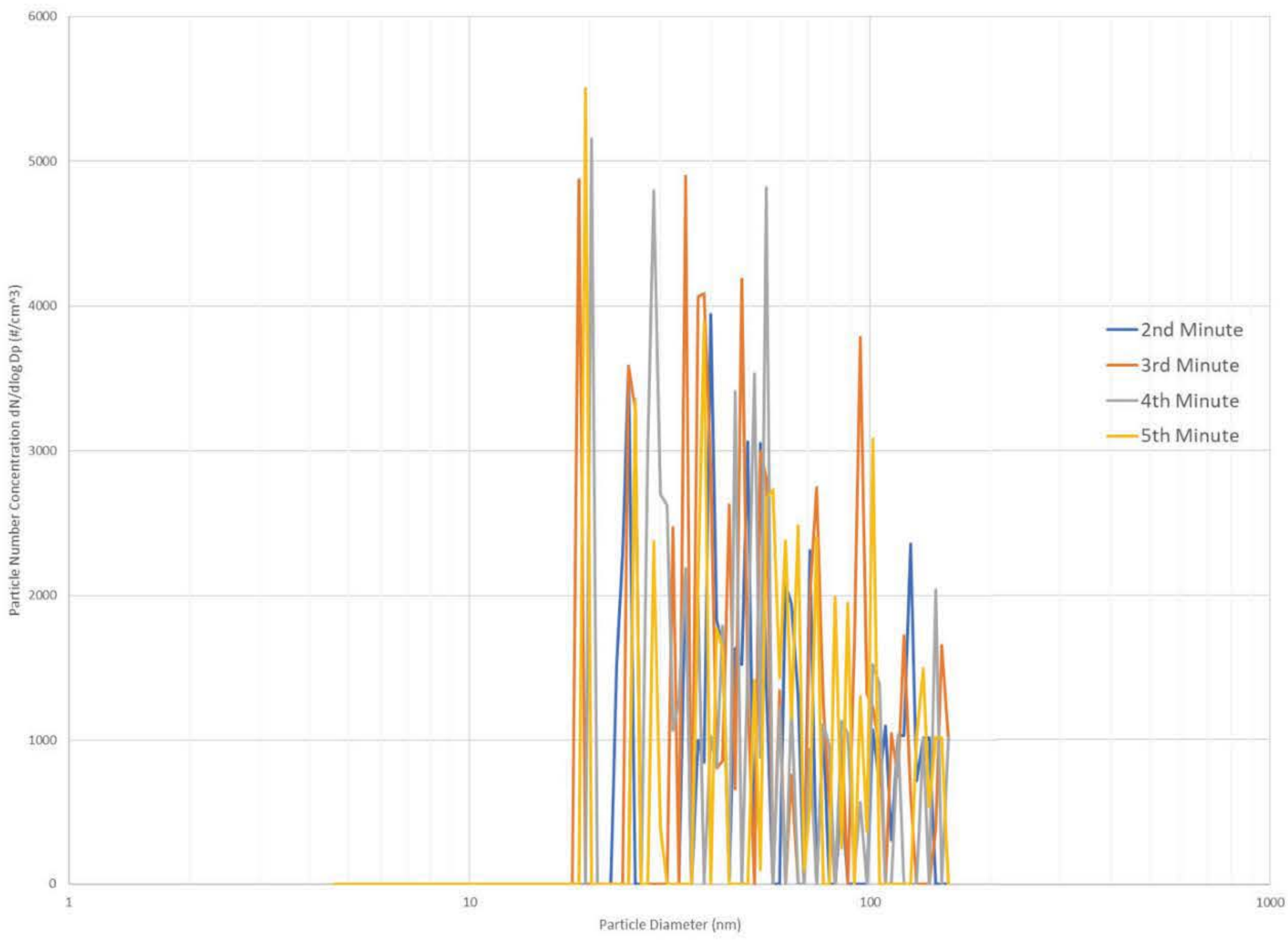

Figure 128: Particle size distribution of particles generated from drill from "No drill chamber run 1" (CPC data shown in Figure 126 and 127), after drill is started, as recorded on SMPS.

The particle size distribution demonstrates that a substantial number of particles are produced within the SMPS size range of 4.61 -156.8 nm. The data collected from the SMPS produces a representation of the particle size distribution over a 45s period followed by 10s for the classifier to regenerate to its initial voltage and 5s to start the size distribution again. The data therefore is presented as the size distribution over the 4 minutes after the drill and assembly are initiated (from Figure 126 and Figure 127). The data is presented on a logarithmic scale to simplify the data display and the large separation between particle size diameters. The plot can be seen to have sharp jolts between diameters presenting a sinuous shape due to huge differences in particle number concentrations at the different particle diameters.

Across the four minutes, no particles below 18.8 nm were recorded and can be established to be relatively spread out to the limit of the SMPS at 156.8 nm as shown in Figure 128. The mean values for the three runs without the drill chamber are compared and presented in Figure 129.

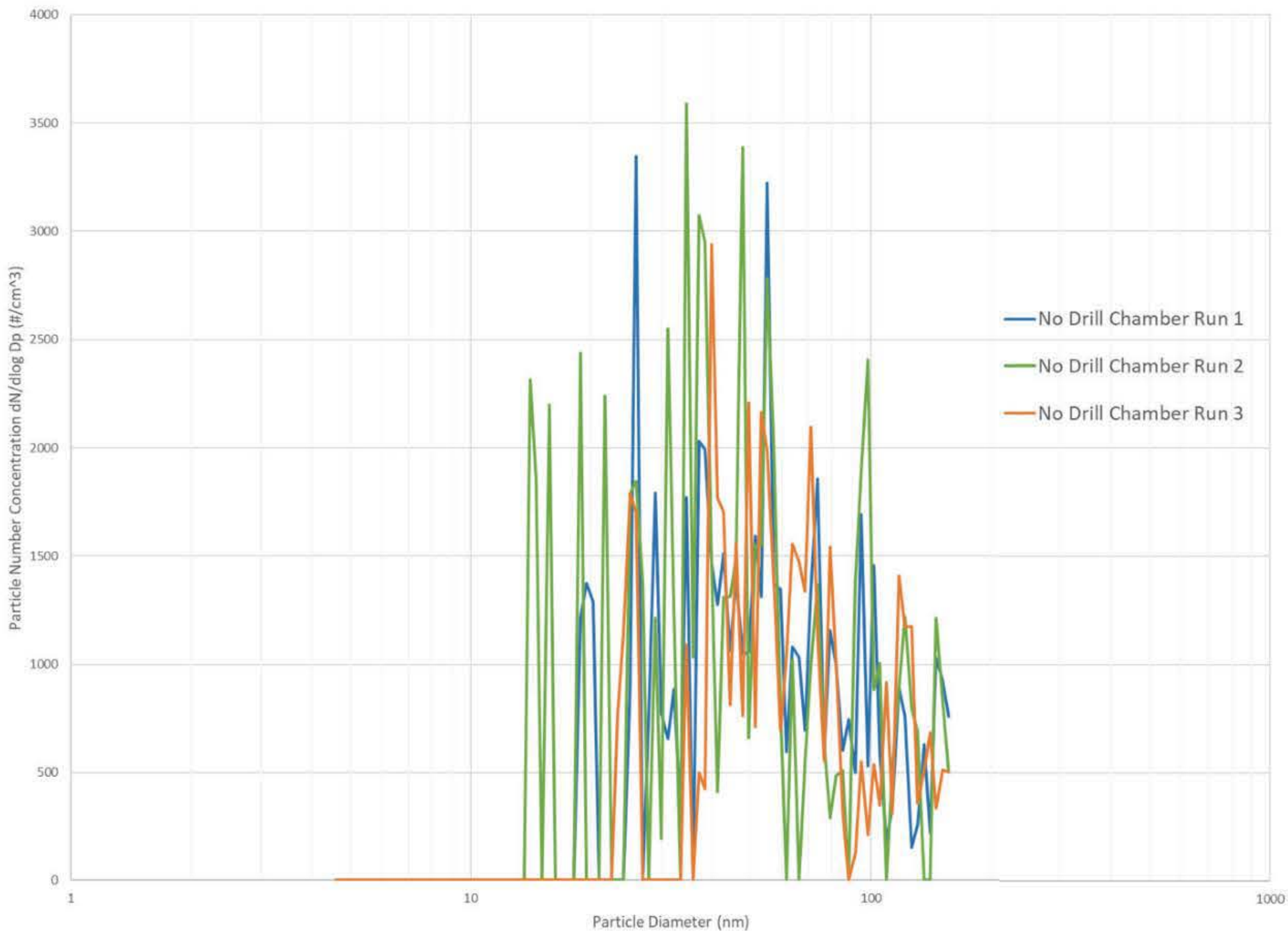

Figure 129: Mean particle size distribution over 4 minutes [n=4] of particles generated from drill runs without drill chamber (shown in Figure 126 and 127), after drill is started, recorded on SMPS.

The data collected on using the drill and assembly without a drill chamber presented similar results. Similar diameters and deviations were observed along with no particles measured below 14.1nm. The

data provides a clear quantification of the particles produced from the Dremel 4000 drilling tool and the assembly as they are the only two objects moving within the steel chamber. The two components combined demonstrate a generation of background particles which would interfere with the measurements and potentially impact the particles released from the nanocomposites. Not only is there an escalation in particle number concentration, but a substantial number of particles within the size ranges of nanoparticles used within this study. The chamber around the drill is therefore needed in order to conceal the particles/background interference. The data shown in Figure 125 and Figure 126 from the CPC exemplify the elimination of the background particles produced from the drill. The clear comparison between the three runs also demonstrate a repetition and confidence in the assembly, drill and instrumentation. This is further evaluated in tests to proceed.

With removal of the background interference, the design meets one of the established necessary requirements identified in the literature review. The other parameter identified to consider is the location of the particle measurements. The process related approach was ascertained as the appropriate initial method as it is a worst-case scenario of the nanoparticles released and is task-based scenario instead of an exposure scenario. The location of the probe to measure the nanoparticles released is therefore positioned above the drilling on the material. A comparison of the probe located above the drilling and as close as possible to the drilling are shown in Figure *130* and Figure *131* for drilling on the polyester based materials. A purpose of the process related approach is to evaluate and ascertain a maximum potential in nanoparticle release from the sample tested.

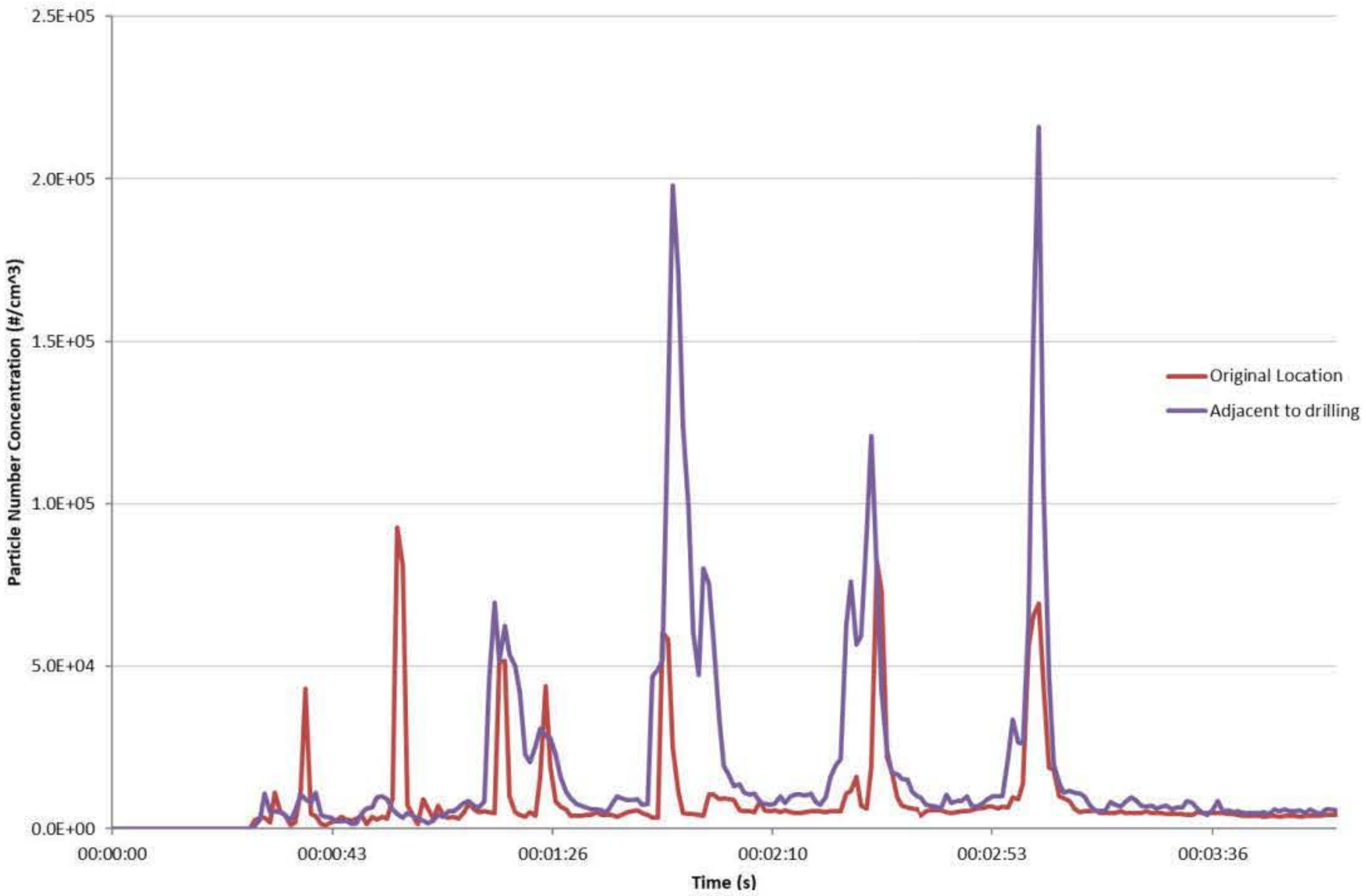

Figure 130: Particle number concentration comparison of probe located above drill (Original Location) and as close as possible without interfering (adjacent to drilling) as measured on CPC.

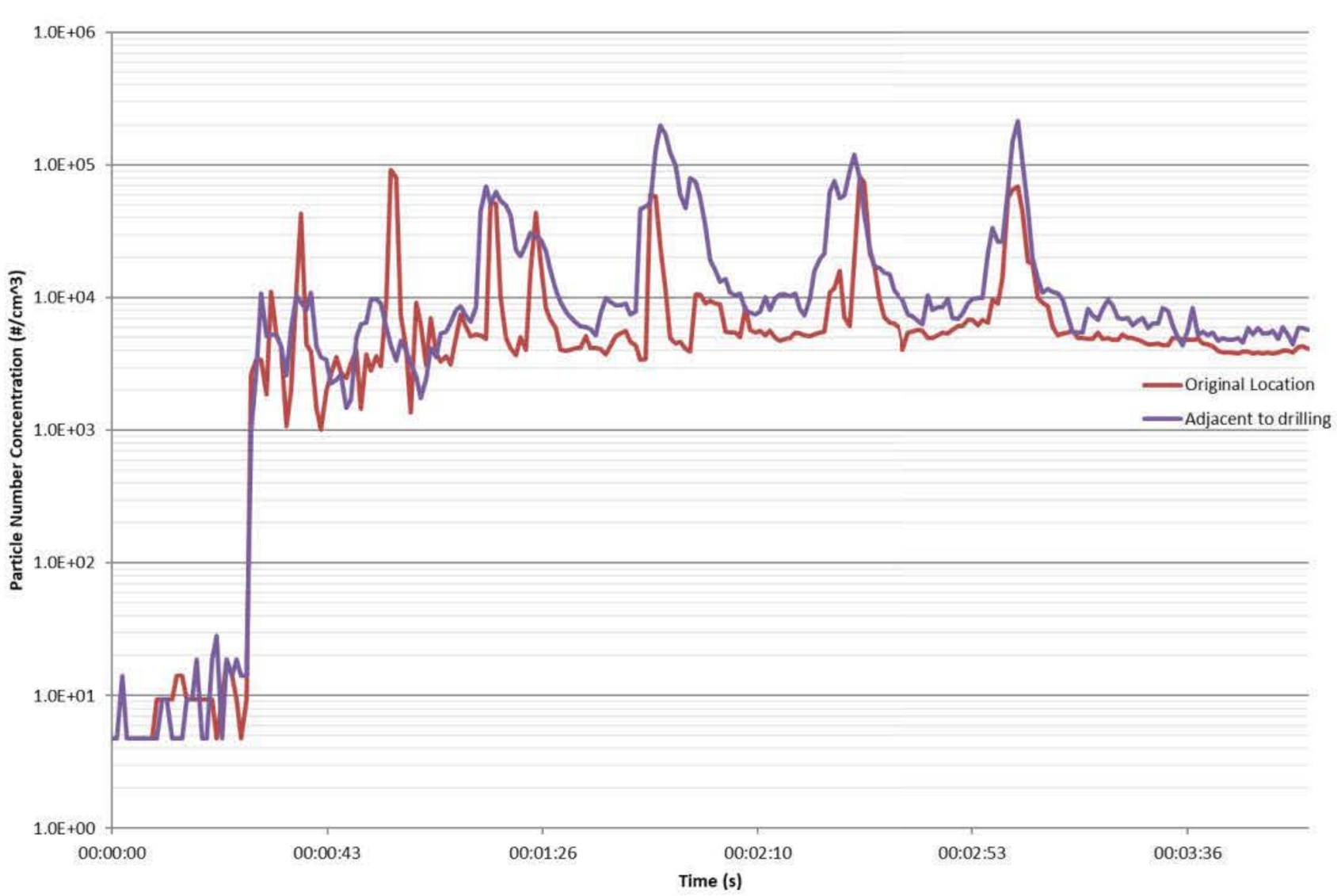

Figure 131: Particle number concentration comparison of probe located above drill (Original Location) and as close as possible without interfering (adjacent to drilling) as measured on CPC on a logarithmic scale.

For the comparison of probe location, a 39mm/min feed rate with a 1.5mm drill bit diameter was used at 10000 RPM. The drilling can be seen to take place over the first 3 minutes followed by 1 minute

without any drilling. The high peaks visible across the 4 minutes reveal a large concentration released into the chamber as the drill goes through the material. Six holes were drilled which can be split into six detached peaks for each drill bit diameter. Some peaks are divided into two peaks each as the drill enters and leaves the material. As the peaks introduced are significantly more than the concentration in-between holes being drilled and the concentration after drilling, a logarithmic scale shows a clear comparison between the two probe locations.

There are some noticeable minor differences between the two probe locations shown in Figure *130* and Figure *131*. A slight change in peak concentration with slightly higher particle number concentrations introduced due to drilling from the Adjacent to Drilling probe location. With a maximum of 9.26×10^3 #/cm^3 at the Original location, and a 21.6×10^3 #/cm^3 at the Adjacent to Drilling location, a 133% increase was observed. The difference in repositioning the probe location (15mm) towards the sample will measure more particles released due to being closer to the both sample and location of the drilling. The highest concentration and therefore a worst-case measured using the setup, is with the probe located as close as possible to the point of release and measured as the drill is in contact with the material. As categorised in the literature review, if the worst-case scenario demonstrates high and potentially dangerous concentrations, then other probe locations (e.g. at worker exposure distances) can be taken. This is in line with the NEAT assessment approaches (*Methner et al., 2010a*, *b*) which can be considered the process related approach to get as close to an absolute value of the maximum particle number concentration introduced from the material due to drilling.

Although the position of the probe has a slight effect on the peak particle number concentration released, the concentrations are seen to stabilise to similar concentrations at the end of the 4 minutes of sampling. This is also represented in the selection of numerical values presented in Table 27. A comparison of the particle number concentration over the 3 minutes of drilling and particles measured during the peaks exhibited a 124 % increase from the Original Location to Adjacent to Drilling. However, when comparing the two locations over the 1 minutes after drilling stopped, only a 36 % increase was observed. Furthermore, the final particle number concentrations demonstrated only a 21% increase. The probe location can therefore be understood to have an effect on the peak particle number concentration released during drilling, but less on the particle number concentration remaining in the chamber after drilling has ceased. This is further substantiated in Table 28, in the inferential statistical representation of the data. The distinction in peaks introduced is apparent with the difference in 95% upper limit of confidence interval, but the similarity in concentration in lower peaks is noticeable with almost identical 5% Lower limit of confidence intervals.

Table 27: Numerical representation of the particle number concentrations comparison of probe located above drill (Original Location) and as close as possible without interfering (adjacent to drilling) as measured on CPC.

	Maximum Particle Number Concentration [#/cm^3]	Mean Particle Number Concentration over entire 4 minutes [#/cm^3]	Mean Particle Number Concentration first 3 minutes [#/cm^3]	Mean Particle Number Concentration during 4th minute [#/cm^3]	Final Particle Number Concentration at 4 minutes [#/cm^3]
Original Location	9.26×10^4	8.50×10^3	9.54×10^3	4.51×10^3	4.33×10^3
Adjacent to drilling	21.6×10^4	18.2×10^3	21.3×10^3	6.12×10^3	5.24×10^3
Percentage Increase	133%	114%	124%	36%	21%

Table 28: Inferential statistical representation of the particle number concentrations introduced at the peaks of probe located above drill (Original Location) and as close as possible without interfering (Adjacent to Drilling). Lower and upper limits represent the 90% confidence interval on a sampling t-distribution.

Sample	Mean: $\bar{\bar{X}}$ [#/cm^3]	Deviation: $S_{\bar{X}}$ [#/cm^3]	Variance: $S_{\bar{X}}{}^2$ [#/cm^3]	5% Lower limit of confidence interval [#/cm^3]	95% upper limit of confidence interval [#/cm^3]
Original Location	6.65×10^4	1.87×10^4	3.48×10^8	5.57×10^4	7.73×10^4
Adjacent to drilling	10.4×10^4	8.99×10^4	80.7×10^8	5.23×10^4	1.56×10^5

The calculated lower tail of 5% and upper tail of 95% give a representation of the data for a 90% confidence interval of a t-distribution. This highlights the disparities between the peak particle number concentrations and therefore, a statistically significant difference with the change in probe location in peak concentration measurements. A two sample t-test of significance of the sample mean and deviation to the original location returned statistically significant differences for the two locations (outside the 95% confidence interval). Since the probe is placed closer, a peak particle number concentration can be expected to be higher due to the proximity to the release. As the probe is distanced away, the particles would disperse and therefore reducing the concentration. These results clearly demonstrate the effect of probe location and therefore, the important consideration needed when setting up a worker exposure scenario. The position of the probe with minor distances will affect the peak particle number concentrations introduced from drilling. Since this is a process related

approach and an attempt to find the worst-case scenario, the closer placed probe (Adjacent to Drilling) is of interest for this study. The finalisation of the probe location completes the setup development for the methodology. Figure 132 displays a design drawing of the chamber and the assembled chamber.

a.)

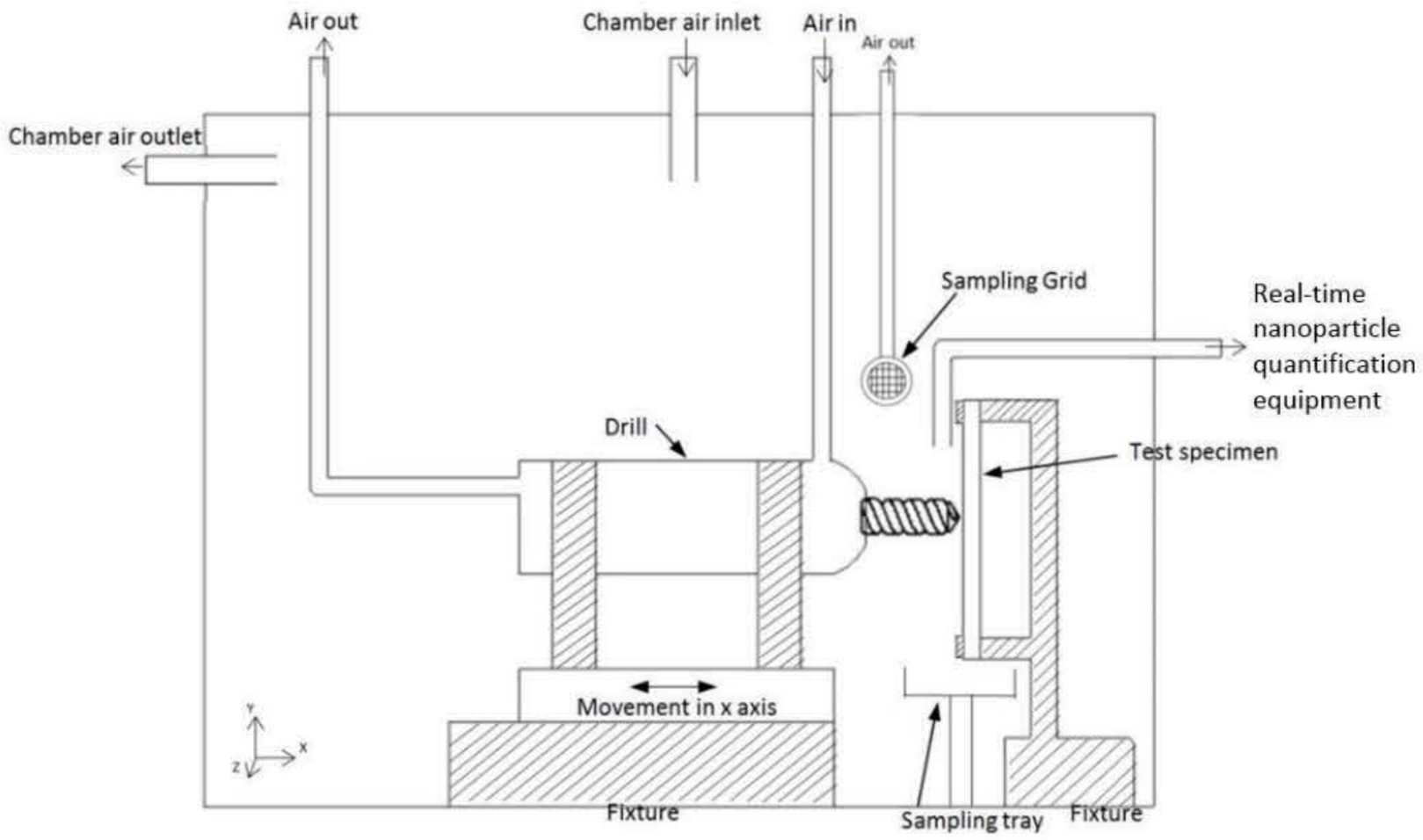

b.)

Figure 132: Drilling setup within enclosed test chamber with cycled airflow to allow for a clean environment removing any background interference represented as a.) design drawing (not to scale) and b.) apparatus setup with front window panel removed and side door open.

An outlet channel is placed adjacent to the test specimen for the nanoparticle release equipment readings. A standard IOM Inhalable Sampler for collection of inhalable particles was placed next the

test specimen with a 2 L/min suction to attract and prevent particles from detaching away from the grid for post-test chemical analysis (Sanchez Jimenez et al., 2012). An additional sampling tray was positioned below the test specimen for collection of the deposited particles for further post-test analysis.

The vital factors for the design of the chamber are that it is controllable and repeatable. The setup permits any drilling test to take place without any interfering background noise. Any material sample can be placed in the chamber and undergo the drilling test and give comparable data if repeated at an alternative time or location, permitting the testing parameters were the same. The only variable or influencing factor in the design is the material being tested, and the setup is therefore process related. The full extent of the repeatability of the methodology is evaluated throughout this thesis. Each set of materials are repeated and demonstrates the consistency of the method.

As evidenced in previous work (*Sachse et al. 2012a, b; Bello et al. 2010; Irfan et al., 2013),* one hole did not provide a full representation of the particles released. Furthermore, the studies reported post-drilling data to show the particle number concentration after drilling ended. The length of data sampling is also relative to the measuring equipment chosen. The data collected from the SMPS for this study produces a representation of the particle size distribution over a 45s period followed by 10s for the classifier to regenerate to its initial voltage and 5s to start the size distribution again. This renders a 1-minute sampling period. In order to determine the length of data collection after drilling, Figure 133 and Figure 134 demonstrate the particle number collection recorded on the polyamide-based samples for 30 minutes after drilling ended.

The particles introduced during drilling and subsequent peak particle number concentrations as holes are being drilled are distinctly evident. Five peaks can be seen, representing the five holes drilled, followed by over 27min after drilling is stopped. The particle number concentration can be seen to stabilise quickly after drilling has ended and there is no significant change visible. However, evaluating the numerical values show there is a slow decrease in particle number concentration. The numerical representation of selected data from the results is presented in Table *29* and Table *30*.

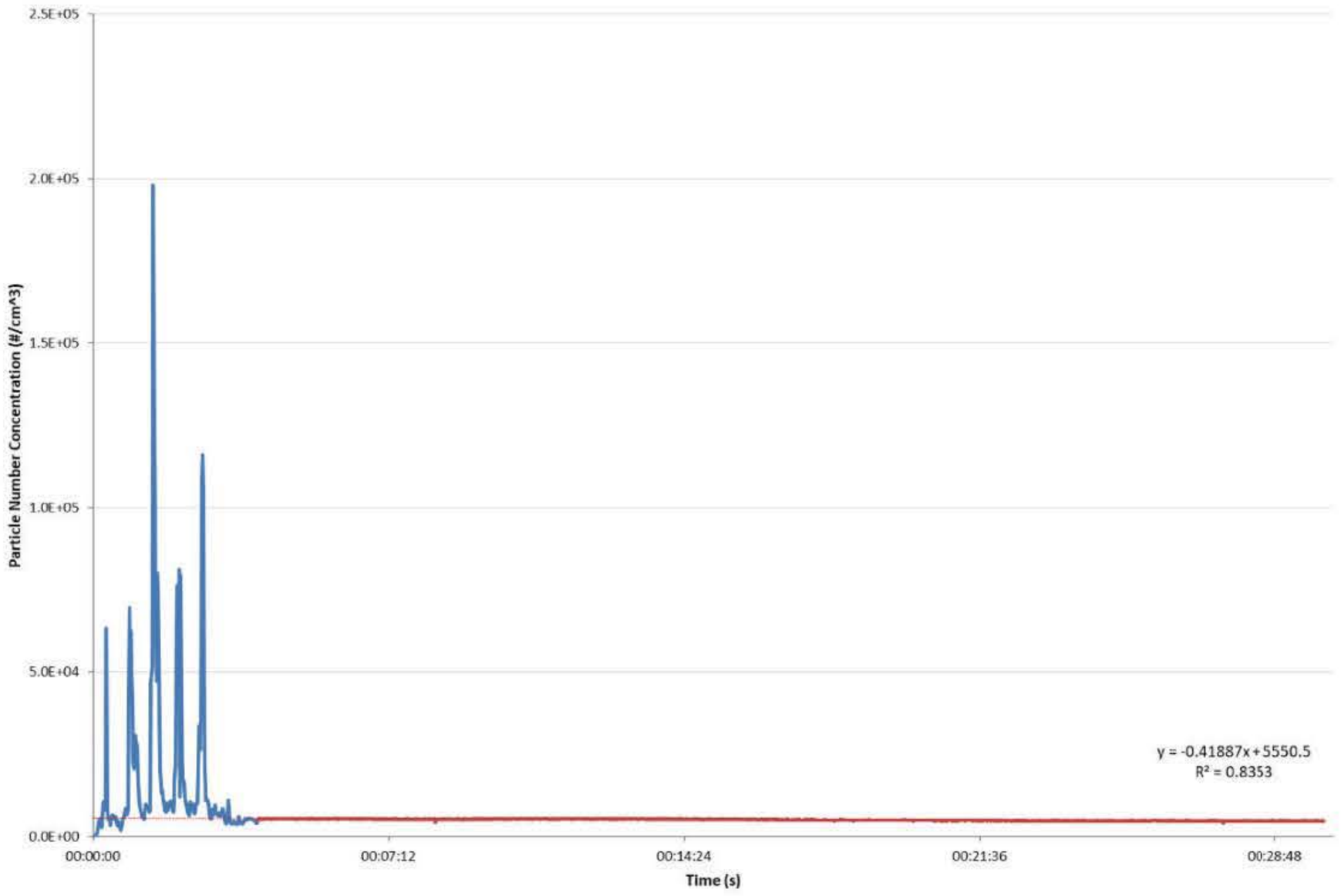

Figure 133: Particle number concentration over a total of 30min as measured on CPC. Polyamide-based materials and 39 mm/min feed rate, 1.5 mm drill bit diameter at 10000 RPM.

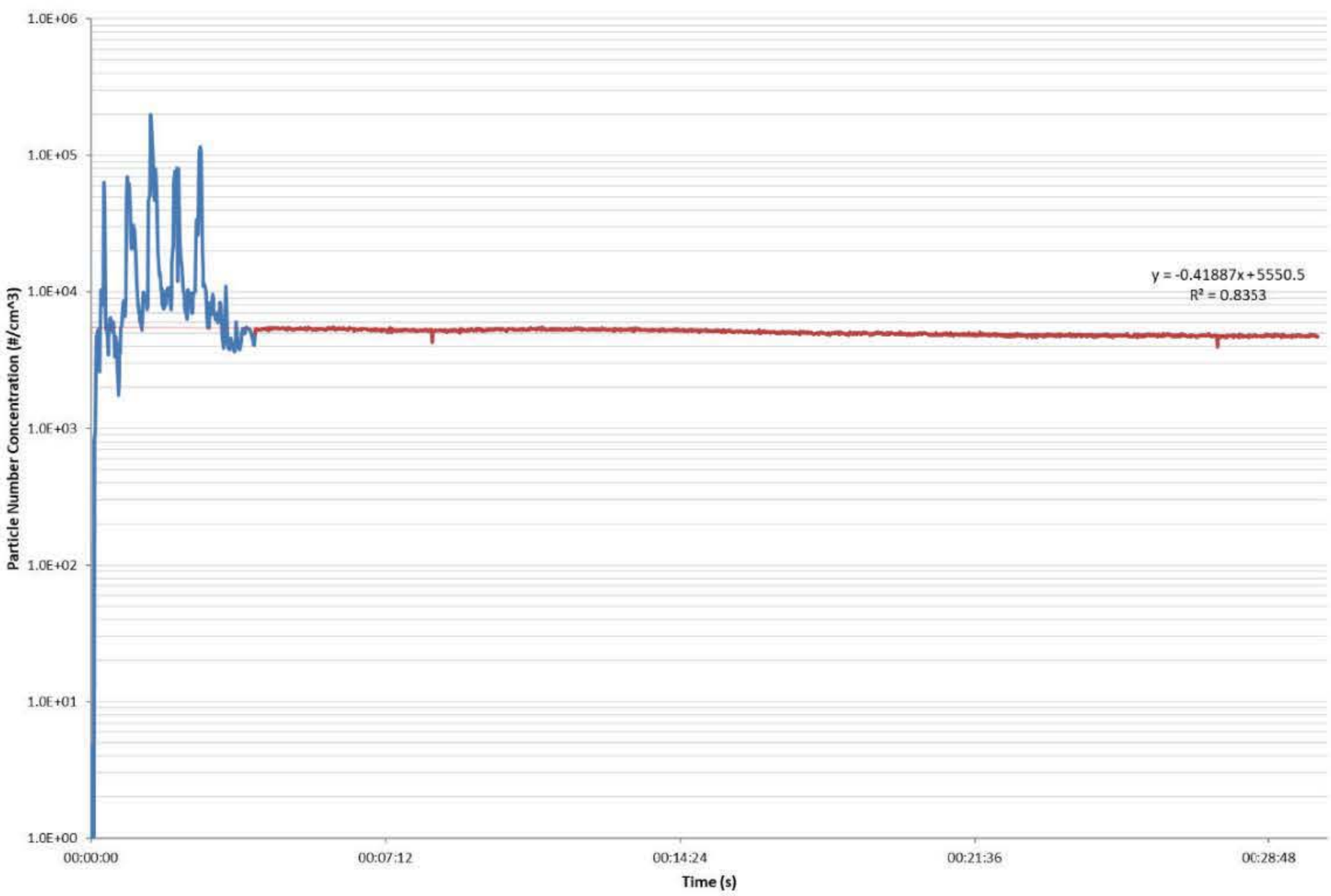

Figure 134: Particle number concentration over a total of 30min as measured on CPC on a logarithmic scale. Polyamide-based materials and 39 mm/min feed rate, 1.5 mm drill bit diameter at 10000 RPM.

Table 29: Numerical representation of the particle number concentration over a total of 30min as measured on CPC.

	Maximum Particle Number Concentration [n = 1800] [#/cm^3]	Mean Peak Particle Number Concentration [n = 5] [#/cm^3]	Mean Particle Number Concentration during minute 4 [n = 60] [#/cm^3]	Particle Number Concentration at 4 minutes [n = 1] [#/cm^3]	Particle Number Concentration at 30 minutes [n = 1] [#/cm^3]
30 min study	1.98 x 10^5	1.06 x 10^5	5.26 x 10^3	4.93 x 10^3	4.71 x 10^3

Table 30: Inferential statistical representation of the particle number concentrations after minute 4 to minute 30 [n= 1560]. Lower and upper limits represent the 90% confidence interval on a sampling t-distribution.

Sample	Mean: $\bar{\bar{X}}$ [#/cm^3]	Deviation: $S_{\bar{X}}$ [#/cm^3]	First-order linear trend line: $S_{\bar{X}}{}^2$ [#/cm^3]	5% Lower limit of confidence interval [#/cm^3]	95% upper limit of confidence interval [#/cm^3]
Original Location	5.05 x 10^3	2.39 x 10^2	y = -0.41887x + 5551	5.03 x 10^3	5.08 x 10^3

Although it is visibly obscure, the number representation of the particle number concentration displays the slight decrease after 4 minutes. The data and comparison between the mean concentrations between minutes 3 to 4 (5.26 x 10^3 #/cm^3) and the mean between minutes 4 and 30 (5.05 x 10^3 #/cm^3), show the slight decrease. However, the inferential statistical analysis and resulting 90% confidence interval reveal how minimal the negative decrease is. As would be expected in a linear decay, the final particle number concentration lays outside of the 90% confidence interval. The decrease can be seen to follow a linear regression. Therefore, a negative trend line of a first-order linear function, y, can be put together to model the decrease (Kahn, 2015):

$$y = ax + b \qquad \textit{Equation A.6}$$

Where:
b = the y intercept: $b = \bar{X}_y - a\bar{X}_x$
a = the slope $a = r\frac{S_y}{S_x}$
r = Pearson's r
S_x = standard deviation of values on the x-axis
$\bar{X}_x$= mean of values on the x-axis
S_y= standard deviation

$\bar{X}_y$ = mean of values on the y-axis

The model trendline of the decrease in particle number concentration emphasise how little is changing over the 30 minutes of sampling. The particles released from the drilling can be understood to disperse and stabilise almost instantly. The small decrease shows that over an extended period of time, some particles are depositing to reduce the particle number concentration.

The purpose and benefit of the evaluation carried out on particle number concentration levels after an extended period of time is to identify how long is necessary to collect data once drilling has ended. The data ascertained that the particle number concentration stabilises within 1 minute after drilling is finished.

The results present the first of data available in literature that demonstrate the peaks introduced at the point of drilling. In the studies thus far by Sachse et al., (20121), Bello et al., (2010) and Irfan et al., (2013) no such level of detail is provided. The data represented an increase over a longer period of time due to measurement sampling periods and unable to develop a method to achieve the level of detail. Therefore, this is completely state-of-the-art in representing the release of nanoparticles from materials due to drilling.

Demonstration of Reproducibility

In order to support the findings within this thesis, the particle number concentration was repeated on two sets of samples to demonstrate the reproducibility of the methodology. Therefore, the neat PP sample underwent the drilling process on two separate occasions. An initial three runs were carried out and are presented within the thesis. A fourth run on the same material, but 7 months later was carried out and compared to the initial three runs. The plot of the particle number concentration across the four minutes of drilling is presented in Figure 135.

The data demonstrates the parallel nanoparticle release during all four runs. ANOVA single factor analysis was performed between the 8 peaks introduced from run 1 and each following run individually. The analysis between run 1 and run 2 returned statistically insignificant differences (F value = 3.48 and F critical value = 4.60) with an 8.3 % probability and therefore accepting a hypothesis that the samples displayed no difference in peak particle number concentrations. The analysis between run 1 and run 3 returned statistically insignificant differences (F value = 0.926 and F critical value = 4.60) with a 35 % probability and therefore accepting a hypothesis that the samples displayed no difference in peak particle number concentrations. The analysis between run 1 and run 4 returned statistically insignificant differences (F value = 0.781 and F critical value = 4.60) with a 39 % probability and therefore accepting a hypothesis that the samples displayed no difference in peak particle number

concentrations. The statistical analysis therefore demonstrates that there was no statistically significant difference between the samples.

To further analyse the data, the 8 peaks introduced from all runs were compared as whole to assess the variability between the run peak means introduced from the same sample. The analysis returned statistically insignificant differences (F value = 1.54 and F critical value = 2.95) with a 22.7 % probability and therefore accepting a hypothesis that the samples displayed no difference in peak particle number concentrations. Therefore, the analysis of the nanoparticle release between the runs on the same sample, and including one run carried out 7 months later, displayed statistically insignificant differences.

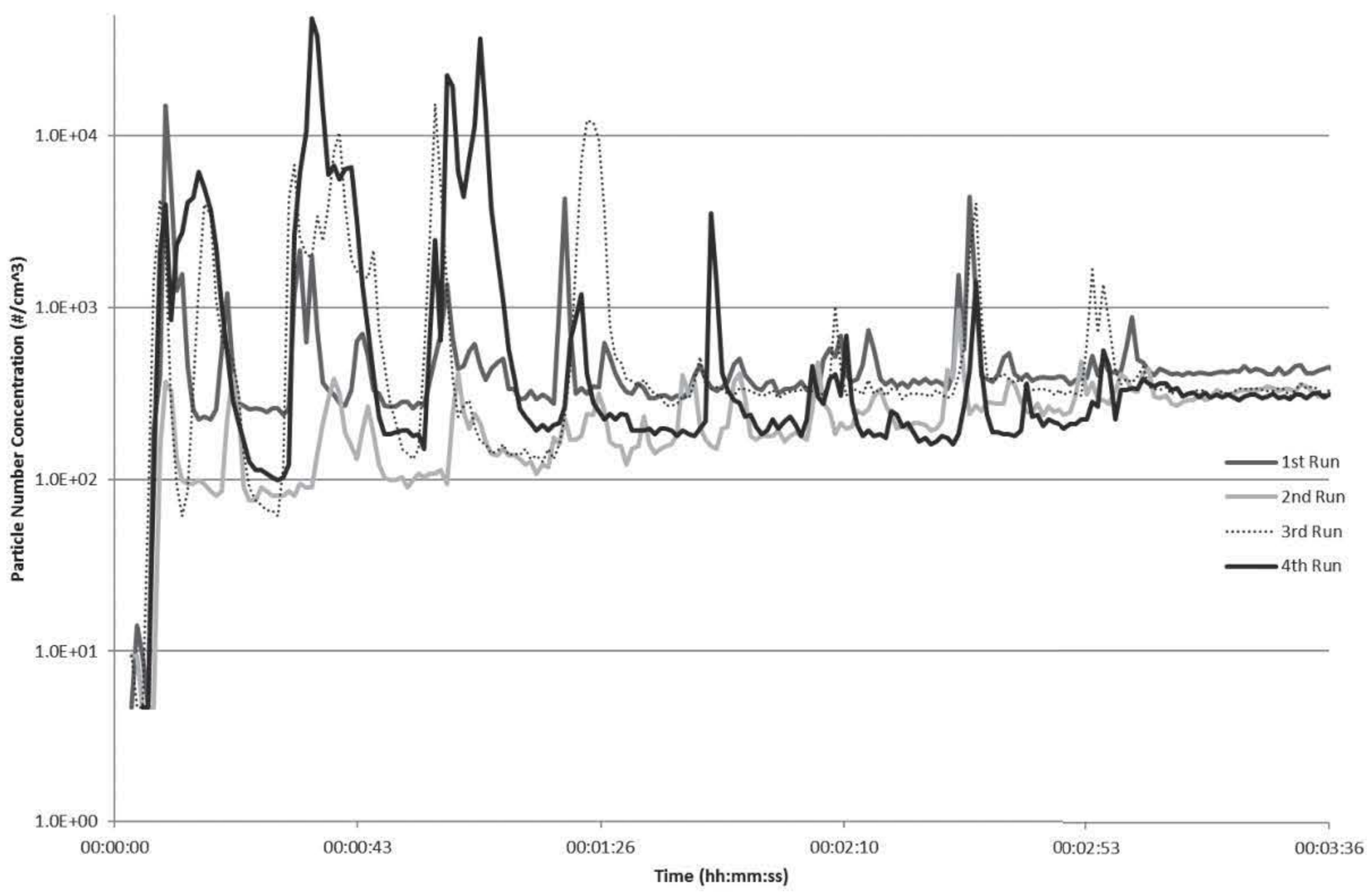

Figure 135: Particle number concentration runs on neat PP sample, as recorded on CPC. First three runs are taken on same day, with the 4th run taken place 7 months after initial test on first three (total of 221 days in-between testing).

As can be seen, the fourth run demonstrated a similar profile in particle number concentration in comparison to the initial three runs. A numerical comparison between the data is presented in Table *31*.

Table 31: Inferential statistical representation of the particle number concentrations introduced at the peaks due to the drilling on neat PP samples. Lower and upper limits represent the 90% confidence interval on a sampling t-distribution.

Run	Mean: $\overline{\overline{X}}$ [#/cm^3]	Deviation: $S_{\overline{X}}$ [#/cm^3]	Minimum [#/cm^3]	Maximum [#/cm^3]	5% Lower limit of confidence interval [#/cm^3]	95% upper limit of confidence interval [#/cm^3]
PP Run 1-3	7.55×10^3	6.33×10^3	0.50×10^3	15.3×10^3	4.38×10^3	10.7×10^3
PP Run 4	7.88×10^3	1.19×10^4	0.56×10^3	47.8×10^3	1.95×10^3	13.8×10^3

The numerical data demonstrates the similarity between the initial three runs and the fourth run. A further two-sample t-test of significance was performed on the drilling run carried out 7 months later and the average of the initial 3 runs. Run 4 displayed a statistically insignificant difference in the mean peak particle number concentration (statistically insignificant). ANOVA single factor analysis was performed to assess the variability between the sample peak means introduced between the first 3 runs and run 4. The analysis returned statistically insignificant differences (F value = 0.004528 and F critical value = 4.60) with a 94.7% probability and therefore accepting a hypothesis that the samples displayed no difference in peak particle number concentrations.

The evaluation of the particle number concentration on the PP samples therefore demonstrates that the methodology is repeatable. The removal of background noise and any interference from the drill demonstrates that the data returned statistically insignificant differences. Furthermore, the time frame in between tests also demonstrates that the material did not undergo any major changes which might affect the particle number concentration. This is also an important finding for the PP samples as the results within the thesis are compared to an investigation on the same materials carried out by Schutz (2010) using a different methodology in a different lab. The results are compared in Chapter Eight.

Similarly, the neat PE sample underwent the same repeated drilling investigated 7 months later and is presented in Figure 136. The fourth run can be seen to display similar peaks and particle number concentration at the end of the four minutes of sampling. The numerical values are represented in Table 32.

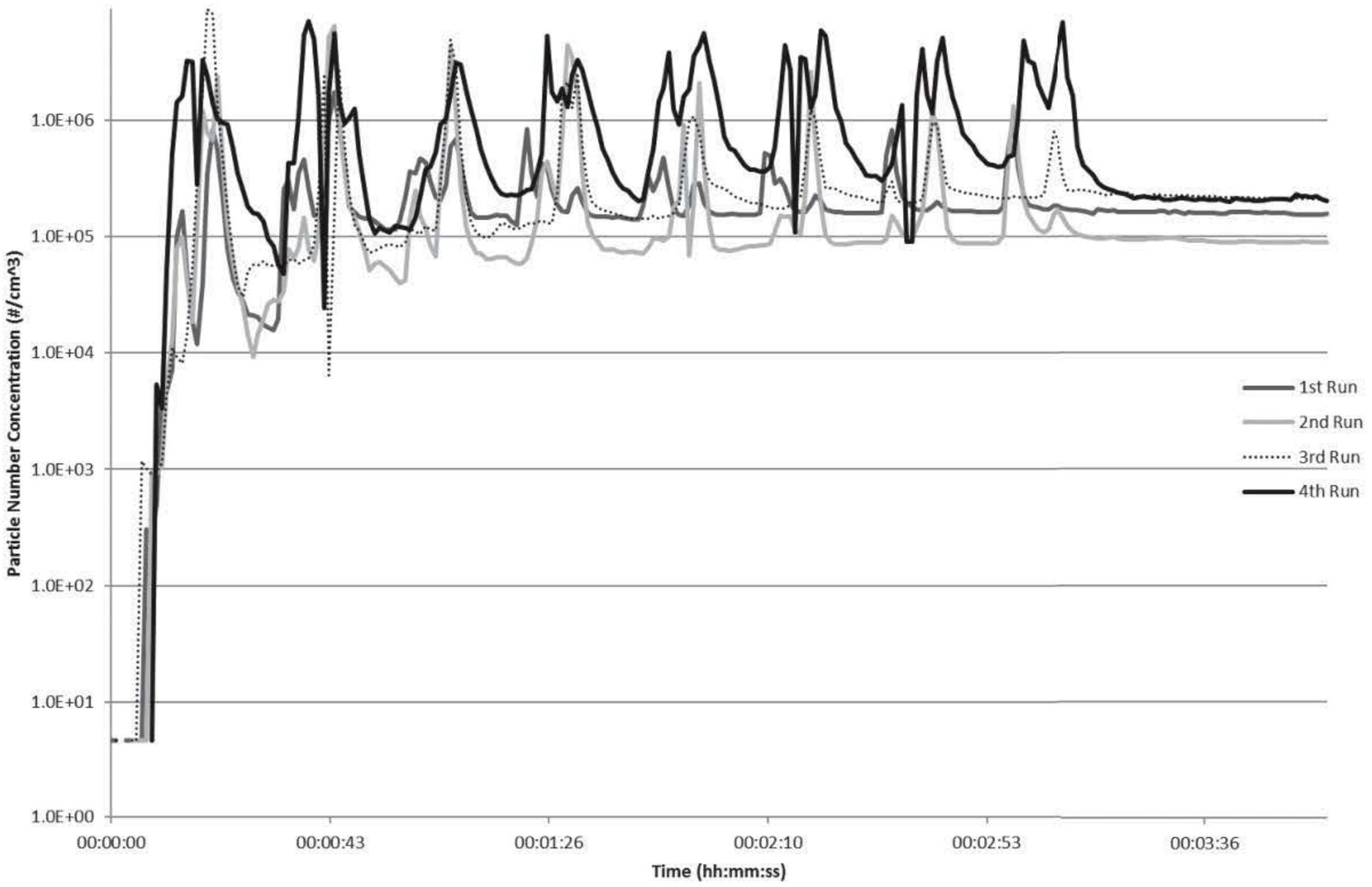

Figure 136: Particle number concentration runs on neat PE sample, as recorded on CPC. First three runs are taken on same day, with the 4th run taken place 7 months after initial test on first three (total of 221 days in-between testing).

Table 32: Inferential statistical representation of the particle number concentrations introduced at the peaks due to the drilling on neat PE samples. Lower and upper limits represent the 90% confidence interval on a sampling t-distribution.

Run	Mean: $\overline{\overline{X}}$ [#/cm^3]	Deviation: $S_{\overline{X}}$ [#/cm^3]	Minimum [#/cm^3]	Maximum [#/cm^3]	5% Lower limit of confidence interval [#/cm^3]	95% upper limit of confidence interval [#/cm^3]
PE Run 1-3	3.97×10^6	2.54×10^6	1.19×10^6	8.88×10^6	2.70×10^6	5.24×10^6
PE Run 4	5.25×10^6	1.35×10^6	3.13×10^6	6.99×10^6	4.58×10^6	5.93×10^6

The fourth run on the PE sample demonstrated a slight increase in the mean peak particle number concentration, in comparison to the same investigation on the neat PP sample. However, the data is still comparable to the first three runs. As with the neat PP sample, a two-sample t-test of significance was performed on the drilling run carried out 7 months later and the average of the initial 3 runs. Run 4 displayed a statistically insignificant difference in the mean peak particle number concentration

(statistically insignificant). ANOVA single factor analysis was performed to assess the variability between the sample peak means introduced between the first 3 runs and run 4. The analysis returned statistically insignificant differences (F value = 1.40 and F critical value = 4.60) with a 25.6% probability and therefore accepting a hypothesis that the samples displayed no difference in peak particle number concentrations. Comparing the statistical analysis with the PP sample, shows the PE displayed a lower probability of showing no difference, but still demonstrated a statistically insignificant difference in run 4 compared to the previous 3 runs.

The repetition of the particle number concentration profiles on the neat PP and neat PE sample therefore have demonstrated a level of repeatability of the methodology. Both samples demonstrate no statistically significant difference from the initial first three runs. However, as is demonstrated in the first three runs, the materials still demonstrate a level of variation and randomness. As is reported within literature (e.g. Brouwer et al., 2012), it is therefore important to carry out statistical analysis on the results. The data therefore is able to account for the variation in particle number concentrations introduced during drilling.

Conclusion

The appendix has demonstrated a specially designed drilling chamber for the nanoparticle release assessment from nanocomposite materials. As stated from the literature review and the introduction of this thesis, there is currently no available standardised method to assess the nanoparticle release from nanocomposite materials during machining. Therefore, in order to carry out the objectives within this thesis, a methodology was designed based on previous studies and literature, to be able to investigate the influence of the nanoparticles on nanoparticles release during drilling.

The methodology is designed to meet the identified criteria to perform a controllable and repeatable assessment of the nanoparticle release. Critically, the automated drilling methodology allows for the elimination of background noise from the measurements. The external numerical control of the drilling permits the monitoring and characterisation of the nanoparticles released from the materials without any interference. Achieving a clean environment within the chamber was a key principle of the testing methodology. Furthermore, the design allows for both real-time and post-analysis of the nanoparticle release quantification and characterisation from a lifecycle scenario. This section has provided a detailed description and demonstration of the methodology utilised in the this thesis to investigate the selected materials.

Emission measurements were taken using a CPC to help develop the methodology and test parameters. The final drilling parameters decided upon are a Dremel 4000 drilling tool with an industrial standard stainless steel 3.5mm twist drill bit was used at 10000 RPM with a feed rate of

78mm/min. The drilling studies are to be carried out by drilling across the width of the sample resulting in eight holes and bearing a time duration of 3 minutes followed by 1 minute of no drilling. This methodology allows for both an investigation into the particles released at the instant of drilling and the remaining emissions airborne post drilling. The eight holes drilled per sample are to be repeated three times to get a statistical average of the aerosols released.

The development of the methodology is presented along with a demonstration of the repeatability achieved. As highlighted within Chapter one, the methodology therefore provides an approach to evaluate the nanoparticle release that has minimalised all possible factors apart from the change in material. The results will therefore be able to assess the influence of nanofillers on nanoparticle release during drilling.

Within the development of the design, an additional best practice for the nanoparticle release assessment was published within this project in collaboration partners of SIRENA. The full report and details can be found in Appendix B. This report was published as an interim guideline when dealing with the potential release of nanomaterials. The manual gives 10 steps to follow based on what was learnt from carrying out the nanoparticle assessment carried out within this project.

The 10 guidelines and ideas are as follows:

1. Do evaluate the release
2. Use a reference material
3. Do not start from scratch… Adapt existing standards whenever available
4. Correlate the specific nano-release process to the specific stages the sample will undergo throughout its life cycle and also to the nature of the sample that is being tested
5. Monitor (and isolate) background and/or alternative emissions not specifically related to the process that is being simulated
6. Use calibrated and sensitive measurement equipment
7. Evaluate both aerosols generated and deposited particles, as both materials are relevant to estimate the release
8. Correlate the emission or release taking place with the actual simulation process under assessment
9. Collection step
10. Protect personnel carrying out the research

The manual is a product based on the experiences through this project and findings within literature. The details of each guideline are provided in the report, and range from the initial guideline of actually

quantifying and evaluating the release of nanoparticles. The research data collected from this project has indicated all materials reinforced with nanoparticles have influenced the nanoparticle release. The initiative should therefore always be taken to assess the release when dealing with nanoparticle reinforcements.

Other key guidelines include monitoring and isolation of background emissions. A core feature of the chamber and methodology designed within this thesis is the development of a clean environment allowing a repeatable experiment. Additional work in the development to improve the ease of use and logistical limitations of the chamber were carried out and are presented in Appendix C.

Appendix B –

SIRENA Best Practice Manual

SIRENA

LIFE 11 ENV/ES 596

SIRENA - SIMULATION OF THE RELEASE OF NANOMATERIALS FROM CONSUMER PRODUCTS FOR ENVIRONMENTAL EXPOSURE ASSESSMENT

BEST PRACTICE MANUAL FOR THE SIMULATION OF THE RELEASE OF NANOMATERIALS FROM POLYMER NANOCOMPOSITE PRODUCTS

DECEMBER 2015

Inkoa

Cranfield UNIVERSITY tecnalia Inspiring Business ROBERT GORDON UNIVERSITY•ABERDEEN

Disclaimer

This guide has been prepared by SIRENA's Project beneficiaries. All pictures have been supplied by SIRENA's Project partners unless otherwise specified.

The SIRENA LIFE Project is partially funded by the LIFE+ financial instrument of the European Commission under contract number LIFE 11 ENV/ES/596. The views expressed in present document are those of the Project beneficiaries. These views have not been adopted or approved by the Commission and should not be relied upon as a statement of the Commission's or its services' views. The European Commission does not guarantee the accuracy of the data included in present guidelines, nor does it accept responsibility for any use made thereof.

The organisations participating in this publication accept no liability whatsoever for damage arising from interpretation or use of the information, or reliance upon views contained herein.

This best practices document is to be regarded as a living document and must be reviewed and modified on a regular basis to assess its validity, accuracy and applicability.

© Partners of the SIRENA LIFE Project 2015

This work is copyrighted. This work may be reproduced in whole or in part, provided that it is not sold or used in any way for commercial benefit and that the source and author of any material used is acknowledged.

Further electronic copies of this guide are available from: http://www.life-sirena.com

Table of contents

List of Abbreviations

CNT – Carbon Nanotube

DMA - Differential Mobility Analyser

EAPNC – Emitted Aerosol Particle Number Concentration

ELPI - Electrical Low Pressure Impactor

ENMs – Egineered Nanomaterials

ESD - ElectroStatic Discharge

ESPs - Electrostatic precipitators

NEPs - Nanotechnology Enabled Products

PSD- Particle Size Distribution

PNC –Particle Number Concentration

POSS – Polyhedral Oligomeric Sisesquioxane

SIMS - Secondary Ion Mass Spectrometry

TRL - Technology Readiness Levels

XPS - X-Ray Photoelectron Spectroscopy

1. Introduction

One of the main applications of nanotechnology is the manufacturing of polymer nanocomposites, reinforced polymers with low quantities of nanosized ingredients dispersed into a thermoplastic or thermoset matrix. The use of engineered nanomaterials in composites production offers enormous advantages over traditional macro- or microsized fillers and applications across a wide range of industrial sectors are currently on the market.

In absence of an international consensus in relation to the (eco)toxicological impact of ENMs, industry must evaluate and, if feasible, quantify the risk of ENMs embedded into composite matrixes release to the environment throughout their life cycle as an integral part of its design processes. This information should be made available to the relevant regulatory authorities and consumers.

The main goal of the SIRENA LIFE Project is to demonstrate and validate a methodology to simulate the unintended release of ENMs from consumer products by replicating different life cycle scenarios to be adopted by a wide number of industrial sectors in order to get the necessary information for exposure assessment. To this aim, nanocomposite samples of different nature representing applications in the Automotive, Aerospace and Renewable Energy sectors have been mechanically degraded –via drilling and crashing- under controlled conditions in order to verify if embedded ENMs are released in these processes.

The present guidelines have been developed on the basis of the experience gained within SIRENA. The document compiles a series of practices that have been found to be successful for the evaluation of the release of ENMs from the plastic matrixes where those are embedded under mechanical stress.

Alternatively, nano-release can take place via chemical decomposition of the host matrix (including UV-assisted, thermal, hydrolytic and biological degradation) which could lead to direct release of ENMs either by exposing embedded particles to the material surface or by indirect release via attenuated diffusion properties. Many of the principles described in the next pages for experimental design are also applicable to this type of release.

2. Basic information

Relevant definitions to understand the information presented on this document are hereby provided:

Item	Definition
Emission	The act of producing or sending out something from a source
Release	To set free from physical restraint or binding
Aerosol	A system of colloidal particles dispersed in a gas, as smoke or fog
Dusts	Solid aerosols generated by the handling, grinding, abrasion, or cutting of a bulk material
Mists	Liquid aerosols generated by condensation from a gaseous state or by the breaking up of a bulk liquid into a dispersed state
Smoke	Solid aerosols resulting from the incomplete combustion of carbonaceous materials
Fumes	Solid aerosols generated by the condensation of vapors or gases from combustion or other high temperature processes
Bioaerosols	Solid or liquid aerosols from biological sources
Fibers	A special (based on toxicological properties) kind of dust that is fibrous in nature (i.e., longer than it is width). Aspect ratio (L:W) defined as 3:1 or 5:1

Additional definitions of relevance to the present document include:

Item	Definition
Nanomaterial	With the aim of ensuring that a nanomaterial is defined consistently in all pieces of EU Regulation, the Commission adopted a Recommendation on the definition on 18 October 2011: "Nanomaterial" means: *A natural, incidental or manufactured material containing particles, in an unbound state or as an aggregate or as an agglomerate and where, for 50 % or more of the particles in the*

Item	Definition
	number size distribution, one or more external dimensions is in the size range 1 nm - 100 nm". Nevertheless, this definition has generated a great controversy due to, fundamentally, the size range and percentage of particles it defines and, the selection of the particle number as the main measurement unit. The SCENIHR (Scientific Committee on Emerging an Newly Identified Health Risks), for example, considers that a material might be considered as a nanomaterial when >0.15% of the material has a size below the designated upper size limit and the Nanotechnology Industries Association (NIA), considers that the 50% threshold should be increased. The Commission is currently waiting on a third part of the report "Towards a review of the EC Recommendation for a definition of the term nanomaterial" from the Joint Research Centre (JRC). The first part (Part 1: Compilation of information concerning the experience with the definition) was published in July 2014 and the second one (Part 2: Assessment of collected information concerning the experience with the definition) in September 2014. The term "nanomaterial" is also defined in ISO/TS 80004-1:2010: "*material with any external dimension in the nanoscale or having internal or surface structure in the nanoscale*". This definition is generic, as it covers both nano-object (any external dimension in the nanoscale) and nanostructured material (internal or surface structure in the nanoscale). Among nanostructured, they define five different subcategories: • Nanostructured powder (including nanostructured aggregate, agglomerate, core-shell particle and capsule) • Nanocomposite (comprising polymer matrix, metal matrix, and ceramic matrix nanocomposite) • Solid nanofoam • Nanoporous material • Fluid nanodisperisons (including nanosuspension, nanoemulsion, liquid nanofoam, nano aerosol. WIESNER et al. (2009) refer that NMs may include individual nanoparticles (NPs), NP composites, macroscopic objects composed of NPs such as thin films, and many other objects composed of materials with the requisite characteristics of having at least one dimension of 1-100nm and displaying novel properties. Engineered nanomaterials (ENM) en engineered nanoparticles (ENPs) are materials intentionally created with specific properties related to shape, size, surface properties and chemistry.
Composite	Combination of two or more different materials mixed in an effort to blend the

Item	Definition
	best properties of both
Nanocomposite	Composite material in which one or more phases of the components has at least one dimension that is nanoscopic in sizeEngineers (). Nanocomposites display enhanced physical, thermal and other unique properties when compared to conventional microscale composites. Nanocomposites based on the nature of matrix phase can be divided into polymeric, ceramic and metallic composites. Nanocomposites can also be classified according to their types of filler material (such as clay nanocomposites, ceramic nanocomposites, carbon nanotube composites, metal and metal oxide nanocomposites and nanobiocomposites). According to the IUPAC, a nanocomposite is a *Composite* in which at least *one* of the phases has at least *one dimension* of the order of nanometers (WORK et al., 2004).

The transition from microparticles to nanoparticles yields dramatic changes in physical properties. Nanoscale materials have a large surface area for a given volume. Since many important chemical and physical interactions are governed by surfaces and surface properties, a nanostructured material can have substantially different properties from a larger-dimensional material of the same composition.

In polymer science, the most relevant classification of ENMs is that related to their geometry, since, depending on the application of interest, high aspect-ratio particles are used for nanocomposites manufacturing. Attending to their geometry, ENMs are classified into three classes: particle, layered and fibrous materials. Examples of particulate materials include metallic and ceramic nanoparticles and POSS; fibrous materials are exemplified by carbon nanotubes and silicates such as sepiolite and wollastonite; finally, graphene and montmorillonite are layered materials.

Nevertheless, some authors (Nowack et al., 2012) argue that when trying to carry out their hazard identification they should be categorized based on the location of the nanoscale structure in the system/ material. In this sense, Hansen (2007) developed a categorization framework depending on where the nanoscaled structure is located.

Figure 1: Categorization framework to aid hazard identification of nanomaterials. S. Foss Hansen, B.H. Larsen, S.I. Olsen, A. Baun. Nanotoxicology, 2007, 1-8. According to this categorization, nanocomposites belong to class III, subcategory c "Nanoparticles suspended in solids".

2.1. Commercial relevance of Nanocomposites

The development of polymer nanocomposites is one of the most active areas of production of nanomaterials and the polymers and nanofillers used to these applications are continuously increasing in the last years.

According to BCC Research (Global Markets for Nanocomposites, Nanoparticles, Nanoclays, and Nanotubes. NANO21F, May 2014) the Global consumption of nanocomposites will reach by 2019 584.984 metric tons/$4.2 billion (a CAGR of 21.1% in unit terms and 24% in value terms between 2014 and 2019).

Although the Asia- Pacific region was the largest geographical market for nanocomposites in 2013, consuming about 36% of the market, it is expected that in 2019, Europe (with the 33.2% of the market) will be the first consuming region as can be seen in the next table:

Market	2013	2014	2019	CAGR% 2014-2019
Asia-Pacific	443.6	502.1	1,356.0	22.0
Europe	409.5	486.7	1,405.8	23.6
U.S.	265.7	325.2	1,163.0	29.0
Rest of World (ROW)	112.5	129.6	303.0	18.5
Total	1,231.3	1,443.6	4,227.8	24.0

Table 1: Consumption of nanocomposites by country/region through 2019 ($ Millions). Source BCC Research

However, as can also see in the table, the US market for nanocomposites has the highest projected growth rate of any major market (29%), followed by Europe and Asia.

Relating the consumption by type, in 2013, clay nanocomposites accounted for 59% of total nanocomposite consumption by value in 2013, followed by carbon nanotube composites (17.7%) and metal/metal oxide nanocomposites (12.8%). For 2019, authors expect that clay nanocomposites'

market share will increase and carbon nanotube composites and metal/metal oxide nanocomposites' share will drop.

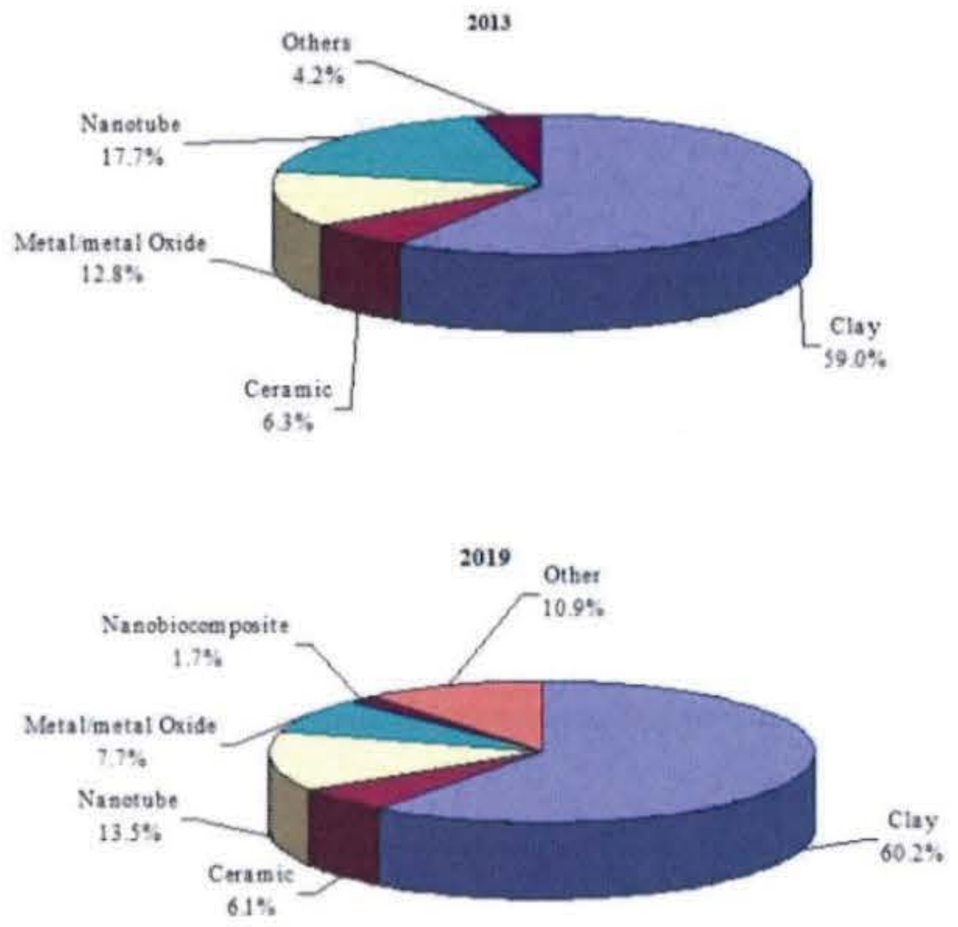

Figure 2: Global nanocomposite consumption by type, 2013 VS 2019 (% of total value) Source: BCC research

Regarding nanocomposite consumption by application, in 2013, automotive area was the main nanocomposite application area with 51.4% of the worldwide market, continued by packaging (22.5%) and electronics/ESD (13.85). In authors' opinion, automotive and electronics/ESD share will drop and packaging while increase slightly. Textiles are going to emerge as the fourth largest nanocomposite application area in 2019.

Polymers used as matrices of nanocomposites, include Nylon, Polyolefin, Polyethylene, Polypropylene, Polyvinyl chloride, Polystyrene, Ethylene- vinyl acetate copolymer, epoxy resins, polyurethanes, polyamides and polyethylene terephthalate.

Nanofillers used in order to improve the properties of the different polymers are applied at rates 1-10% (in mass) and the most common ones are nanoclays, nano oxides, carbon nanotubes and metallic nanoparticles.

Some applications of polymer matrix nanocomposites include:

- Mechanical Reinforcement: By adding nanofillers to polymers an improvement in mechanical properties can be achieved (mechanical stability, stiffness, strength, toughness ...).
- Barrier and membrane separation properties

- Flammability resistance: The addition of some nanofillers to polymers lead to an increased flammability resistance
- Polymer blend compatibilization: It has been demonstrated that the addition of nanoparticles can prevent the coalescence retaining improved dispersion after shear mixing.
- Biomedical applications
- Fuel cell applications
- Electrical/electronics, optoelectronics and sensors

2.2. Who should read this manual

Within the actual regulatory framework, companies do not need to declare the nanoparticles or ENMs used within their consumer products and processes with several exceptions. The EU Cosmetics Regulation and the EU Biocides Regulation contain both specific provisions for nanomaterials according to which the materials used in the nanometric scale need to be identified as such on the product labels. The proposal for a Regulation on medical devices refers that, where applicable, an indication that the device incorporates or consists of nanomaterial is to be included on the label unless the nanomaterial is encapsulated or bound in such a manner that it cannot be released into the patient's or user's body when the device is used within its intended purpose.

It is therefore expected that the regulatory framework affecting the integration of ENMs within a number of fields changes in the next years, integrating specific provisions for nanomaterials.

In accordance with the *Study to Assess the Impact of Possible Legislation to Increase Transparency on Nanomaterials on the Market* (June 2014), there appears to be a widespread (but not universal) view that available information on nanomaterials is insufficient for informed decision-making. This was reflected in the call by the European Parliament[1] in 2009 for the European Commission to compile: "*an inventory of the different types and uses of nanomaterials on the European market, while respecting justified commercial secrets such as recipes, and to make this inventory publicly available*".

Since then, several Member States (most notably France) have launched initiatives for national registries for nanomaterials. Furthermore, Austria, Belgium, the Czech Republic, Denmark, France, Italy, Luxemburg, the Netherlands, Spain, Sweden and Croatia have asked the Commission[2] to "*propose legislation on registration or market surveillance of nanomaterials or products containing nanomaterials*". Various stakeholders and non-governmental organisations have also called for a registry for nanomaterials.

There exists a significant controversy in relation to the present approach and an international consensus has not yet been reached. In case of approval, there exist several options to accomplish with the registry. One of such options is the EU Nanomaterial Registry by Application. This would require manufacturers/importers/downstream users/distributors to submit a new declaration for each new

[1] European Parliament resolution of 24 April 2009 on regulatory aspects of nanomaterials (2008/2208(INI))

[2] As indicated in the Commission's Working Document:
http://ec.europa.eu/DocsRoom/documents/5282/attachments/1/translations/en/renditions/native

nanomaterial-containing mixture or article that they put on the market. This would allow for full traceability of an ENM across the supply chain.

The nano-release assessment serves **the safer-by-design principle,** allowing the reformulation of NEPs (Nanotechnology Enabled Products) with a reduced ENMs content or with different configurations so that release is decreased or eliminated until the associated (eco)toxicological impact of ENMs is cleared out. The most logical step following the registry, would be the evaluation of the potential ENM release of these products, in order to evaluate consumer and environmental exposure beyond manufacturing stages of the so called NEPs (Nanotechnology Enabled Products).

Furthermore, the Article 13 of REACH refers that testing (human toxicity...) may be omitted where justified by information on exposure and implemented risk management measures. On the basis of the present article, if it can be demonstrated that there is no exposure to ENMs throughout their life cycle; ie, no release takes place, no testing is to be carried out.

The present guidelines are addressed to research centres and universities, having conducted the majority of the nano-release assessment studies to date but also to a wide number of industrial sectors. The efforts by BASF in the present area represent an example of industrial leadership in the present area of development.

3. Lessons learnt

The present section describes several ideas that could be taken into account when designing an investigation to evaluate the release of ENMs from polymer nanocomposites. These ideas come from the experimental work conducted within SIRENA and also from the thorough assessment of additional research studies and initiatives at this regard that has been carried out by means of the Technological Surveillance during the implementation of the project.

3.1. Do evaluate the release

The first and fundamental step in the control of hazards is their **recognition**.

ENMs released from products may exhibit a different toxicity than pristine ENM (Nowack et al., 2012) which are used for toxicity tests. Once released in the environment, physical and chemical transformations and biotic metabolism can change the properties of ENM and thus influence their toxicity. Examples of abiotic influences on ENM are; thermal treatment (incineration, heating), dissolution, transportation, agglomeration, aggregation, absorption, sorption, sedimentation, etc. Moreover, chemical changes to released ENM and their functionalized surface can occur (for example by oxidation). Such modifications in natural media influence surface-chemistry-related factors such as mobility, persistence, reactivity, bioavailability and biocompatibility of ENMs ((CIEL) et al., 2015). As a consequence, the associated hazard profile of the released materials will be affected.

Predicting exposure to ENMs and the relevant exposure concentration begins with an assessment of the environmental availability of ENMs throughout their life-cycle. This will largely be determined by the engineered matrices in which these materials are found, such as composites in intermediate or finished consumer goods. ENM could be released during primary production processes (synthesis), formulation and application of intermediate products, waste treatment as well as accidents that may occur at each stage of a product's life cycle.

However, the unintentional release of ENM from products is often not anticipated or taken into account prior to their commercialization, amongst other because no standardized methods and protocols are available to evaluate the release.

A relevant consideration to be made refers to the actual target of the assessment to be carried out. Nano-release evaluation can serve two different purposes:

- Exposure assessment to released nanosized particles: worker, consumer or environmental exposure to articles or processes in which Nanotechnology is present in either way under normal or accidental conditions. We can refer to this part of the assessment as nanosized EMISSION or DUST.
- Nano-release assessment: in present assessment the main target is to verify if Nanotechnology incorporating products actually release these ENMs throughout their life cycle (be it Nanosilver incorporating t-shirts or plastic food containers integrating ENMs). This evaluation can be referred to as RELEASE (and more specifically as NANO-RELEASE).

Different questions are therefore to be answered particularly for the materials of interest of SIRENA:

- What is the physico-chemical nature of the particles released by nano-additivated composites under mechanical stress (in comparison with the traditional formulations –including micro-additivated samples-)? Particle size distribution...
- Do embedded ENMs actually release from nanocomposite samples under mechanically stressing conditions? The answer to this question is challenging, because freely released ENMs may constitute too small a portion of the total released mass that instruments are not sensitive enough to detect them and released ENMs could adhere to the surfaces of larger abraded particles and thus remain hidden from conventional particle sizing experiments.
- If affirmative, what are the specific characteristics of the released materials? Chemical composition of mixed nature, variety of shapes, number distribution...

The World Health Organization published in 1999 (WHO, 1999) that "*Dusts usually originate from larger masses of the same material, through a mechanical breakdown process such as grinding, cutting, drilling, crushing, explosion, or strong friction between certain materials (e.g., rocks). Dust thus generated is often called* ***"primary airborne dust***." The generation of dust from materials under mechanical stressing conditions is therefore a well-known phenomenon. It is also acknowledged that dust particle size is related to the amount of energy involved in creation; the higher the energy, the smaller the particle created; the lower the energy, the larger the particle created.

We can expect dust to be generated in the mechanical degradation processes that are considered within SIRENA, and such dust will convey an environmental and/or human exposure. What we do not know is neither if the exposure associated to these mechanisms on nanocomposite materials is different to the exposure associated to the traditional materials (with microparticles or no particles embedded) nor if ENMs do release from the embedding matrix as isolated or hybrid particles (matrix-ENM).

In most of the studies conducted to date, no free nanofillers have been observed; rather, released particles were agglomerates of the nanofillers and the host matrix. Considering the samples and mechanical processes tested within SIRENA no free nano-fillers have been observed either. However, this conclusion cannot be extrapolated to any polymer nanocomposite material, since nano-release is specific to the type of sample and degradation process investigated and it must therefore be evaluated on a case by case basis.

3.2. Use a reference material

From a life cycle perspective, **samples with the same functionality** should be selected as a reference which sometimes means using samples with traditional macro or microsized fillers and not necessarily with the non-reinforced matrix, which would enable a fair comparison (taking into account functionality issues). This would be especially relevant for assessments related to the changes in particle size distribution and aerosol generation in the samples of interest. If nano-release is the very specific target, the selection would necessarily be nano VS non-nano containing specimens.

The selection of the test materials is crucial. Within SIRENA pre-market materials have been selected considering that the nano-release assessment needs to be performed on materials that are likely to reach the market in their actual configuration. As a matter of fact, within SIRENA we have verified that the performance of the reinforced specimens is increased in contrast with the reference materials and thus, have a real potential to replace the traditional formulations in specific applications.

Bello et al. (2012) refer as sample materials to two types of advanced CNT-hybrid composites. In detail: *(1) "fuzzy fiber" reinforced plastic laminate composite containing woven alumina fibers in each lamina with aligned CNTs grown on the surface of the alumina fibers (referred to here as CNT-alumina [CNT-A]), and (2) a graphite-epoxy prepreg system (aligned and collimated carbon fibers with an epoxy resin arranged in a layered laminate configuration) with aligned CNTs placed at the centre (termed here CNT-carbon [CNTC] composites)*. No practical examples of the type of applications containing these materials are provided; the reader cannot tell from the information on the article whether the selected materials are of commercial relevance or if those have been manufactured for RTD purposes only.

In a different study, Cena and Peters (2012) have not used a reference sample, but, instead, airborne concentrations were measured during two processes: weighing bulk CNTs and sanding epoxy nanocomposite test sticks (2% wt CNT). Though this study can provide data on the emissions associated to the use of CNTs in the referred scenarios, it provides no information on the emissions associated to alternative traditionally used fillers for a relative perception of the associated risk.

3.3. Do not start from scratch... Adapt existing standards whenever available

No specific standard is available to date for nano-release assessment from nanocomposite samples. For instance, the ISO/TS 12025:2012 – *Nanomaterials. Quantification of nano-object release from powders by generation of aerosols* describes how to choose the measurement device and the sampling procedure to follow. However, it only concerns release of nanoobjects from powders and not from actual nanoproducts as solid parts undergone mechanical stress situations.

However, standard tests exist simulating accelerated ageing, mechanical or chemical stress; as most of these protocols serve the purpose of verifying if a certain material or product can perform well under certain use conditions. These standards only cover the equipment to use and procedure to follow in order to carry out the mechanical tests but do not mention the measurement of nanoparticles released or their collection. Notwithstanding with the above mentioned, such standards can be adapted to the purposes of the assessment we are conducting. In fact, in literature, standard methods that have been adapted for nano-release assessment have been reported as hereby exemplified:

- Golanski et al. (2011) refer the use of the ISO 11998 for nano-release assessment in a wet abrasion study on TiO_2 nano-additivated paints.
- Wohlleben et al. (2011) & Wohlleben et al. (2013) refer the Taber Abraser test as an established method of the coatings industry to quantify wear resistance which is described in several national and international standards (e.g. DIN53754:1977, DIN 68861-2:1981, ISO 5470-1:1999 and ASTM D4060-95:2007).
- On a pilot interlaboratory comparison of protocols that simulate aging of nanocomposites and detect released fragments, Wohlleben et at (2014) have simulated the year-long outdoor use by consumers on the basis of ISO-standardised weathering tests established for plastics and coatings, in particular ISO 4892-2 (2013).
- On a different context, the international standard ISO 105-C06:1994, for determining colour fastness in commercial and industrial laundering has been reported for nano-release assessment from textiles incorporating ENMs (Windler et al., 2012).

Simulation of the release of nano-sized particles during experimental processes in several studies have used existing standardized procedures. However, to the best of our knowledge, no standard methods exist to test drilling resistance; due to this fact the typical drilling conditions in an industrial setting have been selected and uniformly applied to all sample materials within SIRENA. However, in the case of the cashing/impact approach, the test conditions described in the Euro NCAP regulation for 'Impact Testing' (http://www.euroncap.com/en/for-engineers/protocols/general/) have been selected.

Automatic processes are preferred over manual process since those can be easily controlled enabling repeatable and reproducible tests. Note that the purpose of the research is to evaluate and quantify the release of ENMs, not the assessment of the consumer exposure in manual DIY operations. Depending on the focus of the assessment, industrial or domestic processes could also be simulated.

In relation to the generation of controlled conditions for nano-aerosol measurement and characterization, to the best of our knowledge, no specific standard exists. Groso et al. (2010) have developed a procedure for managing the occupational safety and health risks relevant to research laboratories producing and using nanomaterials. *The procedure consists of two parts. Using a decision*

tree authors sort the "nano-laboratories" into three hazard classes (Nano 3 = highest hazard to Nano 1 =lowest hazard), which corresponds to analogue approaches applied to other hazard types (biohazard, radioprotection or chemistry). For each hazard level authors then provide a list of required risk mitigation measures (technical, organizational and personal).

Alternative standards to be used as a starting point are the emission chambers used to measuring the discharge of volatile organic compounds in indoor air.

Within SIRENA, the developed prototype by Cranfield University underwent a Local Exhaust Ventilation (LEV) test in order to evaluate if the system is safe towards the operator.

Finally, the chamber should have implemented temperature and relative humidity monitoring/control systems, since these two parameters might affect the agglomeration status of the airborne materials. These two have not been monitored within SIRENA but could be observed in future optimizations of the developed prototypes. Other parameters such as air exchange rate, loading rate, air velocity and clean air supply should be known as they might have an effect on the emitted particles.

3.4. Correlate the specific nano-release process to the specific stages the sample will undergo throughout its life cycle and also to the nature of the sample that is being tested

This tip is especially relevant if the (eco)toxicological potential of the released particles or nanofillers is to be evaluated. It has been written on the basis that the nano-release simulation study should be planned in agreement with the ulterior scenarios the material will go during its life time, for instance a piece of polyamide to be placed inside the car will not undergo hydrolysis or chemical degradation processes in contrast to pieces exposed to environmental stress.

The key issue is to define what type of exposure is to be evaluated: depending on the exposure -worker exposure, consumer exposure, environmental exposure- the forms of the nano-objects will vary. The assessment should focus **the most relevant forms of the released particles when the exposure takes place**.

An additional relevant consideration to be made is related with the **nature of the samples** that is being evaluated. In fact, according to Duncan (2015) the available literature on release of ENMs from nanocomposites as a result of mechanical degradation suggests that the physical properties of the host material (and the types of forces applied) are integral to determining the number and size of particles released.

In agreement with the above statement, within SIRENA, in the drilling experiments noticeable differences were observed when comparing emissions of thermoplastic and thermoset materials, the first ones with a lower release which is attributed to the fact that Polypropylene melts and nanosized particles are retained in this process.

Figure 3: SEM image of the turns collected from a Polyester/Al_2O_3 sample
Thermoset

Figure 4: SEM image of the turns collected from a Polypropylene sample
Thermoplastic*

Figure 5: SEM image of the turns collected from an Epoxy/CNT sample
Thermoset

Images by CRANFIELD UNIVERSITY.

The different behaviour of the two types of materials reacting to the drilling can be observed at the microscale since the turns collected from the drilling of polypropylene (and so thermoplastic) materials appear like an agglomeration of materials that seems to have melted –Figure 2- due to their low thermal conductivity.

Within SIRENA the same drilling conditions for all the samples studied have been applied independently of their thermoplastic or thermoset nature. Considering the heat effect on thermoplastic matrixes, the drilling protocol could have been adapted by extending the machining time with slower feed rates (this is just an example of an alternative approach). This must be seen as a relevant consideration for future studies on nano-release assessment on polymer nanocomposite samples in mechanical degradation studies.

The results obtained within SIRENA suggest that the nature of the host material has a greater influence on the characteristics of particle release from plastic nanocomposites during mechanical abrasion than the characteristics of the nanofillers.

Aligned with the present results, Hirth et al. concluded from their work[3] that CNT protrusions are a material-dependent phenomenon related to the toughness of the host matrix and are likely to occur only in particles released from host materials with elongation-at-break values greater than 10%. In materials with large elongation-at-break values (e.g., thermoplastic polymers such as Nylon, PE, PET, etc.), necking of the host matrix is expected to inhibit the formation of CNT protrusions; that is, the host material will "stretch" around nanofillers rather than simply break off to leave nanofillers exposed.

It must be noted that within SIRENA no CNT protrusion has been observed in epoxy samples (same host matrix, filler and filler quantity -2% weight-) in contrast to the reference cited above. The difference relays in the mechanical process tested, thus nano-release needs to be considered to be specific to the mechanical process under consideration.

Finally, in relation to the nature of the samples of interest, no studies have been identified addressing the release/emissions on recycled polymer nanocomposite samples, for any of the possible degradation processes these might undergo (mechanical, chemical, biological...) depending on their specific application and life cycle stage of consideration. This can be pointed out as a research gap to be addressed in the future.

[3] Hirth et al., Scenarios and methods that induce protruding or released CNTs after degradation of nanocomposite materials. J. Nanopart. Res. 2013, 15, 1504.

3.5. Monitor (and isolate) background and/or alternative emissions not specifically related to the process that is being simulated

Background nanoaerosols from natural and incidental sources are ubiquitous and present major challenges for the characterization of aerosols in simulated scenarios. Several approaches have been proposed and applied, including subtraction of background concentrations, either measured prior to the activity or during the activity away from the source, and statistical techniques. However, concurrent processes (i.e., use of combustion or electro motors) can be a significant source of other (potentially health relevant) particles (Koponen et al. 2011; Szymczak et al. 2007). Furthermore, these techniques for correcting background levels do not account for the interactions between ambient aerosols and the ENM particles.

Instruments to date do not distinguish ambient particles and ultrafine particles from the nanoaerosols generated in mechanical degradation processes on test samples. Furthermore, it is unclear whether background measurements should be subtracted from the measurements taken during simulated scenarios or reported separately.

The use of enclosures facilitates the discrimination of nano-objects from background particles. An additional benefit of using enclosures is the safety of the testing personnel, who is not directly exposed to the released particles with possible hazardous properties not yet clearly determined.

In the preparatory actions conducted within SIRENA, several particle measurements were carried out as blank tests (no nanocomposite samples being mechanically degraded) on different days. The different particle number concentrations can be observed in the Figure 6. Measured particle concentration corresponds to the activation of the drill with no samples being drilled on 7 different days.

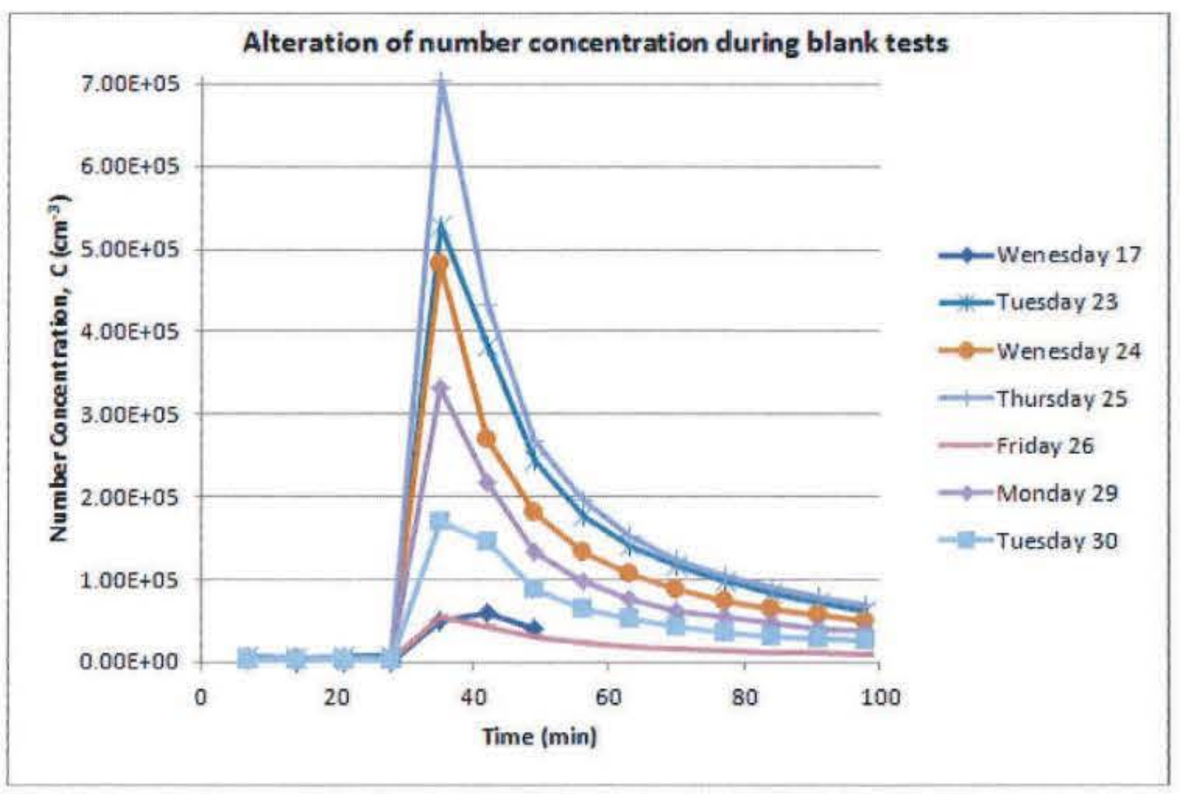

Figure 6: Variations in particle number concentration obtained in blank tests (un-optimized protocol and testing prototype)

Additionally, **emissions associated to the equipment** that is used to generate the release are to be monitored. In fact, several authors (Koponen et al., 2009, van Broekhuizen et al., 2011, Kuhlbusch et al., 2011, Wohlleben et al., 2011) have detected high levels of ultra-fine particles which they attributed to particle emissions from electric motors. Szymczak et al. (2007) and Lioy et al. (1999) showed that certain motors (with carbon brushes sliding over copper commutator contacts) tend to release significant amounts of ultra-fine particles.

Being aware of the present circumstance, a water cooled and sealed spindle drill system to ensure no particles are introduced into the chamber was implemented in the developed prototype by CRANFIELD UNIVERSITY.

Figure 7: Water cooled and sealed spindle drill system implemented in the prototype developed within SIRENA

To address the background noise problem, researchers at RGU and VITO developed a new chamber system that eliminates all the background noise. This new chamber set up includes an enclosed environment which consisted of only "clean air" through a series of HEPA filters. The testing would only initiate once the chamber had cleaned itself and a low concentration of particles was produced on the CPC. The HEPA filters combinations were capable of producing a CPC reading within the chamber of o #/cm^3 particle number concentration.

3.6. Use calibrated and sensitive measurement equipment

Instrument and system calibration are of main importance for the successful measurement of aerosol properties and nano-release assessment in a sampling environment. While there are theoretical means for assessing instrument or system performance, calibration provides information which is more reliable and more applicable for the particular sampling conditions.

The ISO 9001:2008 Quality management systems - Requirements are:

7.6 Control of monitoring and measuring equipment

The organization shall determine the monitoring and measurement to be undertaken and the monitoring and measuring equipment needed to provide evidence of conformity of product to determined requirements.

Where necessary to ensure valid results, measuring equipment shall

- *be calibrated or verified, or both, at specified intervals, or prior to use, against measurement standards traceable to international or national measurement standards;*
- *be adjusted or re-adjusted as necessary;*

In addition, the organization shall assess and record the validity of the previous measuring results when the equipment is found not to conform to requirements. The organization shall take appropriate action on the equipment and any product affected.

Box 1: Extract of the ISO 9001:2008

In general, devices used to assess exposure to nanomaterial or nano-size aerosols can be subdivided into devices that monitor (on-line) a chemical substance or aerosol by "near or quasi" real-time detection and devices that sample (time-aggregated) chemical substances or aerosols on a substrate, followed by off-line analysis.

As a limitation to the state of the art technology it must be noted that the methods and instrumentation generally applied to estimate the particle size distribution make the assumption that the particle's shape is spherical which is usually not the case.

3.7. Evaluate both aerosols generated and deposited particles, as both materials are relevant to estimate the release

Recent publications by Shandilya et al. (2015) and others, have addressed the release of ENMs by means of abrasion but focus only on aerosolized particles (EAPNC – Emitted Aerosol Particle Number Concentration; PSD- Particle Size Distribution, determined on the basis of PNC –Particle Number Concentration).

When aerosolized, ENM coagulate homogeneously or heterogeneously with other ENM, or attach to ambient background particles; all processes effectively alter the particle size distribution, the particle number concentration, and the chemical composition of the background aerosols (Schneider et al. 2011; Seipenbusch et al. 2008). Many studies of aerosolized ENM focus primarily on measuring nano-sized particles (compared to larger particles), yet particles may no longer be in the nano-size range at the time of sampling. CLARK ET AL 2012

Within SIRENA emitted particles are classified as airborne and deposited. Airborne particles are measured by Cranfield University via SMPS+C whereas deposited particles are collected for ulterior characterization studies. In the case of RGU, the particle size distribution was measured using an SMPS and a DMS50.

In fact, data from the SMPS provide information related to the exposure to the emitted particles. Information related to the nano-release assessment –to the date of present report- can be obtained by actively collecting emitted particles and visually inspecting whether ENMs have released or not from the surrounding matrix. As an alternative, Wohlleben et al. (2011) used XPS and SIMS to show that silica nanoparticles were exposed on the surfaces of composite particles released from silica/polyamide PNCs, but only in concentrations similar to what is found in the bulk composition of the PNCs, if silica nanofillers were released in a free state and then adsorbed onto the surface of particles composed of the host material after aerosolization, XPS and SIMS would reveal disparate concentrations of silicon between the postabrasion released particles and the preabrasion bulk material. According to these authors, a wider application of surface analytical techniques such as SIMS and XPS could reveal more about the conditions under which free nanofiller release is likely and confirm the presence of nanofillers on abraded particle surfaces.

It must be noted that indoor particles are subject to aerosol transport processes such as deposition and therefore released nanoparticles in airborne conditions might eventually deposit. Due to this fact, both airborne and deposited particles are of interest as there might be changes from one status to another and emitted nanoparticles might be in either both. Bearing this fact in mind, preliminary testing studies must evaluate the time needed so that most particles are deposited following a mechanical degradation process and particle levels decrease to the pre-experiment levels. Only after this time should deposited particles be collected.

It is also relevant to encompass the measuring time of the instrumentation used with the testing time during which particles are emitted. The SMPS classifies sequentially the different electrical mobilities of the particles in a DMA and determines their number concentrations with a condensation particle counter. The SMPS thus relies on stable concentrations and size distributions for the full length of the measurement (7 min in the case of Cranfield University).

3.8. Correlate the emission or release taking place with the actual simulation process under assessment

In the case of the drilling approach the amount of particles emitted or ENMs released can be correlated with the volume of material removed by the drill (material removal rate). The same can be applied to other physical processes such as abrasion.

There is, however, one relevant consideration that is to be made at this regard, the mechanical degradation of the sample -if the sample is of plastic nature- can generate heat that would melt the material thus decreasing the number of particles emitted. As an alternative to reduce the heat generated in the mechanical degradation process, wet machining (with a cooling effect) has been evaluated in several studies. Not surprisingly, abrasion during wet conditions often results in a significant reduction in the number of aerosolized particles, although perhaps not in the total amount of material released (in the evaluated literature studies, the liquid were not assessed for particle content).

For samples exposed to environmental degradation, emissions/release can be expressed per area of sample that has been in contact with the environmental stressors (light, water...).

3.9. Collection step

Because particles and objects released by machining of nano-composites are potentially of nanoscale it is necessary to use collection equipment that is suited for presenting such objects to the analysing equipment without change of the relevant characteristics. This can be achieved by sampling "cassettes" that contain membranes for stripping solid aerosol objects from an airstream that passes through the membrane, by diffusion cells that collect ultra-fine particles on open mesh structures (PWRAS), by inertial impactors that deposit particles dynamically onto solid target surfaces (ELPI, PWRAS) as well as by thermophoretic (TP) or electrostatic precipitators (ESP, NAS) that achieve the same using thermal gradients or electrostatic attraction, respectively. Large particles can be collected by simply letting them fall into a particle storage container under the influence of gravity (Schutz & Morris, 2013).

Ideally, if emissions and/or released particles are to be evaluated from the ecotoxicological perspective the storage time should be minimal, since samples might undergo changes during storage. ENMs enclosed in particles of a composite matrix are largely isolated from the surroundings, at least temporarily. This has the consequence that they are not equally biologically available and more persistent. It can generally be said that such chemicals have lower bioavailability and consequently a reduced acute toxic effect. Bioavailability may, however, change if surrounding environmental factors affect the material particle so that it erodes, corrodes or is dissolved. The smaller the particles are, the more rapid the ENM can escape from the particle matrix because the surface to area ratio increases.

The preferred scenario would be to conduct any assessment directly with the released particles; be it *in vitro* or *in vivo* testing. This would allow preventing particle loses in the collection stage as well as particle changes undergone during storage periods, depending on the nature of the emitted particles. The particle deposition rate in the air-liquid interface is a relevant parameter if the present approach is considered.

3.10. Protect personnel carrying out the research

Though the present tip has been placed as the last one, it is possibly the most relevant one. In absence of conclusive data related to the (eco)toxicological potential of ENMs, even less of hybrid materials released during the life cycle of NEPs, personnel working on nano-release needs to be protected. In this sense, EC Guidelines for worker protection are recommended:

- Working Safely with Manufactured Nanomaterials – Guidance for Workers (November 2014)
- Guidance on the protection of the health and safety of workers from the potential risks related to nanomaterials at work – Guidance for employers and health and safety practitioners (June 2013)

In addition to evaluating the release and emissions associated to NEPs, such information should be made available to the public and regulatory bodies.

4. Outlook and steps to standardisation

Having established the main principles for nano-release assessment, the next step and basic consideration with standardization purposes would be to conduct **inter-laboratory assays** that would allow comparing the consistency, repeatability and accuracy of the experiments performed. This is the most immediate need to start a standardization process.

Finally, if a research study finds that the degradation (be it physical or chemical) of a ENM/polymer composite releases ENMs, ENM fragments, or ENM/matrix aggregates, an immediate question that arises is whether the released particles pose a real risk to human health or the environment. Such a question can only be answered by assessing the toxicological or ecological impact of ENMs with the exact form and concentration of the ENMs found to be released during the exposure assessment. The present approach is currently being considered in many European projects undertaking a "life cycle" approach in the conception of NEPs, however, there are a number of challenges yet to be overcome so that results obtained can be considered conclusive.

Relevant standards in the area of Nanotechnology are published by standardization committees and EU Projects addressing nanosafety (nanoREG, amongst other). Amongst other, the reader is referred to ISO/TC 229 to access the latest publications at this regard.

5. References List

(CIEL), C. F. I. E. L., ECOS & E.V., Ö.-I. 2015. Toxicity of Engineered Nanomaterials.

BELLO, D., WARDLE, B. L., ZHANG, J., YAMAMOTO, N., SANTEUFEMIO, C., HALLOCK, M. & VIRJI, M. A. 2012. Characterization of exposures to nanoscale particles and fibers during solid core drilling of hybrid carbon nanotube advanced composites. *INT J OCCUP ENVIRON HEALTH* 16.

CENA, L. G. & PETERS, T. M. 2012. Characterization and control of airborne particles emitted during production of epoxy/carbon nanotube nanocomposites. *J Occup Environ Hyg.*, 8.

DUNCAN, T. V. 2015. Release of Engineered Nanomaterials from Polymer Nanocomposites: the Effect of Matrix Degradation. *ACS Appl. Mater. Interfaces*, 7, 20-39.

ENGINEERS, S. O. P.

GOLANSKI, L., GABORIEAU, A., GUIOT, A., UZU, G., CHATENET, J. & TARDIF, F. 2011. Characterization of abrasion-induced nanoparticle release from paints into liquids and air. *J. Phys.: Conf. Ser.*, 304.

GROSO, A., PETRI-FINK, A., MAGREZ, A., RIEDIKER, M. & MEYER, T. 2010. Management of nanomaterials safety in research environment. *Particle and Fibre Toxicology*, 7.

HANSEN, S. F., LARSEN, B. H., OLSEN, S. I. & BAUN., A. 2007. Categorization framework to aid hazard identification of nanomaterials. *Nanotoxicology*, 1-8.

KOPONEN, I. K., JENSEN, K. A. & SCHNEIDER, T. 2009. Sanding dust from nanoparticle-containing paints: physical characterisation. *In:* KENNY, L. (ed.) *Inhaled Particles X.*

KUHLBUSCH, T. A. J., ASBACH, C., FISSAN, H., GOHLER, D. & STINTZ, M. 2011. Nanoparticle exposure at nanotechnology workplaces: A review. *Particle and Fibre Toxicology*, 8.

LIOY, P. J., WAINMAN, T., ZHANG, J. F. & GOLDSMITH, S. 1999. Typical household vacuum cleaners: The collection efficiency and emissions characteristics for fine particles. *Journal of the Air & Waste Management Association*, 49, 200-206.

NOWACK, B., RANVILLE, J., DIAMOND, S., GALLEGO-URREA, J., METCALFE, C., ROSE, J., HORNE, N., KOELMANS, A. & KLAINE, S. 2012. Potential scenarios for nanomaterial release and subsequent alteration in the environment. *Environ Toxicol Chem. 2012 Jan;31(1):50-9. doi:* , 31, 50-9.

S. FOSS HANSEN, B.H. LARSEN, S.I. OLSEN, A. BAUN. (2007) Categorization framework to aid hazard identification of nanomaterials. Nanotoxicology, 2007, 1-8.

SHANDILYA, N., BIHAN, O. L., BRESSOT, C. & MORGENEYER, M. 2015. Emission of Titanium Dioxide Nanoparticles from Building Materials to the Environment by Wear and Weather. *Environ. Sci. Technol.* , 49, 2163–2170

SZYMCZAK, W., MENZEL, N. & KECK, L. 2007. Emission of ultrafine copper particles by universal motors controlled by phase angle modulation. *Journal of Aerosol Science*, 38, 520-531.

VAN BROEKHUIZEN, P., VAN BROEKHUIZEN, F., CORNELISSEN, R. & REIJNDERS, L. 2011. Use of nanomaterials in the European construction industry and some occupational health aspects thereof. *Journal of Nanoparticle Research*, 13, 447-462.

WHO 1999. Hazard prevention and control in the work environment: Airborne dust.

WIESNER, M. R., LOWRY, G. V., JONES, K. L., MICHAEL F. HOCHELLA, J., GIULIO, R. T. D., CASMAN, E. & BERNHARDT, E. S. 2009. Decreasing Uncertainties in Assessing Environmental Exposure, Risk, and Ecological Implications of Nanomaterials. *Environ. Sci. Technol.*, 43, 6458–6462.

WINDLER, L., LORENZ, C., GOETZ, N. V., HUNGERBUHLER, K., AMBERG, M., HEUBERGER, M. & NOWACK, B. 2012. Release of Titanium Dioxide from Textiles during Washing. *Environ. Sci. Technol.*, 46, 8181-8188.

WOHLLEBEN, W., BRILL, S., MEIER, M. W., MERTLER, M., COX, G., HIRTH, S., VON VACANO, B., STRAUSS, V., TREUMANN, S., WIENCH, K., MA-HOCK, L. & LANDSIEDEL, R. 2011. On the Lifecycle of Nanocomposites: Comparing Released Fragments and their In-Vivo Hazards from Three Release Mechanisms and Four Nanocomposites. *Small*, 7, 2384-2395.

WOHLLEBEN, W., MEIER, M. W., VOGEL, S., LANDSIEDEL, R., COX, G., HIRTH, S. & TOMOVIC, Z. 2013. Elastic CNT-polyurethane nanocomposite: synthesis, performance and assessment of fragments released during use. *Nanoscale*, 5, 369-380.

WOHLLEBEN, W., VILAR, G., FERNÁNDEZ-ROSAS, E., GONZÁLEZ-GÁLVEZ, D., GABRIEL, C., HIRTH, S., FRECHEN, T., STANLEY, D., GORHAM, J., SUNG, L.-P., HSUEH, H.-C., CHUANG, Y.-F., NGUYEN, T. & VAZQUEZ-CAMPOS, S. 2014. A pilot interlaboratory comparison of protocols that simulate aging of nanocomposites and detect released fragments. *Environ. Chem.*

WORK, W. J., HORIE, K., HESS, M. & STEPTO, R. F. T. 2004. Definition of terms related to polymer blends, composites, and multiphase polymeric materials (IUPAC Recommendations 2004). *Pure Appl. Chem*, 76, 1985-2007.

Appendix C –

Further Automated Drilling Methodology Development

Whilst the methodology developed undergoes further studies and investigations, this project has also worked towards the improvement of the method. Although the methodology is designed for drilling on nanocomposite materials, one identified improvement on the chamber it to be adaptable for use of other mechanical processes. In order to make the methodology more adaptable, a simplification to the chamber would be needed to allow for more mechanical processes on the materials. A solution to this would be to minimise the size of the chamber and rearrange the mechanical process external to the chamber.

The side of the chamber could then be modified for the necessary machining tools, sealing the mechanical tool away from the measurement of the nanoparticles released from the samples. This could allow for more mechanical process such as grinding, sanding, cutting and milling on the materials. A prototype design is displayed in Figure 137.

a.)

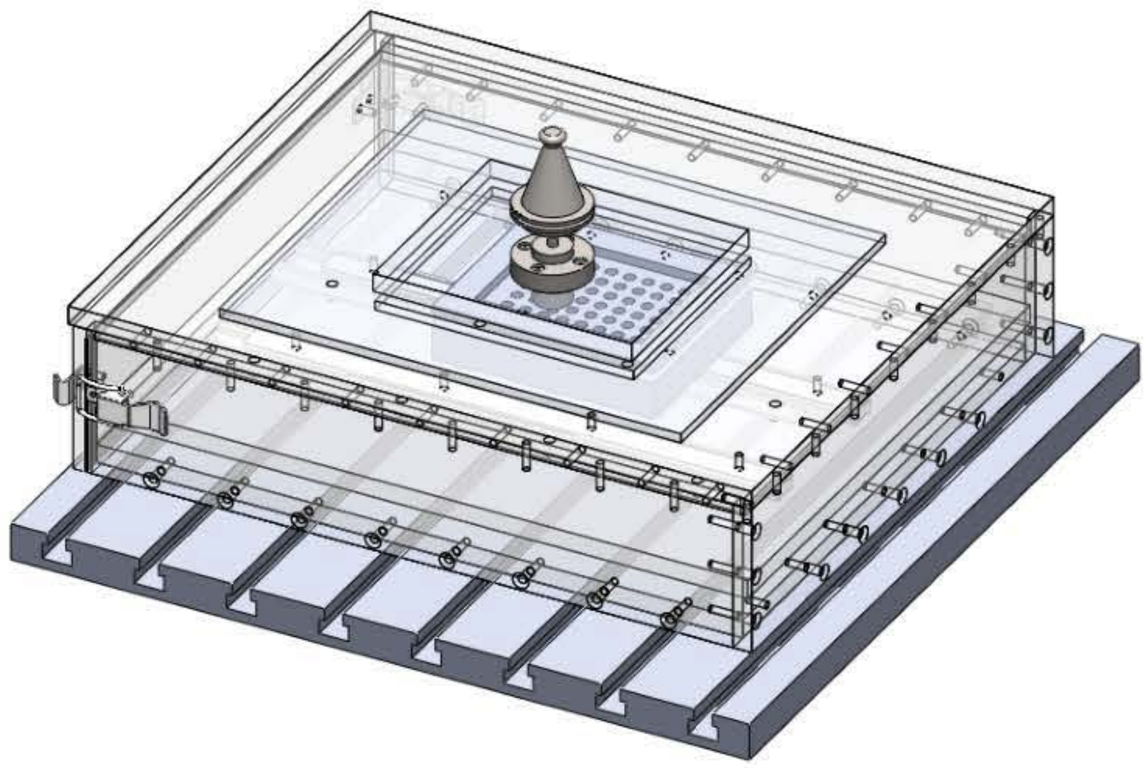

b.)

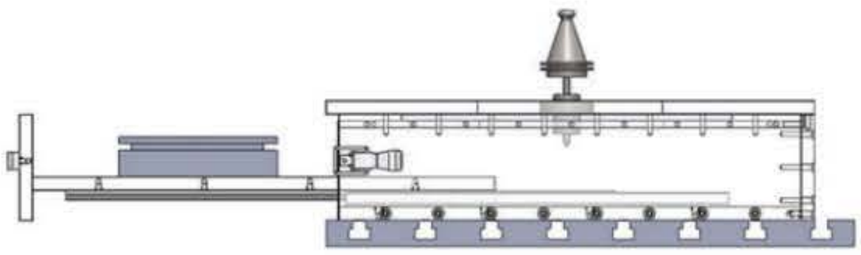

c.)

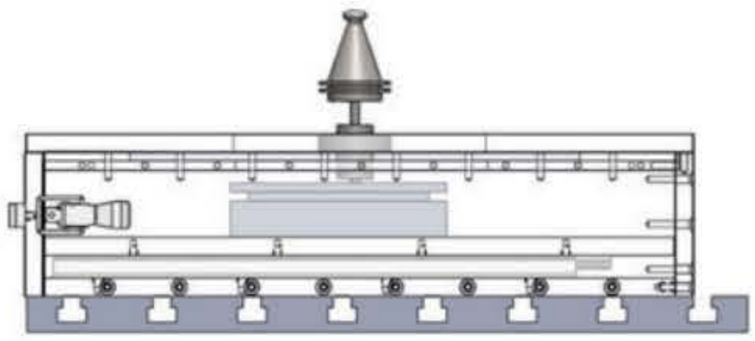

Figure 137*:* Prototype of modified chamber design for automated drilling from a.) isometric view, b.) side view of open draw and c.) side view of closed draw.

The mechanical drill, or alternative mechanical process would be placed external to the chamber, with only the drill bit end positioned through the top panel of the chamber, sealed through a wiper seal. This design is yet to be tested, and is still within the development stages, but allows for the adaptation to multiple mechanical processes. The side draw would open as demonstrated in Figure 137, to input the material to be tested. The inlet and out air flow to clean the chamber are not included within the sketch, as well as the probe to the nanoparticle quantification equipment and sampling collection.

The prototype is a modification of the tested design developed within this thesis. The test method developed within this thesis has been demonstrated for the assessment of nanoparticle release during drilling on nanocomposite materials. This has achieved the objective to design a controllable and repeatable test methodology for the nanoparticle release assessment from drilling.

Appendix D –

Stress vs Strain Graphs of Tensile and Flexural Results for EP-based, PE-based and PP-based samples.

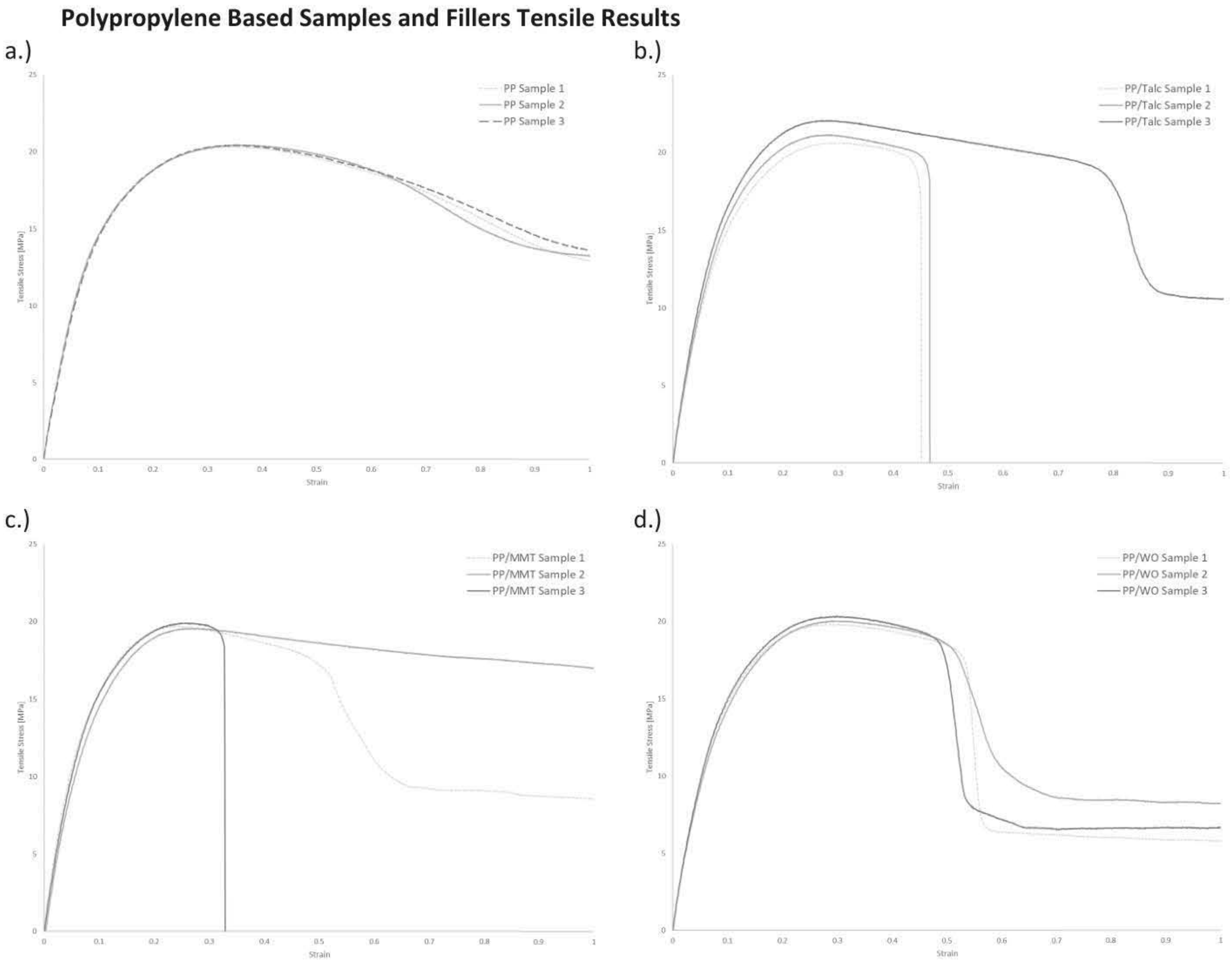

Figure 138: Stress vs strain curves from tensile tests on a.) PP samples b.) PP/Talc samples c.) PP/MMT samples and d.) PP/WO samples.

Polypropylene Based Samples and Fillers Flexural Results

a.)

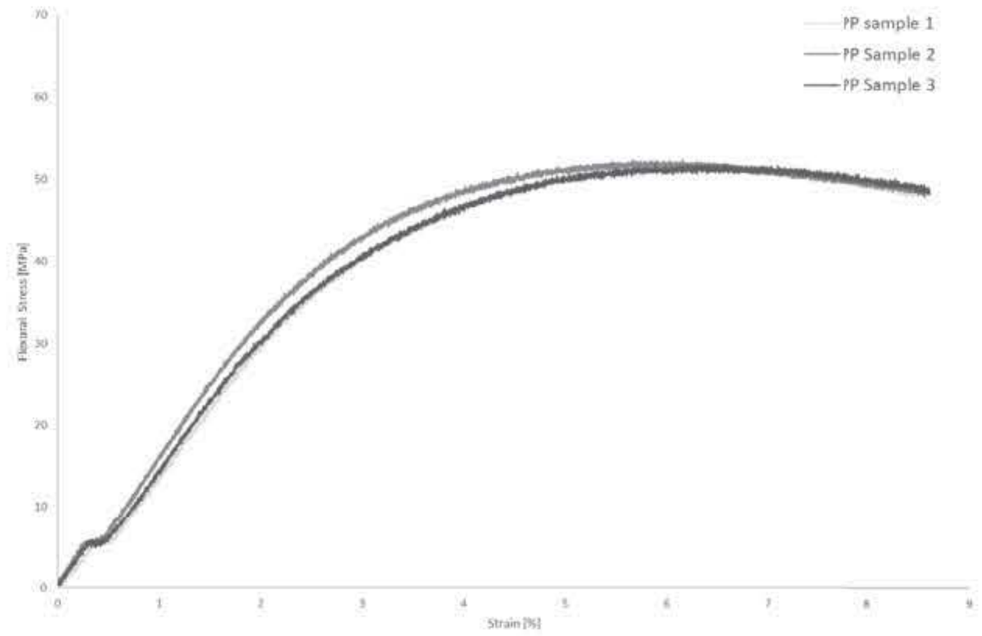

b.)

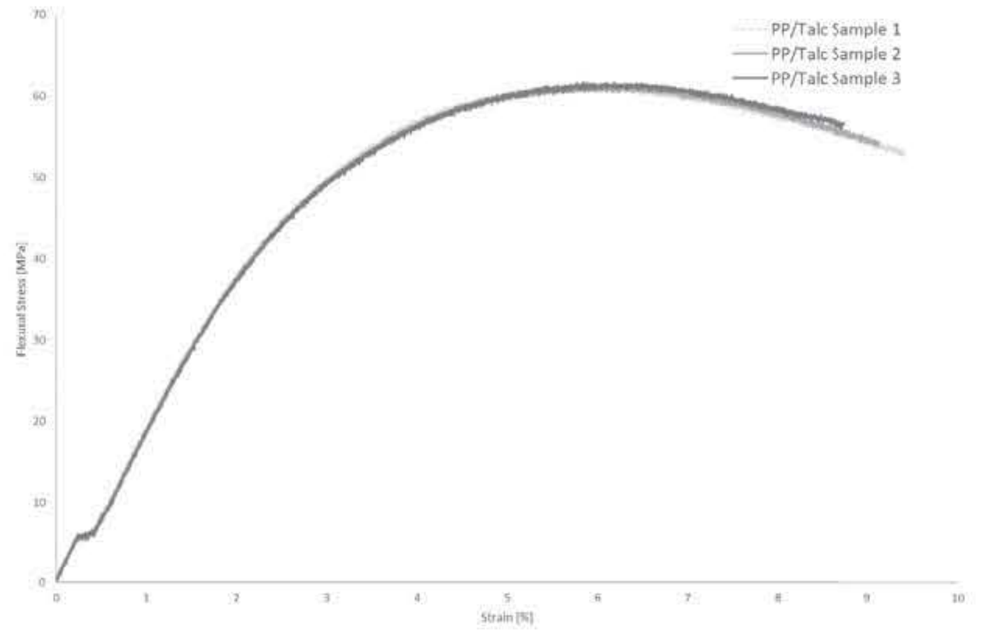

c.)

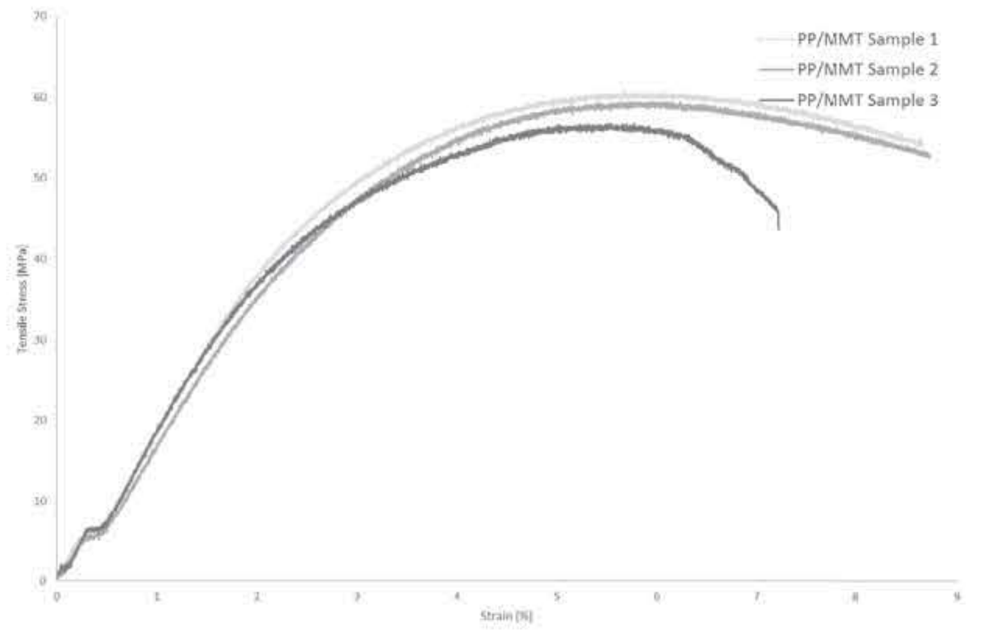

d.)

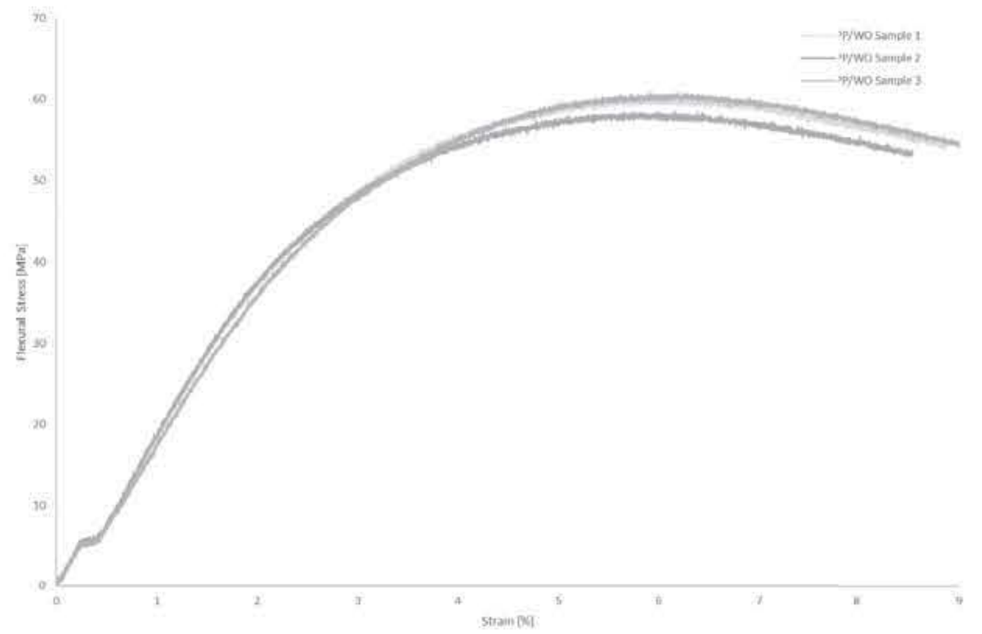

Figure 139: Stress vs strain curves from flexural tests on a.) PP samples b.) PP/Talc samples c.) PP/MMT samples and d.) PP/WO samples.

Polyester Based Samples and Fillers Tensile Results

a.)

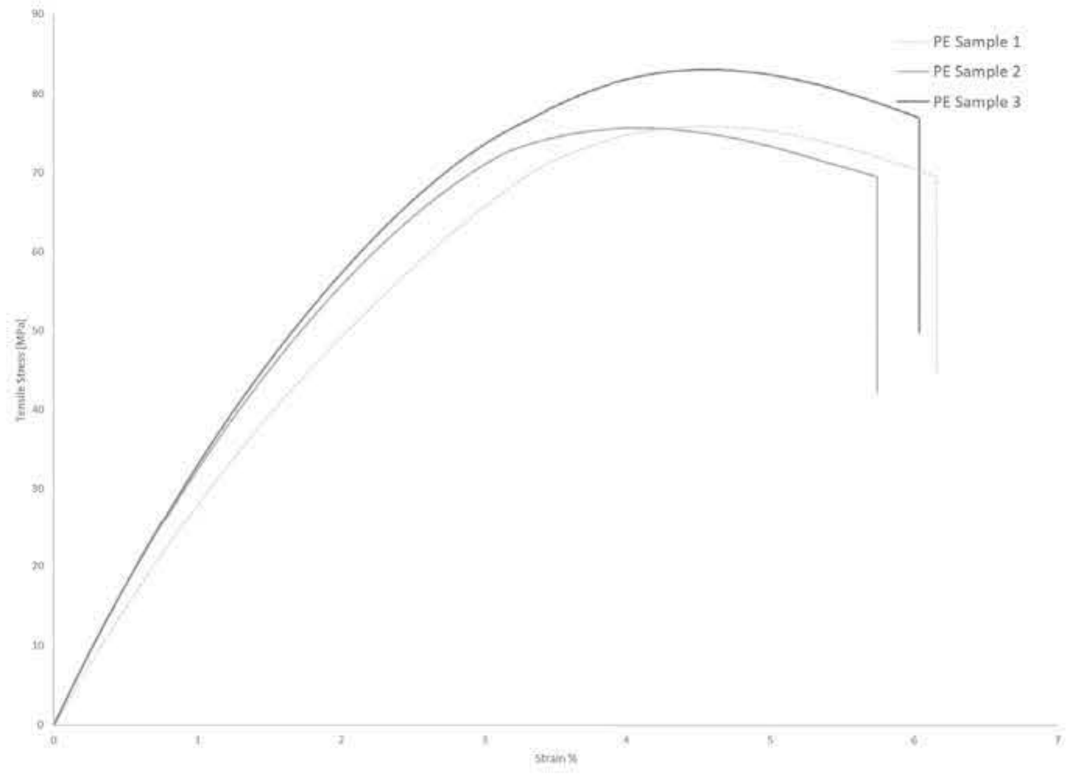

b.)

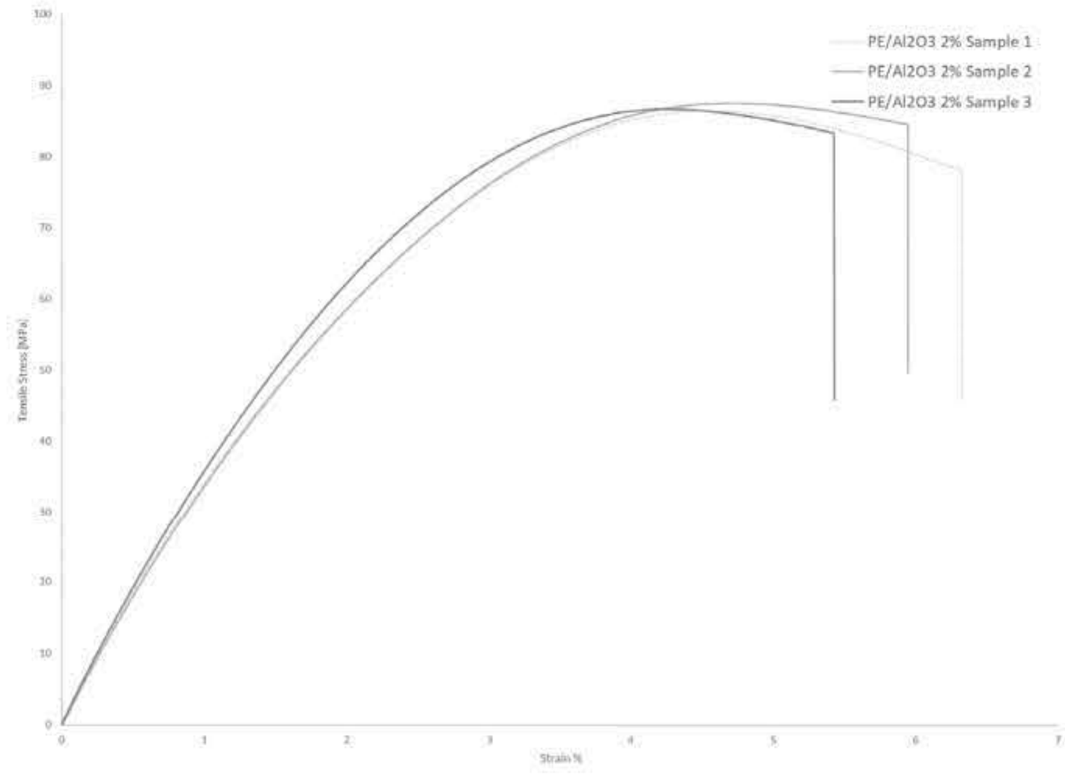

c.)

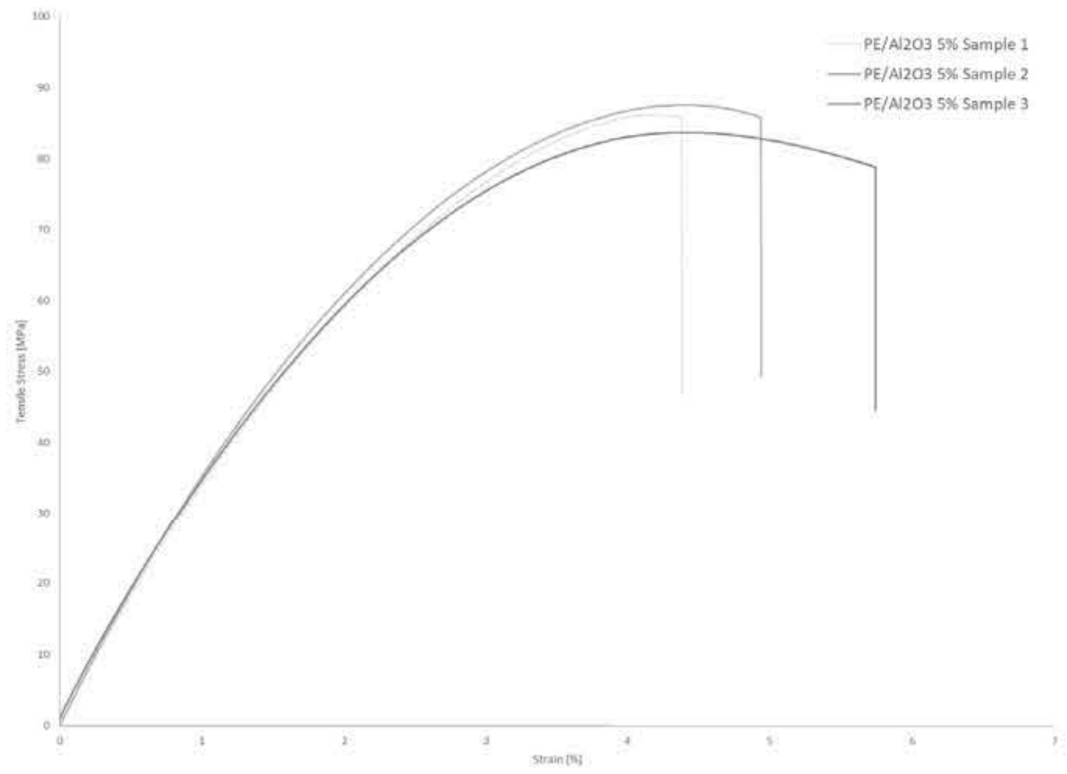

d.)

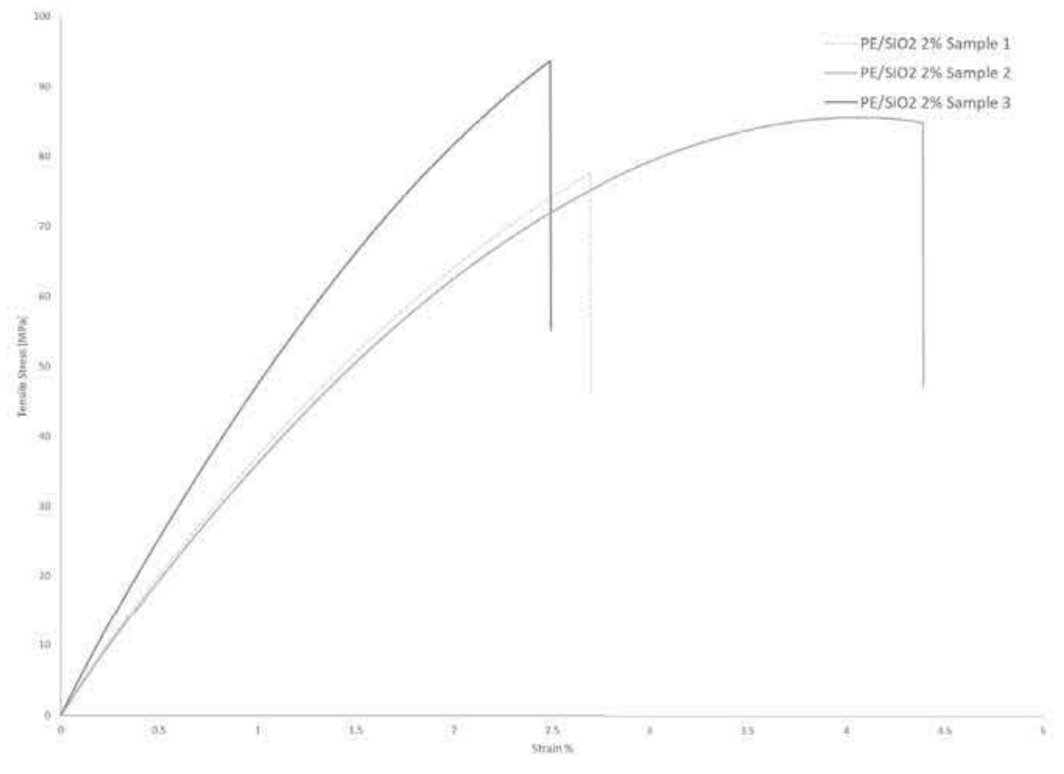

e.)

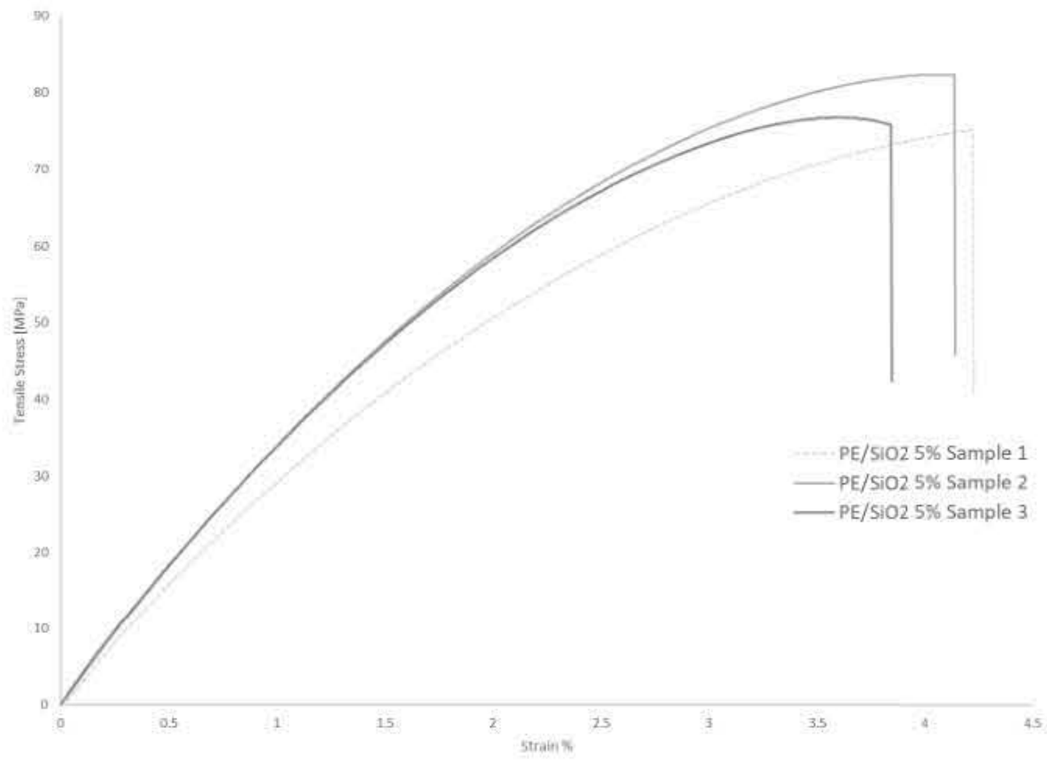

Figure 140: Stress vs strain curves from tensile tests on a.) PE samples b.) PE/Al_2O_3 2% samples c.) PE/Al_2O_3 5% samples d.) PE/SiO_2 2% samples and e.) PE/SiO_2 5% samples

Polyester Based Samples and Fillers Flexural Results

a.)

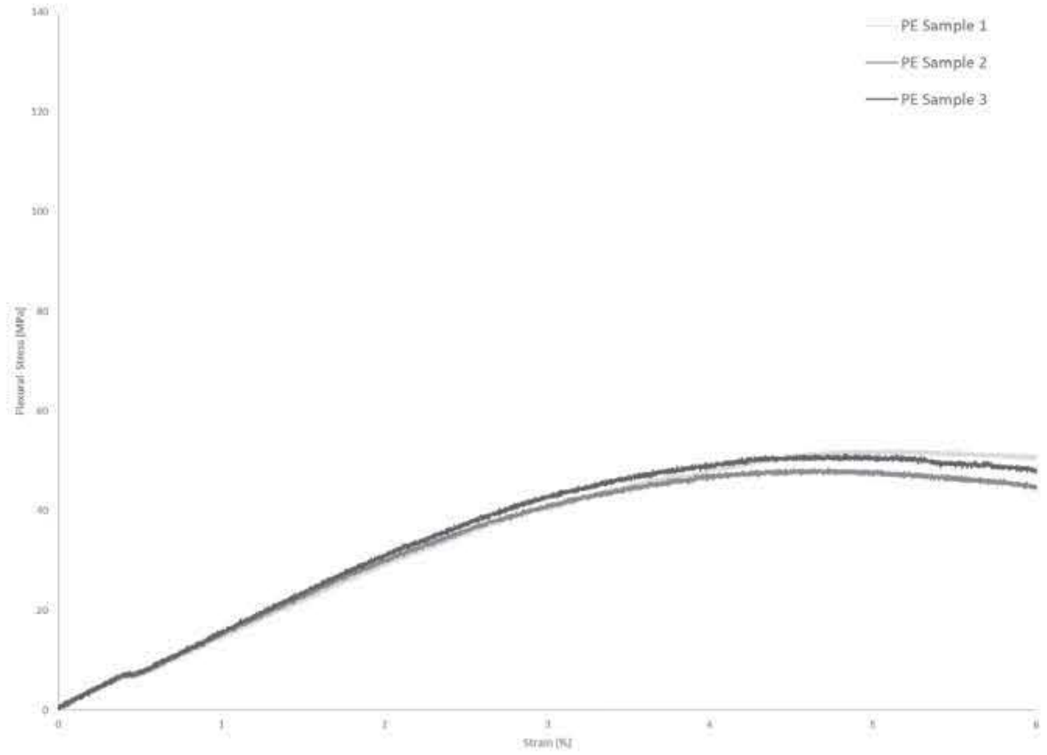

b.)

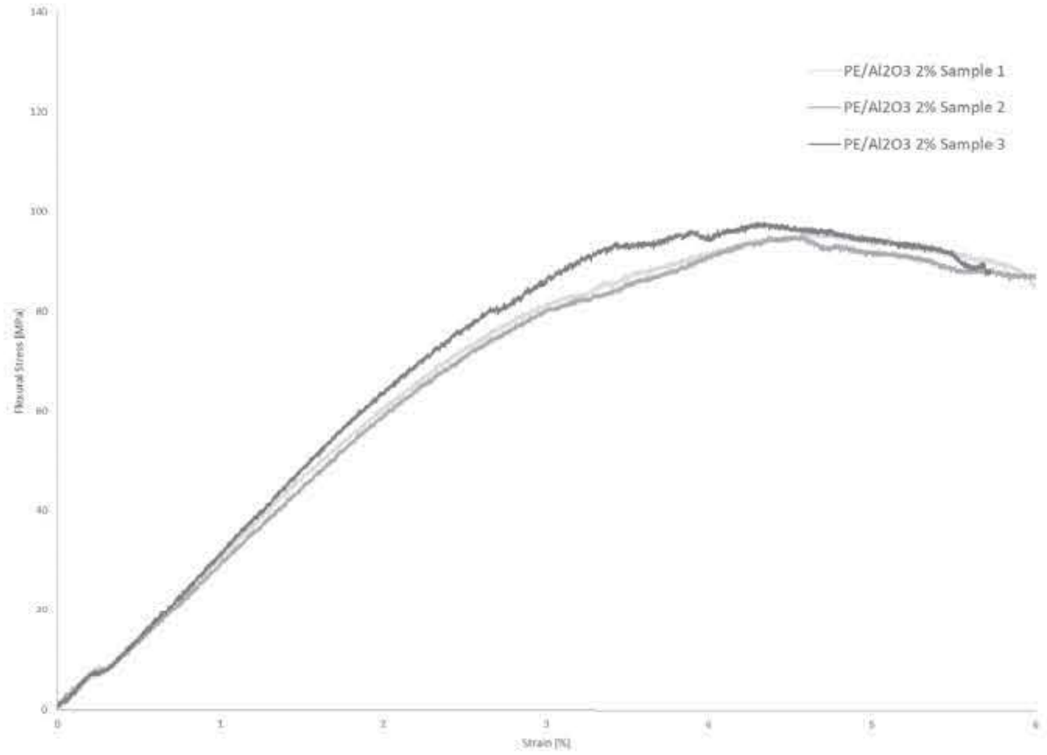

c.)

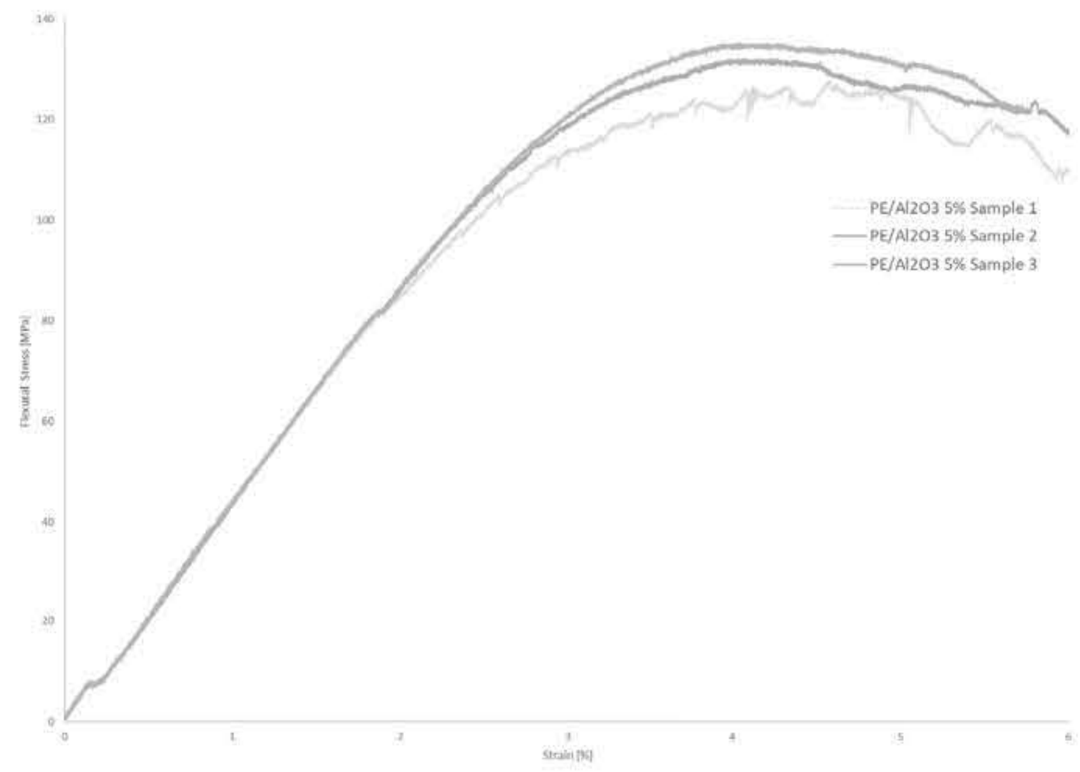

d.)

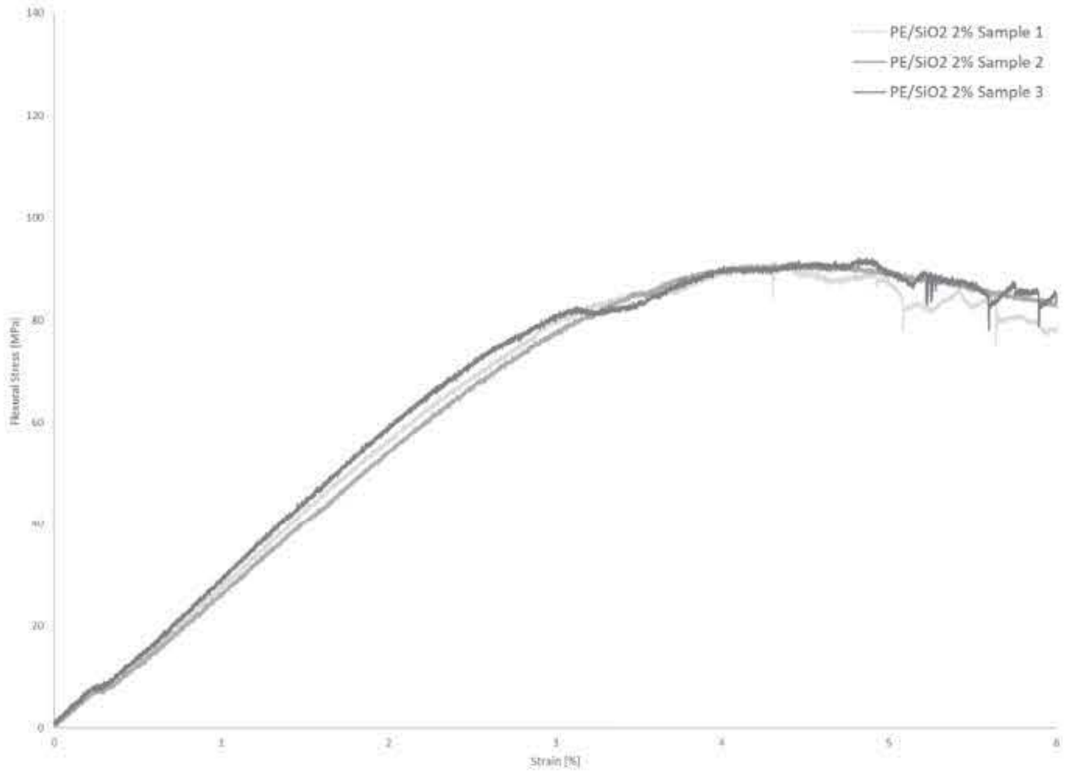

e.)

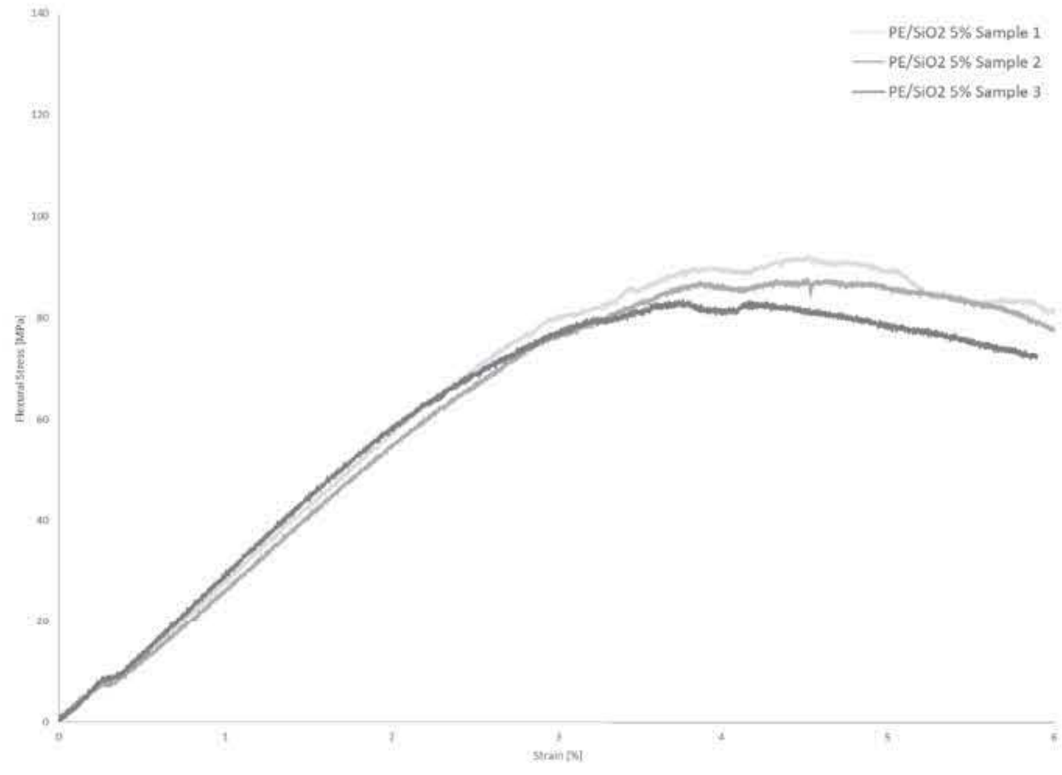

Figure 141: Stress vs strain curves from flexural 3-point bend tests on a.) PE samples b.) PE/Al_2O_3 2% samples c.) PE/Al_2O_3 5% samples d.) PE/SiO_2 2% samples and e.) PE/SiO_2 5% samples

Epoxy reinforced with CNF Fillers Tensile Results

a.)

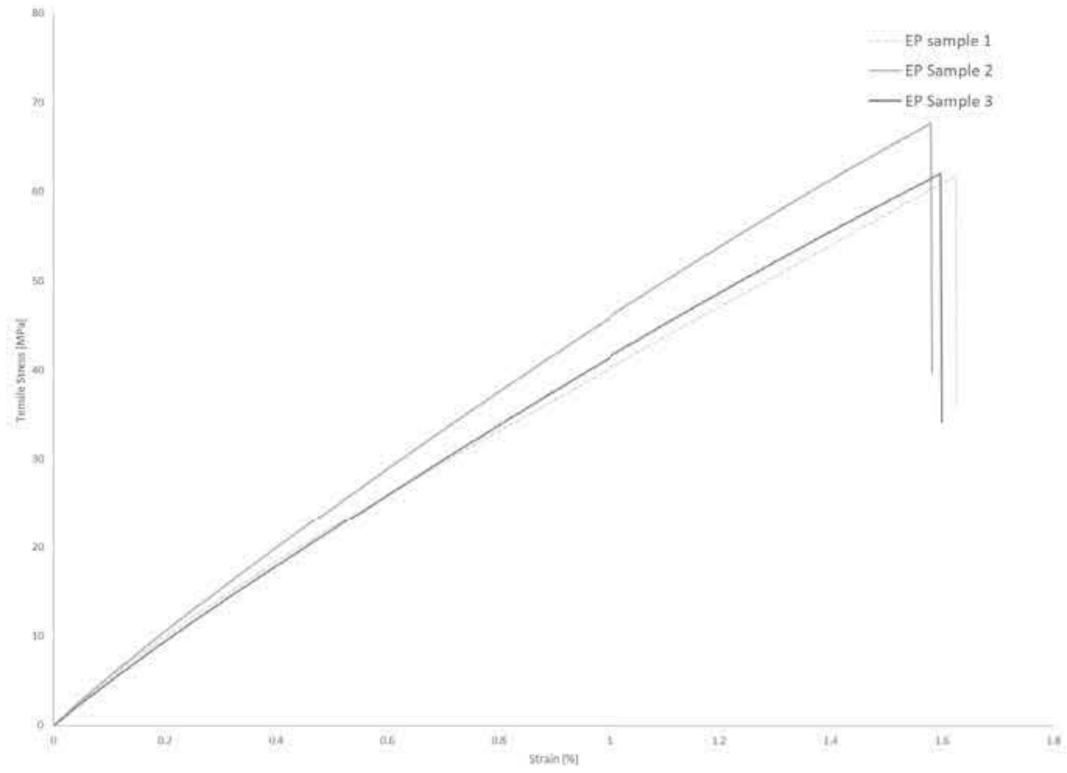

b.)

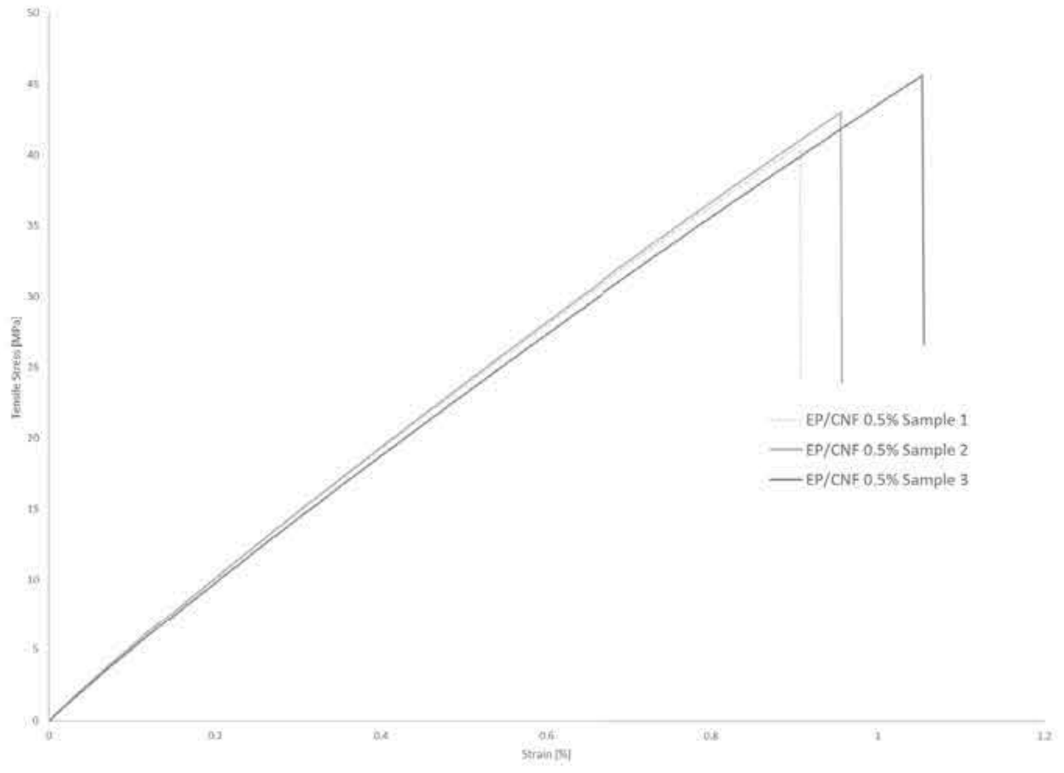

c.)

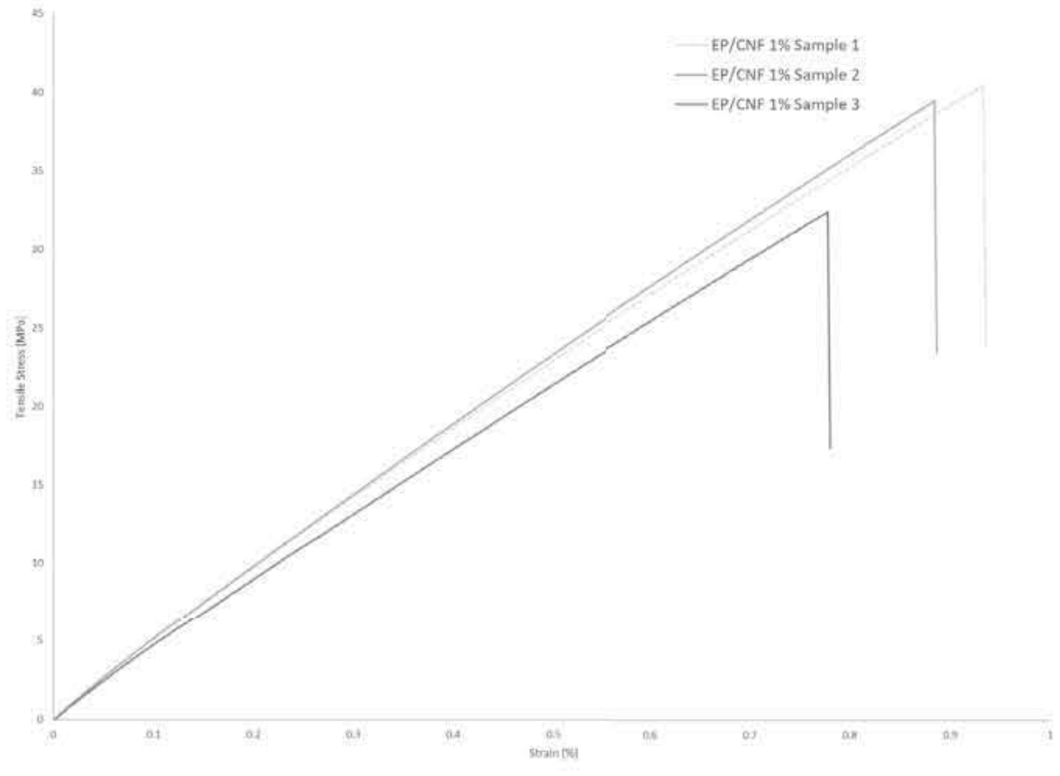

d.)

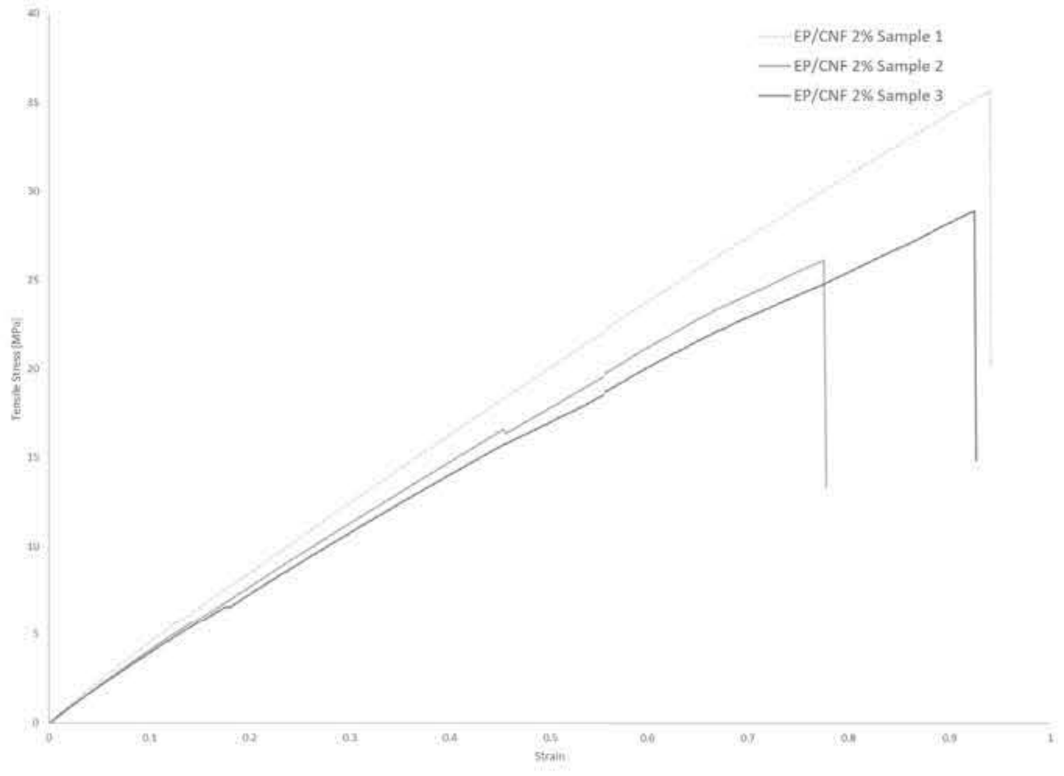

Figure 142: Stress vs strain curves from tensile tests on a.) EP samples b.) EP/CNF 0.5 % samples c.) EP/CNF 1 % samples and d.) EP/CNF 2 % samples.

Epoxy reinforced with CNF Fillers Flexural Results

a.)

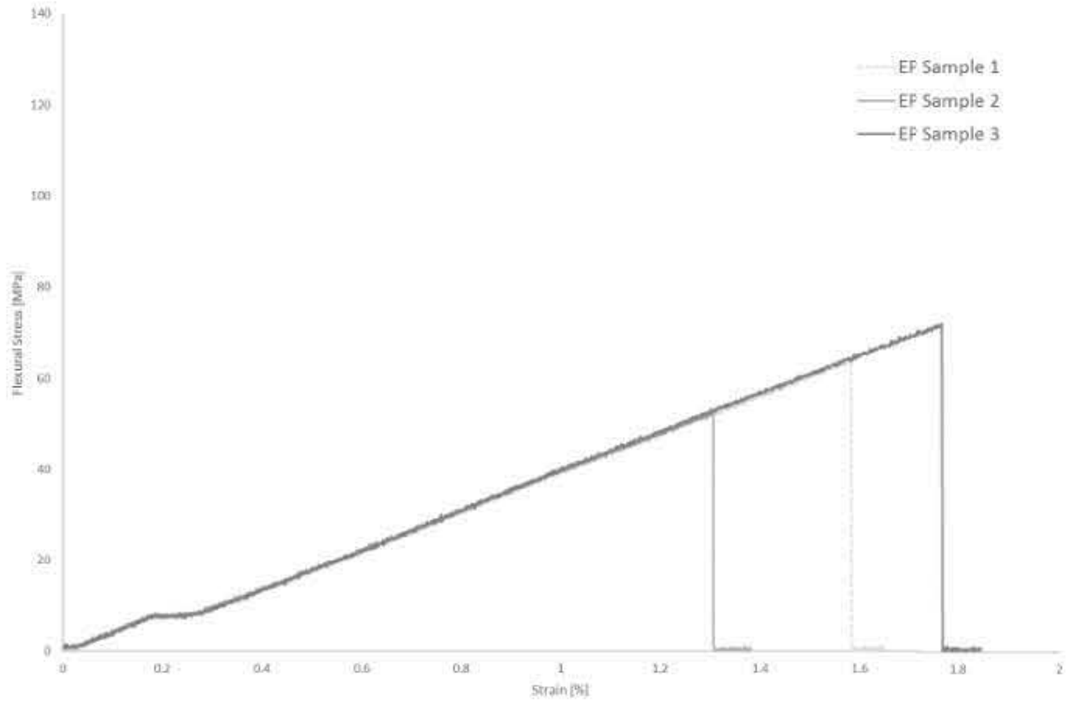

b.)

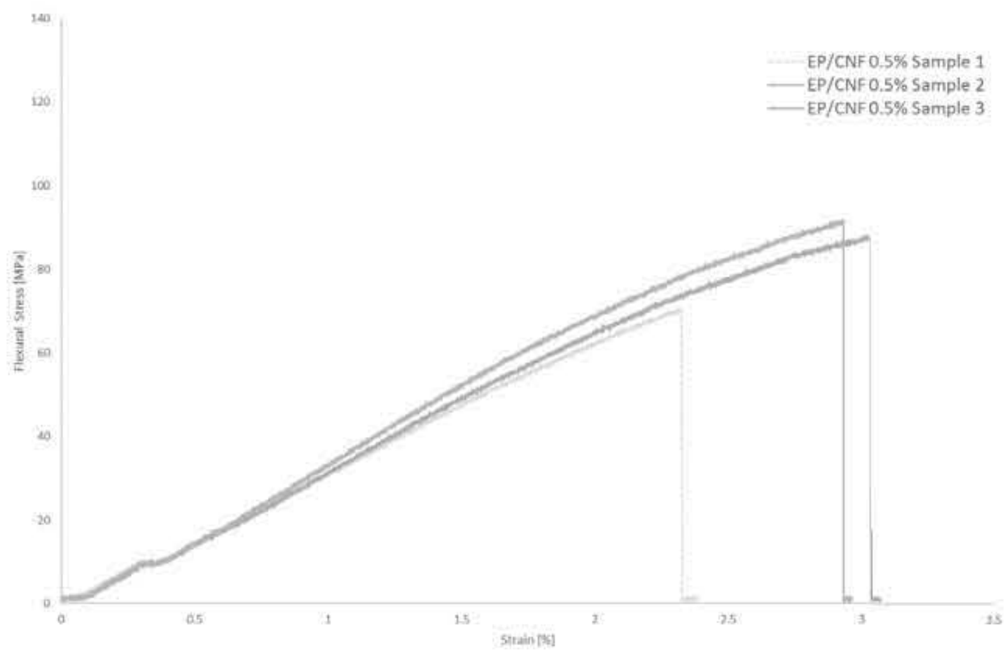

c.)

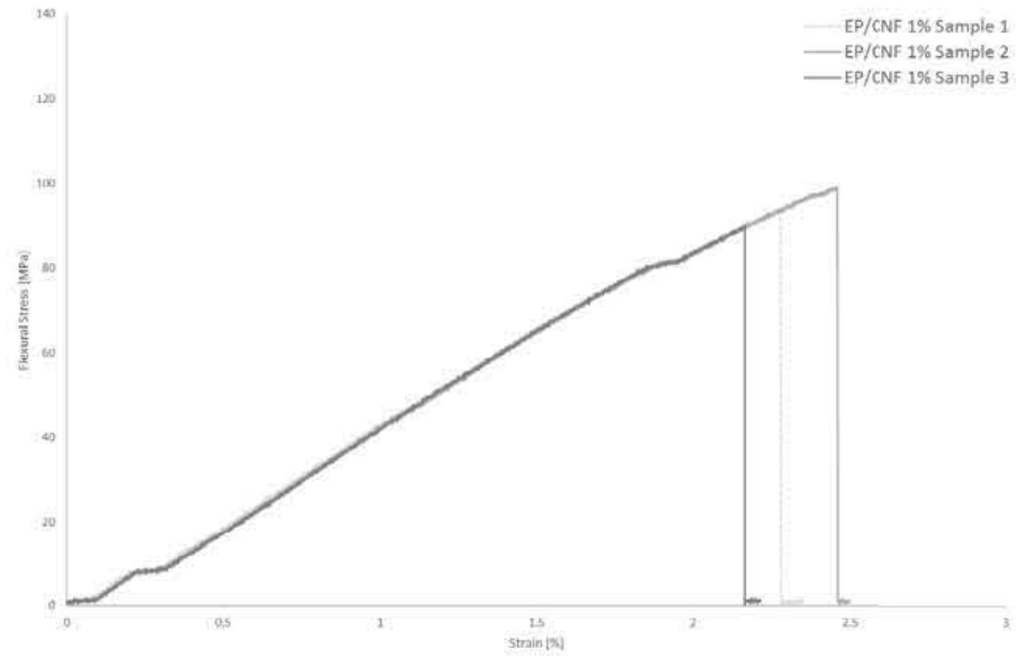

d.)

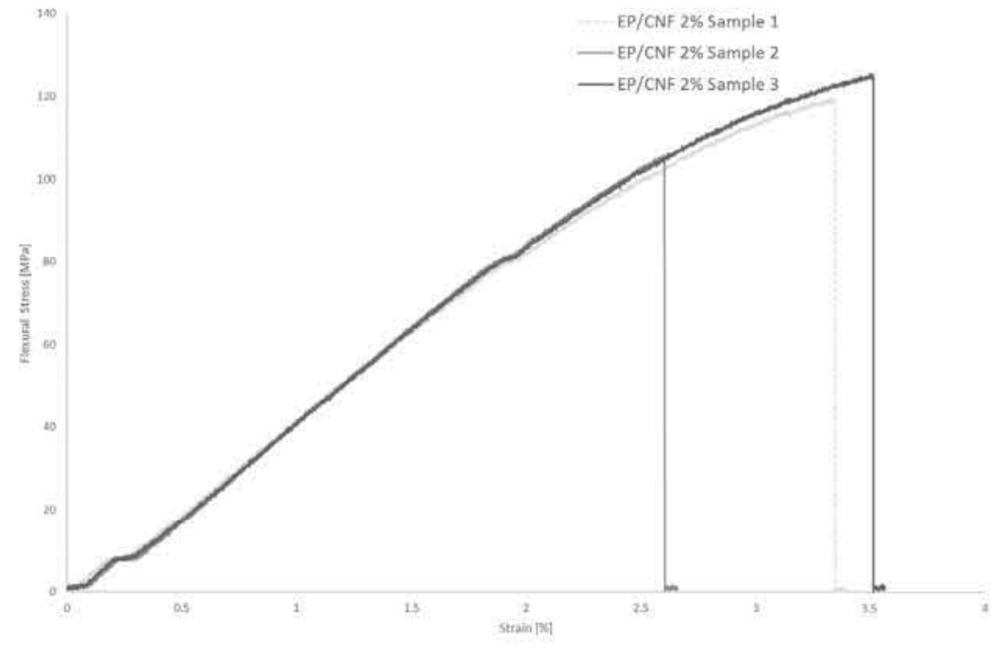

Figure 143: Stress vs strain curves from flexural 3-point bend tests on a.) EP samples b.) EP/CNF 0.5 % samples c.) EP/CNF 1 % samples and d.) EP/CNF 2 % samples.

Epoxy reinforced with CNT Fillers Tensile Results

a.)

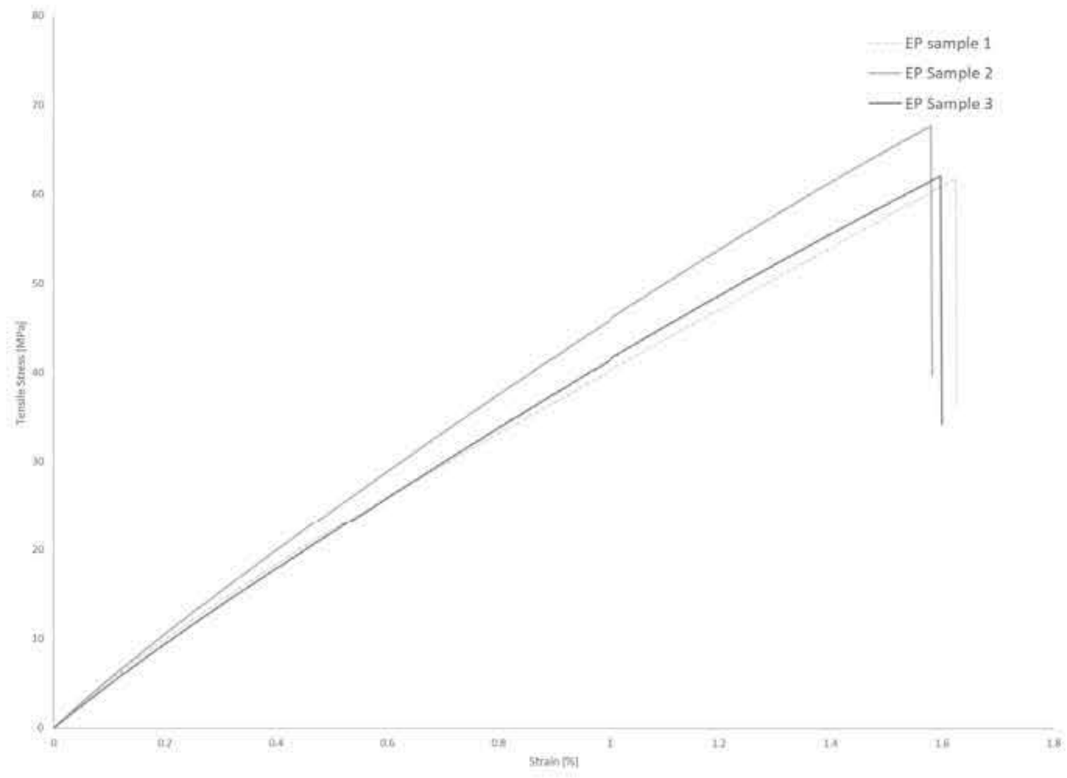

b.)

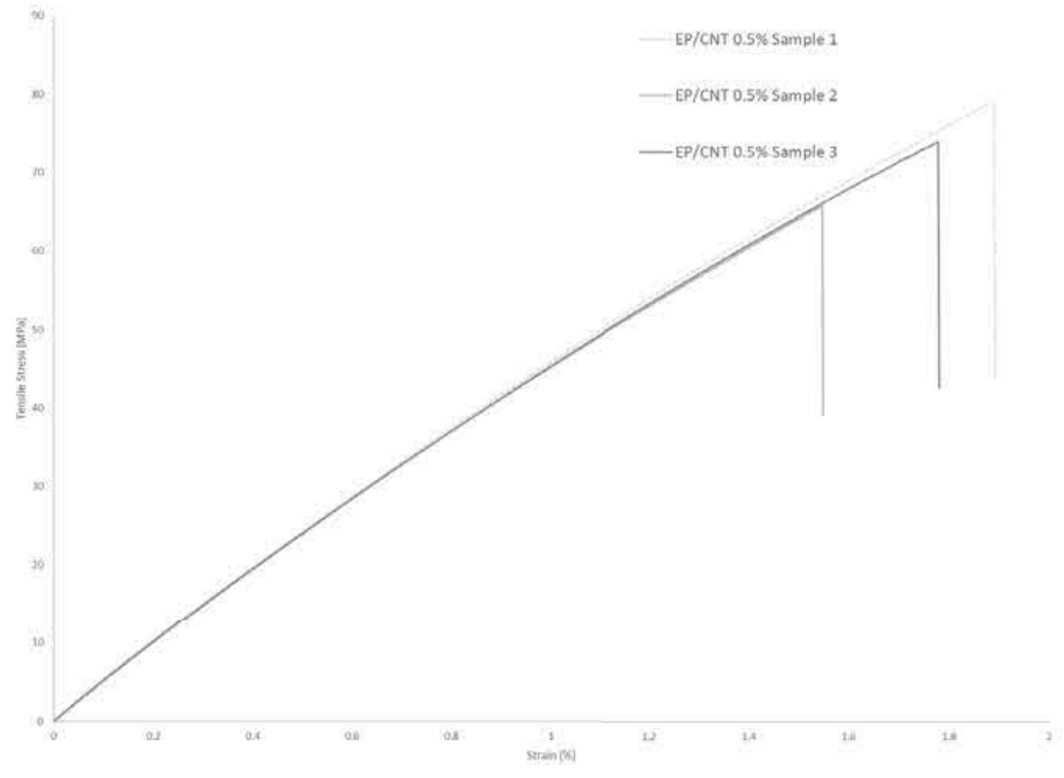

c.)

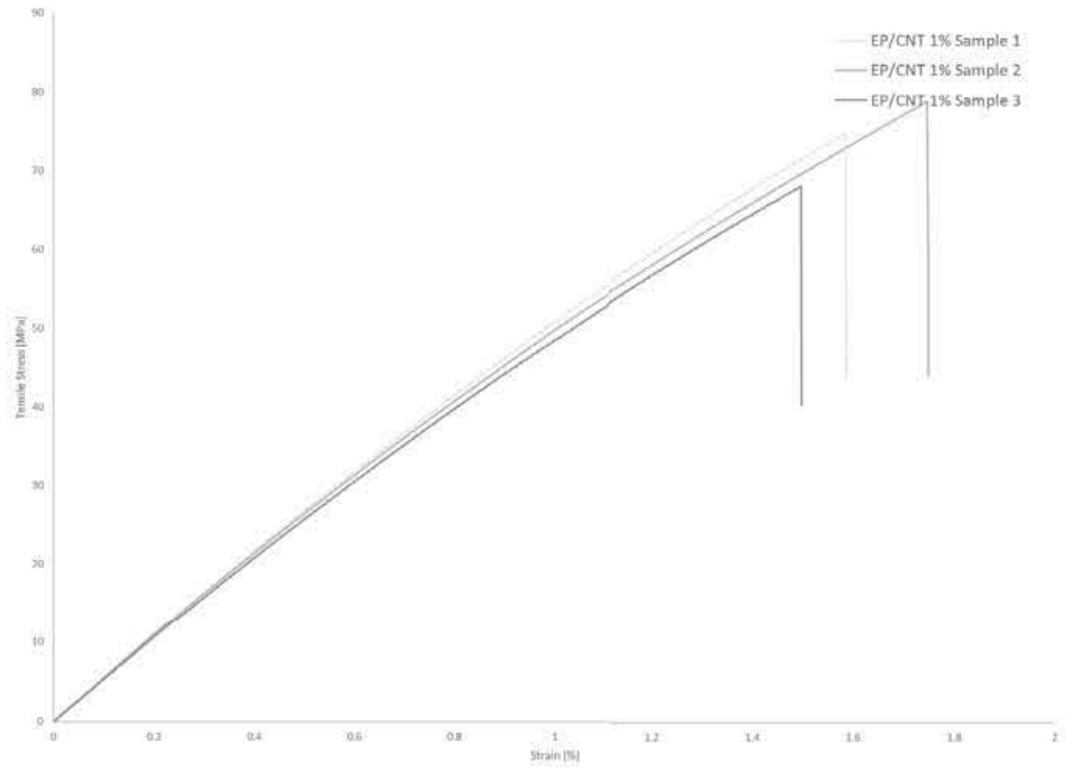

d.)

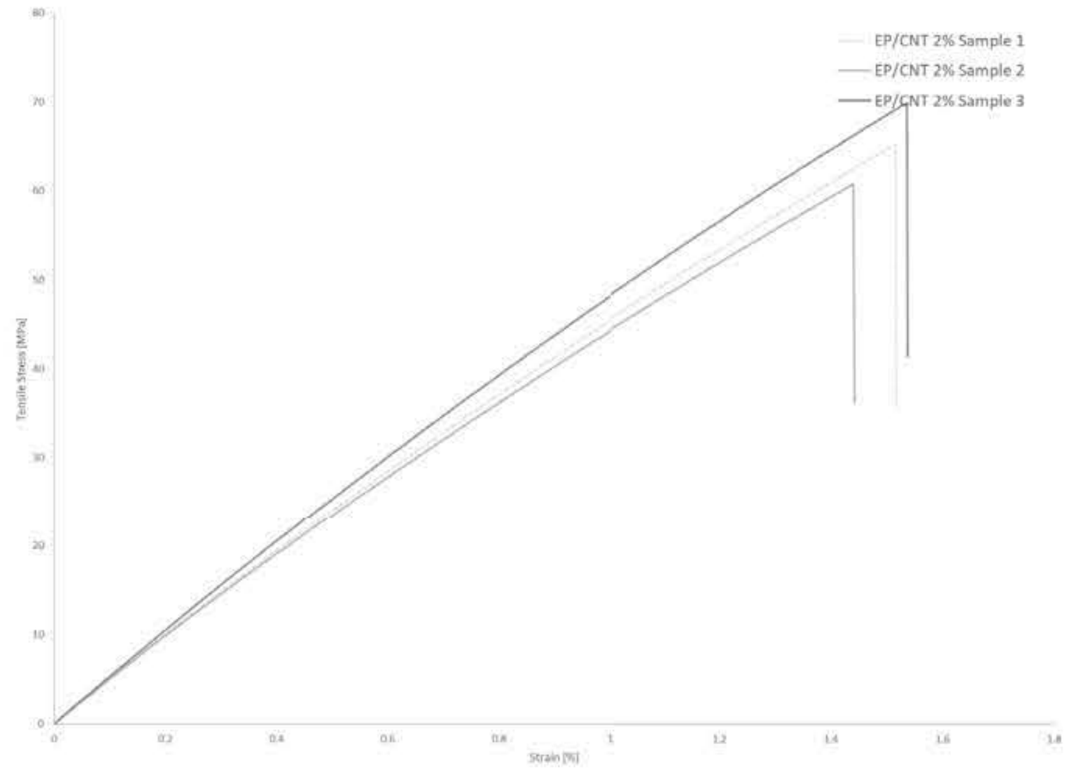

Figure 144: Stress vs strain curves from tensile tests on a.) EP samples b.) EP/CNT 0.5 % samples c.) EP/CNT 1 % samples and d.) EP/CNT 2 % samples.

Epoxy reinforced with CNT Fillers Flexural Results

a.)

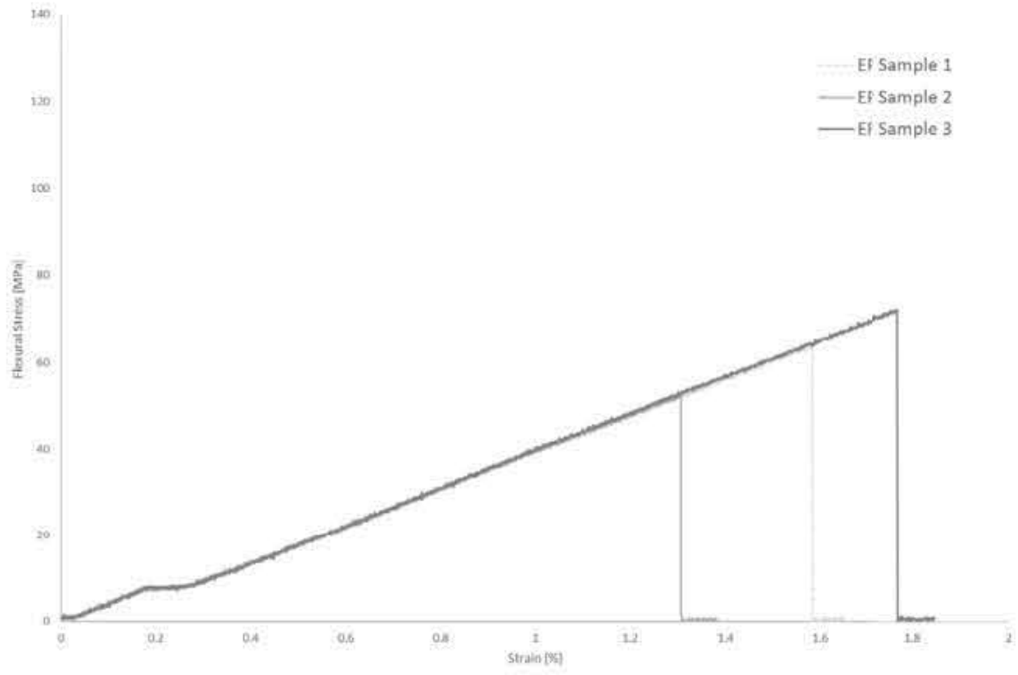

b.)

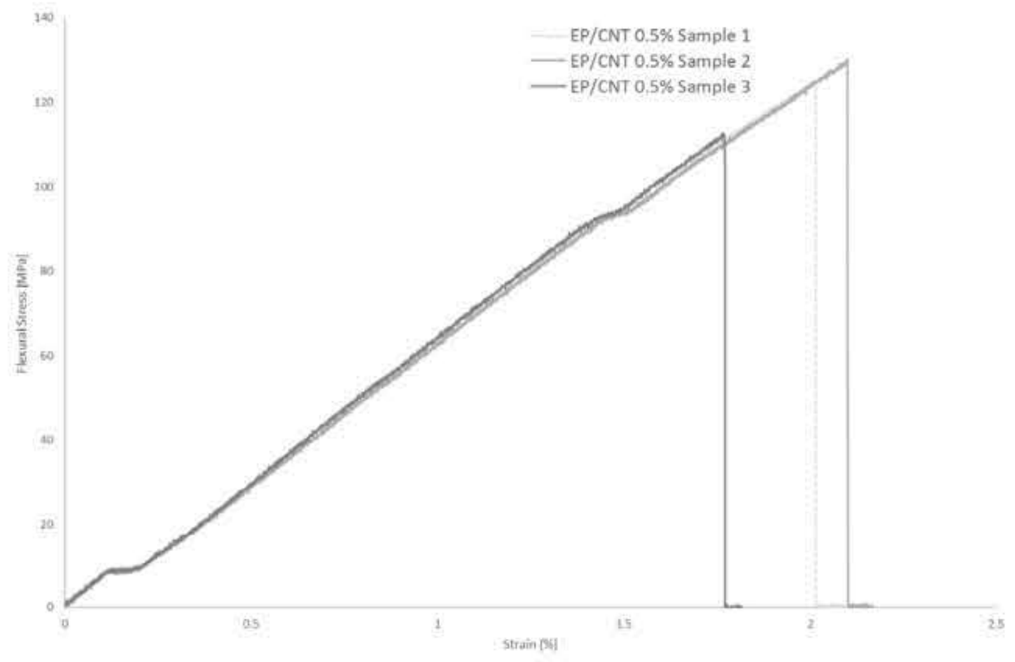

c.)

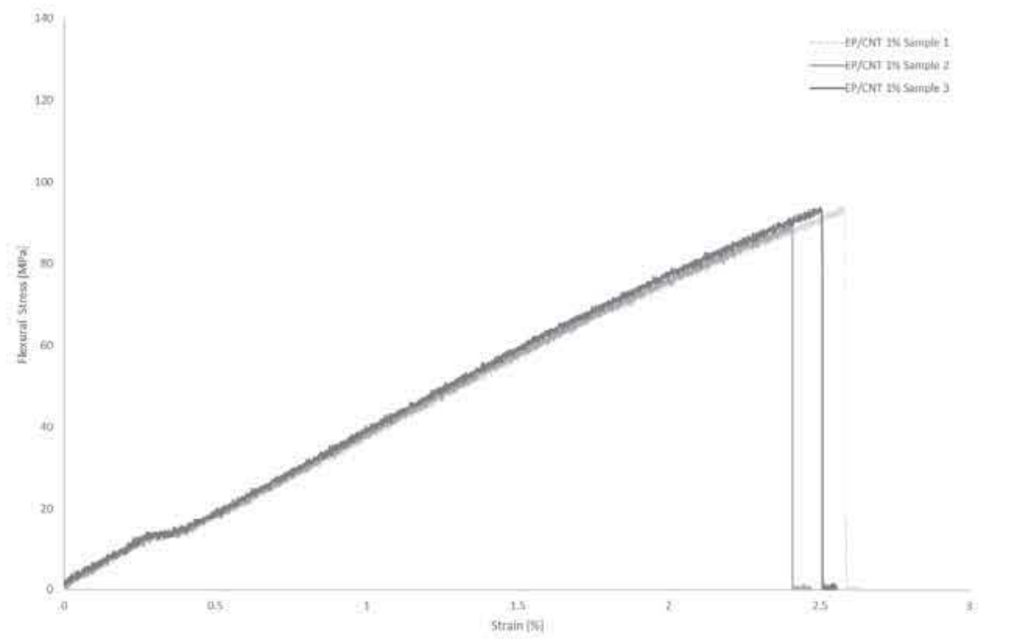

d.)

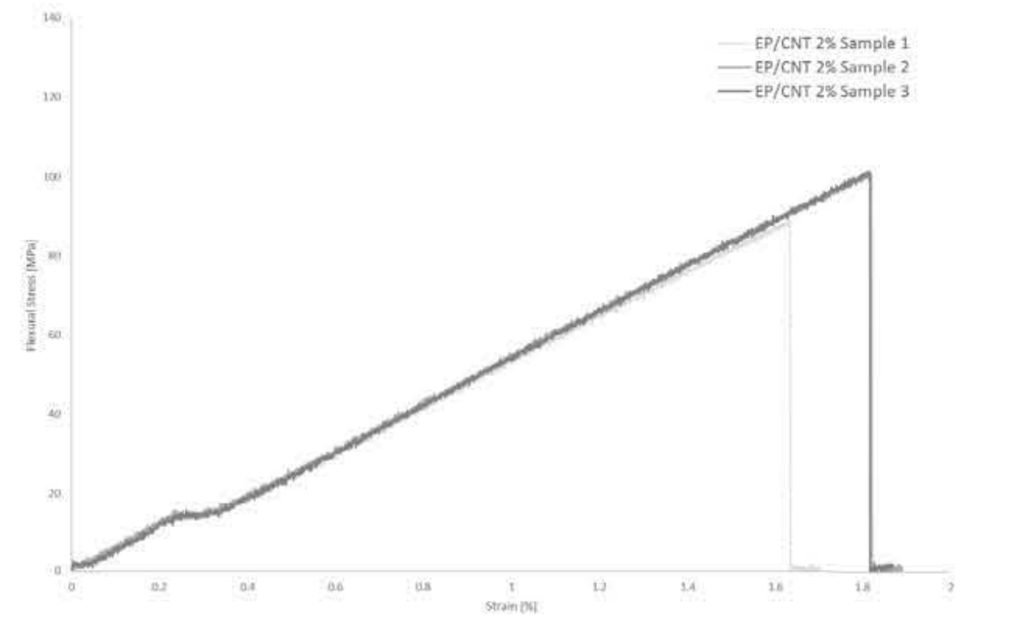

Figure 145: Stress vs strain curves from flexural 3-point bend tests on a.) EP samples b.) EP/CNT 0.5 % samples c.) EP/CNT 1 % samples and d.) EP/CNT 2 % samples.

In addition to the mechanical performance, some of the EP-based samples underwent a surface electrical conductivity test (taken place at Tecnalia) to demonstrate the influence of the CNFs and CNTs. The materials were tested in accordance the standard DC resistance or conductance testing of moderately conductive materials to complement the references on enhanced properties achieved with the use of CNTs and CNFs in surface and volume conductivity. The results are illustrated in Figure 146.

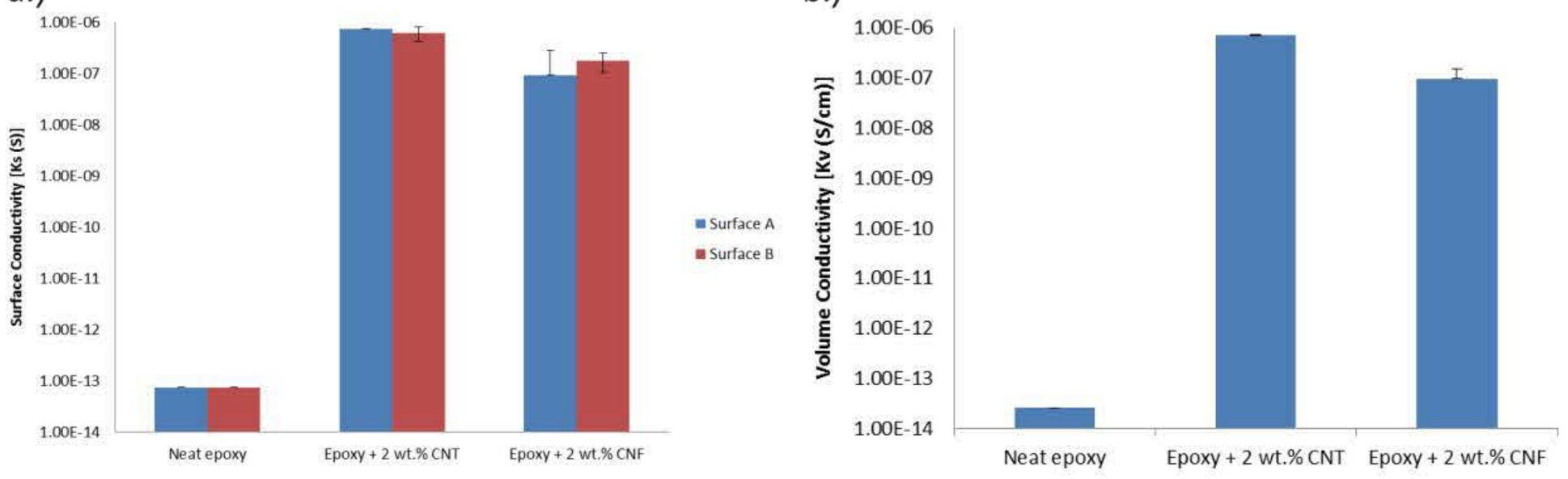

Figure 146: Measurements of EP/CNT and EP/CNF compared to neat EP sample of a.) Surface conductivity and b.) volume conductivity.

With the chosen 2 wt. % of both carbon nanofillers, the surface and volume conductivity of the nanocomposite material significantly improved by up to a factor of 8. A comparable magnitude of improvement is in literature with the same matrix-filler combination (*Bal, 2010; Ladani et al., 2015*). The same weight concentration reported the CNTs with a superior performance than the CNFs.

Epoxy/Carbon Fibre reinforced with GO Fillers Tensile Results

a.)

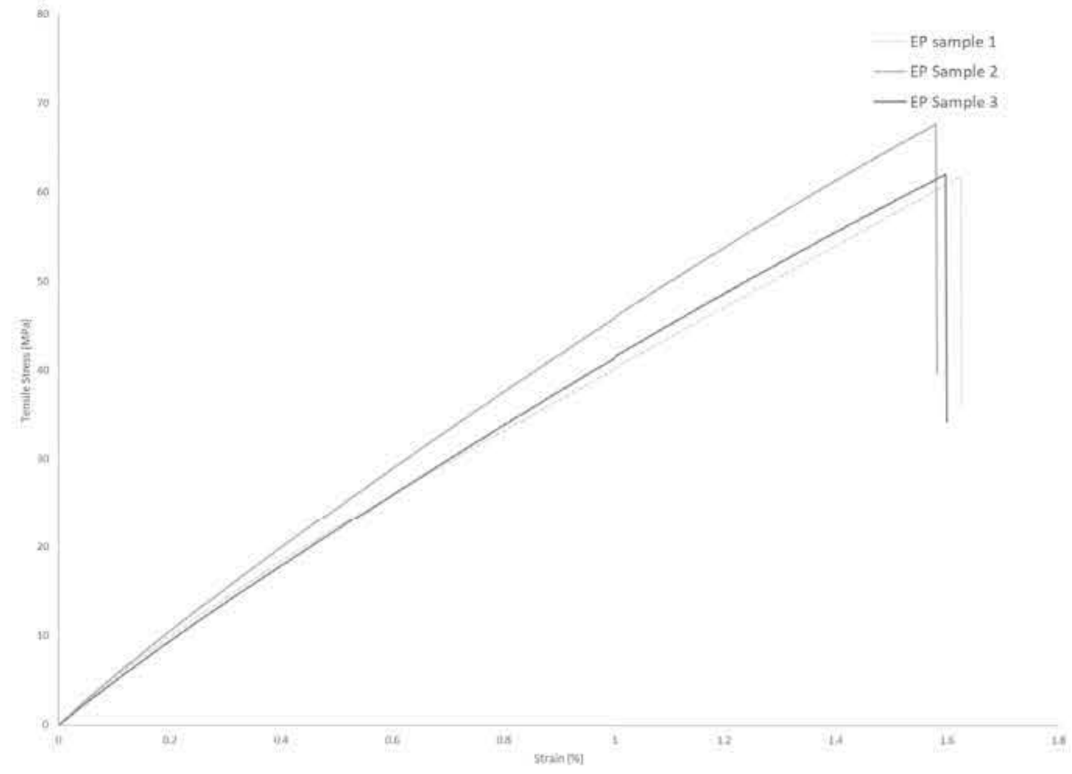

b.)

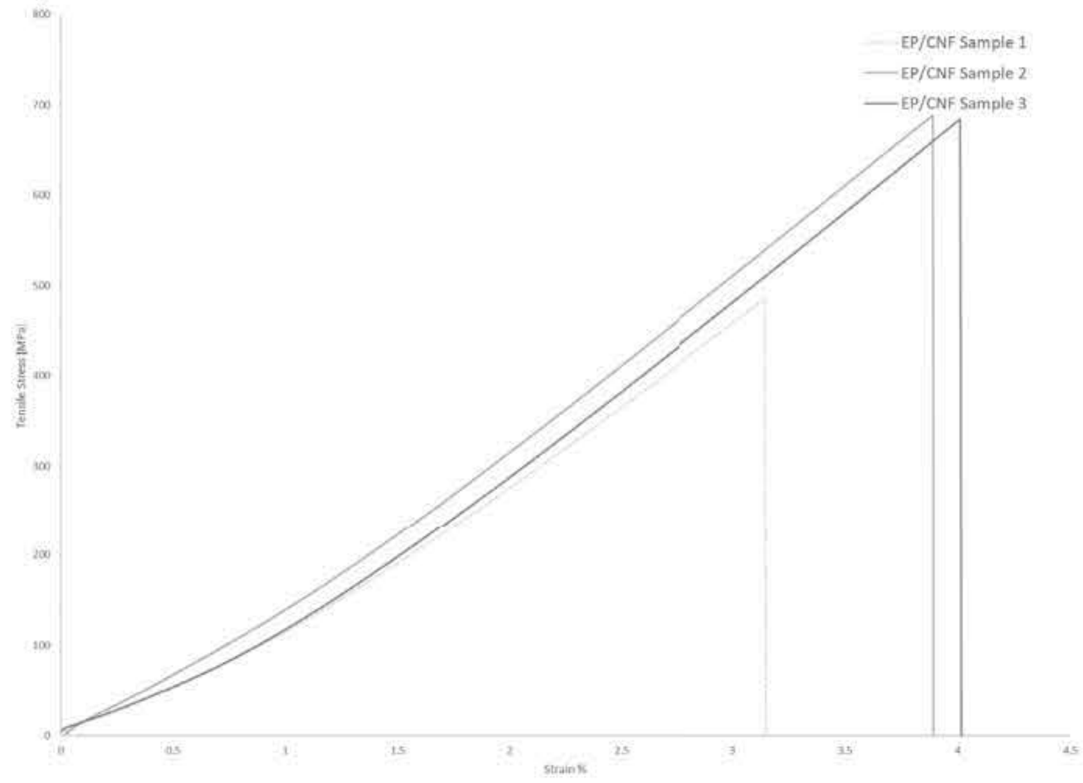

c.)

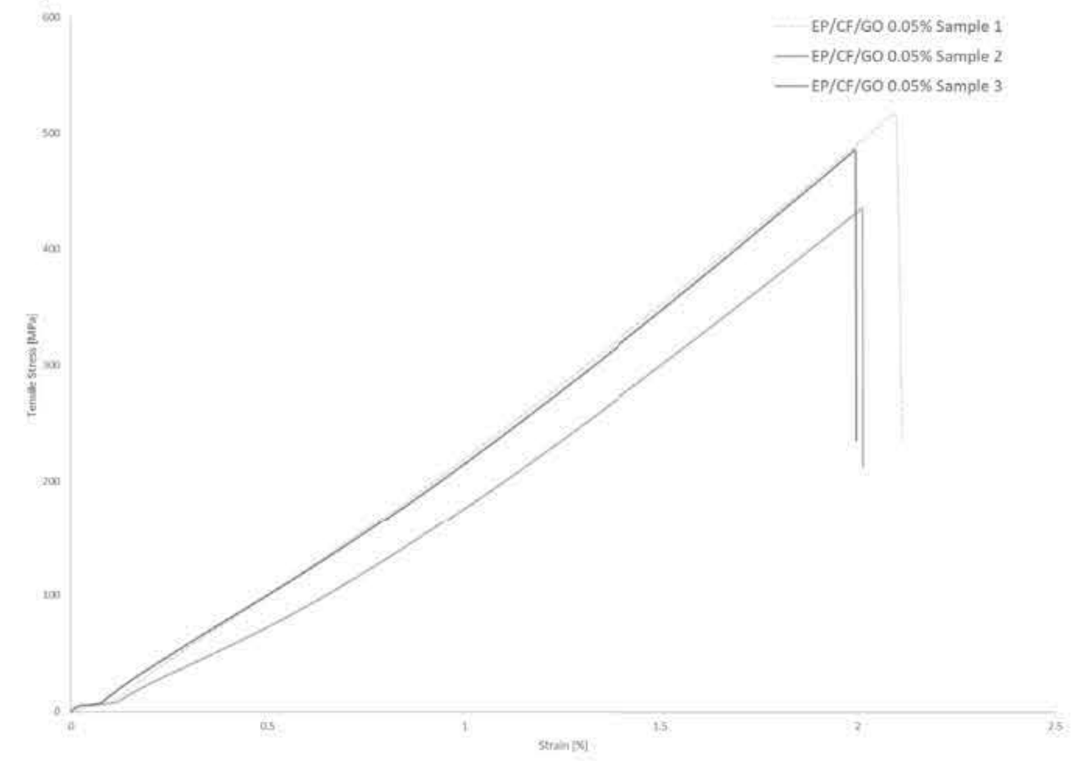

d.)

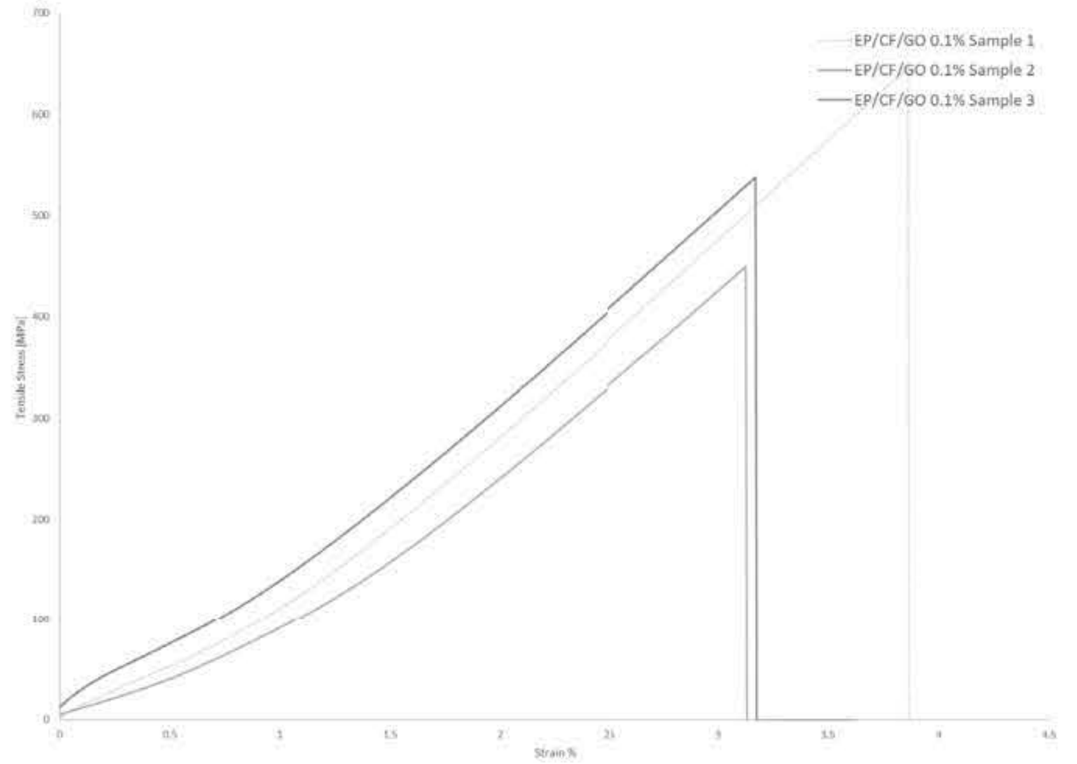

e.)

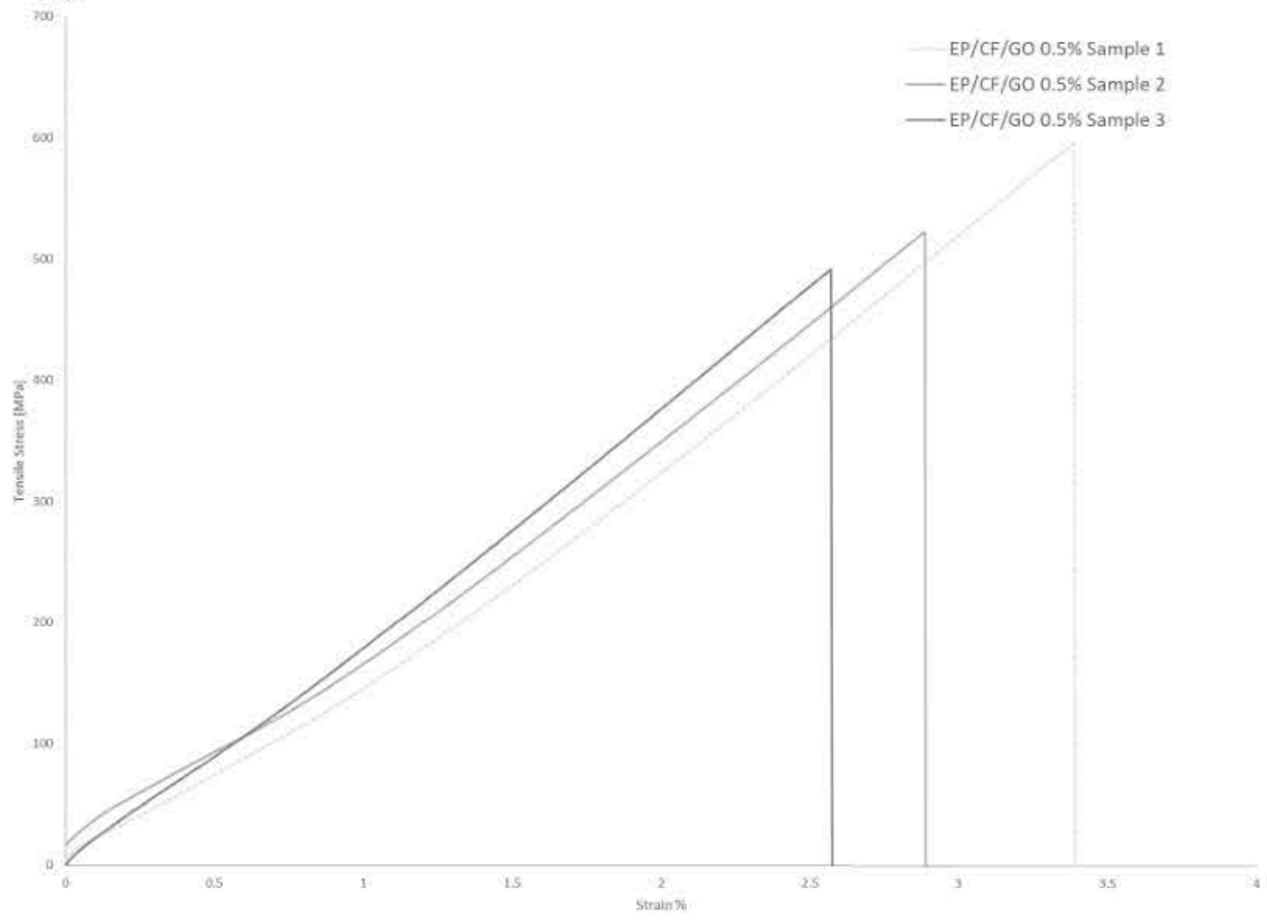

Figure 147: Stress vs strain curves from tensile tests on a.) EP samples b.) EP/CF samples c.) EP/CF/GO 0.05 wt. % samples d.) EP/CF/GO 0.1 wt. % samples and e.) EP/CF/GO 0.5 wt. % samples

Epoxy/Carbon Fibre reinforced with GO Fillers Flexural Results

a.)

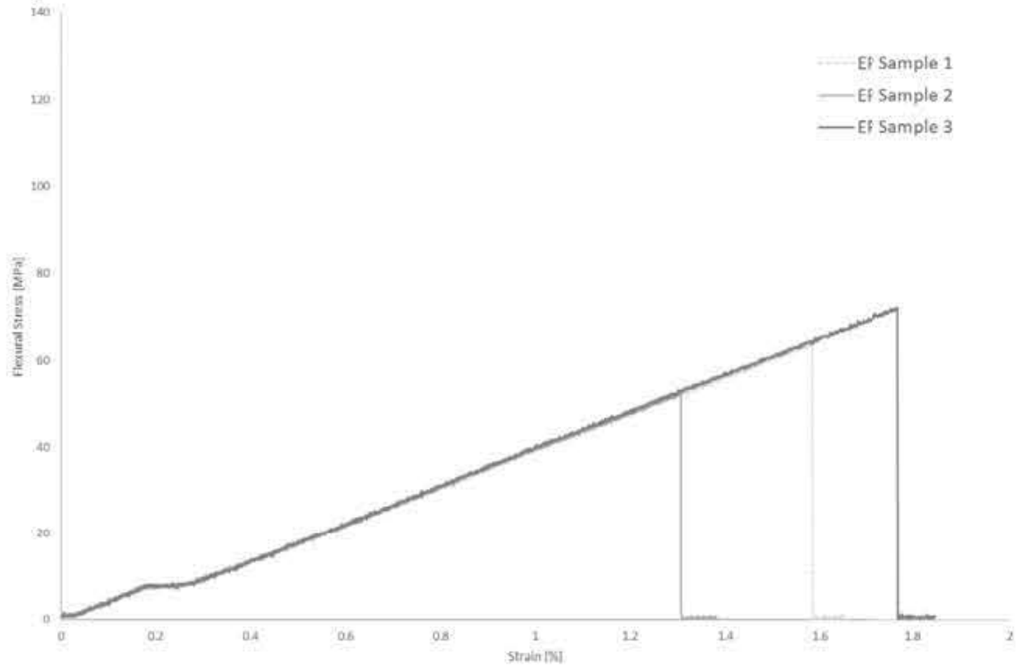

b.)

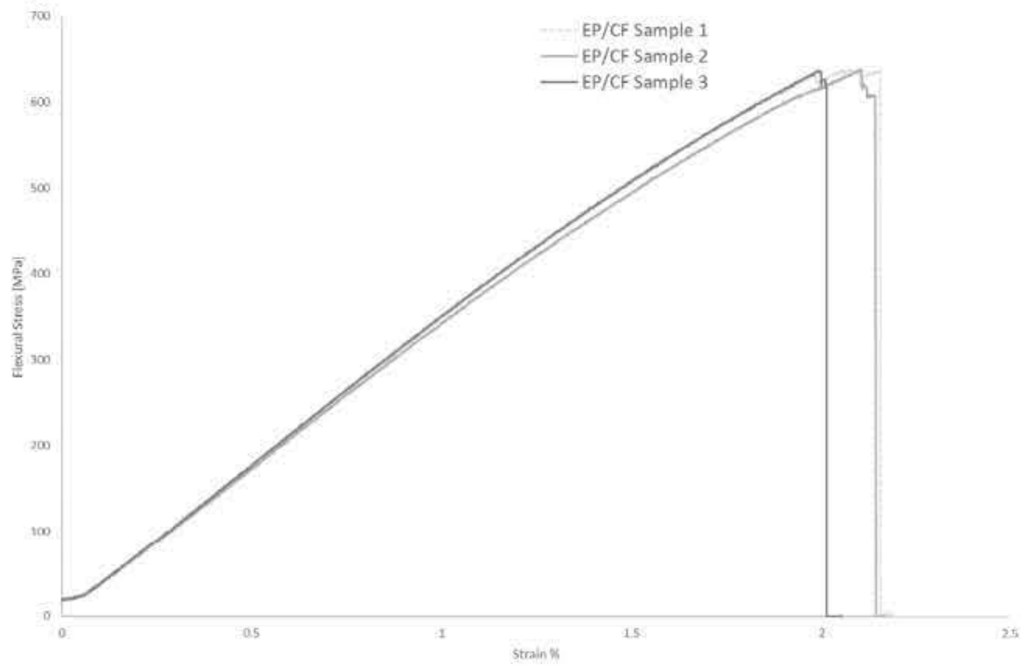

c.)

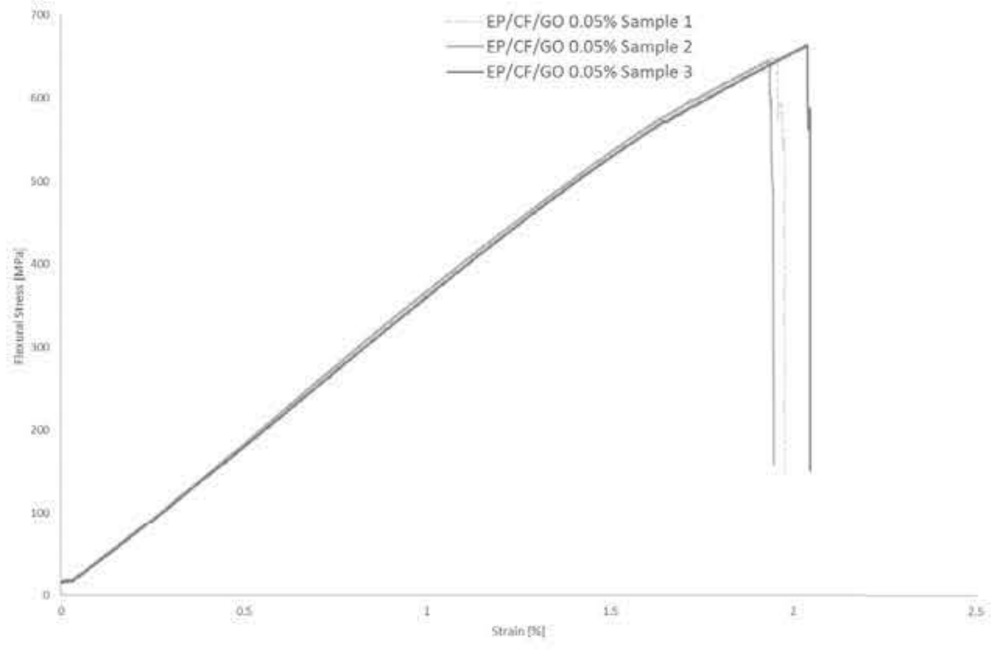

d.)

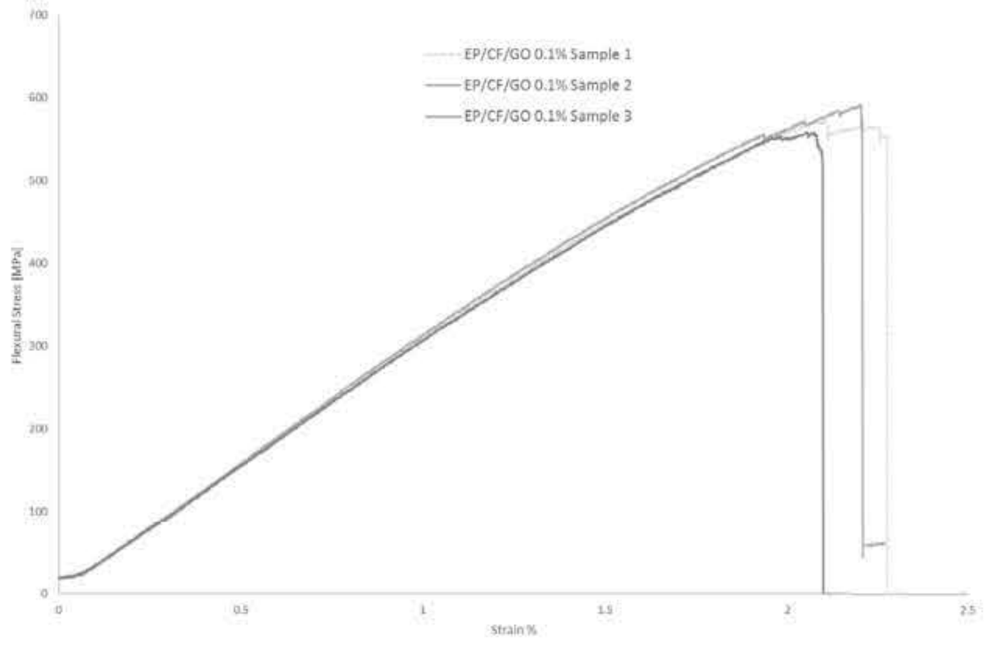

e.)

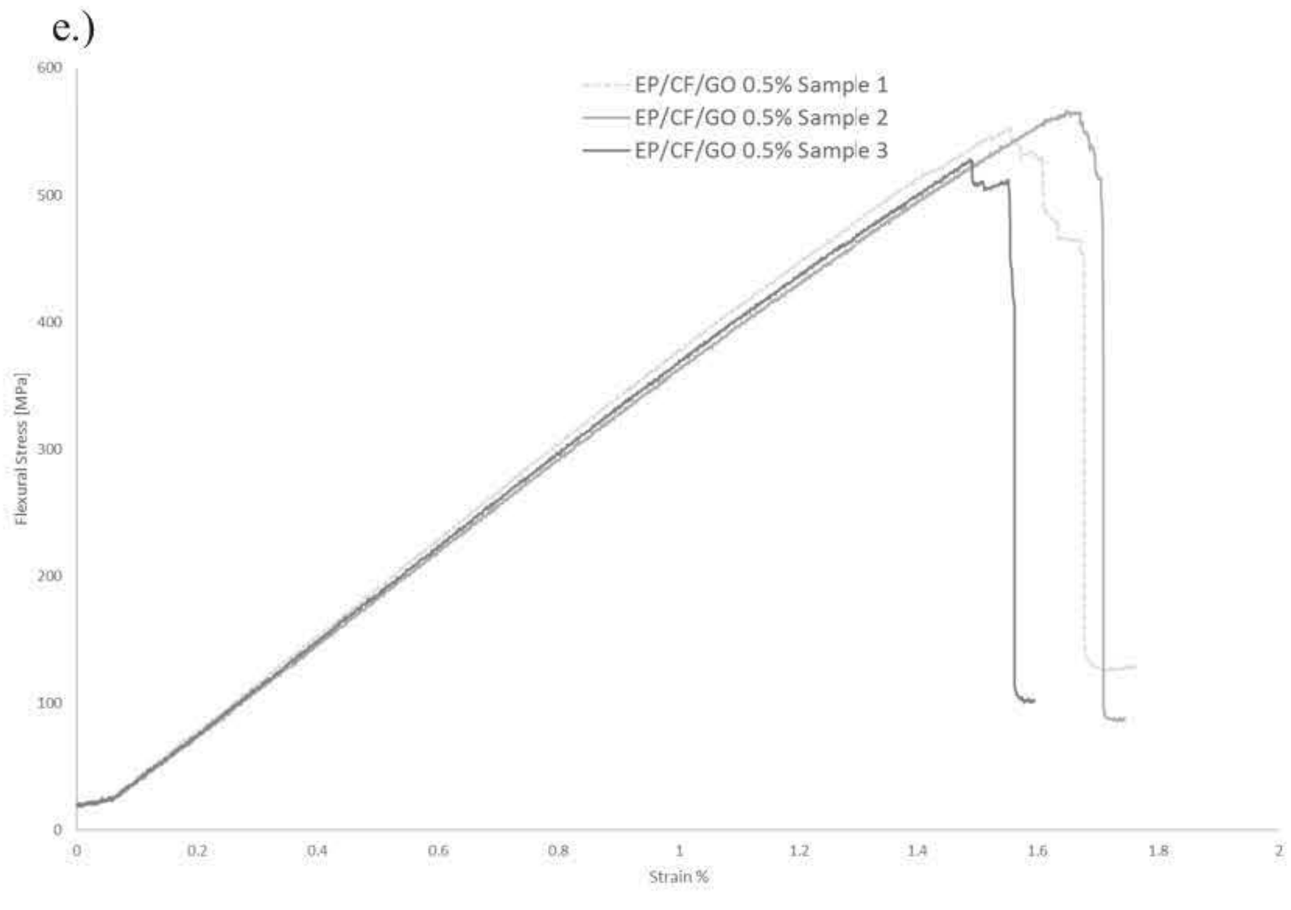

Figure 148: Stress vs strain curves from flexural tests on a.) EP samples b.) EP/CF samples c.) EP/CF/GO 0.05 wt. % samples d.) EP/CF/GO 0.1 wt. % samples and e.) EP/CF/GO 0.5 wt. % samples

Appendix E –

Stress vs Strain of Tensile and Flexural Results Data Calculations.

The data collected from the INSTRON 3382 is measured in terms of load (N) and extension (mm). As per the standard, the data is converted into the tensile stress $\sigma_{Tensile}$, using:

$$\sigma_{Tensile} = \frac{F}{A_{Tensile}} \quad \textbf{- Equation E.1}$$

Where:
F = load [N];
$A_{Tensile}$ = cross-sectional area of tensile samples [mm^2]

The ultimate tensile stress, $\sigma_{Ultimate}$, is therefore calculated using the maximum load, F_{max}, recorded from the equipment for both flexural and tensile tests. The flexural stress $\sigma_{Flexural}$ is calculated using the load, F, measured from the flexural test and the cross-sectional area of flexural samples, $A_{Flexural}$.

$$\sigma_{Flexural} = \frac{F}{A_{Flexural}} \quad \textbf{- Equation E.2}$$

Where:
F = load [N];
$A_{Flexural}$ = cross-sectional area of tensile samples [mm^2]

Correspondingly, the tensile strain, $\varepsilon_{Tensile}$, is calculated as per the standards using:

$$\varepsilon_{Tensile} = \frac{\delta_{Tensile}}{L_{Tensile}} \quad \textbf{- Equation E.3}$$

Where:
$\delta_{Tensile}$ = change in length [mm]
$L_{Tensile}$ = original gauge length [mm]

As per the ASTM D7264 standard, the flexural strain, $\varepsilon_{Flexural}$, for the 3-point bend test is determined using:

$$\varepsilon_{Flexural} = \frac{6\delta_{Flexural}h}{{L_{Flexural}}^2} \quad \textbf{- Equation E.4}$$

Where:
$\delta_{Flexural}$ = mid-span deflection [mm]
h = thickness of beam [mm]
$L_{Flexural}$ = support span [mm]

The modulus of elasticity (also known as Young's Modulus for a tensile test), $E_{Young's}$, was calculated as per the standard using:

$$E_{Young's} = \frac{\Delta\sigma_{Tensile}}{\Delta\varepsilon_{Tensile}} \quad \textbf{- Equation E.5}$$

Where:
$\Delta\sigma_{Tensile}$ = difference in applied tensile stress between two strain points [MPa]
$\Delta\varepsilon_{Tensile}$ = difference between the corresponding two tensile strain points

The flexural chord modulus of elasticity, $E_{Flexural}^{Chord}$, is determined from the 3-point flexural test using:

$$E_{Flexural}^{Chord} = \frac{\Delta\sigma_{Flexural}}{\Delta\varepsilon_{Flexural}} \quad \textbf{- Equation E.6}$$

Where:
$\Delta\sigma_{Flexural}$ = difference in applied flexural stress between two strain points [MPa]
$\Delta\varepsilon_{Flexural}$ = difference between the corresponding two flexural strain points

The data is converted and presented in terms of stress vs strain to compare results.